

Aspects of Critical Behavior of Two Dimensional Electron Systems

A dissertation presented

by

Maxim A. Metlitski

to

The Department of Physics

in partial fulfillment of the requirements

for the degree of

Doctor of Philosophy

in the subject of

Physics

Harvard University

Cambridge, Massachusetts

May 2011

©2011 - Maxim A. Metlitski

All rights reserved.

Thesis advisor

Author

Professor Subir Sachdev

Maxim A. Metlitski

Aspects of Critical Behavior of Two Dimensional Electron Systems

Abstract

This thesis is devoted to the study of strongly correlated electron systems in two spatial dimensions. The main perspective used in this work is that of scaling, implemented by the renormalization group formalism. This thesis can be divided into three main parts. The first part, comprised of chapters 2-5, investigates various aspects of two dimensional insulating quantum antiferromagnets. In particular, chapters 2-4 deal with the phase transition between an ordered antiferromagnet and a valence bond solid on a square lattice. This transition falls outside the conventional Landau-Ginzburg-Wilson paradigm and is described by a so-called “deconfined” quantum critical point. In chapter 2, we present an elegant calculation of the scaling dimension of the valence bond solid order parameter at this quantum critical point. Chapters 3 and 4 investigate signatures of deconfined criticality in the response of an antiferromagnet to non-magnetic impurities. Chapter 5 describes the edge response of a conventional ordered square-lattice antiferromagnet.

The second part of this thesis, comprised of chapters 6 and 7, studies the subject of quantum phase transitions in metallic systems. Such transitions are particularly interesting as Landau Fermi-liquid theory is expected to break down at the critical point. Transitions in metallic systems can be divided into two broad classes based on

whether the wave-vector carried by the order parameter is zero or finite. Chapter 6 studies the first class of transitions, using as an example the critical point involving the onset of Ising-nematic order, which spontaneously breaks the point-group symmetry of the lattice. Chapter 7 studies the second class of transitions, focusing on the critical point involving the onset of spin-density-wave order.

The final part of this thesis, chapter 8, investigates entanglement in a two dimensional system close to a quantum phase transition. Using the $O(N)$ critical point as an example, we explicitly demonstrate the previously hypothesized presence of sub-leading universal corrections to the entanglement entropy. This is the first calculation of the entanglement entropy at a generic, interacting critical point in dimension larger than one.

Contents

Title Page	i
Abstract	iii
Table of Contents	v
Citations to Previously Published Work	ix
Acknowledgments	xi
Dedication	xiv
1 Introduction	1
1.1 Experimental motivation: cuprates and beyond	9
1.2 Magnetic insulators in two dimensions	21
1.2.1 Mott insulators and magnetic exchange	21
1.2.2 Effective theory of a quantum antiferromagnet	23
1.2.3 Long-range ordered state: spin-wave theory	26
1.2.4 Landau-Ginzburg-Wilson criticality	28
1.2.5 Deconfined criticality	30
1.3 Phase transitions in metals	46
1.3.1 Fermi-liquid theory	46
1.3.2 Order onset in a metal	54
1.3.3 Hertz theory	58
1.3.4 Failure of Hertz theory	61
2 Monopoles in CP^{N-1} model via the state-operator correspondence	64
2.1 Introduction	65
2.2 Review of CP^{N-1} model	67
2.3 State-operator correspondence and monopole scaling dimensions	71
2.4 Calculation	76
2.5 Discussion	81
2.6 Conclusion	83

3	Impurity spin textures across conventional and deconfined quantum critical points of two dimensional antiferromagnets	84
3.1	Introduction	85
3.1.1	LGW transition	87
3.1.2	Deconfined transition	89
3.2	LGW criticality	93
3.3	Deconfined criticality	98
3.3.1	Critical point in a finite system	99
3.3.2	Néel phase	113
3.4	Conclusion	122
4	Valence bond solid order near impurities in two-dimensional quantum antiferromagnets	125
4.1	Introduction	126
4.1.1	Modulated exchange	131
4.1.2	Missing spin	133
4.2	$1/N$ Expansion of the CP^{N-1} theory in the presence of monopoles . .	137
4.3	Easy plane model at $N = 1$	143
4.3.1	Duality and Wilson loops	143
4.3.2	Perturbative expansion of the dual theory for $Q \rightarrow 0$	149
4.3.3	Peculiarities of the free theory	152
4.3.4	$1/M$ expansion of the dual theory	159
4.4	Easy plane theory for general N	167
4.4.1	Duality in the Easy Plane Theory	168
4.4.2	Wilson loops in the easy plane theory	171
4.5	Conclusion	176
5	Edge response in two-dimensional quantum antiferromagnets	179
5.1	Introduction	179
5.2	Edge response in the $O(3)$ σ -model	185
5.2.1	Zero Temperature	185
5.2.2	Edge susceptibility at finite temperature	192
5.3	Large S expansion of the Heisenberg model with an edge	196
5.4	The comb structure	202
5.5	Conclusion	206
6	Quantum phase transitions of metals in two spatial dimensions: Ising-nematic order	208
6.1	Introduction	209
6.2	The model	212
6.3	One loop propagators	219
6.4	Scaling and renormalization	221

6.4.1	Rotational symmetry	223
6.4.2	Ward identities	226
6.4.3	RG equations	231
6.5	Anomalous exponents to three loops	238
6.5.1	Dynamical critical exponent	239
6.5.2	Fermion anomalous dimension	243
6.5.3	Fermi surface shift	248
6.6	Conclusion	249
7	Quantum phase transitions of metals in two spatial dimensions: Spin density wave order	253
7.1	Introduction	254
7.2	Low energy field theory	257
7.2.1	The Hertz action	261
7.2.2	Breakdown of the Hertz theory	263
7.2.3	RG interpretation	264
7.3	Field-theoretic RG	265
7.3.1	RG flows	276
7.4	Counting powers of N	279
7.5	Pairing vertex	297
7.6	Density vertices	301
7.7	Conclusion	309
8	Entanglement entropy in the $O(N)$ model	315
8.1	Introduction	316
8.2	The replica trick	324
8.3	Parametric enhancement of correlation length correction	325
8.4	ϵ -expansion: correlation length correction	328
8.4.1	Gaussian theory	328
8.4.2	Interacting theory	329
8.4.3	Beyond the leading order in ϵ	340
8.5	ϵ -expansion: finite size correction	351
8.5.1	Gaussian theory	352
8.5.2	ϵ -expansion	354
8.5.3	Beyond the leading order in ϵ	356
8.6	Large N limit	360
8.7	Conclusion.	371
A	Appendix to Chapter 2	374
A.1	Functions $G_q(b^2)$ and $F_q(b^2)$	374
A.2	Comparison to Murthy-Sachdev expression	378

B	Appendix to Chapter 3	380
B.1	$U(1)$ charge density	380
C	Appendix to Chapter 4	384
C.1	Electric field in the free theory	384
C.2	Integral form of the twisted propagator	386
D	Appendix to Chapter 5	391
D.1	Eigenfunctions of Bogoliubov quasiparticles	391
E	Appendix to Chapter 6	394
E.1	Decoupling of non-collinear momenta	394
E.2	Computations of Feynman diagrams	398
E.2.1	Boson self-energy	398
E.2.2	Fermion self-energy	402
F	Appendix to Chapter 7	411
F.1	RG computations	411
F.1.1	RPA polarization	411
F.1.2	Fermion self energy	413
F.1.3	Boson-fermion vertex	414
F.1.4	Boson self energy	415
F.2	Violations of large- N counting	418
F.2.1	Boson-fermion vertex correction at three loops	418
F.2.2	Quartic vertex	422
F.2.3	Pairing vertex	426
F.2.4	Density vertex	429
	Bibliography	431

Citations to Previously Published Work

Publications related to the particular chapters are as follows

Chapter 2

- Max A. Metlitski, Michael Hermele, T. Senthil, and Matthew P. A. Fisher, “*Monopoles in CP^{N-1} model via the state-operator correspondence,*” Phys. Rev. B **78**, 214418 (2008).

Chapter 3

- Max A. Metlitski and Subir Sachdev, “*Impurity spin textures across conventional and deconfined quantum critical points of two-dimensional antiferromagnets,*” Phys. Rev. B **76**, 064423 (2007).

Chapter 4

- Max A. Metlitski and Subir Sachdev, “*Valence bond solid order near impurities in two-dimensional quantum antiferromagnets,*” Phys. Rev. B **77**, 054411 (2008).
- Max A. Metlitski, “*Wilson loops in non-compact $U(1)$ gauge theories at criticality,*” Phys. Rev. D **77**, 085011 (2008).

Some additional numerical work related to Chapter 4 but not included in this thesis has been presented in

- Ribhu K. Kaul, Roger G. Melko, Max A. Metlitski and Subir Sachdev, “*Imaging bond order near non-magnetic impurities in square lattice antiferromagnets,*” Phys. Rev. Lett. **101**, 187206 (2008).

Chapter 5

- Max A. Metlitski and Subir Sachdev, “*Edge and impurity response in two-dimensional quantum antiferromagnets,*” Phys. Rev. B **78**, 174410 (2008).

Chapter 6

- Max A. Metlitski and Subir Sachdev, “*Quantum phase transitions of metals in two spatial dimensions: I. Ising-nematic order,*” Phys. Rev. B **82**, 075127 (2010).

Chapter 7

- Max A. Metlitski and Subir Sachdev, “*Quantum phase transitions of metals in two spatial dimensions: II. Spin density wave order,*” Phys. Rev. B **82**, 075128 (2010).
- Max A. Metlitski and Subir Sachdev, “*Instabilities near the onset of spin density wave order in metals,*” New J. Phys. **12**, 105007 (2010).

Chapter 8

- Max A. Metlitski, Carlos A. Fuertes and Subir Sachdev, “*Entanglement Entropy in the $O(N)$ model,*” Phys. Rev. B **80**, 115122 (2009).

Some work related to the problem of doping an antiferromagnetic Mott insulator, which is not presented in this thesis for space reasons, has appeared in:

- Ribhu K. Kaul, Max A. Metlitski, Subir Sachdev and Cenke Xu, “*Destruction of Neel order in the cuprates by electron-doping,*” Phys. Rev. B **78**, 045110 (2008).
- Subir Sachdev, Max A. Metlitski, Yang Qi and Cenke Xu, “*Fluctuating spin density waves in metals,*” Phys. Rev. B **80**, 155129 (2009).

Acknowledgments

As hard as it is to believe, with every word I write now my five years at Harvard are drawing to an end. These were undoubtedly the five most exciting years of my life, for which I have many people to thank here. So, let me begin.

First of all, I would like to express my deep gratitude to my advisor, Subir Sachdev. I have been truly lucky to have Subir as my mentor over the past five years: the support and encouragement that I received knew no boundaries. I am humbled by Subir's enthusiasm for my ideas and the unlimited freedom he gave me to explore them. I continue to be amazed by his style of doing physics, marked by deep intuition combined with brilliant technical skill. Subir is always at his best: whether giving a talk, figuring out a problem on the blackboard, barbecuing for his guests or driving fearlessly through a blizzard in the Colorado mountains. I sincerely hope that the completion of this thesis will not mark the end of our collaboration, but rather a new beginning!

Besides Subir, I have been fortunate to collaborate with and learn from a number of remarkable people. In particular, I would like to thank Senthil Todadri, a “scientific sibling” one can truly look up to! It has been great fun to realize that we are working on similar problems and join forces! I am also grateful to Andrey Chubukov, a fearless man in the face of horrendous Feynman diagrams, for many long discussions, as well as for his hospitality in Dresden last summer. Other collaborators that I would like to thank are Cenke Xu, Mike Hermele, Matthew Fisher, Ribhu Kaul, Roger Melko, Yang Qi, Carlos Fuertes, Sean Hartnoll and Diego Hofman. Finally, it is always a pleasure to talk to my friend and fellow graduate student Eun-Gook Moon. I am very happy that we are coherently pair-hopping to Santa-Barbara next year and will have

a chance for many more exciting discussions.

I would also like to thank Bert Halperin and Andy Strominger for kindly agreeing to serve on my thesis committee.

Going further into the past, my undergraduate and Master's thesis advisor Eric Zhitnitsky has undoubtedly played a crucial role in my decision to pursue a career in physics. I distinctly remember Eric's first lecture in my undergraduate quantum mechanics class, which started with the words "Quantum mechanics is not like any other kind of mechanics!" I was hooked by the quantum world ever since. Eric's love of physics and his unwavering optimism are truly inspiring. I am extremely grateful to Eric for his support over both my years at UBC and subsequent PhD years at Harvard. As Michael Forbes, a fellow student of Eric, has succinctly summarized Eric's attitude towards his students: "Yes, Eric is your mother!" I still can't believe I have been so lucky with my mentors!

Over the past five years I have been fortunate to make many friends both in and outside physics. I would especially like to thank my dear friends Michael (Misha) Novick and Alexander (Sasha) Ryabogin. It is difficult for me to imagine life without being able to go to Misha's place for tea (which typically turns into a royal feast). To Sasha I am grateful for helping me rediscover my love of Russian poetry that has greatly influenced my worldview. I have met many friends during various summer schools and conferences. In particular, I would like to thank the Les Houches gang: Lyudmila (Lyudochka) Kushnir, Joern Kupferschmidt, Jonathan Edge, Silvia Viola Kusminskiy and Maria Medvedeva. You guys are amazing and I am looking forward to many new adventures together (where did we decide on next: Morocco?) To

Lyudochka I am additionally grateful for helping me keep my sanity during the time I have been writing this thesis. I would also like to thank another Les Houches friend, Zhenya Burovski, for his hospitality in Paris on two occasions. Which brings me to another friend, Misha Zvonarev (a.k.a. Misha de Paris) to whom I would like to pay a compliment using his own favorite expression: “Misha, you are rock solid!”

Finally, I would like to thank my family. To my grandmother Lilia I am grateful for the daily phone calls and constant encouragement over the past five years. I can only dream to be as involved in life as she is when I get to her age. To my grandfather Misha, I would like to say that I always feel his love even though we live half a world away. He was the first to earn a PhD in my family and I am proud to follow in his footsteps. I would also like to thank my younger brother Daniel for his affection.

Above all, everything I have I owe to my parents. I admire their courage in deciding to immigrate to Canada to give my brother and myself a better future. Their move has enabled me to freely choose my career and enter the academic world. My mother’s devotion to my education has always been extraordinary. I owe her many hours that she spent with me in my childhood going through fun math problems, taking me to various extra-curricular classes etc. To my father I would like to say that he is the most interesting person in the world to talk to and I wish I had a tiny fraction of his intellectual curiosity. As I am finishing writing this I already know what I will predictably do next: I will call my parents.

*10.04.2011
Cambridge, MA*

Dedicated to my father Sasha and my mother Luba.

Chapter 1

Introduction

One of the central themes in modern physics is the idea of universality: the observation that systems, which are very different microscopically, can have identical long distance, low energy properties. Such behavior is typically observed when the correlation length of the system becomes much larger than the microscopic length scale. A system with a divergent correlation length is called “critical.” The classic example of universality is that of finite temperature second order phase transitions, where as one lowers the temperature T , the system goes from a disordered to an ordered phase. The correlation length ξ at such transitions typically diverges as a power law,

$$\xi^{-1} \sim (T - T_c)^\nu \tag{1.1}$$

where T_c is the critical temperature of the transition, and ν is the correlation length exponent. A number of other quantities, such as the expectation value of the order parameter, the susceptibility and the specific heat also show power law behavior close to the transition. Amazingly, the critical exponents governing the power law

behavior are universal. Moreover, the universality class of the transition is determined exclusively by the symmetry properties of the order parameter. A general theory of such transitions, the so-called “Landau-Ginzburg-Wilson paradigm,” is very well developed by now.

Much attention over the recent years has been devoted to the study of critical behavior at zero temperature. Unlike critical systems at finite temperature, where on sufficiently large length scales only classical fluctuations play a role, the physics at zero temperature is inherently quantum-mechanical. Thus, we refer to critical behavior at zero temperature as “quantum criticality.” Quantum critical behavior can occur either close to a phase transition, tuned by a non-thermal parameter, such as pressure, magnetic field or doping, or in a whole stable phase of matter. In the first case, the correlation length of the system diverges as,

$$\xi^{-1} \sim (g - g_c)^\nu \quad (1.2)$$

where g_c is the critical value of the tuning parameter g . To the divergent correlation length there corresponds a vanishing energy scale

$$\Delta \sim \xi^{-z} \quad (1.3)$$

where z is known as the dynamical critical exponent. At the phase transition itself $g = g_c$, also known as the “quantum critical point” (QCP), the correlation length is infinite and the system possesses gapless excitations which disperse as

$$\omega \sim k^z \quad (1.4)$$

In the second case of a stable critical phase, the correlation length is infinite and the system possesses gapless excitations throughout the phase.

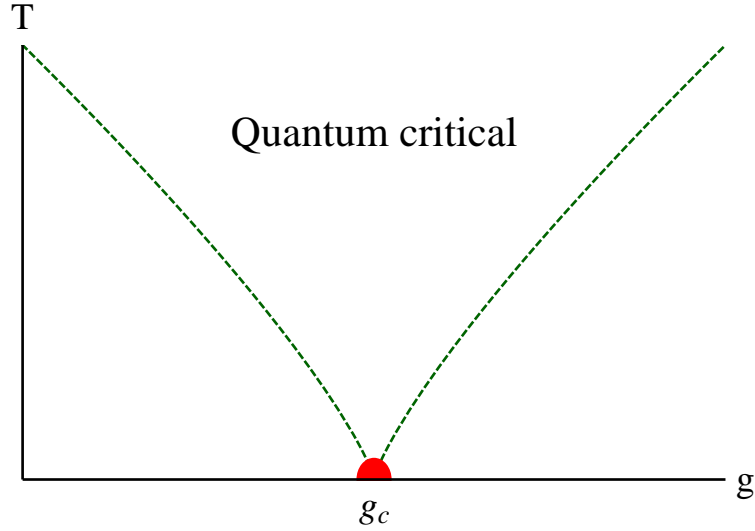


Figure 1.1: A generic phase diagram of a system close to a quantum critical point. The region marked “Quantum critical” is controlled by the $T = 0$ QCP at $g = g_c$. The green lines may be crossovers or sharp phase transitions depending on the system.

In both cases, temperature serves as an additional probe of the quantum critical physics. The role of temperature in the physics of quantum criticality is analogous to that of finite size scaling in the physics of classical criticality. Indeed, temperature enters the partition function of a quantum system through periodic identification of the imaginary time direction $\tau \sim \tau + \beta$, with $\beta = 1/kT$. In the case of a quantum phase transition this gives rise to the appearance of a “quantum critical fan” region located above the quantum critical point in the phase diagram, Fig. 1.1. The boundary of the critical fan is given roughly by $kT \sim \Delta \sim |g - g_c|^{\nu z}$. Deep inside the fan, $kT \gg \Delta$, so the length of the temporal direction $1/kT$ is much smaller than the time scale $1/\Delta$ associated with the gap formation. Hence, the system is unaware of the presence of the energy scale Δ and behaves as if it was directly at the critical point. This leads to a surprising conclusion that as one raises the temperature of the system,

an increasingly larger region of the phase diagram is controlled by the QCP.

It is believed that the universe of quantum critical phenomena is far richer than its classical counterpart. Indeed, we now know that for a quantum phase transition, it is not enough to specify the symmetry properties of the order parameter to determine the universality class. For instance, a quantum phase transition involving the onset of some order in a metal is drastically different from the corresponding transition in an insulator. The reason for this is the presence of additional low energy excitations in a metal, which are absent in an insulator. Even in insulating systems, symmetry considerations do not determine the universality class of the transition. For example, the transition involving the destruction of magnetic order is different in systems with an odd and even number of electrons per unit cell. Finally, some quantum phase transitions, such as the Mott transition between a metal and an insulating spin-liquid, do not involve spontaneous symmetry breaking at all.

As with classical phase transitions the spatial dimensionality of the system plays an important role in the study of quantum criticality. Quantum fluctuations tend to increase as the dimension is lowered. As a result, one dimensional systems often exhibit truly exotic physics, such as spin-charge separation and fractional excitations. Luckily, in one dimension a number of techniques are available, such as bosonization and exact solutions through the so-called “Bethe-ansatz,” which allow one to harness the exotic physics. Moreover, critical one dimensional systems with a dynamical exponent $z = 1$, i.e. with linearly dispersing excitations, possess an infinite dimensional conformal symmetry, which gives one a complete classification of such systems. On the other hand, in higher dimensions exact solutions are largely absent and the con-

formal group is only finite dimensional, making the study of critical behavior much more challenging.

In this thesis, we will explore some aspects of quantum criticality in two dimensional electron systems. Unlike in one dimension, where quantum fluctuations typically prevent the system from spontaneously breaking continuous symmetries, thus excluding phases with true magnetic long range order, in two dimensions quantum fluctuations are weaker making such phases stable at zero temperature. Moreover, Fermi-liquids, which are unstable in the presence of arbitrarily weak interactions in one dimension become stable in two dimensions. The question that will preoccupy us through most of this thesis is how do these conventional phases get destroyed at quantum phase transitions.

The thesis can be divided into three parts. The first part, comprised of chapters 2-5 is devoted to insulating magnetic systems. Chapters 2-4 deal with the subject of the phase transition between an insulating $S = 1/2$ antiferromagnet and a valence-bond-solid on a square lattice. The antiferromagnetic state breaks the $SU(2)$ spin rotation symmetry, while the valence-bond-solid breaks the rotational symmetry of the lattice. Within the classical Landau-Ginzburg-Wilson (LGW) paradigm, a direct second order transition between these phases is prohibited, as the symmetries spontaneously broken on the two sides of the critical point appear unrelated. However, as realized in Refs. [1, 2], in the quantum world, the defects of the order parameter in a phase where one symmetry is broken carry non-trivial quantum numbers under the other symmetry. Namely, skyrmions of the antiferromagnet transform non-trivially under lattice rotations and vortices of the valence-bond-solid carry spin $1/2$. At the

transition, condensation of defects of one order occurs, which leads to the appearance of the other order. In the literature, this transition is known as a “deconfined” quantum critical point, due to its description in terms of strongly interacting $S = 1/2$ excitations.

Chapter 2 presents an elegant calculation of the scaling dimension of the valence-bond-solid order parameter at the deconfined QCP. This calculation utilizes the state-operator correspondence of conformal field theory and confirms the results of a previous direct, but rather cumbersome, calculation in Ref. [3]. It also explicitly demonstrates that skyrmions do, indeed, become massless at the transition.

Chapters 3 and 4 study the response of an antiferromagnet in the vicinity of a deconfined QCP to a non-magnetic, missing spin impurity. Such impurities can be introduced in the cuprate superconductors by substituting a magnetic Cu^{2+} ion, with a non-magnetic Zn^{2+} ion. The impurity is expected to localize the missing spin $S = 1/2$ around it; in chapter 3 we study the associated spin texture. The signature of deconfined criticality is even more dramatic in the response of the local bond order to the missing spin impurity: in chapter 4 we find that such an impurity nucleates a vortex of the local bond order.

Chapter 5 studies the response of a conventional ordered antiferromagnet on a square lattice to the presence of a straight edge boundary. This work was done in parallel with the Monte-Carlo simulations of Ref. [4] and was initially motivated by the observation of an unusual bond pattern close to the edge. We have provided an interpretation for the appearance of this pattern in terms of the proximity of the system to a deconfined critical point. We have also predicted that the magnetic susceptibility

of the system acquires a negative boundary contribution that diverges logarithmically as the temperature $T \rightarrow 0$. This prediction was verified by the simulations in Ref. [4].

The second part of this thesis, consisting of chapters 6 and 7 studies quantum phase transitions associated with ordering in two dimensional metallic systems. This problem is believed to be of great importance for the physics of a variety of correlated electron systems, such as the cuprate and pnictide superconductors, heavy-fermion compounds and some organic materials. The experimental motivation will be briefly reviewed in Sec. 1.1. On the theoretical side, this problem introduces new technical as well as conceptual challenges compared to the study of corresponding transitions in insulators. The reason for this is the presence of low energy critical excitations on the whole Fermi-surface rather than at isolated points.

Phase transitions in metallic systems can be divided into two classes, based on whether the order parameter carries a zero or finite momentum. The fluctuations of the order parameter couple differently to the Fermi-surface for the two classes. In chapter 6, we develop a critical theory of the phase transitions in the first class, using as an example the Ising-nematic transition on a square lattice. Such a transition is associated with the onset of correlations that spontaneously break the four-fold rotational symmetry of the lattice to a two-fold subgroup. In chapter 7, we study the onset of antiferromagnetic, spin-density-wave (SDW) order in a metal, which is an important example of a transition in the second class. For both types of transitions, we show that the previously accepted treatment, known as Hertz theory,[5] fails in two spatial dimensions.

The third part of this thesis, chapter 8, studies the quantum entanglement of the

system close to a QCP. Given a system consisting of two subsystems A and B , a convenient measure of entanglement between A and B is the so-called “entanglement entropy,” defined as the von-Neumann entropy associated with the reduced density matrix of one of the subsystems. The entanglement entropy serves as an inherently quantum mechanical non-local observable. This observable is expected to capture the long-range correlations present in a critical quantum system. In particular, for a conformally invariant one dimensional system, it is known that the entanglement entropy diverges as

$$S = \frac{c}{3} \log \ell/a \quad (1.5)$$

where ℓ is the subsystem size, a is the lattice spacing and c is a universal number characterizing the critical system, known as the central charge.[6] The logarithmic divergence in Eq. (1.5) is a signature of the long-range entanglement present at a quantum critical point. On the other hand, in dimensions larger than one, the leading contribution to the entanglement entropy at a QCP scales as the area (length) of the boundary of the subsystem,

$$S = C \frac{|\partial A|}{a^2} \quad (1.6)$$

This contribution is dominated by the short-range entanglement close to the boundary between A and B and, therefore, has a non-universal coefficient C . However, it has been hypothesized that there exist universal subleading corrections to Eq. (1.6). In chapter 8, we confirm this hypothesis by an explicit calculation of the entanglement entropy at a transition in two dimensions in the $O(N)$ universality class. This is the first calculation of entanglement entropy at a generic, interacting two dimensional critical point.

In the rest of this chapter we review introductory material, which will be used through the rest of this thesis. In Sec. 1.1 we give a brief overview of experiments on cuprate superconductors and other strongly correlated materials, which have motivated the theoretical work in the first two parts of this thesis. Sec. 1.2 reviews the physics of insulating antiferromagnets in two dimensions and serves as an introduction to the first part of this thesis. Sec. 1.3 reviews Landau Fermi-liquid theory and introduces the subject of quantum phase transitions in metals, which will be further discussed in the second part of this thesis.

1.1 Experimental motivation: cuprates and beyond

Much of the work contained in this thesis has been motivated by the enigmatic cuprate superconductors. These materials, discovered in 1986, continue to present a challenge to theoretical understanding. Cuprates are a family of layered compounds with a common structural element of copper-oxygen planes, which are believed to be responsible for the exotic physical properties.

All cuprates possess a similar phase diagram, schematically shown in Fig. 1.2. At stoichiometric doping, these materials are insulators with a gap of order 2 eV. The insulating behavior is not a trivial consequence of band structure. Indeed, each copper-oxygen plane consists of a square lattice of coppers with oxygens situated on the bonds of this lattice, so that each unit cell contains one copper atom and two oxygens, see Fig. 1.3. In the undoped materials, the chemical valence of copper and oxygen is Cu^{2+} and O^{2-} respectively. Hence, the oxygen shell is completely filled, while Cu is in the $3d^9$ configuration. The crystal field lifts the orbital degeneracy,

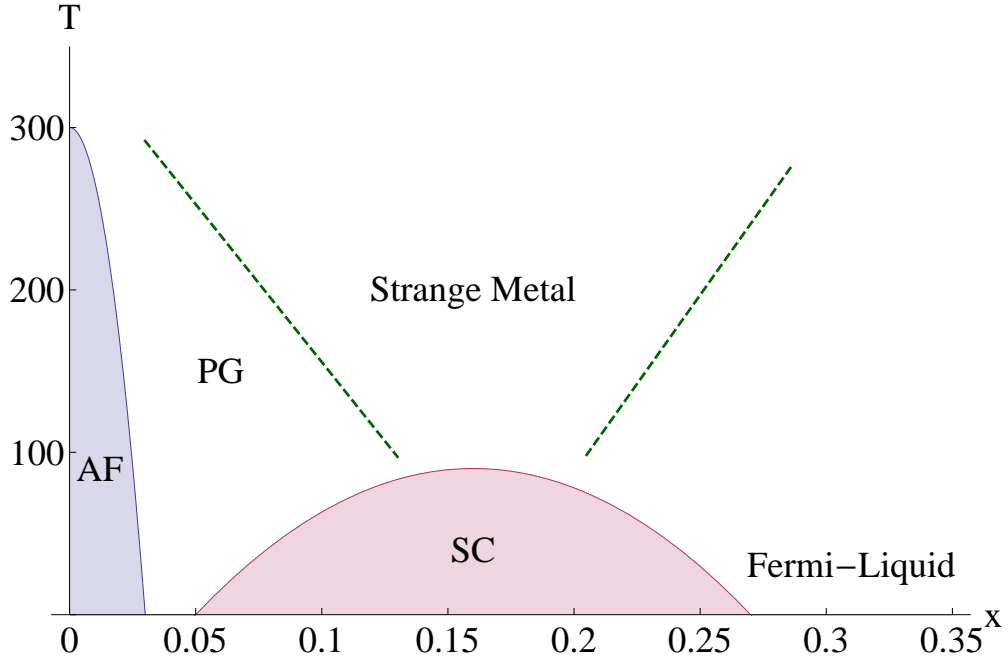


Figure 1.2: A schematic phase diagram of cuprate superconductors as a function of hole-doping x and temperature T . AF denotes the Néel ordered antiferromagnetic state, SC - the d -wave superconducting phase and PG - the pseudogap region.

leaving a half-filled Cu $d_{x^2-y^2}$ orbital. Since the number of electrons per unit cell is odd, band structure would predict that the system is a metal. The experimentally observed insulating behavior is attributed to electron correlations, specifically, a strong Coulomb repulsion on the Cu sites, which quenches the charge motion.

The insulator displays long range antiferromagnetic Néel order shown in Fig. 1.3 with an ordering temperature of $T_N \approx 300$ K. The magnetism is a consequence of the super-exchange interaction mediated by virtual tunneling. The exchange constant between the neighbouring copper sites is of order $J \sim 1500$ K. The large difference between J and T_N is due to the fact that strictly two dimensional systems with $SU(2)$ spin-rotation symmetry don't display long range order at any finite temperature. The

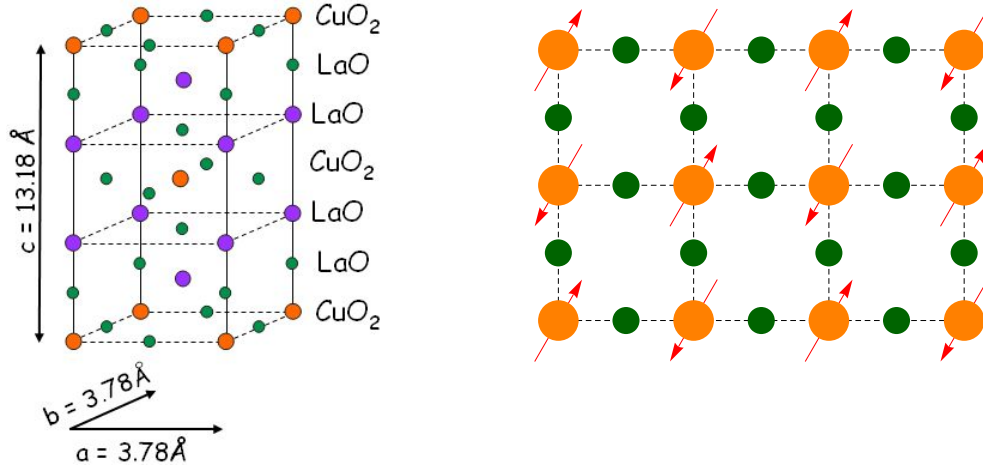


Figure 1.3: Left: crystal structure of the cuprate superconductor $\text{La}_{2-x}\text{Sr}_x\text{CuO}_4$. Cu atoms are shown in orange, O in green and La/Sr in purple. Right: the copper-oxygen plane (same color-coding as in the left figure). Here, we also display the staggered pattern of Cu spins in the antiferromagnetic Néel state.

presence of long range magnetic order in cuprates below T_N is, thus, a consequence of weak interlayer coupling. In the range $T_N \lesssim T \lesssim J$ the system displays the hallmarks of two dimensional antiferromagnetism, such as a correlation length that exponentially diverges as the temperature is lowered.[7] The reader is referred to Sec. 1.2 for a brief review of magnetic insulators.

The stoichiometric material can be doped with either holes or electrons. On the hole doped side, the long-range commensurate antiferromagnetic order disappears at about 3 – 5% doping, and a superconducting phase appears roughly in the 6 – 27% doping range. The pairing symmetry of the superconductor is $d_{x^2-y^2}$ and the maximum critical temperature varies from 35 to 135 K depending on the compound. Upon further doping, the material becomes a fairly conventional metal. The phase diagram is rather similar on the electron doped side, the main difference being that commensurate antiferromagnetism here is more robust and survives up to 14 – 15%

doping. The maximum value of T_c of about 25 K is also lower on the electron doped side. Below, we will focus our attention mainly on the hole doped cuprates.

Perhaps, even more fundamental than the question of the numerically large value of the critical temperature T_c for the onset of superconductivity is the origin of various phenomena observed in the “normal” metallic state of cuprates at temperature above T_c . Here two puzzles are present. The first is the so-called “pseudogap” regime observed on the underdoped side of the phase diagram. Pseudogap refers to a number of anomalies detected by various experimental probes such as specific heat, magnetic susceptibility, optical and dc transport, STM (scanning-tunneling microscopy) and ARPES (angle-resolved photoemission). Note that for many probes the onset of the pseudogap appears as a fairly smooth crossover rather than a sharp transition, so the value of T^* may vary depending on the probe. When the system is strongly underdoped, T^* is as high as 300 K - much higher than the superconducting T_c . Many of the probes suggest a disappearance of low energy quasiparticles near the Fermi-surface in the pseudogap regime. This is in contrast to the behavior in conventional superconductors, where the Fermi-surface becomes gapped only below the superconducting transition temperature.

A number of different orders are detected in the underdoped region of the phase diagram where the pseudogap is realized. First, many cuprate materials display an incommensurate magnetic order. For instance, in $\text{YBa}_2\text{Cu}_3\text{O}_{6+x}$ (YBCO) this order is detected by muon spin-rotation and neutron scattering[8, 9] below about 10% doping, see Fig. 1.4. The order is static below a very low temperature of about 2 K. At higher temperature, the magnetic order is fluctuating, however, there appears

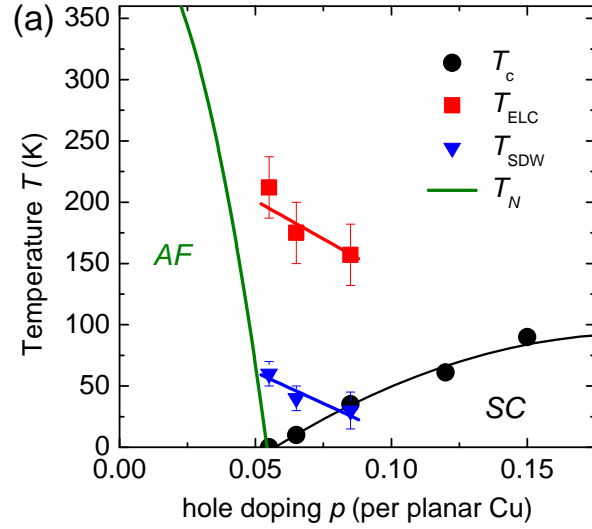


Figure 1.4: Phase diagram of $\text{YBa}_2\text{Cu}_3\text{O}_{6+x}$ as revealed by neutron scattering (from Ref. [8]). Blue triangles mark a crossover associated with the onset of two dimensional incommensurate magnetic (spin-density-wave) order. Red squares mark the onset of Ising-nematic (electron liquid-crystal) order. Phases with commensurate antiferromagnetic order (AF) and superconducting order (SC) are also marked.

a static Ising-nematic order, corresponding to spontaneous breaking of the four-fold rotation symmetry of the square lattice to a two-fold subgroup. The nematic order is also detected by electric transport[10] and Nernst-effect measurements[11] on YBCO, as well as by STM measurements on $\text{Bi}_2\text{Sr}_2\text{CaCu}_2\text{O}_{8+x}$ (Bi-2212).[12, 13] In particular, Nernst effect measurements demonstrate that the nematic order survives all the way to optimal doping and onsets at a temperature which roughly coincides with the pseudogap T^* , see Fig. 1.5.

Besides the incommensurate magnetic and Ising-nematic symmetry breaking, a number of other orders have been detected in the underdoped cuprates. These include incommensurate charge order observed by neutron and X-ray scattering that accompanies the incommensurate magnetic order in $\text{La}_{2-x}\text{Ba}_x\text{CuO}_4$ (LBCO)[14, 15]

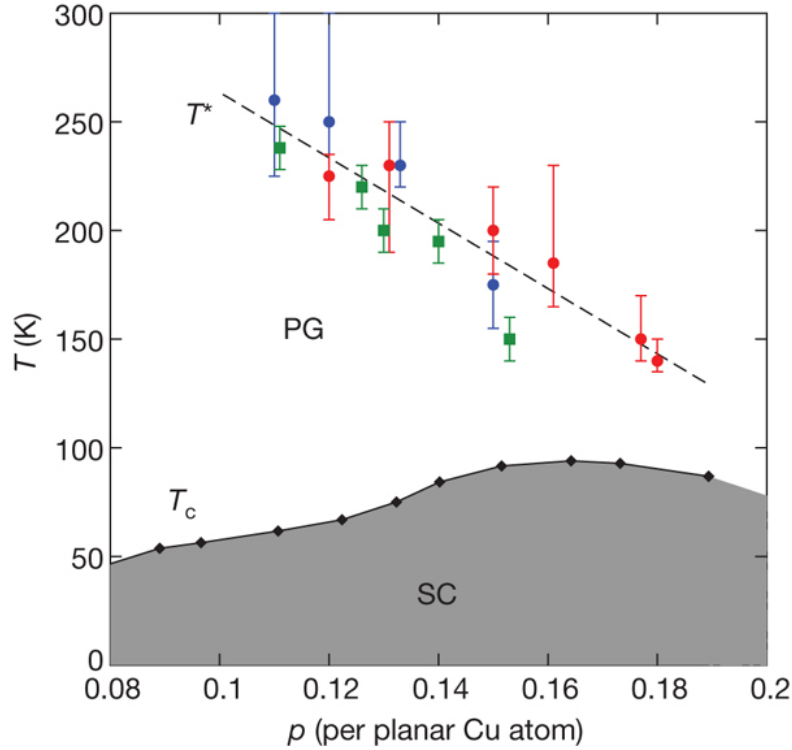


Figure 1.5: Phase diagram of $\text{YBa}_2\text{Cu}_3\text{O}_{6+x}$ from electrical resistivity and Nernst effect measurements (from Ref. [11]). The shaded grey region denotes the superconducting phase. Blue and red dots mark the onset temperature of a strong anisotropic Nernst signal measured along the two crystal axes. Green squares mark the pseudogap temperature as determined from electrical resistivity.

and $\text{La}_{1.6-x}\text{Nd}_{0.4}\text{Sr}_x\text{CuO}_4$ (LNSCO),[16] as well as at least local tendency to charge ordering detected by STM in Bi-2212[12] and $\text{Bi}_{2-y}\text{Pb}_y\text{Sr}_{2-z}\text{La}_z\text{CuO}_{6+x}$ (Bi-2201)[17]. We also mention the observation of time reversal symmetry breaking seen by polarized neutron scattering in YBCO [18] and $\text{HgBa}_2\text{CuO}_{4+x}$ [19] and by Kerr rotation in YBCO.[20]

Many theoretical ideas have been proposed to explain the behavior of underdoped cuprates. One approach is to start with the antiferromagnetically ordered Mott insulator at zero doping and ask how does this state evolves as one adds charge

carriers to the system. This is the philosophy that has partly motivated the work in Chapters 2-4 of this thesis. We must note that in this thesis we have not considered doped Mott insulators, but rather focused on an even simpler question of how does the antiferromagnetic Néel state get destroyed by quantum fluctuations in the undoped system. Even this simplified problem turns out to be highly non-trivial. In particular, as has been realized in Refs. [21, 22, 1, 2] and will be reviewed in Sec. 1.2.5, disordering the antiferromagnet naturally leads to the appearance of valence-bond-solid order, see Fig. 1.13, somewhat akin to the spatial modulations observed by STM in the pseudogap regime of Bi-2212 [12], see Fig. 1.6. Nevertheless, it is clear that to fully explain various orders and phase-transitions appearing at lowest temperatures in the superconducting state of underdoped cuprates and at higher temperature in the metallic pseudogap regime it is crucial to include doping. Extensions of the ideas in Refs. [21, 22, 1, 2] to finite doping have been presented in Refs. [23, 24, 25, 26, 27, 28, 29] and will not be discussed in this thesis.

The second puzzle of the normal state of the cuprate superconductors is the so-called “strange metal” regime realized in a fan-like region around optimal doping above the superconducting dome, see Fig. 1.2. The main characteristic of the strange metal is a resistivity, which grows linearly with temperature, see Fig. 1.8. This linear behavior persists in a very wide temperature window from T_c to 600 K in YBCO and to 1100 K in $\text{La}_{2-x}\text{Sr}_x\text{CuO}_4$ (LSCO). This is in contrast to T^2 Fermi-liquid behavior of resistivity expected in an ordinary metal, which is observed on the overdoped side of the phase diagram. Very naively, a linear in T resistivity corresponds to a linear in T scattering rate, which is in some sense the largest allowed by quantum

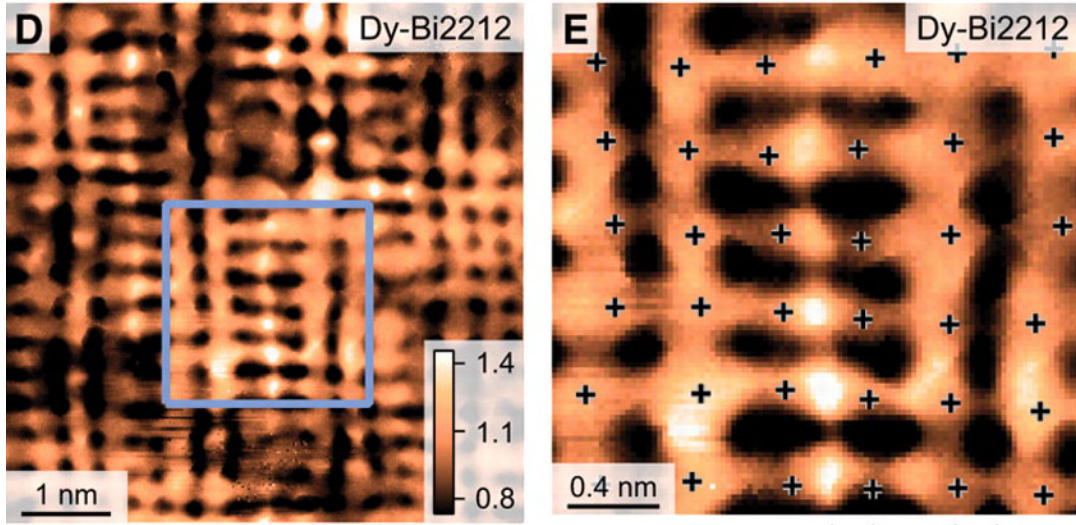


Figure 1.6: STM images of Bi-2212 (from [12]). Crosses denote the copper atoms. A distinct bond-centered pattern is observed.

mechanics.[30] A number of other anomalies appear in the strange metal regime, such as a power law behavior of the optical conductivity $\sigma(\omega) \sim \omega^{-\alpha}$ with $\alpha \approx 2/3$ in the regime $T \ll \omega \lesssim 0.7$ eV.[31] Moreover, ARPES measurements observe very broad excitations in the strange metal region, especially close to the $(\pi, 0)$, $(0, \pi)$ points in the Brillouin zone. On the overdoped side of the phase diagram, as one raises the temperature, the disappearance of coherent quasiparticles in ARPES measurements coincides with the onset of T -linear behavior of the resistivity.[32]

A funnel-like region of the phase diagram with a T -linear resistivity is observed in a number of other strongly correlated electron systems besides the cuprates. Examples include the recently discovered pnictide superconductors, heavy-fermion compounds and some organics. In almost all of these materials, the strange metal region is realized close to the boundary between a metallic antiferromagnetic phase and a conventional metal and is cut-off at low temperature by the presence of a superconducting dome,

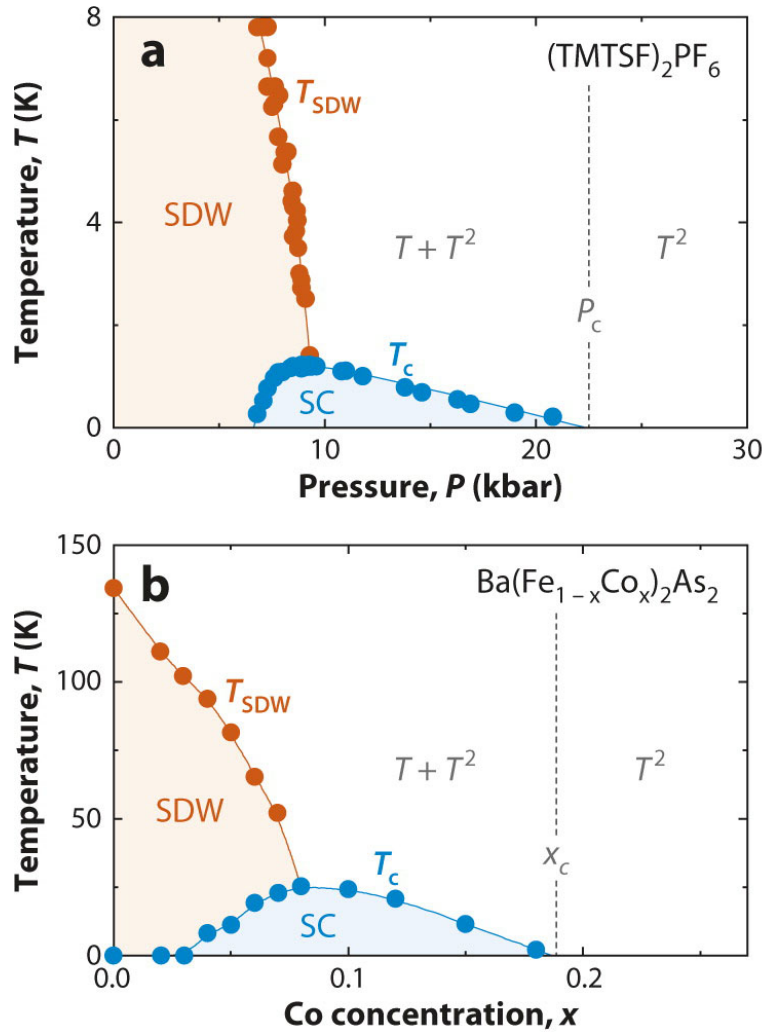


Figure 1.7: Left (from [33]): phase diagram of the organic Bechgaard salt $(\text{TMTSF})_2\text{PF}_6$ as a function of pressure P ; Right (from [34]): phase diagram of the pnictide $\text{Ba}(\text{Fe}_{1-x}\text{Co}_x)_2\text{As}_2$ as a function of Co doping x . In both figures, orange dots mark the phase boundary of a SDW phase and blue dots of a superconducting phase.

see Figs. 1.7, 1.8.

One attractive theoretical idea to explain the strange metal is that there exists a quantum critical point hidden underneath the superconducting dome, see Fig. 1.9.

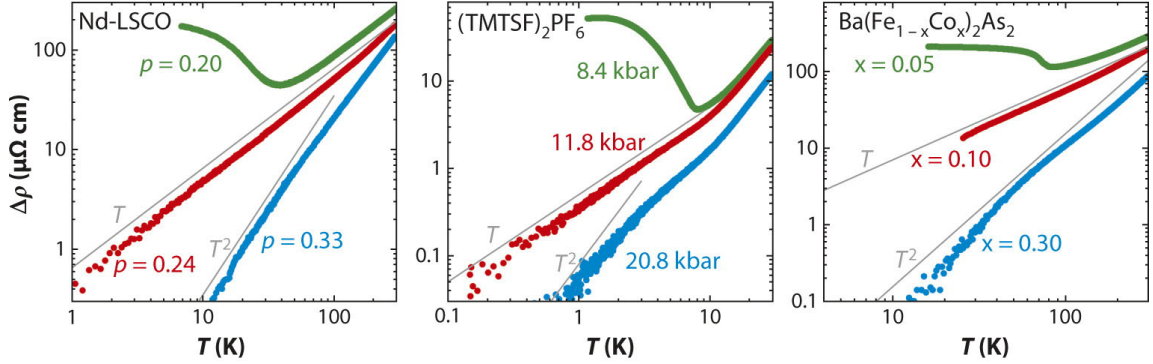


Figure 1.8: Behavior of the resistivity as a function of temperature in various strongly correlated quasi-two dimensional materials (from [35]). Left: data on hole-doped cuprates Nd-LSCO at hole doping $p = 0.20$ and $p = 0.24$ (from [36]) and LSCO at $p = 0.33$ (from [37]); Middle (from [33]): data on the organic Bechgaard salt $(\text{TMTSF})_2\text{PF}_6$ at various values of pressure; Right (from [34]): data on the pnictide $\text{Ba}(\text{Fe}_{1-x}\text{Co}_x)_2\text{As}_2$ at various values of Co doping x . In all three cases, at large values of the tuning parameter (blue curves) the system is a conventional Fermi-liquid with a T^2 resistivity. On the other hand, at small values of the tuning parameter (green curves) the system displays SDW order and an upturn of the resistivity at low temperature. Finally, at a critical intermediate value of the tuning parameter (red curves), strange metal behavior with a T -linear resistivity is observed.

This QCP may be associated with a quantum phase transition involving the onset of some order in the underlying metallic state. The strange metal is then the quantum critical fan associated with the QCP. The strong fluctuations of the order parameter present at this QCP decohere the electronic excitations and naturally lead to non-Fermi-liquid behavior. Note that to access the zero-temperature QCP one must suppress the superconducting order, which is masking it, by e.g. an application of a magnetic field. This has been done in recent experiments on LSCO [38] and LNSCO [36], which show a T -linear resistivity at optimal doping persisting to 1 K temperature.

There are several candidates for the order appearing at the QCP, the most natural being the antiferromagnetic order. When occurring in a metal, antiferromagnetic order

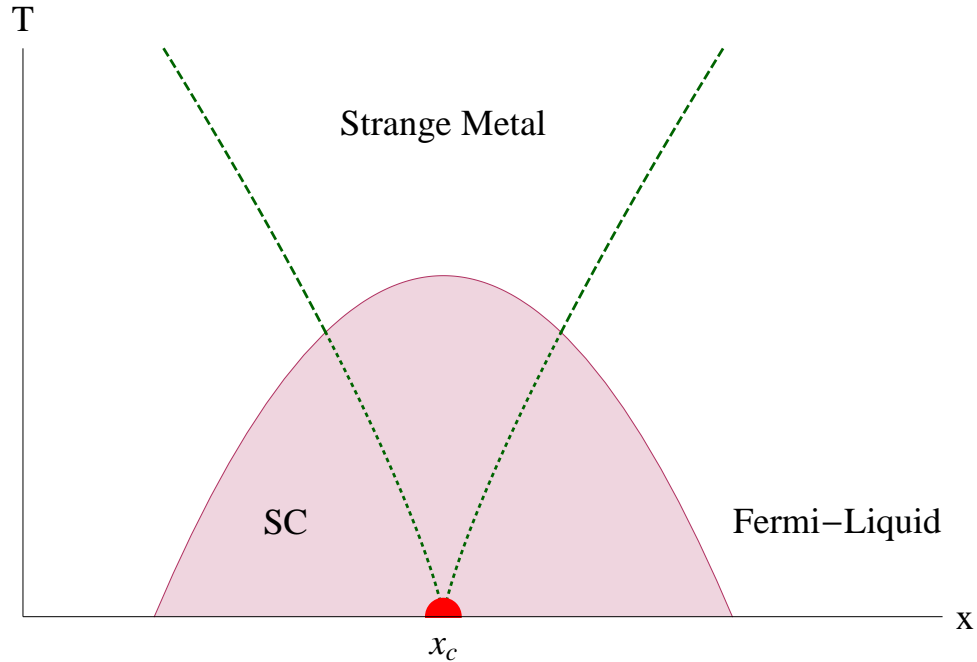


Figure 1.9: A schematic phase diagram of cuprates with a quantum critical point controlling the strange metal regime hidden underneath the superconducting dome.

is also referred to as spin-density-wave (SDW) order. Other candidates for the order appearing at the phase transition include the Ising-nematic order discussed above[39] and the “circulating current” order proposed by Simon and Varma.[40]

In most cuprate superconductors, no static magnetic order is observed close to optimal doping, casting doubt on the idea of a SDW QCP. However, this may be the result of a competition between the superconducting and SDW orders.[42, 41] The appearance of superconductivity then suppresses SDW order and shifts the actual critical point associated with its onset to smaller doping of 10 – 13%, see Fig. 1.10. Support for this scenario is provided by experiments on underdoped LSCO [43] and YBCO,[8] which demonstrate that by partly suppressing superconductivity with a magnetic field, one can enhance and even induce the SDW order. Further support

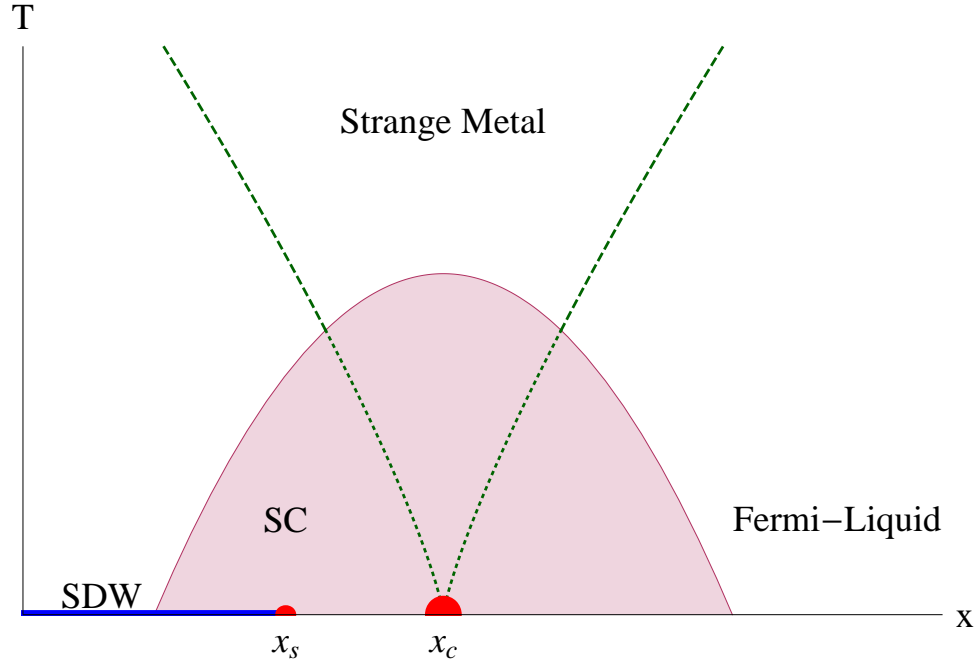


Figure 1.10: Spin-density-wave critical points in the cuprates. The quantum critical point at doping $x = x_c$ is associated with the onset of SDW order in the underlying metallic state and controls the strange metal region. This QCP is masked by the presence of the superconducting dome, but can be revealed by suppressing the superconductor with a large magnetic field. The true QCP for the onset of SDW order in a superconductor is then shifted to smaller doping $x = x_s$. Adapted from Ref. [41].

comes from the observation of small Fermi-surface pockets by quantum oscillation experiments performed on underdoped YBCO in high magnetic fields.[44] Such pockets would naturally appear due to the reconstruction of the Fermi-surface by the SDW order parameter.

Motivated by the above scenario for the strange metal regime, in the third part of this thesis we will study quantum phase transitions in two dimensional metals, focusing on the Ising-nematic transition in chapter 6 and on the SDW transition in chapter 7. Note that a SDW QCP holds the promise to explain not only the strange metal region of the cuprate phase diagram, but also the mechanism for appearance

of superconductivity itself. Indeed, it is known that antiferromagnetic fluctuations mediate an attractive interaction between the electrons in the d -wave channel.[45, 46] Whether, as suggested by experiments, a SDW critical point in a metal is always at lowest temperatures unstable to superconductivity is an important open theoretical problem.

1.2 Magnetic insulators in two dimensions

1.2.1 Mott insulators and magnetic exchange

In this section we review the physics of two dimensional magnetic Mott insulators. As a starting point for our discussion we use the Hubbard model,

$$H = - \sum_{(i,j)} t_{ij} (c_{i\alpha}^\dagger c_{j\alpha} + h.c.) - \mu \sum_i c_{i\alpha}^\dagger c_{j\alpha} + \frac{U}{2} \sum_i n_i (n_i - 1) \quad (1.7)$$

Here i, j labels the sites of the lattice, $c_{i\alpha}^\dagger, c_{i\alpha}$ are creation and destruction operators for an electron on site i with spin $\alpha = \uparrow, \downarrow$ and $n_i = c_{i\alpha}^\dagger c_{i\alpha}$ is the electron density on site i . The parameters t, μ and U are respectively the electron hopping, the electron chemical potential and the strength of onsite repulsion. Below, we assume that the system is at half-filling, i.e. there is on average one electron per lattice site.

When the hopping t is strictly zero, the ground state of the Hamiltonian in Eq. (1.7) has exactly one electron per site, so that the charge excitations are gapped. Thus, the system is referred to as a Mott insulator. The spin on each site, however, can still take any value, leading to a macroscopic degeneracy. This degeneracy is lifted once a finite hopping t is turned on. Indeed, in the limit $t \ll U$, in second order

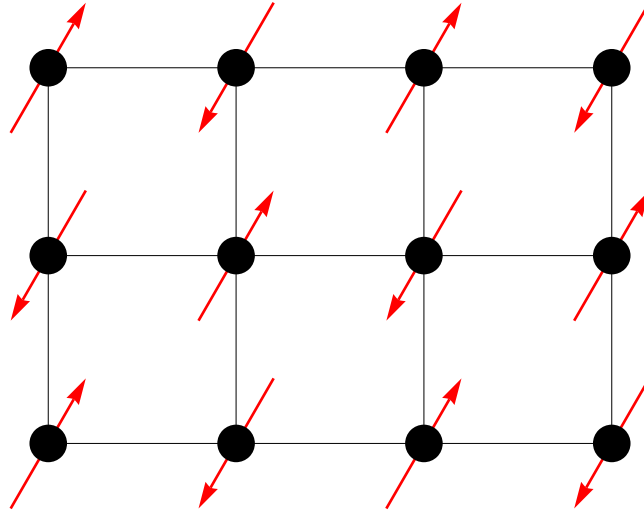


Figure 1.11: The antiferromagnetically ordered Néel state on the square lattice.

perturbation theory one generates a super-exchange interaction,

$$H = \sum_{\langle i,j \rangle} J_{ij} \vec{S}_i \cdot \vec{S}_j \quad (1.8)$$

where $\vec{S}_i = \frac{1}{2} c_{i\alpha}^\dagger \vec{\sigma}_{\alpha\beta} c_{i\beta}$ is the electron spin on site i and the exchange constant $J_{ij} = \frac{4t_{ij}^2}{U}$. Observe that the interaction (1.8) is antiferromagnetic, tending to antialign the spins. Note that by proceeding to higher order in the t/U expansion, one also generates interaction terms in the effective Hamiltonian involving spins on three and more sites. Such terms become progressively important as one increases t/U .

Let us now specialize to a square lattice and begin by considering just the nearest neighbour exchange interaction. This leads to a Heisenberg Hamiltonian,

$$H = J \sum_{\langle ij \rangle} \vec{S}_i \cdot \vec{S}_j \quad (1.9)$$

The square lattice is bipartite: i.e., it can be divided into two sublattices such that the nearest neighbors of any site on one of the sublattices, lie on the other sublattice.

If the spins in Eq. (1.9) were classical vectors, the ground state would be a Néel state, in which all the spins on one sublattice point in one direction and all the spins on the other sublattice point in the opposite direction, see Fig. 1.11. Monte-Carlo simulations indicate that this simple picture remains qualitatively correct in the deep quantum limit when the spin $S = 1/2$. In particular, the ground state carries a finite staggered magnetization,

$$\langle \vec{S}_i \rangle = (-1)^{i_x+i_y} \vec{N} \quad (1.10)$$

The direction of \vec{N} is arbitrary, thus, the system breaks the spin-rotation symmetry $SU(2)$ down to a $U(1)$ subgroup, and so from Goldstone's theorem we expect two gapless modes to be present. The magnitude of the staggered magnetization $|\vec{N}|$ is reduced by quantum fluctuations from its ideal value $|\vec{N}| = 1/2$. Monte-Carlo simulations give,[47]

$$|\vec{N}| \approx 0.30743(1) \quad (1.11)$$

In the following sections we will introduce an effective low energy theory that describes the Néel state. We will then discuss how to generalize this theory to treat the phase transition involving the destruction of magnetic order.

1.2.2 Effective theory of a quantum antiferromagnet

In this section, we introduce an effective theory that describes the fluctuations in a quantum antiferromagnet. In our theory, we will only assume a tendency towards local antiferromagnetic ordering. Thus, the theory will be able not only to describe the long-range ordered Néel state, but also the transition out of this state. Our discussion largely follows Ref. [30].

We begin with a path integral representation of the partition function of the system (1.9),

$$Z = \int \prod_i D\vec{N}_i(\tau) e^{-S[\vec{N}_i(\tau)]} \quad (1.12)$$

where the action \mathcal{S} is given by

$$\mathcal{S} = \sum_i \mathcal{S}_B[\vec{N}_i(\tau)] + \int_0^\beta d\tau H[S\vec{N}_i(\tau)] \quad (1.13)$$

Here $\vec{N}_i(\tau)$ is a unit vector representing the orientation of the spin on site i at imaginary time τ . For now, we will take the magnitude of the spin S to be arbitrary. The term \mathcal{S}_B is the spin Berry phase,

$$\mathcal{S}_B[\vec{N}(\tau)] = iS\mathcal{A}[\vec{N}(\tau)] \quad (1.14)$$

with $\mathcal{A}[\vec{N}(\tau)]$ - the area on the unit sphere swept out by $\vec{N}(\tau)$ during its evolution. If we introduce a function $\vec{N}(u, \tau)$ such that $\vec{N}(u = 0, \tau) = \vec{N}(\tau = 0)$ and $\vec{N}(u = 1, \tau) = \vec{N}(\tau)$, we may express

$$\mathcal{A}[\vec{N}(\tau)] = \int_0^1 du \int_0^\beta d\tau \vec{N} \cdot (\partial_u \vec{N} \times \partial_\tau \vec{N}) \quad (1.15)$$

Let us introduce the local fluctuating antiferromagnetic order parameter $\vec{n}(\vec{x}, \tau)$, which is assumed to vary slowly on scale of the lattice spacing. Then, we may write,

$$\vec{N}(\vec{x}_i, \tau) = (-1)^{i_x+i_y} \vec{n}(\vec{x}_i, \tau) \sqrt{1 - \vec{L}^2(\vec{x}_i, \tau)} + \vec{L}(\vec{x}_i, \tau) \quad (1.16)$$

Here, in addition to the local fluctuations of the staggered magnetization $\vec{n}(\vec{x}, \tau)$, we have also included fluctuations of the uniform component of the magnetization \vec{L} . The fields \vec{n} and \vec{L} satisfy,

$$\vec{n}^2 = 1, \quad \vec{n} \cdot \vec{L} = 0 \quad (1.17)$$

The uniform fluctuations of the magnetization are assumed to be small, $\vec{L}^2 \ll 1$. Now, expanding the action (1.13) to leading order in \vec{L} and in derivatives of \vec{n} we obtain,

$$S = iS \sum_i (-1)^{i_x+i_y} \mathcal{A}[\vec{n}(\vec{x}_i, \tau)] + \int d\tau d^2x \left(\frac{JS^2}{2} (\nabla \vec{n})^2 + \frac{4JS^2}{a^2} \vec{L}^2 - \frac{iS}{a^2} \vec{L} \cdot (\vec{n} \times \partial_\tau \vec{n}) \right) \quad (1.18)$$

Next, performing the integral over the uniform part of the magnetization \vec{L} ,

$$S = iS \sum_i (-1)^{i_x+i_y} \mathcal{A}[\vec{n}(\vec{x}_i, \tau)] + S_n \quad (1.19)$$

with

$$S_n = \frac{1}{2g} \int d\tau d^2x \left(\frac{1}{c^2} (\partial_\tau \vec{n})^2 + (\nabla \vec{n})^2 \right) \quad (1.20)$$

and the parameters

$$g = (JS^2)^{-1}, \quad c = 2\sqrt{2}JSa \quad (1.21)$$

We note that the above derivation of the effective action (1.19) is strictly valid only in the limit $S \rightarrow \infty$. When the value of S is finite one must take into account corrections to (1.19) coming from short distance fluctuations of the magnetization. We expect that such fluctuations renormalize the parameters (1.21), but do not qualitatively alter the form of the effective action.

The second term in Eq. (1.19) is the 2 + 1 dimensional $O(3)$ non-linear σ -model, familiar from the study of classical critical phenomena. We will discuss this model in more detail in the next section. The first term in Eq. (1.19) is the Berry phase contribution of the staggered spin texture. It appears that this term does not survive in the continuum limit due to the rapidly oscillating prefactor $(-1)^{i_x+i_y}$. It is, indeed, true that the Berry phase contribution vanishes when the field $\vec{n}(\vec{x}, \tau)$ is smooth.

However, we will see in Sec. 1.2.5 that the Berry phase term becomes finite when the order parameter \vec{n} forms a topological defect. This fact will play a crucial role in the theory of destruction of magnetic order on a square lattice.

1.2.3 Long-range ordered state: spin-wave theory

In this section we use the effective action (1.19) to discuss the low energy properties of the long-range ordered state. As will be discussed in more detail in Sec. 1.2.5, topological defects are confined in the long-range ordered state and the Berry phase term in Eq. (1.19) can be ignored. The theory, thus, reduces to the $O(3)$ nonlinear σ -model in Eq. (1.20). We may write the action of the theory (1.20) more concisely as,

$$S_n = \frac{1}{2g} \int d^3x (\partial_\mu \vec{n})^2 \quad (1.22)$$

Here, $d^3x = d\tau d^2\vec{x}$, the index μ runs over both the spatial and temporal directions and we have set the spin-wave velocity $c = 1$. Note that space and time enter on an equal footing in Eq. (1.22), so the quantum theory in d dimensions is equivalent to a classical theory in $D = d + 1$ dimensions.

In two spatial dimensions, the theory (1.22) possesses a stable fixed point at $g = 0$ corresponding to a magnetically ordered state. Indeed, let us expand the order parameter \vec{n} about $\vec{n} = (0, 0, 1)$. Writing, $\vec{n} = (\sqrt{g}\vec{\pi}, \sqrt{1 - g\vec{\pi}^2})$, we can express (1.22) as,¹

$$S_n = S_n^0 + S_n^{int} \quad (1.23)$$

¹In principle, there is also a Jacobian of the transformation from \vec{n} to $\vec{\pi}$ that has to be added to the action (1.23). This Jacobian does not modify the power-counting argument given below. Moreover, the Jacobian formally vanishes if one uses dimensional regularization.

$$S_n^0 = \frac{1}{2} \int d^3x (\partial_\mu \vec{\pi})^2 \quad (1.24)$$

$$S_n^{int} = \frac{1}{2} \int d^3x \frac{g}{1 - g\vec{\pi}^2} (\vec{\pi} \cdot \partial_\mu \vec{\pi})^2 \quad (1.25)$$

The action S_n^0 describes two free bosonic modes with a linear dispersion,

$$\omega = c|\vec{q}| \quad (1.26)$$

These are the antiferromagnetic spin-waves. The action S_n^{int} represents the interactions between the spin-waves. To generate a perturbative expansion about the free spin-wave theory S_n^0 , we may expand the prefactor $(1 - g\vec{\pi}^2)^{-1}$ in S_n^{int} in powers of g , generating terms of the form $S_n^{m+1} \sim g^{m+1} \int d^3x (\vec{\pi}^2)^m (\vec{\pi} \cdot \partial_\mu \vec{\pi})^2$. We would like to see if S_n^{m+1} is a relevant perturbation in the RG sense to the free spin-wave theory S_n^0 . Note that S_n^0 is invariant under the scaling,

$$\vec{\pi}(x) \rightarrow s^{1/2} \vec{\pi}(sx) \quad (1.27)$$

Under this scaling S_n^{m+1} transforms as $S_n^{m+1} \rightarrow s^{m+1} S_n^{m+1}$. Hence, each power of the coupling constant g in the perturbative expansion brings in a power of frequency/momentum. Therefore, g flows under RG as,

$$\frac{dg}{d\ell} = -g \quad (1.28)$$

Hence, interactions are irrelevant at the $g = 0$ fixed point and do not destroy the antiferromagnetically ordered state. However, the effects of interactions on the correlation functions of the theory can be systematically calculated in an expansion in the energy/momentum q , with the perturbation S_n^{m+1} entering at order q^{m+1} in the expansion. Note that there exist an infinite number of additional perturbations to the

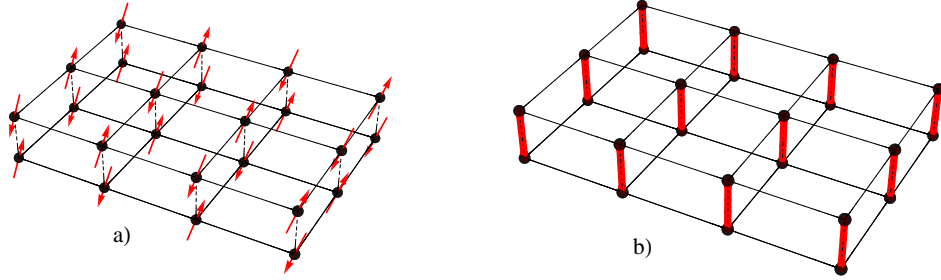


Figure 1.12: A cartoon representation of the two phases of a bilayer antiferromagnet: a) a Néel ordered phase. b) a paramagnetic phase (red tubes represent singlet configurations).

action (1.22) such as e.g. $(\partial_\mu \vec{n})^4$. At each order in the expansion, one must consider all such perturbations which are consistent with symmetry and of the same order in q .

1.2.4 Landau-Ginzburg-Wilson criticality

In this section we discuss phase transitions of $S = 1/2$ antiferromagnets with an even number of electrons per unit cell. We will see that such transitions belong to the conventional Landau-Ginzburg-Wilson paradigm.

As a concrete example, consider a system consisting of two coupled antiferromagnetic layers,

$$H = J \sum_{\langle ij \rangle} (\vec{S}_{i1} \cdot \vec{S}_{j1} + \vec{S}_{i2} \cdot \vec{S}_{j2}) + J_\perp \sum_i \vec{S}_{i1} \cdot \vec{S}_{i2} \quad (1.29)$$

Here \vec{S}_{i1} and \vec{S}_{i2} are the spin operators in the two layers. We take the spin $S = 1/2$. J and J_\perp are the intralayer and interlayer exchange couplings respectively. In the limit, $J_\perp = 0$, each layer forms an independent ordered Heisenberg antiferromagnet. Turning on a finite $J_\perp \ll J$ locks the order parameters in the two layers to point

in opposite directions - this results in a stable antiferromagnetically ordered phase, see Fig. 1.12 a). In the opposite limit, $J_{\parallel} = 0$, the vertical rungs of the bilayer are decoupled. In the ground state, each rung forms a spin singlet, see Fig. 1.12 b). The energy cost to break a singlet and create an excitation with spin $S = 1$ is J_{\perp} . This gap remains robust once a small finite $J_{\parallel} \ll J_{\perp}$ is turned on. Hence, for $J_{\parallel} \ll J_{\perp}$ the system is in a disordered paramagnetic phase with fully gapped $S = 1$ excitations. The two states at $J_{\parallel} \gg J_{\perp}$ and $J_{\parallel} \ll J_{\perp}$ are not continuously connected to each other and must, therefore, be separated by a quantum phase transition. Monte-Carlo simulations show that this phase transition is second order and occurs at a value $J_{\perp}/J_{\parallel} = 2.52181(3)$ [48].

To develop an effective theory of the phase transition, we repeat the procedure in Sec. 1.2.2. It is crucial to note that for the present problem, the Berry phase contribution in Eq. (1.19) cancels between the two layers, as the local spin orientation is opposite in the two layers. Thus, the effective action for the transition is given just by the $O(3)$ non-linear σ -model in Eq. (1.20). Note that the effective theory (1.20) could have been constructed exclusively based on symmetry properties of the order parameter and hence belongs to the LGW paradigm.

It is well known from classical statistical mechanics that the $O(3)$ nonlinear σ -model has a phase transition in $2 + 1$ dimensions at a finite value of g , separating the ordered phase, described in Sec. 1.2.3, and a disordered phase with fully gapped $S = 1$ excitations. This is precisely the kind of transition we are trying to describe! In the statistical mechanics literature the universality class of this transition is known as “3D Heisenberg.” A wealth of information has been accumulated on this universality

class, from both analytical calculations using ϵ and large- N expansions, as well as from classical Monte-Carlo simulations. We refer the reader to Ref. [49] for a contemporary review. The results of quantum Monte-Carlo simulations on the microscopic model (1.29) are in good agreement with the predictions of the 3D Heisenberg universality class.

1.2.5 Deconfined criticality

In this section we discuss the quantum phase transition involving the disappearance of magnetic order in a $S = 1/2$ antiferromagnet on a square lattice. Now the number of electrons per unit cell is odd. As a result, unlike in Sec. 1.2.4, here we will find a phase transition that does not belong to the LGW paradigm. Our discussion below will be based on the original papers [1],[2].

The valence-bond-solid state

Let us imagine starting with the Heisenberg Hamiltonian (1.9) on a square lattice and adding interaction terms that tend to disorder the antiferromagnet. These can come in the form of further neighbour exchange couplings and multisite ring exchange. For now, we will not specify a particular Hamiltonian. Rather, let us picture a caricature magnetically disordered state that such additional terms may induce. We quickly come to the realization that no analogue of the “trivial” paramagnetic state that we encountered in Sec. 1.2.4 exists in the present case. One possible non-magnetic competitor to the Néel state is a valence-bond-solid (VBS), where the spins form local singlets, which crystalize into a regular arrangement, see Fig. 1.13. However, unlike

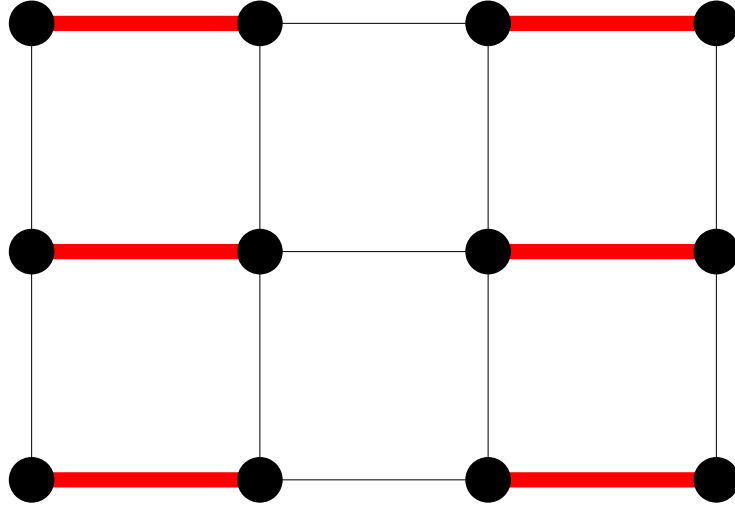


Figure 1.13: A valence-bond-solid state. The red lines denote bonds with a larger value of $-\langle \vec{S}_i \cdot \vec{S}_j \rangle$. In a cartoon picture, the spins form singlets on these bonds.

the paramagnetic state in Sec. 1.2.4, a VBS state breaks the symmetry of the square lattice, so that the ground state is four-fold degenerate, see Fig. 1.14. Note that in addition to the columnar state in Fig. 1.13 one may also imagine a plaquette ground state shown in Fig. 1.15, which is similarly four-fold degenerate.

We may introduce a local VBS order parameter V ,

$$V(\vec{x}_i) = (-1)^{i_x} (\vec{S}_i \cdot \vec{S}_{i+\hat{x}} - \vec{S}_i \cdot \vec{S}_{i-\hat{x}}) + i(-1)^{i_y} (\vec{S}_i \cdot \vec{S}_{i+\hat{y}} - \vec{S}_i \cdot \vec{S}_{i-\hat{y}}) \quad (1.30)$$

The order parameter V is a complex number transforming under the 90° lattice rotation symmetry as,

$$V(\vec{x}) \rightarrow iV(R_{\pi/2}^{-1}\vec{x}) \quad (1.31)$$

where $R_{\pi/2}$ is the 90° rotation matrix.

In the conventional LGW framework, a generic direct second-order transition between an antiferromagnetic state and a valence-bond-solid state is prohibited. Indeed,

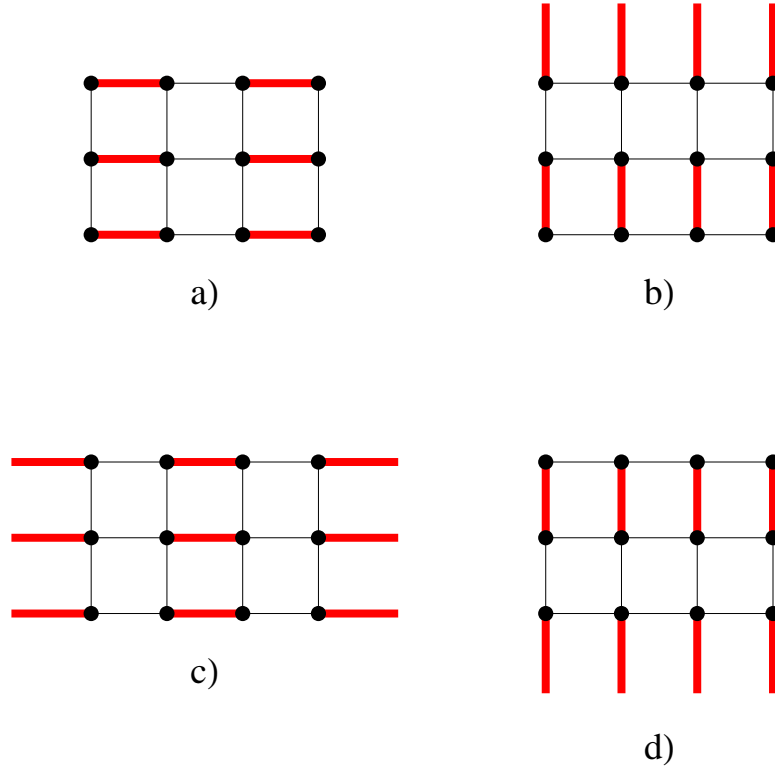


Figure 1.14: Four degenerate valence-bond-solid ground states related by 90° degree rotations.

classically, the Néel and VBS order parameters \vec{n} and V are completely unrelated. Let us write down the Landau-Ginzburg free energy as a function of the two order parameters

$$L = r_\phi \vec{\phi}^2 + r_V |V|^2 + u_\phi (\vec{\phi}^2)^2 + u_V |V|^4 + v \vec{\phi}^2 |V|^2 + \lambda_4 (V^4 + (V^\dagger)^4) \quad (1.32)$$

Here, we have chosen to relax the hard constraint $\vec{n}^2 = 1$ on the Néel order parameter \vec{n} and use an unconstrained “easy-spin” field $\vec{\phi}$ instead. The quartic term with the coupling λ_4 in Eq. (1.32) is allowed by the four-fold lattice rotation symmetry (1.31). Depending on the sign of λ_4 it selects between the columnar state in Fig. 1.13 and the plaquette state in Fig. 1.15. This term will eventually play an important role in

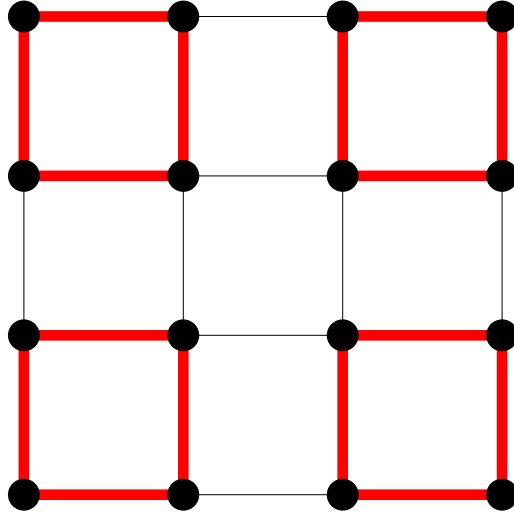


Figure 1.15: A plaquette valence-bond-solid state. The red lines denote bonds with a larger value of $-\langle \vec{S}_i \cdot \vec{S}_j \rangle$. As with the columnar state in Fig. 1.13, there are four degenerate ground states obtained by 90° rotations of the plaquette state.

our discussion below.

In mean-field theory, to have a direct second order transition from a Néel state to the VBS state, we must simultaneously tune both r_ϕ and r_V to zero in Eq. (1.32). Instead, if we tune only one parameter, we generically obtain either a direct first order transition between the two phases, Fig. 1.16 a), a sequence of two second order transitions with a coexistence region in between, Fig. 1.16 b), or a sequence of two second order transitions with a fully disordered state in between, Fig. 1.16 c). In principle, in a given microscopic model the scenarios a) and b) may be realized. However, as has already been mentioned, there does not exist a “trivial” disordered state on a square lattice, so the scenario c) is unphysical. Instead, we will argue below that another scenario of a direct second order transition between the Néel and the VBS states may be realized, once quantum effects are taken into account.

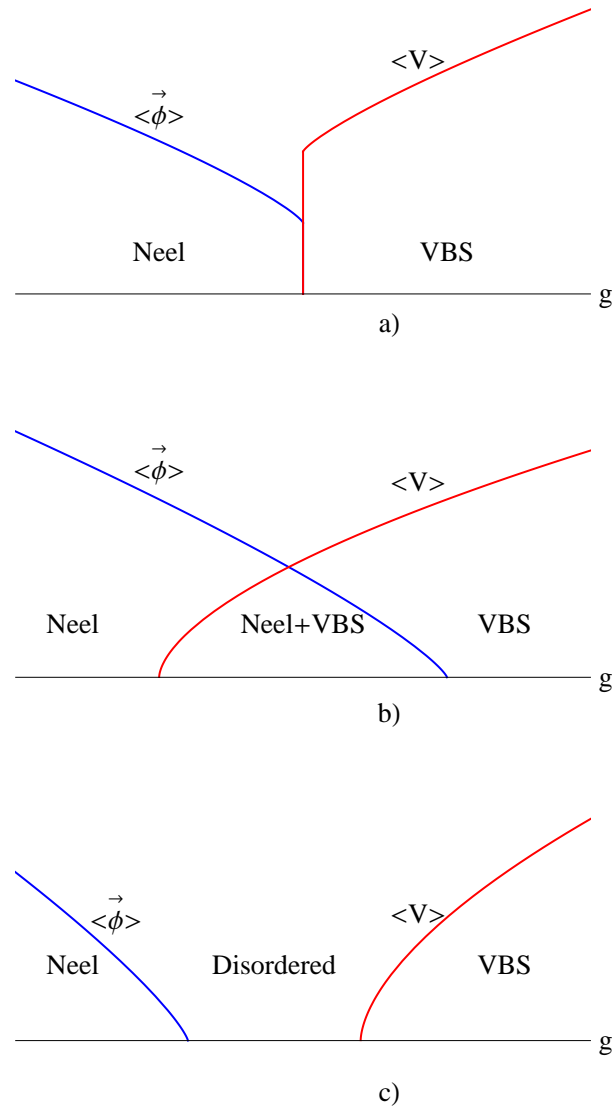


Figure 1.16: A generic phase diagram of the Néel to VBS transition as a function of a tuning parameter g as predicted by the LGW paradigm. The blue and red curves mark the expectation values of the Néel and VBS order parameters.

Skyrmions, Hedgehogs and Berry Phases

Let us return from the phenomenological LGW theory (1.32) to the effective theory of a quantum antiferromagnet in Eq. (1.19). How do the valence-bond-solid

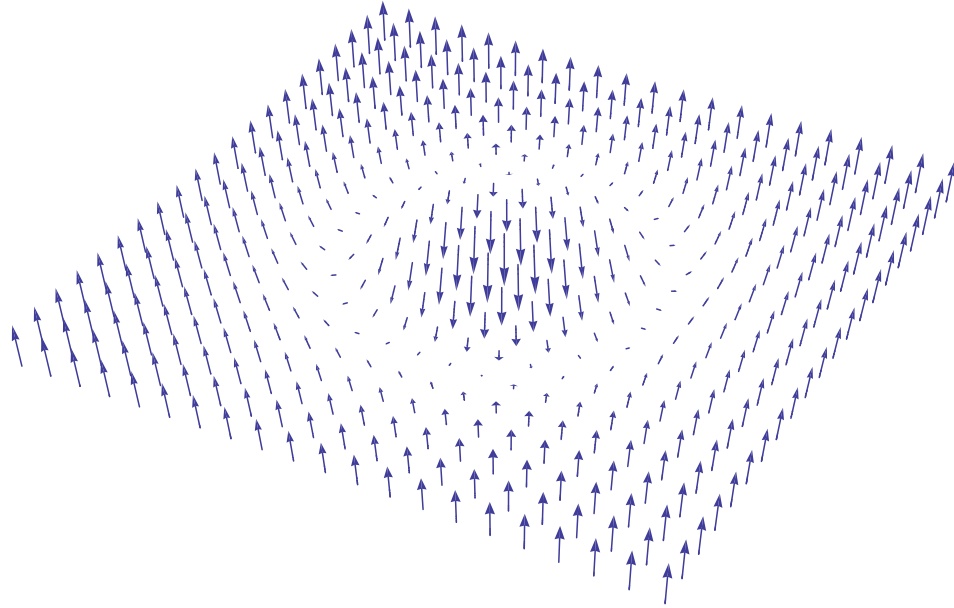


Figure 1.17: A skyrmion configuration of the Néel order parameter $\vec{n}(\vec{x})$ with topological charge $Q = 1$.

correlations emerge out of this theory involving the staggered magnetization \vec{n} alone? To answer this question, let us take a step back and discuss what configurations play a role in disordering the antiferromagnet. Natural candidates for this role are skyrmions. Skyrmions are static configurations where the spatial plane is non-trivially mapped into the order parameter manifold S^2 . For the skyrmion to have a finite energy, we require the order parameter to tend to a constant far away from the skyrmion core. Thus, the spatial plane is effectively compactified to a sphere S^2 and skyrmions can be classified as mappings from the spatial manifold S^2 into the order parameter manifold S^2 . Such mappings are described by the second homotopy group $\pi_2(S^2) = \mathbb{Z}$

and characterized by an integer topological charge,

$$Q = \frac{1}{4\pi} \int d^2x \vec{n} \cdot (\partial_x \vec{n} \times \partial_y \vec{n}) \quad (1.33)$$

A picture of a skyrmion with $Q = 1$ is shown in Fig. 1.17. As long as one considers only smooth evolutions of the order parameter $\vec{n}(\vec{x}, \tau)$, one cannot deform configurations with different values of the topological charge Q into each other and Q is conserved. Moreover, to the global topological charge Q one can associate a local topological current,

$$J_\mu = \frac{1}{8\pi} \epsilon_{\mu\nu\lambda} \vec{n} \cdot (\partial_\nu \vec{n} \times \partial_\lambda \vec{n}) \quad (1.34)$$

such that

$$Q = \int d^2x J_\tau \quad (1.35)$$

For smooth evolutions of the order parameter, the current J_μ is conserved,

$$\partial_\mu J_\mu = 0 \quad (1.36)$$

However, in the microscopic theory, singular configurations of the order parameter $\vec{n}(\vec{x}, \tau)$ are allowed. Such singularities come in the form of space-time defects, known as hedgehogs, see Fig. 1.18. Hedgehogs are characterized by a topological number n ,

$$n = \int J_\mu dS_\mu \quad (1.37)$$

where the integral in Eq. (1.37) is over a surface in space-time enclosing the singularity. A hedgehog can be regarded as a tunneling event between sectors with topological charge Q and topological charge $Q + n$. Thus, topological charge is not conserved in the presence of hedgehogs. In a quantum theory, we can think of a hedgehog with

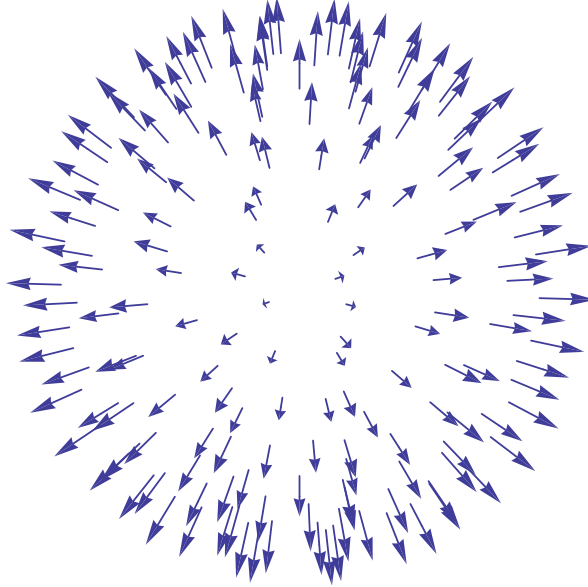


Figure 1.18: A hedgehog configuration of the Néel order parameter $\vec{n}(\vec{x}, \tau)$ with topological number $n = 1$.

charge $n = 1$ at a time τ and position \vec{x} as a skyrmion creation operator. We will denote this operator as $V(\vec{x}, \tau)$ for a reason that will become clear below.

A crucial observation is that the Berry phase term in Eq. (1.19) takes on a non-trivial value in the presence of hedgehog events. As shown in Ref. [50], if the field $\vec{n}(\vec{x}, \tau)$ has hedgehogs with charge n_a localized on plaquettes of the square lattice x_a , the Berry phase term evaluates to

$$e^{-S_B} = \prod_a (e^{-i\varphi_a})^{n_a} \quad (1.38)$$

The phase factors $e^{-i\varphi_a}$ can be chosen to take on values $1, i, -1, -i$, depending on whether the two coordinates of the plaquette x_a are (even, even), (odd, even), (odd, odd), (even, odd).

The Berry phase term, Eq. (1.38), implies that single hedgehog events occurring on nearby sites interfere destructively and do not survive in the continuum limit of the theory. Only the hedgehog events with $n \equiv 0 \pmod{4}$ carry a trivial Berry phase and survive in the continuum. More formally, Berry phases endow the hedgehog operator V with non-trivial transformation properties under the lattice rotation symmetry,

$$V(\vec{x}) \rightarrow iV(R_{\pi/2}^{-1}\vec{x}) \quad (1.39)$$

This symmetry implies that if we start with a hedgehog free theory, a perturbation to the action involving a single hedgehog operator

$$\delta L = \lambda_1(V + V^\dagger) \quad (1.40)$$

is prohibited. On the other hand, a perturbation with a “quadrupled” hedgehog operator

$$\delta L = \lambda_4(V^4 + (V^\dagger)^4) \quad (1.41)$$

is allowed. Moreover, we see that the transformation laws (1.39), (1.31) are identical. This leads to the identification of the hedgehog operator $V(\vec{x}, \tau)$ with a valence-bond-solid order parameter!

We conclude that the critical theory of an $S = 1/2$ antiferromagnet on a square lattice is given by the $O(3)$ non-linear σ -model (1.20) which is regularized at short distances so that only quadrupled hedgehog events are admitted. On the other hand, for the LGW transition of an antiferromagnet with an even number of electrons per unit cell, discussed in Sec. 1.2.4, all hedgehog configurations are allowed in the non-linear σ -model. The two different short distance regularizations of the non-linear σ -model need not lie in the same universality class. Indeed, Monte-Carlo simulations

in which one explicitly suppresses hedgehogs in the σ -model give a transition with critical properties different from the usual 3D Heisenberg class where hedgehogs are allowed.[51]

$U(1)$ gauge theory formulation

To obtain some insight into the transition it will be convenient to use an equivalent representation of the $O(3)$ non-linear σ -model, given by the so-called CP^1 model,

$$L = \frac{1}{g} |(\partial_\mu - iA_\mu)z|^2, \quad z_\alpha^\dagger z_\alpha = 1 \quad (1.42)$$

Here, z_α is a two component complex field and A_μ is a $U(1)$ gauge field. The theory (1.42) possesses a local $U(1)$ gauge symmetry,

$$z_\alpha \rightarrow e^{i\beta(x)} z_\alpha, \quad A_\mu \rightarrow A_\mu + \partial_\mu \beta \quad (1.43)$$

By integrating over A_μ in Eq. (1.42), we recover the $O(3)$ non-linear σ -model, with the identification,

$$\vec{n} = z_\alpha^\dagger \vec{\sigma}_{\alpha\beta} z_\beta \quad (1.44)$$

Note that the field z carries spin-1/2 under the $SU(2)$ spin-rotation symmetry.

In the gauge-theory formulation the topological current in Eq. (1.34) corresponds to the magnetic field,

$$J_\mu = \frac{1}{2\pi} \epsilon_{\mu\nu\lambda} \partial_\nu A_\lambda \quad (1.45)$$

and the topological charge in Eq. (1.35) corresponds to the magnetic flux in units of 2π . The hedgehog events (1.37) correspond to the Dirac magnetic monopoles. A $U(1)$ gauge theory in which monopoles are present (absent) is known as “compact” (“non-compact”). The non-compact theory has an additional global $U(1)$ -symmetry

associated with the conservation of the topological current (1.45). We will refer to this symmetry as the $U(1)_\Phi$ flux symmetry. The monopole operator transforms under this symmetry as,

$$V(x) \rightarrow e^{i\alpha} V(x) \quad (1.46)$$

with α - the phase parameter of the $U(1)_\Phi$ transformation. If we turn on the “quadrupled” monopole operators (1.41), the $U(1)_\Phi$ symmetry is explicitly broken to a \mathbb{Z}_4 subgroup, which can be identified with the physical lattice rotation symmetry.

We begin by considering the non-compact theory. We will then come back to include the effects of the “quadrupled” monopole operator (1.41). In 2+1 dimensions the non-compact theory has two phases, separated by a phase transition at a finite value g_c of the coupling constant g . For $g < g_c$, the theory is in the “Higgs” phase. Here, the field z_α acquires an expectation value, $\langle z_\alpha \rangle \neq 0$. As a result, both the local $U(1)$ gauge symmetry, (1.43), and the global $SU(2)$ spin-rotation symmetry are spontaneously broken. The later is reflected in the non-zero expectation value $\langle \vec{n} \rangle \neq 0$ of the Néel order parameter. Hence, we may identify the Higgs phase as the antiferromagnetically ordered state. Note that the gauge field A_μ acquires a mass in this phase via the Anderson-Higgs mechanism and so disappears from the low energy spectrum, which consists of two Goldstone modes, as expected in an ordered antiferromagnet. Also note that excitations carrying a finite magnetic flux are gapped in this phase. Indeed, here magnetic flux is confined into flux tubes, similar to Abrikosov vortices in a superconductor. A monopole-antimonopole pair in a Higgs phase is separated by a flux-tube, which carries a finite tension. Therefore, the correlation function $\langle V(x)V^\dagger(0) \rangle$ decays exponentially, the $U(1)_\Phi$ symmetry is

unbroken, and so the Higgs phase carries no valence-bond-solid order.

For $g > g_c$ the theory is in the ‘‘Coulomb’’ phase. Here, $\langle z_\alpha \rangle = 0$ and the field z_α creates massive spin-1/2 excitations. Thus, the Néel magnetization $\langle \vec{n} \rangle = 0$ and this phase is magnetically disordered. The gauge field A_μ remains gapless and at the lowest energies can be described by a Maxwell action,

$$L = \frac{1}{2e^2} (\epsilon_{\mu\nu\lambda} \partial_\nu A_\lambda)^2 \quad (1.47)$$

with e^2 - an effective g -dependent coupling constant. The low energy spectrum, therefore, consists of a gapless photon mode! Note, moreover, that excitations with a finite flux Φ now have the flux smeared uniformly over the entire spatial manifold and carry an energy,

$$E(\Phi) = \frac{\Phi^2}{2e^2 L^2} \quad (1.48)$$

where L^2 is the system area. Therefore, the gap to flux excitations vanishes in the thermodynamic limit. In fact, we can interpret Eq. (1.48) as the tower of states associated with a spontaneously broken $U(1)_\Phi$ symmetry. This interpretation is supported by noting that the monopole action is infra-red finite in the Coulomb phase, so that the monopole operator acquires a finite expectation value $\langle V \rangle \neq 0$. Recalling that the $U(1)_\Phi$ symmetry is physically associated with lattice rotations and the monopole operator with the valence-bond-solid order parameter, we identify the Coulomb phase with a valence-bond-solid ordered phase!

Note that in the Coulomb phase the gapless photon is created out of the vacuum by the topological current J_μ ,

$$\langle p | J_\mu(0) | 0 \rangle = -ie p_\mu \quad (1.49)$$

Here $J_\mu(0)$ is the current operator at $x = 0$ and $|p\rangle$ - the photon state with momentum \vec{p} and energy $p_0 = |\vec{p}|$. The relation (1.49) is of the same form as Goldstone's theorem. Therefore, we can think of the photon as a Goldstone's boson associated with the spontaneously broken $U(1)_\Phi$ symmetry.

Let us now discuss the critical point $g = g_c$ between the Coulomb and the Higgs phases. Critical properties can be extracted using a large- N expansion, whereby the field z_α is promoted to have N complex components. Such a theory is believed to describe the Néel to VBS transition in certain $SU(N)$ quantum antiferromagnets.[21, 22] In the large N limit, the phase transition is of second order and the critical exponents can be systematically calculated as a power series in $1/N$. One should note that in the opposite limit $N = 1$ the theory becomes dual to the 2+1 dimensional XY model,[52, 53] which also has a second order transition. Therefore, it is reasonable to guess that in the physical case $N = 2$ the transition is likewise second order. Classical Monte-Carlo simulations on the CP^1 model have been interpreted in terms of both a second order transition[51, 54] and a weakly first order transition.[55]

Let us now complete the discussion by adding the effects of the quadrupled monopole perturbation (1.41). We have already observed that in the Higgs phase monopoles are confined into pairs by flux-tubes. Hence, the perturbation (1.41) will not affect the low energy properties of the antiferromagnetically ordered state. On the other hand, monopoles drastically change the nature of the Coulomb phase. Indeed, monopoles are not confined in the Coulomb phase and form a plasma once a finite density of them is introduced. In such a plasma, a previously gapless photon field acquires a mass.[56] This effect can be understood in the following way. In the ab-

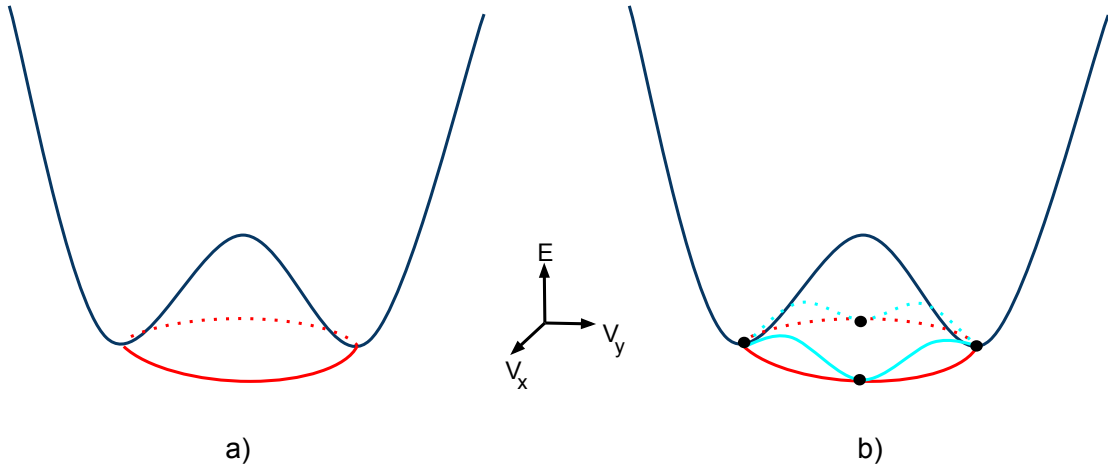


Figure 1.19: Lifting of the $U(1)$ degeneracy of the vacuum manifold in the Coulomb phase by the quadrupled monopole perturbation.

sence of monopoles, the theory has a $U(1)_\Phi$ continuous symmetry. This symmetry is spontaneously broken in the Coulomb phase and the vacuum manifold is a degenerate circle characterized by the phase of the monopole operator condensate $\langle V \rangle$, Fig. 1.19 a). Once the symmetry is explicitly broken from $U(1)_\Phi$ to the discrete subgroup \mathbb{Z}_4 by the perturbation (1.41), the degeneracy of the vacuum manifold is lifted and the ground state is only four-fold degenerate, Fig. 1.19 b). As a result, the photon, which was previously a Goldstone mode of the $U(1)_\Phi$ symmetry, becomes massive. Moreover, previously deconfined $S = 1/2$ excitations created by the z_α field are now confined, and the spinfull excitations are expected to carry $S = 1$. [56] This is in full agreement with what we expect of a physical VBS phase, where all excitations are gapped, the ground state is only four-fold degenerate and magnetic excitations carry $S = 1$.

Finally, let us discuss the fate of the critical point in the presence of quadrupled monopoles. Here the physics depends on the scaling dimension of the quadrupled

monopole operator V^4 at the critical point of the non-compact theory. If $\dim[V^4] > 3$, the perturbation (1.41) is irrelevant at the critical point and the transition can be described by the non-compact theory. Thus, at the transition point, the physical \mathbb{Z}_4 symmetry of the system is dynamically enlarged to a $U(1)_\Phi$ symmetry. This is the scenario of “deconfined” criticality - the transition is described in terms of strongly interacting $S = 1/2$ excitations z_α . Note that in this scenario, the perturbation (1.41) is still relevant in the Coulomb phase. However, the length-scale at which the effects of this perturbation, such as confinement, become important diverges as

$$\xi_{\text{conf}} \sim \xi^{1+(\dim[V^4]-3)/2} \quad (1.50)$$

where ξ is the correlation length associated with the non-compact transition, controlling e.g. the mass of the z_α excitations. For $\dim[V^4] > 3$, $\xi_{\text{conf}} \gg \xi$, so confinement sets in on a length-scale, which is parameterically larger than the correlation length ξ .

In the opposite scenario, if $\dim[V^4] < 3$, the perturbation (1.41) is relevant at the critical point. In this case, the runaway flow of the coupling λ_4 may drive the system to a first order phase transition or a new infra-red fixed point with yet undetermined properties.

We note that as has been originally shown in Ref. [3] and will be derived more elegantly in chapter 2, in the large- N limit the scaling dimension of monopole operators V^n is of order N for all values of the topological number n . Hence, in this limit the quadrupled monopole operator is irrelevant and the deconfined criticality scenario is expected to be realized.

Numerics

We conclude this section by noting that a transition between an antiferromagnet and a VBS is seen in quantum Monte Carlo simulations [57, 58, 59] of a particular model Hamiltonian

$$H = J \sum_{\langle ij \rangle} \vec{S}_i \cdot \vec{S}_j + Q \sum_{\langle ijkl \rangle} (\vec{S}_i \cdot \vec{S}_j - 1/4)(\vec{S}_k \cdot \vec{S}_l - 1/4) \quad (1.51)$$

Here the sum in the second term of Eq. (1.51) is over the plaquettes of the square lattice. Each plaquette contributes two terms to the sum: one where the four sites i, j, k, l of the plaquette are divided into pairs $(i, j), (k, l)$ on horizontal bonds and one with the pairs on vertical bonds. The form (1.51) is dictated by the absence of a sign problem for this Hamiltonian. Monte-Carlo simulations find an antiferromagnetically ordered state for large J/Q and a valence-bond-solid for small J/Q . Latest simulations [59] pin the transition at $J/Q \approx 0.044$. No signature of a first order transition is observed in the simulations[59], however, logarithmic corrections to scaling appear at the critical point. Such corrections can be finite-size manifestations of a numerically small corrections to scaling exponent ω or indicate some yet undiscovered physics. Irrespective of such corrections, an emergent $U(1)_\Phi$ symmetry is seen at the transition, consistent with the irrelevancy of the quadrupled monopole operators at the critical point.[57]

In summary, we have seen in this section that a valence-bond-ordered state naturally emerges when a square lattice quantum antiferromagnet is disordered. The correct framework for describing the phase transition between these two states is different from the conventional LGW formalism. We have discussed the exotic deconfined criticality proposal in this new framework. This scenario almost certainly

occurs for some $SU(N)$ antiferromagnets on a square lattice with N - large.[21, 22] Whether this scenario is ultimately realized for a physical $SU(2)$ antiferromagnet or if the transition in this case is fluctuation induced first order is still a matter of debate.

1.3 Phase transitions in metals

In this section, we will give a brief introduction to phase transitions in metals. We will mainly concentrate on the case of two spatial dimensions. We begin in Sec. 1.3.1 by reviewing Landau Fermi-liquid theory, which is the standard theory of metals. Then in Sec. 1.3.2 we describe how the onset of order affects the metal. In Sec. 1.3.3, we introduce an effective low energy theory to describe the phase transition and present Hertz's analysis of this theory. Finally, in Sec. 1.3.4 we discuss the shortcomings of Hertz theory.

1.3.1 Fermi-liquid theory

To introduce a description of metals, we start with the Hubbard model, Eq. (1.7). Let us begin by switching off the electron interactions U . By going to momentum space, the Hamiltonian may then be written as,

$$H = \sum_{\vec{k}} \epsilon(\vec{k}) c_{\alpha}^{\dagger}(\vec{k}) c_{\alpha}(\vec{k}) \quad (1.52)$$

where $c_{\alpha}^{\dagger}(\vec{k})$, $c_{\alpha}(\vec{k})$ are electron creation/destruction operators with momentum \vec{k} and spin α . The physics is determined by the electron band-structure $\epsilon(\vec{k})$. The electronic states in momentum space with $\epsilon(\vec{k}) < 0$ are filled and the states with $\epsilon(\vec{k}) > 0$ are empty. These regions are separated by a surface $\epsilon(\vec{k}) = 0$, known as the Fermi-surface,

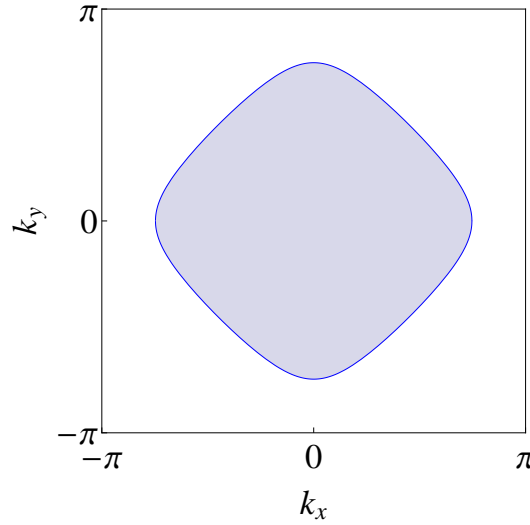


Figure 1.20: Fermi-surface of a two dimensional metal. The shaded states are filled and the unshaded states - empty.

see Fig. 1.20. The low energy excitations take the form of particles and holes in the vicinity of the Fermi-surface, carrying fermion number $+1$ and -1 respectively, and spin $1/2$. The dispersion of the exciations is linear,

$$\omega = v(\hat{k})k \quad (1.53)$$

where $v(\hat{k}) = |\nabla\epsilon(\vec{k})|$ is the Fermi-velocity and k is the distance to the Fermi-surface. Note that the Fermi-velocity is generally dependent on the location on the Fermi-surface. Defining the imaginary time electron Green's function,

$$G(\vec{k}, \omega)\delta_{\alpha\beta} = - \int d\tau \langle c_{\alpha}(\vec{k}, \tau) c_{\beta}^{\dagger}(\vec{k}, 0) \rangle e^{i\omega\tau} \quad (1.54)$$

for momentum \vec{k} close to the Fermi-surface we have

$$G(\vec{k}, \omega) = \frac{1}{i\omega - v(\hat{k})k} \quad (1.55)$$

Next, let us ask to what extent is the free electron picture preserved once electron interactions are turned on. In 1956, L. D. Landau hypothesized that as long as the

interactions are not too strong, the low energy excitations in an interacting electron liquid are continuously connected to those in a non-interacting electron gas. The resulting state of matter is known as a Fermi-liquid. In particular, in a Fermi-liquid, a sharp notion of the Fermi-surface is retained and the particle and hole excitations on this Fermi-surface remain gapless. Note that the shape of the Fermi-surface as well as the Fermi-velocity of the excitations are generally renormalized by the interactions. The “dressed” excitations of the interacting system are known as Landau quasiparticles. The electron Green’s function at low energy and momentum close to the Fermi-surface takes the form

$$G(\vec{k}, \omega) = \frac{Z(\hat{k})}{i\omega - v^*(\hat{k})k} \quad (1.56)$$

Here v^* denotes the interaction renormalized Fermi-velocity. The factor Z is the so-called quasiparticle residue - it measures the overlap between a free electron and a Landau quasiparticle state $|\vec{k}\rangle$,

$$Z(\hat{k}) = |\langle \vec{k} | c_{\alpha}^{\dagger}(\vec{k}) | 0 \rangle|^2 \quad (1.57)$$

(Here, we’ve assumed that \vec{k} lies outside the Fermi-surface). Note that the analytic pole structure of the interacting fermion Green’s function (1.56) is the same as of the free Green’s function (1.55).

The presence of gapless excitations makes the Fermi-liquid a critical phase of matter. The modern renormalization group treatment of this phase has been developed in Refs. [60, 61, 62]. Here, the RG set-up is slightly different from that encountered in classical statistical mechanics due to the fact that gapless excitations are not located at isolated points in momentum space, but on a whole surface. The low energy

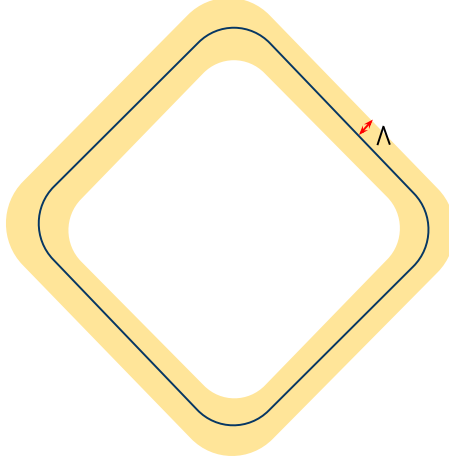


Figure 1.21: Low energy theory of a Fermi-liquid. A thin shell of states of thickness Λ is kept around the Fermi-surface.

theory is written in terms of electron states within a thin momentum shell of width Λ around the Fermi-surface, see Fig. 1.21. All the high-energy states outside this shell are assumed to have been integrated out. In the process of integration, the action of the theory is generally renormalized from its original form, Eq. (1.7). The most general quadratic part of the action consistent with symmetries is,

$$S_2 = \int \frac{d^2\vec{k}d\omega}{(2\pi)^3} \psi_\alpha^\dagger(\vec{k}, \omega) (-i\omega + v^*(\hat{k})k) \psi_\alpha(\vec{k}, \omega) \quad (1.58)$$

Here, we have labeled the electron operator $\psi(\vec{k}) \propto c(\vec{k})$ to remind ourselves that a finite quasiparticle residue will be induced in the process of integrating out electron modes away from the Fermi-surface.

At each step of the RG procedure, one decreases the cut-off Λ by integrating out the electron modes within the momentum shell $s\Lambda < k < \Lambda$. One then rescales coordinates and fields in a way to restore the momentum cut-off back to Λ and

preserve the quadratic action (1.58),

$$\psi(k, \omega, \hat{k}) \rightarrow s^{-3/2} \psi'(k/s, \omega/s, \hat{k}) \quad (1.59)$$

Note that only the component of momentum k perpendicular to the Fermi-surface is scaled, while the coordinate along the Fermi-surface \hat{k} is not affected by the RG.

Next, consider perturbations to the quadratic action (1.58). The most general four-fermi interaction takes the form,

$$S_4 = -\frac{1}{4} \int \prod_{i=1}^4 \frac{d^3 k_i}{(2\pi)^3} U_{\alpha\beta;\gamma\delta}(\hat{k}_1, \hat{k}_2; \hat{k}_3, \hat{k}_4) \psi_\alpha^\dagger(k_1) \psi_\beta^\dagger(k_2) \psi_\gamma(k_3) \psi_\delta(k_4) \\ \times (2\pi)^3 \delta^3(k_1 + k_2 - k_3 - k_4) \quad (1.60)$$

The tensor U , which parameterizes the four-fermi interactions, is fully antisymmetric in spin and momentum variables, and to leading order in energy only depends on the coordinate along the Fermi-surface. Higher order interactions between the fermions will also be generated in the integration process, but are irrelevant under RG.

There are only two types of four-fermi interactions U , which preserve the momentum and keep all the fermions in the vicinity of the Fermi-surface: forward-scattering and BCS scattering,² see Fig. 1.22. (The name BCS stems from the fact that such processes lead to the famous Bardeen-Cooper-Schrieffer superconducting instability, as we will discuss shortly). Thus,

$$U = U^{FS} + U^{BCS} \quad (1.61)$$

$$U_{\alpha\beta;\gamma\delta}^{FS}(\hat{k}, \hat{k}'; \hat{k}, \hat{k}') = \delta_{\alpha\gamma} \delta_{\beta\delta} F^c(\hat{k}, \hat{k}') + (2\delta_{\alpha\delta} \delta_{\beta\gamma} - \delta_{\alpha\gamma} \delta_{\beta\delta}) F^s(\hat{k}, \hat{k}') \quad (1.62)$$

²In principle, for a general Fermi-surface additional ‘‘umklapp’’ processes may be allowed. These, however, are irrelevant under RG.

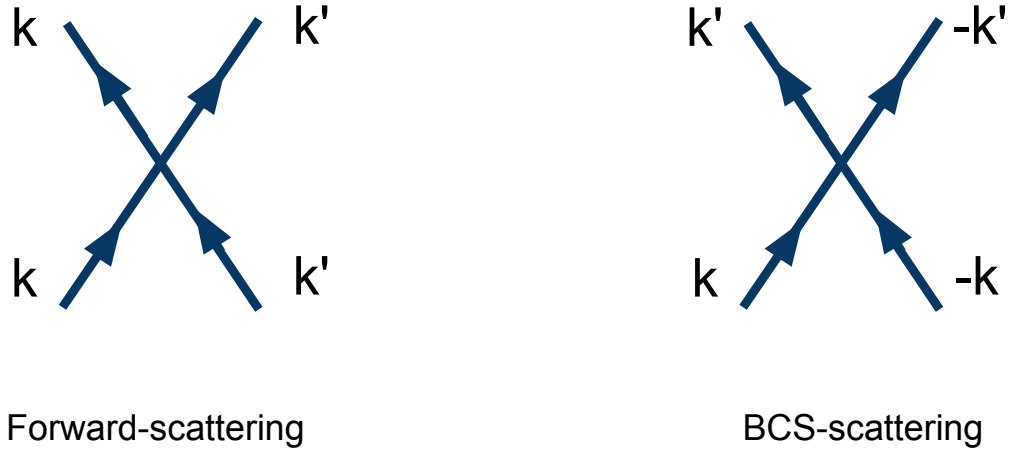


Figure 1.22: Four-fermi interactions in a Fermi-liquid.

$$U_{\alpha\beta;\gamma\delta}^{BCS}(\hat{k}, -\hat{k}; \hat{k}', -\hat{k}') = (\delta_{\alpha\gamma}\delta_{\beta\delta} - \delta_{\alpha\delta}\delta_{\beta\gamma})V^s(\hat{k}, \hat{k}') + (\delta_{\alpha\gamma}\delta_{\beta\delta} + \delta_{\alpha\delta}\delta_{\beta\gamma})V^a(\hat{k}, \hat{k}') \quad (1.63)$$

The parameters F^c and F^s are the forward-scattering amplitudes in the charge and spin channels, while V^s and V^a are the BCS scattering amplitudes in the spin-singlet and spin-triplet channels.

At tree level, both the forward-scattering and BCS scattering interactions are marginal.[62] At one loop order, the forward-scattering interaction remains marginal, while the BCS interaction acquires a flow. The analysis of the flow equation is simplest when the system has rotational symmetry, although the results are qualitatively the same in the general case. In the presence of rotational symmetry, the Fermi-surface is a circle of radius k_F and the scattering amplitudes can be expanded in terms of

angular harmonics,

$$F^{c,s}(\theta, \theta') = \sum_m F_m^{c,s} e^{im(\theta-\theta')} \quad (1.64)$$

$$V^{c,s}(\theta, \theta') = \sum_m V_m^{c,s} e^{im(\theta-\theta')} \quad (1.65)$$

Then, the RG flow equations read,

$$\begin{aligned} \frac{dF_m}{d\ell} &= 0 \\ \frac{dV_m}{d\ell} &= -N(0)V_m^2 \end{aligned} \quad (1.66)$$

where $N(0) = \frac{k_F}{2\pi v^*}$ is the density of states at the Fermi-level. Note that the flow is the same in all angular momentum channels, hence, we drop the subscript m below.

The flow equation in the BCS channel integrates to,

$$V(\ell) = \frac{V}{1 + N(0)V\ell} \quad (1.67)$$

Thus, a repulsive interaction in the BCS channel, $V > 0$, is marginally irrelevant and flows logarithmically to zero. On the other hand, an attractive interaction in the BCS channel, $V < 0$, is marginally relevant and diverges at the energy scale,

$$\Delta \sim \Lambda \exp\left(-\frac{1}{N(0)V}\right) \quad (1.68)$$

This divergence is interpreted as the Bardeen-Cooper-Schrieffer pairing instability that leads to the appearance of superconductivity.

Thus, we see that a Fermi-liquid is stable, as long as the BCS interaction in all angular momentum channels is repulsive. Of course, our analysis above was perturbative and additional instabilities are expected once interactions become sufficiently strong. We would like to note that the flow equations (1.66) are actually exact to

all loops. In fact, if one switches off all irrelevant interactions that are implicitly contained in the action (1.60), the theory becomes exactly solvable.[62]. In particular, even though the forward-scattering interaction is exactly marginal, the fermion Green's function takes the same form as in the free theory, Eq. (1.55). The forward-scattering interactions do, however, affect various susceptibilities of the system. In particular, working with the rotationally invariant system and letting

$$Q_m^c(x) = \frac{1}{k_F^m} \psi_\alpha^\dagger(x) (-i\partial_x + \partial_y)^m \psi_\alpha(x) \quad (1.69)$$

$$Q_m^{s,a}(x) = \frac{1}{k_F^m} \psi_\alpha^\dagger(x) (-i\partial_x + \partial_y)^m \sigma_{\alpha\beta}^a \psi_\beta \quad (1.70)$$

and defining,

$$\chi_m^c = \lim_{\vec{q} \rightarrow 0} \int d^2x d\tau \langle Q_m^c(x) Q_m^{\dagger c}(0) \rangle e^{-i\vec{q} \cdot \vec{x}} \quad (1.71)$$

$$\chi_m^s \delta^{ab} = \lim_{\vec{q} \rightarrow 0} \int d^2x d\tau \langle Q_m^{sa}(x) Q_m^{\dagger sb}(0) \rangle e^{-i\vec{q} \cdot \vec{x}} \quad (1.72)$$

we have

$$\chi_m^{c,s} = \frac{2N(0)}{1 + 2N(0)F_m^{c,s}} \quad (1.73)$$

Note that χ_0^c is the compressibility of the system and χ_0^s - the spin susceptibility. χ 's with $m > 0$ are susceptibilities to deformation of the Fermi-surface in higher angular momentum channels. Observe that the susceptibility $\chi_m^{c,s}$ diverges when $2N(0)F_m^{c,s} \rightarrow -1$. This corresponds to the so-called ‘‘Pomeranchuk’’ instability to a deformation of the Fermi-surface, which will be discussed in more detail in Chapter 6.

We conclude this section by noting that to the order in energy considered above, Landau-quasiparticle excitations have an infinite lifetime, as can be seen from Eq. (1.56). To extract the lifetime one has to go to higher order in the energy expansion of the

theory (i.e. take into account irrelevant scattering processes). This gives a decay rate

$$\Gamma(\omega) \sim \omega^2 \log\left(\frac{\Lambda}{\omega}\right) \quad (1.74)$$

The appearance of the logarithm in Eq. (1.74) is special to two spatial dimensions and is a consequence of forward and BCS scattering interactions with $\theta = 0$ and $\theta = \pi$. [63, 64] In higher dimensions, one obtains simply $\Gamma \sim \omega^2$. In either case, note that $\Gamma \ll \omega$, so the Landau quasiparticles are well-defined.

1.3.2 Order onset in a metal

In this section we consider what happens when a Fermi-liquid undergoes spontaneous symmetry breaking and develops an order. This generally occurs when the strength of the interactions U becomes comparable to the Fermi-energy t . We can divide all orders into two classes: those, which carry a zero wave-vector $\vec{Q} = 0$ and those that carry a finite wave-vector $\vec{Q} \neq 0$. Some examples of orders in the first class are the ferromagnetic order and the nematic order. The latter is associated with spontaneous breaking of the lattice point group symmetry. Orders in the second class include the spin-density-wave order and the charge-density-wave order. The reason for the division into two classes will become apparent shortly.

To be specific, let us focus on two particular examples, which will be further studied in Chapters 6 and 7. As an example of a transition in the first class, we consider the onset of Ising-nematic order on the square lattice. This order corresponds to spontaneous breaking of the 90° rotation symmetry of the square lattice to a 180° rotation symmetry. The order parameter is a real (Ising) field ϕ with the transformation

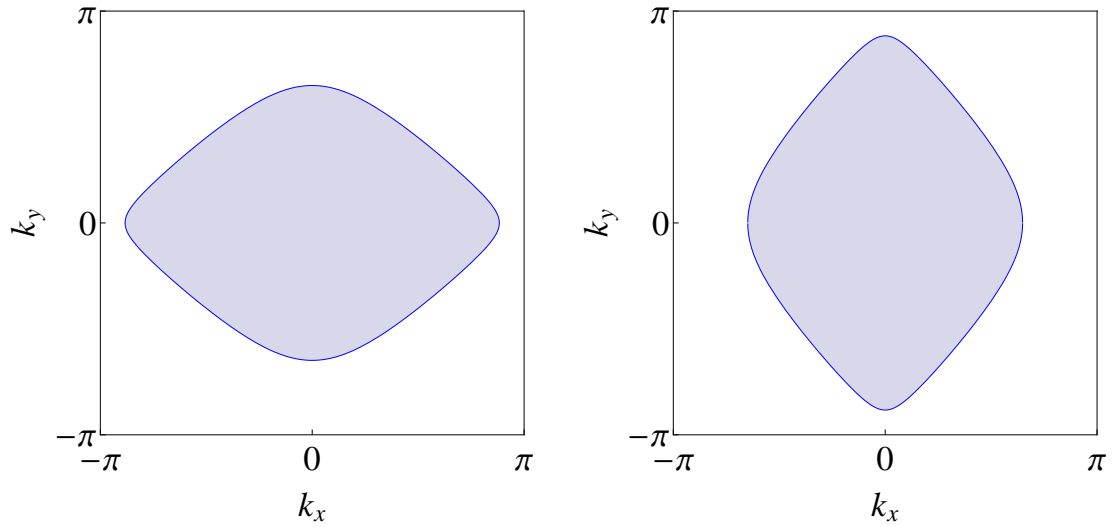


Figure 1.23: Distortion of the Fermi-surface in an Ising-nematic state. The two figures correspond to ground states with opposite values of the Ising-nematic order parameter $\langle\phi\rangle$.

properties under the 90° rotation symmetry

$$R_{\pi/2} : \phi \rightarrow -\phi \quad (1.75)$$

One can express ϕ in terms of electron operators as,

$$\phi \sim \sum_{\vec{k}} d_{\vec{k}} c_{\alpha}^{\dagger}(\vec{k}) c_{\alpha}(\vec{k}) \quad (1.76)$$

Here $d_{\vec{k}}$ is a form-factor with $d_{x^2-y^2}$ symmetry, e.g. $d_{\vec{k}} = \cos k_x - \cos k_y$. Note that even when a finite Ising-nematic order $\langle\phi\rangle \neq 0$ develops in a metal, the system is expected to remain a Fermi-liquid. The Fermi-surface of the metal will, however, distort to reflect the spontaneous breaking of rotational symmetry. As shown in Fig. 1.23, there are then two degenerate ground states corresponding to $\langle\phi\rangle > 0$ and $\langle\phi\rangle < 0$.

As an example of a transition in the second class, consider the onset of spin-

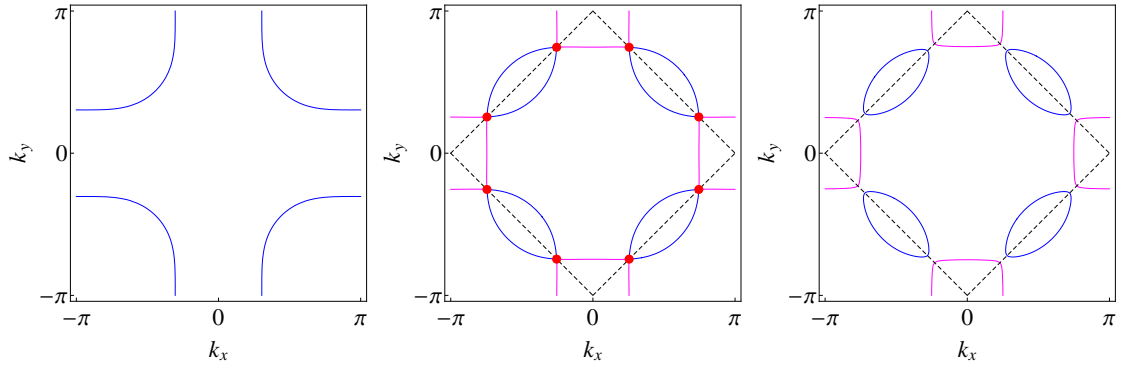


Figure 1.24: Fermi-surface evolution due to the onset of SDW order with wave-vector $\vec{Q} = (\pi, \pi)$. Left: the Fermi-surface in the disordered state (the shape has been chosen to be reminiscent of cuprate Fermi-surface at large doping). Middle: folding of the Brillouin zone by the SDW order. The new Brillouin zone boundary is shown with dashed lines. Red circles represent hot spots - points on the original Fermi-surface connected by the ordering wave-vector \vec{Q} . Right: Fermi-surface in the SDW ordered phase. A gap opens up at the hot spots and the Fermi-surface splits into electron (pink) and hole pockets (blue).

density-wave order with wave-vector $\vec{Q} = (\pi, \pi)$ on the square lattice. In terms of symmetry, this order is the same as the antiferromagnetic Néel order considered in Sec. 1.2.1. The order parameter is a real three-component vector $\vec{\phi}$ related to the local electron spin \vec{S} via

$$\vec{S}(\vec{x}_i) \sim (-1)^{i_x+i_y} \vec{\phi}(\vec{x}) \quad (1.77)$$

The SDW order spontaneously breaks the lattice translational symmetry. Therefore, in the ordered phase the Brillouin zone will be folded. The effect of this folding depends on the geometry of the initial Fermi-surface of the system. If there exist points on the Fermi-surface, known as hot spots, connected by the ordering wave-vector \vec{Q} then the onset of the SDW order will produce a gap at these hot spots, leading to a break-up of the Fermi-surface into electron and hole pockets as shown in Fig. 1.24. This is the case that we will focus on here. On the other hand, if the initial Fermi-surface is

small, such that no hot spots are present, the effect of the transition on the metallic properties are fairly innocuous and won't be considered further in this thesis. In both cases, the ordered phase remains a Fermi-liquid.

Thus, for both classes of orders, the QCP involving the order onset is a transition between two Fermi-liquids. There are two elements that are expected to play a role in the description of the transition: the fluctuations of the order parameter and the low energy electronic excitations close to the Fermi-surface. The first element is familiar to us from the study of classical phase transitions, while the second element is entirely quantum mechanical. At the transition, the fluctuations of the order parameter become soft at a single point in momentum space, which suggests their treatment with conventional renormalization group techniques, where the momentum \vec{q} of the fluctuations is scaled to zero. On the other hand, the presence of the Fermi-surface dictates a rather different RG treatment as has been discussed in Sec. 1.3.1, where the fermion momenta are scaled towards the Fermi-surface. At present, no complete theory which fully marries these two scalings is available. The original treatment of the problem, known as Hertz theory,[5] has tried to evade the difficult conceptual questions associated with the presence of the Fermi-surface, by attempting to integrate the electronic degrees of freedom out. We will review Hertz's theory below and point out where it fails. In Chapters 6 and 7 we will present a more complete approach, which treats the electrons and order-parameter fluctuations on the same footing.

1.3.3 Hertz theory

In this section we set-up an effective theory of phase transitions in metals and review Hertz's treatment of this theory. We will focus on the two examples of Ising-nematic and SDW transitions discussed in Sec. 1.3.2. We begin by considering the following effective action

$$S = S_f + S_\phi + S_{int} \quad (1.78)$$

Here S_f is an action describing free electrons with a dispersion $\epsilon(\vec{k})$

$$S_f = \int d^2x d\tau c_\alpha^\dagger (\partial_\tau + \epsilon(-i\nabla)) c_\alpha \quad (1.79)$$

The action S_ϕ describes fluctuations of the order parameter - it takes the same form for both the Ising-nematic and SDW transitions:

$$S_\phi = \int d^2x d\tau \left(\frac{1}{2c^2} (\partial_\tau \phi)^2 + \frac{1}{2} (\nabla \phi)^2 + \frac{r}{2} \phi^2 + \frac{u}{4} (\phi^2)^2 \right) \quad (1.80)$$

Finally, S_{int} describes the coupling between the order parameter fluctuations and the electronic excitations. It has a somewhat different form for the two transitions. For the Ising-nematic case,

$$S_{int} = \int \frac{d^3q}{(2\pi)^3} \frac{d^3k}{(2\pi)^3} \lambda(\vec{k}) \phi(q) c_\alpha^\dagger(k + q/2) c_\alpha(k - q/2) \quad (1.81)$$

where the coupling constant $\lambda(\vec{k})$ has a $d_{x^2-y^2}$ symmetry. Similarly, for the case of the SDW transition

$$S_{int} = \int \frac{d^3q}{(2\pi)^3} \frac{d^3k}{(2\pi)^3} \lambda(\vec{k}) \phi^a(\vec{q}) c_\alpha^\dagger(k + q/2 + \vec{Q}) \sigma_{\alpha\beta}^a c_\beta(k - q/2) \quad (1.82)$$

In this case, $\lambda(\vec{k})$ has an s -wave symmetry.

Let us consider how the small momentum fluctuations of the order parameter couple to the electronic states in the vicinity of the Fermi-surface for the two classes of transitions. In the class with $\vec{Q} = 0$, if the electron momentum \vec{k} is initially close to the Fermi-surface, it remains so after scattering off an order parameter fluctuation, see Eq. (1.81). Thus, order parameter fluctuations couple to the whole Fermi-surface. On the other hand, for the class with $\vec{Q} \neq 0$, if the initial fermion momentum \vec{k} is close to the Fermi-surface, the final momentum $\vec{k} + \vec{Q}$ after scattering off an order parameter fluctuation will be close to the Fermi-surface only if \vec{k} lies near one of the Fermi-surface hot spots, discussed in Sec. 1.3.2. Thus, order parameter fluctuations couple primarily to the electrons in the hot spot vicinity. This difference between the two classes of transitions will result in rather different low energy theories in chapters 6 and 7.

Let us now review Hertz's treatment of the effective theory (1.78). Hertz's idea was to integrate out the electronic degrees of freedom and work with an effective action for the order parameter fluctuations alone. In principle, by integrating out the electrons one will generate terms in the effective action of all orders in ϕ ,

$$\delta S[\phi] = \sum_{n=2}^{\infty} \frac{1}{n!} \int \prod_{i=1}^n \frac{d^3 q_i}{(2\pi)^3} \Gamma^n(q_1, q_2, \dots, q_n) \phi(q_1) \phi(q_2) \dots \phi(q_n) (2\pi)^3 \delta^3(q_1 + q_2 + \dots + q_n) \quad (1.83)$$

Since the electrons in the vicinity of the Fermi-surface are gapless, one, moreover, expects the coefficients Γ^n of these terms to be non-analytic in the low-frequency and momentum limit, such that the resulting effective action will be non-local. Hertz has truncated the infinite series in Eq. (1.83) at second order. This is equivalent to treating the coupling between the electrons and the order parameter in the random-

phase approximation (RPA) and induces the following term in the action for ϕ

$$\delta S_{RPA} = \frac{1}{2} \int \frac{d^3 q}{(2\pi)^3} \Pi(\omega, \vec{q}) |\phi(\omega, \vec{q})|^2 \quad (1.84)$$

The polarization function $\Pi(\omega, \vec{q})$ has the following behavior in the $q \rightarrow 0$ limit for the two classes of transitions,

$$\Pi(\omega, \vec{q}) = \Pi(\omega = 0, \vec{q} = 0) + \gamma \frac{|\omega|}{|\vec{q}|} + C\vec{q}^2 + \dots, \quad \vec{Q} = 0 \quad (1.85)$$

$$\Pi(\omega, \vec{q}) = \Pi(\omega = 0, \vec{q} = 0) + \gamma|\omega| + C\vec{q}^2 + \dots, \quad \vec{Q} \neq 0 \quad (1.86)$$

Note the non-analytic frequency dependence in Eqs. (1.85), (1.86). This behavior is known as Landau damping and is due to the decay of order parameter fluctuations into particle-hole pairs in the vicinity of the Fermi-surface. We point out that in the $\vec{Q} = 0$ case, the form (1.85) is only valid in the limit $\omega \ll v|\vec{q}|$, however, this will be the regime of interest to us below. Note that expressions (1.85), (1.86) are actually correct in any spatial dimension $d > 1$.

At low energy, the fermion induced dynamics in Eqs. (1.85), (1.86) dominates the tree level analytic dynamics given by the term $(\partial_\tau \phi)^2$ in the action (1.80). Hence, we may drop the tree-level dynamics, obtaining the Hertz action,

$$S_{Hertz} = \frac{1}{2} \int \frac{d^d \vec{q} d\omega}{(2\pi)^3} \left(\frac{\gamma|\omega|}{|\vec{q}|^{z-2}} + \vec{q}^2 + r \right) |\phi(\omega, \vec{q})|^2 + \frac{u}{4} \int d^2 x d\tau (\phi^2)^2 \quad (1.87)$$

where

$$z = \begin{cases} 3 & \vec{Q} = 0 \\ 2 & \vec{Q} \neq 0 \end{cases} \quad (1.88)$$

The quadratic part of Eq. (1.87) dictates that the fluctuations of the order parameter disperse with

$$\omega \sim |\vec{q}|^z \quad (1.89)$$

Hence, we recognize z as the dynamical critical exponent of the system.

Let us begin by setting the quartic coupling $u = 0$ and tuning the system to the transition point $r = 0$. The theory is then invariant under scaling with

$$\phi(\vec{x}, \tau) \rightarrow s^{\frac{d+z-2}{2}} \phi(s\vec{x}, s^z \tau) \quad (1.90)$$

Now, under the scaling (1.90) the quartic coupling u flows as

$$\frac{du}{dl} = -(d + z - 4)u \quad (1.91)$$

Hence, for transitions with $\vec{Q} = 0$, the quartic coupling is irrelevant for $d > 1$ and for transitions with $\vec{Q} \neq 0$ for $d > 2$. In the marginal case of $z = 2$ and $d = 2$, one-loop calculations demonstrate that u is actually marginally irrelevant.[5] Hence, in all cases Hertz theory predicts that the transition is described by mean field exponents.

1.3.4 Failure of Hertz theory

In this section we discuss various problems with Hertz theory. There are several physical reasons to suspect that Hertz theory may be incomplete. The first of these is the feedback of order parameter fluctuations on the eliminated electronic degrees of freedom. Indeed, as will be further discussed in chapters 6 and 7, if one calculates the one-loop fermion self-energy at the phase transition due to electron scattering off order parameter fluctuations, one obtains,[65, 66]

$$\Sigma(\omega, \vec{k}) \sim -i|\omega|^{2/3} \text{sgn}(\omega), \quad \vec{Q} = 0, \quad (1.92)$$

$$\Sigma(\omega, \vec{k} = \vec{k}_{hs}) \sim -i|\omega|^{1/2} \text{sgn}(\omega), \quad \vec{Q} \neq 0 \quad (1.93)$$

In the case of transitions with $\vec{Q} = 0$ the form (1.92) holds everywhere on the Fermi-surface, while for transitions with $\vec{Q} \neq 0$ the form (1.93) only holds at hot spot

momenta $\vec{k} = \vec{k}_{hs}$. In either case, the self energy is not of a Fermi-liquid form and corresponds to a damping rate which is as large as the energy itself. Hence, at the transition, Landau quasiparticles become ill-defined and the system becomes a non Fermi-liquid. This can also be seen by calculating the self-energy in the disordered phase, slightly away from the critical point. Here, at lowest energies the system is a Fermi-liquid, however, at one loop the quasiparticle residue behaves as

$$Z \sim r^{1/2} \quad (1.94)$$

where r is the tuning parameter (For the case of a transition with $\vec{Q} \neq 0$ the behavior (1.94) is realized only at the hot spots). Hence, as one approaches the transition, the quasiparticle residue smoothly goes to zero, until the Landau quasiparticle disappears altogether at the QCP.

The strong modification of the low energy fermionic excitations by the order parameter fluctuations casts doubt on whether one can successfully integrate the fermions out. Technically, the most suspicious step in the derivation of Hertz theory is the truncation of the series in Eq. (1.83) at second order. This step would be justified if the coefficients of higher order terms Γ^n were analytic in frequency and momentum, as one can then represent these terms as a polynomial in ϕ and its derivatives. The lowest order ϕ^4 term in this polynomial is already accounted for in the Hertz theory and shown to be irrelevant. The higher order polynomial terms are even more irrelevant.

However, as was demonstrated for the case of the SDW transition in Ref. [67] and for the nematic transition in Ref. [68], the higher order vertices Γ^n are actually highly singular. This is the technical reason for the breakdown of Hertz theory. A

more complete description of the transition, which treats both the order-parameter fluctuations and the non Fermi-liquid behavior of the low energy fermions will be presented in chapters 6 and 7.

Chapter 2

Monopoles in CP^{N-1} model via the state-operator correspondence

One of the earliest proposed phase transitions beyond the Landau-Ginzburg-Wilson paradigm is the quantum critical point separating an antiferromagnet and a valence-bond-solid on a square lattice. The low energy description of this transition is believed to be given by the $2 + 1$ dimensional CP^1 model - a theory of bosonic spinons coupled to an abelian gauge field. Monopole defects of the gauge field play a prominent role in the physics of this phase transition. In the present chapter, we use the state-operator correspondence of conformal field theory in conjunction with the $1/N$ expansion to study monopole operators at the critical fixed point of the CP^{N-1} model. This elegant method reproduces the result for monopole scaling dimension obtained through a direct calculation by Murthy and Sachdev. The technical simplicity of our approach makes it the method of choice when dealing with monopole operators in a conformal field theory.

2.1 Introduction

Recent theoretical studies have begun to elucidate two remarkable classes of quantum critical phenomena in two-dimensional magnetic insulators. Phase transitions beyond the Landau-Ginzburg-Wilson paradigm make up the first such class.[1, 2, 69, 70] These Landau-forbidden transitions are continuous quantum critical points (QCPs) between two conventional ordered ground states, where a Landau theory description in terms of the two order parameters does not predict a direct continuous transition upon tuning a single parameter. The second class consists of critical spin liquids, which are disordered ground states with gapless excitations and power law correlations, and which can exist as stable zero-temperature phases that can be accessed with no fine-tuning of parameters.[71, 72, 73, 74, 75, 76, 77, 78, 79] Aside from the intrinsic theoretical interest, there is evidence for a Landau-forbidden phase transition in a model of $S = 1/2$ spins, between a Neel antiferromagnet and a valence-bond solid (VBS).[57, 58] Moreover, several materials have emerged as candidates for critical spin liquid ground states.[80, 81, 82, 83, 84, 85, 86, 87, 88, 89]

The field-theoretic description of such phenomena can typically be cast in terms of a gauge field coupled to bosonic and/or fermionic matter fields. In particular, the Landau-forbidden QCP (quantum critical point) between the Neel and VBS ground state is described by the CP^{N-1} model for $N = 2$, [1, 2] which consists of an N -component boson field z coupled to a *compact* $U(1)$ gauge field A_μ . Compactness means that magnetic monopole defects of the gauge field are present and carry the quantized flux $2\pi q$; in two dimensions, these are instanton configurations of the gauge field in space-time. Such topological defects, and the field theory operators (called

monopole operators) that insert them at a particular point in space-time, play an important role in Neel-VBS transition, and in other gauge theories of Landau-forbidden QCPs and critical spin liquids. In the present case, $q = 1$ monopole operators play a particularly important role as the order parameter for the VBS state. Furthermore, $q = 4$ monopole operators are allowed perturbations to the action. Thus it is important to have information about the scaling dimensions of monopole operators, which determine power-law decay of their two-point functions, and whether those operators allowed by symmetry are relevant perturbations to the action.

Many of the gauge theories of interest, including the CP^{N-1} model, are solvable in a large- N limit, where the number of bosonic or fermionic matter fields is taken large. Even in this solvable limit, it is challenging to work with monopole operators, because they cannot be expressed as a polynomial of gauge fields and matter fields. While electric-magnetic duality gives direct access to monopole operators,[90] it is limited to purely bosonic theories with only abelian symmetries. Despite these difficulties, progress has been made: in a technical *tour de force*, by a direct evaluation of the free energy of a monopole-antimonopole pair, Murthy and Sachdev calculated the monopole scaling dimension as a function of q for the CP^{N-1} model in the large- N limit.[3] Much more recently, Borokhov, Kapustin and Wu exploited the state-operator correspondence of conformal field theory to calculate the monopole scaling dimension for massless Dirac fermions coupled to a $U(1)$ gauge field, often referred to as QED3.[91] In the large- N limit, calculation of the scaling dimension was reduced to determining the ground state energy of free Dirac fermions moving on a sphere with a background quantized flux. Although conceptually more sophisticated, this

calculation was technically much simpler than that of Murthy and Sachdev.

In this chapter, we follow Ref. [91] and apply the state-operator correspondence to calculate monopole scaling dimensions in the CP^{N-1} model, and reproduce the result of Murthy and Sachdev in a relatively simple calculation. In addition to the aesthetic advantage of greater simplicity, this result provides a nontrivial check on the correctness of the Murthy-Sachdev result. Furthermore, it illustrates the power of the state-operator correspondence in working with monopole operators of conformal field theories in three space-time dimensions.

The outline of this chapter is as follows. In Sec. 2.2 we begin with a brief review of the solution of the CP^{N-1} model in the large- N limit. Next, in Sec. 2.3 we review the state-operator correspondence in some detail. In Sec. 2.4, we use the state-operator correspondence to calculate the monopole scaling dimension in the CP^{N-1} model, and present the details of the calculation. This is followed by a discussion (Sec. 2.5) and conclusions (Sec. 2.6). Technical details are contained in two appendices.

2.2 Review of CP^{N-1} model

The Lagrangian of the CP^{N-1} model in $D = 3$ Euclidean space-time dimensions is

$$\mathcal{L} = |D_\mu z|^2 + i\lambda(|z|^2 - \frac{1}{g}), \quad (2.1)$$

where z is an N -component complex scalar field, and λ is a local Lagrange multiplier enforcing the constraint $z^\dagger z = 1/g$. The covariant derivative $D_\mu \equiv \partial_\mu - iA_\mu$, where A_μ is a *non-compact* $U(1)$ gauge field. The non-compactness of A_μ is equivalent to the fact that the gauge flux is a conserved $U(1)$ current $j_\mu^G = \epsilon_{\mu\nu\lambda} \partial_\nu A_\lambda$. Conservation of

j_μ^G is equivalent to the absence of monopole events in space-time, or, in other words, to the absence of monopole operators in the Lagrangian. For the purposes of this chapter, there is no need to consider the more complicated *compact* CP^{N-1} model, which can be easily defined on the lattice. The reason is that monopole operators are irrelevant (in the renormalization group sense) at the large- N critical point of the CP^{N-1} model, and so the critical properties will be the same whether we start with a compact or non-compact model.

The global symmetry is thus $(SU(N)/Z_N) \times U(1)$, where the $SU(N)$ rotates among the N components of z , and the $U(1)$ is the symmetry associated with flux conservation (*i.e.* conservation of j_μ^G). The quantized flux q of a monopole operator is its charge under the $U(1)$. A useful way to state the difference between the compact and non-compact CP^{N-1} models is that non-compact model has $U(1)$ flux conservation as an exact microscopic symmetry, while in the compact model this symmetry is not present. However, at least in the large- N limit, this symmetry emerges at long distances at the critical point, corresponding to the irrelevance of monopole operators.

The critical point of the CP^{N-1} model is a continuous transition between an ordered phase where z is condensed (small g), and a disordered phase (large g) where the only low-energy excitation is the photon of the $U(1)$ gauge field. Upon integrating out the z -bosons, we obtain the effective action for the fields A_μ and λ ,

$$S_{\text{eff}} = N \text{Tr} \ln(-D_\mu D_\mu + i\lambda) - \frac{1}{g} \int d^D x i\lambda. \quad (2.2)$$

Taking $g \propto 1/N$, S_{eff} is exactly solved by the saddle-point approximation in the large- N limit, and corrections to any desired quantity can be obtained in the $1/N$ expansion.

In the large- N limit, monopoles appear as the solutions to the saddle point equations where $\partial_\mu j_G^\mu \neq 0$ at a few points in space-time. For example, the lowest action saddle point with a charge- q monopole at the origin has a gauge field A_μ^q , chosen so that

$$\epsilon_{\mu\nu\lambda} \partial_\nu A_\lambda^q = \frac{q}{2} \frac{x_\mu}{x^3}. \quad (2.3)$$

One then needs to solve the saddle point equations to find the saddle-point value of the Lagrange multiplier field, $\bar{\lambda}_q(x)$. The corresponding saddle-point action of the monopole is then

$$S_q = N \text{Tr} \ln(-(\partial_\mu - iA_\mu^q)(\partial_\mu - iA_\mu^q) + i\bar{\lambda}_q) - \frac{1}{g} \int d^D x i\bar{\lambda}_q. \quad (2.4)$$

At the critical point ($g = g_c$), the action S_q is related to the scaling dimension of the monopole operator $m_q^*(x)$, which inserts a charge- q monopole. To see this, we put the theory in a space-time which is a ball of radius R . Then we consider the object

$$f(R) = \langle m_q^*(0) \rangle \quad (2.5)$$

$$= \frac{\int [dz][dA_\mu][d\lambda] m_q^*(0) e^{-\int_{|x|<R} d^3x \mathcal{L}}}{\int [dz][dA_\mu][d\lambda] e^{-\int_{|x|<R} d^3x \mathcal{L}}} \quad (2.6)$$

$$= e^{-(S_q - S_0)}. \quad (2.7)$$

At criticality, the usual scaling considerations applied to this object dictate that

$$f(R) \propto \left(\frac{R}{a}\right)^{-\Delta_q}, \quad (2.8)$$

where Δ_q is the scaling dimension of m_q^* and a is a short-distance cutoff (*e.g.* the lattice spacing). This implies that

$$S_q - S_0 \sim \Delta_q \ln \left(\frac{R}{a}\right). \quad (2.9)$$

In the disordered phase ($g > g_c$) there is a finite correlation length ξ , and for $R \gg \xi$ one has

$$S_q - S_0 \sim \Delta_q \ln \left(\frac{\xi}{a} \right). \quad (2.10)$$

Working in the disordered phase, Murthy and Sachdev directly evaluated S_q and obtained the coefficient of the logarithm in Eq. (2.10), and hence the monopole scaling dimension. In this chapter we will calculate the same quantity by a somewhat less direct but technically much simpler method.

As it will be needed later on, we now compute the $N \rightarrow \infty$ critical coupling g_c , where the phase transition occurs. On the $SU(N)$ -symmetric side of the phase diagram, the lowest action saddle point is expected to be given by $A_\mu = A_\mu^0 = 0$ and $i\lambda = i\bar{\lambda}_0 = m^2$. Thus, the gap equation $\frac{\delta S}{\delta \lambda} = 0$ becomes,

$$\int \frac{d^3 p}{(2\pi)^3} \frac{1}{p^2 + m^2} = \frac{1}{Ng} \quad (2.11)$$

The integral on the left hand side is ultraviolet-divergent and needs to be regularized. We will consistently use throughout this chapter Pauli-Villars regularization, which is obtained by augmenting the operator trace in Eq. (2.2) by

$$\text{Tr} \ln(-D_\mu D_\mu + i\lambda) \rightarrow \text{Tr} \ln(-D_\mu D_\mu + i\lambda) + \sum_i s_i \text{Tr} \ln(-D_\mu D_\mu + i\lambda + M_i^2), \quad (2.12)$$

where M_i^2 are regulator masses to be taken to infinity, and s_i are alternatingly -1 for fermionic regulators and $+1$ for bosonic regulators. To regularize the trace completely in the current problem, we actually need three regulator fields ($i = 1, 2, 3$), satisfying

$$\sum_i s_i = -1 \quad \text{and} \quad \sum_i s_i M_i^2 = 0. \quad (2.13)$$

Thus, the regularized saddle point equation (2.11) is

$$\int \frac{d^3p}{(2\pi)^3} \left(\frac{1}{p^2 + m^2} + \sum_i s_i \frac{1}{p^2 + m^2 + M_i^2} \right) = \frac{1}{Ng}. \quad (2.14)$$

At the critical point, the z -boson mass m vanishes, thus the critical coupling g_c is given by

$$\int \frac{d^3p}{(2\pi)^3} \left(\frac{1}{p^2} + \sum_i s_i \frac{1}{p^2 + M_i^2} \right) = \frac{1}{Ng_c}. \quad (2.15)$$

Evaluating the integrals, the result is

$$\frac{1}{Ng_c} = -\frac{1}{4\pi} \sum_i s_i M_i. \quad (2.16)$$

2.3 State-operator correspondence and monopole scaling dimensions

While the state-operator correspondence is a standard and well-known feature of conformal field theory (CFT), [92] it has not been widely applied in condensed matter physics except in the context $D = 2$ CFTs.¹ For this reason, in this section we introduce in some detail the state-operator correspondence for a CFT in general space-time dimension D .

We consider a CFT in Euclidean space-time invariant under the Euclidean Poincaré group and under scale transformations. (We actually do not need invariance under special conformal transformations for the following discussion.) We shall work in the scaling limit (*i.e.* continuum limit), so that, in particular, we can think of scale transformations as an exact symmetry. By assumption, any local operator can be written

¹One exception is Ref. [78], which used the results of Ref. [91] to study the stability of algebraic spin liquids.

as a linear combination of scaling operators $\mathcal{O}_i(x)$. Scale invariance is the statement that any correlation function of local operators is unchanged upon replacing $\mathcal{O}_i(x)$ by $\mathcal{O}'_i(x) = \lambda^{\Delta_i} \mathcal{O}_i(\lambda x)$, where Δ_i is the scaling dimension of \mathcal{O}_i . The Noether current associated with scale transformations is denoted j_μ^D .

The goal of the ensuing discussion is twofold. First, we shall show that there is a quantum Hamiltonian $\hat{H}_S(R)$ defined on the $(D-1)$ -sphere of radius R . The eigenstates of this Hamiltonian are in one-to-one correspondence with the scaling operators \mathcal{O}_i , and their energies are related to the scaling dimensions by $E_i = \Delta_i/R$. Second, we will give a simple method for constructing $\hat{H}_S(R)$.

We shall define the “spherical Hamiltonian” $H_S(R)$ on a sphere of radius R centered at the origin:

$$H_S(R) \equiv \frac{1}{R} \int d^D x \delta(|x| - R) n_\mu j_\mu^D. \quad (2.17)$$

Note that $H_S(R)$ is not quite the same as the quantum Hamiltonian $\hat{H}_S(R)$, which has not yet been defined. In Eq. (2.17), $n_\mu(x)$ is the outward normal vector of the sphere, and the initial factor of $1/R$ has been inserted for later convenience. The spherical Hamiltonian is useful because it is the generator of infinitesimal scale transformations. This statement is made precise by the Ward identity, which for the scaling operator $\mathcal{O}_i(x)$ can be written

$$H_S(R) \mathcal{O}_i(x) = \frac{1}{R} (\Delta_i + x_\mu \partial_\mu) \mathcal{O}_i(x), \quad (2.18)$$

provided $|x| < R$. (For a development of Ward identities as they are used here, we refer the reader to Chapter 2 of Ref. [93].)

We need to construct the Hilbert space in which $\hat{H}_S(R)$ acts. Suppose the Lagrangian depends on the set of fields ϕ_a . A wavefunction on the $(D-1)$ -sphere of

radius R is a functional $\Psi = \Psi[\phi_a]$, which depends only on $\phi_a(x)$ for $|x| = R$. The operator $\hat{H}_S(R)$ is defined by its action on the wavefunction Ψ :

$$[\hat{H}_S(R)\Psi][\phi_a] = \lim_{\epsilon \rightarrow 0^+} \int \prod_{R-\epsilon \leq |x| < R+\epsilon} [d\phi'_a(x)] \left[\prod_{|x|=R+\epsilon} \delta(\phi_a(x) - \phi'_a(x)) \right] H_S(R) \Psi[\phi'_a; R-\epsilon]. \quad (2.19)$$

For each scaling operator, we can associate a wavefunction Ψ_i by inserting \mathcal{O}_i at the origin, and “cutting open” the path integral at $|x| = R$. This means we integrate over $\phi_a(x)$ for $|x| < R$, with a fixed boundary condition at $|x| = R$. Formally,

$$\Psi_i[\phi_a; R] = \int \prod_{|x| < R} [d\phi'_a(x)] \left[\prod_{|x|=R} \delta(\phi_a(x) - \phi'_a(x)) \right] \mathcal{O}_i(0) e^{-S[\phi'_a]}. \quad (2.20)$$

The action of $\hat{H}_S(R)$ on Ψ_i can be calculated using the Ward identity:

$$\begin{aligned} [\hat{H}_S(R)\Psi_i][\phi_a] &= \lim_{\epsilon \rightarrow 0^+} \int \prod_{|x| < R+\epsilon} [d\phi'_a(x)] \left[\prod_{|x|=R+\epsilon} \delta(\phi_a(x) - \phi'_a(x)) \right] H_S(R) \mathcal{O}_i(0) e^{-S[\phi'_a]} \\ &= \frac{\Delta_i}{R} \int \prod_{|x| < R} [d\phi'_a(x)] \left[\prod_{|x|=R} \delta(\phi_a(x) - \phi'_a(x)) \right] \mathcal{O}_i(0) e^{-S[\phi'_a]} \\ &= \frac{\Delta_i}{R} \Psi_i[\phi_a]. \end{aligned} \quad (2.21)$$

Thus we have shown that Ψ_i is an eigenstate of $\hat{H}_S(R)$, where the energy E_i is simply related to the scaling dimension of \mathcal{O}_i by $E_i = \Delta_i/R$. Furthermore, this result can be used to argue that for each \mathcal{O}_i there is a unique state Ψ_i . First, if two \mathcal{O}_i have different scaling dimensions, then the corresponding states have different energies and are clearly distinct (*i.e.* they are orthogonal). Suppose that a set of \mathcal{O}_i have the same scaling dimension. Generically, this will only occur if these operators form an irreducible multiplet under the global symmetries of the CFT. The corresponding states must transform under the same multiplet; therefore, they must be linearly independent, and can be chosen to be mutually orthogonal.

To complete this discussion we still need to show that wavefunctions $\Psi[\phi_a]$ and scaling operators \mathcal{O}_i are in one-to-one correspondence. We have already shown that for each scaling operator there is a unique state Ψ_i . It remains to be shown that every eigenstate of $\hat{H}_S(R)$ corresponds to a unique scaling operator. First, on general grounds of scale invariance, there must be a one-to-one linear mapping relating eigenstates of $\hat{H}_S(R)$ to those of $\hat{H}_S(r)$. Consider an eigenstate $\Psi[\phi_a; R]$ of $\hat{H}_S(R)$ with energy E , whose image under this mapping is $\Psi[\phi_a; r]$ with energy $E' = ER/r$. (E' must have this form because the energies scale with inverse radius of the sphere, as is apparent, for example, from the form of the Ward identity.) We shall be interested in $r < R$, and we may make r as small as we like (as long as it is not so small that we are no longer in the scaling limit). We consider a functional integral where we insert this state at radius r , that is

$$Z_\Psi = \int \prod_{r < |x| < \infty} [d\phi_a(x)] \Psi[\phi_a; r] e^{-S[\phi_a]}. \quad (2.22)$$

As r becomes small, we can view this as the insertion of some local operator \mathcal{O} at the origin. That is,

$$\lim_{r \rightarrow 0} Z_\Psi = \int \prod_x [d\phi_a(x)] \mathcal{O}(0) e^{-S[\phi_a]}. \quad (2.23)$$

Now we can apply the Ward identity to an insertion of $H_S(R)$ inside Z_Ψ :

$$\begin{aligned} & \int \prod_{r < |x| < \infty} [d\phi_a(x)] \Psi[\phi_a; r] H_S(R) e^{-S[\phi_a]} = \\ &= \frac{r}{R} \lim_{\epsilon \rightarrow 0^+} \int \prod_{r < |x| < \infty} [d\phi_a(x)] \Psi[\phi_a; r] H_S(r + \epsilon) e^{-S[\phi_a]} \\ &= \frac{E'r}{R} \int \prod_{r < |x| < \infty} [d\phi_a(x)] \Psi[\phi_a; r] e^{-S[\phi_a]} \\ &= E \int \prod_{r < |x| < \infty} [d\phi_a(x)] \Psi[\phi_a; r] e^{-S[\phi_a]}. \end{aligned} \quad (2.24)$$

Taking the limit $r \rightarrow 0$, the above relations imply the operator equation $H_S(R)\mathcal{O}(0) = E\mathcal{O}(0)$, and \mathcal{O} is a scaling operator, as desired.

Now that we have established the basic facts of the state-operator correspondence, we will outline a simple procedure to actually construct $\hat{H}_S(R)$. It is useful to recall how this can be done for the usual Hamiltonian. Starting from a quantum state defined on the space-like hypersurface at constant imaginary time τ , the Hamiltonian, which generates time translations, can be defined in terms of the transfer matrix $e^{-\delta\tau\hat{H}}$ that evolves to the hypersurface at $\tau + \delta\tau$. In principle, the transfer matrix can be obtained from the functional integral by integrating over the fields between τ and $\tau + \delta\tau$.

Similarly, in the present case we can start with a quantum state defined on the $(D - 1)$ -sphere of radius R . It is useful to work in polar coordinates $x = (r, \Omega)$, where Ω includes the $D - 1$ angular coordinates, and make the change of variables $r = Re^{\tau/R}$ for a fixed value of R . In these variables, scale transformations are realized as “time” translations $\tau \rightarrow \tau + \delta\tau$. An infinitesimal scale transformation sends $R \rightarrow Re^{\delta\tau/R} = R + \delta\tau$. Therefore the spherical Hamiltonian, which generates scale transformations, can be obtained from the transfer matrix $e^{-\delta\tau\hat{H}_S(R)}$ that evolves the state at R to one at radius $R + \delta\tau$.

Now, as illustrated in Fig. 2.1, for a small patch of the $(D - 1)$ sphere of radius R , the infinitesimal scale transformation is indistinguishable from an infinitesimal time translation, in the radial direction. On this small patch, then, the scale transformation will simply be generated by the Hamiltonian density (for appropriately defined local time and space directions). In order to obtain the generator of scale transformations

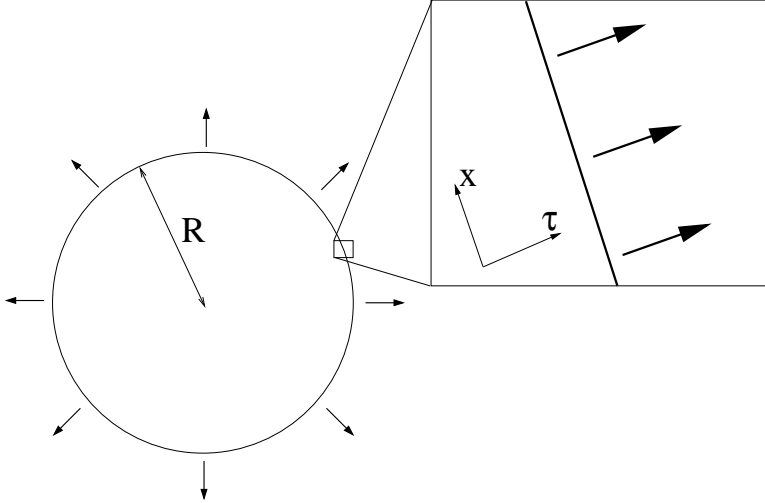


Figure 2.1: Depiction of a scale transformation as an evolution from the sphere at radius R to an expanded sphere with larger radius. In the magnified region, we illustrate that this evolution is locally equivalent to a time translation, with the locally defined time (τ) and space (x) coordinates shown.

for the entire sphere, we simply need to wrap the flat-space Hamiltonian onto the sphere. In practice, it is often easier to work with the functional integral corresponding to $\hat{H}_S(R)$, which is defined on the space $S^{D-1}(R) \times \mathbb{R}$. Here $S^{D-1}(R)$ is the $(D-1)$ -sphere of radius R , and \mathbb{R} is the imaginary time direction parametrized by τ .

2.4 Calculation

Our objective is to compute the scaling dimension Δ_q of the monopole operator of charge q . Such an operator will create states with flux $2\pi q$ out of the vacuum. Therefore, by the state-operator correspondence, to find Δ_q we must tune the theory to the critical coupling g_c , compactify the spatial manifold to a two-sphere S^2 of radius R and find the energy of the state carrying a flux $2\pi q$ over the sphere.

As a first step we need to find the saddle point of the theory on a sphere with flux. We expect the saddle point for the gauge field A_μ to be given by a uniform distribution of the flux over the spatial sphere (in particular $A_\tau = 0$). We also expect the Lagrange multiplier λ to go to a finite constant, $i\lambda = m_q^2$. Note that even though for an infinite system $i\lambda = m^2 = 0$ at the critical point, finite size effects lead to a non-vanishing $m_q^2 \sim O(R^{-2})$ on a sphere of radius R . In fact, as we will see shortly, $\sqrt{m_q^2 + q/2}$ is just the minimal energy to create a spinon above the state with flux q . In particular, for $q = 0$, we expect $m_0 R$ to be the scaling dimension Δ_z of the operator z .² We know that for $N \rightarrow \infty$, this conformal dimension is just the engineering dimension for the field z – namely $\Delta_z = 1/2$. We will verify shortly that $m_0 R = 1/2$.

By varying the effective action [*i.e.* the analog of Eq. (2.2) on the sphere] with respect to λ we obtain the gap equation on a sphere with flux,

$$\text{Tr} \left[\frac{1}{-D_\mu D_\mu + m_q^2} \right] + \sum_i s_i \text{Tr} \left[\frac{1}{-D_\mu D_\mu + m_q^2 + M_i^2} \right] = \frac{4\pi R^2 \beta}{Ng_c}. \quad (2.25)$$

where β is the length of the temporal direction. Using translational invariance along the time direction,

$$\int \frac{d\omega}{2\pi} \left(\text{Tr}_\perp \left[\frac{1}{-D_\perp^2 + \omega^2 + m_q^2} \right] + \sum_i s_i \text{Tr}_\perp \left[\frac{1}{-D_\perp^2 + \omega^2 + m_q^2 + M_i^2} \right] \right) = \frac{4\pi R^2}{Ng_c}, \quad (2.26)$$

where $-D_\perp^2$ is the square of the covariant derivative along spatial directions, and Tr_\perp is the trace over the space of functions on the sphere of radius R . We may take the ω -integral, obtaining

$$\frac{1}{2} \left(\text{Tr}_\perp \left[\frac{1}{(-D_\perp^2 + m_q^2)^{\frac{1}{2}}} \right] + \sum_i s_i \text{Tr}_\perp \left[\frac{1}{(-D_\perp^2 + m_q^2 + M_i^2)^{\frac{1}{2}}} \right] \right) = \frac{4\pi R^2}{Ng_c}. \quad (2.27)$$

²Because z is not gauge invariant, it only makes sense to talk about its scaling dimension in the $N = \infty$ limit, where gauge fluctuations are completely suppressed.

To evaluate the traces in (2.27) we need the spectrum of $-D_{\perp}^2$. Fortunately, this problem of a particle moving on a sphere with a monopole of charge q at the origin was solved a long time ago by Wu and Yang.[94] The eigenfunctions are the monopole harmonics, $Y_{q/2,l,m}$ with $l = q/2, q/2 + 1, \dots$ and $m = -l, -l + 1, \dots, l$. The corresponding eigenvalue of $-D_{\perp}^2 R^2$ is $l(l + 1) - (q/2)^2$. Note that, for $q = 0$, we recover the usual spherical harmonics. Thus, Eq. (2.27) becomes

$$\frac{1}{2} \sum_{l=q/2}^{\infty} \frac{2l+1}{4\pi R} \left(\frac{1}{(l(l+1) - (q/2)^2 + (m_q R)^2)^{\frac{1}{2}}} + \sum_i s_i \frac{1}{(l(l+1) - (q/2)^2 + (m_q R)^2 + (M_i R)^2)^{\frac{1}{2}}} \right) = \frac{1}{Ng_c}. \quad (2.28)$$

We would like to isolate the cutoff dependence of the left-hand side of Eq. (2.28). For this purpose, we rewrite Eq. (2.28) as

$$\frac{4\pi R}{Ng_c} = G_q(a_q^2) + \sum_i s_i G_q(b_{qi}^2), \quad (2.29)$$

where

$$G_q(b^2) = \sum_{l=q/2}^{\infty} \left(\frac{l+1/2}{((l+1/2)^2 + b^2)^{\frac{1}{2}}} - 1 \right) \quad (2.30)$$

$$a_q^2 = (m_q R)^2 - \frac{1}{4}(q^2 + 1), \quad b_{qi}^2 = a_q^2 + (M_i R)^2. \quad (2.31)$$

Here we have used the fact $\sum_i s_i = -1$. The ultraviolet cutoffs M_i now appear only in the second term on the right hand side of Eq. (2.29). To finish isolating the cutoff dependence we need to find the behavior of the function $G_q(b^2)$ in the limit $b^2 \rightarrow \infty$. This is easily accomplished using Poisson resummation (see Appendix A.1), and we obtain

$$G_q(b^2) \sim -b + q/2, \quad b \rightarrow \infty. \quad (2.32)$$

Here, we have dropped terms decaying as b^{-1} or faster. Substituting this into Eq. (2.29), we have

$$\frac{4\pi R}{Ng_c} = G_q(a_q^2) - \sum_i s_i b_{qi} - q/2 \quad (2.33)$$

Now, eliminating g_c using equation Eq. (2.16), we see that the ultraviolet-divergent terms cancel, and we obtain

$$G_q(a_q^2) = q/2. \quad (2.34)$$

This is precisely Eq. (3.23) of Murthy and Sachdev,[3] with the identification $\alpha_q = -a_q^2 - q^2/4 = 1/4 - (m_q R)^2$. Also, notice that $G_q(0) = 0$. So for $q = 0$, we immediately obtain $a_0^2 = 0$ as the solution to Eq. (2.34), and $m_0 R = 1/2$ as expected.

Now we proceed to the calculation of the energy of a state with flux $2\pi q$. Namely, let

$$T_q = \frac{1}{\beta} \left(\text{Tr} \ln(-D_\mu D_\mu + m_q^2) + \sum_i s_i \text{Tr} \ln(-D_\mu D_\mu + m_q^2 + M_i^2) \right). \quad (2.35)$$

The saddle-point action of the configuration with flux $2\pi q$ is given by

$$S_q = \beta N T_q - \frac{1}{g_c} \int dx m_q^2 = N \beta \left(T_q - \frac{4\pi R^2}{Ng_c} m_q^2 \right), \quad (2.36)$$

and, therefore, the energy E_q is given by

$$\frac{E_q R}{N} = T_q R - \frac{4\pi R}{Ng_c} (m_q R)^2. \quad (2.37)$$

The desired scaling dimension of the charge- q monopole operator is $\Delta_q = (E_q - E_0)R$.

We now evaluate T_q . Going to frequency space, we have

$$\begin{aligned} T_q &= \int \frac{d\omega}{2\pi} \left(\text{Tr}_\perp \ln(-D_\perp^2 + \omega^2 + m_q^2) + \sum_i s_i \text{Tr}_\perp \ln(-D_\perp^2 + \omega^2 + m_q^2 + M_i^2) \right) \\ &= \text{Tr}_\perp (-D_\perp^2 + m_q^2)^{\frac{1}{2}} + \sum_i s_i \text{Tr}_\perp (-D_\perp^2 + m_q^2 + M_i^2)^{\frac{1}{2}}. \end{aligned} \quad (2.38)$$

Recalling the form of the spectrum of $-D_{\perp}^2$,

$$T_q R = \sum_l (2l+1) \left((l(l+1) - (q/2)^2 + (m_q R)^2)^{\frac{1}{2}} + \sum_i s_i (l(l+1) - (q/2)^2 + (m_q R)^2 + (M_i R)^2)^{\frac{1}{2}} \right). \quad (2.39)$$

We rewrite this in the form

$$T_q R = 2F_q(a_q^2) + 2 \sum_i s_i F_q(b_{qi}^2), \quad (2.40)$$

where

$$F_q(b^2) = \sum_{l=q/2}^{\infty} \left((l+1/2)((l+1/2)^2 + b^2)^{\frac{1}{2}} - (l+1/2)^2 - \frac{1}{2}b^2 \right). \quad (2.41)$$

It should be noted that the sum over l in Eq. (2.41) converges. As in the analysis of the gap equation, only the second term of Eq. (2.40) depends on the ultraviolet cutoff. Also as before, we consider the $b \rightarrow \infty$ limit of $F_q(b^2)$. After a short calculation (see Appendix A.1), we obtain

$$F_q(b^2) \sim -\frac{1}{3}b^3 + \frac{q}{4}b^2 + \left(\frac{1}{24} - \frac{q^2}{8}\right)b + \frac{1}{24}q(q^2 - 1), \quad b \rightarrow \infty. \quad (2.42)$$

Substituting this result into Eq. (2.40) and noting that $b_{qi}^3 = (M_i R)^3 + \frac{3}{2}a_q^2(M_i R) + \mathcal{O}[(M_i R)^{-1}]$, we find

$$T_q R = -\frac{2}{3} \sum_i s_i (M_i R)^3 + \left(\frac{1}{12} - \frac{q^2}{4} - a_q^2\right) \sum_i s_i M_i R + 2F_q(a_q^2) - \frac{q}{2}a_q^2 - \frac{1}{12}q(q^2 - 1). \quad (2.43)$$

Now, we can bring everything together. Substituting the critical coupling g_c [Eq. (2.16)] into Eq. (2.37) and recalling that $(m_q R)^2 = a_q^2 + \frac{1}{4}(q^2 + 1)$, we find

$$\frac{E_q R}{N} = -\frac{2}{3} \sum_i s_i (M_i R)^3 + \frac{1}{3} \sum_i s_i (M_i R) + 2F_q(a_q^2) - \frac{q}{2}a_q^2 - \frac{1}{12}q(q^2 - 1) \quad (2.44)$$

The cutoff-dependent (and also ultraviolet-divergent) terms in $E_q R/N$ comprise a q -independent constant. Hence, the energy differences are finite:

$$\frac{(E_q - E_0)R}{N} = 2(F_q(a_q^2) - F_0(a_0^2)) - \frac{q}{2}a_q^2 - \frac{1}{12}q(q^2 - 1) \quad (2.45)$$

Recalling that $a_0^2 = 0$ and noting that $F_q(0) = 0$, we obtain the final result,

$$\frac{\Delta_q}{N} = \frac{(E_q - E_0)R}{N} = 2F_q(a_q^2) - \frac{q}{2}a_q^2 - \frac{1}{12}q(q^2 - 1). \quad (2.46)$$

It is easy to show this result is precisely that of Murthy and Sachdev (see Appendix A.2).

2.5 Discussion

Let us put our calculation into the context of the role of U(1) flux symmetry in the noncompact CP^{N-1} model. In the ordered phase of the theory ($g < g_c$) the flux symmetry is unbroken, as the Meissner effect leads to flux confinement. The configurations carrying magnetic flux in this phase have a finite energy and, in fact, are quantum descendants of instantons of the two-dimensional CP^{N-1} model.[95] Close to the critical point these instantons are strongly dressed by the interaction: their size grows and their energy decreases as $g \rightarrow g_c$. Precisely at the QCP the instantons become massless. The condition that flux and spin gaps vanish at the same critical point is at the heart of deconfined criticality. We have verified this fact explicitly here by showing that the energy of a flux q instanton goes as Δ_q/R on a sphere of radius R . The observation that on a finite sphere the energy scales as $1/R$ at the QCP follows from dimensional analysis arguments. However, the fact

that Δ_q coincides with the scaling dimension of the monopole operator is a non-trivial prediction of the state-operator correspondence of conformal field theory. The agreement between our result and the more direct computation of Δ_q by Murthy and Sachdev is a strong check that the monopole operator survives in the scaling limit.

Now, to complete our discussion, once the coupling $g > g_c$ and we are in the disordered phase, the instantons, having become massless at the phase transition, condense. As a result, the U(1) flux symmetry is spontaneously broken; the photon is a Goldstone boson associated with this symmetry, since it is created out of the vacuum by the current j_μ^G . What is the fate of configurations carrying finite flux in this phase? We can compute their energy directly from the effective action for the photon field,

$$S = \frac{1}{2e^2} \int d^3x (\epsilon_{\mu\nu\lambda} \partial_\nu A_\lambda)^2 \quad (2.47)$$

where to leading order in $1/N$, $e^2 = 24\pi m/N$, with m the spinon mass. For simplicity we work with a flat spatial manifold here (e.g. a torus). Then, smearing the flux $2\pi q$ uniformly over the space,

$$\epsilon_{ij} \partial_i A_j = \frac{2\pi q}{V} \quad (2.48)$$

where V is the spatial volume. The energy becomes,

$$E = \frac{(2\pi q)^2}{2e^2 V} \quad (2.49)$$

Indeed, as always occurs when a continuous global symmetry is spontaneously broken, the states of finite charge (flux) form a tower, with energies scaling as inverse volume.

Thus, in the $N = \infty$ limit, we have a detailed quantitative understanding of the flux sector of the CP^{N-1} model at the critical point and in the disordered phase. It

would be interesting to extend the quantitative description to the ordered phase. In particular, it would be interesting to compute the finite instanton mass, m_i , which we expect to govern the long distance decay of monopole-antimonopole correlation functions. From general scaling arguments, we expect $m_i \sim (g - g_c)^\nu$, where ν is the correlation length exponent. Moreover, we expect the ratio m_i/ρ_s , where ρ_s is the spin-stiffness, to be a universal number. Unfortunately, it is rather difficult to analyze the instantons in the ordered phase even at $N = \infty$, since the saddle point value of the fields A_μ and z_α is no longer dictated by symmetry as it was at the critical point.

2.6 Conclusion

In this chapter we have used the state-operator correspondence of conformal field theory to compute the monopole scaling dimension in the CP^{N-1} model at $N = \infty$. Our result agrees with the more direct calculation by Murthy and Sachdev;[3] however, our approach has the advantage of technical simplicity. In fact, one can even envision using this method to compute the $1/N$ corrections to the monopole scaling dimension. From the conceptual point of view our result demonstrates the vanishing of the flux gap at the QCP and confirms the survival of the monopole operator in the scaling limit.

Chapter 3

Impurity spin textures across conventional and deconfined quantum critical points of two dimensional antiferromagnets

We describe the spin distribution in the vicinity of a non-magnetic impurity in a two dimensional antiferromagnet undergoing a transition from a magnetically ordered Néel state to a paramagnet with a spin gap. The quantum critical ground state in a finite system has total spin $S = 1/2$ (if the system without the impurity had an even number of $S = 1/2$ spins), and recent numerical studies in a double layer antiferromagnet[96] have shown that the spin has a universal spatial form delocalized across the entire sample. We present the field theory describing the uniform and staggered magnetizations in this spin texture for two classes of antiferromagnets: (*i*) the transition from a Néel state to a paramagnet with local spin singlets, in models with an even number of $S = 1/2$ spins per unit cell, which are described by a $O(3)$ Landau-Ginzburg-Wilson field theory; and (*ii*) the transition from a Néel state to a valence bond solid, in antiferromagnets with a single $S = 1/2$ spin per unit cell,

which are described by a “deconfined” field theory of spinons.

3.1 Introduction

There have been many experimental studies of non-magnetic Zn impurities substituting for the spin $S = 1/2$ Cu ions in spin-gap and superconducting compounds [97, 98, 99, 100, 101, 102, 103]. These have stimulated many theoretical studies of the spin dynamics in the vicinity of a vacancy (*i.e.* a site with no spin) in $S = 1/2$ square lattice antiferromagnets [104, 105, 106, 107, 108, 109, 110, 111, 112, 113, 114, 115, 116, 96, 117].

An important feature of the impurity-response escaped¹ theoretical attention until recently [96]. Consider the regime where the bulk antiferromagnet preserves global rotational symmetry and has a $S = 0$ ground state. Such states can be reached by deforming the nearest-neighbor antiferromagnet into a coupled-ladder or coupled-dimer antiferromagnet [118, 119], in a double-layer antiferromagnet [48], or by adding additional ring-exchange interactions while preserving full square lattice symmetry[57]. Now remove a single $S = 1/2$ spin in a system with an even number of spins, leaving an antiferromagnet with a vacancy and an odd number of $S = 1/2$ spins. We expect this antiferromagnet to have a doubly-degenerate ground state with total spin $S = 1/2$. Without loss of generality, we can examine the ground state with spin-projection $S_z = 1/2$. In such a state, even though there is no broken symmetry and no applied magnetic field (the Hamiltonian has full SU(2) spin symmetry), the ex-

¹Section II.B.3 of Ref. [112] contains results which can be used to extract the spin textures in zero field.

pectation values of the spin projection on the site i , $\langle S_{zi} \rangle$, is non-zero on all i for any finite system of size L . The question of interest in this chapter is the following: What is the spatial form of $\langle S_{zi} \rangle$? It is possible that the $S = 1/2$ magnetization is pushed out to the boundaries of the system, far from the impurity: in this case, it will not be relevant to the impurity properties in the limit $L \rightarrow \infty$. However, we will find this is not the case for the antiferromagnets examined here. For the spin-gap antiferromagnets we consider, the $S = 1/2$ magnetization is bound to the impurity over a length scale inversely proportional to the spin gap. At the quantum critical points separating the spin gap states from the Néel state, which define ‘algebraic spin liquids’, we will find, as in Ref. [96], that the impurity magnetization is delocalized over the entire system, forming a spin texture with a universal spatial form determined only by the system size L .

We will divide our introductory discussion here into two subsections. The first subsection will consider the models which have been numerically studied in Ref. [96]. These are antiferromagnets which have an even number of $S = 1/2$ spins per unit cell (such as the coupled-dimer[118, 119] or double layer[48] models), which exhibit a transition between a Néel state and a simple spin gap state; the latter state is adiabatically connected to a state in which the spins in each unit cell are separately locked into singlets, with negligible resonance between unit cells. This is a ‘conventional’ transition, described by a Landau-Ginzburg-Wilson (LGW) theory.

In the second subsection, we consider the more interesting and much more subtle case of a “deconfined” critical point [1, 2]. Here we are considering antiferromagnets with a single $S = 1/2$ spin per unit cell, and so there is no simple spin-gap state

with local singlets. For the models studied in Refs. [1, 2, 57], the spin gap state has singlet valence bonds which crystallize into a regular arrangement, breaking the space group symmetry of the square lattice, while preserving spin rotation invariance. Such a state is a valence bond solid (VBS), and we will be interested in the impurity response across the Néel-VBS transition.

3.1.1 LGW transition

As noted above, we consider a transition in a dimerized antiferromagnet (with an even number of $S = 1/2$ spins per unit cell of the Hamiltonian) from a spin gap state to a Néel state. A convenient description of both phases and the quantum phase transition is provided by the O(3) non-linear sigma model, expressed in terms of a unit vector field $\mathbf{n}(\vec{x}, \tau)$ representing the local orientation of the Néel order parameter. Here \vec{x} is the two dimensional spatial position, τ is imaginary time, and $\mathbf{n}^2 = 1$ everywhere in spacetime. The bulk action in the absence of the impurity is the O(3) non-linear sigma model

$$\mathcal{S}_b^n = \frac{1}{2g} \int d\tau \int d^2x (\partial_\mu \mathbf{n})^2, \quad (3.1)$$

where g is the coupling constant which tunes the antiferromagnet from the Néel state ($g < g_c$) to the spin gap state ($g > g_c$), μ is a 3-dimensional spacetime index and a spin-wave velocity has been set to unity. In this formulation, the influence of the impurity is represented universally by the following Berry phase term alone[112] (provided the antiferromagnet is not too far from the critical point)

$$\mathcal{S}_{\text{imp}}^n = iS \int d\tau \mathbf{A}[\mathbf{n}(0, \tau)] \cdot \frac{d\mathbf{n}(0, \tau)}{d\tau}, \quad (3.2)$$

for a spin $S = 1/2$ antiferromagnet, where \mathbf{A} is the Dirac monopole function in spin space with $\nabla_{\mathbf{n}} \times \mathbf{A} = \mathbf{n}$. Note that $\mathcal{S}_{\text{imp}}^{\mathbf{n}}$ does not include any coupling constants, and it depends upon the value of \mathbf{n} only at $\vec{x} = 0$, which is the position of the impurity.

Now we need to describe the $S = 1/2$ ground state of $\mathcal{S}_b^{\mathbf{n}} + \mathcal{S}_{\text{imp}}^{\mathbf{n}}$ for $g \geq g_c$. First, we need a proper discussion of the rotationally invariant $S = 0$ ground state without the impurity. While it may be possible to do this within the context of a small g expansion of the $O(3)$ non-linear sigma model, the procedure is quite cumbersome and delicate, requiring a global average over all possible locally ordered states. We shall instead follow a simpler procedure which is described in more detail in Section 3.2: we use an alternative soft-spin, LGW formulation of $\mathcal{S}_b^{\mathbf{n}}$ in terms of a vector order parameter, ϕ , whose length is unconstrained. The $\phi = 0$ saddle point then is an appropriate starting point for describing the physics of the $S = 0$ ground state of the bulk theory and its excitations. Next, we include the impurity term described by $\mathcal{S}_{\text{imp}}^{\mathbf{n}}$, and also apply an infinitesimal magnetic field in the z direction. As we will show in Section 3.2, the Berry phase effectively localizes the order parameter at the impurity site, $\mathbf{n}(\vec{x} = 0, \tau)$, to a specific orientation on the unit sphere; in particular, for the $S_z = 1/2$ state chosen by the applied field, we may perform an expansion about a saddle point with $\mathbf{n}(\vec{x} = 0, \tau) = (1, 0, 0)$. This expansion quantizes, at each order, the total spin at $S_z = 1/2$: this was established in Section II.C.2 of Ref. [107] for $g < g_c$, and the same result also applies here for $g \geq g_c$. The infinitesimal magnetic field is set to zero at the end, but the spin density of the $S_z = 1/2$ state remains non-zero in this limit.

The results in Section 3.2 provide an explicit analytic realization for the scaling

forms presented in Ref. [96] for the spin texture near the impurity. For the magnetization density, \mathbf{Q} , which is the conserved Noether “charge” density associated with the O(3) symmetry of the antiferromagnet, we have at $g = g_c$ and zero temperature (T) and in the $S_z = 1/2$ state:

$$\langle Q_z(\vec{x}) \rangle = \frac{1}{L^2} \Phi_Q \left(\frac{\vec{x}}{L} \right) \quad (3.3)$$

where $\Phi_Q(\vec{r})$ is a universal function obeying the quantized total spin condition

$$\int d^2r \Phi_Q(\vec{r}) = S. \quad (3.4)$$

Similarly, the staggered magnetization associate with the Néel order parameter obeys the scaling form

$$\langle n_z(\vec{x}) \rangle = \frac{1}{L^{(1+\eta)/2}} \Phi_n \left(\frac{\vec{x}}{L} \right) \quad (3.5)$$

at $g = g_c$, where $\Phi_n(\vec{r})$ is another universal function, but its overall scale is non-universal. The exponent η is the anomalous dimension of \mathbf{n} at $g = g_c$ in the absence of the impurity.

3.1.2 Deconfined transition

Now let us turn to the more interesting case of a transition in an antiferromagnet with an odd number of $S = 1/2$ spins per unit cell, such as the square lattice antiferromagnet. In this case, there is no a priori obvious choice for the spin gap state, and the paramagnetic state exhibits spin liquid behavior over all but the largest length scales [1, 2]. The spin liquid state has a bosonic spinon excitation represented by a complex spinor field $z_\alpha(\vec{x}, \tau)$, where $\alpha = \uparrow, \downarrow$, and the constraint $\sum_\alpha |z_\alpha|^2 = 1$ is obeyed everywhere in spacetime. There is also a non-compact U(1) gauge field A_μ

which encodes collective singlet excitations. As argued in Refs. [1, 2] the vicinity of the quantum critical point to the Néel phase is described by the CP^1 field theory of these degrees of freedom. The Néel order parameter, \mathbf{n} is related to z_α by

$$\mathbf{n} = z_\alpha^\dagger \vec{\sigma}_{\alpha\beta} z_\beta, \quad (3.6)$$

where $\vec{\sigma}$ are the Pauli matrices. Also, in our analysis, we find it useful to generalize to the CP^{N-1} model with $SU(N)$ symmetry, where $\alpha = 1 \dots N$, and then the Pauli matrices are replaced by the generators of $SU(N)$. The action of the CP^{N-1} model also involves a non-compact $U(1)$ gauge field A_μ , and is given by

$$\mathcal{S}_b^z = \int d\tau \int d^2x \left[\frac{1}{g} |(\partial_\mu - iA_\mu)z_\alpha|^2 + \frac{1}{2e^2} (\epsilon_{\mu\nu\lambda} \partial_\nu A_\lambda)^2 \right]. \quad (3.7)$$

This theory describes a Néel-ordered phase for $g < g_c$, and a spin-gap state with VBS order for $g \geq g_c$ (additional Berry phase terms are needed to obtain the four-fold square-lattice symmetry of the VBS order[21, 22]). It is crucial to note that, unlike the situation in 1+1 dimensions [95, 120], the models $\mathcal{S}_b^{\mathbf{n}}$ (in Eq. (3.1)) and \mathcal{S}_b^z are *not* equivalent to each other in 2+1 dimensions. This was established in Ref. [51], and is a consequence of the proliferation of ‘hedgehog’ or ‘monopole’ defects at the critical point of $\mathcal{S}_b^{\mathbf{n}}$; such defects are absent in the \mathcal{S}_b^z theory.

Now let us add an impurity to the field theory in Eq. (3.7). It was argued in Ref. [121] that the impurity is now represented by a source term for a static charge $Q = 2S$ at $\vec{x} = 0$. Thus

$$\mathcal{S}_{\text{imp}}^z = iQ \int d\tau A_\tau(\vec{x} = 0, \tau) \quad (3.8)$$

As before, we are now interested in describing the ground state of $\mathcal{S}_b^z + \mathcal{S}_{\text{imp}}^z$, which we expect carries total spin $S = 1/2$. However, now the projection onto the state

with $S = 1/2$ cannot be done by the method used for the LGW theory. For $g \geq g_c$, we begin with a $S = 0$ ground state of \mathcal{S}_b^z , but now don't find that the impurity term in Eq. (3.8) introduces any net spin: the total spin remains at $S = 0$ to all orders in perturbation theory. Clearly, we need the impurity charge Q to non-perturbatively bind a $S = 1/2$ z_α spinon. For $g > g_c$, such binding can be addressed via a non-relativistic Schrödinger equation [23], the analysis does not appear appropriate at the main point of interest, $g = g_c$, where we have a conformal field theory (CFT) with no sharp quasiparticle excitations. Here we expect the spinon to be smeared over the whole system of size of L . We shall describe this spinon state by explicitly beginning with a $S = 1/2$ state of \mathcal{S}_b^z and then perturbatively examining the influence of $\mathcal{S}_{\text{imp}}^z$: this is expected to yield correlations in the true $S = 1/2$ ground state of $\mathcal{S}_b^z + \mathcal{S}_{\text{imp}}^z$.

Using the language of general $\text{SU}(N)$, let the ground states of $\mathcal{S}_b^z + \mathcal{S}_{\text{imp}}^z$ be $|\alpha\rangle$; these transform under the fundamental representation of $\text{SU}(N)$. To find the matrix element of some operator $O(\vec{x})$ between states $|\alpha\rangle$ and $|\beta\rangle$ of the $\text{SU}(N)$ multiplet, we compute,

$$\langle \alpha | O(\vec{x}) | \beta \rangle = \lim_{\mathcal{T} \rightarrow \infty} \frac{\left\langle z_\alpha(0, \mathcal{T}/2) \exp\left(-i \int_{-\mathcal{T}/2}^{\mathcal{T}/2} A_\tau(0, \tau) d\tau\right) O(\vec{x}, 0) z_\beta^\dagger(0, -\mathcal{T}/2) \right\rangle_{\mathcal{S}_b^z}}{\left\langle z_\alpha(0, \mathcal{T}/2) \exp\left(-i \int_{-\mathcal{T}/2}^{\mathcal{T}/2} A_\tau(0, \tau) d\tau\right) z_\alpha^\dagger(0, -\mathcal{T}/2) \right\rangle_{\mathcal{S}_b^z}}. \quad (3.9)$$

Effectively, we start with external charge free vacuum, and then at time $\tau = -\mathcal{T}/2$ create a spinon together with the Wilson line, the latter representing the effect of the external charge $Q = 1$. We wait for a long time $\mathcal{T}/2$ to single out the lowest energy state with the quantum numbers of the operator z_α^\dagger . We then measure the operator $O(\vec{x})$, again wait time $\mathcal{T}/2$ and annihilate our spinon together with the external charge. The denominator in Eq. (3.9) serves to cancel out the matrix element for

creating the spinon - external charge bound state out of the vacuum (no sum over α is implied in the denominator). Expressions of type (3.9) are common when studying the properties of heavy-light mesons in quantum chromodynamics.

The time \mathcal{T} must be much larger than the gap between states with the quantum numbers that we are studying. In the spin gap phase, $g > g_c$, this gap is finite in the infinite volume limit. However, at the critical point the gap will be of order $1/L$. So one has to choose $\mathcal{T} \gg L$. Although unusual, this condition can always be satisfied as we work at zero temperature.

To discuss higher charge impurity ($Q > 1$) one needs to act on the vacuum with higher $U(1)$ charge composite operators of the z field. The resulting states can form higher representations of $SU(N)$ symmetry. For simplicity, we limit ourselves to $Q = 1$ below.

Details of our evaluation of Eq. (3.9) in the $1/N$ expansion appear in Section 3.3.1. We will obtain results for the scaling functions appearing in Eq. (3.3) and (3.5) describing the spin distribution at the deconfined quantum critical point.

In addition, in Section 3.3.2 we compute the uniform and staggered spin distributions in the Néel phase of the CP^{N-1} model. We find that the short distance behaviour of spin distributions both at the critical point and in the Neel phase is in agreement with the impurity scaling theory postulated in Ref. [121]. In particular, we obtain substantial additional evidence that the uniform and staggered spin operators flow to the same impurity spin operator upon approaching the impurity site. Results of the $1/N$ expansion for the impurity critical exponents of uniform and staggered magnetization are obtained.

3.2 LGW criticality

This section will study the field theory $\mathcal{S}_b^n + \mathcal{S}_{\text{imp}}^n$ describing an impurity in an antiferromagnet with an even number of $S = 1/2$ spins per unit cell. As discussed in Section 3.1, the $O(3)$ non-linear sigma model formulation in Eqs. (3.1) and (3.2) is not appropriate for our purposes. Instead, we shall use a ‘soft-spin’ approach which yields a convenient description of the rotationally-invariant state of the bulk antiferromagnet for $g \geq g_c$, and of its impurity-induced deformations. The universal results appear in an expansion in

$$\epsilon = (3 - d), \tag{3.10}$$

where d is the spatial dimensionality.

This dimensionality expansions allow us to compute, in principle, the universal scaling functions, appearing in Eqs. (3.3) and (3.5), which were numerically computed recently in Ref. [96]. The scaling functions clearly depend upon the geometry of the sample, and the nature of the finite-size boundary conditions. Such features are not easily captured in a dimensionality expansion. Consequently the results in this section are more a “proof of principle” that the scaling results apply. Direct comparison of the results below for scaling functions to the numerical results are not very useful.

As discussed in Ref. [107], the ϵ expansion is obtained by replacing the fixed length field \mathbf{n} by a field ϕ whose amplitude is allowed to vary freely. However, we do not have the freedom to relax the length constraint on the impurity site because the Berry phase term is only defined for a unit length field. Consequently, we retain an independent field $\mathbf{n}(\tau)$ representing the impurity spin, which is now linearly coupled

to ϕ . So we consider the theory

$$\begin{aligned}\mathcal{Z}_\phi &= \int \mathcal{D}\phi(\vec{x}, \tau) \mathcal{D}\mathbf{n}(\tau) \delta(\mathbf{n}^2 - 1) \exp\left(-\mathcal{S}_b^\phi - \mathcal{S}_{\text{imp}}^\phi\right) \\ \mathcal{S}_b^\phi &= \int d^d x d\tau \left[\frac{1}{2} ((\partial_\mu \phi)^2 + s\phi^2) + \frac{g_0}{4!} (\phi^2)^2 \right] \\ \mathcal{S}_{\text{imp}}^\phi &= iS \int d\tau \mathbf{A}[\mathbf{n}(\tau)] \cdot \frac{d\mathbf{n}(\tau)}{d\tau} - \gamma_0 S \mathbf{n}(\tau) \cdot \phi(0, \tau)\end{aligned}\quad (3.11)$$

Here $s \sim g$ is the coupling that tunes the system across the bulk quantum phase transition, and g_0 and γ_0 are the couplings which were shown in Ref. [107] to approach fixed point values in the vicinity of the quantum critical point. In the $(3-d)$ expansion, these fixed point values are small with $g_0 \sim \gamma_0^2 \sim \epsilon$. It was argued in Ref. [112] that this fixed point is identical to that obtained from the O(3) non-linear sigma model theory appearing in Eqs. (3.1,3.2).

We will be interested here in the $s \geq s_c$ regime of \mathcal{Z}_ϕ here, where $\langle \phi \rangle = 0$ and full rotational symmetry is preserved in the absence of the impurity. As discussed in Section 3.1, we need to project on to the state with total $S_z = 1/2$ in the presence of the impurity. This is easily done here by choosing the following parameterization for the impurity degree of freedom $\mathbf{n}(\tau)$ in terms of a complex scalar $\psi(\tau)$:

$$\mathbf{n} = \left(\frac{\psi + \psi^*}{2} \sqrt{2 - |\psi|^2}, \frac{\psi - \psi^*}{2i} \sqrt{2 - |\psi|^2}, 1 - |\psi|^2 \right). \quad (3.12)$$

The advantage of the representation (3.12) is that with the gauge choice

$$\mathbf{A}(\mathbf{n}) = \frac{1}{1 + n_z} (-n_y, n_x, 0), \quad (3.13)$$

the Berry phase takes the following form

$$i\mathbf{A}(\mathbf{n}) \cdot \frac{d\mathbf{n}}{d\tau} = \frac{1}{2} \left(\psi^* \frac{\partial \psi}{\partial \tau} - \psi \frac{\partial \psi^*}{\partial \tau} \right), \quad (3.14)$$

Furthermore, the measure term in the functional integral also has the simple form

$$\int \mathcal{D}\mathbf{n} \delta(\mathbf{n}^2 - 1) = \int \mathcal{D}\psi \mathcal{D}\psi^* \quad (3.15)$$

Now, an expansion of the correlators of \mathcal{Z}_ϕ , in a functional integral over ϕ and ψ about the saddle point with $\phi = 0$ and $\psi = 0$, in powers of the couplings γ_0 and g_0 , automatically projects onto the state with total spin projection $S_z = 1/2$. This is easily established by applying a uniform magnetic field, and verifying by the methods of Ref. [107, 112] that the total magnetization is quantized by a Ward identity associated with the conservation of spin.

We can now use the above perturbative expansion, using methods explained at length elsewhere[107, 112], to compute the expectation values of the magnetization density $\langle Q_z(\vec{x}) \rangle$ and the Néel order parameter $\langle \phi_z(\vec{x}) \rangle$. We perform this computation on a sample with periodic boundary conditions and length L in each spatial dimension, *i.e.* a torus T^d . The main effect of the finite boundary conditions is that the momenta \vec{p} are discrete, and each momentum component is quantized in integer multiples of $2\pi/L$. The results below are easily generalized to other finite size geometries and boundary conditions. To leading order in ϵ , the results are

$$\begin{aligned} \langle Q_z(\vec{x}) \rangle &= S\delta^d(\vec{x}) - \gamma_0^2 S\delta^d(\vec{x}) \int \frac{d\omega}{2\pi} \frac{1}{(i\omega + \epsilon)^2} G(\omega, 0) + 2\gamma_0^2 S \int \frac{d\omega}{2\pi} G(\omega, \vec{x}) G(\omega, -\vec{x}) \\ \langle \phi_z(\vec{x}) \rangle &= \gamma_0 S G(0, \vec{x}) \left[1 - \gamma_0^2 \int \frac{d\omega}{2\pi} \frac{1}{(i\omega + \epsilon)^2} G(\omega, 0) \right] \end{aligned} \quad (3.16)$$

where ϵ is a positive infinitesimal proportional to an applied magnetic field which selects the $S_z = 1/2$ state. We may set $\epsilon = 0$ after the frequency integrals have been performed. The Green's function of the ϕ field is

$$G(\omega, \vec{x}) = \frac{1}{L^d} \sum_{\vec{p}} \frac{e^{i\vec{p}\cdot\vec{x}}}{\omega^2 + \vec{p}^2 + \Delta^2}, \quad (3.17)$$

where Δ is the spin gap of the bulk antiferromagnet in the absence of the impurity. Other boundary conditions will only change the form of G , requiring expressions involving different normal mode wavefunctions, but the form in Eq. (3.16) will remain unchanged. It is easy to check that the spatial integral of $\langle Q_z \rangle$ is quantized at S .

To leading order in ϵ , it would appear that we can set Δ equal to the spin gap in the infinite bulk antiferromagnet, and in particular, set $\Delta = 0$ at the critical point $s = s_c$. However, we will see below that for the particular boundary conditions we are using here, there are infrared divergencies at $\Delta = 0$ in the expressions for the impurity-induced spin textures. In such a situation we have to examine the finite L corrections to the value of Δ at $s = s_c$, which yield a non-zero Δ even at the bulk quantum critical point. The value of Δ can be computed as described elsewhere[122], and to leading order in ϵ , the equation determining Δ at the quantum critical point $s = s_c$ is

$$\Delta^2 = \frac{5g_0}{6} \frac{1}{L^d} \sum_{\vec{p}} \int \frac{d\omega}{2\pi} \frac{1}{\omega^2 + \vec{p}^2 + \Delta^2} \quad (3.18)$$

To leading order in ϵ , only the $\vec{p} = 0$ term on the right-hand-side has to be included; setting g_0 equal to its fixed point value[122] we find for small ϵ

$$\Delta = \left(\frac{20\pi^2\epsilon}{11} \right)^{1/3} \frac{1}{L}. \quad (3.19)$$

Note that $L\Delta$ is a universal number at $s = s_c$, which is the main result we will need below to establish the universality of the spin texture.

Returning to the expressions in Eq. (3.16), we now want to manipulate them into the forms of Eq. (3.3) and (3.5). However, the presence of the $\delta^d(\vec{x})$ in Eq. (3.16) makes the \vec{x} dependence singular. These singularities are in fact an artifact of the present perturbative expansion in real space, and are not expected to be present once

the expansion is resummed. This is evident by examining the results in momentum space, where the results are a smooth function of momentum. In this manner we obtain after applying Eq. (3.17) to Eq. (3.16)

$$\begin{aligned}\langle Q_z(\vec{p}) \rangle &= S \left[1 - \frac{\gamma_0^2}{L^d} \sum_{\vec{q}} \frac{1}{2E_{\vec{q}}} \left(\frac{1}{E_{\vec{q}}^2} - \frac{2}{E_{\vec{p}+\vec{q}}(E_{\vec{p}+\vec{q}} + E_{\vec{q}})} \right) \right] \\ \langle \phi_z(\vec{p}) \rangle &= \frac{\gamma_0 S}{\vec{p}^2 + \Delta^2} \left[1 - \frac{\gamma_0^2}{L^d} \sum_{\vec{q}} \frac{1}{2E_{\vec{q}}^3} \right]\end{aligned}\quad (3.20)$$

where $E_{\vec{p}} = \sqrt{\vec{p}^2 + \Delta^2}$. Now Eqs. (3.20) can be evaluated at the fixed point value of γ_0 , and to leading order in ϵ they are seen to yield results consistent with the following scaling forms which can be deduced from Eqs. (3.3,3.5)

$$\begin{aligned}\langle Q_z(\vec{p}) \rangle &= \tilde{\Phi}_Q(\vec{p}L) \\ \langle \phi_z(\vec{p}) \rangle &= L^{(d+1-\eta)/2} \tilde{\Phi}_n(\vec{p}L)\end{aligned}\quad (3.21)$$

The explicit results for the scaling functions to leading order in ϵ are

$$\begin{aligned}\tilde{\Phi}_Q(\vec{y}) &= S \left[1 - 2\pi^2\epsilon \sum_{\vec{x}} \frac{1}{2\mathcal{E}_{\vec{x}}} \left(\frac{1}{\mathcal{E}_{\vec{x}}^2} - \frac{2}{\mathcal{E}_{\vec{y}+\vec{x}}(\mathcal{E}_{\vec{y}+\vec{x}} + \mathcal{E}_{\vec{x}})} \right) \right] \\ \tilde{\Phi}_n(\vec{y}) &= \frac{\pi S \sqrt{2\epsilon}}{\vec{y}^2 + L^2 \Delta^2} [1 - 2\pi^2\epsilon (\text{a finite number})]\end{aligned}\quad (3.22)$$

where now \vec{x} and \vec{y} are *three* dimensional momenta whose components are quantized in integer multiples of 2π (except in the integral in the second equation), and $\mathcal{E}_{\vec{x}} = \sqrt{\vec{x}^2 + L^2 \Delta^2}$. It is easily checked that these expressions are free of infrared and ultraviolet divergencies, and so yield universal results because $L\Delta$ is a universal number.

From the above expression, we observe that $\tilde{\Phi}_Q(|\vec{y}| \rightarrow \infty) = S(1 - (\epsilon/2) \ln |\vec{y}|)$, which we assume exponentiates to $\tilde{\Phi}_Q(|\vec{y}| \rightarrow \infty) \sim |\vec{y}|^{-\epsilon/2}$. From the short distance

behavior of the spin texture discussed in Ref. [96], we expect that $\tilde{\Phi}_Q(|\vec{y}| \rightarrow \infty) \sim |\vec{y}|^{-\eta'/2}$, where η' is the scaling dimension of the boundary spin[107]. So we obtain the value $\eta' = \epsilon$, which is consistent with earlier results[107]. Similarly, from the short distance behavior discussed in Ref. [96], we also have $\tilde{\Phi}_n(|\vec{y}| \rightarrow \infty) \sim |\vec{y}|^{-2+(\epsilon+\eta-\eta')/2}$. So with $\eta \sim \mathcal{O}(\epsilon^2)$ and $\eta' = \epsilon$, we have $\tilde{\Phi}_n(|\vec{y}| \rightarrow \infty) \sim |\vec{y}|^{-2}$, which is consistent with Eq. (3.22).

3.3 Deconfined criticality

This section describes the Néel-VBS transition in square lattice quantum antiferromagnets with a single $S = 1/2$ per unit cell. As discussed in Section 3.1, the response of a non-magnetic impurity is described by the action $\mathcal{S}_b^z + \mathcal{S}_{\text{imp}}^z$ in Eqs. (3.7,3.8) for a complex $SU(N)$ spinon field z_α and a non-compact $U(1)$ gauge field A_μ . Here we will describe the $1/N$ expansion of its universal critical properties. Note that in what follows we have rescaled the spinon field z , to remove the coupling constant g from the action (3.7), in favour of a rescaled constraint $z_\alpha^\dagger z_\alpha = 1/g$. This constraint is enforced with a local Lagrange multiplier λ , so that the bulk action becomes,

$$\mathcal{S}_b^z = \int d\tau \int d^2x \left[|(\partial_\mu - iA_\mu)z_\alpha|^2 + i\lambda(|z_\alpha|^2 - \frac{1}{g}) + \frac{1}{2e^2}(\epsilon_{\mu\nu\lambda}\partial_\nu A_\lambda)^2 \right]. \quad (3.23)$$

It is useful to define $SU(N)$ generalizations of the $SU(2)$ observables introduced in Section 3.1. The uniform magnetization density \mathbf{Q} generalizes to Q^a , which is the temporal component of a current associated with the $SU(N)$ rotation symmetry,

$$Q^a = z^\dagger T^a D_\tau z - (D_\tau z)^\dagger T^a z \quad (3.24)$$

(where $D_\mu = \partial_\mu - iA_\mu$ is the covariant derivative) while the Néel order \mathbf{n} in Eq. (3.6) becomes the staggered magnetization operator

$$n^a = z^\dagger T^a z \tag{3.25}$$

where T^a are generators of the $SU(N)$ algebra. We will describe the spatial dependence of the expectation values of these operators for two cases: a finite system of size L at the critical point $g = g_c$ in Section 3.3.1, and the infinite system in the Néel phase with broken $SU(N)$ symmetry in Section 3.3.2.

3.3.1 Critical point in a finite system

We tune the system to the critical point $g = g_c$ of the infinite volume zero temperature model, and then consider the system on a spatial torus of length L . We use periodic boundary conditions for all fields.² As we discussed in Section 3.1, the ground state in the absence of an impurity is a spin-singlet, while adding an impurity yields a ground state which transforms under the fundamental representation of $SU(N)$. This ground state has a single spinon in it, and we argued that the projection onto this state can be performed by Eq. (3.9). For an additional test of our projection formalism, see the appendix, where we compute the $U(1)$ (electric) charge density in the presence of the impurity.

Before we address the explicit computation of (3.9), we discuss scaling forms that our results should obey.

²In principle, on a spatial torus, we can certainly have a finite magnetic (F_{ij}) flux, which would correspond to non-periodic boundary conditions. However, finite flux sectors are expected to be separated from vacuum by an energy gap, and hence are suppressed at $T = 0$.

Scaling forms

We are interested in computing the uniform and staggered magnetization densities. Recall, that since the uniform magnetization is a zeroth component of a conserved current, it receives no renormalizations. Therefore, utilizing the $SU(N)$ symmetry, we have the general scaling form,

$$\langle \alpha | Q^a(\vec{x}) | \beta \rangle = \frac{1}{L^2} \Phi_Q\left(\frac{\vec{x}}{L}\right) T_{\alpha\beta}^a. \quad (3.26)$$

The leading $1/L^2$ prefactor corresponds to the scaling dimension $\Delta_Q = d = 2$ of the magnetization density. Moreover, by conservation of total $SU(N)$ charge,

$$\int d^2r \Phi_Q(\vec{r}) = -1 \quad (3.27)$$

where the integral is over $0 < r_1, r_2 < 1$. Similarly, for the case of the staggered magnetization,

$$\langle \alpha | n^a(\vec{x}) | \beta \rangle = \Lambda^{\eta_n} \left(\frac{1}{L}\right)^{1-\eta_n} \Phi_n\left(\frac{\vec{x}}{L}\right) T_{\alpha\beta}^a \quad (3.28)$$

Here η_n is the anomalous dimension of the staggered magnetization operator $n^a(x)$, $\Delta_n = \dim[n^a] = 1 - \eta_n$. This exponent is related to the exponent η in Eq. (3.5), and their values were computed previously [123] in the $1/N$ expansion for arbitrary spacetime dimension $2 < D < 4$:

$$\eta_n = \frac{1}{2}(D - 2 - \eta) = \frac{1}{N} \frac{16\Gamma(D - 2)}{\Gamma(2 - D/2)\Gamma(D/2 - 1)^3} + O(1/N^2) \stackrel{D=3}{=} \frac{16}{\pi^2 N} + O(1/N^2). \quad (3.29)$$

The function Φ_Q is completely universal, whereas Φ_n is universal only up to an overall scale. In particular, Φ_n does not have any property analogous to (3.27).

Of particular interest is the behavior of the functions $\Phi_Q(\vec{r})$, $\Phi_n(\vec{r})$ for $\vec{r} \rightarrow 0$. We make a hypothesis that $n^a(\vec{x}, \tau)$ and $Q^a(\vec{x}, \tau)$ flow to the same operator $S^a(\tau)$ as \vec{x}

approaches the Wilson line,

$$\begin{aligned} \lim_{|\vec{x}| \rightarrow 0} Q^a(\vec{x}, \tau) &= \frac{c_Q}{|\vec{x}|^{-\Delta_{\text{imp}}^Q}} S^a(\tau) \\ \lim_{|\vec{x}| \rightarrow 0} n^a(\vec{x}, \tau) &= \frac{c_n}{|\vec{x}|^{-\Delta_{\text{imp}}^n}} S^a(\tau) \end{aligned} \quad (3.30)$$

Calculations in the ϵ expansion supporting this hypothesis have been given in Ref. [121].

We have performed analogous calculations in the $1/N$ expansion again confirming the OPE (3.30). Technically, this impurity OPE program consists of the following steps. First one considers the (multiplicative) renormalization of the operator $n^a(\vec{x} = 0)$, by studying its insertion into the two point function of the z field (this consist of the usual bulk renormalization, plus an additional renormalization of the logarithmic divergences that appear as $\vec{x} \rightarrow 0$). Once $n^a(\vec{x} = 0)$ operator is renormalized, one considers the insertion of $Q^a(\vec{x} \rightarrow 0)$ into the two point function of the z field. The highest divergence as $|\vec{x}| \rightarrow 0$ is power-like, $1/|\vec{x}|$, modified by logarithms at higher orders in $1/N$. This leading divergence can be cancelled by a $n^a(\vec{x} = 0)$ counterterm (with a coefficient that diverges as $\vec{x} \rightarrow 0$). This procedure gives one a way to construct order by order in $1/N$, the impurity operator $S^a(\tau)$ (which is essentially a regularized $n^a(\vec{x} = 0, \tau)$), and compute the anomalous dimensions Δ_{imp}^Q , Δ_{imp}^n as well as coefficients c_Q , c_n (the later are renormalization scheme dependent). As the computation of the OPE in the $1/N$ expansion essentially follows that in the ϵ expansion presented in Ref. [121], we shall not include it here. We only note that in this way, we have been able to explicitly check the OPE (3.30) to order $1/N^2$, obtaining Δ_{imp}^n to order $1/N^2$ and Δ_{imp}^Q to order $1/N$ (this is lower order than the corresponding result for Δ_{imp}^n as c_Q/c_n is of order $1/N$). Explicit results in this expansion will appear in Section 3.3.2.

Calculations of Φ_Q and Φ_n given below provide additional support for the OPE (3.30). Note that the exponents Δ_{imp}^Q and Δ_{imp}^n are not independent. Indeed, let the correlator

$$\langle S^a(\tau)S^b(0) \rangle \sim \frac{1}{\tau^{2\Delta_S}} \delta_{ab}. \quad (3.31)$$

The exponent Δ_S is related to the boundary spin exponent η' used in Refs. [107, 96] by $\eta' = 2\Delta_S$. Then,

$$\Delta_S = \Delta_Q + \Delta_{\text{imp}}^Q = \Delta_n + \Delta_{\text{imp}}^n \quad (3.32)$$

Recalling, $\Delta_Q = 2$, $\Delta_n = 1 - \eta_n$,

$$\Delta_{\text{imp}}^Q = \Delta_{\text{imp}}^n - 1 - \eta_n. \quad (3.33)$$

Our explicit results for the profiles Φ_Q, Φ_n confirm the relation (3.33) to leading (zeroth) order in $1/N$, see below. We have also been able to check this relation to order $1/N$ using the impurity OPE program summarized above: to this order, $\Delta_{\text{imp}}^Q = -1 - \eta_n$, as $\Delta_{\text{imp}}^n \sim O(1/N^2)$. The result of our evaluation of Δ_{imp}^n to $O(1/N^2)$ will appear later in Eqs. (3.120),(3.121).

Note that the OPE (3.30) is sensitive only to short distance physics, and, thus, coefficients c_Q, c_n should be independent of the system size L as well as the deviation from the critical point (all this IR information is, however, contained in the impurity operator S^a). Thus, the ratio,

$$\frac{c_Q}{c_n} = \lim_{|\vec{x}| \rightarrow 0} |\vec{x}|^{\Delta_{\text{imp}}^n - \Delta_{\text{imp}}^Q} \frac{\langle Q^a(\vec{x}) \rangle}{\langle n^a(\vec{x}) \rangle} = \lim_{|\vec{x}| \rightarrow 0} |\vec{x}|^{1+\eta_n} \frac{\langle Q^a(\vec{x}) \rangle}{\langle n^a(\vec{x}) \rangle} \quad (3.34)$$

although non-universal, should be constant throughout the scaling regime (once the regularization scheme is chosen). We shall check this fact below to leading order in

$1/N$ by comparing the short distance behaviour (controlled by the OPE) of uniform and staggered magnetization densities at the critical point and in the Néel phase.

Projection onto the single spinon state

Now we return to the evaluation of the matrix elements (3.9). Although it is possible to obtain all the results presented below directly from Eq. (3.9) it is technically somewhat simpler to use instead,

$$\langle \alpha | O(\vec{x}) | \beta \rangle = \lim_{\mathcal{T} \rightarrow \infty} \frac{\langle z_\alpha(\vec{k}, \mathcal{T}/2) O(\vec{x}, 0) z_\beta^\dagger(\vec{k}', -\mathcal{T}/2) \rangle_{\text{imp}}}{\langle z_\alpha(\vec{k}, \mathcal{T}/2) z_\alpha^\dagger(\vec{k}', -\mathcal{T}/2) \rangle_{\text{imp}}} \quad (3.35)$$

Here, $z_\alpha(\vec{k}, \tau) = \int d^2x z_\alpha(\vec{x}, \tau) e^{-i\vec{k}\vec{x}}$ and the subscript “imp” indicates that the correlator should be computed in a theory with the action $\mathcal{S}_b^z + \mathcal{S}_{\text{imp}}^z$ which includes the impurity term. Effectively, we have extended the Wilson line, which in (3.9) stretched from the point where a spinon was created to the point where it was destroyed, to run from $\tau = -\infty$ to $\tau = \infty$. In addition, we have taken our “incoming” and “outgoing” spinon to be in momenta \vec{k} and \vec{k}' states. This makes the numerator and denominator of (3.35) non-gauge invariant. Nevertheless, we expect that this non-gauge invariance comes solely from the matrix element for creating the ground state of the system by acting on the vacuum with z^\dagger and cancels out between the numerator and denominator of (3.35).

Since the impurity term Eq. (3.8) breaks spatial (but not temporal) translational invariance, for $\mathcal{T} \rightarrow \infty$ we expect to obtain the ground state irrespective of which \vec{k}, \vec{k}' we started with. Nevertheless, it will be most convenient in our perturbative treatment to work with $\vec{k} = \vec{k}' = 0$.

Since the external charge does not break $SU(N)$ symmetry and time translation

symmetry, we have,

$$\langle z_\alpha(x) z_\beta^\dagger(x') \rangle_{\text{imp}} = \delta_{\alpha\beta} D(\vec{x}, \vec{x}', \tau - \tau') \quad (3.36)$$

We let,

$$D(\vec{x}, \vec{x}', \tau) = \frac{1}{L^2} \sum_{\vec{p}, \vec{p}'} \int \frac{d\omega}{2\pi} D(\vec{p}, \vec{p}', \omega) e^{i\vec{p}\vec{x}} e^{-i\vec{p}'\vec{x}'} e^{i\omega\tau} \quad (3.37)$$

We write,

$$\langle z_\alpha(y) O(x) z_\beta^\dagger(y') \rangle_{\text{imp}} = \int dv dv' D(y, v) O_{\alpha\beta}(v, x, v') D(v', y') \quad (3.38)$$

Fourier transforming,

$$O_{\alpha\beta}(v, x, v') = \frac{1}{L^2} \sum_{\vec{p}} \frac{1}{L^2} \sum_{\vec{p}'} \int \frac{d\omega}{2\pi} \int \frac{d\omega'}{2\pi} O_{\alpha\beta}(\vec{p}, \vec{q}, \vec{p}', \omega, \omega') \times e^{i\vec{p}\vec{v}} e^{-i\vec{p}'\vec{v}'} e^{i\vec{q}\vec{x}} e^{i\omega v_\tau} e^{-i\omega' v'_\tau} e^{i(\omega - \omega')x_\tau} \quad (3.39)$$

where we use the notation that the three-vector x has spatial components \vec{x} and temporal component x_τ . So,

$$\langle z_\alpha(\vec{k}, \mathcal{T}/2) O(\vec{x}, 0) z_\beta^\dagger(\vec{k}', -\mathcal{T}/2) \rangle_{\text{imp}} = \sum_{\vec{p}, \vec{p}', \vec{q}} \int \frac{d\omega}{2\pi} \int \frac{d\omega'}{2\pi} D(\vec{k}, \vec{p}, \omega) O_{\alpha\beta}(\vec{p}, \vec{q}, \vec{p}', \omega, \omega') D(\vec{p}', \vec{k}', \omega') e^{i\omega\mathcal{T}/2} e^{i\omega'\mathcal{T}/2} e^{i\vec{q}\vec{x}} \quad (3.40)$$

As we perform the integral over ω, ω' , we pick up poles of the propagators D in the $\Im(\omega) > 0, \Im(\omega') > 0$ planes (we expect that $O_{\alpha\beta}$ is analytic in ω). In the limit $\mathcal{T} \rightarrow \infty$ only the contribution from the pole with smallest imaginary part survives. Let this pole be at $\omega = im$ and denote by $\text{Res}(\vec{k}, \vec{p})$ the residue of $D(\vec{k}, \vec{p}, \omega)$ at this pole. Then,

$$\langle z_\alpha(\vec{k}, \mathcal{T}/2) O(\vec{x}, 0) z_\beta^\dagger(\vec{k}', -\mathcal{T}/2) \rangle_{\text{imp}} \rightarrow \sum_{\vec{p}, \vec{p}', \vec{q}} (i\text{Res}(\vec{k}, \vec{p})) (i\text{Res}(\vec{p}', \vec{k}')) \times O_{\alpha\beta}(\vec{p}, \vec{q}, \vec{p}', im, im) e^{i\vec{q}\vec{x}} e^{-m\mathcal{T}} \quad (3.41)$$

Similarly, the denominator of (3.35) is,

$$\langle z_\alpha(\vec{k}, \mathcal{T}/2) z_\alpha^\dagger(\vec{k}', -\mathcal{T}/2) \rangle_{\text{imp}} \rightarrow L^2 i \text{Res}(k, k') e^{-m\mathcal{T}} \quad (3.42)$$

Finally,

$$\langle \alpha | O(\vec{x}) | \beta \rangle = \frac{1}{L^2} \sum_q \langle \alpha | O(\vec{q}) | \beta \rangle e^{i\vec{q}\vec{x}} \quad (3.43)$$

with,

$$\langle \alpha | O(\vec{q}) | \beta \rangle = \sum_{\vec{p}, \vec{p}'} \frac{(i \text{Res}(\vec{k}, \vec{p}))(i \text{Res}(\vec{p}', \vec{k}'))}{i \text{Res}(k, k')} O_{\alpha\beta}(\vec{p}, \vec{q}, \vec{p}', im, im) \quad (3.44)$$

Large N expansion of CP^{N-1} theory in finite volume

We now compute the expression (3.44) using the large N expansion in finite volume. First, consider the $N = \infty$ limit. The gap equation reads,

$$\frac{1}{L^2} \sum_{\vec{p}} \int \frac{d\omega}{2\pi} \frac{1}{\omega^2 + \vec{p}^2 + m_0^2} = \frac{1}{gN} \quad (3.45)$$

and to this order in N , $m_0^2 = i\langle \lambda \rangle$. In the infinite volume, the critical coupling $g = g_c$ is obtained when the gap m_0 vanishes,

$$\frac{1}{g_c N} = \int \frac{d^3 p}{(2\pi)^3} \frac{1}{p^2} \quad (3.46)$$

However, once we make the spatial volume finite, a non-zero m_0 is generated even at the critical point. Thus, setting $g = g_c$, using Eq. (3.46) and poisson resummung, we obtain,

$$\sum_{\vec{n} \in \mathbf{Z}^2} \int \frac{d\omega}{2\pi} \int \frac{d^2 p}{(2\pi)^2} e^{i\vec{p}\vec{n}L} \frac{1}{\omega^2 + \vec{p}^2 + m_0^2} = \int \frac{d\omega}{2\pi} \int \frac{d^2 p}{(2\pi)^2} \frac{1}{\omega^2 + \vec{p}^2} \quad (3.47)$$

On the left-hand side, only the $\vec{n} = 0$ term diverges in the UV. However, this divergence cancels with the divergence of the right-hand side. Thus, performing all

integrals,

$$\sum_{\vec{n} \neq 0} \frac{1}{4\pi|\vec{n}|} e^{-m_0|\vec{n}|L} = \frac{m_0 L}{4\pi} \quad (3.48)$$

The solution of the Eq. (3.48) is,

$$m_0 = \theta \frac{1}{L} \quad (3.49)$$

where θ is a constant that can be obtained by solving (3.48) numerically to be, $\theta \approx 1.51196$.

Thus, at leading order the propagator,

$$D_0(\vec{k}, \vec{k}', \omega) = \delta_{\vec{k}, \vec{k}'} \frac{1}{\omega^2 + \vec{k}^2 + m_0^2} \quad (3.50)$$

and the lowest pole is at $\vec{k} = 0$, $\omega = im_0$ and, $i\text{Res}(\vec{k}, \vec{p}) = \delta_{\vec{k}, 0} \delta_{\vec{p}, 0} \frac{1}{2m_0}$.

To develop the $1/N$ expansion, we will need to find the A_μ and λ propagators.

The dynamically generated self-energy for A_μ is to leading order,

$$K_{\mu\nu}(p) = -N \frac{1}{L^2} \sum_{\vec{q}} \int \frac{dq_\tau}{2\pi} \left(\frac{(2q-p)_\mu (2q-p)_\nu}{((q-p)^2 + m_0^2)(q^2 + m_0^2)} - \frac{2\delta_{\mu\nu}}{(q^2 + m_0^2)} \right) \quad (3.51)$$

This self energy is always more singular near the critical point than the bare Maxwell term in \mathcal{S}_b^z , and so we will work with $e^2 = \infty$ for the rest of this chapter. To find the photon propagator, $\mathcal{D}_{\mu\nu}(p)$, we also need to fix a gauge. Practically, for the calculations to follow, we will only need the static electromagnetic propagator $\mathcal{D}_{\tau\tau}(\vec{p}, p_\tau = 0) = K_{\tau\tau}(\vec{p}, p_\tau = 0)^{-1}$, which is a gauge invariant quantity. We also note that in the infinite volume limit,

$$K_{\mu\nu}(q) = K(q)(q^2 \delta_{\mu\nu} - q_\mu q_\nu) \quad (3.52)$$

$$K(q) = NA q^{D-4} \quad (3.53)$$



Figure 3.1: The insertion of Q^a into the z propagator.

where the constant A is given by,

$$A = \frac{1}{(4\pi)^{D/2}} \frac{(D-2)\Gamma(2-D/2)\Gamma(D/2-1)^2}{\Gamma(D)} \quad (3.54)$$

Here D is the space-time dimension. In our case, $D = 3$ and $A = \frac{1}{16}$.

Likewise, the self-energy for λ is to leading order,

$$\Pi(p) = N \frac{1}{L^2} \sum_{\vec{q}} \int \frac{dq_\tau}{2\pi} \frac{1}{(q^2 + m_0^2)((q-p)^2 + m_0^2)} \quad (3.55)$$

In the infinite volume limit,

$$\Pi(p) = NBp^{D-4} \quad (3.56)$$

where the constant B is given by,

$$B = \frac{1}{(4\pi)^{D/2}} \frac{\Gamma(2-D/2)\Gamma(D/2-1)^2}{\Gamma(D-2)} \quad (3.57)$$

For $D = 3$, $B = \frac{1}{8}$.

Matrix elements

Now, let us compute the matrix elements of operator $Q^a(x)$. The insertion of Q^a into the z propagator, to leading order in $1/N$ is given by diagram in Fig. 3.1, so

$$Q_{\alpha\beta}^a(\vec{p}, \vec{q}, \vec{p}', \omega, \omega') = i(\omega + \omega') T_{\alpha\beta}^a \delta_{\vec{q}, \vec{p}' - \vec{p}} \quad (3.58)$$

So utilizing formula (3.44), with $\vec{k} = \vec{k}' = 0$, we obtain,

$$\langle \alpha | Q^a(\vec{q}) | \beta \rangle = -T_{\alpha\beta}^a \delta_{\vec{q}0} \quad (3.59)$$

i.e.,

$$\langle \alpha | Q^a(\vec{x}) | \beta \rangle = -\frac{1}{L^2} T_{\alpha\beta}^a \quad (3.60)$$

and the function $\Phi_Q(\vec{r}) = -1$, satisfies the normalization condition (3.27). So at leading order in the $1/N$ expansion the magnetization in the presence of an impurity is spatially uniform. The system with the impurity simply consists of a free spinon in the zero momentum state. The effects of the interaction with the impurity appear only at next order in $1/N$.

Similarly, for the staggered magnetization, the insertion of $n^a(x)$ into the z propagator, to leading order is given by the same diagram in Fig. 3.1, except the cross now stands for n^a .

$$n_{\alpha\beta}^a(\vec{p}, \vec{q}, \vec{p}', \omega, \omega') = \delta_{\vec{q}, \vec{p}' - \vec{p}} T_{\alpha\beta}^a \quad (3.61)$$

so that,

$$\langle \alpha | n^a(\vec{q}) | \beta \rangle = \frac{1}{2m_0} \delta_{\vec{q}0} T_{\alpha\beta}^a \quad (3.62)$$

and,

$$\langle \alpha | n^a(\vec{x}) | \beta \rangle = \frac{1}{2\theta L} T_{\alpha\beta}^a \quad (3.63)$$

So the staggered magnetization at leading order in $1/N$ is also uniform, $\Phi_n(\vec{r}) = \frac{1}{2\theta}$.

Now, let's include the $1/N$ corrections.

We will concentrate on corrections to $\langle \alpha | O(\vec{q}) | \beta \rangle$, for $O = Q^a, n^a$, with $\vec{q} \neq 0$ (where the leading $O(1)$ term vanishes). These turn out to be much simpler to


 Figure 3.2: $1/N$ corrections to z self-energy.

compute than corrections for $\vec{q} = 0$. Moreover, for Q^a , we know by $SU(N)$ charge conservation that the $N = \infty$ result (3.59) at $\vec{q} = 0$ receives no further corrections. Thus, to order $1/N$,

$$\begin{aligned}
 \langle \alpha | O(\vec{q}) | \beta \rangle &\stackrel{\vec{q} \neq 0}{=} i\text{Res}(0, -\vec{q})_1 O_{\alpha\beta}(-\vec{q}, \vec{q}, 0, im_0, im_0)_0 \\
 &+ i\text{Res}(\vec{q}, 0)_1 O_{\alpha\beta}(0, \vec{q}, \vec{q}, im_0, im_0)_0 \\
 &+ i\text{Res}(0, 0)_0 O_{\alpha\beta}(0, \vec{q}, 0, im_0, im_0)_1
 \end{aligned} \tag{3.64}$$

where the subscripts 0, 1 indicate the order in $1/N$ to which the quantity has to be computed.

The $1/N$ corrections to the z self-energy are shown in Fig. 3.2 (we drop λ tadpole diagrams). Of these only the last one couples to the impurity and, therefore, breaks translational invariance. So, letting,

$$D(\vec{k}, \vec{k}', \omega) = D_0(\vec{k}, \vec{k}', \omega) - \sum_{\vec{p}, \vec{p}'} D_0(\vec{k}, \vec{p}, \omega) \Sigma(\vec{p}, \vec{p}', \omega) D(\vec{p}', \vec{k}', \omega) \tag{3.65}$$

$$\Sigma(\vec{k}, \vec{k}', \omega) \stackrel{\vec{k} \neq \vec{k}'}{=} \frac{1}{L^2} 2i\omega \mathcal{D}_{\tau\tau}(\vec{k} - \vec{k}', 0) + O(1/N^2) \tag{3.66}$$

and

$$D(\vec{k}, \vec{k}', \omega) \stackrel{\vec{k} \neq \vec{k}'}{=} -\frac{1}{L^2} 2i\omega \mathcal{D}_{\tau\tau}(\vec{k} - \vec{k}', 0) \frac{1}{\omega^2 + \vec{k}^2 + m_0^2} \frac{1}{\omega^2 + \vec{k}'^2 + m_0^2} + O(1/N^2) \tag{3.67}$$

So the residue,

$$i\text{Res}(0, -\vec{q}) = i\text{Res}(\vec{q}, 0) \stackrel{\vec{q} \neq 0}{=} \frac{1}{L^2} \frac{1}{\vec{q}^2} \mathcal{D}_{\tau\tau}(\vec{q}, 0) + O(1/N^2) \quad (3.68)$$

Note that at this order renormalization of the location of the pole $\omega = im \stackrel{N=\infty}{=} im_0$ can be neglected.

The $1/N$ corrections to the insertion of Q^a into the z propagator are shown in Fig. 3.3.

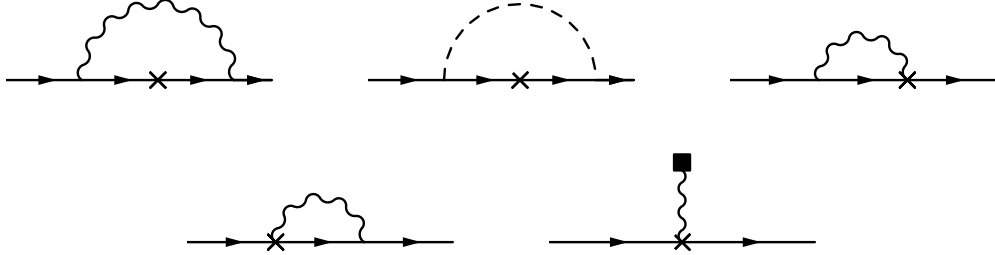


Figure 3.3: $1/N$ corrections to the insertion of Q^a into the z propagator.

Again, only the last one of these couples to the impurity and breaks translational invariance, so,

$$Q_{\alpha\beta}^a(\vec{p}, \vec{q}, \vec{p}', \omega, \omega') \stackrel{\vec{q} \neq \vec{p}' - \vec{p}}{=} -2 \frac{1}{L^2} \mathcal{D}_{\tau\tau}(\vec{q} + \vec{p} - \vec{p}', 0) T_{\alpha\beta}^a + O(1/N^2) \quad (3.69)$$

Combining (3.64),(3.68),(3.69),

$$\langle \alpha | Q^a(\vec{q}) | \beta \rangle = - \left(\delta_{\vec{q},0} + (1 - \delta_{\vec{q},0}) \frac{1}{\theta L} \left(1 + \frac{4m_0^2}{\vec{q}^2} \right) \mathcal{D}_{\tau\tau}(\vec{q}, 0) \right) T_{\alpha\beta}^a + O(1/N^2) \quad (3.70)$$

The calculation of $1/N$ corrections to result (3.62) for impurity induced staggered magnetization $n^a(x)$ proceed in the same fashion. The corrections to insertion of

$n^a(x)$ into the z propagator are given by the first two diagrams in Fig. 3.3 (except now the cross stands for n^a insertion). None of these break translational invariance (as the last diagram in Fig. 3.3 is present only for Q^a , but not for n^a). Therefore,

$$\langle \alpha | n^a(\vec{q}) | \beta \rangle = \frac{1}{2m_0} \left(\delta_{\vec{q},0} (1 + O(1/N)) + (1 - \delta_{\vec{q},0}) \frac{1}{L^2} \frac{4m_0}{q^2} \mathcal{D}_{\tau\tau}(\vec{q}, 0) \right) T_{\alpha\beta}^a + O(1/N^2) \quad (3.71)$$

Note again that in the case of $\langle \alpha | n^a(\vec{q}) | \beta \rangle$ we have computed the $1/N$ corrections only to $\vec{q} \neq 0$. Unlike the case of uniform magnetization, here the $N = \infty$ result for $\langle \alpha | n^a(\vec{q} = 0) | \beta \rangle$ is expected to receive corrections.

Thus, the scaling functions,

$$\Phi_Q(\vec{x}/L) = -1 - \frac{1}{\theta L} \sum_{\vec{q} \neq 0} \left(1 + \frac{4m_0^2}{q^2} \right) \mathcal{D}_{\tau\tau}(\vec{q}, 0) e^{i\vec{q}\vec{x}} + O(1/N^2) \quad (3.72)$$

$$\Phi_n(\vec{x}/L) = \frac{1}{2\theta} + c_1 + \frac{1}{L^3} \sum_{\vec{q} \neq 0} \frac{2}{q^2} \mathcal{D}_{\tau\tau}(\vec{q}, 0) e^{i\vec{q}\vec{x}} + O(1/N^2) \quad (3.73)$$

where c_1 is an \vec{x} -independent constant of order $1/N$ (c_1 should be also independent of Λ ; we have not verified this fact as we did not compute the $1/N$ corrections to $\langle \alpha | n^a(\vec{q} = 0) | \beta \rangle$). We may write,

$$\Phi_Q(\vec{r}) = -\left(1 + \frac{1}{N} f_Q(\vec{r}) \right) + O(1/N^2) \quad (3.74)$$

$$\Phi_n(\vec{r}) = \frac{1}{2\theta} \left(1 + 2c_1\theta + \frac{1}{N} f_n(\vec{r}) \right) + O(1/N^2) \quad (3.75)$$

We have evaluated the functions f_Q , f_n numerically and plotted them along the diagonal of our spatial torus in Fig. 3.4.

Now, we would like to find the $\vec{q} \rightarrow \infty$, $\vec{x} \rightarrow 0$ asymptotes of (3.72), (3.73). For this purpose, we may replace the finite box propagator $\mathcal{D}_{\tau\tau}(q)$ by the infinite box propagator,

$$\mathcal{D}_{\tau\tau}(\vec{q}, 0) \xrightarrow{\vec{q} \rightarrow \infty} \frac{1}{NA} \frac{1}{|\vec{q}|} \quad (3.76)$$

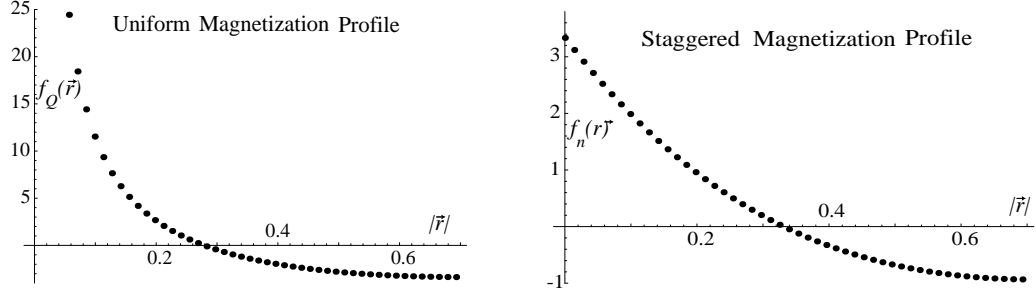


Figure 3.4: Uniform (a) and Staggered (b) magnetization distribution functions $f_Q(\vec{r})$, $f_n(\vec{r})$ plotted along the torus diagonal.

Writing, $\Phi_{Q,n}(\vec{x}/L) = \frac{1}{L^2} \sum_{\vec{q}} \Phi_{Q,n}(\vec{q}) e^{i\vec{q}\vec{x}}$,

$$\Phi_Q(\vec{q}) \xrightarrow{\vec{q} \rightarrow \infty} -\frac{1}{NA\theta} \frac{L}{|\vec{q}|} + O(1/N^2) \quad (3.77)$$

$$\Phi_n(\vec{q}) \xrightarrow{\vec{q} \rightarrow \infty} \frac{2}{NA} \frac{1}{L|\vec{q}|^3} + O(1/N^2) \quad (3.78)$$

Fourier transforming,

$$\Phi_Q(\vec{r}) \xrightarrow{|\vec{r}| \rightarrow 0} -\frac{1}{2\pi\theta NA} \frac{1}{|\vec{r}|} + O(1/N^2) \quad (3.79)$$

$$\Phi_n(\vec{r}) \xrightarrow{|\vec{r}| \rightarrow 0} \frac{1}{2\theta} + c_2 + O(1/N^2) \quad (3.80)$$

where c_2 is a constant of order $1/N$.

Thus, we conclude that,

$$\Delta_{\text{imp}}^Q = -1 + O(1/N) \quad \Delta_{\text{imp}}^n = O(1/N^2) \quad (3.81)$$

which is consistent with the relation between impurity exponents (3.33). Note that the present calculation shows that Δ_{imp}^n is zero to order $1/N$. We shall verify this fact in a different way in Section 3.3.2, and compute Δ_{imp}^n to order $1/N^2$.

Moreover, the ratio,

$$\frac{c_Q}{c_n} = -\frac{1}{\pi NA} + O(1/N^2) \quad (3.82)$$

is independent of regularization at this order in N .

3.3.2 Néel phase

In this section, we compute the uniform and staggered magnetization in the presence of an impurity of charge Q in the symmetry broken phase, $g < g_c$. We work in infinite volume. We develop the $1/N$ expansion around the symmetry broken vacuum,

$$\langle z_1 \rangle = \frac{1}{\sqrt{2}}v \quad (3.83)$$

Note that in general v is not a gauge invariant quantity. However, this fact does not manifest itself at the order at which we are working. To leading order in N ,

$$\frac{1}{2}v^2 = \frac{1}{g} - \frac{1}{g_c} \quad (3.84)$$

Note that $v^2 \sim O(N)$. Moreover, we take $Q \sim O(1)$ in N .

We now must quantize our theory around the symmetry broken state. We write,

$$z_1 = \frac{1}{\sqrt{2}}(h + v + i\phi), \quad z_\alpha = \pi_\alpha, \quad \alpha = 2..N \quad (3.85)$$

We work in the so-called R_ξ gauge, in which the mixing between the goldstone ϕ and the photon A_μ is absent, at the expense of introducing a ghost field c . In what follows, we have eliminated the mixing only to leading order in $1/N$. This is achieved by using the gauge-fixing condition,

$$\partial_\mu A_\mu = \xi v K^{-1} \phi + w \quad (3.86)$$

where the action for the auxillary field w , which appears in the Fadeev-Poppov formalism, is

$$\mathcal{S}_w = \frac{1}{2\xi} \int dx dy w(x) K(x-y) w(y) \quad (3.87)$$

Here, $K(x - y)$ is the photon polarization function given by Eq. (3.53). Similarly, in what follows $\Pi(x - y)$ is the λ self energy given by Eq. (3.55).

At the end of the day, the action one obtains is,

$$\begin{aligned}
 \mathcal{S}_\xi &= \frac{1}{2} \int dx dy A_\mu(x) \left(K_{\mu\nu}(x - y) - \frac{1}{\xi} \partial_\mu \partial_\nu K(x - y) + \delta_{\mu\nu} v^2 \right) A_\nu \\
 &+ \frac{1}{2} \int dx dy \phi(x) \left(-\partial^2 \delta(x - y) + \xi v^2 K^{-1}(x - y) \right) \phi(y) \\
 &+ \frac{1}{2} \int dx dy \lambda(x) \Pi(x - y) \lambda(y) \\
 &+ \int dx dy \left(\bar{c} \left(-\partial^2 \delta(x - y) + \xi v^2 K^{-1}(x - y) \right) c(y) + \xi v \bar{c}(x) K^{-1}(x - y) h(y) c(y) \right) \\
 &+ \int dx \left(|D_\mu \pi|^2 + \frac{1}{2} (\partial_\mu h)^2 + i v \lambda h + (\phi \partial_\mu h - \partial_\mu \phi h) A_\mu + (v h + \frac{1}{2} h^2 + \frac{1}{2} \phi^2) A_\mu^2 \right) \\
 &+ \int dx \left(i \lambda |\pi|^2 + \frac{1}{2} i \lambda (\phi^2 + h^2) \right) \tag{3.88}
 \end{aligned}$$

As usual, we avoid double counting by dropping any diagrams, which are already included in the dynamically generated $N = \infty$ self-energies for A_μ , λ etc. The propogators for our fields are shown in Fig. 3.5. Note that in the Néel phase, we get mixing between the λ and h fields.

Now, having set up the perturbation theory, we wish to compute, $\langle Q^a(\vec{x}) \rangle$, $\langle n^a(\vec{x}) \rangle$. Utilizing the pattern of spontaneous symmetry breaking, $U(N) \rightarrow U(N - 1)$ (here we look only at global symmetry), one can show that,

$$\langle n^a \rangle = T_{11}^a \langle n^0 \rangle \tag{3.89}$$

where $n^0 = z^\dagger T^0 z$ and T^0 is any generator of $SU(N)$ with $T_{11}^0 = 1$. Similarly for Q^a . For definiteness, we may choose $T_{11}^0 = 1$, $T_{1\alpha}^0 = T_{\alpha 1}^0 = 0$, $T_{\alpha\beta}^0 = -\frac{1}{N-1} \delta_{\alpha\beta}$, $\alpha, \beta = 2 \dots N$.



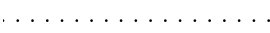
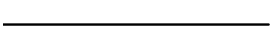



A_μ  A_ν	$D_{\mu\nu}(p) = \frac{1}{p^2 K(p) + v^2} \left(\delta_{\mu\nu} + \frac{(\xi-1)K(p)p_\mu p_\nu}{p^2 K(p) + \xi v^2} \right)$
ϕ  ϕ	$D_\phi(p) = \frac{1}{p^2 + \xi v^2 K^{-1}(p)}$
\bar{c}  c	$D_c(p) = \frac{1}{p^2 + \xi v^2 K^{-1}(p)}$
π_β^*  π_α	$D_{\pi_{\alpha\beta}}(p) = \frac{\delta_{\alpha\beta}}{p^2}$
h  h	$D_h(p) = \frac{\Pi(p)}{p^2 \Pi(p) + v^2}$
λ  λ	$D_\lambda(p) = \frac{p^2}{p^2 \Pi(p) + v^2}$
h  λ	$D_{h\lambda}(p) = \frac{-iv}{p^2 \Pi(p) + v^2}$

Figure 3.5: Propagators in the Néel phase.

Let's start with computing the uniform magnetization.

$$Q^0 = \frac{N}{N-1} j_\tau^1 - \frac{1}{N-1} j_\tau \quad (3.90)$$

where

$$j_\tau^1 = z_1^\dagger D_\tau z_1 - (D_\tau z_1)^\dagger z_1 \quad (3.91)$$

and j_τ is the $U(1)$ charge density discussed in the appendix, see Eq. (B.1). By equation of motion (B.4),

$$\langle j_\tau(\vec{x}) \rangle = -J_\tau^{\text{ext}}(\vec{x}) = -Q\delta^2(\vec{x}) \quad (3.92)$$

So, it remains to compute $\langle j_\tau^1(\vec{x}) \rangle$. Expanding j_τ^1 in terms of ϕ , h and A_μ ,

$$j_\tau^1 = -iv^2 A_\tau + iv(\partial_\tau \phi - 2A_\tau h) + i(h\partial_\tau \phi - \phi\partial_\tau h - A_\tau(h^2 + \phi^2)) \quad (3.93)$$



Figure 3.6: Leading contribution to uniform magnetization in the symmetry broken phase.

In the $1/N$ expansion the leading contribution to $\langle j_\tau^1 \rangle$ is of $O(1)$ and comes from the first term on the r.h.s of (3.93), see Fig. 3.6.

$$\langle j_\tau^1(\vec{p}) \rangle = -Qv^2 \mathcal{D}_{\tau\tau}(\vec{p}, 0) = -Qv^2 \frac{1}{\vec{p}^2 K(\vec{p}) + v^2} \quad (3.94)$$

Thus, $\langle Q^0(\vec{p}) \rangle = \langle j_\tau^1(\vec{p}) \rangle + O(1/N)$. Fourier transforming,

$$\langle Q^0(\vec{x}) \rangle = -\frac{Qv^2}{2\pi NA} \frac{1}{|\vec{x}|} + \frac{Qv^4}{4N^2 A^2} \left(\mathbf{H}_0 \left(\frac{v^2 |\vec{x}|}{NA} \right) - Y_0 \left(\frac{v^2 |\vec{x}|}{NA} \right) \right) + O(1/N), \quad (3.95)$$

where \mathbf{H}_0 is the Struve function and Y_0 is the Bessel function. Taking the short and long distance asymptotes,

$$\langle Q^0(\vec{x}) \rangle \xrightarrow{|\vec{x}| \rightarrow 0} -\frac{Qv^2}{2\pi NA} \frac{1}{|\vec{x}|} \quad (3.96)$$

$$\langle Q^0(\vec{x}) \rangle \xrightarrow{|\vec{x}| \rightarrow \infty} -\frac{QNA}{2\pi v^2} \frac{1}{|\vec{x}|^3} \quad (3.97)$$

The long distance decay is a consequence of the Goldstone physics of the spin waves, and the $1/|\vec{x}|^3$ decay is expected to be exact. At short distances, we have the physics of the critical point, and the exponent will have corrections at higher order. From the present result we can conclude that the impurity exponent

$$\Delta_{\text{imp}}^Q = -1 + O(1/N), \quad (3.98)$$

which is consistent with the result obtained at the critical point (3.81).

Now, let's discuss the staggered magnetization,

$$n^0 = \frac{N}{N-1} z_1^\dagger z_1 - \frac{1}{N-1} z^\dagger z \quad (3.99)$$

By equations of motion,

$$z^\dagger z = \frac{1}{g} \quad (3.100)$$

thus,

$$n^0 = \frac{N}{N-1} z_1^\dagger z_1 - \frac{1}{(N-1)g} \quad (3.101)$$

and

$$z_1^\dagger z_1 = \frac{1}{2} v^2 + v h + \frac{1}{2} (h^2 + \phi^2) \quad (3.102)$$

Thus, at leading order, $\langle z_1^\dagger z_1(\vec{x}) \rangle = \frac{1}{2} v^2$, and

$$\langle n^0(\vec{x}) \rangle = \frac{1}{2} v^2 + O(1) \quad (3.103)$$

Moreover, the \vec{x} -dependent corrections to $\langle n^0(\vec{x}) \rangle$ come only at $O(1/N)$, with diagrams of Fig. 3.7 (the part of n^0 which contributes at this order, denoted by \times , is vh).

We will discuss the diagrams in Fig. 3.7 shortly. For now, we can conclude that,

$$\Delta_{\text{imp}}^n = O(1/N^2) \quad (3.104)$$

in agreement with the result (3.81) obtained at the critical point. Moreover, we can now compute the ratio,

$$\frac{c_Q}{c_n} = -\frac{Q}{\pi N A} + O(1/N^2) \quad (3.105)$$

which exactly agrees with the result obtained at the critical point (3.82) for $Q = 1$.

Notice, that this is a highly nontrivial check of the OPE (3.30) as $\langle Q^a \rangle$, $\langle n^a \rangle$ depend

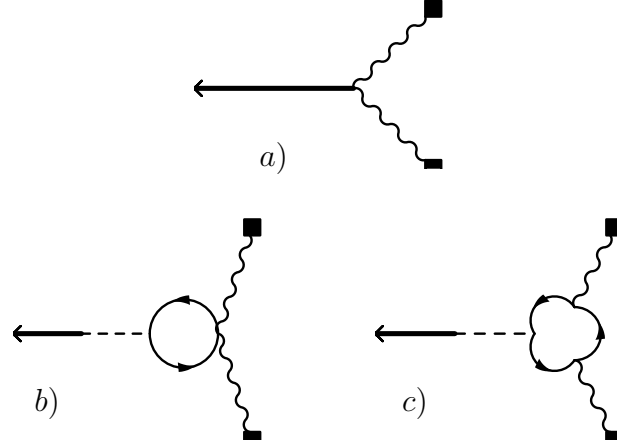


Figure 3.7: Leading \vec{x} -dependent contribution to staggered magnetization in the symmetry broken phase.

on v in the Néel phase and on L at the critical point. Nevertheless, all the dependence on the IR scale cancels out in the ratio c_Q/c_n , which is constant throughout the scaling regime.

Coming back to the diagrams in Fig. 3.7,

$$\begin{aligned} \langle n^0(\vec{q}) \rangle \stackrel{\vec{q} \neq 0}{\approx} & Q^2 v^2 \mathcal{D}_h(\vec{q}, 0) \int \frac{d^{D-1}p}{(2\pi)^{D-1}} \left(1 + \frac{i}{2} \Pi^{-1}(\vec{q}, 0) \Gamma^{\tau\tau}(\vec{q}, 0, \vec{p}, 0, \vec{q} - \vec{p}, 0) \right) \\ & \times \mathcal{D}_{\tau\tau}(\vec{p}, 0) \mathcal{D}_{\tau\tau}(\vec{q} - \vec{p}, 0) \end{aligned} \quad (3.106)$$

We keep the space-time dimension D arbitrary in what follows, as we wish to compare our result for Δ_{imp}^n obtained in the $1/N$ expansion, with the result obtained using ϵ expansion[121]. Here, $\Gamma^{\mu\nu}(q, p, q - p)$ is the lowest order contribution to the A_μ, A_ν, λ vertex, given by the sum of the loops in Fig. 3.8. The diagram in Fig. 3.8 a) is given by,

$$\Gamma_1^{\mu\nu}(q, p, q - p) = 2i\delta_{\mu\nu}\Pi(q) \quad (3.107)$$

Thus, diagrams in Fig. 7 a) and b) cancel (by the way, these diagrams are individually UV divergent for $D \leq 3$). So, calling the diagram in Fig. 3.8 b), $\Gamma_2^{\mu\nu}(q, p, q - p)$,

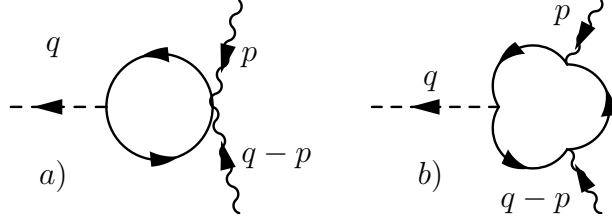


Figure 3.8: Leading contribution to the three point vertex of A_μ , A_ν and λ fields, $\Gamma^{\mu\nu}(q, p, q - p)$.

$$\begin{aligned} \langle n^0(\vec{q}) \rangle \stackrel{\vec{q} \neq 0}{\equiv} & Q^2 v^2 D_h(\vec{q}, 0) \int \frac{d^{D-1}p}{(2\pi)^{D-1}} \frac{i}{2} \Pi^{-1}(\vec{q}, 0) \Gamma_2^{\tau\tau}(\vec{q}, 0, \vec{p}, 0, \vec{q} - \vec{p}, 0) \\ & \times \mathcal{D}_{\tau\tau}(\vec{p}, 0) \mathcal{D}_{\tau\tau}(\vec{q} - \vec{p}, 0) \end{aligned} \quad (3.108)$$

Evaluating $\Gamma_2^{\mu\nu}$,

$$\begin{aligned} \Gamma_2^{\mu\nu}(q, p, q - p) &= -2iN \int \frac{d^D l}{(2\pi)^D} \frac{(2l - p)_\mu (2l - p - q)_\nu}{l^2 (l - p)^2 (l - q)^2} \\ &= -\frac{4iN\Gamma(2 - D/2)}{(4\pi)^{D/2}} \int dx_1 dx_2 dx_3 \delta(1 - x_1 - x_2 - x_3) (\Delta^2)^{D/2-2} \\ & \quad \left(\delta_{\mu\nu} + \frac{(4 - D)(2x_1 q + (2x_2 - 1)p)_\mu ((2x_1 - 1)q + (2x_2 - 1)p)_\nu}{4\Delta^2} \right) \end{aligned} \quad (3.109)$$

where,

$$\Delta^2 = x_1(1 - x_1)q^2 + x_2(1 - x_2)p^2 - 2x_1 x_2 p \cdot q \quad (3.110)$$

We are interested only in $\Gamma_2^{\tau\tau}$, with $p^0 = q^0 = 0$. Thus,

$$\begin{aligned} & \Gamma_2^{\tau\tau}(\vec{q}, 0, \vec{p}, 0, \vec{q} - \vec{p}, 0) = \\ &= -\frac{4iN\Gamma(2 - D/2)}{(4\pi)^{D/2}} \int dx_1 dx_2 dx_3 \delta(1 - x_1 - x_2 - x_3) (\Delta^2)^{D/2-2} \end{aligned} \quad (3.111)$$

For $|\vec{p}| \gg |\vec{q}|$, $\Gamma_2^{\tau\tau}(\vec{q}, 0, \vec{p}, 0, \vec{q} - \vec{p}, 0) \sim |\vec{p}|^{D-4}$, so for $\vec{p} \rightarrow \infty$ the integrand in Eq. (3.108) behaves as $|\vec{p}|^{-D}$ and the integral is UV convergent.

We now attempt to understand the behaviour of (3.108) for $\vec{q} \rightarrow \infty$, from which we should be able to extract the impurity anomalous dimension Δ_{imp}^n . For this purpose, we may set $v = 0$ in the propagators $D_h(\vec{q}, 0)$, $\mathcal{D}_{\tau\tau}(\vec{p}, 0)$, $\mathcal{D}_{\tau\tau}(\vec{q} - \vec{p}, 0)$ (this does not introduce any IR divergences).

$$\langle n^0(\vec{q}) \rangle \stackrel{\vec{q} \rightarrow \infty}{=} \frac{Q^2 v^2}{N^3 A^2 B} |\vec{q}|^{2-D} \int \frac{d^{D-1}p}{(2\pi)^{D-1}} \frac{i}{2} \Gamma_2^{\tau\tau}(\vec{q}, 0, \vec{p}, 0, \vec{q} - \vec{p}, 0) \frac{1}{|\vec{p}|^{D-2}} \frac{1}{|\vec{p} - \vec{q}|^{D-2}} \quad (3.112)$$

Let us first discuss the limit $D = 4 - \epsilon$, $\epsilon \rightarrow 0$. In this regime, to leading order in ϵ ,

$$\Gamma_2^{\tau\tau}(\vec{q}, 0, \vec{p}, 0, \vec{q} - \vec{p}, 0) = -2iN \frac{1}{(4\pi)^2} \Gamma(2 - D/2) \quad (3.113)$$

and,

$$\langle n^0(\vec{q}) \rangle \stackrel{\vec{q} \rightarrow \infty}{=} \frac{72\pi^4 \epsilon^2 Q^2 v^2}{N^2} \frac{1}{|\vec{q}|^3} \quad (3.114)$$

Fourier transforming,

$$\langle n^0(\vec{x}) \rangle \stackrel{\vec{x} \rightarrow 0}{=} \frac{1}{2} v^2 + c_3 - \frac{36\pi^2 \epsilon^2 Q^2}{N^2} v^2 \log(v|\vec{x}|) + c_4 + O(1/N^2) \quad (3.115)$$

where c_3, c_4 do not depend on \vec{x} and are of order 1 and $1/N$ respectively. Thus, to leading order in $1/N, \epsilon$,

$$\Delta_{\text{imp}}^n = -\frac{72\pi^2 Q^2 \epsilon^2}{N^2} \quad (3.116)$$

in agreement with the calculations of Ref. [121], where the impurity exponents were obtained by performing the impurity operator renormalizations as summarized in Section 3.3.1.³

³Note that in the ϵ expansion of Ref. [121] only the analogue of the diagram in Fig. 3.7 a) appears,

For arbitrary D , Δ_{imp}^n is difficult to calculate analytically, as $\Gamma^{\tau\tau}$ is no longer a constant. However, combining Eqs. (3.108), (3.111) and introducing a new set of Feynman parameters,

$$\langle n^0(\vec{q}) \rangle \stackrel{\vec{q} \rightarrow \infty}{=} \frac{Q^2 v^2}{N^2} \frac{1}{|\vec{q}|^{D-1}} f(D) \quad (3.117)$$

where the numerical constant $f(D)$ is given by,

$$f(D) = \frac{1}{A^2 B (4\pi)^{D-1} \Gamma(D/2 - 1)^2} \int_0^1 dx_1 \int_0^{1-x_1} dx_2 \int_0^1 dy_1 \int_0^{1-y_1} dy_2 \\ x_2^{(D-3)/2} (1-x_2)^{D/2-1} y_1^{1-D/2} y_2^{D/2-2} (1-y_1-y_2)^{D/2-2} \\ (x_2(1-x_2)^2 y_2(1-y_2) + x_1 y_1 ((1-x_1)(1-x_2) - 2y_2 x_2(1-x_2) - y_1 x_1 x_2))^{-\frac{1}{2}} \quad (3.118)$$

Consequently,

$$\langle n^0(\vec{x}) \rangle \stackrel{\vec{x} \rightarrow 0}{=} \frac{1}{2} v^2 + c_3 - \frac{2}{(4\pi)^{(D-1)/2} \Gamma((D-1)/2)} f(D) \frac{Q^2}{N^2} v^2 \log(v^{2/(D-2)} |\vec{x}|) + c_4 + O(1/N^2) \quad (3.119)$$

and

$$\Delta_{\text{imp}}^n = -\frac{4}{(4\pi)^{(D-1)/2} \Gamma((D-1)/2)} f(D) \frac{Q^2}{N^2} + O(1/N^3) \quad (3.120)$$

Evaluating $f(D)$ numerically for $D = 3$,

$$\Delta_{\text{imp}}^n \approx -25.9 \frac{Q^2}{N^2} + O(1/N^3) \quad (3.121)$$

while the diagrams in Figs. 3.7 b), c) do not appear at leading order in ϵ , as they are higher order in coupling constant. Nevertheless in the $1/N$ expansion, we saw that the answer comes entirely from the diagram in Fig. 3.7 c), with diagrams in Fig. 3.7 a) and Fig. 3.7 b) canceling for all D . The reason is the following: in the $1/N$ expansion all diagrams in Fig. 3.7 are individually of same order in ϵ . Moreover, to leading order in ϵ , the diagrams b) and c) cancel, so a) = - b) $\stackrel{\epsilon \rightarrow 0}{=} c)$. In the ϵ expansion, this fact is foreseen in advance: the $1/\epsilon$ pole must cancel between diagrams b) and c) (the 4-point diagram with two photons and two scalars is not divergent). Thus, we can obtain the answer to leading order in ϵ either from a) alone or from c) alone.

We note that we have separately verified the result (3.120) by performing the impurity OPE program as summarized in Section 3.3.1.

3.4 Conclusion

A recent numerical study [96] examined the spin distribution in the vicinity of a non-magnetic impurity in a double-layer, $S = 1/2$ square lattice antiferromagnet at its quantum critical point. The ground state of the system has total spin $S = 1/2$, and the spin distribution of this $S = 1/2$ was found to be extended across the entire system. Universal scaling forms (Eqs. (3.3) and (3.5)) for the uniform and staggered spin distributions were postulated[96], and found to be in excellent agreement with the numerical results.

This chapter has presented the field-theoretic foundation of the above results. Using the soft-spin $O(3)$ LGW field theory in Eq. (3.11), we found that the universal scaling forms in Eqs. (3.3) and (3.5) were indeed obeyed in an expansion in $(3 - d)$ (where d is the spatial dimensionality), and explicit results for the universal scaling functions appear in Eq. (3.22).

Next, we examined a similar non-magnetic impurity in $S = 1/2$ antiferromagnets which have a single $S = 1/2$ spin per unit cell. Such antiferromagnets can display a deconfined quantum phase transition[1, 2] between Néel and valence bond solid (VBS) states. An explicit example of such a transition was found recently in Ref. [57]. The field theory for this situation in $\mathcal{S}_b^z + \mathcal{S}_{\text{imp}}^z$ in Eqs. (3.7,3.8). It describes the dynamics of a $SU(N)$ spinor field, z_α (the spinon), and we obtained its critical properties in a $1/N$ expansion. Projecting onto the total spin $S = 1/2$ sector of this theory (which

contains the ground state in the presence of the impurity) was not straightforward here, and we achieved this by the relation Eq. (3.9). Our results obey scaling forms which appear in Section 3.3.1. The scaling functions are in Eqs. (3.72) and (3.73), and are plotted in Fig. 3.4. The boundary spin exponent for the deconfined critical point appears in Eqs. (3.120), (3.121). We also obtained substantial evidence for the structure of the operator product expansion near the impurity, and the fact that the staggered and uniform magnetizations flow to the same impurity spin operator.

After the theoretical work presented above was completed, the numerical simulations in Ref. [57] of the $SU(2)$ antiferromagnet with a single $S = 1/2$ spin per unit cell were extended to include the response to a non-magnetic impurity.[124] It was found that the universal scaling forms (3.3),(3.5) acquire logarithmic corrections. Similar logarithmic violations have been found in other response functions.[59] The precise origin of such corrections is not completely settled. Note that in a model of a $SU(3)$ antiferromagnet,[125] the scaling forms (3.3),(3.5) are seen to hold, albeit with large finite size corrections. This suggests that the theory possesses an operator, which becomes nearly marginal in the vicinity of $N = 2$.

In the context of the present study, the basic scaling structure of the uniform and staggered magnetization for the conventional LGW and the unconventional deconfined transitions is quite similar. In both cases, there is a single impurity spin operator which determines the exponents characterizing the spatial form of the spin texture. The main observable difference is in the very different values of the exponents. However, a more significant difference arises when we consider the form of the VBS order near the impurity, as this is an issue only for the deconfined critical point.

Results on the structure of the VBS order will be presented in Chapter 4.

Chapter 4

Valence bond solid order near impurities in two-dimensional quantum antiferromagnets

Recent scanning tunnelling microscopy (STM) experiments on underdoped cuprates have displayed modulations in the local electronic density of states which are centered on a Cu-O-Cu bond.[12] As a paradigm of the pinning of such bond-centered ordering in strongly correlated systems, we present the theory of valence bond solid (VBS) correlations near a single impurity in a square lattice antiferromagnet. The antiferromagnet is assumed to be in the vicinity of a quantum transition from a magnetically ordered Néel state to a spin-gap state with long-range VBS order. We identify two distinct classes of impurities: (*i*) local modulation in the exchange constants, and (*ii*) a missing or additional spin, for which the impurity perturbation is represented by an uncompensated Berry phase. The “boundary” critical theory for these classes is developed: in the second class we find a “VBS vortex” around the impurity, accompanied by a suppression in the VBS susceptibility. Implications for numerical studies of quantum antiferromagnets and for STM experiments on the cuprates are noted.

4.1 Introduction

A number of recent scanning tunnelling microscopy experiments have highlighted spatial modulations in the local density of states in the cuprate compounds, nucleated by external perturbations. In Ref. [126], the spatial modulation was observed in the normal state above T_c , presumably nucleated by impurities. In Refs. [127, 128, 129], the order was found in a halo around vortices, which were in turn pinned by impurities. Most recently, in Ref. [12], similar charge-ordering patterns were found to be ubiquitous in the underdoped cuprates at low temperatures, and it was established that the charge ordering was “bond-centered”, and had an anisotropic structure similar to a valence bond solid state [130, 131, 132, 133].

In the light of these observations, it is of general interest to study the appearance of varieties of charge order (including “valence bond solid” (VBS) order [132, 133])¹ near impurities in strongly correlated systems. For superfluid states, such a theory has been presented in earlier work [134, 135], and compared quantitatively with some of the above experiments. It was argued that the charge order was linked to quantum fluctuations of vortices/anti-vortices in the superfluid order. Consequently, the problem mapped onto the pinning of the vortices by impurities, and the quantum zero-point motion of vortices about the pinning site. In both zero and non-zero mag-

¹In an antiferromagnet of $S = 1/2$ degrees of freedom, VBS order is associated with modulations in the expectation values of the bond exchange energy $\vec{S}_1 \cdot \vec{S}_2$, where $\vec{S}_{1,2}$ are the spin operators on the ends of the bond. While this is the best physical interpretation of VBS order, in a symmetry classification VBS order can also be considered to be a particular realization of “charge order”. This is because in the underlying Hubbard-like model (with a repulsive energy U and hopping matrix element t), from which the antiferromagnet descends, the VBS state will have modulations of order t/U in the charge density in the bonding orbital between the two sites. For a discussion of how the VBS characterization of the charge order can explain the experimental observations in the cuprates, see Ref. [132, 133].

netic fields, enhanced charge order was found in the spatial region over which the vortex executed its zero-point motion [134]. This charge order was present even when the net vorticity was zero everywhere (as is the case in zero magnetic field): the vorticity cancelled between the vortex and anti-vortex fluctuations, but the charge order did not.

This chapter will present an extensive field-theoretic analysis of a paradigm of the problem of charge order near impurities in correlated systems. We will consider insulating $S = 1/2$ antiferromagnets on the square lattice, across a quantum phase transition from the magnetically ordered Néel state, to a spin-gap valence bond solid (VBS) state [21, 22, 1, 2]. By representing the $S = 1/2$ spins as hard-core bosons, our results can be reinterpreted as applying to the superfluid-insulator transition of bosons at half-filling on the square lattice: the Néel state of the antiferromagnet maps onto the superfluid state of the bosons, while the VBS state maps onto a Bose insulator with bond-centered charge order. The bond-centered charge correlations in the underdoped cuprates now appear to have two possible physical mechanisms (“disordered” antiferromagnet/superfluid), but it was argued in Ref. [136] that they represent the same underlying physics. Our results here will go beyond the earlier work [134, 135] in two important respects:

- (i) We will describe the critical singularities in the impurity-induced VBS/charge order at the quantum critical point, and
- (ii) We will consider a wider class of impurity perturbations. In the previous work [134, 135], an “impurity” was assumed to be a generic deformation of the underlying Hamiltonian which broke its space group symmetry. For the Néel-VBS transition,

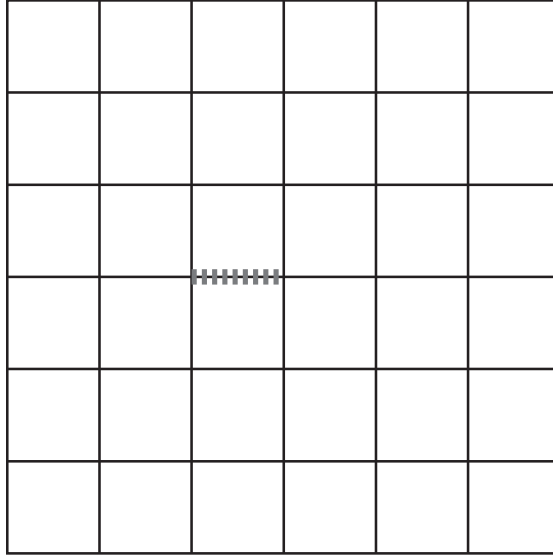


Figure 4.1: A modulated exchange impurity which is described in Section 4.1.1. The dashed line indicates a different value of the antiferromagnetic exchange constant. We expect VBS order to be enhanced near such an impurity, because the modulated exchange will lock in a preferred orientation and offset of the VBS state.

such an impurity is realized *e.g.* by the modulation in the magnitude of a particular exchange coupling – see Fig 4.1. We briefly will discuss the critical singularities describing the *enhancement* of VBS order near such an impurity in Section 4.1.1 below; these results have a natural extension to the models of charge order near the superfluid-insulator transition discussed above. However, the primary focus of the present chapter is on a distinct class of impurities, in which the valence-bond structure of the non-magnetic ground state of the antiferromagnet is more strongly disrupted, and a “Berry phase” contribution of an unpaired spin is the crucial impurity-induced perturbation [106, 121]. Such impurities are realized by replacing the $S = 1/2$ Cu spins in antiferromagnets by a non-magnetic Zn ion, or a $S = 1$ Ni ion (see Fig. 4.2). For the superfluid-insulator transition, such an impurity is a site from which parti-

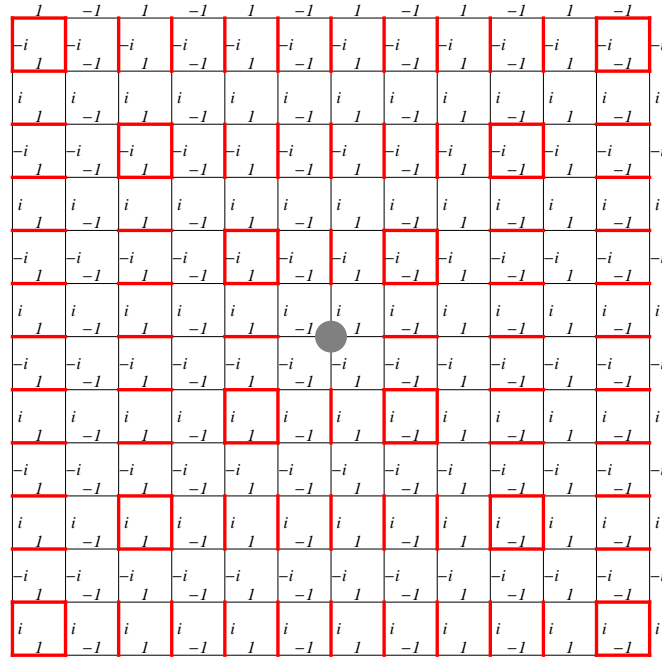


Figure 4.2: A vacancy (the shaded circle) in a square lattice quantum antiferromagnet which is described in Section 4.1.2 and the remainder of the chapter. The red lines represent singlet bonds between the spins. The red squares can be thought of as a resonance between a pair of horizontal and a pair of vertical singlet bonds. The local value of the VBS order is measured by the phase factors on the singlet bonds. Moving anti-clockwise from the right, we observe that VBS order cycles as $-1 \rightarrow -i \rightarrow 1 \rightarrow i$. Thus, this configuration is a “vortex” of the VBS order (this VBS vortex is “dual” to the vortex in the superfluid/Néel order that is discussed in the beginning of the chapter). Anti-vortices in the VBS order appear only around vacancies on the other sublattice; in other words, VBS vortices transform to VBS anti-vortices under translation by a single site—see Fig 4.3 later.

cles are excluded, and so a local “phase-shift” is induced in the charge order of the insulating state (replacing a Cu atom by Zn or Ni is expected to have the desired “Cooper pair” exclusion effect[136]). Our main results will include a description of the *suppression* of VBS order near such “Berry phase” impurities: these results are summarized in Section 4.1.2 below, and described in the body of the chapter. A simple sketch of how such an impurity disrupts the VBS order is shown in Fig. 4.2; this

figure builds upon the dual theory of spinons in the VBS state developed by Levin and Senthil [137]. The bulk of this chapter will describe how quantum fluctuations of the type sketched in Fig. 4.2 lead to a modification of the scaling dimension of the VBS order in the vicinity of the vacancy.

The remainder of the chapter will be presented in the language of the Néel-VBS transition in quantum antiferromagnets. For this model, a field theoretic description of the vicinity of the quantum critical point [1, 2, 3, 51] is provided by the CP^{N-1} theory at $N = 2$:

$$\mathcal{S} = \int d^2x d\tau \left[|(\partial_\mu - iA_\mu)z_\alpha|^2 + s|z_\alpha|^2 + \frac{g}{2} (|z_\alpha|^2)^2 + \frac{1}{2e^2} (\epsilon_{\mu\nu\lambda} \partial_\nu A_\lambda)^2 \right]. \quad (4.1)$$

Here μ, ν, λ are spacetime indices, z_α , $\alpha = 1 \dots N$ is a complex scalar which is a $SU(N)$ fundamental, and A_μ is a non-compact $U(1)$ gauge field. The Néel order of the antiferromagnet is $n^a = z^\dagger T^a z$, where T^a is a $SU(N)$ generator. The $SU(N)$ symmetry is spontaneously broken in the Néel phase, $\langle n^a \rangle \neq 0$, which is realized for $s < s_c$, where s_c is the critical value of the tuning parameter, s , for the quantum phase transition. For $s > s_c$, the CP^{N-1} theory above describes a $U(1)$ spin liquid state of the antiferromagnet, with gapped spinons z_α and a gapless, $U(1)$ photon. However, as has been argued at length elsewhere [21, 22], lattice effects not included in the continuum field theory (4.1) eventually render the $U(1)$ spin liquid unstable to spinon confinement and fully gapped state with VBS order. The VBS order parameter, V , is an operator [21, 2] which creates a *Dirac monopole* with total flux 2π in the $U(1)$ gauge field A_μ . This chapter will therefore be concerned with correlations of the monopole/VBS operator V under the field theory \mathcal{S} after including the impurity perturbations described below. The bulk scaling dimension of the monopole operator

at the $s = s_c$ critical point will make frequent appearances in our analysis, and so we define this as

$$\Delta^V = \dim[V(\vec{x}, \tau)] \text{ in the theory } \mathcal{S} \text{ without an impurity.} \quad (4.2)$$

The following subsections will now describe the two classes of impurity perturbations to the theory \mathcal{S} shown in Figs. 4.1 and 4.2 respectively.

4.1.1 Modulated exchange

A modulation in the magnitude of an exchange constant in the underlying antiferromagnet (see Fig. 4.1) breaks the lattice space group symmetry, but preserves the spin rotation symmetry. Also, the number of spins on each sublattice is preserved, so no “Berry phase” term is expected. Consequently, we need to consider all local perturbations to \mathcal{S} which preserve the required symmetries. The simplest allowed possibility is a local shift in the position of the critical point. For an impurity at the spatial origin, $x = 0$, this would lead to a term

$$\tilde{s} \int d\tau |z_\alpha(\vec{x} = 0, \tau)|^2 \quad (4.3)$$

However, a simple computation [107] shows that \tilde{s} is very likely an irrelevant perturbation at the bulk critical point. We have $\dim[\tilde{s}] = 1 - (D - 1/\nu)$, where $D = 3$ is the spacetime dimension, and ν is the correlation length exponent of \mathcal{S} . Because it is almost certainly the case that $\nu > 1/2$, we conclude that \tilde{s} is irrelevant. However, a more interesting perturbation is that considered in previous work [134, 135] on the superfluid-insulator transition. In the present context, this perturbation follows from the fact that with broken space group symmetry, a linear coupling to the monopole

operator is permitted. So we have the impurity action

$$\tilde{\mathcal{S}}_{\text{imp}} = \int d\tau [h^* V(\vec{x} = 0, \tau) + \text{c.c.}] \quad (4.4)$$

where h is a complex-valued constant whose value depends upon the details of the modulated exchange near $x = 0$. Now the renormalization group (RG) flow of h follows from Eq. (4.2) to linear order

$$\frac{dh}{d\ell} = (1 - \Delta^V)h + \mathcal{O}(h^2) \quad (4.5)$$

The remainder of this subsection will analyze the correlations of the monopole/VBS operator $V(\vec{x}, \tau)$ in the theory $\mathcal{S} + \tilde{\mathcal{S}}_{\text{imp}}$.

First, let us consider the likely possibility that $\Delta^V < 1$. In this case, h is a relevant perturbation, and higher order corrections to Eq. (4.5) cannot be ignored. By analogy with results in the theory of boundary critical phenomena [138], and in particular with the theory of the “extraordinary” transition [139, 140, 141], we conclude that a likely possibility is that the RG flow is to strong coupling, to a fixed point with $|h| = \infty$. In this, case some powerful statements on the correlations of $V(\vec{x}, \tau)$ can be immediately made. It is useful to express the correlations in the vicinity of the impurity by an operator product expansion (OPE). In general, this expansion will have the structure

$$\lim_{|\vec{x}| \rightarrow 0} V(\vec{x}, \tau) \sim |\vec{x}|^{\Delta_{\text{imp}}^V} V_{\text{imp}}(\tau) \quad (4.6)$$

where V_{imp} is an operator localized on the impurity site, and Δ_{imp}^V is the difference in scaling dimensions between V and V_{imp} . Specifically, Eq. (4.6) implies

$$\Delta^V = -\Delta_{\text{imp}}^V + \dim[V_{\text{imp}}]. \quad (4.7)$$

Now at a $|h| = \infty$ fixed point, we expect that fluctuations of V near the impurity are strongly suppressed, and so it is a reasonable conclusion that V_{imp} is just the identity operator

$$V_{\text{imp}} = \mathbb{1}. \quad (4.8)$$

Consequently, $\dim[V_{\text{imp}}] = 0$, and we have our main result

$$\Delta_{\text{imp}}^V = -\Delta^V. \quad (4.9)$$

The combination of Eq. (4.6) and (4.9) appears to be a promising route to measuring the scaling dimension of a monopole operator in numerical studies of quantum antiferromagnets.

To complete our analysis of modulated exchange, we also address the case with $\Delta^V > 1$. In this situation, by Eq. (4.5), the perturbation h is irrelevant, and so we may compute the consequences of h by perturbation theory. Computing correlations to first order in h we see that Eq. (4.6) is now replaced by

$$\lim_{|\vec{x}| \rightarrow 0} V(\vec{x}, \tau) \sim h |\vec{x}|^{-2\Delta^V + 1} \quad (4.10)$$

4.1.2 Missing spin

Next we will consider the behavior of the monopole/VBS operator V near the missing spin impurity illustrated in Fig. 4.2. As discussed in some detail in Ref. [121], the dominant consequent of such an impurity is an exactly marginal perturbation to \mathcal{S} given by

$$\mathcal{S}_{\text{imp}} = iQ \int d\tau A_\tau(\vec{x} = 0, \tau) \quad (4.11)$$

where Q is a “charge” characterizing the impurity. The value of Q does not flow under the RG, and so Q is a pure number which controls all universal characteristics of the impurity response. For an impurity of Fig. 4.2 with a single missing spin, $Q = \pm 1$. The remainder of this chapter presents an analysis of the critical properties of the $\mathcal{S} + \mathcal{S}_{\text{imp}}$ defined in Eqs. (4.1) and (4.11).

The magnetic correlations of the theory $\mathcal{S} + \mathcal{S}_{\text{imp}}$ (and of a related theory [142]) have been computed in chapter 3, which obtained the scaling dimensions of the Néel order parameter, n^a , and of the uniform magnetization density in the vicinity of the impurity. It was found that the impurity significantly enhanced the local magnetic susceptibilities. For the case of double-layer antiferromagnets, which have magnetic ordering transitions described by Landau-Ginzburg-Wilson theory, such impurity magnetic correlations have also been computed by similar methods [106, 107, 112], and found to be in excellent agreement with numerical studies [144, 96, 117].

This chapter will describe the “charge-order” correlations of the theory $\mathcal{S} + \mathcal{S}_{\text{imp}}$ by a computation of the OPE of the monopole/VBS operator $V(\vec{x}, \tau)$ as $\vec{x} \rightarrow 0$. Our principal result is that the OPE is modified from the form in Eq. (4.6) to

$$\lim_{|\vec{x}| \rightarrow 0} V(\vec{x}, \tau) \sim |\vec{x}|^{\Delta_{\text{imp}}^V} e^{-iQ\theta} V_{\text{imp}}(\tau) \quad (4.12)$$

where θ is the azimuthal angle of \vec{x} . There are two important changes from Eq. (4.6). The first is that V_{imp} is no longer a trivial unit operator, but a fluctuating impurity degree of freedom with a non-trivial scaling dimension. The second is the presence of the $e^{-iQ\theta}$ factor, which indicates a Q -fold winding in the phase of the VBS order parameter around the impurity. The sketch in Fig. 4.2 gives a simple physical interpretation of this winding in terms of the valence bond configurations of the underlying

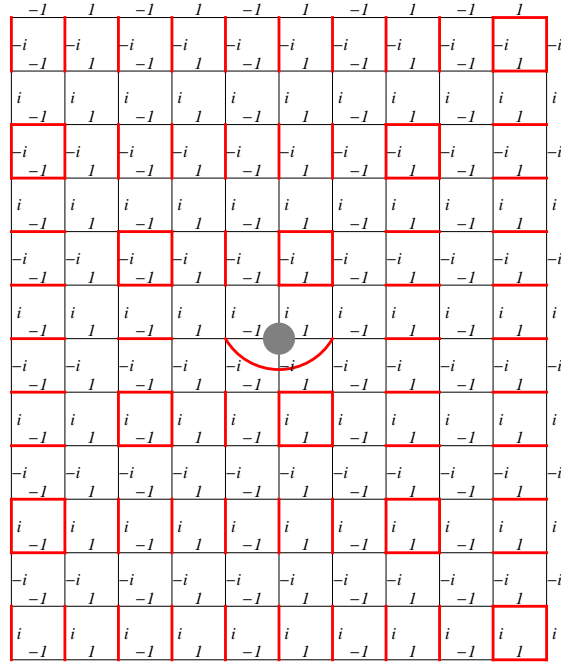


Figure 4.3: A VBS *anti*-vortex in the presence of an impurity with a charge Q opposite in sign to that required by Eq. (4.12). This configuration has a higher energy cost than the VBS vortex configurations in Fig. 4.2.

antiferromagnet. Also, as we discussed earlier [121], the sign of Q is determined by the sublattice location of the missing spin. Thus, the result Eq. (4.12) indicates that VBS vortices will occur preferentially around impurities on one sublattice, while VBS anti-vortices occur around impurities on the other sublattice. This same result is also obtained from the intuitive microscopic picture in Fig. 4.2. Also, we show in Fig. 4.3 an illustration of an anti-vortex in the presence of an impurity on the disfavored sublattice: the same sublattice bond indicates that this configuration has a higher energy.

Apart from establishing the form of Eq. (4.12), we will also describe computations of the exponent Δ_{imp}^V . There are general reasons for expecting that $\Delta_{\text{imp}}^V > 0$, and this will be the case in the explicit result we obtain. This positive value of Δ_{imp}^V char-

acterizes the *suppression* of VBS order near the impurity, and should be contrasted with the negative value in Eq. (4.9) for the impurity in Fig. 4.1.

Our analysis will begin in Section 4.2 by a large N analysis of the theory $\mathcal{S} + \mathcal{S}_{\text{imp}}$ with full $SU(N)$ spin symmetry. We will establish Eq. (4.12) in this limit. We will also find that the $N = \infty$ limit (at fixed Q) of the exponent Δ_{imp}^V vanishes, but we will not evaluate the subleading correction in the $1/N$ expansion here.

The remainder of the chapter will explore another approach to estimating Δ_{imp}^V . This relies [1, 2] on examining the “easy-plane” limit of the CP^{N-1} model, in which the global $SU(N)$ spin symmetry is reduced to $U(1)^{N-1}$. With this simplification to an abelian global symmetry, an explicit duality transformation of the theory becomes possible. In the dual theory, the monopole/VBS operator V has a local expression in terms of the dual fields, and so this facilitates the analysis of the impurity critical property. We will begin the dual analysis in Section 4.3 by considering the simplest $N = 1$ case [145]: this model describes the onset of VBS order in a $S = 1/2$ quantum antiferromagnet in the presence of a staggered magnetic field [2], and is the simplest setting in which several technical issues can be described. We then extend the analysis to general N in Section 4.4. The exponent Δ_{imp}^V will be estimated in these sections by a self-consistent theory of Gaussian fluctuations about a mean-field state; in the physically interesting case of $N = 2$ and $Q = 1$, which describes both the easy plane antiferromagnet and the boson superfluid/insulator transition, we obtain the estimate

$$\Delta_{\text{imp}}^V \approx 0.57, \quad N = 2, Q = 1 \quad (4.13)$$

Our analysis of the easy plane theory in Section 4.4 also exhibits certain features which we do not expect to be shared by the case with global $SU(N)$ symmetry: for

$Q/N = 1/2$, we find VBS-vortex solutions in which the $e^{-iQ\theta}$ factor in Eq. (4.12) is replaced by $e^{-i\ell\theta}$ with the integer $-Q \leq \ell \leq Q$. In the self-consistent theory we present here, all the values of ℓ are degenerate, but we expect these degeneracies are partially lifted in the full easy-plane theory. These issues are discussed further in Section 4.4.

4.2 $1/N$ Expansion of the CP^{N-1} theory in the presence of monopoles

The insertion of one monopole into the partition function of CP^{N-1} model in the disordered phase has been originally considered in Ref. [3]. The $1/N$ expansion proceeds by replacing the quartic self-interactions in Eq. (4.1) by a fixed-length constraint on the spinors; so we consider the action

$$\mathcal{S} = \int d^2x d\tau \left[|(\partial_\mu - iA_\mu)z_\alpha|^2 + i\lambda \left(|z_\alpha|^2 - \frac{1}{g} \right) \right] \quad (4.14)$$

where λ is a fluctuating Lagrange multiplier field. The procedure for generating the $1/N$ expansion is now simple. One first integrates over the z fields obtaining an effective action for A_μ and λ . However, instead of expanding this effective action around the trivial classical vacuum $A_\mu = 0$, one expands around the monopole (instanton) solution, A_μ^i , with

$$F_\mu^i = 2\pi q \frac{(x - x_0)_\mu}{4\pi|x - x_0|^3} \quad (4.15)$$

where $F_\mu = \epsilon_{\mu\nu\lambda} \partial_\nu A_\lambda$, q is the monopole charge and x_0 is the monopole position. In practice, integrating out the z fields in the background of spatially varying monopole

fields is quite complicated (even more so due to the appearance of UV and IR divergences), so that only the leading term in the $1/N$ expansion has been computed in the past (that is fluctuations of A_μ about the monopole solution have not been taken into account). At this order, one finds,

$$\langle V^q(x) \rangle \sim \left(\frac{m}{\Lambda} \right)^{2N\rho_q} \quad (4.16)$$

where $V^q(x)$ is the monopole operator of charge q , m is the mass gap of the theory, Λ is the ultraviolet cut-off and ρ_q is a collection of universal numbers (depending only on the charge of the monopole) which have been computed in Ref. [3]. Thus, the dimension of operator $V^q(x)$, $\dim[V^q] = 2N\rho_q$.

If finding the expectation value of a monopole operator (and its scaling dimension) was very complicated, finding correlators of $V(x)$ with Wilson loops at $N = \infty$ turns out to be exceedingly simple. Indeed, we notice that at leading order in $1/N$ it is sufficient to simply replace A_μ in the Wilson loop by its monopole value,

$$\frac{\langle V^q(x) \exp(-iQ \int_{\mathcal{C}} A_\mu dx_\mu) \rangle}{\langle V^q \rangle} \rightarrow \exp\left(-iQ \int_{\mathcal{C}} A_\mu^i dx_\mu\right) = \exp\left(-iQ \int_{\mathcal{S}} F_\mu^i dS_\mu\right) \quad (4.17)$$

provided that we take the charge Q to be $\mathcal{O}(1)$ in N (otherwise, if $Q \sim \mathcal{O}(N)$ the Wilson line will change the background monopole field and the problem becomes intractable). Here \mathcal{C} is some closed contour and \mathcal{S} is any surface such that $\partial\mathcal{S} = \mathcal{C}$. Thus, all we have to do is find the flux of our monopole through the Wilson loop that we are considering. Fluctuations of A_μ about the monopole field (4.15) will contribute at $\mathcal{O}(1/N)$ to the correlator (4.17). Likewise, if we denote the Wilson loop operator by $W(\mathcal{C})$, then in the absence of the monopole field $\langle W(\mathcal{C}) \rangle \sim 1 + \mathcal{O}(1/N)$ (saturated

by fluctuations of A_μ around the trivial vacuum), so

$$\frac{\langle V^q(x)W(\mathcal{C}) \rangle}{\langle W(\mathcal{C}) \rangle} = \langle V^q \rangle \exp \left(-iQ \int_{\mathcal{S}} F_\mu^i dS_\mu \right) \quad (4.18)$$

and at leading order in $1/N$ the external charge only changes the phase of the expectation value of monopole operator but not its magnitude.

In principle we are interested in finding the correlator of the monopole operator (that we place at a point $x = (r \cos \theta, r \sin \theta, 0)$) and a straight, temporal Wilson line of charge Q (which we place at the origin). However, to regularize possible IR divergences let's also place a charge $-Q$ on the positive x axis far away from the origin. As usual, we may connect the two oppositely directed Wilson lines in the far past and far future. Then, according to (4.17) we have to compute the magnetic flux due to the monopole field (4.15) through the $y = 0, x > 0$ half-plane,

$$\int \vec{F} \cdot d\vec{S} = -\frac{q}{2} \int_{-\infty}^{\infty} d\tau \int_0^{\infty} dx \frac{r \sin \theta}{((x - r \cos \theta)^2 + r^2 \sin^2 \theta + \tau^2)^{\frac{3}{2}}} \quad (4.19)$$

$$= -q \int_0^{\infty} dx \frac{r \sin \theta}{(x - r \cos \theta)^2 + r^2 \sin^2 \theta} \quad (4.20)$$

$$= -q(\pi - \theta) \quad (4.21)$$

We see that the flux through the Wilson loop changes by $2\pi q$ as the monopole crosses the surface of the loop. However, the expectation value,

$$\langle V^q(x) \rangle_{\text{imp}} = \frac{\langle V^q(x)W(\mathcal{C}) \rangle}{\langle W(\mathcal{C}) \rangle} = \langle V^q \rangle e^{iQq(\pi - \theta)} \quad (4.22)$$

remains single valued, as by Dirac's condition Q is an integer (in what follows, we shall also often discuss Wilson loops with non-integer charge Q , which in the presence of monopole operators are defined by specifying a surface \mathcal{S} , $W(\mathcal{S}) = e^{-iQ \int_{\mathcal{S}} F_\mu dS_\mu}$). The correlation functions then explicitly depend on the choice of the surface, as can

be seen from (4.22)). Thus, we see that the phase of the monopole operator winds by $-2\pi Q$ as we move it in a full circle around the Wilson line, i.e. an external charge creates a vortex of the monopole field, consistent with the OPE in Eq. 4.12. We expect that once we go beyond the leading order in N , this vortex will also get a nontrivial spatial profile,

$$\langle V^q(x) \rangle_{\text{imp}} = \langle V^q \rangle f(m|\vec{x}|) e^{-iQq\theta} e^{i\chi} \quad (4.23)$$

Here $f(r)$ is the vortex profile function and $e^{i\chi}$ is some overall phase (discussed below). We expect that far away from the external charge, the monopole field tends to its vacuum expectation value so that $f(\infty) = 1$. Moreover, by continuity we expect the monopole field to vanish at the origin, $f(0) = 0$. To the order to which we were working, $f(r) = 1$, which implies that the impurity exponent $\Delta_{\text{imp}}^V \sim \mathcal{O}(1/N)$.

Notice that the result (4.22) is sensitive to the angular position of the distant charge relative to the one at the origin (we introduced the variable θ as the angle between the plane of the Wilson loop and the monopole operator). This is not unexpected: the monopole field is the order parameter for the flux symmetry, which is spontaneously broken in the disordered phase. As we rotate the distant charge, the overall phase $e^{i\chi}$ of the expectation value of the monopole operator changes - that is we explore different states in our vacuum manifold.

If we were instead considering a correlation function of a string of monopole operators $\prod_i V^{q_i}(x_i)$ such that the overall combination is invariant under the flux symmetry (that is $\sum_i q_i = 0$) we expect the dependence on the angular position of the distant charge to drop out. We can check this in the limit $m|x_i - x_j| \gg 1$, $m|\vec{x}_i| \gg 1$,

assuming clustering,

$$\langle \prod_i V^{q_i}(x_i) \rangle_{\text{imp}} \rightarrow \prod_i \langle V^{q_i}(x_i) \rangle_{\text{imp}} \rightarrow \prod_i \langle V_i^q \rangle e^{-iQq_i\theta_i} \quad (4.24)$$

which is invariant under $\theta_i \rightarrow \theta_i + \chi$. Alternatively, in the same limit of far separated monopoles and at $N = \infty$, the classical magnetic field will just be a linear superposition of magnetic fields due to each monopole. Thus, the flux Φ through the Wilson loop will be given by, $\Phi = -\sum_i q_i(\pi - \theta_i) = \sum_i q_i\theta_i$ and using the equivalent of (4.18) for a string of monopole operators, we arrive at the same expression (4.24).

We expect the general form (4.23) to be preserved at any finite order in $1/N$. Nevertheless, in the flux-broken phase of the theory, there are also non-perturbative effects that should be taken into consideration. Indeed, the $U(1)_\Phi$ vortex nucleated by the external charge is global, and thus, will have a logarithmically divergent energy. Put into a more conventional language, the external charge creates a Coulomb potential, which is logarithmic in two dimensions, $V(r) \approx -\frac{e^2 Q}{2\pi} \log(mr)$ for $mr \gg 1$. The effective coupling constant e^2 can be calculated in the $1/N$ expansion to be $e^2 \sim \frac{1}{N}m$. Thus, it will be energetically favourable for the external charge to bind a dynamical spinon (we concentrate on the case $Q = 1$ here for simplicity). This process can be analyzed by means of a non-relativistic Schrodinger equation[23]. One finds a bound state of size $r_b \sim N^{\frac{1}{2}}m^{-1}$. We expect that for $r \gg r_b$ the external charge will be screened by the dynamical spinon. On the other hand for $r \ll r_b$ this logarithmic confinement should generally have little effect on the physics. However, there is one notable exception: the expectation value of the monopole operator V^q (4.22) will be drastically altered on all distance scales by the screening. Indeed, if we assume that screening takes place, $\langle V^q(\vec{x}) \rangle$ has to tend to its vacuum expectation value for

$|\vec{x}| \gg r_b$, and should experience no phase winding. We don't expect the winding number to change abruptly as we decrease $|\vec{x}|$, so we won't see a phase winding of $\langle V^q(\vec{x}) \rangle$ on short distances $|\vec{x}| \ll r_b$ as well.

A toy model for the disappearance of winding when screening effects are taken into account can be constructed as follows. We can use the charge $-Q$ that we previously put far away from the origin to represent the dynamical spinon that gets bound to the external charge. We first freeze the location of this spinon at some position \vec{x}' away from the origin and compute the resulting expectation value of $V^q(\vec{x})$ using eq. (4.18). We then average the resulting $\langle V^q(\vec{x}) \rangle$ over the spinon positions x' with the probability distribution $|\psi(\vec{x}')|^2$, where $\psi(\vec{x})$ is the spinon wave-function. Since this wave-function will be azimuthally symmetric, one immediately learns that upon averaging over the angular position of the spinon, $\langle V^q(\vec{x}) \rangle$ loses its finite winding number and will, in fact, carry a constant phase for all \vec{x} . This same averaging will also lead to an additional suppression $\langle V^q(\vec{x}) \rangle \sim |\vec{x}|$ as $\vec{x} \rightarrow 0$ (recall that at $N = \infty$ there was no suppression of the vortex profile for $x \rightarrow 0$ before screening effects were taken into account). The origin of this suppression is easy to see - for an external charge located infinitely far away, the averaging over the azimuthal position of the charge is identical to averaging of the phase χ in eq. (4.23) producing a zero result for $\langle V^q \rangle$.

Do the above findings invalidate the OPE (4.12)? The answer is no. The above discussion simply implies that $\langle V_{\text{imp}} \rangle = 0$ and, thus, the expectation value $\langle V(\vec{x}) \rangle$ for $\vec{x} \rightarrow 0$ is controlled by higher order terms in the OPE (namely, by the impurity operator with angular momentum zero). However, higher correlation functions of V

operator, e.g. the VBS susceptibility $\langle V(x)V^\dagger(x') \rangle$, are still controlled by the OPE (4.12). Such correlators are invariant under the $U(1)_\Phi$ symmetry, so as we argued above, their short distance properties are not sensitive to the location of the distant charge, and hence, to screening physics.

4.3 Easy plane model at $N = 1$

This section, and the next, will examine a simplified version of the theory $\mathcal{S} + \mathcal{S}_{\text{imp}}$ in which the non-abelian global $SU(N)$ symmetry is reduced to an abelian $U(1)^{N-1}$ symmetry. This enables us to use the tools of abelian particle-vortex duality [52, 53] to obtain a theory expressed in terms of fields which are locally related to the monopole/VBS operator V . The present section will consider the simplest case [145] with $N = 1$. This model describes the onset of VBS order in a $S = 1/2$ quantum antiferromagnet in the presence of a staggered magnetic field [2], and is useful in resolving a number of key technical questions in their simplest setting. For $N = 1$, the theory \mathcal{S} does not have any global continuous symmetry, and becomes equivalent to scalar electrodynamics. With the results for the $N = 1$ theory obtained in the present section, we will be able to rapidly analyze the general N case in the next section.

4.3.1 Duality and Wilson loops

It is well known that in three space-time dimensions, near its critical point, non-compact $N = 1$ scalar electrodynamics is dual to a theory of a complex (pseudo)scalar field with a global $U(1)$ symmetry [52, 53]. The Lagrangians of these two theories are

as follows,

$$L_{QED} = \frac{1}{2e^2} F_\mu^2 + |(\partial_\mu - iA_\mu)z|^2 + m^2|z|^2 + \frac{g}{2}|z|^4 \quad (4.25)$$

$$L_{XY} = |\partial_\mu V|^2 + \tilde{m}^2|V|^2 + \frac{\tilde{g}}{2}|V|^4 \quad (4.26)$$

Here z and V are complex one component fields. The duality is understood as being true for the range of parameters where L_{QED} has a second order phase transition (which at weak coupling is believed to occur for g/e^2 sufficiently large). One way to understand the duality is by noting that the phase transition in scalar QED is driven by spontaneous breaking of flux symmetry $U(1)_\Phi$, which is precisely the global symmetry of L_{XY} . The order parameter for the flux symmetry is the monopole operator $V(x)$ - that is the dynamical field of L_{XY}^2 . As we know, to each continuous symmetry there corresponds a conserved current. In the case of flux symmetry of QED, this pseudo-vector current is just the magnetic field F_μ , which is trivially conserved in the absence of monopoles, $\partial_\mu F_\mu = 0$. Let's introduce an external field H_μ that would couple to this current,

$$\delta L_{QED} = iH_\mu F_\mu \quad (4.27)$$

Suppose we are calculating some correlation function with insertion of a string of monopole operators of charge q_i at points x_i . The gauge field A_μ in the path integral is then subject to the condition, $\partial_\mu F_\mu = \sum_i 2\pi q_i \delta(x - x_i)$. Then under the transformation,

$$H_\mu \rightarrow H_\mu + \partial_\mu \alpha \quad (4.28)$$

²Here we use the notation that $V^{q=1}(x) \sim V(x)$ and $V^{q=-1}(x) \sim V^\dagger(x)$. The precise proportionality factor between V 's in the direct and dual picture is a delicate matter (related in part to the precise definition of the monopole operator in the direct picture), which shall not be very important to us here.

$$S_{QED} \rightarrow S_{QED} + i \int dx \partial_\mu \alpha F_\mu = S_{QED} - i \int dx \alpha \partial_\mu F_\mu = S_{QED} - 2\pi i \sum_i q_i \alpha(x_i) \quad (4.29)$$

Hence, by introducing the field H_μ we can enlarge the global $U(1)_\Phi$ symmetry to a fictitious local symmetry, provided that the monopole operators transform as,

$$V^q(x) \rightarrow e^{2\pi i q \alpha(x)} V^q(x) \quad (4.30)$$

The dual Lagrangian L_{XY} has to possess this local symmetry. Hence, to introduce the field H_μ into the dual Lagrangian we simply have to covariantize the derivative of the dynamical monopole field V ,

$$\partial_\mu V \rightarrow D_\mu V = (\partial_\mu - 2\pi i H_\mu) V \quad (4.31)$$

in eq. (4.26). Other “gauge invariant” operators can also be added to L_{XY} , e.g. $H_{\mu\nu}^2$; however, their contribution will, generally, either cancel out in correlation functions or be less singular near the critical point.

Thus, the dual Lagrangian in the presence of a background source field H_μ is given by,

$$L_{XY} = |(\partial_\mu - 2\pi i H_\mu) V|^2 + \tilde{m}^2 |V|^2 + \frac{\tilde{g}}{2} |V|^4 \quad (4.32)$$

The covariantization procedure (4.31) was explicitly written down in Ref. [146]. Similar arguments for the case of a constant imaginary H_μ , which physically represents an external magnetic field in the QED language and translates into a chemical potential for the flux symmetry in the XY language, have been given in Ref. [147]. In Ref. [148] we have also given an argument based on an exact duality transformation on the lattice, which support (4.32).

Having learned how to incorporate the source field H_μ into the dual Lagrangian, it is now trivial to dualize Wilson loops. Indeed, insertion of a Wilson loop $W(\mathcal{C})$ into a correlation function is equivalent to adding into the Lagrangian the source term

$$\delta L = iQ \int_{\mathcal{C}} dx_\mu A_\mu = iQ \int_{\mathcal{S}} dS_\mu F_\mu = i \int dx H_\mu F_\mu \quad (4.33)$$

where

$$H_\mu(x) = Q \int_{y \in \mathcal{S}} dS_\mu \delta(x - y) \quad (4.34)$$

That is H_μ is a field that lives on the surface of the Wilson loop and is directed perpendicular to this surface.

Another benefit of introducing the source field H_μ is that by differentiating with respect to it we can compute correlation functions of the magnetic field F_μ . For instance,

$$\langle -iF_\mu(x) \rangle_H = \frac{\delta \log Z[H]}{\delta H_\mu(x)} = -2\pi i \langle (V^\dagger D_\mu V - (D_\mu V)^\dagger V)(x) \rangle_H \quad (4.35)$$

That is the topological flux current F_μ of QED gets mapped into the Noether's current associated with the global $U(1)$ symmetry of the dual model. Differentiating once again,

$$\begin{aligned} \langle F_\mu(x) F_\nu(y) \rangle_{H, conn} &= -\frac{\delta Z[H]}{\delta H_\mu(x) \delta H_\nu(y)} \\ &= (2\pi)^2 \left(\langle V^\dagger \overleftrightarrow{D}_\mu V(x) V^\dagger \overleftrightarrow{D}_\nu V(y) \rangle_{H, conn} + 2\delta_{\mu\nu} \delta(x - y) \langle V^\dagger V(x) \rangle_H \right) \end{aligned} \quad (4.36)$$

The first term in (4.36) is the expected correlator of two $U(1)_\Phi$ currents, while the second term is a tadpole that ensures the overall transversality of the correlation function.

Having discussed the duality at length, we now return to our original problem: what is the influence of the external charge (Wilson line) on various physical observables. The observable of most interest to us is the monopole operator $V(x)$. However, this observable is physical only for integer-valued charge Q of the Wilson line (Dirac's condition). Indeed, recall that in the dual language the field H depends on a choice of surface \mathcal{S} of the Wilson loop. If we pick a different surface \mathcal{S}' then the field H_μ undergoes a gauge transformation $H_\mu \rightarrow H'_\mu = H_\mu + \partial_\mu \alpha$ with $\alpha(x) = -Q \mathbb{1}_{x \in \mathcal{V}}$ where \mathcal{V} is the volume bounded by the two surfaces \mathcal{S} and \mathcal{S}' . Hence,

$$\langle V(x) \dots \rangle_{H'} = e^{2\pi i \alpha(x)} \langle V(x) \dots \rangle_H \quad (4.37)$$

where ellipses denote some other operators. Thus, the operator $V(x)$ is invariant under changing the surface of the Wilson loop if and only if Q is an integer. However, if the charge Q is a rational number, $Q = p/q$ where p and q are integers then the flux $2\pi q$ monopole operator $V^q(x) \sim (V(x))^q$ is physical. Moreover, a theory with arbitrary irrational Q is still sensible provided that we confine our attention to correlation functions of operators which are invariant under the fictitious $U(1)_\Phi$ local symmetry, e.g. the magnetic field operator $-iF_\mu = -2\pi i V^\dagger \overleftrightarrow{D}_\mu V$. In fact, if we are dealing with such gauge invariant operators we don't necessarily have to use the precise form of H given by (4.34); defining γ_μ to be a field living on the perimeter of the Wilson loop and directed along it,

$$\gamma_\mu(x) = Q \int_{y \in \mathcal{C}} dy_\mu \delta(x - y) \quad (4.38)$$

we see that,

$$\epsilon_{\mu\nu\lambda} \partial_\nu H_\lambda = \gamma_\mu \quad (4.39)$$

Then, by performing a suitable gauge transformation on H_μ and V we can choose H_μ to be any field with curl given by γ_μ . Thus, we see that the duality maps a Wilson loop of charge Q in the QED language to an external magnetic flux tube of flux $2\pi Q$ in the XY language. This correspondence has been noted in Ref. [149], but the consequences of this correspondence for the critical properties of Wilson loops were not discussed.

Now we can address the problem that we originally posed in a dual language. Let's place an charge external charge Q at the spatial origin. For now we don't insist that this charge be an integer. The dual source field H_μ must, therefore, satisfy

$$\nabla \times \vec{H} = Q\delta^2(\vec{x})\hat{z} \quad (4.40)$$

Thus, we basically have to solve an Aharonov-Bohm problem with flux $2\pi Q$. One choice for the source field H_μ is

$$H_\mu(x) = Q\delta_{\mu,2}\theta(x)\delta(y) \quad (4.41)$$

This is the so-called string gauge, which corresponds to (4.34), with the surface of the Wilson loop being the plane $y = 0, x > 0$. As is well known, the string gauge is equivalent to $H_\mu = 0$ and the boundary condition,

$$V(\theta = 2\pi) = e^{-2\pi i Q}V(\theta = 0) \quad (4.42)$$

where θ is the azimuthal angle. Thus, we have to solve the theory (4.26) with the twisted boundary condition (4.42). We observe that the physics is, therefore, a periodic function of Q . For integer Q the boundary condition (4.42) is trivial - there is no twist. So our argument indicates that integral external charges do not affect

correlation functions on distances of order of the correlation length of the theory: screening of integral charges takes place on distance scales of order of microscopic UV cutoff. This surprising fact is discussed in more detail in Ref. [148].

The behaviour at non-integer Q is less unexpected. One physical question that we may ask is what is the magnetic (electric) field induced by the charge Q (we define the electric field $E_i = F_{i3} = -\epsilon_{ij}F_j$ where latin letters i, j, k run over spatial indices). Although this is a departure from our original goal, we will see that a lot of the results that we will obtain along the way will be useful when we return to discuss correlators of monopole field for the planar theory with N fields. Another question that we will address for non-integer, rational, values of $Q = p/q$ is the behaviour of higher flux monopole operators $V(x)^q$.

4.3.2 Perturbative expansion of the dual theory for $Q \rightarrow 0$

The magnetic field $-iF_\mu$ is a conserved current and receives no renormalizations and, thus, has conformal dimension 2. Therefore, at the critical point we expect,

$$\langle -i\vec{E} \rangle = C(Q) \frac{1}{r^2} \hat{r} \quad (4.43)$$

The electric field is imaginary as we are working in Euclidean space. The coefficient $C(Q)$ is a universal number that is a periodic function of charge Q . We shall be interested in determining this function.

For $Q \rightarrow 0$ we can perform a perturbative expansion in $H_\mu \sim \mathcal{O}(Q)$.

$$\langle -iF_\mu(x) \rangle_H = \frac{\delta \log Z[H]}{\delta H_\mu(x)} \approx \int dy \frac{\delta^2 \log Z}{\delta H_\mu(x) \delta H_\nu(y)} H_\nu(y) = - \int dy \langle F_\mu(x) F_\nu(y) \rangle H_\nu(y) \quad (4.44)$$

As we have learned, the correlation function of magnetic field F_μ dualizes to,

$$K_{\mu\nu}(x-y) = \langle F_\mu(x)F_\nu(y) \rangle = (2\pi)^2 \left(\langle V^\dagger \overleftrightarrow{\partial}_\mu V(x) V^\dagger \overleftrightarrow{\partial}_\nu V(y) \rangle + 2\delta_{\mu\nu}\delta(x-y)\langle V^\dagger V \rangle \right) \quad (4.45)$$

By transversality,

$$K_{\mu\nu}(p) = K(p)\left(\delta_{\mu\nu} - \frac{p_\mu p_\nu}{p^2}\right) \quad (4.46)$$

By RG $K(p)$ should have the form,

$$K(p) = Mg(p/M) \quad (4.47)$$

where M is some physical scale in the theory (e.g. in the $U(1)_\Phi$ disordered phase, the mass of the monopole field V). At the critical point,

$$K(p) = A|p| \quad (4.48)$$

where A is some universal number. On the XY side of the theory, this universal number has been computed before using both ϵ expansion[150] and large M expansion[151]. The large M expansion is obtained by replacing the complex scalar V in the action for the XY theory (4.26) by an M component complex field. In the large M expansion the coefficient A is found to be at next to leading order in M ,

$$A = (2\pi)^2 \frac{M}{16} \left(1 - \frac{1}{M} \frac{32}{9\pi^2} \right) \stackrel{M=1}{\approx} 1.6 \quad (4.49)$$

while in the ϵ expansion one obtains $A \approx 2.0$ at $\mathcal{O}(\epsilon^2)$. Monte-Carlo simulations on the XY model[151] indicate $A \approx 1.8$.³ The coefficient A can also be computed by performing a large N expansion in the original QED, whereby the field z is promoted

³Given our normalization of A one has to multiply the value of universal conductance presented in Refs. [150, 151] by 2π .

to have N components. At leading order one obtains $A = 16/N \stackrel{N=1}{=} 16$ (as usual, direct large N expansion in QED produces results, which are numerically notoriously inaccurate for $N \sim 1$).

For completeness, we also discuss the behaviour of $K(p)$ at small momenta on both sides of the critical point. In the phase where the $U(1)_\Phi$ symmetry is spontaneously broken the spectrum of the theory should contain a goldstone, which can be created out of the vacuum by the $U(1)_\Phi$ current,

$$\lim_{p \rightarrow 0} \langle p | F_\mu(x) | 0 \rangle = 2\pi \lim_{p \rightarrow 0} \langle p | -iV^\dagger \overleftrightarrow{\partial}_\mu V(x) | 0 \rangle = 2\pi i f p_\mu e^{ipx} \quad (4.50)$$

where in three dimensions f^2 defines a physical energy scale. Note that equation (4.50) is written in Minkowski space. We see that the goldstone is nothing but the photon of the original QED. Then $K_{\mu\nu}(p)$ should have a pole at $p^2 = 0$ and using spectral decomposition,

$$\lim_{p \rightarrow 0} K(p) = (2\pi f)^2 \quad (4.51)$$

On the other hand, in the the phase where the $U(1)_\Phi$ symmetry is unbroken (that is in the “superconducting” phase of QED) the V field is massive and all the excitations have a gap. Therefore, $K_{\mu\nu}(p)$ cannot have a pole at $p^2 = 0$ and

$$\lim_{p \rightarrow 0} K(p) \sim \frac{p^2}{M} \quad (4.52)$$

Having discussed the expected form of $K_{\mu\nu}$ in different phases we can go back to eq. (4.44) for electric field induced by the charge Q . Introducing the kernel $\mathcal{D}(p) = K(p)/p^2$, and using eq. (4.40),

$$\langle -iF_\mu(x) \rangle = - \int dy K_{\mu\nu}(x-y) H_\nu(y) = -Q \int d\tau' \epsilon_{\mu\nu 3} \partial_\nu^x \mathcal{D}(\vec{x}, \tau') \quad (4.53)$$

Hence,

$$\langle -i\vec{E}(\vec{x}) \rangle = Qh(|\vec{x}|)\hat{r} \quad (4.54)$$

where

$$h(|\vec{x}|) = -\frac{\partial}{\partial|\vec{x}|} \int d\tau' \mathcal{D}(\vec{x}, \tau') \quad (4.55)$$

Substituting the expression (4.48) for $K(p)$ at the critical point we obtain,

$$\langle -i\vec{E}(\vec{x}) \rangle = Q \frac{A}{2\pi|\vec{x}|^2} \hat{r} \quad (4.56)$$

Hence we identify,

$$C(Q) \approx QA/(2\pi), \quad Q \rightarrow 0 \quad (4.57)$$

Similarly, in the $U(1)_\Phi$ ordered phase,

$$\langle -i\vec{E}(\vec{x}) \rangle = Q \frac{2\pi f^2}{|\vec{x}|} \hat{r} \quad (4.58)$$

So in this phase, as expected, the external electric charge produces the usual Coulomb-like electric field, $\vec{E} = \frac{e_{eff}^2 Q}{2\pi r}$, as appropriate to two spatial dimensions with the identification $e_{eff} = 2\pi f$.

4.3.3 Peculiarities of the free theory

So far we have only discussed the leading term in $C(Q)$ for $Q \rightarrow 0$. In principle, we could continue the expansion in Q to higher orders: then the problem reduces to finding correlators of current operators $-iF_\mu = iV^\dagger \overleftrightarrow{\partial}_\mu V$. These correlators can be found by performing either ϵ or $1/M$ expansion of the XY model. In either case, going beyond the leading order in Q is not simple. So, instead, we choose to return to the formulation of the problem involving the twisted boundary condition (4.42).

In the next section we will use this formulation to compute $C(Q)$ for all Q (albeit numerically) at $M = \infty$. However, before we do so, we will solve a slightly simpler problem: namely we find the form of $C(Q)$ at the gaussian fixed point $\tilde{g} = 0, \tilde{m}^2 = 0$ of the Lagrangian (4.26). The reason for studying the free theory is that the calculations in it are, technically, very similar to those in the strongly coupled $M = \infty$ theory addressed in the next section (even though the physical results are quite different).

In the free theory, $C(Q)$ can be determined exactly, and, surprisingly, turns out to be a non-analytic function of Q at $Q = 0$. We have not been able to see any hints of this non-analyticity from the perturbative expansion of the free theory in Q (perhaps because we could go perturbatively only to linear order in Q , whereas the non-analyticity of $C(Q)$ starts only at order $|Q|^2$). On the other hand, once we go in the next section to the strongly interacting fixed point (obtained in the $M = \infty$ limit), the theory cures itself of all *IR* divergences and $C(Q)$ becomes analytic in Q .

So, let's compute,

$$\langle -iF_\mu(x) \rangle = \langle -2\pi i V^\dagger \overleftrightarrow{\partial}_\mu V(x) \rangle = -2\pi i \lim_{x \rightarrow y} (\partial_\mu^x - \partial_\mu^y) \langle V(x) V^\dagger(y) \rangle \quad (4.59)$$

in the free theory, $L = |\partial_\mu V|^2$ subject to boundary condition (4.42). As eq. (4.59) shows, to find the $U(1)_\Phi$ current it is sufficient to determine the propagator, $D(x - y) = \langle V(x) V^\dagger(y) \rangle$. The propagator will also determine the correlation function of operators $(V(x))^q$ for rational $Q = p/q$,

$$\langle (V(x))^q (V^\dagger(y))^q \rangle = q! D(x - y)^q \quad (4.60)$$

We note that our problem is invariant under translations along the temporal direction,

so,

$$D(\vec{x}, \vec{x}', \tau - \tau') = \int \frac{d\omega}{2\pi} D_2(\vec{x}, \vec{x}', \omega^2) e^{i\omega(\tau - \tau')} \quad (4.61)$$

where $D_2(\vec{x}, \vec{x}', \omega^2)$ denotes the two-dimensional propagator with mass $m^2 = \omega^2$ and twisted b.c. (4.42). We use spectral decomposition to find D_2 ,

$$D_2(\vec{x}, \vec{x}', m^2) = \sum_l \frac{e^{il\theta}}{2\pi} \int_0^\infty dE \frac{1}{m^2 + E} \phi_{l,E}(\vec{r}) \phi_{l,E}^*(\vec{r}') \quad (4.62)$$

where we sum over states with fixed azimuthal angular momentum $l = n - Q$, $n \in \mathbb{Z}$. Note that the angular momenta are not integral due to the twisted b.c. (4.42). The radial eigenfunctions $\phi_{l,E}(r)$ satisfy,

$$\left(-\frac{1}{r} \frac{\partial}{\partial r} \left(r \frac{\partial}{\partial r} \right) + \frac{l^2}{r^2} \right) \phi_{l,E}(r) = E \phi_{l,E}(r) \quad (4.63)$$

and are normalized as,

$$\int_0^\infty dr r \phi_{l,E}^*(r) \phi_{l,E'}(r) = \delta(E - E') \quad (4.64)$$

The solution to ODE (4.63) is,

$$\phi_{l,E}(r) = \frac{1}{\sqrt{2}} J_{|l|}(\sqrt{E}r) \quad (4.65)$$

where $J_n(u)$ is the n-th order Bessel function. Hence,

$$D(r, r', \theta - \theta', \tau - \tau') = \sum_l e^{il(\theta - \theta')} \int \frac{d\omega}{2\pi} e^{i\omega(\tau - \tau')} \int_0^\infty \frac{du}{2\pi} \frac{u}{u^2 + \omega^2} J_{|l|}(ur) J_{|l|}(ur') \quad (4.66)$$

where we made the substitution $u = \sqrt{E}$. Integrating over ω ,

$$D(r, r', \theta, \tau) = \frac{1}{4\pi r'} \sum_l e^{il\theta} \int_0^\infty dv J_{|l|}\left(\frac{r}{r'}v\right) J_{|l|}(v) \exp\left(-\frac{|\tau|}{r'}v\right) \quad (4.67)$$

Now we can ask, what is the behaviour of the propagator $D(r, r', \theta, \tau)$ for $r \rightarrow 0$, i.e. for $r \ll r'$. Recalling, $J_{|l|}(r) \approx \frac{1}{2^{|l|}\Gamma(|l|+1)}r^{|l|}$,

$$\int_0^\infty dv J_{|l|}\left(\frac{r}{r'}v\right) J_{|l|}(v) \exp\left(-\frac{|\tau|}{r'}v\right) \approx \left(\frac{r}{r'}\right)^{|l|} B_l\left(\frac{|\tau|}{r'}\right) \quad (4.68)$$

with

$$B_l(u) = \frac{1}{2^{|l|}\Gamma(|l|+1)} \int dv v^{|l|} J_{|l|}(v) \exp(-uv) = \frac{\Gamma(|l| + \frac{1}{2})}{\Gamma(|l| + 1)} \left(1 + \frac{\tau^2}{r'^2}\right)^{-|l| - \frac{1}{2}} \quad (4.69)$$

Thus, for $r \rightarrow 0$ the contribution of states with angular momentum l to the propagator scales as $r^{|l|}$. So, the largest contribution comes from smallest $|l| = |n - Q|$. For $-\frac{1}{2} < Q < \frac{1}{2}$ smallest $|l|$ is given by setting $n = 0$, $l = -Q$. Hence, for $|Q| < 1/2$, and $r/r' \ll 1$,

$$D(r, r', \theta, \tau) \approx \frac{1}{4\pi r'} \left(\frac{r}{r'}\right)^{|Q|} e^{-iQ\theta} B_Q\left(\frac{\tau}{r'}\right) \quad (4.70)$$

For values of $|Q| > 1/2$ we simply periodize the eq. (4.70), since all physics in XY model is periodic in Q with period 1 (see discussion in previous section). From here on, we therefore confine our attention to $|Q| < 1/2$.

Thus, if we were to perform the OPE in Eq. (4.12) in the XY model

$$V(\vec{x}, \tau) \sim |\vec{x}|^{\Delta_{\text{imp}}^V} e^{-iQ\theta} V_{\text{imp}}(\tau) \quad \text{for } |\vec{x}| \rightarrow 0 \quad (4.71)$$

we would obtain for $|Q| < \frac{1}{2}$ in the free XY model,

$$\Delta_{\text{imp}}^V = |Q|. \quad (4.72)$$

We immediately see that the free theory is non-analytic in Q at $Q = 0$. By periodizing in Q , we also see that Δ_{imp}^V is non-analytic at $Q = \pm 1/2$. However, this later non-analyticity appears only after we take $r \rightarrow 0$ limit of the propagator, while we expect the non-analyticity at $Q = 0$ to persist in the propagator for arbitrary r, r' .

In fact, $Q = \frac{1}{2}$ is a very special point. At this point the $n = 0, l = -Q$ and $n = 1, l = 1 - Q$, i.e. $l = \pm 1/2$ terms in the sum (4.67) become equally important for $r/r' \rightarrow 0$. Thus, for $Q \rightarrow 1/2$ it makes sense to keep both terms in the asymptotic expansion of the propagator,

$$D(r, r', \theta, \tau) \approx \frac{1}{4\pi r'} \left(\left(\frac{r}{r'} \right)^Q e^{-iQ\theta} B_Q\left(\frac{\tau}{r'}\right) + \left(\frac{r}{r'} \right)^{1-Q} e^{-i(Q-1)\theta} B_{Q-1}\left(\frac{\tau}{r'}\right) \right) \quad (4.73)$$

and we may hypothesize the impurity OPE, for $Q \rightarrow 1/2$,

$$V(\vec{x}, \tau) \sim c_Q |\vec{x}|^{\Delta_Q^V} e^{-iQ\theta} V_Q(\tau) + c_{Q-1} |\vec{x}|^{\Delta_{Q-1}^V} e^{-i(Q-1)\theta} V_{Q-1}(\tau), \quad \text{for } |\vec{x}| \rightarrow 0 \quad (4.74)$$

where V_Q and V_{Q-1} are two impurity operators, with impurity anomalous dimensions Δ_Q^V and Δ_{Q-1}^V . In the free theory, $\Delta_Q^V = Q$ and $\Delta_{Q-1}^V = 1 - Q$. Hence, for $Q < 1/2$, $\Delta_Q^V < \Delta_{Q-1}^V$ and the operator V_Q is the most relevant as $|\vec{x}| \rightarrow 0$, while the operator V_{Q-1} provides a subleading correction. For $Q > 1/2$ the roles of these two operators are reversed. Finally, for $Q = 1/2$ the two operators have degenerate anomalous dimensions, $\Delta_{1/2}^V = \Delta_{-1/2}^V$ and,

$$V(\vec{x}, \tau) \sim c_{1/2} |\vec{x}|^{\Delta_{1/2}^V} e^{-i\theta/2} V_{1/2}(\tau) + c_{-1/2} |\vec{x}|^{\Delta_{-1/2}^V} e^{i\theta/2} V_{-1/2}(\tau), \quad \text{for } |\vec{x}| \rightarrow 0 \quad (4.75)$$

Physically, the $Q = 1/2$ point is special because the CP symmetry is effectively restored at it.⁴ Indeed, under CP, $Q \rightarrow -Q$. However, as already discussed, the universal physics is periodic in Q , so the points $Q = \pm 1/2$ are identified. Thus, the two impurity operators, $V_{\pm 1/2}$ are just CP conjugates of each other and must have the same impurity anomalous dimensions. Hence, although our original analysis was

⁴In $D = 3$ we take the P -parity symmetry to correspond to a reflection about one spatial axis, $\theta \rightarrow -\theta$ (a complete spatial inversion $\vec{x} \rightarrow -\vec{x}$ is a rotation in $2+1$ dimensions). The monopole field V is a pseudoscalar, which means that under charge conjugation C , $V \rightarrow V^\dagger$ and under P -parity, $V(x_1, x_2, x_3) \rightarrow V^\dagger(x_1, -x_2, x_3)$.

performed for the case of the free theory, we expect the conclusions to remain valid in the strongly interacting theory.

We remind the reader that even though the operator $V(x)$ is mathematically well defined by specifying the surface \mathcal{S} of the Wilson loop for arbitrary Q , it is not physical for non-integral Q . Indeed, a physical operator cannot obey twisted boundary conditions. However, for rational $Q = p/q$, the flux $2\pi q$ monopole operator $V^q(x) \sim (V(x))^q$ is well-defined on both sides of the duality. Using (4.60) and (4.70), we obtain the OPE,

$$V^q(\vec{x}, \tau) \sim |\vec{x}|^{\Delta_{\text{imp}}^V(q)} e^{-iqQ\theta} V_{\text{imp}}^q(\tau) \quad \text{for } |\vec{x}| \rightarrow 0 \quad (4.76)$$

with

$$\Delta_{\text{imp}}^V(q) = q|Q| \quad (4.77)$$

in the free XY theory for $|Q| < 1/2$. Since $qQ = p$ is an integer, the OPE (4.76) is invariant under $\theta \rightarrow \theta + 2\pi$, making the operator $V^q(x)$ single-valued, as required.

Having discussed the impurity OPEs, let us return to the calculation of electric field. Since we know that the electric field will be radial, we only need the $\hat{\theta}$ component of the magnetic field,

$$\begin{aligned} \langle -iF_\theta \rangle &= -2\pi i \frac{1}{r} \lim_{\theta \rightarrow \theta'} (\partial_\theta - \partial_{\theta'}) D(r = r', \theta - \theta', \tau = \tau') \\ &= -4\pi i \frac{1}{r} \lim_{\theta \rightarrow 0} \partial_\theta D(r = r', \theta, \tau = \tau') \end{aligned} \quad (4.78)$$

For this purpose, we don't need the propagator with $r/r' \ll 1$, but rather with $r \rightarrow r'$, $\tau \rightarrow \tau'$. We denote, $D(r, \theta) = D(r = r', \theta, \tau = \tau')$. Unfortunately, if we plug $r = r'$, $\tau = \tau'$ into the expression for propagator (4.67), the integral over v diverges. We expect that if we instead first keep $r - r'$, $\tau - \tau'$ finite, perform the integration over

v , sum over angular momenta l and only then take $r = r'$, $\tau = \tau'$, the divergence disappears. There are also other ways to regularize the propagator: e.g. make the integral over ω in (4.61) run over $D - 2$ dimensions. This would correspond to the XY model in D dimensions coupled to an external flux-tube (the flux-tube is a defect in 2 dimensions, so its world-volume is $D - 2$ dimensional). One then takes the limit $D \rightarrow 3$ at the end of the calculation. We have successfully used this method to compute the electric field (see Appendix C.1). The result for the coefficient $C(Q)$ of eq. (4.43) is,

$$C(Q) = \frac{1}{8}(1 - 2|Q|)^2 \tan(\pi Q), \quad |Q| < 1 \quad (4.79)$$

Thus, we see that the function $C(Q)$ is non-analytic at $Q = 0$. This analyticity occurs at non-leading order in Q ,

$$C(Q) \approx \frac{\pi}{8} Q(1 - 4|Q|), \quad Q \rightarrow 0 \quad (4.80)$$

The leading order term, $C(Q) \approx \frac{\pi}{8} Q$ is the one which would have been predicted by expanding the free theory perturbatively in Q .

One can also derive the result (4.79) in a different way, which can be more easily generalized from the free theory to the $1/M$ expansion in a strongly interacting theory. This calculation is based on the integral representation of the propagator of the twisted theory derived in Ref. [152]. We repeat the calculations of Ref. [152] in Appendix C.2 as in the next section we will need to generalize them for application in $1/M$ expansion. The result is,

$$D(r, \theta) = \frac{1}{4\pi r} \int_0^\infty d\nu \tanh(\pi\nu) U_\nu(\theta) \quad (4.81)$$

with,

$$U_\nu(\theta) = \frac{e^{-2\pi i Q \text{sgn}(\theta)} \sinh(\nu|\theta|) + \sinh(\nu(2\pi - |\theta|))}{\cosh(2\pi\nu) - \cos(2\pi Q)} \quad (4.82)$$

from which one recovers eq. (4.79) by using eq. (4.78), see Appendix C.2.

4.3.4 $1/M$ expansion of the dual theory

We now progress from the free XY model to the $1/M$ expansion of the strongly interacting theory. We take the Lagrangian to be,

$$L = |\partial_\mu V|^2 + i\lambda(|V|^2 - \frac{1}{g}) \quad (4.83)$$

Here V is an M component complex scalar and λ is a Lagrange multiplier, which enforces the local constraint,

$$|V|^2 = \frac{1}{g} \quad (4.84)$$

This hard constraint replaces the self-interaction of the V field. In the presence of an external charge in the direct theory, we take V to satisfy the twisted boundary conditions (4.42). In principle, we would like to solve the theory (4.83) in the limit $M \rightarrow 1$. However, practically we will only be able to perform computations at $M = \infty$.

We will be interested in the properties of the theory (4.42) at its critical point $g = g_c$. As is well known from standard $1/M$ expansion techniques, at $M = \infty$ the critical coupling is given by,

$$\frac{1}{Mg_c} = \frac{1}{M} \langle V^\dagger V \rangle = D(x = x') \quad (4.85)$$

where D is the usual massless 3D propagator,

$$D(x, x') = \frac{1}{4\pi|x - x'|} \quad (4.86)$$

Of course, the propagator with $x = x'$ in (4.85) is UV singular and has to be regularized. Since we will perform calculations of propagator in position space, it is convenient for us to use point-splitting regularization.

In the absence of the twisted boundary condition (4.42) and at the critical point, we perform the expansion around $\langle i\lambda \rangle = 0$ (so that the effective mass for the V particles vanishes). However, once Q is finite, $\lambda = 0$ is no longer sufficient to make the constraint (4.84) satisfied. Instead, the Lagrange multiplier acquires a spatial dependence

$$\langle i\lambda(\vec{x}, \tau) \rangle = \frac{a(Q)}{|\vec{x}|^2} \quad (4.87)$$

Here a is a universal function of the charge Q . The dependence on \vec{x} is determined from the canonical dimension of λ (λ acquires a non-trivial anomalous dimension only at order $1/M$). Thus, at finite Q , the propagator of V field satisfies,

$$\left(-\partial^2 + \frac{a(Q)}{|\vec{x}|^2}\right)D(x, x', Q) = \delta(x - x') \quad (4.88)$$

and $a(Q)$ should be determined self-consistently from the equation,

$$\frac{1}{Mg_c} = \frac{1}{M} \langle V^\dagger V \rangle_Q = D(x = x', Q) \quad (4.89)$$

Combining eqs. (4.85), (4.89),

$$\lim_{x \rightarrow x'} (D(x, x', Q) - D(x, x', Q = 0)) = 0 \quad (4.90)$$

Thus, the problem is reduced to finding the propagator $D(x, x', Q)$. Just as in the free case, we use spectral decomposition (4.62), and the radial functions $\phi_{l,E}(r)$ now satisfy,

$$\left(-\frac{1}{r} \frac{\partial}{\partial r} \left(r \frac{\partial}{\partial r}\right) + \frac{l^2 + a}{r^2}\right) \phi_{l,E}(r) = E \phi_{l,E}(r) \quad (4.91)$$

where again due to the twisted boundary conditions $l = n - Q$, $n \in \mathbb{Z}$. The solution to (4.91) is,

$$\phi_{l,E}(r) = \frac{1}{\sqrt{2}} J_{\sqrt{l^2+a}}(\sqrt{E}r) \quad (4.92)$$

Comparing the result above to free theory (4.65), we see that the only difference is in the replacement of the indices of Bessel functions $|l| \rightarrow \sqrt{l^2+a}$. Going from 2D to 3D propagator as in the free case (4.67),

$$D(r, r', \theta, \tau) = \frac{1}{4\pi r'} \sum_l e^{il\theta} \int_0^\infty dv J_{\sqrt{l^2+a}}\left(\frac{r}{r'}v\right) J_{\sqrt{l^2+a}}(v) \exp\left(-\frac{|\tau|}{r'}v\right) \quad (4.93)$$

Finally, expanding the propagator (4.93) for $r \ll r'$, we obtain the equivalent of (4.70),

$$D(r, r', \theta, \tau) \approx \frac{1}{4\pi r'} \left(\frac{r}{r'}\right)^{\sqrt{Q^2+a(Q)}} e^{-iQ\theta} B_{\sqrt{Q^2+a(Q)}}\left(\frac{\tau}{r'}\right), \quad |Q| < 1/2 \quad (4.94)$$

Thus, we recover the OPE (4.71), but the impurity exponent now becomes some nontrivial function of Q ,

$$\Delta_{\text{imp}}^V = \sqrt{Q^2 + a(Q)}, \quad |Q| < 1/2 \quad (4.95)$$

We note that, similar to the free case, as Q passes $1/2$, the most relevant angular momentum l in the sum (4.93) changes from $l = -1/2$ to $l = 1/2$, and at $Q = 1/2$ we have the OPE (4.75) with two degenerate impurity operators.

To find the nontrivial impurity exponent we need to solve eq. (4.90) for $a(Q)$. We are, therefore, after the propagator $D(x, x', Q)$ with $x \rightarrow x'$. We could, in principle proceed as in the free case. Namely, make our flux-tube uniform along $D - 2$ spatial dimensions (introducing a convergence factor v^{D-3} into (4.93)), perform the integrals in (4.93) with $r = r'$, $\tau = 0$, perform the sum over the angular momenta l , take

$\theta \rightarrow 0$ and $D \rightarrow 3$. However, unlike in the free case, the sums over angular momenta cannot be now performed analytically in terms of hypergeometric functions (with nice analytic continuation for $\theta \rightarrow 0$). The sum over l can still be performed numerically, however, the convergence is rather slow. Nevertheless, we have been able to determine $a(Q)$ numerically using this method. However, this method is less suitable for finding the electric field coefficient $C(Q)$, which requires us to differentiate the propagator at $\theta = 0$, making the convergence properties of the series even worse.

Instead, we shall use a different method, generalizing the integral form of the propagator (4.81) derived in Ref. [152] to the present problem. As shown in Appendix C.2, the twisted propagator at $M = \infty$ is given by,

$$D(r, \theta) = \frac{1}{4\pi r} \int_0^\infty d\nu \tanh(\pi\nu) \frac{\nu}{\sqrt{\nu^2 + a}} U_{\sqrt{\nu^2 + a}}(\theta) \quad (4.96)$$

with $U_\nu(\theta)$ still given by eq. (4.82).

Now, $a(Q)$ can be determined from (4.90),

$$\begin{aligned} 0 &= \lim_{\theta \rightarrow 0} (D(r, \theta, Q) - D(r, \theta, Q = 0)) \quad (4.97) \\ &= \frac{1}{4\pi r} \int_0^\infty d\nu \tanh(\pi\nu) \left(\frac{\nu}{\sqrt{\nu^2 + a}} \frac{\sinh(2\pi\sqrt{\nu^2 + a})}{\cosh(2\pi\sqrt{\nu^2 + a}) - \cos(2\pi Q)} - \frac{\sinh(2\pi\nu)}{\cosh(2\pi\nu) - 1} \right) \quad (4.98) \end{aligned}$$

Eq. (4.97) can be solved numerically for $a(Q)$. However, before we do this, let's verify our claim that $\langle i\lambda \rangle = 0$ (i.e. $a = 0$) is not sufficient to satisfy (4.89) for finite Q .

Indeed, from (4.97) we obtain

$$\begin{aligned} &\lim_{x \rightarrow x'} (D(x, x', Q, a = 0) - D(x, x', Q = 0)) = \frac{1}{M} (\langle V^\dagger V(x) \rangle_Q - \langle V^\dagger V(x) \rangle_{Q=0}) \\ &= \frac{1}{4\pi r} \int_0^\infty d\nu \frac{\cos(2\pi Q) - 1}{\cosh(2\pi\nu) - \cos(2\pi Q)} = -\frac{1}{8\pi r} (1 - 2|Q|) \tan(\pi|Q|), \quad |Q| < 1 \quad (4.99) \end{aligned}$$

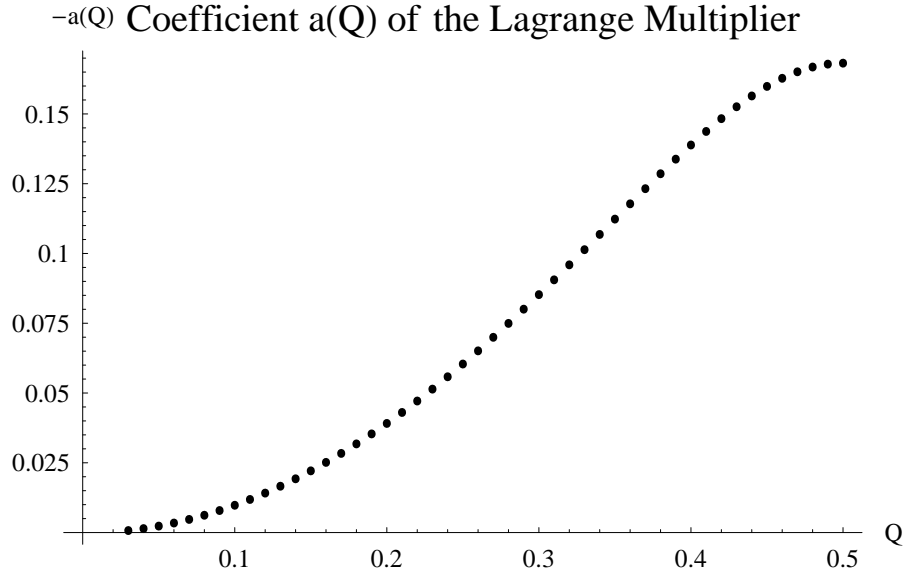


Figure 4.4: Coefficient $a(Q)$ of the Lagrange multiplier $\langle i\lambda(x) \rangle$, see eq. (4.87), in the $M = \infty$ generalization of the dual theory.

where expectation values in the first line of (4.99) are computed in the free theory. The precise value of expression (4.99) is not very important for our purposes (although it is curious to note that like many quantities in the free theory it is non-analytic in Q at $Q = 0$). What is important for us is that expression (4.99) is negative. This means that the twisted boundary condition effectively creates a repulsive barrier, leading to a decrease in $V^\dagger V$ compared to untwisted theory. To compensate for this decrease in the strongly interacting theory, we need $\langle i\lambda(x) \rangle$ to provide an attractive potential for V particles. Hence, we conclude that $a(Q) < 0$ for Q finite. One may be concerned that the square roots in expressions (4.96), (4.97) are ambiguous for $a < 0$ and $\nu^2 < |a|$. However, it turns out that these expressions do not depend on our choice of the sign for the square root as long as it is consistent. The numerical

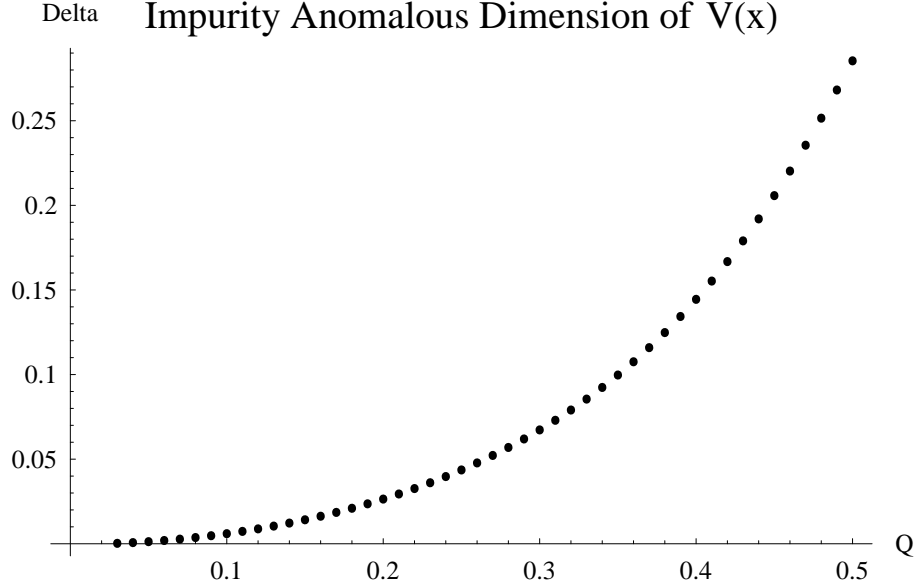


Figure 4.5: Impurity anomalous dimension Δ_{imp}^V of the monopole operator $V(x)$, see Eq. (4.71), computed in the $M = \infty$ generalization of the dual theory.

solution for $a(Q)$ is shown in Fig. 4.4. We note that this solution agrees with the one obtained using the spectral form of propagator (4.93).

One can also attempt to use eq. (4.97) to find a series solution for $a(Q)$ near $Q = 0$. It is easy to convince oneself that,

$$a(Q) \approx -Q^2, \quad Q \rightarrow 0 \tag{4.100}$$

Unfortunately, the integrand in eq. (4.97) is quite singular at $\nu \rightarrow 0$ for $a \rightarrow 0, Q \rightarrow 0$, so that a systematic series expansion beyond the leading order is not straight-forward. Nevertheless, we believe that such an expansion exists and $a(Q)$ is an analytic function of Q near $Q = 0$. Assuming such analyticity and using charge conjugation symmetry, $a(Q) = a(-Q)$, one obtains, $a(Q) \approx -Q^2 + c_4 Q^4$ for $Q \rightarrow 0$. Here c_4 is a positive constant as the integral (4.97) diverges for $a < -Q^2$.

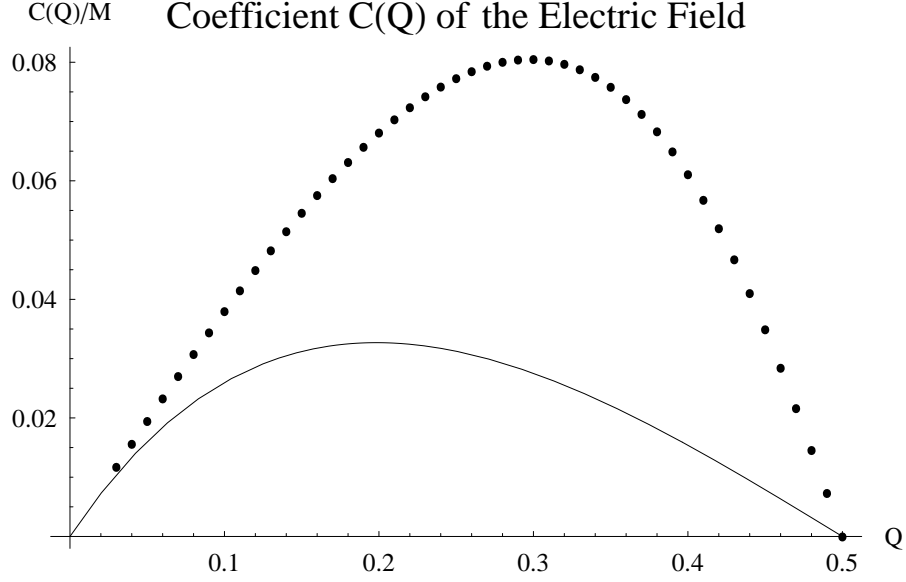


Figure 4.6: Coefficient $C(Q)$ of the electric field, see eq. (4.43). The dotted and solid curves correspond to the strongly interacting theory at $M = \infty$ and the free theory respectively.

Having found $a(Q)$ we immediately obtain the impurity anomalous dimension of the operator V (given by eq. (4.95)), see Fig. 4.5. This anomalous dimension is no longer the trivial value $\Delta_{\text{imp}}^V = |Q|$ of the free theory (4.72). Given the leading behaviour of $a(Q)$ as $Q \rightarrow 0$ (4.100) and assuming analyticity of $a(Q)$ we conclude that Δ_{imp}^V will also be analytic at $Q = 0$ (as opposed to the situation in the free theory). Moreover,

$$\Delta_{\text{imp}}^V \approx \sqrt{c_4} Q^2, \quad Q \rightarrow 0 \quad (4.101)$$

Finally, we can now compute the coefficient of the electric field $C(Q)$. For the M -field generalization of the dual theory, we define the magnetic field by the same equation (4.59) as for $M = 1$ theory, that is we consider the current associated with

the global $U(1)$ symmetry,

$$\begin{aligned} \langle -iF_\mu(x) \rangle &= \langle -2\pi i V_\alpha^\dagger \overleftrightarrow{\partial}_\mu V_\alpha(x) \rangle = -2\pi i \lim_{x \rightarrow y} (\partial_\mu^x - \partial_\mu^y) \langle V_\alpha(x) V_\alpha^\dagger(y) \rangle = \\ &- 2\pi i M \lim_{x \rightarrow y} (\partial_\mu^x - \partial_\mu^y) D(x, y) \end{aligned} \quad (4.102)$$

Due to our normalization of the $U(1)$ current, the electric field induced will be of order M . Now, differentiating $D(r, \theta)$ in (4.96) and taking the symmetric limit as $\theta \rightarrow 0$,

$$-i\partial_\theta D(r, 0) = -\frac{1}{4\pi r} \int_0^\infty d\nu \nu \tanh(\pi\nu) \frac{\sin(2\pi Q)}{\cosh(2\pi\sqrt{\nu^2 + a}) - \cos(2\pi Q)} \quad (4.103)$$

Using the values of $a(Q)$ found earlier (Fig. 4.4) and evaluating the integral (4.103) numerically we obtain the coefficient $C(Q)$, shown in Fig. 4.6 (dotted curve). Fig. 4.6 also shows the value of $C(Q)$ in the free theory (4.79) for comparison (solid line).

Alternatively, we can use (4.103) to expand $C(Q)$ in a series in Q . Using the leading behaviour (4.100), we find,

$$C(Q) \approx M \left(\frac{\pi Q}{8} + \mathcal{O}(Q^3) \right), \quad Q \rightarrow 0 \quad (4.104)$$

We see that the leading term in (4.104) agrees with the one, which would be obtained by perturbation theory in Q in the large M limit (4.49), (4.57). It is also interesting to compare eq. (4.104) to asymptotic behaviour of $C(Q)$ in the free theory (4.80). We see that the leading term $C(Q)/M \approx \pi Q/8$ in both cases is the same, however, the subleading terms are different. The first subleading term in the free theory is non-analytic $\sim |Q|Q$, as opposed to the strongly interacting theory's analytic $\mathcal{O}(Q^3)$. Thus, we have been able to verify that the leading non-analyticity of $C(Q)$ in the free theory disappears in the interacting theory. We actually expect that the interacting theory cures itself of non-analyticities in Q at all orders in Q .

Finally, let us discuss impurity anomalous dimensions of higher flux operators $V^q(x)$ for rational $Q = p/q$, as these are actual physical observables on the QED side of the duality. Once we go from $M = 1$ dual theory to its large M counterpart, there are many possible generalizations of the $V^q(x)$ operator. Indeed, we can form different $SU(M)$ multiplets out of q instances of $SU(M)$ fundamental $V_\alpha(x)$. We expect that these multiplets will have different (impurity) anomalous dimensions for M finite. However, for $M = \infty$ all of these operators will have degenerate (impurity) anomalous dimensions. We can consider, for instance, the completely symmetric representation $V_S^q(x) = (V_\alpha(x))^q$, where α is some fixed index (no summation over α). Then, for $M = \infty$,

$$\langle V_S^q(x)(V_S^q(y))^\dagger \rangle = q!(D(x-y))^q \quad (4.105)$$

Hence, just as in the free case, the operator $V_S^q(x)$ has the impurity OPE (4.76) with the corresponding impurity anomalous dimension,

$$\Delta_{\text{imp}}^V(q) = q\Delta_{\text{imp}}^V \quad (4.106)$$

4.4 Easy plane theory for general N

We now turn to the general case of the model $\mathcal{S} + \mathcal{S}_{\text{imp}}$ with a global $U(1)^{N-1}$ symmetry. The results of the previous section with $N = 1$ can be rapidly generalized, and will lead to a quantitative result for the scaling dimension of the monopole/VBS operator V near the impurity.

4.4.1 Duality in the Easy Plane Theory

In this section, we consider a theory with N flavours of spinon fields z_α (N does not necessarily have to be large),

$$L = \frac{1}{2e^2} F_\mu^2 + |(\partial_\mu - iA_\mu)z_\alpha|^2 + U(z_\alpha) \quad (4.107)$$

Here, U is some potential with the global $U(1)^N$ symmetry under independent phase rotations of the z_α fields. The singlet component of this symmetry is actually gauged by the field A_μ ,

$$U(1) : z_\alpha \rightarrow e^{i\theta(x)} z_\alpha, \quad A_\mu \rightarrow A_\mu + \partial_\mu \theta \quad (4.108)$$

while the non-singlet components are true global symmetries of the theory,

$$U(1)^{N-1} : z_\alpha \rightarrow e^{i\theta^a t_\alpha^a} z_\alpha \quad (4.109)$$

where t^a , $a = 1..N-1$ are the generators of the $U(1)^{N-1}$ symmetry satisfying, $\sum_\alpha t_\alpha^a = 0$. We require U to have a symmetry under the permutation of labels of z_α fields. We choose U in such a fashion that in the “condensed” phase of the theory, it favours non-zero expectation values of all components of the z_α field, so that the vacuum manifold of the theory is a torus, $(S^1)^N$ (here we temporarily forget that the singlet symmetry is gauged). For $N = 2$ the theory under consideration is believed to describe the phase transition in the easy-plane antiferromagnet.

We would like to dualize the theory (4.107). Similar theories were dualized in Ref. [134, 51, 153, 154, 155], and here we will present a related discussion. An exact duality on the lattice appears in Ref. [148], but we can write down the form of the dual action from very general considerations. Let us first identify the dual degrees of freedom. We go to the condensed phase of the theory (4.107), where all $\langle z_\alpha \rangle \neq 0$.

Then, we can have vortices in any component of the z_α field. Formally, the homotopy group, $\pi_1((S^1)^N) = \mathbb{Z}^N$. So, we have N types of vortices, which become the degrees of freedom of the dual theory V_α , $\alpha = 1..N$.

These vortices are global, rather than local. Indeed, let's consider a vortex in the first component z_1 ,

$$z_1(\vec{x}) \sim v e^{i\lambda(\vec{x})}, \quad z_\alpha \sim v, \alpha \neq 1, \quad |\vec{x}| \rightarrow \infty \quad (4.110)$$

where $\lambda(\vec{x})$ winds from 0 to 2π as one goes around a contour out at infinity surrounding the vortex. Then, this vortex corresponds to a space-time dependent transformation of the vacuum (4.108), (4.109), with, $\theta(\vec{x}) = \frac{1}{N}\lambda(\vec{x})$ and $\theta^a(\vec{x})t^a = (1-1/N, -1/N, \dots -1/N)\lambda(\vec{x})$. Thus, our vortex possesses a winding both in the local and in the global symmetry group. The winding in the local $U(1)$ group will be canceled by the gauge field,

$$A_\mu(x) = \partial_\mu\theta(x) = \frac{1}{N}\partial_\mu\lambda(x) \quad (4.111)$$

hence our global vortices carry a magnetic flux $\Phi = 2\pi/N$. [156, 157] Therefore, under the flux symmetry (4.28), the fields V_α should transform as,

$$V_\alpha(x) \rightarrow e^{2\pi i\alpha(x)/N} V_\alpha(x) \quad (4.112)$$

This fact will be crucial for the analysis to follow.

The winding in the global group will lead to a long-range Coulombic interaction between our vortices. We will need dynamical gauge fields in the dual theory to give rise to this interaction. However, if we have a unit winding in each component of the z field, our vortex becomes completely local, and carries total flux 2π . We can think of such a local vortex as a composite of N global vortices of different types. The

creation operator for this flux-tube, therefore, will be,

$$\mathcal{V}(x) = \prod_{\alpha} V_{\alpha}(x) \quad (4.113)$$

Since the local vortex carries flux 2π , we can also associate the operator (4.113) with the monopole operator of the direct theory. Indeed, given (4.112), under the flux symmetry (4.28),

$$\mathcal{V}(x) \rightarrow e^{2\pi i \alpha(x)} \mathcal{V}(x) \quad (4.114)$$

which is the correct transformation law for the monopole operator (4.30).

We expect local vortices to interact by short range forces. Therefore, the operator (4.113) should not be charged under the emergent gauge fields of the dual theory.

We are now ready to write down the dual theory,

$$L = \frac{1}{2\tilde{e}^2} \sum_i (F_{\mu}^{\alpha})^2 + |(\partial_{\mu} - iB_{\mu}^{\alpha} - \frac{2\pi i}{N} H_{\mu}) V_{\alpha}|^2 + \tilde{U}(V_{\alpha}) \quad (4.115)$$

Here $B_{\mu}^{\alpha} = B_{\mu}^a t_{\alpha}^a$, $a = 1..N - 1$, are emergent dual gauge fields, which couple to the non-singlet currents. $F^{\alpha} = \epsilon_{\mu\nu\lambda} \partial_{\nu} B_{\lambda}^{\alpha}$ are the corresponding field strengths. The dual potential $\tilde{U}(V_{\alpha})$ is chosen to have the same properties as the direct potential U : it has a $U(1)^N$ symmetry under independent phase rotations of the fields V_{α} and a symmetry under permutation of labels of V_{α} fields. Moreover, it favours $\langle V_{\alpha} \rangle \neq 0$ for all α in the condensed phase of the dual theory. Thus, the theory (4.115) has a local $U(1)^{N-1}$ symmetry,

$$U(1)^{N-1} : \quad V_{\alpha}(x) \rightarrow e^{i\phi^{\alpha}(x)t_{\alpha}^a} V_{\alpha}(x), \quad B_{\mu}^a \rightarrow B_{\mu}^a + \partial_{\mu}\phi^a \quad (4.116)$$

as well as the global $U(1)$ flux symmetry of the direct theory (4.112) (which we have promoted to a local symmetry by introducing a non-dynamical source field H_{μ}).

As required, the monopole operator (4.113) is invariant under the local $U(1)^{N-1}$ symmetry of the dual theory (4.116).

The theory (4.115) also has a global $U(1)^{N-1}$ symmetry associated with conservation of fluxes of the $N - 1$ emergent gauge fields. This topological symmetry can be identified with the Noether's symmetry (4.109) of the direct theory.

4.4.2 Wilson loops in the easy plane theory

Now, we would like to apply the duality discussed in the previous sections to study the properties of Wilson loops in the $U(1)^{N-1}$ symmetric theory (4.107). Recall, that to represent Wilson loops we must use a source field H_μ given by (4.34). As discussed for the case of $N = 1$ theory, the effect of such a source field on the dual action (4.115) is to introduce a twisted boundary condition for the vortex fields,

$$V_\alpha(\theta = 2\pi) = e^{-2\pi i Q/N} V_\alpha(\theta = 0) \quad (4.117)$$

where Q is the charge of our Wilson line. The physical origin of the factor $1/N$ is the fractional charge $2\pi/N$ of the vortex fields V_α under the flux symmetry. Thus, we come to the amazing conclusion that the universal physics in the planar model is periodic in the charge Q of the Wilson line, with period $Q = N$. This is a generalization of the $Q = 1$ periodicity of single flavour QED discussed before. As explained in Ref. [148], we expect that this $Q \sim N$ periodicity is a feature of the easy plane theory and does not generalize to the case with the full $SU(N)$ invariance.

Now, we would like to discuss more quantitative features of Wilson loops in the planar model. In particular, we would like to find the impurity anomalous dimension of the monopole operator (4.71) and the coefficient of the electric field (4.43) at the

critical point of the theory. We note that as in the $N = 1$ case, we can easily dualize the magnetic field by differentiating the dual action with respect to the source field H_μ ,

$$\langle -iF_\mu \rangle = \frac{(-2\pi i)}{N} \langle V_\alpha^\dagger \overleftrightarrow{D}_\mu V_\alpha \rangle \quad (4.118)$$

with $D_\mu V_\alpha = (\partial_\mu - iB_\mu^\alpha - \frac{2\pi i}{N} H_\mu) V_\alpha$.

To find Δ_{imp}^V and $C(Q)$, we follow the procedure established for the $N = 1$ case in section 4.3.4 and perform a large M expansion of the dual theory (4.115). Namely, we promote each field V_α to an $SU(M)$ multiplet, V_α^i , $i = 1..M$. Moreover, we replace the soft potential $\tilde{U}(V_\alpha)$ by a hard constraint, $\sum_i |V_\alpha^i|^2 = 1/g$, for each $\alpha = 1..N$. This constraint will be enforced by a set of N Lagrange multipliers λ_α . Thus, our Lagrangian becomes,

$$L = \sum_{\alpha,i} |(\partial_\mu - iB_\mu^\alpha - \frac{2\pi i}{N} H_\mu) V_\alpha^i|^2 + \sum_{\alpha,i} i\lambda_\alpha (|V_\alpha^i|^2 - \frac{1}{g}) \quad (4.119)$$

In (4.119) we have also dropped the kinetic term for the gauge fields, as near the critical point such operators will be irrelevant. In addition to the $U(1)_\Phi$ global flux symmetry and the $U(1)^{N-1}$ local symmetry of the original $M = 1$ action, the theory (4.119) also has a $SU(M)^N$ global symmetry under independent $SU(M)$ rotations of the N M -tuplets V_α^i . We note that the various $SU(M)$ multiplets talk to each other only through the gauge fields B_μ^α .

We would like to generalize the observables of the $M = 1$ theory to the large M case. The magnetic field (4.118) is generalized trivially,

$$\langle -iF_\mu \rangle = \frac{(-2\pi i)}{N} \langle (V_\alpha^i)^\dagger \overleftrightarrow{D}_\mu V_\alpha^i \rangle \quad (4.120)$$

The monopole operator (4.113) on the other hand, now carries indices under the

$SU(M)^N$ group,

$$\mathcal{V}(x)_{i_1..i_N} = \prod_{\alpha} V_{\alpha}^{i_{\alpha}}(x) \quad (4.121)$$

The insertion of the Wilson loop source H_{μ} is again equivalent to the twisted boundary condition (4.117).

We now perform a large M expansion of the theory (4.119) with the twisted boundary condition (4.117), keeping N fixed. We will be only able to make computations for $M = \infty$. We are interested in the physics at the critical point. We expand the theory about the saddle point $B_{\mu}^{\alpha} = 0$ (this is a saddle point as the twisted boundary condition (4.117) does not couple to the non-singlet sectors of the theory⁵). As usual, the fluctuations of these gauge fields about the saddle point will be suppressed by powers of $1/M$. Thus, at $M = \infty$, we are left with N decoupled instances of the Lagrangian (4.83) that has been discussed at length for the case of $N = 1$ theory. The only difference is the replacement, $Q \rightarrow Q/N$ in the boundary condition (4.42). Hence, we conclude,

$$\langle \mathcal{V}(x)_{i_1..i_N} \mathcal{V}^{\dagger}(x')_{j_1..j_N} \rangle \stackrel{M \rightarrow \infty}{=} \prod_{\alpha} \langle V_{\alpha}^{i_{\alpha}}(x) (V_{\alpha}^{j_{\alpha}})^{\dagger}(x') \rangle = D(x, y, Q/N)^N \prod_{\alpha} \delta_{i_{\alpha} j_{\alpha}} \quad (4.122)$$

where $D(x, x', Q)$ is the propagator in the $N = 1$ theory (4.83) with the twisted boundary condition (4.42) at $M = \infty$. The asymptotic behaviour of this propagator for $r \ll r'$ is given in eq. (4.94). Thus, the asymptotic behaviour of the correlation

⁵In reality, we expect a non-zero B_{μ}^{α} , corresponding to finite flavour charge density of the direct theory. Indeed, we expect that the external charge will be screened in the direct theory by a flavoured spinon z_{α} . The associated flavour charge density (magnetization) in the $SU(N)$ symmetric case has been discussed in Ref. [143]. However, at the critical point, the screening cloud will be distributed over the whole size of the system. Therefore, the corresponding (finite) flux density will be non-intensive and will not affect intensive observables such as Δ_{imp}^V and $C(Q)$.

function (4.122) for $r \ll r'$ is

$$\langle \mathcal{V}(x)_{i_1 \dots i_N} \mathcal{V}^\dagger(x')_{j_1 \dots j_N} \rangle \approx \left(\frac{1}{4\pi r'} \right)^N \left(\frac{r}{r'} \right)^{N\sqrt{(Q/N)^2 + a(Q/N)}} e^{-iQ\theta} G(\tau/r') \prod_{\alpha} \delta_{i_{\alpha} j_{\alpha}},$$

$|Q/N| < 1/2$

where G is some (known) function. Hence, the monopole operator $\mathcal{V}(x)$ in the planar N component theory has the impurity OPE,

$$\mathcal{V}(\vec{x}, \tau) \sim |\vec{x}|^{\Delta_{\text{imp}}^{\mathcal{V}}} e^{-iQ\theta} \mathcal{V}_{\text{imp}}(\tau) \quad \text{for } |\vec{x}| \rightarrow 0 \quad (4.123)$$

with

$$\Delta_{\text{imp}}^{\mathcal{V}} = N\sqrt{(Q/N)^2 + a(Q/N)} = N\Delta_{N=1}^{\mathcal{V}}(Q/N), \quad |Q/N| < 1/2 \quad (4.124)$$

where the monopole impurity anomalous dimension $\Delta_{N=1}^{\mathcal{V}}(Q)$ in the $N = 1, M = \infty$ theory is given by Fig. 4.5.

From OPE (4.123), we observe that for integer Q the monopole operator is single valued under $\theta \rightarrow \theta + 2\pi$, even though the dynamical fields of the theory V_{α} obey twisted boundary conditions (4.117). We also note that formulas (4.123) and (4.124) are correct only for $|Q/N| < 1/2$; for other values of Q they should be extended by periodicity $Q \sim Q + N$.

We can now take the $N \rightarrow \infty, Q$ -fixed limit of (4.124). Using the asymptotic behaviour (4.101), $\Delta_{\text{imp}}^{\mathcal{V}} \sim Q^2/N$. Thus, the impurity anomalous dimension of the monopole operator is of order $\mathcal{O}(1/N)$ for $N \rightarrow \infty$ in the easy plane theory. It is interesting to note that, as discussed in section 4.2, this is also true of the theory with a full $SU(N)$ symmetry. At this point, it is not clear whether this is just a coincidence.

Finally, let us discuss the special point $Q/N = 1/2$. Our interest in this point is not purely academic, as we expect $N = 2$, $Q = 1$ to correspond to the physical case of a single impurity in an easy plane antiferromagnet or superfluid. We recall that at this point the propagator $D(r, r', \theta, \tau)$ for $r \ll r'$ is dominated by two angular momenta, $l = \pm 1/2$,

$$D(r, r', \theta, \tau) \approx \frac{1}{4\pi r'} \left(\frac{r}{r'}\right)^{\sqrt{1/4+a(1/2)}} (e^{i\theta/2} + e^{-i\theta/2}) B_{\sqrt{1/4+a(1/2)}}\left(\frac{\tau}{r'}\right) \quad (4.125)$$

So that

$$D(r, r', \theta, \tau)^N \approx \left(\frac{1}{4\pi r'}\right)^N \left(\frac{r}{r'}\right)^{N\sqrt{1/4+a(1/2)}} \sum_{m=0}^{2Q} \binom{2Q}{m} e^{i(m-Q)\theta} G(\tau/r') \quad (4.126)$$

Hence, using (4.122), the correlation function of two monopole operators is dominated by angular momenta $l = -Q, -Q + 1, \dots, Q - 1, Q$ for $r \ll r'$. So, we conjecture the operator product expansion,

$$\mathcal{V}(\vec{x}, \tau) \sim \sum_{l=-Q}^Q c_l |\vec{x}|^{\Delta_l^{\mathcal{V}}} e^{-il\theta} \mathcal{V}_l(\tau) \quad \text{for } |\vec{x}| \rightarrow 0 \quad (4.127)$$

At $M = \infty$ all the operators \mathcal{V}_l have degenerate impurity anomalous dimensions $\Delta_l^{\mathcal{V}}$. As discussed in section 4.3.3, the anomalous dimensions of operators with opposite angular momenta are equal by CP symmetry emergent at the $Q/N = 1/2$ point. However, there is no fundamental reason why anomalous dimensions of operators with different values of l should be equal. Thus, we expect the degeneracy to be lifted at higher orders in $1/M$ expansion. Therefore, unfortunately, the question of whether the OPE (4.127) will be dominated by $l = 0$ or by finite l is beyond the reach of our calculation. Nevertheless, our calculation at $M = \infty$ predicts for the physically relevant case of $N = 2$, $Q = 1$,

$$\Delta_{\text{imp}}^{\mathcal{V}} \approx 0.57, \quad N = 2, Q = 1 \quad (4.128)$$

The emergent CP symmetry at the point $Q/N = 1/2$ means that quantum fluctuations manage to render the states of Figs. 4.2 and Fig. 4.3 degenerate in the long-wavelength limit. We remind the reader the CP symmetry is due to the emergent $Q \sim N$ periodicity of the easy plane theory. No such periodicity is expected to occur in the full $SU(N)$ symmetric theory, where the impurity OPE is dominated by a single operator with a definite angular momentum as in eq. (4.12).

For completeness sake, we also discuss the coefficient $C(Q)$ of the electric field. From eq. (4.120) at $M = \infty$ we obtain,

$$C(Q) = C_{N=1}(Q/N) \tag{4.129}$$

where the coefficient $C_{N=1}(Q)$ in the $N = 1, M = \infty$ theory is given by Fig. 4.6. We note that for $Q/N = 1/2$ the electric field vanishes, as it should, by the emergent CP symmetry.

4.5 Conclusion

This chapter began with the theory \mathcal{S} in Eq. (4.1) for square lattice quantum antiferromagnets in the vicinity of a Néel-VBS quantum phase transitions. We considered generic local deformations of the antiferromagnet, and argued that they could be classified into two categories. The first category, illustrated in Fig. 4.1, is a modulated exchange impurity: we found an enhancement of VBS order, characterized by the exponent in Eq. 4.9. The second category was realized by a missing or additional spin (*e.g.* Zn or Ni impurities on Cu sites), shown in Fig. 4.2. For this case we found that VBS order was suppressed by the appearance of a VBS vortex, as in Fig. 4.2,

and characterized by the scaling properties discussed in Section 4.1.2.

The results of this chapter should be useful in numerical studies of the quantum phase transition between the Néel and VBS state [57, 58]. By enhancing an exchange constant as in Fig. 4.1, and measuring the decay of the average VBS order parameter away from the impurity, the exponent Δ^V can be estimated from Eqs. (4.6-4.9). There will be no mean VBS order in the vicinity of a missing spin impurity as in Fig. 4.2. However, the spatial dependence in the VBS susceptibility is fixed by Δ_{imp}^V in Eq. (4.12). The positive value of Δ_{imp}^V indicates that the VBS susceptibility should be suppressed near such an impurity.

In STM studies of the cuprates, we have noted earlier the demonstration of bond-centered charge order in the local density of states by Kohsaka *et al.* [12]. A numerical analysis of the pinning of such charge order by modulated exchange impurities (in the class in Section 4.1.1) has also been carried out [130, 131]. However, it is also experimentally possible to induce “missing spin” impurities (in the class of Section 4.1.2) by replacing the Cu sites with Zn and Ni impurities. There have been STM studies of such impurities [100, 101, 102], and it would be of great interest to carefully examine the nature of the bond-centered modulations in the vicinity of such impurities. If we assume that the “stripe” instability is primarily associated with the appearance of magnetic order [158, 159, 160, 161, 162], then the theory of the enhancement of magnetic order near such impurities [121, 143] should apply: we should therefore expect an increase in the strength of the density of states modulations in this model. In contrast, if we assume a VBS theory of the modulations, then in the impurity model of Section 4.1.2, the bond-centered modulations should be suppressed. The

experimental situation could well include both effects, complicating the interpretation. However, evidence for VBS vortex configurations like those in Fig. 4.2 would lend strong support to the VBS theory.

Chapter 5

Edge response in two-dimensional quantum antiferromagnets

Motivated by recent Monte-Carlo simulations of Höglund and Sandvik[4], we study edge response in square lattice quantum antiferromagnets. We use the $O(3)$ non-linear σ -model to compute the decay asymptotics of the staggered magnetization, energy density and local magnetic susceptibility away from the edge. We find that the total edge susceptibility is negative and diverges logarithmically as the temperature $T \rightarrow 0$. We confirm the predictions of the continuum theory by performing a $1/S$ expansion of the microscopic Heisenberg model with the edge. We propose a qualitative explanation of the edge dimerization seen in Monte-Carlo simulations by a theory of valence-bond-solid correlations in the Néel state.

5.1 Introduction

The Heisenberg antiferromagnet on a square lattice is one of the best known model magnetic systems. It has been studied extensively both numerically by quantum Monte-Carlo and analytically by $1/S$ expansion and field-theoretic methods. It

is known to have an ordered ground state at zero temperature with the staggered magnetization reduced by quantum fluctuations to $N_b = \langle N \rangle = 0.307$ for the spin $S = 1/2$. [47]

Despite many years of study, the simple Heisenberg model does not cease to surprise us. Recent Monte-Carlo simulations [4] on the $S = 1/2$ model have shown that the edge response in this system is very peculiar. In particular, a negative edge susceptibility is observed at low temperatures. This result is in contrast with an intuitive picture of a “dangling” edge spin. In this picture a spin at the edge, having fewer neighbors than bulk spins, is more loosely coupled and, hence, fluctuates more, leading to an enhancement in the susceptibility. The simulation of local susceptibility near the edge shows that the negative sign of edge susceptibility does not come from the edge spins per se, whose susceptibility is, indeed, enhanced, but rather from a tail in the response decaying away from the edge. Another curious effect observed in Ref. [4] is the dimerization of bond response near the edge, leading to the appearance of a comb-like structure, as in Fig. 5.1. The tendency to dimerize into singlets near the edge was argued in Ref. [4] to be the source of negative edge susceptibility.

In the present chapter, we study large-distance asymptotics of the edge response of a square lattice quantum antiferromagnet by means of an effective $O(3)$ σ -model description. This field-theoretic method is an expansion in powers of energy and momentum, with the microscopic physics entering at each order through a finite number of parameters, such as the spin-wave velocity c , the spin stiffness ρ_s and the value of the staggered moment N_b .¹ The $O(3)$ σ -model has proved powerful

¹We will use the subscript b from here on to denote bulk properties.

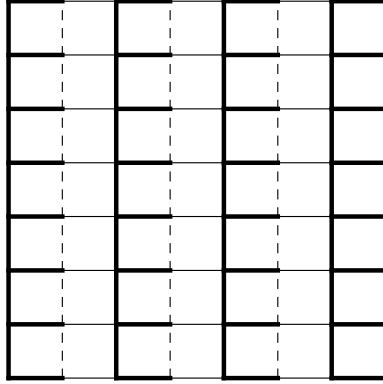


Figure 5.1: A schematic picture of the comb structure in bond strengths observed in Monte-Carlo simulations [4], with a free edge on the left side.

for studying finite temperature/size effects, which typically lead to a crossover into an $O(3)$ model of lower dimension.[7] It turns out to be also useful for studying the edge behaviour, particularly as no new parameters beyond the bulk ones are needed to describe the leading low temperature, large distance asymptotics in the edge response. We concentrate our attention on the staggered moment $\langle N(\mathbf{x}) \rangle$, the local energy density $\langle \epsilon(\mathbf{x}) \rangle$ and the local magnetic susceptibility $\chi_{\perp}(\mathbf{x})$. We show that at zero temperature these quantities approach their bulk values away from the edge with simple power law forms,

$$\frac{\langle N(\mathbf{x}) \rangle - N_b}{N_b} = -\frac{c}{8\pi\rho_s x} \quad (5.1)$$

$$\langle \epsilon(\mathbf{x}) \rangle - \epsilon_b = \frac{c}{16\pi x^3} \quad (5.2)$$

$$\chi_{\perp}(\mathbf{x}) - \chi_{\perp,b} = -\frac{1}{8\pi x c} \quad (5.3)$$

where x is the distance to the edge. Integrating eq. (5.3), we conclude that the total edge susceptibility per unit edge length is negative and diverges logarithmically with

the system size,

$$\chi_{\perp,\text{edge}} = -\frac{1}{8\pi c} \log(L/a) \quad (5.4)$$

We show that at finite temperature the $1/x$ power law in the susceptibility (5.3) is cut-off for distances larger than the thermal wave-length, $x \gtrsim c/T$, leading to the total edge susceptibility,

$$\chi_{\perp,\text{edge}} = -\frac{1}{8\pi c} \log(c/Ta) \quad (5.5)$$

Such a log divergent susceptibility is indeed seen in the Monte Carlo simulations [4]. For the co-efficient of the logarithm in $\chi_{\text{edge}} = (2/3)\chi_{\perp,\text{edge}}$, with $c = 1.69J$, we find $-0.0157/J$, while the Monte Carlo has a best fit value of $-0.0182/J$ (see Fig. 5.2). This is in reasonable agreement, with the difference probably attributable

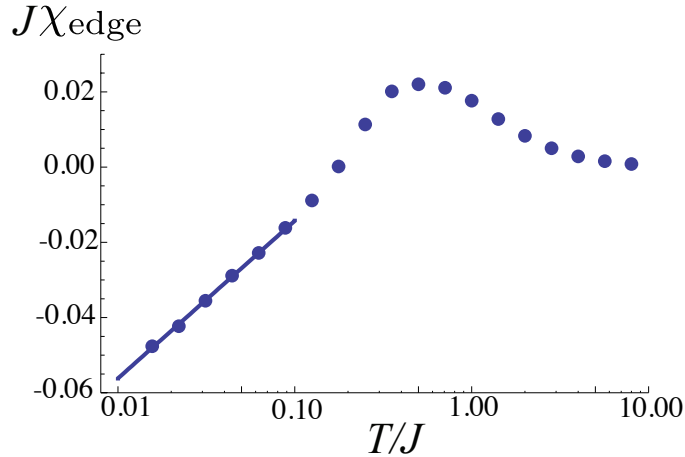


Figure 5.2: Edge susceptibility: Comparison of the Monte Carlo data of Ref. [4] (dots) with the best fit line $J\chi_{\text{edge}} = -0.0182 \log(0.219J/T)$ to the low T data.

to difficulties in numerically reaching the asymptotic low T limit.

As for the edge comb structure seen in Ref. [4], this is a short distance phenomenon, which cannot be studied within our continuum $O(3)$ σ -model. In fact, the

standard, “perturbative” treatment of the $O(3)$ model describes only the low-energy excitations which live near the wave-vector (π, π) and cannot provide any information about valence-bond-solid correlations, which live near $(\pi, 0)$ and $(0, \pi)$. Because these correlations are gapped in the antiferromagnet, they must decay exponentially away from the edge, as seen in Monte-Carlo. To capture the short-distance physics, we have performed a $1/S$ expansion of the Heisenberg model on the lattice with an edge. We find the large-distance asymptotics in agreement with the predictions of our continuum theory. However, we don’t reproduce the multiple short-distance oscillations of bond energies away from the edge seen by Monte-Carlo. Instead, we find that the bonds touching the edge are stronger than the bulk ones, while all the subsequent bonds are weaker. We conclude that the edge dimerization is, likely, a *non-perturbative effect* in $1/S$, which is invisible in the spin-wave expansion. It is remarkable that such non-perturbative effects are present in the simple $S = 1/2$ Heisenberg model, where the $1/S$ expansion yields quantitatively accurate results for many quantities.

In principle, one may be able to explicitly incorporate the non-perturbative physics in the form of hedgehogs into the semi-classical, large S treatment of the Heisenberg model. The hedgehog configurations are relevant for the dimerization physics, as they carry Berry phases,[50] which endow them with non-trivial quantum numbers under the lattice symmetry.[21, 22] However, studying the hedgehog contribution to the edge physics is technically intractable.

Instead, we pursue a more phenomenological approach, in which we assume that the system possesses a dynamical valence-bond-solid order parameter with a large

correlation length. This assumption is justified close to a phase transition into a valence-bond-solid phase, which can be tuned by adding additional frustrating interactions to the Heisenberg model.[57, 58] Moreover, even for the pure, nearest neighbour Heisenberg model with $S = 1/2$, it has been argued long ago[163] that the quantum fluctuations are strong enough that the system is “proximate” to a phase transition at which the magnetic order is lost. This proximity is manifested by the existence of an intermediate temperature window, dominated by the quantum critical point (the low temperature physics is dominated by the antiferromagnet, while the high temperature physics is dominated by the non-universal lattice effects). The observation of edge dimerization over more than 5 lattice spacings in the latest Monte Carlo simulations implies that the correlation length of the valence-bond-solid order parameter in the $S = 1/2$ Heisenberg model is rather large, further supporting the proximity to a phase transition.

We show that the comb structure of the bond order seen in Monte-Carlo simulations can be qualitatively understood in the quantum critical language. The particular details of the critical theory are not very important for this purpose - the physics can be read off straight-forwardly from the transformation properties of observables under the lattice symmetry. In particular, we demonstrate that close to the critical point the oscillations of bonds perpendicular to the edge and lines parallel to the edge in the comb can be related to each other.

This chapter is organized as follows. Section 5.2.1 is devoted to the description of the edge in the framework of the $O(3)$ model at zero temperature. In section 5.2.2 we discuss the crossover of edge susceptibility to finite temperature. In section 5.3

we perform the large S expansion of the Heisenberg model with an edge. In section 5.4 we discuss edge dimerization in a quantum antiferromagnet in the proximity to a phase transition into a valence-bond-solid. Some concluding remarks are presented in section 5.5.

5.2 Edge response in the $O(3)$ σ -model

5.2.1 Zero Temperature

In this section we discuss the large distance asymptotic behaviour away from the edge of the staggered moment, local uniform susceptibility and the bond energies using the continuum $O(3)$ σ -model. The advantage of this approach is that the results obtained are exact, depending only on a few phenomenological parameters, such as spin-wave velocity c , spin-stiffness ρ_s and bulk staggered moment N_b . These parameters are known from $1/S$ -expansion and Monte-Carlo simulations.

The σ -model action for the local order parameter \vec{n} , satisfying $\vec{n}^2 = 1$, is

$$S = \frac{\rho_s^0}{2} \int d^3x (\partial_\mu \vec{n})^2 \quad (5.6)$$

Here, μ runs over the three indices of the space-time coordinate $x = (\mathbf{x}, y, \tau)$, ρ_s^0 is the “bare” spin stiffness (we will discuss the renormalization process shortly) and we have set $c = 1$, we will restore c at the end of the computations. To introduce the edge, we consider this model on the half-plane $x \geq 0$. Thus, x is the coordinate perpendicular to the edge and y is the coordinate along the edge. In addition to the bulk action (5.6), we also have to consider boundary perturbations. The simplest terms allowed

by symmetries are,

$$S_{\text{bound}} = \sum_{\mu} g_{\mu} \int dy d\tau (\partial_{\mu} \vec{n})^2 \Big|_{x=0} \quad (5.7)$$

where g_{μ} are some coupling constants. These terms are irrelevant by power counting (the coupling has scaling dimension -1), and can be ignored for the leading asymptotic behaviour calculations performed below. Note that the “lower dimension” surface term $\vec{n} \partial_x \vec{n}$ vanishes identically due to the constraint $\vec{n}^2 = 1$. The absence of a boundary term implies that \vec{n} obeys free boundary conditions,

$$\partial_x \vec{n} \Big|_{x=0} = 0 \quad (5.8)$$

as can be seen by varying the action (5.6) with respect to \vec{n} , integrating by parts and requiring that the surface term be zero.

To set up perturbation theory, we write $\vec{n} = (\vec{\pi}, \sqrt{1 - \vec{\pi}^2})$ and expand the action in $\vec{\pi}$, obtaining,

$$S = \frac{\rho_s^0}{2} \int d^3x \left((\partial_{\mu} \vec{\pi})^2 + \frac{1}{1 - \vec{\pi}^2} (\vec{\pi} \partial_{\mu} \vec{\pi})^2 \right) \quad (5.9)$$

The second term in brackets above can be expanded as a power series in $\vec{\pi}$ - yielding terms with couplings of scaling dimension -1 and lower. These terms again will not influence the leading asymptotic behaviour of observables discussed below.

We are, thus, left with the free theory for the Goldstone fields $\vec{\pi}$, supplemented by the free boundary condition $\partial_x \vec{\pi} = 0$. The propagator with these boundary conditions is,

$$\begin{aligned} & \langle \pi^a(\vec{x}, \tau) \pi^b(\vec{x}', \tau') \rangle = \\ &= \frac{\delta^{ab}}{\rho_s^0} \int \frac{d\omega}{2\pi} \frac{dk_y}{2\pi} \frac{dk_x}{\pi} \frac{1}{\omega^2 + k_x^2 + k_y^2} e^{i\omega(\tau - \tau')} e^{ik_y(y - y')} \cos(k_x x) \cos(k_x x') \\ &= \frac{\delta^{ab}}{\rho_s^0} (D(x - x', y - y', \tau - \tau') + D(x + x', y - y', \tau - \tau')) \end{aligned} \quad (5.10)$$

where $D(x)$ is the standard $3d$ massless propagator,

$$D(x) = \frac{1}{4\pi|x|} \quad (5.11)$$

Now, we can calculate the observables. Let's start with the staggered moment $\langle \vec{N} \rangle$. The microscopic $\vec{N}(x)$ is related to the $O(3)$ field $\vec{n}(x)$ via a multiplicative renormalization, $\vec{N}(x) = N_b Z_N \vec{n}(x)$ where N_b is the exact value of the bulk staggered magnetization and Z_N is a formal power series in ρ_s^{-1} , adjusted order by order to give $\langle N^3 \rangle = N_b$ in the bulk.

Hence, the staggered moment, to leading order is,

$$\langle n^3(x) \rangle = \langle 1 - \frac{\vec{\pi}^2}{2} \rangle = 1 - \frac{1}{\rho_s^0} (D(0) + D(2x, 0, 0)) = 1 - \frac{1}{\rho_s^0} (D(0) + \frac{1}{8\pi x}) \quad (5.12)$$

Thus, as $\lim_{x \rightarrow \infty} Z_N \langle n^3(x) \rangle = 1$, and to leading order $\rho_s^0 = \rho_s$,

$$Z_N = 1 + \frac{1}{\rho_s} D(0) = 1 + \frac{1}{\rho_s} \int \frac{d^3k}{(2\pi)^3} \frac{1}{k^2} \quad (5.13)$$

which is the familiar expression known from calculations with no boundary. So,

$$\langle N^3(x) \rangle = N_b \left(1 - \frac{c}{8\pi\rho_s x} \right) \quad (5.14)$$

where we've reinserted the spin-wave velocity c . The result (5.14) is asymptotically exact and shows suppression of the Néel moment near the edge. We can check the result (5.14) against the large distance asymptotics of the $1/S$ expansion performed in section 5.3. The parameters ρ_s , c and N_b are known in $1/S$ expansion to be at leading order,

$$\rho_s = JS^2, \quad c = 2\sqrt{2}JSa, \quad N_b = S \quad (5.15)$$

where a is the lattice spacing. Substituting these parameters into (5.14) and comparing to our numeric integration results from $1/S$ expansion on the lattice with an edge, we find very reasonable asymptotic agreement (see Fig. 5.3).

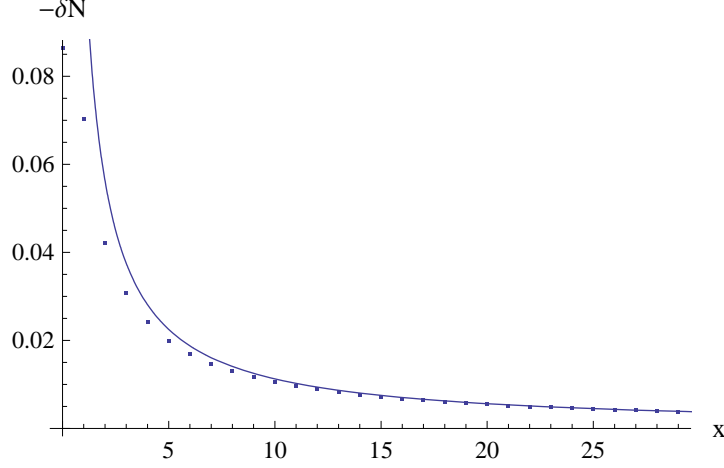


Figure 5.3: Depletion of the staggered moment, $-\delta N(x) = -(\langle N^3(x) \rangle - N_b)$, near the edge. The dotted line is the calculation in the $1/S$ expansion. The solid line is the $O(3)$ σ -model result for asymptotic behaviour, with phenomenological parameters ρ_s , c , N_b matched to $1/S$ expansion.

Next we consider the uniform transverse susceptibility χ_\perp . Recall, the uniform magnetic field \vec{H} enters (5.6) as,

$$S_H = \frac{\rho_s^0}{2} \int d^3x \left((\partial_\tau n^a - i\epsilon^{abc} H^b n^c)^2 + (\partial_i \vec{n})^2 \right) \quad (5.16)$$

The corresponding response function is,

$$\begin{aligned} \chi^{ab}(x, x') &= \frac{\delta^2 \log Z}{\delta H^a(x) \delta H^b(x')} = \rho_s^0 (\delta^{ab} - \langle n^a n^b(x) \rangle) \delta^3(x - x') \\ &\quad - (\rho_s^0)^2 \epsilon^{acd} \epsilon^{bef} \langle n^c \partial_\tau n^d(x) n^e \partial_\tau n^f(x') \rangle \end{aligned} \quad (5.17)$$

Specializing to the transverse susceptibility, $a, b = 1, 2$ and expanding in $\vec{\pi}$,

$$\begin{aligned} \chi^{ab}(x, x') &\approx \delta_{\mu\nu} \rho_s^0 (\delta^{ab} - \langle \pi^a(x) \pi^b(x') \rangle) \delta^2(\vec{x} - \vec{x}') \delta(\tau - \tau') \\ &\quad - (\rho_s^0)^2 \epsilon^{ac} \epsilon^{bd} (\langle \partial_\tau \pi^c(x) \partial_\tau \pi^d(x') \rangle + (\langle \partial_\tau \pi^c(x) (\pi^d \vec{\pi} \partial_\tau \vec{\pi} - \frac{1}{2} \vec{\pi}^2 \partial_\tau \pi^d)(x') \rangle \\ &\quad + (x \leftrightarrow x', c \leftrightarrow d))) \end{aligned} \quad (5.18)$$

Now, we are actually interested in local response to a static, uniform external field,

$$\chi_{\perp}^{ab}(x) = \lim_{\vec{q} \rightarrow 0} \int d^3x' \chi^{ab}(x, x') e^{-i\vec{q}\vec{x}'} \quad (5.19)$$

Note that for a finite system size/temperature relevant for Monte-Carlo simulations, at zero external field, there is no distinction between parallel and transverse susceptibility, and we expect,

$$\chi(x) = \frac{2}{3} \chi_{\perp}(x) \quad (5.20)$$

Since we are working with the static susceptibility, the contribution of the terms in the last two lines of (5.18) is zero, and

$$\chi_{\perp}^{ab}(x) = \rho_s^0 (\delta^{ab} - \langle \pi^a(x) \pi^b(x) \rangle) = \rho_s^0 \delta^{ab} (1 - \frac{1}{\rho_s^0} (D(0) + D(2x, 0, 0))) \quad (5.21)$$

We know that in the bulk, $\chi_{\perp,b} = \lim_{x \rightarrow \infty} \chi_{\perp}(x) = \rho_s$ by Lorentz invariance. The bare spin-stiffness $\rho_s^0 = \rho_s Z_{\rho}$ where Z_{ρ} is a formal power series in $1/\rho_s$. Thus,

$$Z_{\rho} = 1 + \frac{1}{\rho_s} D(0) = 1 + \frac{1}{\rho_s} \int \frac{d^3k}{k^2} \quad (5.22)$$

and we recognize the standard renormalization factor for ρ_s . Note that the equality of the first non-trivial terms in Z_N and Z_{ρ} is an accident, which occurs in the $O(3)$ model (for $O(N)$ the coefficients are generally different). Thus,

$$\chi_{\perp}(x) = \frac{\rho_s}{c^2} - \frac{1}{8\pi x c} \quad (5.23)$$

where we've reinserted c . Note that the deviation of $\chi_{\perp}(x)$ from its bulk value is negative, in agreement with the simulations of Höglund and Sandvik.[4] Moreover, the long distance contribution to the total edge susceptibility (per edge length) is given by,

$$\chi_{\perp, \text{edge}} = \int_0^{\infty} dx (\chi_{\perp}(x) - \chi_{\perp,b}) \sim -\frac{1}{8\pi c} \log(L_x/a) \quad (5.24)$$

At zero temperature, the log divergence of the long-distance tail will always overpower any short-distance contribution (which can be positive as suggested by the $1/S$ calculation in section 5.3), leading to a negative total edge susceptibility, as seen by Høglund and Sandvik.[4] At a finite temperature T (and in the infinite volume limit) the $\log L_x$ divergence will be cut-off at the “thermal length,” cT^{-1} , leading to

$$\chi_{\perp, \text{edge}} \sim -\frac{1}{8\pi c} \log\left(\frac{c}{Ta}\right) \quad (5.25)$$

This result will be confirmed by an explicit calculation in the next section.

Finally, we come to the behaviour of the bond energies. We observe that the sum of bonds energies along the x and y directions is just the local energy density

$$\epsilon(x) \sim \frac{J}{a^2} (\vec{S}_i \vec{S}_{i+\hat{x}} + \vec{S}_i \vec{S}_{i+\hat{y}}) \quad (5.26)$$

For the free field theory describing our Goldstones, in Minkowski space,

$$\epsilon(x) = \frac{\rho_s^0}{2} ((\partial_i \vec{\pi})^2 + (\partial_i \vec{\pi})^2) \quad (5.27)$$

Continuing this to Euclidean space,

$$\epsilon(x) = \frac{\rho_s^0}{2} (-(\partial_\tau \vec{\pi})^2 + (\partial_i \vec{\pi})^2) \quad (5.28)$$

Now,

$$\frac{\rho_s^0}{2} \langle \partial_\mu \vec{\pi}(x) \partial_\nu \vec{\pi}(x) \rangle = \lim_{x \rightarrow x'} \frac{\partial^2}{\partial x^\mu \partial x'^\nu} (D(x-x', y-y', \tau-\tau') + D(x+x', y-y', \tau-\tau')) \quad (5.29)$$

The first term on the righthandside is independent of the distance from the edge and, therefore, we drop it. Noting,

$$\partial_\mu \partial_\nu D(x) = -\frac{1}{4\pi|x|^3} \left(\delta_{\mu\nu} - 3 \frac{x_\mu x_\nu}{|x|^2} \right) \quad (5.30)$$

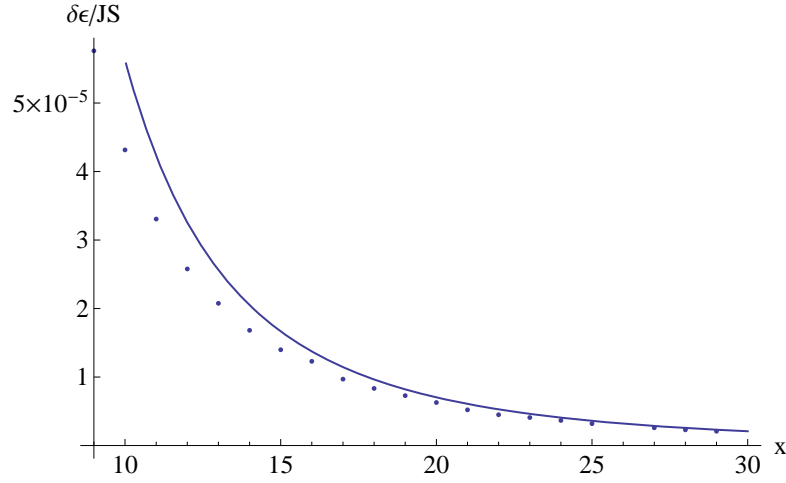


Figure 5.4: Asymptotic increase of local bond energy near the edge. The dotted line is the calculation in the $1/S$ expansion. The solid line is the $O(3)$ σ -model result for asymptotic behaviour, with phenomenological parameters ρ_s , c , N_b matched to $1/S$ expansion.

the second term in (5.29) yields,

$$\frac{\rho_s^0}{2} \langle (\partial_\tau \vec{\pi})^2(x) \rangle = -\partial_\tau^2 D(2x, 0, 0) = \frac{1}{4\pi(2x)^3} \quad (5.31)$$

$$\frac{\rho_s^0}{2} \langle (\partial_x \vec{\pi})^2(x) \rangle = +\partial_x^2 D(2x, 0, 0) = \frac{2}{4\pi(2x)^3} \quad (5.32)$$

$$\frac{\rho_s^0}{2} \langle (\partial_y \vec{\pi})^2(x) \rangle = -\partial_y^2 D(2x, 0, 0) = \frac{1}{4\pi(2x)^3} \quad (5.33)$$

Collecting terms we obtain,

$$\langle \epsilon(x) \rangle = \frac{c}{16\pi x^3} \quad (5.34)$$

Note that energy density is enhanced near the edge, corresponding to a decrease of bond strengths, $-\langle \vec{S}_i \vec{S}_j \rangle$. We can again compare the asymptotically exact expression (5.34) to the results of the $1/S$ expansion in section 5.3, by using the parameters (5.15). We see from Fig. 5.4 that the agreement is rather good.

5.2.2 Edge susceptibility at finite temperature

To compute the uniform susceptibility at finite temperature $T \ll \rho_s$, we follow the usual strategy of dividing the field $n(\vec{x}, \tau)$ into zero frequency piece, $n(\vec{x})$ and finite frequency modes $\pi_\alpha(\vec{x}, \tau)$,

$$n^a(\vec{x}, \tau) = \sqrt{1 - \pi_\alpha \pi_\alpha} n^a(\vec{x}) + \pi_\alpha(\vec{x}, \tau) e_\alpha^a(\vec{x}) \quad (5.35)$$

where $\alpha = 1, 2$ and $\vec{e}_\alpha(\vec{x})$ and $\vec{n}(\vec{x})$ form an orthonormal basis. The strategy is to first integrate over the “fast” modes π_α to obtain an effective action for the slow \vec{n} field. Expanding the action in powers of π to leading order,

$$S \approx \frac{\rho_s^0}{2} \int d^3x (\partial_\mu \pi_\alpha)^2 + \frac{\rho_s^0}{2} \int d^3x ((\partial_i n^a)^2 (1 - \vec{\pi}^2) + \partial_i e_\alpha^a \partial_i e_\beta^a \pi_\alpha \pi_\beta + 2 \partial_i e_\alpha^a e_\beta^a \pi_\alpha \partial_i \pi_\beta) \quad (5.36)$$

In setting up the perturbation theory in π the first term above is treated as the free piece, while the coupling of π to the slow fields in the second term is treated as a perturbation. Thus, in a theory with the edge at finite temperature, the bare propagator for the π field still satisfies free boundary conditions,

$$\langle \pi_\alpha(\vec{x}, \tau) \pi_\beta(\vec{x}', \tau') \rangle = \frac{1}{\rho_s^0} \delta_{\alpha\beta} D_n(x, x') \quad (5.37)$$

where,

$$D_n(x, x') = \hat{D}(x - x', y - y', \tau - \tau') + \hat{D}(x + x', y - y', \tau - \tau') \quad (5.38)$$

with

$$\hat{D}(\vec{x}, \tau) = \frac{1}{\beta} \sum_{\omega_n \neq 0} \int \frac{d^2k}{(2\pi)^2} \frac{1}{k^2 + \omega_n^2} e^{i(\vec{k}\vec{x} + \omega_n \tau)} \quad (5.39)$$

Now, expanding the susceptibility (5.17),

$$\begin{aligned}\chi^{ab}(x) &= \rho_s^0(\delta^{ab} - \langle n^a n^b(x) \rangle) \\ &- (\rho_s^0)^2 \epsilon^{acd} \epsilon^{bef} \int d^3 x' \langle e_\alpha^c e_\beta^d(\vec{x}) e_\gamma^e e_\delta^f(\vec{x}') \pi_\alpha \partial_\tau \pi_\beta(x) \pi_\gamma \partial_\tau \pi_\delta(x') \rangle\end{aligned}\quad (5.40)$$

At leading order, we may factorize the correlator of slow e and fast π fields in (5.40).

Moreover, since at finite temperature rotational invariance is restored,

$$\langle n^a n^b(x) \rangle = \frac{\delta^{ab}}{3} \langle \vec{n}^2(x) \rangle = \frac{\delta^{ab}}{3}\quad (5.41)$$

Hence, the local susceptibility becomes,

$$\chi^{ab}(x) = \frac{2}{3} \rho_s^0 \delta^{ab} - (\rho_s^0)^2 \epsilon^{acd} \epsilon^{bef} \int d^3 x' \langle e_\alpha^c e_\beta^d(\vec{x}) e_\gamma^e e_\delta^f(\vec{x}') \rangle \langle \pi_\alpha \partial_\tau \pi_\beta(x) \pi_\gamma \partial_\tau \pi_\delta(x') \rangle\quad (5.42)$$

We see that the susceptibility involves a convolution of correlators of slow and fast fields. Evaluating the correlation function of the fast fields explicitly,

$$\begin{aligned}\chi^{ab}(x) &= \frac{2}{3} \rho_s^0 \delta^{ab} - \epsilon^{acd} \epsilon^{bef} (\delta_{\alpha\gamma} \delta_{\beta\delta} - \delta_{\alpha\delta} \delta_{\beta\gamma}) \int d^3 x' \langle e_\alpha^c e_\beta^d(\vec{x}) e_\gamma^e e_\delta^f(\vec{x}') \rangle (\partial_\tau D_n(x, x'))^2 \\ &\quad (5.43)\end{aligned}$$

We note,

$$\begin{aligned}\int d\tau' (\partial_\tau D_n(x, x'))^2 &= \frac{1}{\beta} \sum_{\omega_n} \omega_n^2 D_n(\vec{x}, \vec{x}', \omega_n)^2 \\ &= \frac{1}{\beta} \sum_{\omega_n} \omega_n^2 (D(\vec{x} - \vec{x}', \omega_n)^2 + 2D(\vec{x} - \vec{x}', \omega_n)D(\vec{x} - R\vec{x}', \omega_n) + D(\vec{x} - R\vec{x}', \omega_n)^2)\end{aligned}\quad (5.44)$$

where R denotes reflection across the edge at $x = 0$. In the absence of an edge, we can drop the last two terms in (5.44). Then we note that the correlation function of π 's decays exponentially for large distances, hence only $|\vec{x} - \vec{x}'| \lesssim T^{-1}$ contribute to

the integral in (5.42). The slow degrees of freedom $\vec{n}(\vec{x})$ and $\vec{e}_\alpha(\vec{x})$ fluctuate only on much larger distances (in fact T^{-1} serves as an effective short-distance cut-off for the slow degrees of freedom), hence we can to leading order set $\vec{x} = \vec{x}'$ in the correlation function of the e 's. This leads to a considerable simplification as,

$$e_\alpha^a e_\alpha^b = \delta^{ab} - n^a n^b \quad (5.45)$$

and,

$$(\delta_{\alpha\gamma}\delta_{\beta\delta} - \delta_{\alpha\delta}\delta_{\beta\gamma}) \langle e_\alpha^c e_\beta^d(\vec{x}) e_\gamma^e e_\delta^f(\vec{x}) \rangle = \frac{1}{3} (\delta^{ec}\delta^{df} - \delta^{cf}\delta^{de}) \quad (5.46)$$

and

$$\chi^{ab}(x) = \frac{2}{3} \delta^{ab} \left(\rho_s^0 - 2 \int d^3x' (\partial_\tau D_n(x, x'))^2 \right) \quad (5.47)$$

Now let's introduce the edge back. We wish to compute the deviation of local susceptibility from its bulk value. The major difference from the situation in the bulk is that eq. (5.44) no longer depends just on the difference $\vec{x} - \vec{x}'$. For $xT \lesssim 1$, the integral over \vec{x}' in (5.43) is saturated with $x'T \lesssim 1$ and hence, we can effectively set $x = x' = 0$, $y = y'$ in the correlation function of the e 's and recover the simple form (5.47). However, for $xT \gg 1$, the part of the integral in (5.43) that represents $\chi(x) - \chi_b$ is no longer saturated at $x' \sim x$. Hence, one really has to compute the correlation function of the slow degrees of freedom. For $T^{-1} \ll x \ll \xi$, we expect this to modify $\chi(x) - \chi_b$ (which, as we shall see, is exponentially suppressed as $e^{-4\pi T x}$) by logarithmic corrections. On the other hand, for $x \gtrsim \xi$, we expect additional exponential suppression coming from the slow degrees of freedom. As we shall see, the total edge susceptibility is saturated by $xT \lesssim 1$ and, hence, can be computed directly from (5.47).

Keeping the above remarks in mind and setting $\vec{x} = \vec{x}'$ for the slow degrees of freedom in (5.43), we obtain from (5.44) and (5.47),

$$\chi(x) = \frac{2}{3} \left(\rho_s^0 - 2 \frac{1}{\beta} \sum_{\omega_n \neq 0} \omega_n^2 \int_{-\infty}^{\infty} dx' \int_{-\infty}^{\infty} dy' (D(\vec{x} - \vec{x}', \omega_n)^2 + D(\vec{x} - \vec{x}', \omega_n) D(\vec{x} - R\vec{x}', \omega_n)) \right) \quad (5.48)$$

The first term under the integral in (5.48) is the familiar temperature dependent correction to bulk susceptibility, while the second term represents the edge contribution.

Performing the integral over \vec{x}' ,

$$\chi(x) = \chi_b(T) - \frac{4}{3} \frac{1}{\beta} \sum_{\omega_n \neq 0} \frac{d^2 k}{(2\pi)^2} \frac{\omega_n^2}{(k^2 + \omega_n^2)^2} e^{2ik_{xx}} \quad (5.49)$$

where,

$$\chi_b(T) = \frac{2}{3} \left(\rho_s^0 - 2 \frac{1}{\beta} \sum_{\omega_n \neq 0} \int \frac{d^2 k}{(2\pi)^2} \frac{\omega_n^2}{(k^2 + \omega_n^2)^2} \right) = \frac{2}{3} \frac{\rho_s}{c^2} \left(1 + \frac{T}{2\pi\rho_s} \right) \quad (5.50)$$

Now, we can compute the asymptotics of (5.49). For $xT/c \ll 1$, we can replace the sum over ω_n by an integral,

$$\begin{aligned} \chi(x) &\rightarrow \chi_b(T) - \frac{4}{3} \int \frac{d^3 k}{(2\pi)^3} \frac{\omega^2}{(k^2 + \omega^2)^2} e^{2ik_{xx}} = \chi_b(T) - \frac{1}{3} \int \frac{d^2 k}{(2\pi)^2} \frac{1}{k} e^{2ik_{xx}} \\ &= \chi_b(T) - \frac{1}{12\pi xc} \end{aligned} \quad (5.51)$$

which agrees with our earlier $T = 0$ result (5.23) upon the usual replacement (5.20).

In the opposite limit $xT/c \gg 1$, the sum in (5.49) is going to be dominated by the smallest thermal mass, $\omega_{n=1}$, and,

$$\chi(x) \rightarrow \chi_b - \frac{2}{3} \frac{T}{c^2} \left(\frac{xT}{2c} \right)^{\frac{1}{2}} e^{-4\pi T x/c} \quad (5.52)$$

As noted earlier, this result will be modified by logarithmic corrections for $x \ll \xi$ and additional exponential suppression for $x \gg \xi$. It is also now clear from (5.52) that the

total edge susceptibility is saturated by $xT \lesssim 1$, so that the corrections mentioned above can be ignored for its computation, and we can use eq. (5.49), which obeys the scaling form,

$$\chi(x) - \chi_b = T f_\chi(Tx) \quad (5.53)$$

Thus,

$$\chi_{\text{edge}} = \int_a^\infty dx (\chi(x) - \chi_b) = \int_{Ta}^\infty du f_\chi(u) \quad (5.54)$$

where a is a short distance cut-off. We observe that the singular behaviour of χ_{edge} for $T \rightarrow 0$ can be extracted from the short distance asymptotic of $\chi(x)$ (5.51). Noting, $f_\chi(u) \rightarrow -\frac{1}{12\pi u}$ for $u \rightarrow 0$,

$$\chi_{\text{edge}} \sim -\frac{1}{12\pi} \int_{Ta}^\infty \frac{du}{u} = -\frac{1}{12\pi c} \log\left(\frac{c}{Ta}\right) \quad (5.55)$$

as predicted from $T = 0$ behaviour in the previous section.

5.3 Large S expansion of the Heisenberg model with an edge

In this section we perform the large S expansion of the Heisenberg model on a square lattice with an edge. We start with the usual nearest neighbour Hamiltonian,

$$H = J \sum_{\langle ij \rangle} \vec{S}_i \vec{S}_j \quad (5.56)$$

and use the Holstein-Primakoff representation of spin operators, which at leading order in $1/S$ reads,

$$S_i^z = S - b_i^\dagger b_i, \quad S_i^+ = \sqrt{2S} b_i, \quad S_i^- = \sqrt{2S} b_i^\dagger, \quad i \in A \quad (5.57)$$

$$S_i^z = -S + c_i^\dagger c_i, \quad S_i^+ = \sqrt{2S} c_i^\dagger, \quad S_i^- = \sqrt{2S} c_i, \quad i \in B \quad (5.58)$$

where A and B are the two sublattices. We place the edge at $i_x = 0$. Utilizing the translational invariance along the y direction,

$$b_{i_x, i_y} = \frac{1}{\sqrt{N_y/2}} \sum_{k_y} b_{i_x, k_y} e^{ik_y i_y}, \quad c_{i_x, i_y} = \frac{1}{\sqrt{N_y/2}} \sum_{k_y} c_{i_x, k_y} e^{ik_y i_y} \quad (5.59)$$

where $-\pi/2 < k_y < \pi/2$ and N_y is the number of sites in the y direction, we obtain the Hamiltonian,

$$H = 4SJ \sum_{k_y} \sum_{i_x, i'_x} \begin{pmatrix} b_{i_x, k_y} \\ c_{i_x, -k_y}^\dagger \end{pmatrix}^\dagger h_{i_x, i'_x} \begin{pmatrix} b_{i'_x, k_y} \\ c_{i'_x, -k_y}^\dagger \end{pmatrix} \quad (5.60)$$

with

$$h_{ii'} = \begin{pmatrix} A_{ii'} & B_{ii'} \\ B_{ii'} & A_{ii'} \end{pmatrix}, \quad A_{ii'} = \delta_{ii'} \left(1 - \frac{1}{4} \delta_{i0}\right), \quad B_{ii'} = \frac{1}{2} \cos k_y \delta_{ii'} + \frac{1}{4} (\delta_{i', i+1} + \delta_{i', i-1}) \quad (5.61)$$

We perform a Bogoliubov transformation by writing,

$$\begin{pmatrix} b_{i_x, k_y} \\ c_{i_x, -k_y}^\dagger \end{pmatrix} = \sum_{\lambda > 0} \left(\phi^{+\lambda}(i_x) \beta_{\downarrow \lambda, k_y} + \phi^{-\lambda}(i_x) \beta_{\uparrow \lambda, -k_y}^\dagger \right) \quad (5.62)$$

where the β 's obey canonical commutation relations and the two component vectors $\phi^\lambda(i_x) = (u^\lambda(i_x), v^\lambda(i_x))$ are eigenstates of $\tau^3 h$,

$$\tau^3 h \phi^{+\lambda} = \lambda \phi^{+\lambda} \quad (5.63)$$

$$\tau^3 h \phi^{-\lambda} = -\lambda \phi^{-\lambda} \quad (5.64)$$

Explicitly, $\phi^{-\lambda} = \tau^1 \phi^{+\lambda}$. We normalize the ϕ 's as,

$$\langle \phi^{+\lambda} | \tau^3 | \phi^{+\lambda'} \rangle = \delta_{\lambda, \lambda'} \quad (5.65)$$

Then, up to a constant,

$$H = 4SJ \sum_{k_y} \sum_{\lambda > 0} \lambda (\beta_{\uparrow\lambda, k_y}^\dagger \beta_{\uparrow\lambda, k_y} + \beta_{\downarrow\lambda, k_y}^\dagger \beta_{\downarrow\lambda, k_y}) \quad (5.66)$$

The solutions to the eigenvalue problem (5.63) with positive eigenvalues can be divided into the normalizable and non-normalizable branches. The normalizable branch has dispersion

$$\lambda = \frac{1}{\sqrt{2}} |\sin k_y| \quad (5.67)$$

The continuum branch can be parameterized by momentum $0 < k_x < \pi - k_y$ and has dispersion,

$$\lambda = \sqrt{1 - \frac{1}{4}(\cos k_x + \cos k_y)^2} \quad (5.68)$$

We normalize our continuum solutions to,

$$\langle \phi(k_x) | \tau^3 | \phi(k'_x) \rangle = (2\pi) \delta(k_x - k'_x) \quad (5.69)$$

Explicit forms of the eigenstates are given in Appendix D.1. We note that for fixed $k_y \rightarrow 0$, the energies of both the normalizable state and the continuum threshold tend to $\frac{1}{\sqrt{2}}|k_y|$, with the splitting between these two energies of order k_y^3 . This is the reason why the bound state does not show up in the effective low energy $O(3)$ description - it is treated as being part of the continuum.

Now, we can compute the observables. The staggered magnetization is given by,

$$\langle N_j \rangle = S - \langle c_j^\dagger c_j \rangle = S - \int_{-\pi/2}^{\pi/2} \frac{dk_y}{\pi} \sum_{\lambda > 0} |v^\lambda(j_x)|^2 \quad (5.70)$$

We have evaluated the sum (integral) over the eigenstates numerically - the result is plotted in Fig. 5.3. The staggered moment is depleted near the edge and approaches its bulk value monotonically. If we plug $S = 1/2$ into our expansion, the staggered

moment at the edge is $N_{\text{edge}} = 0.217$ compared to $N_b = 0.303$ in the bulk. As already noted, the long distance asymptotics of the staggered moment are in good agreement with the predictions of the $O(3)$ continuum theory.

Similarly, we can compute the bond energies,

$$\begin{aligned}
\langle \vec{S}_j \vec{S}_{j+\hat{x}} \rangle &= -S^2 + S(\langle b_j^\dagger b_j \rangle + \langle c_{j+\hat{x}}^\dagger c_{j+\hat{x}} \rangle + \langle b_j c_{j+\hat{x}} \rangle + \langle b_j^\dagger c_{j+\hat{x}}^\dagger \rangle) \\
&= -S^2 + S \int_{-\pi/2}^{\pi/2} \frac{dk_y}{\pi} \sum_{\lambda>0} (|v^\lambda(j_x)|^2 + |v^\lambda(j_x+1)|^2 \\
&\quad + v^\lambda(j_x+1)^* u^\lambda(j_x) + u^\lambda(j_x)^* v^\lambda(j_x+1)) \\
\langle \vec{S}_j \vec{S}_{j+\hat{y}} \rangle &= -S^2 + S(\langle b_j^\dagger b_j \rangle + \langle c_{j+\hat{y}}^\dagger c_{j+\hat{y}} \rangle + \langle b_j c_{j+\hat{y}} \rangle + \langle b_j^\dagger c_{j+\hat{y}}^\dagger \rangle) \\
&= -S^2 + S \int_{-\pi/2}^{\pi/2} \frac{dk_y}{\pi} \sum_{\lambda>0} (2|v^\lambda(j_x)|^2 \\
&\quad + (u^\lambda(j_x)^* v^\lambda(j_x) + v^\lambda(j_x)^* u^\lambda(j_x)) \cos k_y)
\end{aligned} \tag{5.71}$$

The short distance behaviour of the bond energies is shown in Fig. 5.5. We see that both the perpendicular and parallel bonds touching the edge are stronger than in the bulk ($\langle \vec{S}_i \vec{S}_j \rangle$ is more negative), while all the subsequent bonds are weaker than in the bulk. Substituting $S = 1/2$ into our expansion, we find that at the edge $\langle \vec{S}_j \vec{S}_{j+\hat{x}} \rangle = -0.352$, $\langle \vec{S}_j \vec{S}_{j+\hat{y}} \rangle = -0.368$, while in the bulk, $\langle \vec{S}_j \vec{S}_{j+\hat{\rho}} \rangle = -0.329$. Thus, comparing to the results of quantum Monte Carlo, the $1/S$ expansion reproduces qualitatively the behaviour of the first two rows of bonds away from the edge, but fails to capture the subsequent oscillations in bond strengths on short distances. We expect that these oscillations cannot be seen in the perturbative $1/S$ expansion. In the next section, we will argue that the appearance of such oscillations can be linked to the existence of a competing valence-bond-solid order parameter. As for the long distance asymptotics, we can compare the sum of bond strengths along x and y

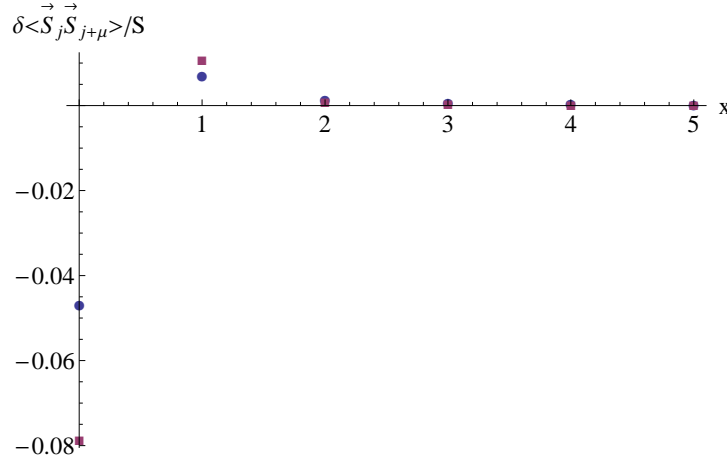


Figure 5.5: Bond strength deviation from bulk value $\delta \langle \vec{S}_j \vec{S}_{j+\hat{\mu}} \rangle = \langle \vec{S}_j \vec{S}_{j+\hat{\mu}} \rangle - \lim_{j_x \rightarrow \infty} \langle \vec{S}_j \vec{S}_{j+\hat{\mu}} \rangle$ along $\mu = x$ (circle) and $\mu = y$ (square) directions computed in the $1/S$ expansion.

directions to the local energy density computed in the continuum $O(3)$ model; the two are in good agreement (see Fig. 5.4).

Now we turn our attention to the local transverse magnetic susceptibility

$$\chi_{\perp}(j_x) = \frac{1}{2TN_y} \lim_{q_y \rightarrow 0} \sum_{j'_x} \langle S^+(j_x, q_y) S^-(j'_x, -q_y) \rangle \quad (5.72)$$

where

$$S^+(j_x, q_y) = \sum_{j_y} S^+(j_x, j_y) e^{-iq_y j_y} \quad (5.73)$$

A finite momentum \vec{q} is needed as a regulator, since we are working in an infinite volume; it is convenient to choose \vec{q} along the y direction (the limit $q_y \rightarrow 0$ is assumed in what follows). At leading order in the $1/S$ expansion,

$$\chi_{\perp}(j) = \frac{1}{2T} S \sum_{j'_x} \langle (b_{j_x, q_y} + c_{j_x, -q_y}^{\dagger})(b_{j'_x, q_y}^{\dagger} + c_{j'_x, -q_y}^{\dagger}) \rangle \quad (5.74)$$

$$= \frac{1}{2T} S \sum_{j'_x} \sum_{\lambda > 0} (u^{\lambda}(j_x, q_y) + v^{\lambda}(j_x, q_y))(u^{\lambda}(j'_x, q_y) + v^{\lambda}(j'_x, q_y))^* (1 + 2n(\lambda)) \quad (5.75)$$

where $n(\lambda) = (e^{\lambda/T} - 1)^{-1}$ is the bose distribution. As expected, for $q_y \rightarrow 0$, the form-factor in (5.75) vanishes upon summing over j'_x , unless $\lambda \rightarrow 0$. Thus, we may replace, $n(\lambda) \rightarrow T/\lambda$, obtaining,

$$\chi_{\perp}(j) = S \sum_{j'_x} \sum_{\lambda > 0} \frac{1}{\lambda} (u^{\lambda}(j_x, q_y) + v^{\lambda}(j_x, q_y))(u^{\lambda}(j'_x, q_y) + v^{\lambda}(j'_x, q_y))^* \quad (5.76)$$

A short calculation then yields,

$$\chi_{\perp}(j) = \frac{1}{8J} (1 + (-1)^{j_x} (\sqrt{2} + 1)^{-(2j_x+1)}) \quad (5.77)$$

This result is saturated by normalizable modes and states at the bottom of the continuum band. We see that as $j_x \rightarrow \infty$, the susceptibility approaches its bulk value $\chi_{\perp,b} = \frac{1}{8J}$. We can define the edge susceptibility (per unit edge length) as,

$$\chi_{\perp,\text{edge}} = \sum_{j_x} (\chi_{\perp}(j) - \chi_{\perp,b}) = \frac{1}{8J} 2^{-3/2} \quad (5.78)$$

So, at leading order in $1/S$ the edge susceptibility is positive, moreover, the approach of $\chi_{\perp}(j)$ to its bulk value is governed by an oscillating exponential decay. Based on our continuum treatment in the previous section, we expect these results to be strongly modified at higher orders in $1/S$. Indeed, at $T = 0$, from eq. (5.23) on large distances $\chi_{\perp}(x) - \chi_{\perp,b}$ falls off as $1/x$. However, the coefficient of this power law is of order $1/S$ and, hence, is not captured by the leading order result (5.77). When integrated over all space, the large distance power law, which is subleading in the $1/S$ expansion, will lead to a logarithmic divergence in the size/inverse temperature of the system, which would overpower the leading term in $1/S$ coming from short distances. Thus, the combination of eqs. (5.23), (5.77) naturally explains the results of Monte Carlo simulations, which see a positive susceptibility of the “dangling” edge

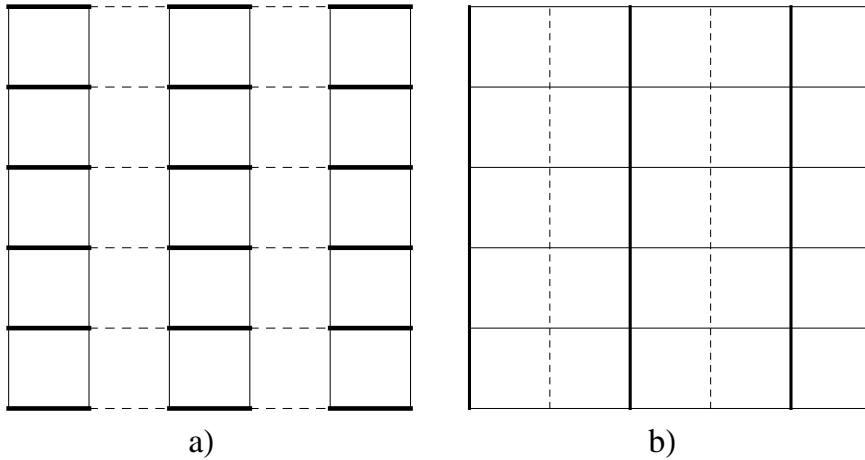


Figure 5.6: a) Lattice order with $\langle V_x \rangle \neq 0$. b) Bond order with $\langle O_x \rangle \neq 0$.

spin combined with the negative total edge susceptibility coming from a large distance tail in $\chi(x)$.

5.4 The comb structure

In this section we explain the appearance of the comb structure (Fig. 5.1), seen near the edge in recent Monte Carlo simulations. In our description, we assume the existence of a dynamic valence-bond-solid (VBS) order parameter $V(x)$ with a large correlation length in the Néel state. Our treatment becomes exact near a phase transition into a valence-bond-solid phase. This phase transition has attracted a lot of attention in the recent years as it lies outside the Landau-Ginzburg paradigm.[1, 2] It is described by the hedgehog suppressed $O(3)$ σ -model, with the valence-bond-solid order parameter $V(x)$ being the hedgehog insertion operator. However, the particular details of the phase transition will not be important for our discussion below.

We begin by defining a microscopic VBS order parameter (which lives on the direct lattice),

$$V_x(i) = (-1)^{i_x+1/2} \left(\vec{S}(i)\vec{S}(i + \hat{x}) - \vec{S}(i)\vec{S}(i - \hat{x}) \right) \quad (5.79)$$

$$V_y(i) = (-1)^{i_y+1/2} \left(\vec{S}(i)\vec{S}(i + \hat{y}) - \vec{S}(i)\vec{S}(i - \hat{y}) \right) \quad (5.80)$$

In this section, we take the origin to lie on the dual lattice. It is customary to group V_x, V_y into a complex order parameter $V = V_x + iV_y$ which has the following transformation properties under elements of the square lattice space group:

$$T_x^\dagger V(i_x, i_y) T_x = -V^\dagger(i_x - 1, i_y) \quad (5.81)$$

$$T_y^\dagger V(i_x, i_y) T_y = V^\dagger(i_x, i_y - 1) \quad (5.82)$$

$$I_x^{\dagger \text{dual}} V(i_x, i_y) I_x^{\text{dual}} = V(-i_x, i_y) \quad (5.83)$$

$$I_y^{\dagger \text{dual}} V(i_x, i_y) I_y^{\text{dual}} = V(i_x, -i_y) \quad (5.84)$$

$$R_{\pi/2}^{\dagger \text{dual}} V(i_x, i_y) R_{\pi/2}^{\text{dual}} = iV^\dagger(i_y, -i_x). \quad (5.85)$$

Here $T_{x,y}$ are translations by one lattice spacing in the x, y directions, $I_{x,y}^{\text{dual}}$ are x, y, reflections about a dual lattice point, and $R_{\pi/2}^{\text{dual}}$ is a 90° rotation about a dual lattice point. For completeness we also list the transformation property of V under rotations about a direct lattice point $(-1/2, -1/2)$,

$$R_{\pi/2}^{\dagger \text{dir}} V(i_x, i_y) R_{\pi/2}^{\text{dir}} = iV(i_y, -1 - i_x) \quad (5.86)$$

A non-zero expectation value of the VBS order parameter V would lead to a bond pattern shown in Fig. 5.6 a). As already noted, the operator $V(x)$ is represented by the hedgehog insertion operator in the continuum description of the antiferromagnet - valence bond solid transition.

Clearly, the order parameter V is adequate for describing the oscillations of horizontal bonds in the comb structure (Fig. 5.1). However, the oscillations of the vertical lines in the comb structure (Fig. 5.1), shown separately in Fig. 5.6 b) are not of the “dimer form.” To describe them, we introduce a new order parameter,

$$\begin{aligned} O_x(i) &= (-1)^{i_x} \left(\vec{S}(i + \frac{1}{2}\hat{x} + \frac{1}{2}\hat{y})\vec{S}(i + \frac{1}{2}\hat{x} - \frac{1}{2}\hat{y}) - \vec{S}(i - \frac{1}{2}\hat{x} + \frac{1}{2}\hat{y})\vec{S}(i - \frac{1}{2}\hat{x} - \frac{1}{2}\hat{y}) \right) \\ O_y(i) &= (-1)^{i_y} \left(\vec{S}(i + \frac{1}{2}\hat{y} + \frac{1}{2}\hat{x})\vec{S}(i + \frac{1}{2}\hat{y} - \frac{1}{2}\hat{x}) - \vec{S}(i - \frac{1}{2}\hat{y} + \frac{1}{2}\hat{x})\vec{S}(i - \frac{1}{2}\hat{y} - \frac{1}{2}\hat{x}) \right) \end{aligned}$$

O_x describes vertical bond lines which are oscillating in strength along the x direction (see Fig. 5.6 b)). Similarly, O_y describes horizontal bond lines, which are oscillating in strength along the y direction.

We can group O_x and O_y into a single complex order parameter $O = O_x + iO_y$.

The transformation properties of O are,

$$T_x^\dagger O(i_x, i_y) T_x = -O^\dagger(i_x - 1, i_y) \quad (5.87)$$

$$T_y^\dagger O(i_x, i_y) T_y = O^\dagger(i_x, i_y - 1) \quad (5.88)$$

$$I_x^{\dagger\text{dual}} O(i_x, i_y) I_x^{\text{dual}} = -O^\dagger(-i_x, i_y) \quad (5.89)$$

$$I_y^{\dagger\text{dual}} O(i_x, i_y) I_y^{\text{dual}} = O^\dagger(i_x, -i_y) \quad (5.90)$$

$$R_{\pi/2}^{\dagger\text{dual}} O(i_x, i_y) R_{\pi/2}^{\text{dual}} = iO(i_y, -i_x) \quad (5.91)$$

and for rotations about direct lattice point $(-1/2, -1/2)$:

$$R_{\pi/2}^{\dagger\text{dir}} O(i_x, i_y) R_{\pi/2}^{\text{dir}} = iO^\dagger(i_y, -1 - i_x) \quad (5.92)$$

Now we may ask whether it is possible in the continuum to construct an operator with the transformation properties of $O(x)$ out of $V(x)$. Clearly, any function of V

with no derivatives cannot do the job, since under dual lattice reflections $I_{x,y}^{\text{dual}}$, O transforms non-trivially, while V transforms trivially. Thus, a static uniform condensate of V (not surprisingly) cannot give rise to the order in Fig. 5.6 b). However, we can obtain an expression with the transformation properties of O if we allow for derivatives of V . Considering expressions with one power of V and one derivative, we obtain,

$$O_x \sim \partial_x V_x, \quad O_y \sim \partial_y V_y \quad (5.93)$$

(with the same proportionality constant).

Thus, if dimerization of horizontal bonds is present and is inhomogeneous along the x direction then we automatically obtain the “secondary” order in Fig. 5.6 b).

Now, we may ask, how a non-zero expectation value of the VBS order is generated? Indeed, in the Néel phase, in the bulk, the \mathbb{Z}_4 lattice rotation symmetry is unbroken and $\langle V \rangle = 0$. However, the edge possesses a smaller lattice symmetry group than the bulk - in particular, the lattice rotation symmetry is explicitly broken. This is manifested in the continuum formulation by the appearance of an edge perturbation,

$$\delta S = \frac{1}{2}h \int d\tau dy (V + V^\dagger) \Big|_{x=0} = h \int d\tau dy V_x \Big|_{x=0} \quad (5.94)$$

In the phase where V is gapped, we expect such a coupling will lead to an appearance of $\langle V_x(x,y) \rangle$ decaying away from the edge. Hence, we will also have $\langle O_x(x,y) \rangle \neq 0$, which close to the critical point can just be obtained from (5.93). Thus, the appearance of the comb structure is very natural.

Based on the known results on boundary critical behaviour,[138] we may write down the scaling forms for $\langle V(x) \rangle$, $\langle O(x) \rangle$ in the critical region. The edge perturbation δS is relevant at the critical point provided that $\Delta^V < 2$, where Δ^V is the scaling

dimension of operator $V(x)$. Then the scaling forms become universal (up to overall multiplicative factors),

$$\langle V_x(x) \rangle \sim \frac{1}{\xi^{\Delta_V}} g(x/\xi) \quad (5.95)$$

$$\langle O_x(x) \rangle \sim \frac{1}{\xi^{\Delta_V+1}} g'(x/\xi) \quad (5.96)$$

Here ξ is the correlation length of the VBS order parameter in the Neel phase (which is proportional to the inverse spin stiffness c/ρ_s with some universal amplitude). In the deconfined criticality scenario, ξ will be given by the inverse skyrmion mass. Note that due to the extra derivative in O compared to V , the modulations of lines parallel to the edge become parametrically weaker than those of dimers perpendicular to the edge as we approach the phase transition. We may also write down short and long distance asymptotics of $g(u)$,

$$g(u) \sim \frac{1}{u^{\Delta_V}}, \quad u \rightarrow 0 \quad (5.97)$$

$$g(u) \sim e^{-u}, \quad u \rightarrow \infty \quad (5.98)$$

where we have not specified the likely power-law prefactor for the long distance asymptotic (5.98).

5.5 Conclusion

In this chapter we have addressed two puzzles raised by recent Monte Carlo simulations of edge response in square lattice quantum antiferromagnets. The first puzzle is the appearance of negative edge susceptibility - we have shown that this effect is due to low energy spin-waves. We predicted that the total edge susceptibility diverges

logarithmically as inverse temperature/system size goes to infinity, and found this to be in good agreement with the Monte Carlo simulations of Ref. [4]. We would like to note here that our results on the low temperature behaviour of susceptibility apply equally well to a clean and rough edge, as our continuum $O(3)$ σ -model description does not assume translational invariance along the edge. (However, for the rough edge, there may be additional important contributions to the susceptibility coming from Berry phase effects, not present in the $O(3)$ σ -model.) The second puzzle is the observation of a comb structure in the bond response near the edge. We have argued that this is likely a purely quantum mechanical effect, which cannot be captured by the naive $1/S$ expansion. We have shown that the appearance of the comb structure can be understood in the framework of a continuum theory involving a dynamical valence-bond-solid order parameter. Such a description becomes exact in the neighbourhood of a quantum phase transition to a valence-bond-solid phase. We hope that the simulations of edge response in Heisenberg model[4] will be extended to the so-called JQ model where such a phase transition is observed.[57, 58] We have made a few predictions regarding the behaviour of the comb structure near criticality, e.g. the relation between the behaviour of bonds parallel and perpendicular to the edge in the comb. Edge response near the quantum critical point might also be a viable way to extract the scaling dimension of the valence-bond-solid order parameter, see eqs. (5.95),(5.97).

Chapter 6

Quantum phase transitions of metals in two spatial dimensions: Ising-nematic order

We present a renormalization group theory for the onset of Ising-nematic order in a Fermi liquid in two spatial dimensions. This is a quantum phase transition, driven by electron interactions, which spontaneously reduces the point-group symmetry from square to rectangular. The critical point is described by an infinite set of 2+1 dimensional local field theories, labeled by points on the Fermi surface. Each field theory contains a real scalar field representing the Ising order parameter, and fermionic fields representing a time-reversed pair of patches on the Fermi surface. We demonstrate that the field theories obey compatibility constraints required by our redundant representation of the underlying degrees of freedom. Scaling forms for the response functions are proposed, and supported by computations up to three loops. Extensions of our results to other transitions of two-dimensional Fermi liquids with broken point-group and/or time-reversal symmetry are noted. Our results extend also to the problem of a Fermi surface coupled to a $U(1)$ gauge field.

6.1 Introduction

A number of recent experiments [10, 9, 12, 11] have noted the presence of Ising-nematic order in the enigmatic normal state of the cuprate superconductors. This order is associated with electronic correlations which spontaneously break the square lattice symmetry to that of a rectangular lattice: *i.e.* the symmetry of 90° rotations is lost, and the x and y directions become inequivalent. This broken symmetry is associated with an Ising order parameter, which we will represent below by a real scalar field ϕ .

Of particular interest are recent experiments on the anisotropy of the Nernst signal [11] in $\text{YBa}_2\text{Cu}_3\text{O}_y$, which indicate that the Ising-nematic order has its onset at the temperature $T = T^*$, which also marks the boundary between the ‘pseudogap’ region and the ‘strange metal’. These results call for the theory of the quantum phase transition involving Ising-nematic ordering in a Fermi liquid metal. Such a quantum critical point would play an important role in the theory of the strange metal. The metallic Ising-nematic critical point is also of importance in experiments [166] on $\text{Sr}_3\text{Ru}_2\text{O}_7$, where the observations of resistance anisotropies have demonstrated spontaneous Ising-nematic ordering. Finally, there are clear indications of Ising-nematic order driven by electron correlations in the pnictides. [167, 168, 169, 170]

One approach to the Ising-nematic ordering is to take a liquid-crystalline perspective [39], and view it among a class of phases with broken square lattice symmetry [171, 162, 172, 173]. Ising nematic phases are also a generic feature of frustrated and doped antiferromagnets, because the Ising-nematic order survives after antiferromagnetism (at wavevectors $\neq (\pi, \pi)$) has been disrupted by thermal [174, 175] or

quantum [176, 177] fluctuations.

A complementary point of view [178, 179, 180, 181, 182, 183, 184, 185, 186, 187, 188, 189, 190, 191] is to start from the Fermi liquid with perfect square lattice symmetry and look for the Pomeranchuk instability of Landau's Fermi liquid theory in the angular momentum $\ell = 2$ channel. Almost all of these works rely on the perspective of Hertz [192], in which the electrons are integrated out to yield a Landau-damped effective action for the scalar order parameter ϕ ; the low energy particle-hole excitations near the Fermi surface lead to long-range interactions in the action for ϕ . However, this procedure of successive integration of fermionic and then bosonic degrees of freedom is clearly dangerous. A systematic renormalization group analysis requires that all excitations at a given energy scale be treated together. Consequently, a complete scaling analysis of the Ising nematic critical point is lacking: such an analysis should be based on a local field theory, and provide a scheme for computing the scaling dimensions of all perturbations of the critical point.

We can also consider the onset of Ising-nematic order in a superconductor, rather than in a Fermi liquid. In a *s*-wave superconductor, the fermionic excitations are fully gapped, and so the theory for ϕ has no long-range interactions: consequently the transition is in the universality class of the 2+1 dimensional pure Ising model. A *d*-wave superconductor does have gapless fermionic excitations at special 'nodal points' in the Brillouin zone, and these nodal fermions do modify the universality of the transition away from pure Ising [193, 194]. A fairly complete understanding of the Ising-nematic transition in *d*-wave superconductors has been reached in recent work [195, 196] using a large- N expansion, where N is the number of fermion components.

This chapter provides a scaling theory of the Ising-nematic quantum critical point in two-dimensional metals, satisfying the requirements stated above. Our theory builds upon the work in the d -wave superconductor [195, 196], and also on advances by Polchinski[75], Altshuler, Ioffe, and Millis[197], and Sung-Sik Lee[79, 198] on a closely-related problem: the dynamics of a Fermi surface with the fermions coupled minimally to a U(1) gauge field.

We focus on a pair of time-reversed patches on the Fermi surface and describe their vicinity by a local 2+1 dimensional field theory. In principle, there are separate critical theories for each pair of time-reversed points on the Fermi surface, as is also the case in the Fermi surface ‘bosonization’ methods.[199, 200, 201, 202, 203, 188, 187] However, a key difference from the latter methods is that each Fermi surface point is associated with a 2+1 dimensional theory, and not a 1+1 dimensional theory. This means that there is a redundancy in our description, and sowing the theories together is not trivial: we show in Section 6.4.1 how this is done in a consistent manner.

Apart from their application to the Ising-nematic transition of interest, simple extensions of our results apply also to the U(1) gauge field case, and to other symmetry breaking transitions in Fermi liquids involving order parameters which carry momentum $\vec{Q} = 0$. We will describe these cases in Section 6.2 below, and briefly indicate the needed extensions in the body of the chapter.

Transitions with order parameters which carry momentum $\vec{Q} \neq 0$ lead to different field theories, which will be described in Chapter 7.

After a discussion of the one loop results in Section 6.3, we present our main scaling analysis in Section 6.4. This includes a discussion of Ward identities which

strongly constrain the structure of renormalization group flow. Finally, explicit three loop computations appear in Section 6.5 and Appendix E.2.

6.2 The model

We consider quantum phase transitions in metals of electrons c_σ ($\sigma = \uparrow, \downarrow$), involving an onset of a real order parameter $\phi(x)$ at wave-vector $\vec{Q} = 0$. The order parameter is taken to have the same transformation properties under lattice symmetries and time reversal as,

$$O(\vec{x}) = \frac{1}{V} \sum_{\vec{q}} \sum_{\vec{k}\sigma} d_{\vec{k}\sigma} c_{\vec{k}-\vec{q}/2,\sigma}^\dagger c_{\vec{k}+\vec{q}/2,\sigma} e^{i\vec{q}\cdot\vec{x}} \quad (6.1)$$

For definiteness, we consider a system on a square lattice. Then, ϕ can describe the following patterns of symmetry breaking:

1. Breaking of the point-group symmetry with $d_{\vec{k}\uparrow} = d_{\vec{k}\downarrow}$ and $d_{\vec{k}\sigma} = d_{-\vec{k}\sigma}$. In these cases $d_{\vec{k}}$ has either $d_{x^2-y^2}$, d_{xy} , or g -wave symmetry. The Ising-nematic transition of most interest to us here corresponds to the $d_{x^2-y^2}$ or d_{xy} cases. These cases all belong to one-dimensional representations of the square lattice point group, and we will argue that these transitions are all in the same universality class.
2. Breaking of time-reversal and point-group symmetry with $d_{\vec{k}\uparrow} = d_{\vec{k}\downarrow}$ and $d_{\vec{k}\sigma} = -d_{-\vec{k}\sigma}$. In this case $d_{\vec{k}}$ transforms under the two-dimensional p -wave representation, and so requires a two component order parameter $\vec{\phi} = (\phi_x, \phi_y)$. We will not consider the two-component case explicitly, but our results have an immediate generalization to this transition. This case corresponds to the ‘‘circulating

current” order parameters proposed by Simon and Varma [40], as was argued in Refs. [193, 204].

3. Breaking of spin-inversion symmetry with $d_{\vec{k}\uparrow} = -d_{\vec{k}\downarrow}$. In this case, $d_{\vec{k}}$ can have either s -wave symmetry (Ising ferromagnet), d -wave symmetry (Ising spin-nematic) or g -wave symmetry. Unlike transitions i) and ii), which respect the full $SU(2)$ spin rotation symmetry, in the present case we assume this symmetry is explicitly broken to a $U(1)$ “easy axis” subgroup.

Notice that in all cases, there is a Z_2 symmetry (either $\pi/2$ rotation, reflection or time-reversal) under which $\phi \rightarrow -\phi$.

Apart from the above symmetry breaking cases, we will also consider the problem of a Fermi surface minimally coupled to a $U(1)$ gauge field [198, 79, 75, 74, 205, 206, 207, 197, 208, 209, 210, 211, 212, 78, 213, 214]. This case is similar to case 2 above, as we describe below Eq. (6.4). Such models arise in theories [78, 213, 214] of certain $U(1)$ spin liquid phases in which c_σ describe the fermionic spinons. We will therefore refer to this model as the “spin-liquid” case below. The same theory also describes [24, 28, 29] “algebraic charge liquids” in which case the c_σ are spinless, charge $-e$ fermions, and σ represents the charge of the fermion under the emergent $U(1)$ gauge field; we will not refer to this case explicitly below.

Given the order parameter in Eq. (6.1), we may write down an effective spacetime Lagrangian describing the interactions of the order parameter ϕ with the fermions as,

$$L = c_\sigma^\dagger \left(\partial_\tau + \epsilon(-i\nabla) \right) c_\sigma - O(x)\phi(x) + \frac{1}{2}(\nabla\phi)^2 + \frac{r_0}{2}\phi^2 \quad (6.2)$$

Here, we have added by hand a gradient term and a mass for the bosonic mode ϕ . Such terms will be generated automatically after integrating out the high-energy fermions. The absence of higher order terms in ϕ and gradients of ϕ will be justified below.

The Lagrangian L in Eq. (6.2) is not yet in a form suitable for our analysis of quantum criticality. The main point is that the fermion spectrum $\epsilon(\vec{k})$ has zeros along the entire Fermi surface of large momenta \vec{k} : so, as is well known, we are not in a position to make a low momentum expansion needed for a field theory. One strategy is to use the Hertz approach [192] of integrating out all the c fermions to obtain a non-local effective action for the order parameter ϕ . The latter is singular only at small momenta \vec{q} and ω , and so it is then at least permissible to make a low momentum and frequency expansion. However, the terms in the effective for ϕ turn out to be highly singular as $\vec{q} \rightarrow 0$ (see Ref. [186] and Appendix E.1). Moreover, in $d = 2$, the strength of the singularity increases with increasing powers of ϕ in the effective action. The situation now seems hopeless, but progress becomes possible after a key observation: the leading singularities in the ϕ effective action appear only when all the ϕ fields have their momenta nearly collinear to each other, as is explained in Appendix E.1, and as will become clear from the structure of our analysis below (by nearly collinear we mean that the angle θ between the momenta is of order $\theta \sim |\vec{q}|/k_F$). In other words, if we are interested only in leading critical behavior, ϕ fields with non-collinear momenta effectively decouple from each other. The couplings between ϕ fields with non-collinear momenta are then irrelevant corrections to the critical theory. The argument supporting this statement is presented in Appendix E.1. More generally,

consider an n -point function

$$\langle \phi(\vec{q}_1)\phi(\vec{q}_2)\phi(\vec{q}_3)\dots\phi(\vec{q}_n)\rangle.$$

In a Gaussian theory for ϕ , which is the claim of Hertz [192], such a correlator would decouple into products over pairs of momenta which sum to zero. However, such a decoupling is too drastic: rather, the decoupling is only over sets of momenta which are collinear with each other, so that the leading critical singularity of the above correlator takes the form

$$\prod_a \langle \phi(\vec{q}_{a1})\phi(\vec{q}_{a2})\dots \rangle.$$

Here all the momenta \vec{q}_{ai} in a group Q_a are collinear to each other, while being non-collinear to momenta in groups Q_b with $b \neq a$. We can therefore limit ourselves to ϕ fields with momenta along a fixed direction \vec{q} . We will now argue that for each such direction \vec{q} , there is a sensible and powerful continuum limit of Eq. (6.2).

It is now clear that we may restrict our search for a field theory to that describing the singularities in the ϕ correlations for a *single* group of collinear momenta Q_a . So let us pick a direction \vec{q} for ϕ . It is believed that a bosonic mode with momentum \vec{q} interacts most strongly with the patches of the Fermi-surface to which it is tangent [198, 79, 75, 197]. Assuming that only a single Fermi surface is present, for each \vec{q} there will be two such points with opposite Fermi-momenta \vec{k}_0 and $-\vec{k}_0$, see Fig. 6.1. We will denote fermions at these momenta as ψ_+ and ψ_- :

$$\psi_{+\sigma}(\vec{k}) = c_{\vec{k}_0+\vec{k},\sigma} \quad , \quad \psi_{-\sigma}(\vec{k}) = c_{-\vec{k}_0+\vec{k},\sigma}. \quad (6.3)$$

We choose coordinate vectors \hat{x} and \hat{y} to be respectively perpendicular and parallel to \vec{q} . Then, expanding the fermion energy near \vec{k}_0 and $-\vec{k}_0$, the needed, low energy,

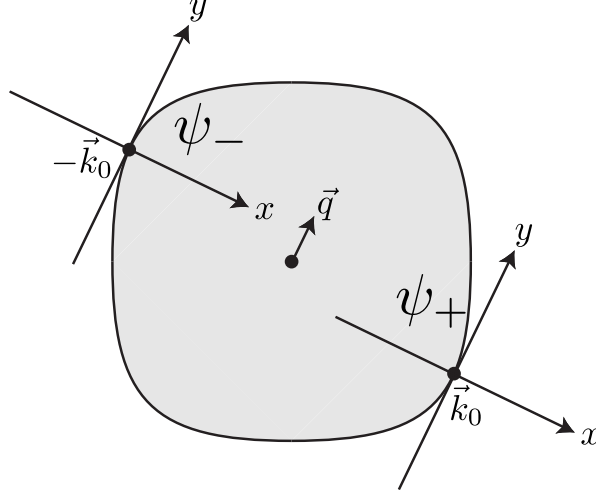


Figure 6.1: The shaded region represents the occupied states inside a Fermi surface. Fluctuations of the order parameter ϕ at wavevectors parallel to \vec{q} couple most strongly to fermions near the Fermi surface points $\pm\vec{k}_0$. These fermions are denoted ψ_{\pm} .

continuum Lagrangian becomes

$$\begin{aligned}
 L_{k_0} = & \psi_{+\sigma}^\dagger \left(\partial_\tau - iv_F \partial_x - \frac{1}{2m} \partial_y^2 \right) \psi_{+\sigma} + \psi_{-\sigma}^\dagger \left(\partial_\tau + iv_F \partial_x - \frac{1}{2m} \partial_y^2 \right) \psi_{-\sigma} \\
 & - d_{+\sigma} \phi \psi_{+\sigma}^\dagger \psi_{+\sigma} - d_{-\sigma} \phi \psi_{-\sigma}^\dagger \psi_{-\sigma} + \frac{1}{2} (\partial_y \phi)^2 + \frac{r_0}{2} \phi^2
 \end{aligned} \tag{6.4}$$

Here v_F and m are the Fermi velocity and the band mass at k_0 , while $d_{\pm\sigma} = d_{\pm k_0\sigma}$, and we have added a subscript k_0 to L emphasize that this is the Lagrangian for the patch near $\pm\vec{k}_0$.

We should emphasize here that all the fields in Eq. (6.4) are 2+1 dimensional quantum fields, with full dependence upon x , y , and τ *i.e.* the fields are $\phi(x, y, \tau)$ and $\psi_{\pm\sigma}(x, y, \tau)$. In principle, we should also add a term $(\partial_x \phi)^2$ to Eq. (6.4); however, we omit it at the outset because it will later be seen to be irrelevant near criticality.

Further, because of this full dependence on x , and y , the fermion fields $\psi_{\pm\sigma}$ describe an extended patch of the Fermi surface near the points $\pm\vec{k}_0$, and not just the two points $\pm\vec{k}_0$. We place some finite cutoff Λ on the size of this patch, and will be interested in the scaling behavior at momenta much smaller than this cutoff.

We now discuss the structure of the couplings $d_{\pm\sigma}$ in Eq. (6.4). For the transitions in s , d and g channels in case 1 above $d_{+\sigma} = d_{-\sigma}$ by inversion symmetry, and $d_{\pm\sigma}$ is σ independent. For case 2, we have $d_{+\sigma} = -d_{-\sigma}$ and also σ independent, although the fermions now couple to a projection of the two component order parameter $\vec{\phi} \cdot \vec{d}$, while the bosonic gradient term generally involves both components of the order parameter. The spin liquid case also has $d_{+\sigma} = -d_{-\sigma}$ and σ independent, and ϕ is associated with the transverse component of the spatial gauge field in the Coulomb gauge [198, 79, 75, 197]; moreover the spin-liquid has $r = 0$ by gauge invariance. Finally, the Ising ferromagnet case 3 has $d_{+\sigma} = d_{-\sigma}$ and $d_{\pm\uparrow} = -d_{\pm\downarrow}$.

We note that for transitions in non-zero angular momentum channels, the coupling d vanishes along certain axes in the Brillouin zone. The intersections of these axes with the Fermi surface are known as cold-spots, as the fermion coupling to the order parameter at these points involves additional derivatives and is much weaker. The scaling theory that follows only describes the Fermi surface away from cold spots.

It is convenient to rescale coordinates and fields in (6.4), $x = (2mv_F)^{-1}\tilde{x}$, $\psi = v_F^{-1/2}\tilde{\psi}$, $\phi = \frac{1}{2m|d|}\tilde{\phi}$. We drop the tildes in what follows. Then,

$$\begin{aligned}
 L = & \psi_{+\sigma}^\dagger \left(\eta \partial_\tau - i \partial_x - \partial_y^2 \right) \psi_{+\sigma} + \psi_{-\sigma}^\dagger \left(\eta \partial_\tau + i \partial_x - \partial_y^2 \right) \psi_{-\sigma} \\
 & - \lambda_{+\sigma} \phi \psi_{+\sigma}^\dagger \psi_{+\sigma} - \lambda_{-\sigma} \phi \psi_{-\sigma}^\dagger \psi_{-\sigma} + \frac{1}{2e^2} (\partial_y \phi)^2 + \frac{r}{2} \phi^2
 \end{aligned} \tag{6.5}$$

with $e^2 = 2md^2/v_F$, $r = r_0/(2md^2)$, $\eta = 2m$, and $\lambda_{s\sigma} = d_{s\sigma}/|d|$, and we will henceforth drop the subscript k_0 on L . We note that as usual, the relation between the parameters of the effective theory and the original model should not be taken literally. Rather, in the critical regime, we have $r_0 - r_{0c} = Z_r(r - r_c)$, where r_c and r_{0c} denote the critical points of the effective theory and the microscopic theory respectively. Moreover, the original fields and the fields defined in each patch of the Fermi surface are related by,

$$\phi(\vec{q}, \omega) \sim Z_\phi^{1/2} K \phi_{patch}(Kq_x, q_y, \omega), \quad \psi(\vec{q}, \omega) \sim Z_\psi^{1/2} K \psi_{patch}(Kq_x, q_y, \omega) \quad (6.6)$$

Note that the “metric factors” K , Z_r , e^2 , Z_ψ , Z_ϕ are generally dependent on the direction of the boson momentum \hat{q} and the cut-off of the low-energy theory Λ .

For brevity, we will only present explicit calculations for the case that does not involve spin (Ising-nematic transition and spin-liquid); the extension of the results to the Ising ferromagnet case will be noted. Moreover, we extend the number of spin components (flavours) to N from the physical value $N = 2$ with the view towards performing a large- N expansion. For this purpose, it is convenient to rescale e^2 and r , yielding our Lagrangian in its final form

$$L = \sum_{s=\pm} \psi_s^\dagger \left(\eta \partial_\tau - is \partial_x - \partial_y^2 \right) \psi_s - \sum_{s=\pm} \lambda_s \phi \psi_s^\dagger \psi_s + \frac{N}{2e^2} (\partial_y \phi)^2 + \frac{Nr}{2} \phi^2. \quad (6.7)$$

Here and below we suppress the flavour index. To reiterate, the Ising-nematic case has $\lambda_+ = \lambda_-$ and the spin-liquid case (*i.e.* Fermi surface coupled to U(1) gauge field) has $\lambda_+ = -\lambda_-$.

6.3 One loop propagators

To gain some insight into the low energy properties of the theory (6.7), it is useful to compute the one loop boson and fermion self-energies.



Figure 6.2: One loop contributions to the boson a) and fermion b) self-energies.

The one-loop boson polarization in Fig. 6.2 a) is given by,

$$\Pi_0(q) = N \int \frac{dl_\tau d^2\vec{l}}{(2\pi)^3} G_s^0(l) G_s^0(l+q) \quad (6.8)$$

We first evaluate this diagram with a bare fermion propagator,

$$G_s^0(k) = \frac{1}{-i\eta k_\tau + s k_x + k_y^2} \quad (6.9)$$

The resulting polarization function takes on a characteristic Landau-damped form,

$$\begin{aligned} \Pi_0(q) &= N \int \frac{dl_\tau dl_y}{(2\pi)^2} \frac{i [\theta(l_\tau) - \theta(l_\tau + q_\tau)]}{-i\eta q_\tau + 2q_y l_y + q_x + q_y^2} + (\vec{q} \rightarrow -\vec{q}) \\ &= \frac{N q_\tau}{2\pi} \int \frac{dl_y}{2\pi} \frac{(-i)}{-i\eta q_\tau + 2q_y l_y + q_x + q_y^2} + (\vec{q} \rightarrow -\vec{q}) = c_b N \frac{|q_\tau|}{|q_y|}, \quad c_b = \frac{1}{4\pi}. \end{aligned} \quad (6.10)$$

Note that η has dropped out of the final result. We are interested above only in the singular contribution to Π_0 , and this is insensitive to orders of integration: so unlike

the conventional order, we have integrated over l_x before l_τ . We include the RPA polarization bubble (6.10) into the bosonic propagator to obtain

$$D(q) = \frac{1}{N} \left(c_b \frac{|q_\tau|}{|q_y|} + \frac{q_y^2}{e^2} + r \right)^{-1}. \quad (6.11)$$

Note that the q_y^2 term is not renormalized by the polarization contribution at this order, and the bare co-efficient represents the phenomenological contribution of higher energy modes.

The one-loop correction to the fermion propagator is given by Fig. 6.2 b). For simplicity, we work at the critical point and set $r = 0$. Then, the fermion self-energy assumes a non-Fermi liquid form

$$\begin{aligned} \Sigma_s(k) &= - \int \frac{dl_\tau d^2\vec{l}}{(2\pi)^3} D(l) G_s^0(k-l) \\ &= - \frac{i}{2N} \int \frac{dl_\tau dl_y}{(2\pi)^2} \left(c_b \frac{|l_\tau|}{|l_y|} + \frac{l_y^2}{e^2} \right)^{-1} \times \text{sgn}(k_\tau - l_\tau) \\ &= - \frac{i c_f}{N} \text{sgn}(k_\tau) |k_\tau|^{2/3}, \quad c_f = \frac{2}{\sqrt{3}} \left(\frac{e^2}{4\pi} \right)^{2/3}. \end{aligned} \quad (6.12)$$

Note, again, that η has dropped out of the result. Incorporating this correction into the fermion propagator,

$$G_s(k) = \left(- \frac{i c_f}{N} \text{sgn}(k_\tau) |k_\tau|^{2/3} + s k_x + k_y^2 \right)^{-1} \quad (6.13)$$

Here we have dropped the bare fermion time derivative term proportional to η , which is irrelevant at low energies compared to the dynamically induced self-energy (6.12).

As is well known,[75] the one-loop expressions (6.10), (6.12) actually satisfy the Eliashberg-like equations, in which the lines of Fig. 6.2 become self-consistent propagators. In what follows, we will use these self-consistent propagators (6.11), (6.13) in our calculations and drop self-energy corrections like those in Fig. 6.2.

6.4 Scaling and renormalization

As has been argued by a number of authors [75, 198, 79, 197], a useful starting point for the renormalization group analysis of the theory (6.7) is obtained by using the scaling,

$$\begin{aligned}
 k_x &\rightarrow s^2 k_x, \quad k_y \rightarrow s k_y, \quad \omega \rightarrow s^3 \omega, \\
 \psi(x, y, \tau) &\rightarrow s^2 \psi(s^2 x, s y, s^3 \tau), \quad \phi(x, y, \tau) \rightarrow s^2 \phi(s^2 x, s y, s^3 \tau)
 \end{aligned} \tag{6.14}$$

This scaling is suggested by the one-loop calculation of fermion and boson propagators in Eqs. (6.11), (6.13). The bare fermion time derivative term $\psi^\dagger \partial_\tau \psi$ is irrelevant under this scaling, and so we will take the limit $\eta \rightarrow 0^+$. Note that neither of the one loop corrections Eqs. (6.10), (6.12) depend upon η .

Alternatively, note that the scaling of time in (6.14) could also have been derived by demanding that the ‘Yukawa coupling’ λ_s be invariant. This avoids the somewhat unnatural appeal to the one-loop self-energy to set bare scaling dimensions, and yields all the scaling dimensions in (6.14) by a simple rescaling of the bare Lagrangian L in Eq. (6.7). Of course, once we have set λ_s to be invariant, then the coupling η becomes irrelevant. These features of the scaling analysis are shared by the theory of the nematic transition in d -wave superconductors in Ref. [196].

Note also the different scaling of spatial momenta k_x and k_y in Eq. (6.14). The main physical consequence of such momentum anisotropy is the effective decompactification of the Fermi surface, which allows one to focus on a theory with two Fermi patches. Also observe that under (6.14) the $(\partial_x \phi)^2$ part of the boson tree level action is irrelevant, which justifies omitting this term in eqs. (6.4), (6.7).

Apart from the fermion time derivative term and the relevant mass perturbation ($r \rightarrow s^{-2}r$), all the terms in the Lagrangian (6.7) are marginal. Higher order perturbations to (6.7), consistent with the Z_2 symmetry of the order parameter, such as a ϕ^4 term, are irrelevant.

We would like to note that for the case of the Ising-nematic (or g -wave) transition the low-energy action (6.7) does not possess a $\phi \rightarrow -\phi$ symmetry. This is due to the fact that the direction of bosonic momentum \vec{q} is transformed under $\pi/2$ rotations (reflections) and hence the physics is controlled by a different pair of patches of the Fermi surface. Hence, in principle, it is possible that in the kinematic regime of interest a ϕ^3 term is generated by the renormalization group process. Such a term would be marginal under the scaling (6.14). A linear term in ϕ can also be generated by the effective theory. However, the one-point function has momentum $\vec{q} = 0$ and, hence, does not belong to any particular kinematic regime. In practice, we can demand that the expectation value of ϕ is zero in the disordered phase by tuning the coefficient of the ϕ -linear term. In any case, as we will show below, there exists a Ward identity, which guarantees that if these terms are initially zero, they are not generated by the RG of the low-energy theory (6.7). Note that for the case of the spin-liquid or Ising ferromagnet transitions, the low energy theory (6.7) respects the time reversal symmetry which maps Fermi patches at k_0 and $-k_0$ into each other and, hence, terms odd in ϕ are prohibited.

An important observation is that the theory (6.7) lacks an expansion parameter. To see this, note that due to the rescaling performed in section 6.2, the engineering dimensions, $[k_x] = [k_y]^2$, but the dimension of ω is kept independent. Then, the

coupling constant e^2 has the dimensions $[k_y]^3/[\omega]$. Therefore, e^2 is a dimensionful quantity and cannot be used as an expansion parameter. Moreover, e^2 is actually the only parameter in the theory relating frequencies and momenta. Hence, its flow under RG is equivalent to an appearance of a non-trivial dynamical critical exponent.

Note that up to this point we have dropped an allowed relevant fermion chemical potential term,

$$\Delta L = -\delta \psi_s^\dagger \psi_s \tag{6.15}$$

This term can be absorbed into the definition of the momentum \vec{k}_0 about which the theory is expanded and, thus, is redundant (note, the scaling dimension $[\delta] = [k_x] = 2$). Nevertheless, it is convenient to leave this term in the Lagrangian for renormalization group purposes. We assume that when the theory is tuned to the criticality $r = r_c$ and the coefficient δ is set to $\delta = \delta_c$, the Fermi surface passes through the points $\vec{k}_0, -\vec{k}_0$.

We now discuss the renormalization of our theory. The Lagrangian contains four marginal operators, which each requires a renormalization constant. However, as we will argue below, emergent low-energy symmetries of the theory (6.7) imply certain relations between these constants. Moreover, the two relevant operators, have the same bare dimension, $[r] = [\delta] = 2$. Thus, we need to consider possible mixing between these operators.

6.4.1 Rotational symmetry

Observe that the initial shape of the Fermi surface does not enter the low-energy theory (6.7). In fact, we could have started with a circular Fermi surface with

$k_F = mv_F$. This is reflected by the fact that Eq. (6.7) has an emergent continuous “rotational symmetry”,

$$\phi(x, y) \rightarrow \phi(x, y + \theta x), \quad \psi_s(x, y) \rightarrow e^{-is(\frac{\theta}{2}y + \frac{\theta^2}{4}x)}\psi_s(x, y + \theta x) \quad (6.16)$$

Equivalently in momentum space,

$$\phi(q_x, q_y) \rightarrow \phi(q_x - \theta q_y, q_y), \quad \psi_s(q_x, q_y) \rightarrow \psi_s\left(q_x - \theta q_y - s\frac{\theta^2}{4}, q_y + s\frac{\theta}{2}\right) \quad (6.17)$$

Note that the rotation angle θ becomes non-compact and the rotation group becomes \mathbb{R} instead of $U(1)$. This is a consequence of the effective decompactification of the Fermi surface. Moreover, due to the anisotropic scaling θ is now dimensionful $[\theta] = [k_y]$. In fact, the situation is analogous to the transformation of the Lorentz symmetry to Galilean invariance in the non-relativistic limit $\omega \ll c|\vec{q}|$. Here the role of ω is played by q_x and the role of $|\vec{q}|$ by q_y .

The symmetry (6.17) implies the following form of the bosonic and fermionic Green’s functions (we suppress the frequency dependence):

$$D(q_x, q_y) = D(q_y) \quad (6.18)$$

$$G_s(q_x, q_y) = G(sq_x + q_y^2). \quad (6.19)$$

In particular, the form of the fermionic Green’s function implies that the terms $\psi_s^\dagger(-is\partial_x)\psi_s$ and $\psi_s(-\partial_y^2)\psi_s$ in the Lagrangian (6.7) must renormalize in the same way. Physically, this means that the curvature radius of the Fermi surface K does not flow under RG (*i.e.* K has a limit as the cutoff $\Lambda \rightarrow 0$).

The identities (6.18,6.19) ensure that the Green’s functions at a given physical momentum remain invariant under small changes in the choice of the points $\pm\vec{k}_0$ on

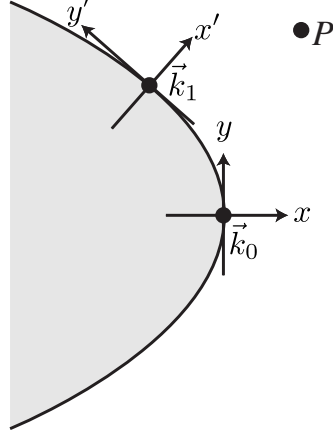


Figure 6.3: The momentum of the fermion at point P can be measured with respect to either the co-ordinate system at \vec{k}_0 , or that at \vec{k}_1 .

the Fermi surface about which the field theory is defined. Let us demonstrate this explicitly using Fig. 6.3. We set the co-ordinate system so that $\vec{k}_0 = (0, 0)$, and measure the momentum of a fermion at the point P to be (q_x, q_y) . Now let us shift to the field theory defined at the Fermi surface point $\vec{k}_1 = (\kappa_x, \kappa_y)$. As this point has to be on the Fermi surface, we have $\kappa_x + \kappa_y^2 = 0$. We denote the co-ordinates of the point P in the new co-ordinate system by (q'_x, q'_y) . These are obtained from the old co-ordinates by a shift in origin followed by a rotation by an angle θ , where $\tan \theta = 2\kappa_y$; this yields

$$\begin{aligned} q'_x &= q_x - \kappa_x + 2\kappa_y(q_y - \kappa_y) \\ q'_y &= q_y - \kappa_y \quad , \end{aligned} \tag{6.20}$$

where we only keep terms to the needed accuracy of $\mathcal{O}(x, y^2)$. It can now be verified that $q'^2_x + q'^2_y = q_x^2 + q_y^2$, and so by Eq. (6.19) the fermion Green's function remains

invariant under the change in the Fermi surface reference point. Also, by choosing $\kappa_y = q_y$ we can set $q'_y = 0$, and then $q_x + q_y^2$ is identified as the invariant measuring the distance between P and the closest point on the Fermi surface. For the boson Green's function, there is no shift in origin of the co-ordinates, and the corresponding transformation is $q'_x = q_x + 2\kappa_y q_y$, $q'_y = q_y$, and this remains invariant under Eq. (6.18).

These invariances are essential in ensuring the consistency of our description of each pair of time-reversed Fermi surface points by a separate 2+1 dimensional field theory. Note that such a consistency requirement would not have arisen if we had used a 1+1 dimensional field theory at each Fermi surface point,[199, 200, 201, 202, 203, 188, 187] because then every fermion momentum would appear only in the theory defined at the closest point on the Fermi surface. In our case, we are free to use the 2+1 dimensional theory at this closest point, or at any of the neighboring points.

Before concluding this section, we would like to point out that in the case of the Ising-nematic transition, the “rotational symmetry” (6.17) is not related in any way to “large” rotations by $\pi/2$, which are actually not implemented in the low-energy theory.

6.4.2 Ward identities

We now examine the consequences of Ward identities associated with the global symmetries of Eq. (6.7). Similar consequences were implicit in the analysis of the superconducting case in Ref. [196]. Here we will present a more formal analysis, which also shows that Eq. (3.20) in Ref. [196] holds to all orders in $1/N$.

The low energy theory (6.7) has two continuous global $U(1)$ symmetries. The first

of these is related to the conservation of particle number,

$$U(1)_F : \psi_+ \rightarrow e^{i\alpha}\psi_+, \quad \psi_- \rightarrow e^{i\alpha}\psi_- \quad (6.21)$$

The conserved current associated with this symmetry is,

$$(j_\tau, j_x, j_y)_F = (i\eta(\psi_+^\dagger\psi_+ + \psi_-^\dagger\psi_-), \psi_+^\dagger\psi_+ - \psi_-^\dagger\psi_-, -i(\psi_+^\dagger\overleftrightarrow{\partial}_y\psi_+ + \psi_-^\dagger\overleftrightarrow{\partial}_y\psi_-)) \quad (6.22)$$

For the spin-liquid problem, the gauge field ϕ couples precisely to the x component of j_F .

The second $U(1)$ symmetry is lattice translation. Indeed, ψ_+ and ψ_- come from opposite points in the Brillouin zone and, hence, transform under general lattice translations as,

$$U(1)_T : \psi_+ \rightarrow e^{i\alpha}\psi_+, \quad \psi_- \rightarrow e^{-i\alpha}\psi_- \quad (6.23)$$

The conserved current associated with this symmetry is

$$(j_\tau, j_x, j_y)_T = (i\eta(\psi_+^\dagger\psi_+ - \psi_-^\dagger\psi_-), \psi_+^\dagger\psi_+ + \psi_-^\dagger\psi_-, -i(\psi_+^\dagger\overleftrightarrow{\partial}_y\psi_+ - \psi_-^\dagger\overleftrightarrow{\partial}_y\psi_-)) \quad (6.24)$$

Observe that the Ising-nematic order parameter ϕ couples to the x component of j_T . Note that despite the similarity of the spin-liquid and Ising-nematic problems, there is an important difference. In the spin-liquid case, the gauge field couples to the fermion current on all energy scales. In the case of the Ising-nematic transition, the order parameter couples to a conserved current only at low energies.

We note in passing that for an Ising ferromagnet transition, the current to which the order parameter couples is related to the symmetry,

$$U(1)_I : \psi_{+\uparrow} \rightarrow e^{i\alpha}\psi_{+\uparrow}, \quad \psi_{-\uparrow} \rightarrow e^{-i\alpha}\psi_{-\uparrow}, \quad \psi_{+\downarrow} \rightarrow e^{-i\alpha}\psi_{+\downarrow}, \quad \psi_{-\downarrow} \rightarrow e^{i\alpha}\psi_{-\downarrow} \quad (6.25)$$

In fact, this is not a symmetry of the underlying theory, but only of the low-energy Lagrangian (6.4). The symmetry is broken by four-Fermi interactions, which are however irrelevant under (6.14).

Current conservation implies that the insertion of $\partial_\tau j_\tau + \partial_x j_x + \partial_y j_y$ into any correlation function is zero, up to contact terms (we have dropped the current subscript; the current, which couples to the order parameter is implicitly assumed). We note that the temporal component of the currents (6.22), (6.24) has a coefficient η in front and, therefore, can be set to zero in the kinematic regime of interest. We, thus, have $\partial_x j_x + \partial_y j_y \sim 0$. Defining the one-particle irreducible polarization function,

$$\Pi_{ij}(q) = \int d\tau d^2x e^{iq_\tau \tau - i\vec{q}\cdot\vec{x}} \langle j_i(x) j_j(0) \rangle_{1PI} \quad (6.26)$$

we have

$$q_x \Pi_{xx}(q) + q_y \Pi_{yx}(q) = 0 \quad (6.27)$$

We note that $\Pi_{xx}(q) = \Pi_{xx}(q_\tau, q_y)$ is precisely the irreducible boson self-energy. Hence,

$$\Pi_{yx}(q_\tau, q_x, q_y) = -\frac{q_x}{q_y} \Pi_{xx}(q_\tau, q_y)$$

Power counting indicates that Π_{xx} has the following UV structure

$$\Pi_{xx}(q_\tau, q_y) \stackrel{UV}{=} K_1 + K_2 r + K_3 q_y^2 \quad (6.28)$$

where $K_1 \sim \Lambda^2$, $K_2, K_3 \sim \log \Lambda$ and Λ is the UV cut-off with dimensions of q_y . For $\Pi_{yx}(q_\tau, q_x, q_y)$ to have an analytic UV behaviour (as again expected from power counting), we must have

$$K_1 = K_2 = 0$$

Thus, the coefficient of the mass operator ϕ^2 requires no renormalization (*i.e.* the metric factor Z_r has a limit as $\Lambda \rightarrow 0$).

An interesting question is whether the polarization function Π_{xx} actually vanishes for $q_y \rightarrow 0$ as suggested by Eq. (6.27). However, for finite q_r we already know from one-loop calculations that such a limit does not exist within the scaling regime, as

$$\Pi_{xx}(q_r, q_y)_{1loop} = c_b \frac{|q_r|}{|q_y|}, \quad \Pi_{yx}(q_r, q_x, q_y)_{1loop} = -c_b \frac{q_x |q_r|}{q_y |q_y|}$$

However, one might hope that the limits $\lim_{q_y \rightarrow 0} \lim_{q_r \rightarrow 0} \Pi_{xx}(q_r, q_y)$, $\Pi_{xy}(q_r, q_x, q_y)$ do exist. In this case, we would conclude,

$$\lim_{q_y \rightarrow 0} \lim_{q_r \rightarrow 0} \Pi_{xx}(q_r, q_y) = 0 \tag{6.29}$$

which would be a stronger statement than the non-renormalization of the mass term. Otherwise, if the limit above exists only for Π_{xx} by not Π_{xy} then,

$$\lim_{q_y \rightarrow 0} \lim_{q_r \rightarrow 0} \Pi_{xx}(q_r, q_y) = c_r r \tag{6.30}$$

with c_r - some universal constant. We have explicitly checked that to three loop order $c_r = 0$ and the strong form of the non-renormalization identity Eq. (6.29) holds.

One can generalize the discussion above to higher order correlation functions of the order parameter. Ward-identities imply that the effective potential for the ϕ field is not renormalized from its tree-level form,

$$V(\phi) = \frac{r}{2} \phi^2 \tag{6.31}$$

This property is also shared by the theory of the nematic transition in a d -wave superconductor.[195, 196] In particular, no ϕ^3 term is induced in the Lagrangian by

the renormalization group process if this term is originally zero. (Note that if a ϕ^3 term is initially present, correlation functions of currents no longer coincide with the correlation functions of the order parameter, and the Ward identities do not constrain the renormalization properties of the theory). The effective potential (6.31) becomes unstable for $r < 0$. Thus, we expect that in the ordered phase the theory is controlled by dangerously irrelevant operators, such as ϕ^4 .

Finally, one can derive a Ward identity for the fermion boson vertex,

$$q_x \Gamma_x(q, p, p + q) + q_y \Gamma_y(q, p, p + q) = G^{-1}(p + q) - G^{-1}(p) \quad (6.32)$$

with

$$\Gamma_i(q, p, p + q) = \int dx_\tau d^2x dy_\tau d^2y e^{-iq_\tau x_\tau + i\vec{q}\cdot\vec{x}} e^{i(p+q)_\tau y_\tau - i(\vec{p}+\vec{q})\cdot\vec{y}} \langle j_i(x) \psi(y) \psi^\dagger(0) \rangle_{1PI} \quad (6.33)$$

$$G(p) = \int d\tau d^2x e^{iq_\tau \tau - i\vec{q}\cdot\vec{x}} \langle \psi(x) \psi^\dagger(0) \rangle \quad (6.34)$$

Γ_x is precisely the irreducible fermion-boson vertex. Power counting gives UV structure of Γ_x and G^{-1} as,

$$\Gamma_x(q, p, p + q) = C_1 \quad (6.35)$$

$$G^{-1}(p) = C_2 + C_3(p_x + p_y^2) \quad (6.36)$$

Thus, for the UV behaviour of Γ_y to be analytic in external momenta, $C_1 = C_3$. Therefore, the vertex and the fermion self-energy renormalize in the same way. Hence, the boson field requires no field-strength renormalization (*i.e.* the metric factor Z_ϕ has a limit as $\Lambda \rightarrow 0$).

Before concluding this section, we would like to note that perturbation theory based on self-consistent propagators (6.11), (6.13) actually does not respect the Ward

identities. This is due to the fact that these one-loop propagators include the fermion self-energy correction, but not the vertex correction. However, since the fermion self-energy is only frequency dependent, Ward identities involving currents at zero external frequency are still respected.

6.4.3 RG equations

From the discussion above, we conclude that at criticality, our theory needs only two renormalizations: a rescaling of the field strength of the fermion field ψ and a renormalization of e^2 ,

$$\psi = Z_\psi^{1/2} \psi_r, \quad e^2 = Z_e e_r^2 \quad (6.37)$$

Here the subscript r denotes renormalized quantities and we define renormalized irreducible correlation functions of n_b boson and n_f fermion fields as,

$$\Gamma_r^{n_b, n_f} = Z_\psi^{n_f/2} \Gamma^{n_b, n_f} \quad (6.38)$$

Both Z_ψ and Z_e are functions of Λ/μ where μ is a renormalization scale (which we choose to have dimensions of q_y) and of the number of fermion flavours N . As e^2 is dimensionful, Z_ψ and Z_e cannot depend on it. We introduce the anomalous dimensions,

$$b = \Lambda \frac{\partial}{\partial \Lambda} \log Z_e \quad (6.39)$$

$$\eta_\psi = -\Lambda \frac{\partial}{\partial \Lambda} \log Z_\psi \quad (6.40)$$

The constants η_ψ and b are expected to be pure universal numbers, independent of Λ/μ .

Away from criticality, we recall that by the Ward identity, the coupling r does not renormalize. On the other hand, the coupling δ can pick up a renormalization linear in r ,

$$\delta = \delta_c + \delta_r + Z_{r\delta} e_r^2 r \quad (6.41)$$

with $Z_{r\delta}$ again a function of Λ/μ only. In what follows, we denote $\delta - \delta_c$ as δ for brevity. Note that there is no renormalization constant in front of δ_r since a finite change in δ only shifts the value of k_x in correlation functions:

$$\Gamma^{n_b, n_f}(\{p\}, \delta + a) = \Gamma^{n_b, n_f}(\{p - sa\hat{x}\}, \delta) \quad (6.42)$$

where $s = \pm 1$ for momenta of fermions ψ_{\pm} and $s = 0$ for boson momenta. We let,

$$\alpha = Z_e^{-1} \Lambda \frac{\partial}{\partial \Lambda} Z_{r\delta} \quad (6.43)$$

Now, differentiating Eq. (6.38) we obtain the renormalization group equations

$$\left(\Lambda \frac{\partial}{\partial \Lambda} + be^2 \frac{\partial}{\partial e^2} + \alpha e^2 r \frac{\partial}{\partial \delta} - \frac{n_f}{2} \eta_{\psi} \right) \Gamma^{n_b, n_f}(\{p_y\}, \{p_x\}, \{\omega\}, r, \delta, e^2, \Lambda) = 0 \quad (6.44)$$

It is convenient to get rid of the derivative with respect to δ in Eq. (6.44). To do so, let the location of the Fermi-surface of fermion ψ_+ at finite δ and r be given by $k_x + k_y^2 = \Delta k(r, \delta, e^2, \Lambda)$. Then, Δk is clearly a physical quantity and must satisfy,

$$\left(\Lambda \frac{\partial}{\partial \Lambda} + be^2 \frac{\partial}{\partial e^2} + \alpha e^2 r \frac{\partial}{\partial \delta} \right) \Delta k(r, \delta, e^2, \Lambda) = 0. \quad (6.45)$$

We will solve this equation shortly. However, first note that

$$\frac{\partial \Delta k}{\partial \delta} = 1. \quad (6.46)$$

Now, it is convenient to expand momenta around the physical Fermi-surface, defining,

$$\tilde{\Gamma}^{n_b, n_f}(\{p\}, r, \delta, e^2, \Lambda) = \Gamma^{n_b, n_f}(\{p + s\Delta k(r, \delta, e^2, \Lambda)\hat{x}\}, r, \delta, e^2, \Lambda) \quad (6.47)$$

The resulting $\tilde{\Gamma}$ is independent of δ and by Eqs. (6.42), (6.44), (6.45), (6.46) satisfies,

$$\left(\Lambda \frac{\partial}{\partial \Lambda} + be^2 \frac{\partial}{\partial e^2} - \frac{n_f}{2} \eta_\psi \right) \tilde{\Gamma}^{n_b, n_f}(\{p_y\}, \{p_x\}, \{\omega\}, r, e^2, \Lambda) = 0 \quad (6.48)$$

By dimensional analysis,

$$\tilde{\Gamma}^{n_b, n_f} = \Lambda^{6-2n_f-2n_b} (e^2)^{n_f/2-1} f^{n_b, n_f} \left(\left\{ \frac{p_y}{\Lambda} \right\}, \left\{ \frac{p_x}{\Lambda^2} \right\}, \left\{ \frac{\omega e^2}{\Lambda^3} \right\}, \frac{\Lambda^2 r}{\mu^2} \right) \quad (6.49)$$

and solving the RG equation, we obtain

$$f^{n_b, n_f}(s\{\tilde{p}_y\}, s^2\{\tilde{p}_x\}, s^{3-b}\{\tilde{\omega}\}, s^{2-b}\tilde{r}) = s^{6-b+(b-\eta_\psi-4)n_f/2-2n_b} f^{n_b, n_f}(\{\tilde{p}_y\}, \{\tilde{p}_x\}, \{\tilde{\omega}\}, \tilde{r}) \quad (6.50)$$

Hence, the critical theory is invariant under,

$$p_y \rightarrow sp_y, \quad p_x \rightarrow s^2 p_x, \quad \omega \rightarrow s^z \omega \quad (6.51)$$

with

$$z = 3 - b, \quad (6.52)$$

where z is the dynamic critical exponent. Note that we have defined z with reference to length scales associated with directions tangent to the Fermi surface (y); as indicated in (6.51), length scales orthogonal to the Fermi surface scale as the square of length scales tangent to the Fermi surface. Moreover, if we define ξ as the correlation length along the y direction then upon approaching the critical point, $\xi \sim r^{-\nu}$, with

$$\nu = \frac{1}{z-1}. \quad (6.53)$$

Note that by combining Eqs. (6.37,6.39,6.52) we can write down the RG equation for the coupling e :

$$\Lambda \frac{\partial e^2}{\partial \Lambda} \Big|_{e^2, \mu} = -(z-3)e^2. \quad (6.54)$$

This shows that the renormalization of the coupling e is directly related to the dynamic critical exponent, as we had claimed earlier.

Now, let us consider a few explicit examples of correlation functions. For the bosonic two-point function we have,

$$D^{-1}(q_y, \omega) = rg \left(q_y (re^2 \Lambda^{z-3})^{-\frac{1}{z-1}}, \omega (r^z e^2 \Lambda^{z-3})^{-\frac{1}{z-1}} \right) \quad (6.55)$$

Note that,

$$\lim_{q_y \rightarrow 0} \lim_{\omega \rightarrow 0} D^{-1}(q_y, \omega) = rg(0, 0) \quad (6.56)$$

i.e. the Ising-nematic susceptibility satisfies $\chi \sim r^{-\gamma}$ with the exponent

$$\gamma = 1. \quad (6.57)$$

We may also write more succinctly,

$$D^{-1}(q_y, \omega) \propto \xi^{-(z-1)} g(q_y \xi, \omega e^2 \Lambda^{z-3} \xi^z) \quad (6.58)$$

So far, we have been concentrating on a fixed direction of bosonic momentum \vec{q} . Now let us study the dependence of the result on \hat{q} . Using Eq. (6.6)

$$D^{-1}(\vec{q}, \omega) = Z_\phi^{-1} K^{-1} Z_r^{-1} r_0 g \left(|\vec{q}| (Z_r^{-1} e^2 \Lambda^{z-3} r_0)^{-\frac{1}{z-1}}, \omega (Z_r^{-z} e^2 \Lambda^{z-3} r_0^z)^{-\frac{1}{z-1}} \right) \quad (6.59)$$

where for brevity r_0 is taken to denote the deviation from the critical point. We concentrate on the static limit $\omega = 0$. In a Fermi liquid, the susceptibility must have a continuous limit as $\vec{q} \rightarrow 0$. Therefore, we conclude that the combination $Z_\phi K Z_r$ must be independent of the direction \hat{q} . This is quite plausible, as neither of the constants run under RG.

Now let us look at the behaviour of susceptibility at the critical point,

$$D^{-1}(q_y, \omega) = \frac{q_y^{z-1}}{e^2 \Lambda^{z-3}} h \left(\frac{\omega e^2 \Lambda^{z-3}}{q_y^z} \right) \quad (6.60)$$

In particular, the static susceptiblity satisfies,

$$D^{-1}(\vec{q}, 0) \sim a(\hat{q}) |\vec{q}|^{z-1} \quad (6.61)$$

In the context of the spin-liquid problem, many studies [205, 208, 209, 210, 211, 212] examined the structure of the higher loop corrections to the susceptibility. In particular, Kim *et al.* [205] examined two-loop corrections to $\text{Im } D^{-1}(\vec{q}, \omega)$ for real frequencies $|\omega| \ll |\vec{q}|$, and found no corrections to the leading answer $\sim \omega/|q_y|$ in Eq. (6.11); Fermi liquid arguments were made [205, 208, 209, 210, 211] that this functional form held at higher orders. However, this result by itself does not fix the value of z ; indeed, $\text{Im } D^{-1}(\vec{q}, \omega) \sim \omega/|q_y|$ is consistent with the scaling form (6.60) for *any* z . These studies also implicitly assumed a Fermi liquid picture with $D^{-1}(\vec{q}, \omega = 0) \sim \vec{q}^2$, and this does imply $z = 3$. We will examine $D^{-1}(\vec{q}, \omega = 0)$ up to 3 loops in Section 6.5.1, and find no correction to $z = 3$.

Proceeding to the fermion Green's function,

$$G_s^{-1}(\vec{k}, \omega) = \Lambda^2 \left(\frac{r e^2}{\Lambda^2} \right)^{\frac{2-\eta_\psi}{z-1}} L \left(k (r e^2 \Lambda^{z-3})^{-\frac{2}{z-1}}, \omega (r^z e^2 \Lambda^{z-3})^{-\frac{1}{z-1}} \right) \quad (6.62)$$

with $k = s k_x + k_y^2$ - the distance to the Fermi surface. More compactly,

$$G^{-1}(\vec{k}, \omega) \propto \xi^{-(2-\eta_\psi)} L(k \xi^2, \omega e^2 \Lambda^{z-3} \xi^z) \quad (6.63)$$

A crucial property of the theory that is manifested by the above expression is that the “fermionic correlation length” scales as the square of the “bosonic correlation length”.

For $\omega \ll \xi^{-z}$, $k \ll \xi^{-2}$ we expect the fermion Green's function to assume a Fermi-liquid form,

$$G(\vec{k}, \omega) = \frac{Z}{-i\omega + v_F k} \quad (6.64)$$

By matching to the scaling form,

$$v_F \sim \xi^{-(z-2)}, \quad Z \sim \xi^{-(z+\eta_\psi-2)} \quad (6.65)$$

Notice that both the Fermi velocity v_F and the residue Z tend to zero as we approach the critical point, albeit with different power laws. Finally, at the quantum critical point,

$$G^{-1}(\vec{k}, \omega) = \Lambda^{\eta_\psi} k^{1-\eta_\psi/2} P\left(\frac{\omega e^2 \Lambda^{z-3}}{k^{z/2}}\right), \quad (6.66)$$

where we reiterate that $k = sk_x + k_y^2$ is the distance to the Fermi surface. In particular, the self-energy on the Fermi surface scales as,

$$G^{-1}(0, \omega) \sim \omega^{(2-\eta_\psi)/z} \quad (6.67)$$

and the static self energy,

$$G^{-1}(\vec{k}, 0) \sim k^{1-\eta_\psi/2} \quad (6.68)$$

Moreover, from Eq. (6.66) we can obtain the tunneling density of states,

$$N(\omega) = \int \frac{d^2 k}{(2\pi)^2} A(\vec{k}, \omega) \quad (6.69)$$

where

$$A(\vec{k}, \omega) = -\frac{1}{\pi} \text{Im} G(\vec{k}, i\omega \rightarrow \omega + i0^+) \quad (6.70)$$

The \vec{k} integral in Eq. (6.69) factorizes into integrals over components along and perpendicular to the Fermi surface. The former gives a factor proportional to the

perimeter of the Fermi surface, while the later yields the frequency dependence,

$$N(\omega) \sim \omega^{\eta_\psi/z} \quad (6.71)$$

We remind the reader that the expression in Eq. (6.71) corresponds to the physically observable electron tunneling density of states only in the case of a nematic transition, as for the spin/charge-liquid problem, the physical electron operator is a product of ψ and a boson operator.

Related scaling forms for the fermion Green's function were discussed on a phenomenological basis by Senthil.[213, 214] However his definition of z differs from ours. We define it using the fermion momentum parallel to the Fermi surface, because this is the natural momentum scale appearing also in the boson correlations. He defines it by the fermion momentum orthogonal to the Fermi surface, which scales as the square of the parallel momentum.

Finally, let us discuss the shift of the Fermi surface Δk . Using Eq. (6.46) in the RG equation (6.45), we obtain,

$$\Delta k = \frac{\alpha}{z-3} r e^2 + C_k (r e^2 \Lambda^{z-3})^{2\nu} + \delta \quad (6.72)$$

Thus, the shift of the Fermi surface upon deviation from the critical point receives two contributions: one analytic in r and the other non-analytic. Reexpressing the second contribution in terms of the correlation length,

$$\Delta k = \frac{\alpha}{z-3} r e^2 + \tilde{C}_k \xi^{-2} + \delta \quad (6.73)$$

where the coefficient \tilde{C}_k is expected to be universal. We would like to point out that the case $z = 3$ has to be treated separately. In this situation one obtains,

$$\Delta k = \frac{\alpha r e^2}{2} \log \frac{r e^2}{\Lambda^2} = -\hat{C}_k \xi^{-2} \log(\Lambda \xi) + \delta \quad (6.74)$$

with \hat{C}_k again universal.

The value of the Fermi surface shift Δk can be used to compute the compressibility, $\frac{\partial n}{\partial \mu}$, where μ is the physical chemical potential. Indeed, by Luttinger's theorem the change in density can be obtained as,

$$\delta n = \frac{N}{(2\pi)^2} \int ds \Delta k(\theta) \quad (6.75)$$

where the integral is over the circumference of the Fermi-surface. The main question is how does the chemical potential enter our low-energy theory. If μ only couples to the operator $\psi^\dagger \psi$, renormalizing the value of δ , then from Eqs. (6.72), (6.74) we would conclude that the compressibility tends to a constant and has no interesting corrections near the quantum critical point. On the other hand, if the coupling r has a non-trivial μ dependence, then we would conclude,

$$\frac{\partial n}{\partial \mu} = \kappa_0 + \kappa_1 \xi^{z-3}, \quad z \neq 3 \quad (6.76)$$

$$\frac{\partial n}{\partial \mu} = \kappa_0 + \hat{\kappa}_1 \log \Lambda \xi, \quad z = 3 \quad (6.77)$$

Note that for $z \geq 3$ the above forms imply that the compressibility diverges as we approach the critical point.

6.5 Anomalous exponents to three loops

In this section, we evaluate the exponents z and η_ψ to three loop order. We find that the exponent η_ψ is non-zero at this order. The value of η_ψ is not suppressed in the large- N limit. On the other hand, the dynamical critical exponent z remains unrenormalized from its RPA value $z = 3$ to this order. Moreover, in the large- N

limit, the boson self energy acquires a finite correction of order $N^{3/2}$, which is larger than the bare value (order N). Finally, we find that the constant α in Eq. (6.43) associated with the shift of the Fermi-surface away from criticality is non-zero at three loop order. We note that the $N^{3/2}$ correction to the boson self-energy and the non-zero η_ψ are only present for the Ising-nematic and spin-liquid universality classes, and are absent for the Ising ferromagnet transition.

6.5.1 Dynamical critical exponent

Let us first address the question of renormalization of e^2 . At two-loops the only correction to the static boson-self energy $\Pi(q_\tau = 0, \vec{q})$, which is not already taken into account by the solution to self-consistent Eliashberg equations is given in Fig. 6.4. However, this diagram vanishes when the external frequency is equal to zero. Indeed, as pointed out in Ref. [198], any diagram with fermions from a single patch, in which the fermion propagators involve a sum of two or less internal momenta, vanishes in the static limit (one picks the internal frequency with the largest absolute value and integrates over the corresponding x component of the momentum. All poles will be in the same half-plane). Actually, a calculation presented in Appendix E.2 shows that the diagram in Fig. 6.4 vanishes for any external frequencies and momenta.

The three loop corrections to $\Pi(q)$ are shown in Figs. 6.5 and 6.6. By the argument described above, all of these diagrams vanish when the external frequency is zero if all the fermions are from the same patch. Hence, the only non-zero corrections to $\Pi(q_\tau = 0, \vec{q})$ come from the Aslamazov-Larkin type diagrams, Fig. 6.6,

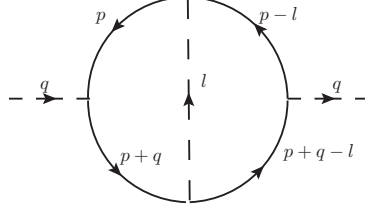


Figure 6.4: Two loop corrections to the polarization.

$$\delta^3\Pi(q) = -\frac{1}{2} \int \frac{dl_\tau d^2\vec{l}}{(2\pi)^3} \Gamma^3(q, l, -(l+q)) \Gamma^3(-q, -l, l+q) D(l) D(l+q) \quad (6.78)$$

Here Γ^3 is the fermion-induced cubic boson vertex, which receives contribution from the two fermion patches,

$$\Gamma^3 = \Gamma_+^3 + \Gamma_-^3 \quad (6.79)$$

$$\Gamma_s^3(l_1, l_2, l_3) = N\lambda_s^3(f_s(l_1, l_2, l_3) + f_s(l_2, l_1, l_3)) \quad (6.80)$$

$$f_s(l_1, l_2, l_3) = \int \frac{dp_\tau d^2\vec{p}}{(2\pi)^3} G_s(p) G_s(p-l_1) G_s(p+l_2) \quad (6.81)$$

The diagrams where the fermions in the two loops come from the same patch give a vanishing contribution to $\Pi(q_\tau = 0, \vec{q})$. Thus, to three loops,

$$\begin{aligned} \delta^3\Pi(q_\tau = 0, \vec{q}) &= -\frac{1}{2} \int \frac{dl_\tau d^2\vec{l}}{(2\pi)^3} \Gamma_+^3(q, l, -(l+q)) \Gamma_-^3(-q, -l, l+q) D(l) D(l+q) \\ &+ (q \rightarrow -q) \\ &= -\lambda_+^3 \lambda_-^3 N^2 \int \frac{dl_\tau d^2\vec{l}}{(2\pi)^3} \left[f_+(q, l, -(l+q)) (f_-(-q, -l, l+q) \right. \\ &\quad \left. + f_-(-q, l+q, -l)) D(l) D(l+q) \right] + (q \rightarrow -q). \quad (6.82) \end{aligned}$$

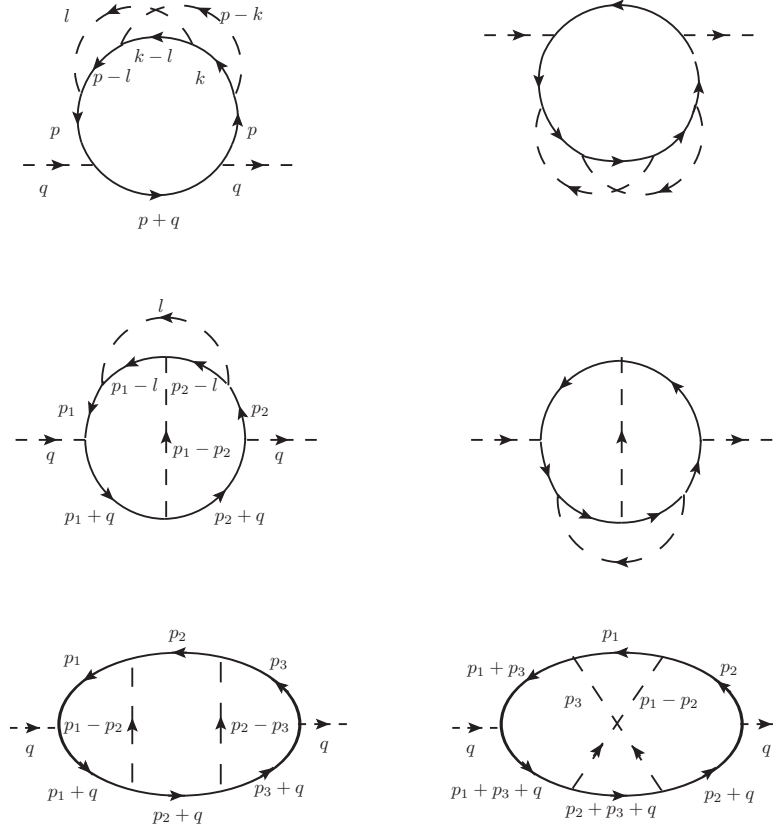


Figure 6.5: Three loop corrections to the boson self-energy with one fermion loop.

The two terms in brackets in the equation above originate respectively from diagrams in Figs. 6.6 a) and b). Converting these diagrams into the double line representation of Ref. [198], we obtain Figs. 6.7 a) and b). [We remark that the genus expansion of Ref. [198] was developed for a theory with only a single Fermi-surface patch. The extension to the present case of a pair of time reversed patches is simple: a reversal of the direction of loops with fermions from the second patch reduces the problem to that with one patch only. The diagrams in Fig. 6.7 have their lines reversed precisely

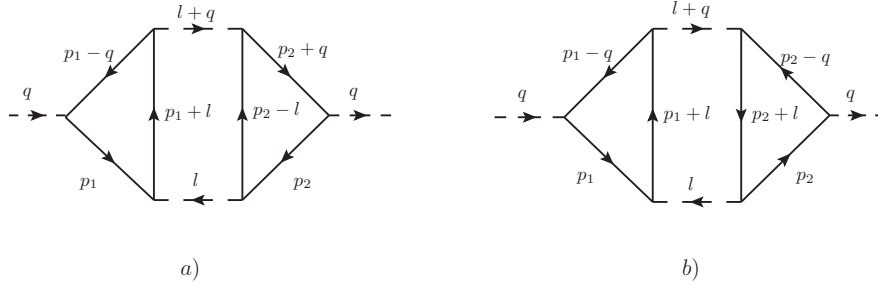


Figure 6.6: Aslamazov-Larkin type three loop contributions to the boson self-energy.

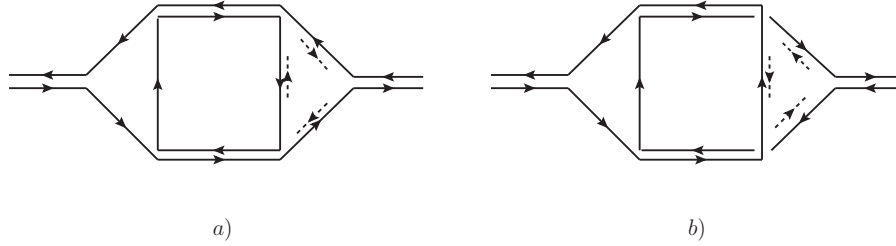


Figure 6.7: Double line representation of Ref. [198] applied to the Aslamazov-Larkin diagrams in Fig. 6.6. The fermions in the two loops are assumed to come from opposite patches. We have reversed the directions of the fermion propagators from the second patch, and the dotted arrows indicate the true directions of the fermion momenta.

in this way. The additional dotted arrow besides each propagator indicates the true direction of fermion momentum.] In this representation, the graph a) contains a loop while the graph b) does not. As a result, in the genus expansion of Ref. [198], the diagram in Fig. 6.6 a) is enhanced to $O(N)$, while the diagram in Fig. 6.6 b) is of $O(1)$. However, we will see that the diagrams are actually individually ultra-violet divergent, as a result the counting of Ref. [198] is inapplicable here. It turns out that the sum of the diagrams is UV finite and of $O(N^{3/2})$.

We give details of the evaluation of Eq. (6.82) in Appendix E.2, where we find

$$\delta^3 \Pi(q_\tau = 0, \vec{q}) = C \lambda_+ \lambda_- \frac{q_y^2}{e^2} \quad (6.83)$$

In the large- N limit, the coefficient C is given by,

$$C \approx -0.09601 N^{3/2}, \quad N \rightarrow \infty \quad (6.84)$$

while for the physical value $N = 2$,

$$C \approx -0.04455, \quad N = 2 \quad (6.85)$$

The $N^{3/2}$ behaviour in Eq. (6.84) indicates a breakdown of the genus expansion of Ref. [198]. Moreover, since this correction is parametrically larger than the tree level value, the existence of the large- N limit of the theory is cast into doubt. In particular, it is not clear if there are higher loop graphs with even stronger divergences in the large- N limit. Moreover, we expect contributions to the bosonic self-energy analytic in q_y to be generated from kinematic regimes involving the whole Fermi-surface and not just the two Fermi patches. Such analytic contributions might also exhibit anomalous scaling with N .

Note that there is no logarithmic dependence on Λ/μ in Eq. (6.83), and so we have $z = 3$ at this order. For the physical value of $N = 2$, the finite three-loop correction turns out to be rather small numerically.

6.5.2 Fermion anomalous dimension

The Feynman diagrams for the fermion self-energy up to three loop order are shown in Figs. 6.8, 6.9 and 6.10. By reasons explained in the previous section, the

diagrams in Figs. 6.8 and 6.9 vanish when the external frequency is zero and, hence, do not contribute to the fermion anomalous dimension.

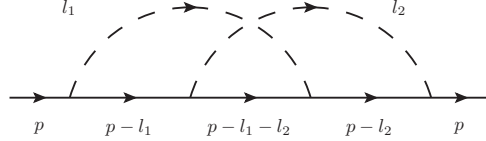


Figure 6.8: Fermion self-energy at two loops.

Thus, the only fermion self-energy diagrams that can give UV divergences are shown in Fig. 6.10. Actually, the diagram in Fig. 6.10 a) is zero since the polarization correction in Fig. 6.4 vanishes. Thus, we only need to consider the two diagrams in Fig. 6.10 b) and c). For these graphs to be UV divergent, the fermions running in the loop and the external fermions must come from different patches. The diagram in Fig. 6.10 b) contains two loops in the double line representation (Fig. 6.11 a)) and is expected to be of order $1/N$, while the one in Fig. 6.10 c) has no loops in the double line representation (Fig. 6.11 b)) and, hence, is expected to scale as $1/N^2$.

A calculation presented in Appendix E.2 gives the *UV* divergent contribution,

$$\delta^{3b}\Sigma_+(\omega = 0, \vec{p}) = \lambda_+\lambda_-J_b(p_x + p_y^2) \log \left(\frac{\Lambda_y}{|p_x + p_y^2|^{1/2}} \right), \quad (6.86)$$

$$\delta^{3c}\Sigma_+(\omega = 0, \vec{p}) = \delta^{3c}\Sigma_+(\omega = 0, \vec{p} = 0) + \lambda_+\lambda_-J_c(p_x + p_y^2) \log \left(\frac{\Lambda_y}{|p_x + p_y^2|^{1/2}} \right) \quad (6.87)$$

The constant J_b is independent of N and given numerically by,

$$J_b \approx 0.1062 \quad (6.88)$$

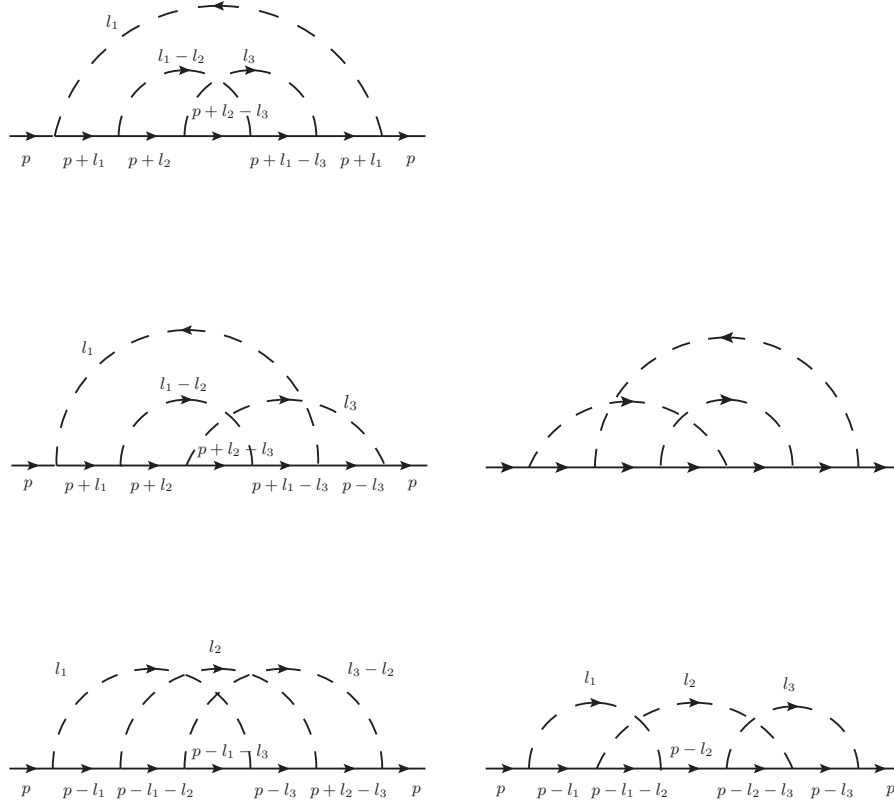


Figure 6.9: Three loop fermion self-energy diagrams with no fermion loops.

On the other hand, the constant J_c is N -dependent. For $N = 2$ we obtain,

$$J_c \approx -0.03795, \quad N = 2 \quad (6.89)$$

while in the large- N limit,

$$J_c \approx \frac{9}{4\pi^2 N^2} \log^3 N, \quad N \rightarrow \infty \quad (6.90)$$

Notice that there is no $1/N$ suppression in Eq. (6.86). A way to interpret this, is that the diagram is really of order $1/N$ (as the genus expansion predicts), however, it is a function of $N(p_x + p_y^2)$. Indeed, recall that the genus expansion assumes

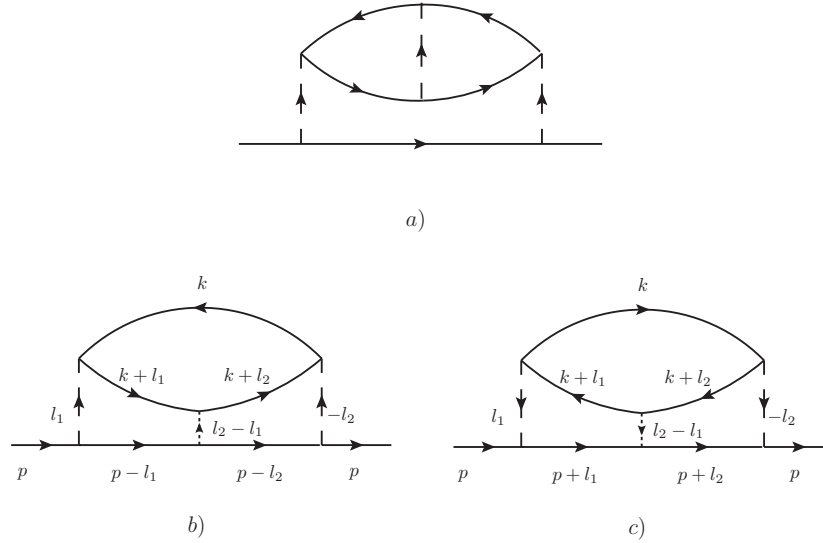


Figure 6.10: Three loop fermion self-energy diagrams with one fermion loop.

$N(p_x + p_y^2) \sim 1$. However, the UV divergent piece of the diagram cannot depend on the magnitude of $p_x + p_y^2$ and is valid for any external momentum or frequency. On the other hand, the infrared scale under the log is expected to become $\omega^{1/3}$ once $\omega \gg N^{3/2}|p_x + p_y^2|^{3/2}$. Also observe that up to a logarithmic enhancement, the non-planar diagram 6.10 c) (6.11 b)) is of order $1/N^2$, as expected from the genus expansion.

Note that the UV divergence in Eqs. (6.86), (6.87) is logarithmic, as expected from power counting, and comes from a region where both internal momenta and frequencies diverge in accordance with the scaling (6.14). This is unlike the anomalous linear divergences of the Aslamazov-Larkin diagrams that occur when the internal momenta q_y are of order of external momenta, while internal q_x, q_τ diverge.

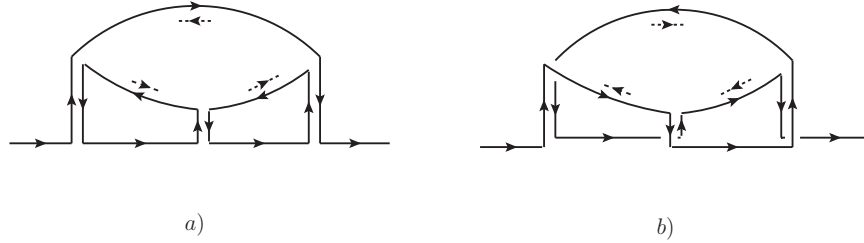


Figure 6.11: Double line representation of fermion self-energy diagrams in Figs. 6.10 b),c), as in Fig. 6.7. The external fermions and the fermions inside the loop are assumed to come from opposite patches.

Thus, to three loop order,

$$\delta^3 \Sigma_+(\omega = 0, \vec{p}) = \delta^3 \Sigma_+(\omega = 0, \vec{p} = 0) + \lambda_+ \lambda_- J (p_x + p_y^2) \log \left(\frac{\Lambda_y}{|p_x + p_y^2|^{1/2}} \right) \quad (6.91)$$

$$J = J_b + J_c \approx \begin{cases} 0.06824 & N = 2 \\ 0.10619 & N = \infty \end{cases} \quad (6.92)$$

Although the self-energy correction (6.91) is not parameterically suppressed compared to the bare value even when $N = \infty$, it appears to be suppressed numerically. Thus, we may estimate,

$$\begin{aligned} Z_\psi &= 1 - \lambda_+ \lambda_- J \log \Lambda / \mu \\ \eta_\psi &= \lambda_+ \lambda_- J = \pm 0.06824 \end{aligned} \quad (6.93)$$

where the upper sign refers to the Ising-nematic transition and the lower sign to the spin-liquid and we have used the value of J at $N = 2$.

6.5.3 Fermi surface shift

We now evaluate the coefficient α , Eq. (6.43), associated with the renormalization of chemical potential δ away from criticality. This coefficient can be obtained from the insertion of the ϕ^2 operator into the two-point fermion Green's function at criticality. By setting all external frequencies to zero, we find that at three loop order the only UV divergent contribution can originate from the diagrams in Figs. 6.10 b) c) with the ϕ^2 operator inserted into the boson propagators. The details of the calculation are presented in appendix E.2. We find,

$$\delta^3 \frac{\partial \Sigma}{\partial r} \stackrel{UV}{=} J_r e^2 \log \Lambda_y \quad (6.94)$$

with

$$\begin{aligned} J_r &= 0.00208, \quad N = 2 \\ J_r &\sim O\left(\frac{1}{N^3}\right), \quad N \rightarrow \infty \end{aligned} \quad (6.95)$$

Absorbing this divergence into the chemical potential,

$$Z_{r\delta} = J_r \log \Lambda_y / \mu \quad (6.96)$$

and

$$\alpha = J_r \quad (6.97)$$

Thus, the ϕ^2 operator mixes with the $\psi^\dagger \psi$ operator. If the dynamical critical exponent $z = 3$, this leads to a logarithmic divergence of the compressibility, Eq. (6.77). Note that the magnitude of the mixing α is suppressed in the large N limit and is also numerically small for $N = 2$.

6.6 Conclusion

This chapter has presented the scaling properties of the field theory in Eq. (6.7) which describes a number of problems involving the breakdown of Landau Fermi liquid theory at all points on a two dimensional Fermi surface. The main motivation was provided by the quantum phase transition caused by the onset of Ising-nematic order, which reduces the point-group symmetry from square to rectangular. However our theory also directly applies or can be generalized to breaking of other point-group and/or time-reversal symmetries, and these were described in Section 6.2. One of these cases is the “circulating current” order parameter of Simon and Varma [193, 40, 204]. Apart from applications to quantum critical points, our theory also described non-Fermi liquid phases associated with spin liquids [78, 213, 214] or algebraic charge liquids [24, 28, 29], which have Fermi surfaces coupled to U(1) gauge fields.

Our critical theory was formulated in terms of a time-reversed pair of patches on the Fermi surface, centered at the wavevectors $\pm\vec{k}_0$ (see Fig. 6.1). The value of \vec{k}_0 was determined by requiring that the tangent to the Fermi surface at \vec{k}_0 be parallel to the wavevector \vec{q} carried by the order parameter insertion in the correlation function being computed. However, in general, there is nothing special about the point \vec{k}_0 , and neighboring points on the Fermi surface should behave in a similar manner. This key feature was implemented in our theory by the rotational symmetry discussed in Section 6.4.1, and the identities (6.18,6.19), which show that the Green’s function remains invariant as we move along the Fermi surface.

We emphasize that although we have critical theories associated with every pair of points on the Fermi surface, the Lagrangian (6.7) and all the fields are 2+1 dimen-

sional *i.e.* ϕ and ψ_σ are integrated over arbitrary functions of x , y , and τ . Thus, as we noted earlier, our approach and results differ from studies using a ‘tomographic’ representations of the Fermi surface, in which every point on the Fermi surface is described by a 1+1 dimensional field theory.[199, 200, 201, 202, 203, 188, 187] Our 2+1 dimensional representation leads to a redundancy in our description of the degrees of freedom, and the identities of Section 6.4.1 ensure the consistency of this redundant description.

Our main results include the scaling relations for the order parameter susceptibility in Eq. (6.58), and for the fermion Green’s function in Eq. (6.63). These are associated with only two independent exponents, the dynamic scaling exponent z , and the fermion anomalous dimension η_ψ . The correlation length exponent ν was given by exact scaling relation in Eq. (6.53), while the susceptibility exponent $\gamma = 1$. For the spin-liquid case, Fermi liquid arguments were made [74, 205, 208, 209, 210, 211] suggesting that $z = 3$; we found $z = 3$ to three loop order in Section 6.5, although we did not prove this to all orders, and our scaling theory is compatible with a general value of z . Our three loop computation also gave a non-zero value of η_ψ , with opposite signs for the Ising-nematic and spin-liquid cases. In the case of the nematic transition, a non-zero positive η_ψ implies the suppression of the electron tunneling density of states, Eq. (6.71). Another striking effect that we find for the case of a nematic transition is the power law divergence of the compressibility for $z > 3$, which turns into a logarithmic divergence if $z = 3$.

Our scaling results were expressed in terms of correlators of the fermionic field $\psi_{+\sigma}$ carrying momentum \vec{q} as measured from the point \vec{k}_0 from the Fermi surface,

implying from (6.3) that the electron c_σ has momentum $\vec{k}_0 + \vec{q}$ (and similarly for $\psi_{-\sigma}$). However, note that (after appropriate rescaling of momenta, and for a circular Fermi surface) $|\vec{k}| - k_F \approx q_x + q_y^2$. Thus the identity (6.19) implies that the scaling function (6.63) for the two-point fermion Green's function depends only on $|\vec{k}| - k_F$. This is similar to the dependence found in other treatments *e.g.* in the recent critical theories [215, 216, 217, 218, 219] obtained by applying the AdS/CFT duality to fermions propagating near a Reissner-Nordstrom black hole. The latter theories, in their current classical gravity formulation, find [217] $\eta_\psi = 0$.

It is also interesting to compare the structure of the critical theory in the AdS/CFT framework to that found here. We have an infinite set of 2+1 dimensional field theories labeled by pairs of momenta on a one-dimensional Fermi surface *i.e.* a $\mathbb{S}^1/\mathbb{Z}_2$ set of 2+1 dimensional field theories. In the low-energy limit, the AdS/CFT approach yields [217] a $\text{AdS}_2 \times \mathbb{R}^2$ geometry: this can be interpreted as an infinite set of chiral 1+1 dimensional theories labeled by a \mathbb{R}^2 set of two-dimensional momenta \vec{k} . It is notable, and perhaps significant, that both approaches have an emergent dimension not found in the underlying degrees of freedom. We began with a 2+1 dimensional Hamiltonian, and ended up with a $\mathbb{S}^1/\mathbb{Z}_2$ set of 2+1 dimensional field theories. In AdS/CFT, there is the emergent radial direction representing energy scale. These emergent dimensions imply redundant descriptions, and require associated consistency conditions: we explored such consistency conditions in Section 6.4.1, while in AdS/CFT the consistency conditions are Einstein's equations representing the renormalization group flow under changes of energy scale. It would be interesting to see if fluctuations about the classical gravity theory yield corrections to the $\text{AdS}_2 \times \mathbb{R}^2$

geometry which clarify the connection to our theory.

In the analysis of the spin-liquid problem, Ref. [198] considered a single patch of the Fermi surface, and argued that the $1/N$ expansion should be organized by the genus of the Feynman graph (after the propagators are written in a suitable double line representation, and the graph is interpreted as lying on a two-dimensional surface). In our two-patch theory here, we have shown that this genus counting is violated. This is the implication of the $N^{3/2}$ dependence of the boson self-energy in Eq. (6.83). In fact, at present, it is not clear how to take the large- N limit of the theory. On the other hand, for the physical value $N = 2$, we found that the higher loop contributions are numerically small, which suggests that the critical exponents are close to the Hertz mean-field values. However, because the loop-wise expansion does not possess even a formal expansion parameter, it is not clear if there is a systematic way to extract corrections to the mean-field exponents. Thus, our value of the fermion anomalous dimension η_ψ , Eq. (6.93), should be regarded as an estimate only.

Chapter 7

Quantum phase transitions of metals in two spatial dimensions: Spin density wave order

We present a field-theoretic renormalization group analysis of Abanov and Chubukov's model of the spin density wave transition in two dimensional metals. We identify the independent field scale and coupling constant renormalizations in a local field theory, and argue that the damping constant of spin density wave fluctuations tracks the renormalization of the local couplings. The divergences at two-loop order overdetermine the renormalization constants, and are shown to be consistent with our renormalization scheme. We describe the physical consequences of our renormalization group equations, including the breakdown of Fermi liquid behavior near the "hot spots" on the Fermi surface. In particular, we find that the dynamical critical exponent z receives corrections to its mean-field value $z = 2$. At higher orders in the loop expansion, we find infrared singularities similar to those found by S.-S. Lee for the problem of a Fermi surface coupled to a gauge field. A treatment of these singularities implies that an expansion in $1/N$, (where N is the number of fermion flavors) fails for the present problem. We also discuss the renormalization of the pairing vertex,

and find an enhancement which scales as logarithm-squared of the energy scale. A similar enhancement is also found for a modulated bond order which is locally an Ising-nematic order.

7.1 Introduction

There is little doubt that the quantum transition involving the onset of spin density wave (SDW) order in a metal is of vital importance to the properties of a variety of correlated electron metals. This is amply illustrated by some recent experimental studies. In the cuprates, Daou *et al.* [36] argued that the Fermi surface change associated with such a transition was the key in understanding the physics of the strange metal. In the pnictide superconductors, experiments [220, 221, 222] have explored the interesting coupling between the onsets of SDW order and superconductivity. In CeRhIn₅ (and other ‘115’ compounds), Knebel *et al.* [223] have described the suppression of the SDW order by pressure, and the associated enhancement of superconductivity.

The theory of Hertz [5, 224, 192] has formed much of the basis of the study of the spin density wave transition in the literature. The central step of this theory is the derivation of an effective action for the spin density wave order parameter, after integrating out all the low energy excitations near the Fermi surface. A conventional renormalization group (RG) is then applied to this effective action, and this can be extended to high order using standard field-theoretic techniques [225]. However, it has long been clear that the full integration of the Fermi surface excitations is potentially dangerous, because the Fermi surface structure undergoes a singular renormalization

from the SDW fluctuations.

Important advances were subsequently made in the work of Abanov and Chubukov [226, 67]. They argued that the Hertz analysis was essentially correct in spatial dimension $d = 3$, but that it broke down seriously in $d = 2$. They proposed an alternative low energy field theory for $d = 2$, involving the bosonic SDW order parameter and fermions along arcs of the Fermi surface; the arcs are located near Fermi surface “hot spots” which are directly connected by SDW ordering wavevector. They also presented a RG study of this field theory, and found interesting renormalizations of the Fermi velocities at the arcs.

This chapter will present a re-examination of the model of Abanov and Chubukov, using a field-theoretic RG method. We will begin in Section 7.2 by introducing the low energy field theory for the SDW transition in two dimensional metals, and reviewing the Abanov-Chubukov argument for the breakdown of the Hertz theory. Section 7.3 will define the independent renormalization constants using the structure of the local field theory, and determine their values using the divergences in a $1/N$ expansion (where N is the number of fermion flavors) to two loop order. Actually, the two-loop divergences overdetermine the renormalization constants, but we will find a consistent solution: this is a significant check on the consistency of our renormalization procedure. While our renormalizations of the Fermi velocities agree with those of Abanov and Chubukov, we find significant differences in the other renormalizations, and associated physical consequences. Specifically, the RG-improved computations at two-loop order yield:

- a fermion self energy at the hot spot given by Eq. (7.63);

- moving away from the hot spot, we find that Fermi liquid behavior is restored, but the quasiparticle residue and the Fermi velocity vary strongly as a function of the momentum (p_{\parallel}) along the Fermi surface: these are given in Eq. (7.64);
- the bosonic SDW spectrum does not obey dynamic scaling with $z = 2$, but instead obeys the ‘super power-law’ form in Eq. (7.65), and the amplitude of the spectrum scales as in Eq. (7.66).

In Section 7.4, we describe the structure of the field theory at higher loop order. Similar to the effects pointed out recently by S.-S. Lee [198] for the problem of a Fermi surface coupled to a gauge field, we find that there are infrared singularities which lead to a breakdown in the naive counting of powers of $1/N$. However, unlike in the problem of a gauge field coupled to a single patch of the Fermi surface [198], we find that the higher order diagrams cannot be organized into an expansion in terms of the genus of a surface associated with the graph. Rather, diagrams that scale as increasingly higher powers of N are generated upon increasing the number of loops.

In Section 7.5, we consider the onset of pairing near the SDW transition, a question examined previously by Abanov, Chubukov, Finkel’stein, and Schmalian [227, 228, 229]. Like them, we find that the corrections to the d -wave pairing vertex are enhanced relative to the naive counting of powers of $1/N$. However, we also find an enhancement factor which scales as the logarithm-squared of the energy scale: this is the result in Eq. (7.90). We will discuss the interpretation of this log-squared term in Section 7.5.

In Section 7.6 we show that a similar log-squared enhancement is present for the vertex of a bond order which is locally an Ising-nematic order; this order parameter is illustrated in Figs. 7.22 and 7.23. The unexpected similarity between this order, and

the pairing vertex, is a consequence of emergent $SU(2)$ pseudospin symmetries of the continuum theory of the SDW transition, with independent pseudospin rotations on different pairs of hot spots. One of the pseudospin rotations is the particle-hole transformation, and the other pseudospin symmetries will be described more completely in Section 7.2.

7.2 Low energy field theory

We will study the generic phase transition between a Fermi liquid and a SDW state in two spatial dimensions, and our discussion also easily generalizes to charge density wave order. The wavevector of the density wave order is \vec{Q} , and we assume that there exist points on the Fermi surface connected by \vec{Q} ; these points are known as hot spots. We assume further that the Fermi velocities at a pair of hot spots connected by \vec{Q} are not parallel to each other; this avoids the case of ‘nested Fermi surfaces’, which we will not treat here.

A particular realization of the above situation is provided by the case of SDW ordering on the square lattice at wavevector $\vec{Q} = (\pi, \pi)$. We also take a Fermi surface appropriate for the cuprates, generated by a tight-binding model with first and second neighbor hopping. We will restrict all our subsequent discussion to this case for simplicity.

At wavevector $\vec{Q} = (\pi, \pi)$ the SDW ordering is collinear, and so is described by a three component real field ϕ^a , $a = x, y, z$. There are $n = 4$ pairs of hot spots, as shown in Fig. 7.1. We introduce fermion fields $(\psi_{1\sigma}^\ell, \psi_{2\sigma}^\ell)$, $\ell = 1 \dots n$, $\sigma = \uparrow \downarrow$ for each pair of hot spots. Lattice rotations map the pairs of hot spots into each other, acting

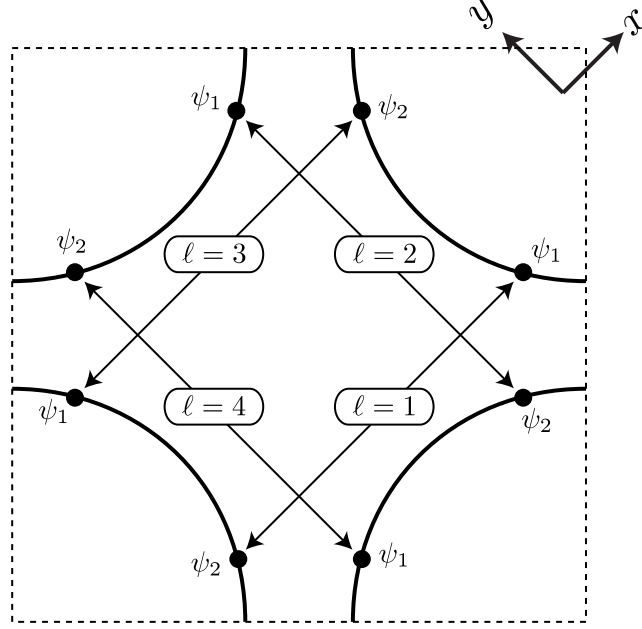


Figure 7.1: Square lattice Brillouin zone showing the Fermi surface appropriate to the cuprates. The filled circles are the hot spots connected by the SDW wavevector $\vec{Q} = (\pi, \pi)$. The locations of the continuum fermion fields ψ_1^ℓ and ψ_2^ℓ is indicated.

cyclically on the index ℓ . Moreover, the two hot spots within each pair are related by a reflection across a lattice diagonal. It will be useful to promote each field ψ to have N -flavors with an eye to performing a $1/N$ expansion. (Note that in Ref. [229], the total number of hot spots $2nN$ is denoted as N .) The flavor index is suppressed in all the expressions. The low energy effective theory is given by the Lagrangian,

$$\begin{aligned}
 L &= \frac{N}{2c^2}(\partial_\tau \vec{\phi})^2 + \frac{N}{2}(\nabla \vec{\phi})^2 + \frac{Nr}{2}\vec{\phi}^2 + \frac{Nu}{4}(\vec{\phi}^2)^2 \\
 &+ \psi_1^{\dagger \ell}(\partial_\tau - i\vec{v}_1^\ell \cdot \nabla)\psi_1^\ell + \psi_2^{\dagger \ell}(\partial_\tau - i\vec{v}_2^\ell \cdot \nabla)\psi_2^\ell \\
 &+ \lambda\phi^a \left(\psi_{1\sigma}^{\dagger \ell} \tau_{\sigma\sigma'}^a \psi_{2\sigma'}^\ell + \psi_{2\sigma}^{\dagger \ell} \tau_{\sigma\sigma'}^a \psi_{1\sigma'}^\ell \right)
 \end{aligned} \tag{7.1}$$

The first line in Eq. (7.1) is the usual $O(3)$ model for the SDW order parameter, the second line is the fermion kinetic energy and the third line is the interaction

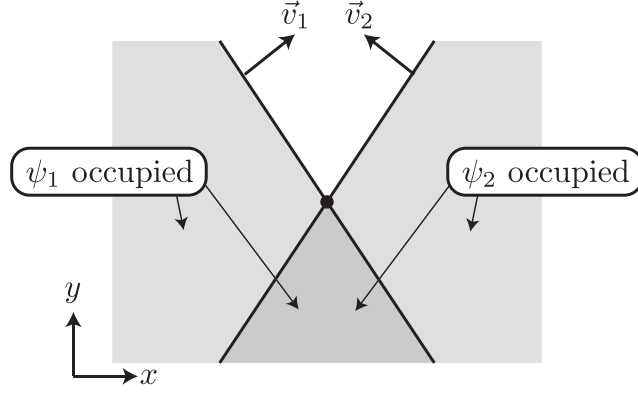


Figure 7.2: Configuration of the $\ell = 1$ pair of hot spots, with the momenta of the fermion fields measured from the common hot spot at $\vec{k} = 0$, indicated by the filled circle. The Fermi velocities $\vec{v}_{1,2}$ of the $\psi_{1,2}$ fermions are indicated.

between the SDW order parameter and the fermions at the hot spots. Here, we have linearized the fermion dispersion near the hot spots and \vec{v}^ℓ are the corresponding Fermi velocities. It is convenient to choose coordinate axes along directions $\hat{x} = \frac{1}{\sqrt{2}}(1, 1)$ and $\hat{y} = \frac{1}{\sqrt{2}}(-1, 1)$, so that

$$\vec{v}_1^{\ell=1} = (v_x, v_y) \quad , \quad \vec{v}_2^{\ell=1} = (-v_x, v_y); \quad (7.2)$$

these Fermi velocities are indicated in Fig. 7.2. The other Fermi velocities are related by rotations, $\vec{v}^\ell = (R_{\pi/2})^{\ell-1} \vec{v}^{\ell=1}$.

We choose the coefficient λ of the fermion-SDW interaction to be of $\mathcal{O}(1)$ in N . As a result, the coefficients in the first line of Eq. (7.1) are all scaled by N as this factor will automatically appear upon integrating out the high-momentum/frequency modes of the fermion fields.

Before proceeding with the analysis of the theory (7.1), let us note its symmetries. Besides the microscopic translation, point-group, spin-rotation and time-reversal symmetries, the low energy theory possesses a set of four emergent $SU(2)$ pseudospin

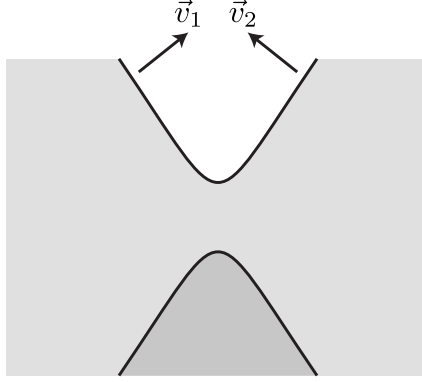


Figure 7.3: Modification of the Fermi surfaces in Fig. 7.2 by SDW order with $\langle \phi \rangle \neq 0$. The full lines are the Fermi surfaces, and the white, light shaded, and dark shaded regions denote momenta where 0, 1, and 2 of the bands are occupied. The upper and lower lines are boundaries of hole and electron pockets respectively.

symmetries associated with particle-hole transformations. Let us introduce a four-component spinor,

$$\Psi_i^\ell = \begin{pmatrix} \psi_i^\ell \\ i\tau^2 \psi_i^{\dagger\ell} \end{pmatrix} \quad (7.3)$$

We will denote the particle-hole indices in the four-component spinor by α, β . The spinor (7.3) satisfies the hermiticity condition,

$$i\tau^2 \begin{pmatrix} 0 & -1 \\ 1 & 0 \end{pmatrix} \Psi_i^\ell = \Psi_i^{*\ell} \quad (7.4)$$

Then, the fermion part of the Lagrangian (7.1) can be rewritten as,

$$L_\psi = \frac{1}{2} \Psi_1^{\dagger\ell} (\partial_\tau - i\vec{v}_1^\ell \cdot \nabla) \Psi_1^\ell + \frac{1}{2} \Psi_2^{\dagger\ell} (\partial_\tau - i\vec{v}_2^\ell \cdot \nabla) \Psi_2^\ell + \frac{1}{2} \lambda \vec{\phi} \cdot (\Psi_1^{\dagger\ell} \vec{\tau} \Psi_2^\ell + \Psi_2^{\dagger\ell} \vec{\tau} \Psi_1^\ell) \quad (7.5)$$

Now the Lagrangian (7.5) and the condition (7.4) are manifestly invariant under,

$$SU(2)_\ell : \Psi_i^\ell \rightarrow U_\ell \Psi_i^\ell \quad (7.6)$$

with $U_\ell - SU(2)$ matrices. We note that the diagonal subgroup of (7.6) is associated with independent conservation of the fermion number at each hot spot pair. The

symmetry (7.6) is a consequence of linearization of the fermion spectrum near the hot spots and is broken by higher order terms in the dispersion. The diagonal subgroup noted above is preserved by higher order terms in the dispersion, but is broken by four-fermi interactions, which map fermion pairs from opposite hot spots into each other. Both symmetry breaking effects are irrelevant in the scaling limit discussed below.

The pseudospin symmetry (7.6) constrains the form of the fermion Green's function to be,

$$-\langle \Psi_{i\alpha\sigma}^\ell \Psi_{j\beta\sigma'}^{m\dagger} \rangle = \delta^{\ell m} \delta_{ij} \delta_{\alpha\beta} \delta_{\sigma\sigma'} G_i^\ell(x - x') \quad (7.7)$$

which implies,

$$G_i^\ell(x - x') = -G_i^\ell(x' - x) \quad (7.8)$$

The corresponding expression in momentum space, $G_i^\ell(k) = -G_i^\ell(-k)$, implies that the location of hot spots in the Brillouin zone is not renormalized by the spin wave fluctuations in the low energy theory.

Another important manifestation of the particle-hole symmetry is the equality of any Feynman graphs, which are related by a reversal of a fermion loop direction.

7.2.1 The Hertz action

The Hertz action is derived by working in the metallic phase, and integrating out the fermions in Eq. (7.1), leaving an effective theory for ϕ alone. In particular, the one-loop self-energy of the field ϕ is evaluated in Appendix F.1.1, and is given by

$$\Pi^0(\omega, \vec{q}) = \Pi^0(\omega = 0, \vec{q} = 0) + N\gamma|\omega| + \dots, \quad \gamma = \frac{n\lambda^2}{2\pi v_x v_y} \quad (7.9)$$

The presence of the non-analytic term $|\omega|$ is due to the fact that the density of particle-hole pairs with momentum \vec{Q} and energy ω scales as ω . As usual, the constant piece $\Pi^0(q=0)$ is eliminated by tuning the coefficient r . The ellipses in Eq. (7.9) denote terms analytic in ω and \vec{q} , starting with ω^2 and \vec{q}^2 . These terms formally disappear when we take the cut-off of the effective theory (7.1) to infinity. Thus, the quadratic part of the effective action for the field ϕ reads

$$S_2 = \frac{N}{2} \int \frac{d\omega d^2k}{(2\pi)^3} \phi^a(-k, -\omega) \left(\gamma|\omega| + \frac{1}{c^2}\omega^2 + \vec{k}^2 + r \right) \phi^a(k, \omega) \quad (7.10)$$

At sufficiently low energies, the analytic term ω^2 in the boson self-energy coming from the bare action, Eq. (7.1), can be neglected compared to the dynamically generated $|\omega|$ term. Thus, at low energies the propagation of collective spin excitations becomes diffusive, due to the damping by the fermions at the hot spots.

Hertz [5] proceeds by neglecting all the quartic and higher order self-interactions of the field ϕ , which are generated when the fermions are eliminated. This is justified if such interactions are local, as one can then absorb them into operators, which are polynomial in the order parameter and its derivatives (the simplest of which is just the operator $(\vec{\phi}^2)^2$). The theory then reduces to,

$$S_H = \frac{N}{2} \int \frac{d\omega d^2k}{(2\pi)^3} \phi^a(-k, -\omega) \left(\gamma|\omega| + \vec{k}^2 + r \right) \phi^a(k, \omega) + \frac{Nu}{4} \int d\tau d^2x (\vec{\phi}^2)^2 \quad (7.11)$$

The quadratic part of the action (7.11) is invariant under scaling with the dynamical critical exponent $z = 2$,

$$\vec{k} \rightarrow s\vec{k}, \quad \omega \rightarrow s^2\omega, \quad \phi(\vec{x}, \vec{\tau}) \rightarrow s\phi(s\vec{x}, s^2\vec{\tau}) \quad (7.12)$$

Thus the theory is effectively $d + z = 4$ dimensional and the quartic coupling u is marginal by power-counting in $d = 2$.

At one loop order, the flow of u follows easily from the conventional momentum shell RG [230]

$$\frac{du}{d\ell} = -\frac{11}{2\pi^2 N\gamma} u^2, \quad (7.13)$$

where $s = e^{-\ell}$ is the renormalization scale. Thus u is marginally irrelevant, and flows to the Gaussian fixed point with $u = 0$ in the infrared. This stability of the Gaussian fixed point has formed the basis of much of the subsequent work [192, 225, 230] on the Hertz theory.

7.2.2 Breakdown of the Hertz theory

The analysis in Section 7.2.1 is valid only under the assumption that the fermion-induced quartic and higher order couplings of the field ϕ can be neglected. In fact, as observed in Refs. [229, 67], this assumption is not justified in spatial dimension $d = 2$. Indeed, as shown in Ref. [229], the fermion-induced four-point vertex is given by,

$$\Gamma_4^{a_1 a_2 a_3 a_4}(q_1, q_2, q_3, q_4) = \lambda^4 f^{a_1 a_2 a_3 a_4}(q_1, q_2, q_3, q_4) + \text{permutations of } 2, 3, 4 \quad (7.14)$$

$$\begin{aligned} & f^{a_1 a_2 a_3 a_4}(q_1, q_2, q_3, q_4) = \\ & = \sum_{\ell} \frac{N(\delta^{a_1 a_2} \delta^{a_3 a_4} - \delta^{a_1 a_3} \delta^{a_2 a_4} + \delta^{a_1 a_4} \delta^{a_2 a_3})(|\omega_1| - |\omega_2| + |\omega_3| - |\omega_4|)}{2\pi v_x v_y (i(\omega_2 + \omega_3) - \vec{v}_1^\ell \cdot (\vec{q}_2 + \vec{q}_3))(i(\omega_1 + \omega_2) - \vec{v}_2^\ell \cdot (\vec{q}_1 + \vec{q}_2))} \end{aligned} \quad (7.15)$$

We see that the vertex (7.14) is highly non-local. Moreover, under the $z = 2$ scaling (7.12), we can neglect the frequency dependence in the denominators of Eq. (7.15), obtaining $\Gamma_4 \sim |\omega|/\vec{q}^2 \sim \mathcal{O}(1)$, which produces a marginal interaction. Similarly, one can show that all the higher order fermion-induced vertices behave as $\Gamma_{2n} \sim$

$|\omega|/|\vec{q}|^{2n-2} \sim |\vec{q}|^{4-2n}$, which is again marginal under (7.12) when combined with the scaling of the field-strength. Thus, the Hertz-Millis theory has an infinite number of non-local marginal perturbations and the standard action (7.11) is incomplete.

7.2.3 RG interpretation

An RG interpretation of the results of Section 7.2.2 follows by performing a scaling analysis directly on the spin-fermion model (7.1). As before, we will scale the boson fields according to Eq. (7.12). Correspondingly, it is natural to scale the fermion momenta towards the hot spots,

$$\psi_{12}^\ell(\vec{x}, \tau) \rightarrow s^{3/2}\psi_{12}^\ell(s\vec{x}, s^2\tau) \quad (7.16)$$

Here the field-strength rescaling has been chosen to preserve the spatial gradient terms in the fermion action. We now see that the boson-fermion coupling λ in (7.1) is *marginal* under the field scalings in Eqs. (7.12) and (7.16); a similar analysis in $d = 3$ would show that λ is irrelevant.

The marginality of λ , and the infinite number of marginal couplings in Section 7.2.2 indicate that all subsequent RG should be performed direction on the spin-fermion model (7.1). Further, with the scalings as in (7.12) and (7.16), we should not expand in powers of λ , but rather analyze the theory at a *fixed* boson-fermion “Yukawa” coupling. A similar strategy was followed in Refs. [195, 196] for the Ising-nematic transition in a d -wave superconductor.

An important consequence of the scalings (7.12) and (7.16) on (7.1) is that both the boson kinetic term $(\partial_\tau\phi)^2$ and the fermion kinetic term $\psi^\dagger\partial_\tau\psi$ are irrelevant. We may safely drop the boson kinetic energy. However, the fermion kinetic energy must

be retained - otherwise, the theory does not possess any dynamics. We will return to this point shortly. Let us now rescale the fermion fields $\psi = \tilde{\psi}/\sqrt{\lambda}$ to eliminate the marginal coupling λ . We define, $\eta = 1/\lambda$ and $\vec{v} = \vec{v}/\lambda$. Note that \tilde{v} has the unusual dimensions of $[\omega]^{1/2}/[k]$. We drop the tildes in what follows. Then,

$$\begin{aligned}
 L &= \frac{N}{2}(\nabla\vec{\phi})^2 + \frac{Nr}{2}\vec{\phi}^2 + \frac{Nu}{4}(\vec{\phi}^2)^2 \\
 &+ \psi_1^{\dagger\ell}(\eta\partial_\tau - i\vec{v}_1^\ell \cdot \nabla)\psi_1^\ell + \psi_2^{\dagger\ell}(\eta\partial_\tau - i\vec{v}_2^\ell \cdot \nabla)\psi_2^\ell \\
 &+ \phi^a \left(\psi_{1\sigma}^{\dagger\ell}\tau_{\sigma\sigma'}^a\psi_{2\sigma'}^\ell + \psi_{2\sigma}^{\dagger\ell}\tau_{\sigma\sigma'}^a\psi_{1\sigma'}^\ell \right)
 \end{aligned} \tag{7.17}$$

As already remarked, the coupling constant η is irrelevant. Thus, we take the limit $\eta \rightarrow 0^+$ in all our calculations. In practice, η gives the prescription for integrating over the poles of the fermion propagator. We will work with the action (7.17) for the rest of this chapter. At criticality it is characterized by two dimensionless constants,

$$\alpha = \frac{v_y}{v_x}, \quad \tilde{u} = \frac{u}{\gamma} \tag{7.18}$$

and a dimensionful constant γ , Eq. (7.9),

$$\gamma = \frac{n}{2\pi v_x v_y}. \tag{7.19}$$

Thus, in the critical regime, the theory (7.17) does not possess an expansion in any coupling constant.

7.3 Field-theoretic RG

We begin by discussing the general renormalization structure of (7.17). In the absence of a coupling constant, we will use the RPA based scaling (7.12) and (7.16)

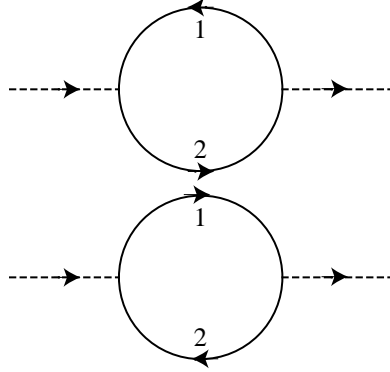


Figure 7.4: The boson self-energy at $N = \infty$. The full lines represent the $\psi_{1,2}$ fermions, and the dashed lines represent the boson ϕ^a .

as the starting point of our analysis. Naively, one expects that this scaling is also obeyed by the $N = \infty$ limit of the theory and that corrections to it can be calculated in a systematic expansion in $1/N$. Indeed, the usual arguments would indicate that at $N = \infty$, the boson self-energy is given by the RPA bubble in Fig. 7.4, Eq. (7.9), (see the Appendix F.1.1 for details of the calculation). Hence, the bosonic propagator

$$\langle \phi^a(x) \phi^b(x') \rangle = \delta^{ab} D(x - x') \quad (7.20)$$

at $N = \infty$ takes the form,

$$D(x) = \frac{1}{N} \int \frac{d\omega d^2q}{(2\pi)^3} \frac{1}{\gamma|\omega| + \bar{q}^2 + r} e^{-i\omega\tau + i\bar{q}\vec{x}} \quad (7.21)$$

which respects the scaling (7.12). On the other hand, the fermion propagator

$$-\langle \psi_{i\sigma}^\ell(x) \psi_{j\sigma'}^{\dagger m}(x') \rangle = \delta^{\ell m} \delta_{ij} \delta_{\sigma\sigma'} G_i^\ell(x - x')$$

at $N = \infty$ is given by its free value,

$$G_i^\ell(x) = \int \frac{d\omega d^2k}{(2\pi)^3} \frac{1}{i\eta\omega - \bar{v}_i^\ell \cdot \vec{k}} e^{-i\omega\tau + i\vec{k}\cdot\vec{x}} \quad (7.22)$$

Applying scaling (7.16) to this propagator indicates η scales to zero; we will eventually take this limit, but need a non-zero η for now to properly define the fermion loop integrals.

As we will see later in Section 7.4, the $N = \infty$ limit in the present theory turns out to be much more subtle and is not given by the simple forms in Eqs. (7.21),(7.22). Moreover, the anomalous dimensions in this limit are not expected to be parametrically small. Nevertheless, we can reasonably expect that the RG structure presented here remains valid, even though we are not able to accurately compute higher loop corrections to the renormalization constants. In addition, the difficulties with the $1/N$ expansion appear only at high loop order, which enables us to check the consistency of our approach to the order discussed below.

With the above remarks in mind, we are ready to discuss the renormalization of the theory in Eq. (7.17). The theory contains five operators that are marginal by power counting at $z = 2$, and not related by symmetry. Two of these are eliminated by field-strength renormalizations,

$$\phi = Z_\phi^{1/2} \phi_r, \quad \psi = Z_\psi^{1/2} \psi_r \tag{7.23}$$

As is conventional, we can fix Z_ϕ by demanding that the coefficient of $(\nabla\phi)^2$ remains invariant. For fermion field, it is convenient to allow both velocities to flow, and so we renormalize these as

$$v_x = Z_v^x v_x^r, \quad v_y = Z_v^y v_y^r. \tag{7.24}$$

The fermion spatial gradient terms are then not available to fix Z_ψ , and we cannot use the fermion temporal gradient term because its coefficient η scales to zero. Instead we demand the invariance of the boson-fermion coupling term to fix the fermion field

strength renormalization; it is thus consistent to use a unit coefficient for this term, as we have done in Eq. (7.17). The quartic boson coupling renormalizes

$$\tilde{u} = \frac{Z_u Z_v^x Z_v^y}{Z_\phi^2} \tilde{u}_r. \quad (7.25)$$

It is also useful to track the renormalization of the dimensionless velocity ratio α in Eq. (7.18)

$$\alpha = \frac{Z_v^y}{Z_v^x} \alpha_r. \quad (7.26)$$

All the renormalization factors Z depend only on N , α_r , \tilde{u}_r and the ratio μ/Λ , where μ is a renormalization scale and Λ is a UV cutoff.

An important point is that the damping parameter γ appearing in the boson propagator does not have an independent renormalization constant. It is not a coupling in a local field theory, and only appears in certain correlation functions as a measure of the strength of the particle-hole continuum, as determined by Eq. (7.19). This implies that when we consider the renormalization of the boson propagator, the renormalization of the parameter γ should track the the renormalizations of the velocities $v_{x,y}$ obtained from the renormalization of the fermion propagator; in other words, the renormalization of γ is

$$\gamma = \frac{1}{Z_v^x Z_v^y} \gamma_r. \quad (7.27)$$

This tight coupling between the boson and fermion sectors is a key feature of the theory (7.17), and a primary reason for strong coupling physics in $d = 2$.

The theory (7.17) contains two relevant perturbations. One of these is the usual $\vec{\phi}^2$ operator, whose coefficient renormalizes as,

$$r = \frac{Z_r}{Z_\phi} r_r \quad (7.28)$$

Here, r always denotes the deviation from the critical point. The other relevant perturbation, whose discussion we have omitted thus far, is the chemical potential,

$$\delta L = -\mu \psi_{i\sigma}^{\ell\dagger} \psi_{i\sigma}^{\ell} \quad (7.29)$$

However, this perturbation is redundant, as it can be absorbed into a shift of hot spot location. Moreover, as already observed in section 7.2, the location of the hot spots is not renormalized in the low-energy theory, which implies that there is no mixing between the two relevant operators. This is unlike the situation for the Ising-nematic transition in a metal studied in Ref. [68], where such mixing leads to a nontrivial shift of the Fermi surface as a function of deviation r from the critical point.

Introducing the renormalized one-particle irreducible correlation functions of n_f fermion and n_b boson fields

$$\Gamma_r^{n_f, n_b} = Z_\psi^{n_f/2} Z_\phi^{n_b/2} \Gamma^{n_f, n_b} \quad (7.30)$$

we can write down the renormalization group equations,

$$\begin{aligned} & \left(\mu \frac{\partial}{\partial \mu} + \beta_\alpha \frac{\partial}{\partial \alpha_r} + \beta_u \frac{\partial}{\partial \tilde{u}_r} + \eta_\gamma \gamma_r \frac{\partial}{\partial \gamma_r} - \eta_2 r_r \frac{\partial}{\partial r_r} - \frac{n_b \eta_\phi}{2} - \frac{n_f \eta_\psi}{2} \right) \times \\ & \times \Gamma_r^{n_b, n_f}(\{p\}, \alpha_r, \tilde{u}_r, \gamma_r, r_r, \mu) = 0 \end{aligned} \quad (7.31)$$

Here, the β -functions and anomalous dimensions are functions of α_r and \tilde{u}_r given by,

$$\beta_\alpha = \mu \frac{\partial \alpha_r}{\partial \mu} \Big|_{\alpha, \tilde{u}, \Lambda}, \quad \beta_u = \mu \frac{\partial \tilde{u}_r}{\partial \mu} \Big|_{\alpha, \tilde{u}, \Lambda}, \quad \eta_\gamma = \frac{1}{\gamma_r} \mu \frac{\partial \gamma_r}{\partial \mu} \Big|_{\alpha, \tilde{u}, \gamma, \Lambda}, \quad (7.32)$$

$$\eta_\phi = \mu \frac{\partial}{\partial \mu} \log Z_\phi \Big|_{\alpha, \tilde{u}, \Lambda}, \quad \eta_\psi = \mu \frac{\partial}{\partial \mu} \log Z_\psi \Big|_{\alpha, \tilde{u}, \Lambda}, \quad \eta_2 = \mu \frac{\partial}{\partial \mu} \log \frac{Z_r}{Z_\phi} \Big|_{\alpha, \tilde{u}, \Lambda} \quad (7.33)$$

Using dimensional analysis,

$$\begin{aligned} \Gamma_r^{n_b, n_f}(\{\omega\}, \{\vec{p}\}, \alpha_r, \tilde{u}_r, \gamma_r, r_r, \mu) &= \gamma_r^{n_b/2 + n_f/4 - 1} \mu^{4 - n_b - 3n_f/2} \\ & f^{n_b, n_f} \left(\left\{ \frac{\gamma_r \omega}{\mu^2} \right\}, \left\{ \frac{\vec{p}}{\mu} \right\}, \alpha_r, \tilde{u}_r, \frac{r_r}{\mu^2} \right) \end{aligned} \quad (7.34)$$

Now, solving the RG equation (7.31),

$$\begin{aligned}
 f^{n_b, n_f}(\{\hat{\omega}\}, \{\hat{p}\}, \alpha_r, \tilde{u}_r, \hat{r}) &= s^{4-3n_f/2-n_b} Z_\phi(s)^{-n_b/2} Z_\psi(s)^{-n_f/2} Z_\gamma(s)^{n_b/2+n_f/4-1} \\
 &\times f^{n_b, n_f}(s^{-2} Z_\gamma(s)\{\hat{\omega}\}, s^{-1}\{\hat{p}\}, \alpha_r(s), \tilde{u}_r(s), Z_r(s)\hat{r})
 \end{aligned} \tag{7.35}$$

with

$$\begin{aligned}
 s \frac{d\alpha_r}{ds} &= \beta_\alpha(\alpha_r(s), \tilde{u}_r(s)), \quad \alpha_r(1) = \alpha_r, \quad s \frac{d\tilde{u}_r}{ds} = \beta_u(\alpha_r(s), \tilde{u}_r(s)), \quad \tilde{u}_r(1) = \tilde{u}_r \\
 Z_\phi(s) &= \exp\left(\int_1^s \frac{ds'}{s'} \eta_\phi(\alpha_r(s'), \tilde{u}_r(s'))\right), \\
 Z_\psi(s) &= \exp\left(\int_1^s \frac{ds'}{s'} \eta_\psi(\alpha_r(s'), \tilde{u}_r(s'))\right), \\
 Z_\gamma(s) &= \exp\left(\int_1^s \frac{ds'}{s'} \eta_\gamma(\alpha_r(s'), \tilde{u}_r(s'))\right), \\
 Z_r(s) &= \exp\left(-\int_1^s \frac{ds'}{s'} \eta_2(\alpha_r(s'), \tilde{u}_r(s'))\right)
 \end{aligned} \tag{7.36}$$

Now, let us construct the scaling forms of the correlation functions assuming that the couplings α_r , \tilde{u}_r have a stable fixed point. Actually, as we will see below, this assumption is not supported by explicit calculations of low loop contributions to the β -functions and anomalous dimensions. However, as already remarked, higher loop diagrams, which are naively suppressed by powers of $1/N$, actually scale as progressively higher powers of N and might modify the RG flow significantly. Thus, the fixed-point form of the correlation functions satisfies,

$$f(s^{2-\eta_\gamma}\{\hat{\omega}\}, s\{\hat{p}\}, s^{2+\eta_2}\hat{r}) = s^{4-\eta_\gamma-(3+\eta_\psi-\eta_\gamma/2)n_f/2-(2+\eta_\phi-\eta_\gamma)n_b/2} f(\{\hat{\omega}\}, \{\hat{p}\}, \hat{r}) \tag{7.37}$$

Hence, typical frequencies and momenta are related by $\omega \sim |\vec{p}|^z$, with the dynamical critical exponent z being given by,

$$z = 2 - \eta_\gamma \tag{7.38}$$

Moreover, the correlation length ξ away from the critical point scales as $\xi \sim r^{-\nu}$ with

$$\nu = \frac{1}{2 + \eta_2} \quad (7.39)$$

Specializing to boson and fermion two-point functions,

$$D^{-1}(\omega, \vec{p}) \sim \xi^{-(2-\eta_\phi)} K(\omega\xi^z, \vec{p}\xi) \xrightarrow{\xi \rightarrow \infty} |\vec{p}|^{2-\eta_\phi} \tilde{K}(\omega/|\vec{p}|^z, \hat{p}) \quad (7.40)$$

$$G^{-1}(\omega, \vec{p}) \sim \xi^{-(z/2-\eta_\psi)} L(\omega\xi^z, \vec{p}\xi) \xrightarrow{\xi \rightarrow \infty} |\vec{p}|^{z/2-\eta_\psi} \tilde{L}(\omega/|\vec{p}|^z, \hat{p}) \quad (7.41)$$

Here, the expressions on the right give the correlation functions at the critical point to which we confine our attention from here on. From Eq. (7.41) we may infer the fate of the Fermi surface at the critical point. We expect that as $\xi \rightarrow \infty$ the Fermi-surface remains sharply defined. Close to the hot spots, the Fermi surfaces of fermions ψ_1 and ψ_2 will evolve into straight lines with a fixed angle between them. At the hot spot, the fermion self-energy takes the form,

$$G^{-1}(\omega, \vec{p} = 0) \sim \omega^{1/2-\eta_\psi/z} \quad (7.42)$$

which is generally non Fermi-liquid like. On the other hand, away from the hot spot, if we define p_\perp as the distance to the Fermi surface and p_\parallel as the distance to the hot spot, for $p_\perp \ll p_\parallel$ and $\omega \ll p_\parallel^z$, we expect well-defined Landau quasi-particles,

$$G(\omega, \vec{p}) \sim \frac{\mathcal{Z}}{i\omega - v_F p_\perp} \quad (7.43)$$

with the Fermi velocity v and quasiparticle residue \mathcal{Z} vanishing as we approach the hot spot as,

$$v_F(p_\parallel) \sim p_\parallel^{z-1}, \quad \mathcal{Z}(p_\parallel) \sim p_\parallel^{z/2+\eta_\psi} \quad (7.44)$$

The remainder of this section will provide a computation of the 4 renormalization constants $Z_\phi, Z_\psi, Z_v^x, Z_v^y$ to leading order in $1/N$. At this order, the constants will

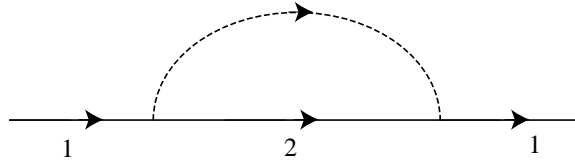


Figure 7.5: The leading contribution to the fermion self-energy.

depend only upon the dimensionless constant α , and do not involve u . We discuss the renormalization of u in Appendix F.2.2. Thus our considerations here will involve the RG flow only of the single coupling α , the ratio of the velocities, and a discussion of its physical implications. For completeness, we will also compute the renormalization constant Z_r , which determines the scaling of the correlation length away from the critical point. This constant will depend upon both α and u already at leading order in $1/N$.

As we will see below, the 4 renormalization constants will be overdetermined from the structure of the $1/N$ corrections to the fermion self energy, the boson-fermion vertex, and the boson self energy. Computations of these quantities are provided in the appendix, and we use the results here to compute the Z 's.

The first correction to the self-energy of the fermion $\psi_1^{\ell=1}$ is given by Fig. 7.5, and computed in Appendix F.1.2.

$$\Sigma_1(\omega, \vec{p}) = -\frac{3}{2\pi N|\vec{v}|\gamma} \left(i\text{sgn}(\omega)(\sqrt{\gamma|\omega| + (\hat{v}_2 \cdot \vec{p})^2} - |\hat{v}_2 \cdot \vec{p}|) + \frac{2}{\pi} \hat{v}_2 \cdot \vec{p} \log \frac{\Lambda}{|\hat{v}_2 \cdot \vec{p}|} \right) \quad (7.45)$$

Note that unless otherwise stated, we will discuss the $\ell = 1$ hot spot and drop the index ℓ . We see that at the hot spot, $\vec{p} = 0$, the self-energy has a non-Fermi liquid

form, [66, 226]

$$\Sigma(\vec{p}=0) = -i \frac{3}{(2\pi n)^{1/2} N} \left(\frac{1}{\alpha} + \alpha \right)^{-1/2} |\omega|^{1/2} \text{sgn}(\omega) \quad (7.46)$$

This result is consistent with our scaling form (7.42); to this order the anomalous dimension $\eta_\psi = 0$. On the other hand, away from the hot spot, in the regime $\gamma|\omega| \ll (\hat{v}_2 \cdot \vec{p})^2$, the fermion propagator takes the Fermi-liquid form (7.43). To leading order, the Fermi surface is given by $\hat{v}_1 \cdot \vec{p} = 0$. The Fermi velocity and quasiparticle residue vanish with the distance p_{\parallel} along the Fermi-surface to the hot spot as,

$$v_F = \frac{4nN}{3\gamma} p_{\parallel}, \quad \mathcal{Z} = \frac{4N}{3} (2\pi n)^{1/2} \gamma^{-1/2} \left(\frac{1}{\alpha} + \alpha \right)^{-1/2} p_{\parallel} \quad (7.47)$$

consistent with the scaling form (7.44) with mean-field exponents $z = 2$, $\eta_\psi = 0$.

The last term in Eq. (7.45) contributes to the renormalization of v_x, v_y , and so constrains the renormalization constants by

$$Z_\psi Z_v^x = 1 - \frac{6}{\pi n N} \frac{\alpha}{1 + \alpha^2} \log(\Lambda/\mu) \quad (7.48)$$

$$Z_\psi Z_v^y = 1 + \frac{6}{\pi n N} \frac{\alpha}{1 + \alpha^2} \log(\Lambda/\mu) \quad (7.49)$$

Next we consider the correction to the boson-fermion vertex,

$$-\langle \psi_{2\sigma}(p') \psi_{1\sigma'}^\dagger(p) \phi^a(-q) \rangle_{1PI} = \tau_{\sigma\sigma'}^a \Gamma_{\phi\psi_2\psi_1^\dagger}(p, q) (2\pi)^3 \delta^3(p' - p - q) \quad (7.50)$$

This is given by Fig. 7.6 and computed in Appendix F.1.3. We need only the UV divergent part, which is

$$\Gamma_{\phi\psi_2\psi_1^\dagger}(p, q) = 1 + \frac{2}{\pi n N} \tan^{-1} \frac{1}{\alpha} \log \Lambda \quad (7.51)$$

Eq. (7.51) constrains the renormalizations by

$$Z_\phi^{1/2} Z_\psi = 1 - \frac{2}{\pi n N} \tan^{-1} \frac{1}{\alpha} \log(\Lambda/\mu) \quad (7.52)$$

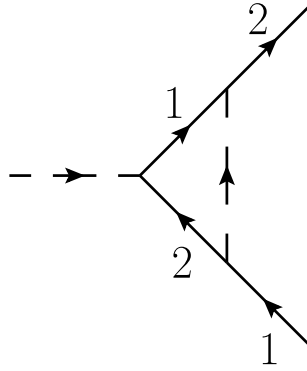


Figure 7.6: The leading correction to the boson-fermion vertex.

Finally, we consider the corrections to the boson two-point function, shown in Fig. 7.7, and computed in Appendix F.1.4. These yield

$$\begin{aligned}
 D^{-1}(\omega, \vec{q}) &= N\gamma|\omega| \left[1 + \frac{4}{\pi nN} \tan^{-1} \frac{1}{\alpha} \log \Lambda \right] \\
 &+ N\vec{q}^2 \left[1 + \frac{2}{\pi nN} \left(\frac{1}{\alpha} - \alpha + \left(\frac{1}{\alpha^2} + \alpha^2 \right) \tan^{-1} \frac{1}{\alpha} \right) \log \Lambda \right] \\
 &+ Nr \left[1 + \left(\frac{4}{\pi nN} \tan^{-1} \frac{1}{\alpha} - \frac{5}{2\pi^2 N} \tilde{u} \right) \log \Lambda \right] \quad (7.53)
 \end{aligned}$$

Note that both the frequency and momentum dependent parts of the boson propagator receive renormalization corrections. As we discussed earlier, the corrections to the coefficient of $|\omega|$ should not be considered as renormalizations of an independent coupling γ , but should rather track the renormalizations of the fermion velocities. Consequently, from Eqs. (7.27) and (7.53), we conclude that

$$Z_\phi (Z_v^x Z_v^y)^{-1} = 1 - \frac{4}{\pi nN} \tan^{-1} \frac{1}{\alpha} \log(\Lambda/\mu) \quad (7.54)$$

From the momentum dependent part of (7.53) we immediately obtain the bosonic

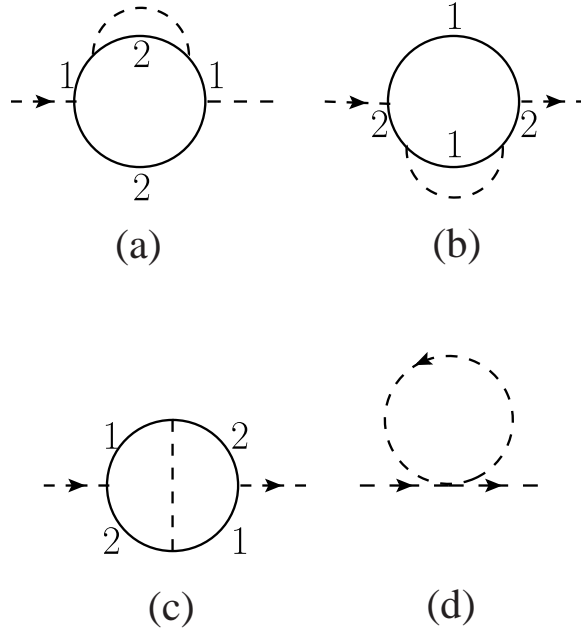


Figure 7.7: The leading correction to the boson polarization. A sum over both directions of the fermion loop is implied.

field strength renormalization,

$$Z_\phi = 1 - \frac{2}{\pi n N} \left(\frac{1}{\alpha} - \alpha + \left(\frac{1}{\alpha^2} + \alpha^2 \right) \tan^{-1} \frac{1}{\alpha} \right) \log(\Lambda/\mu) \quad (7.55)$$

while the r dependent part of (7.53) yields the renormalization constant Z_r ,

$$Z_r = 1 - \left(\frac{4}{\pi n N} \tan^{-1} \frac{1}{\alpha} - \frac{5}{2\pi^2 N} \tilde{u} \right) \log(\Lambda/\mu) \quad (7.56)$$

We note that while our results for the fermion self-energy (7.45) and the vertex (7.51) are in agreement with Ref. [229], the expression for the boson two-point function Eq. (7.53) differs from that of Ref. [229]. More precisely, the frequency dependent part of our D^{-1} agrees with Ref. [229], while the momentum dependent part does not. As already noted, the renormalization of the frequency dependent part of D^{-1} is constrained by that of the fermion self-energy and the vertex. On the other

hand, the renormalization of the momentum dependent part is completely independent. The authors of Ref. [229] found that both the frequency and the momentum parts are renormalized by the same factor, which would imply that the dynamical critical exponent $z = 2$ to this order. However, our calculations indicate that the two renormalizations are equal only at $\alpha = 1$ and, as we will see below, the dynamical critical exponent z receives corrections already at the present order in $1/N$.

We now have 5 equations for 4 renormalization constants: Eqs. (7.48), (7.49), (7.52), (7.54), and (7.55). It is easily verified that they are consistent with each other. This is a strong check on our renormalization procedure, and verifies the consistency of tying γ to the velocities by Eq. (7.19). We can solve these equations to obtain

$$\begin{aligned} \frac{Z_v^y}{Z_v^x} &= 1 + \frac{12}{\pi n N} \frac{\alpha}{1 + \alpha^2} \log(\Lambda/\mu) \\ Z_v^x Z_v^y &= 1 - \frac{2}{\pi n N} \left(\frac{1}{\alpha} - \alpha \right) \left(1 + \left(\frac{1}{\alpha} - \alpha \right) \tan^{-1} \frac{1}{\alpha} \right) \log(\Lambda/\mu) \\ Z_\psi &= 1 + \frac{1}{\pi n N} \left(\frac{1}{\alpha} - \alpha \right) \left(1 + \left(\frac{1}{\alpha} - \alpha \right) \tan^{-1} \frac{1}{\alpha} \right) \log(\Lambda/\mu) \end{aligned} \quad (7.57)$$

7.3.1 RG flows

The renormalization constants in Eq. (7.57) determine the flow of the dimensionless coupling α with the β -function

$$\beta(\alpha_r) = \frac{12}{\pi n N} \frac{\alpha_r^2}{\alpha_r^2 + 1} \quad (7.58)$$

The β function for the velocity anisotropy α has an infrared stable fixed point $\alpha = 0$ and an infrared unstable fixed point $\alpha = \infty$. Physically, both fixed points correspond to a nested Fermi surface. For $\alpha = 0$, the Fermi-velocities at the two hot spots are

anti-parallel, while for $\alpha = \infty$ they are parallel. The flows to the two fixed points are logarithmic. In particular, near the infrared stable fixed point $\alpha = 0$,

$$\alpha_r(s) = \frac{\alpha_r}{1 + \frac{12\alpha_r}{\pi nN} \log(1/s)} \quad (7.59)$$

Here we've assumed that the starting point of the flow $\alpha_r \ll 1$. Note that the logarithmic flow to $\alpha \rightarrow 0$ in the infrared, with vanishing velocity ratio, is similar to that found recently in Ref. [196] in a different physical context.

Let us now discuss the physics of the $\alpha = 0$ fixed point. The renormalization constants in (7.55),(7.56), (7.57) also determine the renormalization of the velocities, the anomalous dimensions of the bosons, fermions and of the ϕ^2 operator. For the velocities, the ratio is already specified by α , and it is convenient to take γ as the other independent combination of the velocities. We have therefore

$$\begin{aligned} \eta_\gamma &= \frac{2}{\pi nN} \left(\frac{1}{\alpha_r} - \alpha_r \right) \left(1 + \left(\frac{1}{\alpha_r} - \alpha_r \right) \tan^{-1} \frac{1}{\alpha_r} \right) \\ \eta_\phi &= \frac{2}{\pi nN} \left(\frac{1}{\alpha_r} - \alpha_r + \left(\frac{1}{\alpha_r^2} + \alpha_r^2 \right) \tan^{-1} \frac{1}{\alpha_r} \right) \\ \eta_\psi &= -\frac{1}{\pi nN} \left(\frac{1}{\alpha_r} - \alpha_r \right) \left(1 + \left(\frac{1}{\alpha_r} - \alpha_r \right) \tan^{-1} \frac{1}{\alpha_r} \right) \\ \eta_2 &= -\frac{2}{\pi nN} \left(\frac{1}{\alpha_r} - \alpha_r \right) \left(1 + \left(\frac{1}{\alpha_r} - \alpha_r \right) \tan^{-1} \frac{1}{\alpha_r} \right) - \frac{5}{2\pi^2 N} \tilde{u}_r \end{aligned} \quad (7.60)$$

Note that as can be seen from Eqs. (7.35),(7.38) the flow of the dimensionful constant γ_r described by the exponent η_γ is equivalent to an anomalous dynamical critical exponent z . Since η_γ is non-zero, the dynamical behaviour of the theory deviates from the simple Hertz-Millis scaling with $z = 2$.

As α flows slowly to 0, the critical exponents in Eq. (7.60) slowly vary:

$$\eta_\phi \rightarrow \frac{1}{nN} \frac{1}{\alpha_r^2}, \quad \eta_\psi \rightarrow -\frac{1}{2nN} \frac{1}{\alpha_r^2}, \quad \eta_\gamma \rightarrow \frac{1}{nN} \frac{1}{\alpha_r^2}, \quad \eta_2 \rightarrow -\frac{1}{nN} \frac{1}{\alpha_r^2}, \quad \alpha_r \rightarrow 0 \quad (7.61)$$

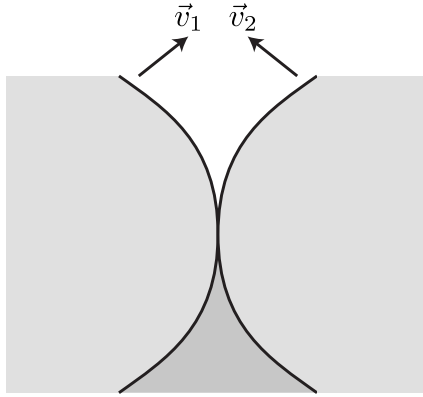


Figure 7.8: Modification of the Fermi surfaces in Fig. 7.2 at the SDW quantum critical point. As in Figs. 7.2 and 7.3, the full lines are the Fermi surfaces, and the white, light shaded, and dark shaded regions denote momenta where 0, 1, and 2 of the bands are occupied. The equation of one of the Fermi surfaces is given in (7.62).

Observe that the corrections to the critical exponents diverge as $\alpha_r \rightarrow 0$. Thus, for sufficiently small momenta the $1/N$ expansion breaks down. From Eq. (7.61) we see that this will happen when $\alpha \sim 1/\sqrt{N}$; from Eq. (7.59), we can estimate that this occurs at a momentum scale $k \sim \exp(-N^{3/2})$. This is parametrically smaller than the scale $k \sim \exp(-N)$ at which the direct expansion in $1/N$ (without RG improvement) becomes invalid.

Despite the breakdown of the RG at the longest scales, there is an intermediate asymptotic regime, $1/\sqrt{N} \ll \alpha_r \ll 1$, where Eq. (7.61) remains valid, and we can integrate the RG equations and find interesting consequences for both the fermionic and bosonic spectra.

For the fermions, the location of the ψ_1 Fermi surface is given at tree-level by $\hat{v}_1 \cdot \vec{p} = 0$, or $p_y = -v_x p_x / v_y = -p_x / \alpha$. Evaluating α at $s = \mu / p_x$, we find the Fermi surface at

$$p_y = -\frac{12}{\pi n N} p_x \log(\mu / |p_x|) \quad (7.62)$$

The resulting Fermi surface distorts from the shape shown in Fig. 7.1 to that in Fig. 7.8. We may also use RG to improve the one-loop result for the fermion self-energy (7.45). From Eq. (7.35), the fermion self-energy at the hot spot is,

$$\Sigma(\omega, \vec{p} = 0) \sim -i \exp\left(-\frac{3}{\pi^2 n^3 N^3} \log^3 \frac{\mu^2}{\gamma_r |\omega|}\right) |\omega|^{1/2} \text{sgn}(\omega), \quad (7.63)$$

Along the Fermi surface away from the hot spot, the quasiparticle residue and Fermi velocity behave as,

$$v_F \sim \exp\left(\frac{48}{\pi^2 n^3 N^3} \log^3 \frac{\mu}{p_{\parallel}}\right) p_{\parallel}, \quad \mathcal{Z} \sim \left(\log \frac{\mu}{p_{\parallel}}\right)^{-1/2} p_{\parallel} \quad (7.64)$$

The characteristic frequency of the bosonic spectrum is $\omega \sim \bar{q}^2/\gamma_r$; evaluating γ_r at $s = \mu/|\bar{q}|$, we find that it scales with a ‘super power-law’ of the momentum

$$\omega \sim \bar{q}^2 \exp\left(\frac{48}{\pi^2 n^3 N^3} \log^3 \frac{\mu}{|\bar{q}|}\right). \quad (7.65)$$

From Eq. (7.35) we also obtain the static and dynamic scaling of the bosonic propagator,

$$\begin{aligned} D^{-1}(\omega, \vec{q} = 0) &\sim |\omega|^{1-\frac{1}{nN}} \exp\left(\frac{6}{\pi^2 n^4 N^4} \log^3 \frac{\mu^2}{\gamma_r |\omega|}\right) \left(\log \frac{\mu^2}{\gamma_r |\omega|}\right)^{-1/3} \\ D^{-1}(\omega = 0, \vec{q}) &\sim |\vec{q}|^2 \exp\left(\frac{48}{\pi^2 n^3 N^3} \log^3 \frac{\mu}{|\vec{q}|}\right) \end{aligned} \quad (7.66)$$

Note that the unusual super-power law dependencies in Eqs. (7.63)-(7.66) are consequences of the scaling of $\alpha_r \rightarrow 0$ in the infrared and associated divergences of the anomalous dimensions.

7.4 Counting powers of N

As written in Eq. (7.17), our field theory offers a potentially simple way of organizing perturbation theory in powers of $1/N$: each boson propagator comes with a

power of $1/N$, each fermion loop yields a power of N , and each u interaction yields a factor N : we refer to this as the “naive” $1/N$ expansion, and it has been the basis of our computations so far.

However, because we have to take $\eta \rightarrow 0$ in the scaling limit, there is a danger that some of the higher order diagrams will have a singular dependence on η . The fermion propagators in such diagrams need to include self-energy corrections for the diagrams to be finite in the $\eta \rightarrow 0$ limit. The price we will pay for this regularization is that the diagram will acquire additional powers of N , and the naive counting of powers of $1/N$ will break down.

Recently, in the context of a theory of a Fermi surface interacting with a gauge field, S.-S. Lee [198] has given a procedure for identifying diagrams with a breakdown of naive $1/N$ counting, and shown that the expansion in powers of $1/N$ is actually an expansion in the genus of a surface defined by the graph. Using his methods we will show that many similar issues appear in our theory for the SDW transition of a Fermi surface, although subtle differences in RG properties imply that in the present case no genus expansion exists, and diagrams of increasingly higher order in N are generated as the number of loops is increased.

In the absence of an external pairing vertex (see section 7.5), the simplest diagrams exhibiting the above effect are the three-loop corrections to the boson-fermion vertex, see Fig. 7.9. In fact, the two diagrams are equal as they are related by particle-hole symmetry. The external fermions are taken to have hot spot index $\ell = 1$, while the fermions running in the loop can come from any hot spot ℓ' , although we will see that the singular contributions will originate from $\ell' = 1$ and $\ell' = 3$. The diagram is given

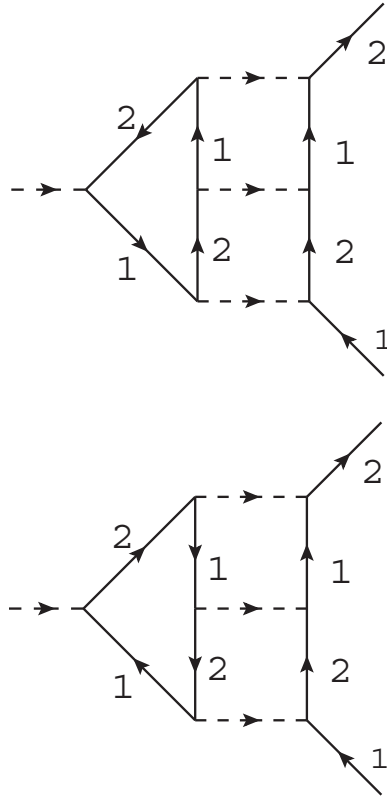


Figure 7.9: Three loop corrections to the boson-fermion vertex that are enhanced in N , scaling as $\mathcal{O}(N^0)$.

by,

$$\delta\Gamma_{\phi\psi_2\psi_1^\dagger}(p, q)\tau^a = -\tau^{a_1}\tau^{a_2}\tau^{a_3} \int \frac{dk_\tau d\vec{k} d\vec{k}' d\vec{k}'}{(2\pi)^6} f^{aa_1 a_2 a_3}(q, p - k', k' - k, k - p - q) \times G_1(k)G_2(k')D(k' - p)D(k - k')D(p + q - k)$$

Substituting the four-point boson vertex f , Eq. (7.15),

$$\begin{aligned}
 \delta\Gamma_{\phi\psi_2\psi_1^\dagger}(p, q) &= -\frac{7N}{2\pi v_x v_y} \sum_{\ell'} \int \frac{dk_\tau d\vec{k} dk'_\tau d\vec{k}'}{(2\pi)^6} \\
 &\quad (|q_\tau| - |p_\tau - k'_\tau| + |k'_\tau - k_\tau| - |k_\tau - p_\tau - q_\tau|) \\
 &\quad \times \frac{1}{(i\eta(p_\tau - k_\tau) - \vec{v}_1^{\ell'} \cdot (\vec{p} - \vec{k}))(i\eta(q_\tau + p_\tau - k'_\tau) - \vec{v}_2^{\ell'} \cdot (\vec{q} + \vec{p} - \vec{k}'))} \\
 &\quad \times \frac{1}{(i\eta k_\tau - \vec{v}_1 \cdot \vec{k})(i\eta k'_\tau - \vec{v}_2 \cdot \vec{k}')} D(k' - p) D(k - k') D(p + q - k)
 \end{aligned} \tag{7.67}$$

Observe that if $\ell' = 2$ or $\ell' = 4$ the four denominators in Eq. (7.67) involve four linearly independent combinations of internal momenta \vec{k} , \vec{k}' . As a result, the integral has a well defined limit when $\eta \rightarrow 0$. On the other hand, when $\ell' = 1$ or $\ell' = 3$ (which we will also denote as $\ell' = -1$), $\vec{v}^{\ell'}$ and \vec{v} are parallel. Keeping only these two hot spots, let us integrate over the momentum components $\vec{v}_1 \cdot \vec{k}$, $\vec{v}_2 \cdot \vec{k}'$. We focus on the contribution from the fermionic poles, which, as we will see, is infrared singular.

$$\begin{aligned}
 \delta\Gamma_{\phi\psi_2\psi_1^\dagger}(p, q) &= \frac{7N}{2\pi v_x v_y |\vec{v}|^2} \sum_{\ell'=\pm 1} \int \frac{dk_\tau dk_\parallel dk'_\tau dk'_\parallel}{(2\pi)^4} \\
 &\quad (|q_\tau| - |p_\tau - k'_\tau| + |k'_\tau - k_\tau| - |k_\tau - p_\tau - q_\tau|) \\
 &\quad \times \frac{(\theta(k_\tau) - \theta(\ell'(k_\tau - p_\tau)))(\theta(k'_\tau) - \theta(\ell'(k'_\tau - p_\tau - q_\tau)))}{(i\eta((1 - \ell')k_\tau - p_\tau) + \ell' \vec{v}_1 \cdot \vec{p})(i\eta((1 - \ell')k'_\tau - p_\tau - q_\tau) + \ell' \vec{v}_2 \cdot (\vec{p} + \vec{q}))} \\
 &\quad \times D(k' - p) D(k - k') D(p + q - k).
 \end{aligned}$$

Here k_\parallel , k'_\parallel denote the components of \vec{k} , \vec{k}' along the Fermi surface of ψ_1 and ψ_2 respectively, and the arguments of boson propagators are evaluated at $\vec{v}_1 \cdot \vec{k} = \vec{v}_2 \cdot \vec{k}' = 0$. (Strictly speaking, only one pair of poles has $\vec{v}_1 \cdot \vec{k} = \vec{v}_2 \cdot \vec{k}' = 0$, while the other pair has $\vec{v}_1 \cdot \vec{k} = \vec{v}_1 \cdot \vec{p}$ and $\vec{v}_2 \cdot \vec{k}' = \vec{v}_2 \cdot (\vec{p} + \vec{q})$. However, in situations of interest to us discussed below the above difference may be neglected in the bosonic propagators).

Note that if we take the initial and final fermion momenta to lie on the Fermi surface, *i.e.* $\vec{v}_1 \cdot \vec{p} = 0$, $\vec{v}_2 \cdot (\vec{p} + \vec{q}) = 0$, then $\delta\Gamma$ diverges as η^{-2} . Since the dimension of η is $\omega^{-1/2}$, this is synonymous to an infra-red divergence,

$$\delta\Gamma_{\phi\psi_2\psi_1^\dagger} \sim \eta^{-2} N^{-2} \omega^{-1}. \quad (7.68)$$

This behavior can be easily checked by, for instance, setting all the external momenta to zero (*i.e.* taking the external fermions to be at the hot spots). We also note that in the case when the external fermion momenta do not lie on the Fermi surface, the limit $\eta \rightarrow 0$ can be taken in the contribution of hot spot pair $\ell' = 1$, but not $\ell' = -1$, as the latter contains a non-local UV divergence. Keeping η finite, we obtain,

$$\delta\Gamma_{\phi\psi_2\psi_1^\dagger} \sim \eta^{-1} N^{-2} p_\perp^{-1}. \quad (7.69)$$

where p_\perp schematically denotes the distance of external fermion momenta to the Fermi surface.

The infra-red divergences in Eqs. (7.68), (7.69) are a product of the bare fermion propagator having $z = 1$ dynamics, whereas we expect that the full fermion propagator has the same dynamics as the spin-density wave excitations. We saw that this, indeed, holds at the one-loop level, where both the boson (7.21) and fermion (7.45) propagators are invariant under scaling with $z = 2$ (up to logarithmic corrections in the latter case). As in Ref. [198], the divergence can be cured by including the one-loop fermion self-energy within the fermion propagators, before taking the $\eta \rightarrow 0$ limit. This is the approach that will be adopted below. From Eq. (7.46), we know that the self-energy is $\sim \sqrt{\omega}/N$. Therefore, mapping $\eta\omega \rightarrow \sqrt{\omega}/N$, we find from

Eq. (7.68) that

$$\delta\Gamma_{\phi\psi_2\psi_1^\dagger} \sim \mathcal{O}(1) \quad (7.70)$$

Thus, the vertex correction is not suppressed relative to the bare value, and the naive $1/N$ expansion has broken down. In the appendix F.2.1, we compute the vertex correction in Fig. 7.9 with dressed fermion propagators and find to logarithmic accuracy,

$$\delta\Gamma_{\phi\psi_2\psi_1^\dagger} \sim X(\alpha) \log \frac{\Lambda}{|\vec{q}|} \quad (7.71)$$

where X is a finite negative function of α . Note that the strong infra-red divergence of Eq. (7.68) is now replaced by a mild logarithmic divergence that one may hope to treat with renormalization group. However, the price one has to pay for curing the strong infra-red divergence is the enhancement of the diagram with N , as anticipated in Eq. (7.70). This enhancement occurs for any external fermion momenta (not only for momenta on the Fermi surface). Finally, the presence of a logarithm implies that not only is the diagram itself unsuppressed relative to its bare value, but also that the anomalous dimensions are not expected to be suppressed with N .

Having seen an explicit example of violation of naive large- N counting, we would like to investigate the general scaling of diagrams with N in our theory, when a one-loop dressed fermion propagator is used. Our procedure closely follows that of Ref. [198]. A general diagram can be schematically written as,

$$\mathcal{D} = N^{L_f} \int \prod_{i=1}^L d^2 p_i d\omega_i \prod_{j=1}^{I_f} \frac{1}{\Sigma_{1loop}(l_j) + \vec{v} \cdot \vec{l}_j} \prod_{k=1}^{I_b} D(q_k) \quad (7.72)$$

Here, I_f and I_b are numbers of fermion and boson propagators respectively, L_f is the number of fermion loops and L is the number of total loops. The momenta l_j and

q_k are linear combinations of p_i entering the fermion and boson propagators. The “naive” scaling of the diagram with N is given by $\mathcal{D} \sim N^{Q_0}$,

$$Q_0 = L_f - I_b \quad (7.73)$$

It is clear that the enhancement of diagrams with N comes from the dangerous factor of $1/N$ in the fermion self-energy. However, in order to access this factor the fermion momentum must be on the Fermi surface. Given a diagram, let us call the phase-space for all internal fermion momenta to lie on the Fermi surface, the “singular manifold.” Having identified this manifold, one can divide the momentum integration variables into components parallel p_{\parallel} and perpendicular p_{\perp} to the manifold,

$$\prod_{i=1}^L d^2 p_i = \prod_{a=1}^n dp_{\parallel a} \prod_{b=1}^{2L-n} dp_{\perp b} \quad (7.74)$$

where n is the dimension of the manifold. Linear combinations of p_{\perp} ’s enter the fermion energy $\vec{v} \cdot \vec{l}_j$ and hence scale as $1/N$, making the fermion propagators scale as N . On the other hand, the components p_{\parallel} only enter the bosonic propagators and the one-loop fermion self-energy Σ_{1loop} and scale as N^0 . Hence, the diagram acquires an enhancement, $\mathcal{D} \sim N^Q$, $Q = Q_0 + \Delta Q$,

$$\Delta Q = [I_f - 2L + n] \quad (7.75)$$

where $[x] = x$ if $x \geq 0$ and $[x] = 0$ if $x < 0$.

Thus, to find the degree of a diagram in N , one has to find the singular manifold and compute its dimension n . This can be done diagrammatically by introducing a double-line representation, originally used in the study of electron-phonon interactions.[231] Below, we will consider diagrams involving opposite hot spot pairs

$\ell = 1$ and $\ell = -1$ only. Substitution of fermions from hot spots $\ell = 2$ and $\ell = -2$ into these diagrams is expected to reduce the dimension of the singular manifold. Moreover, we for simplicity consider diagrams without the quartic bosonic vertex u . Finally, we take all the external fermion momenta to be on the Fermi surface.

Now, we are ready to introduce the double-line representation. We would like to find under what conditions do all the fermions in a diagram go to the Fermi surface. Observe, that any momentum can be uniquely decomposed into components along the Fermi surface of fermion 1 and fermion 2. Thus, we fatten bosonic propagators into double lines, one carrying momentum along the Fermi surface of fermion 1, and the other along the Fermi surface of fermion 2. If a fermion is to absorb this bosonic momentum and stay on the Fermi surface, its incoming and outgoing momenta are fixed in terms of the components of the double line. Hence, the boson-fermion vertices can be redrawn as shown in Fig. 7.10. Note that if a certain momentum is along the Fermi surface of fermion 1 from hot spot $\ell = 1$, it is also along the Fermi surface of fermion 1 from hot spot $\ell = -1$. Thus, the fermion lines in our diagrams can come from either of these hot spots. Also, the direction of lines in the double-line representation is not fixed, and need not coincide with that in the single line representation. If the two are opposite, then it is understood that the physical fermion momentum \vec{p} is the negative of the momentum carried by the fermion in the double-line representation, see Fig. 7.11. Because we are neglecting the Fermi surface curvature in the low-energy theory, a particle with momentum \vec{p} is on the Fermi surface if and only if a particle with momentum $-\vec{p}$ is on the Fermi surface, and the above representation is consistent. (We remind the reader that here all the fermion momenta are

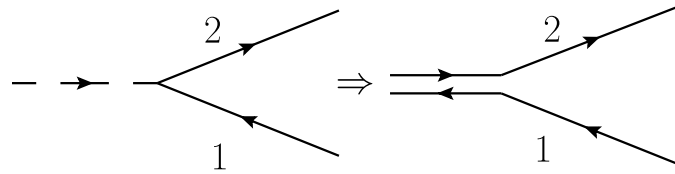


Figure 7.10: Double line representation for the boson-fermion vertex.

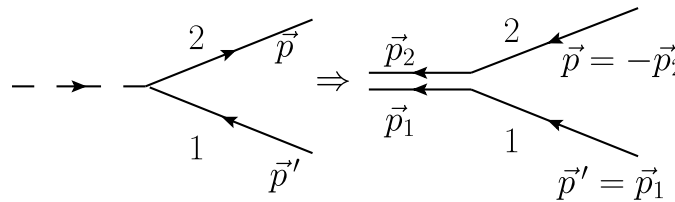


Figure 7.11: Double line representation for the boson-fermion vertex. The direction of momentum and particle flow need not coincide.

defined relative to hot spot locations).

Thus, the double line representation completely specifies the singular manifold. In particular, the dimension of the manifold n is just given by the number of loops in this representation. As an example, consider the double line representation of the diagrams in Fig. 7.9 shown in Fig. 7.12. We see that Fig. 7.12 contains two closed loops, which implies that the singular manifold is two-dimensional. From Eq. (7.75), the enhancement of the diagram is $\Delta Q = 2$, which combined with the naive degree of the diagram, Eq. (7.73), $Q_0 = -2$, gives $Q = 0$, consistent with the explicit calculation in Eq. (7.71). In Fig. 7.13 we also give an example of a vertex correction which is not enhanced in N . Here, the double line representation contains no loops so the dimension of the singular manifold is zero, $\Delta Q = 0$ and the degree of the diagram is given by the naive N counting, $Q = -2$.

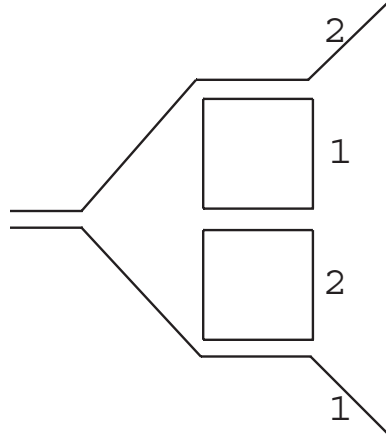


Figure 7.12: Double line representation applied to the diagrams in Fig. 7.9. The enhancement of the diagram in N is related to the number of loops n in the double line-representation via Eq. 7.75.

It is easy to see that the violations of naive large- N counting are not confined to vertex corrections alone. In Fig. 7.14 we show a fermion self-energy diagram that acquires an enhancement. Indeed, the naive degree of the graph is $Q_0 = -3$. However, since the double line representation contains three loops, the graph receives an enhancement $\Delta Q = 2$, so that the total degree of the graph is $Q = -1$. Hence, the graph is of the same order $\mathcal{O}(1/N)$ as the one-loop fermion self-energy. Similarly, in Fig. 7.15 we show an enhanced diagram for the boson self-energy. In this case, $Q_0 = -1$, $\Delta Q = 2$, $Q = 1$. Hence, the diagram is of $\mathcal{O}(N)$, again the same as the tree level contribution.

A remarkable feature of the large- N counting in Eqs. (7.73), (7.75), pointed out in Ref. [198], is that the degree of a diagram is related to its topology. Let us first apply the topological classification to vacuum energy diagrams, *i.e.* graphs with no external lines. We can convert these diagrams into two-dimensional surfaces in the following way. First, let us introduce fermion loops back into the double line

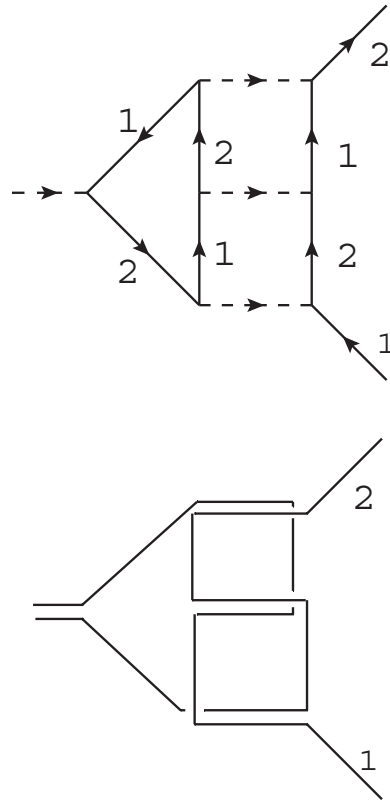


Figure 7.13: A three loop vertex correction with no enhancement in N .

representation (they will appear dotted in our diagrams, see Fig. 7.16). Then attach a face to each solid loop of the double-line representation and a face to each dotted loop (*i.e.* fermion loop). As a result, each boson propagator is shared by two faces with solid boundaries, while each fermion propagator is shared by a face with a solid boundary and a face with a dotted boundary. Therefore, if we glue the faces along propagators we obtain a closed surface. Now consider the Euler characteristic of this surface,

$$\chi = F - E + V \tag{7.76}$$

where F is the number of faces, E is the number of edges and V is the number of

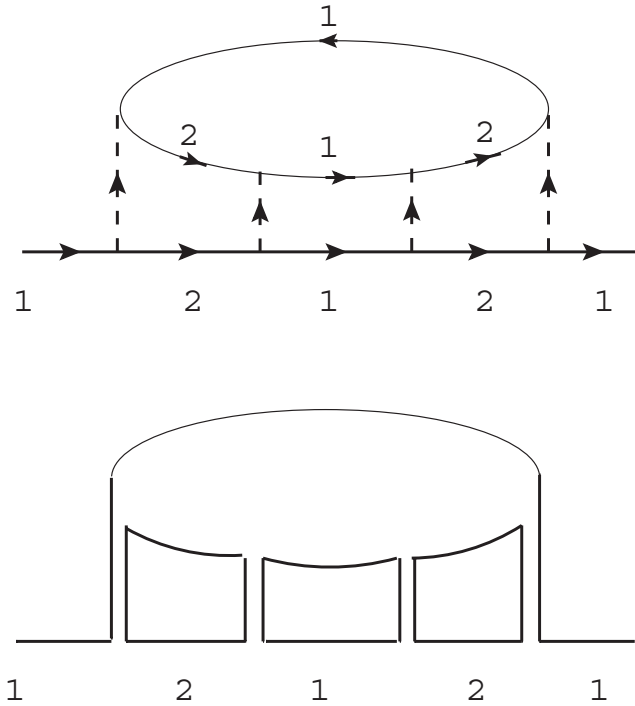


Figure 7.14: A diagram for the fermion self-energy that is of $\mathcal{O}(1/N)$ as a result of enhancement.

vertices of the surface. We have, $F = L_f + n$, $E = I_b + I_f$ and V is just the number of vertices in the original Feynman graph. Now, using $V = 2I_b$, $2V = 2I_f$ we obtain,

$$\chi = L_f + n - \frac{V}{2} \tag{7.77}$$

However, using $L = I_b + I_f - V + 1$, we see that the degree of a diagram in N given by Eqs. (7.73), (7.75), is,

$$Q = L_f - \frac{V}{2} + n - 2 \tag{7.78}$$

where we've assumed that the argument of $[\]$ in Eq. (7.75) is positive. Thus, we arrive at the relation,

$$Q = \chi - 2 \tag{7.79}$$

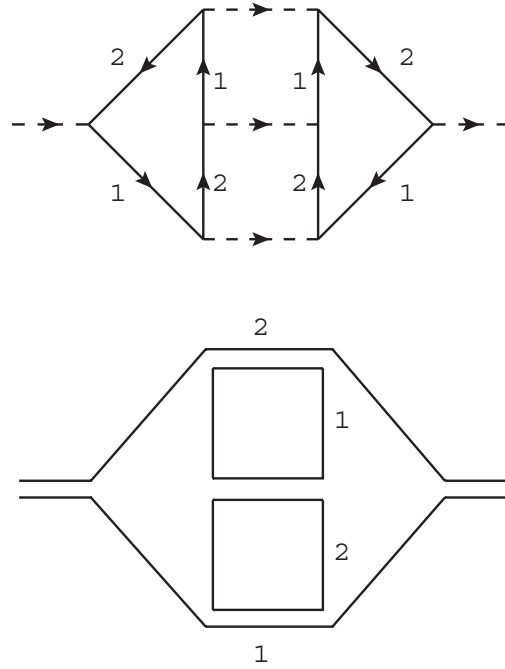


Figure 7.15: A diagram for the boson self-energy that is of $\mathcal{O}(N)$ as a result of enhancement.

This result means that at each order in $1/N$ one has to sum an infinite set of diagrams with a given Euler characteristic. In particular, at $N = \infty$ the theory is dominated by diagrams with $\chi = 2$, *i.e.* those whose double-line representation can be drawn on a sphere. Such graphs are often referred to as planar diagrams.

It is straightforward to extend the classification above to diagrams with external legs. For instance, fermion self-energy diagrams can be obtained by cutting one fermion propagator in a vacuum graph. This results in $I_b \rightarrow I_b$, $L_f \rightarrow L_f - 1$, so $Q_0 \rightarrow Q_0 - 1$, and $I_f \rightarrow I_f - 1$, $L \rightarrow L - 1$, $n \rightarrow n - 1$, as cutting a fermion propagator destroys a solid loop in the double line representation. Hence, $\Delta Q \rightarrow \Delta Q$ and $Q \rightarrow Q - 1$, *i.e.*

$$Q = \chi - 3 \tag{7.80}$$

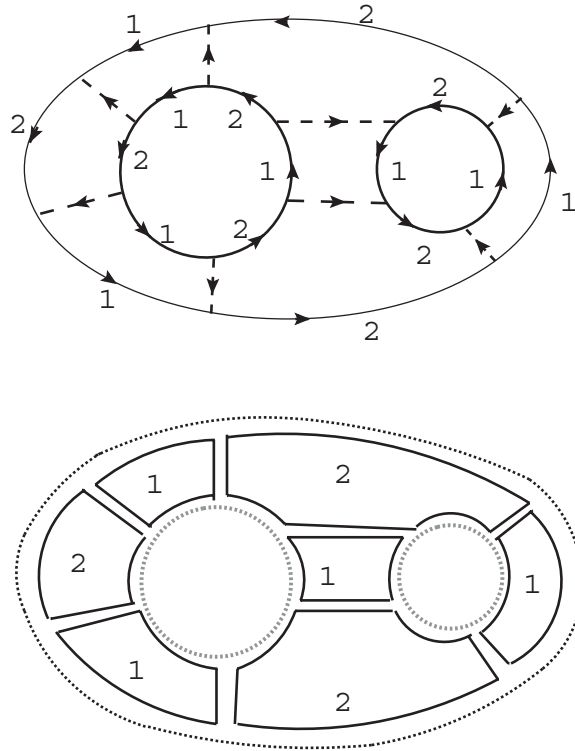


Figure 7.16: Converting vacuum energy diagrams into surfaces: a face is attached to each solid and grey loop in the double-line representation (on the right). In the present case, the resulting surface is a sphere.

with χ the Euler characteristic of the initial vacuum diagram. In particular, planar vacuum graphs give rise to fermion self-energy diagrams of $\mathcal{O}(1/N)$.

Similarly, to obtain a boson self-energy diagram, we cut a boson propagator in a vacuum bubble. This gives $I_b \rightarrow I_b - 1$, $L_f \rightarrow L_f$, so $Q_0 \rightarrow Q_0 + 1$, and $I_f \rightarrow I_f$, $L \rightarrow L - 1$, $n \rightarrow n - 2$, as we now destroy two solid loops in the double line representation. Hence, $\Delta Q \rightarrow \Delta Q$ and $Q \rightarrow Q + 1$, *i.e.*

$$Q = \chi - 1 \tag{7.81}$$

Hence, planar graphs give rise to boson self-energy diagrams of $\mathcal{O}(N)$.

Likewise, to obtain vertex correction diagrams, we remove a vertex in a vacuum

bubble. As a result, $I_b \rightarrow I_b - 1$, $L_f \rightarrow L_f - 1$, so $Q_0 \rightarrow Q_0$, and $I_f \rightarrow I_f - 2$, $L \rightarrow L - 2$, $n \rightarrow n - 2$, as we again destroy two solid loops in the double line representation. Hence, $\Delta Q \rightarrow \Delta Q$ and $Q \rightarrow Q$, *i.e.*

$$Q = \chi - 2 \tag{7.82}$$

and all planar graphs give rise to vertex diagrams of $\mathcal{O}(1)$.

At this point, we would like to make a remark about conditions on external momenta in diagrams needed for the enhancements to occur. Up to now we have been assuming that all the external fermion momenta in a diagram are on the Fermi surface. If all the diagrams in our theory were UV finite then this condition would, indeed, be required. However, as we have seen, some of the diagrams actually contain logarithmic divergences, *i.e.* they receive contributions from momenta, which are much larger than the external momenta. For the purpose of computing the UV divergent contribution to these diagrams and estimating its scaling with N , we can set the external momenta to zero (which certainly puts the external fermions on the Fermi surface). This explains why the vertex correction in Figs. 7.9,7.12 receives an enhancement for any external fermion momentum, as can be explicitly seen in Eq. (7.71).

So far, we have left out one type of diagram which is important from the point of view of RG properties of the theory, namely diagrams for the boson four-point function. Such diagrams can be obtained by cutting two boson propagators in a vacuum bubble. This results in $I_b \rightarrow I_b - 2$, $L_f \rightarrow L_f$, so $Q_0 \rightarrow Q_0 + 2$. Now let us discuss the change in the enhancement ΔQ . We see that $I_f \rightarrow I_f$, $L \rightarrow L - 2$. The change in the dimension of the singular manifold δn depends on how many loops

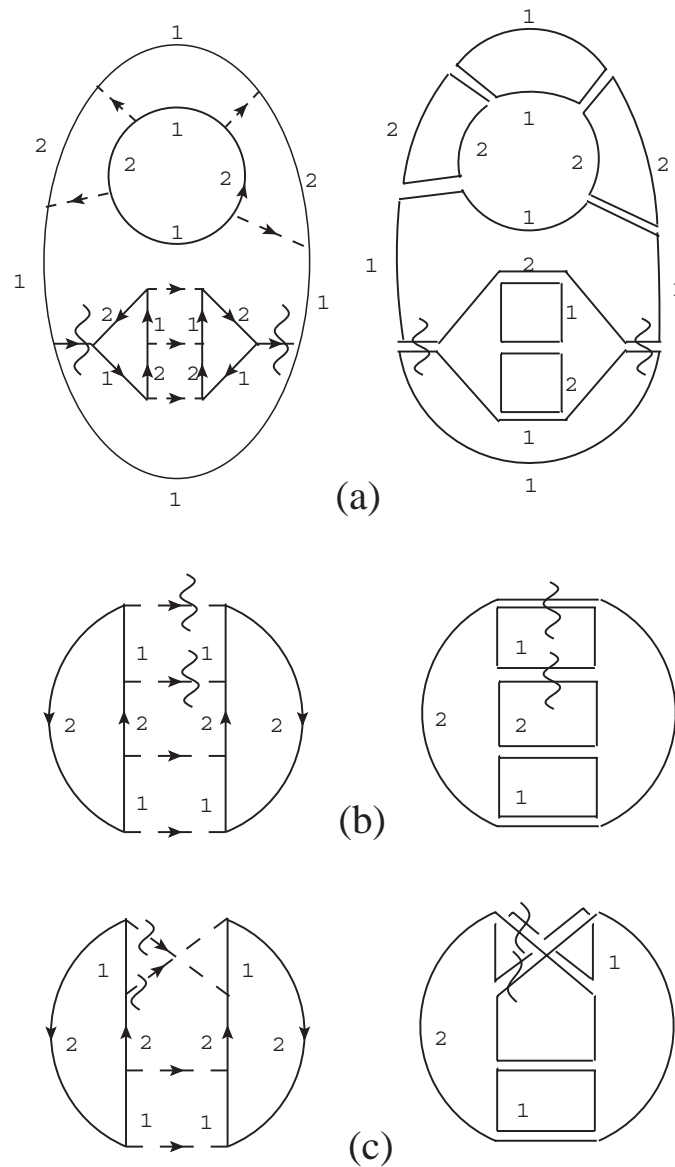


Figure 7.17: Producing a boson four-point function from a vacuum bubble by cutting two boson propagators. If the initial diagram is planar and only two solid lines are cut in the double-line representation then the resulting diagram is disconnected, as in (a). Diagrams of highest degree are obtained by starting with a planar diagram and cutting three solid line loops, as in (b), or starting with a diagram with $\chi = 1$ and cutting two solid line loops, as in (c).

in the double line representation the two propagators that we cut share. If both the components 1 and 2 of the two propagators are part of the same two solid loops, see Fig. 7.17c, then the change in the dimension of the singular manifold $\delta n = -2$. If these two propagators share only one solid loop, see Fig. 7.17b, then $\delta n = -3$. Finally, if the two propagators don't share any solid loops, then $\delta n = -4$. Thus, we obtain, $\Delta Q \rightarrow \Delta Q + 4 + \delta n$ and $Q \rightarrow Q + 6 + \delta n$, *i.e.*

$$Q = \chi + 4 + \delta n \quad (7.83)$$

It appears that the highest possible degree of the four-point vertex corresponds to starting with a planar graph and cutting two bosonic propagators, which are part of the same double-line loop, to obtain, $Q = 4$. However, it is easy to see that this always produces a diagram, which is disconnected, see Fig. 7.17a. To obtain a connected diagram for the four-point function starting from a planar graph, we must cut at least three solid loops, such that the highest possible degree of a four-point function is $Q = 3$. The fact that the four-point vertex scales as N^3 could be anticipated from the simple one-loop result in Eq. (7.15). Indeed, for special kinematic conditions, $\vec{v}_1 \cdot (\vec{q}_2 + \vec{q}_3) = 0$, $\vec{v}_2 \cdot (\vec{q}_1 + \vec{q}_2) = 0$, Eq. (7.15) diverges as $N(\eta^2\omega)^{-1}$, which after including the one-loop fermion self-energy is expected to become of order N^3 . Such kinematic conditions are automatically assumed in our double line representation that led to the large- N counting in Eq. (7.83). However, as was already noted, diagrams that have ultraviolet divergences are expected to receive the enhancement in Eq. (7.75) independent of external momenta. The simplest diagram for the boson four-point vertex that is expected to scale as N^3 and exhibits such a divergence is shown in Fig. 7.18. In the appendix, we explicitly evaluate this diagram obtaining to

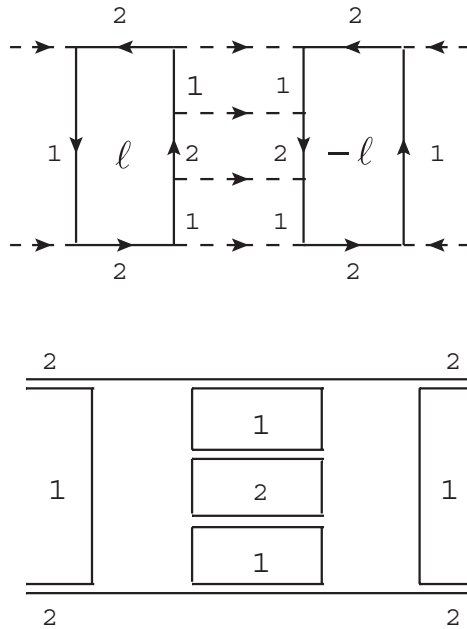


Figure 7.18: A diagram for the boson four-point function that diverges logarithmically and scales as N^3 .

logarithmic accuracy,

$$\delta\Gamma^4 = N^3 Y(\alpha) \gamma \log \frac{\Lambda}{|\vec{q}|} \quad (7.84)$$

with Y a finite function of α .

The fact that there are diagrams for the four-point boson function that scale as N^3 for arbitrary external momenta has drastic consequences for the theory. Indeed, a diagram with just quartic internal vertices (which can themselves have a non-trivial internal structure), will scale as N^Q , with $Q = V_4 + \frac{E_b}{2}$, where V_4 is the number of quartic vertices and E_b is the number of external bosons. Thus, the degree of the diagram in N grows with the number of quartic vertices. This means that perturbation theory based on the one-loop dressed fermion propagator is not a good starting point for taking the large- N limit, and no genus expansion similar to that of Ref. [198]

exists in the present case. Note that this effect was not captured in our initial large- N counting, as we have ignored the possible presence of UV divergent subdiagrams.

7.5 Pairing vertex

In this section we will study the renormalization properties of the BCS order parameter to one loop order. We consider pairing in the spin singlet, parity even, momentum zero channel. There are four order parameters that one can form out of our four pairs of hot spots,

$$V_{\mu\nu} = \epsilon_{\sigma\sigma'}(\psi_{1\sigma}^{\ell=-1}\psi_{1\sigma'}^{\ell=1} + \mu\psi_{2\sigma}^{\ell=-1}\psi_{2\sigma'}^{\ell=1}) + \nu\epsilon_{\sigma\sigma'}(\psi_{1\sigma}^{\ell=-2}\psi_{1\sigma'}^{\ell=2} + \mu\psi_{2\sigma}^{\ell=-2}\psi_{2\sigma'}^{\ell=2}) \quad (7.85)$$

Here the minus sign in the hot spot labels $\ell = -1 \equiv 3$ and $\ell = -2 \equiv 4$ denotes the opposite hot spot pair. The geometry of the pairing operators for $\ell = 1$ is illustrated in Fig. 7.19. The coefficients $\mu = \pm 1$, $\nu = \pm 1$ determine the transformation properties of V under the lattice rotation symmetry $R_{\pi/2}$ and the reflection symmetry $I_{(-1,1)}$ about the $(-1, 1)$ axis:

$$R_{\pi/2} : V_{\mu\nu} \rightarrow \nu V_{\mu\nu} \quad (7.86)$$

$$I_{(-1,1)} : V_{\mu\nu} \rightarrow \mu V_{\mu\nu} \quad (7.87)$$

These properties are summarized in Table 7.1. Since the theory (7.17) conserves the number of fermions at each hot spot pair ℓ , the parts of the order parameter involving $\ell = \pm 1$ and $\ell = \pm 2$ renormalize independently. Hence, the scaling dimension of the pairing vertex in the low-energy theory is independent of ν and is sensitive only to μ , i.e the operators with s and d_{xy} , and g and $d_{x^2-y^2}$ symmetries are degenerate.

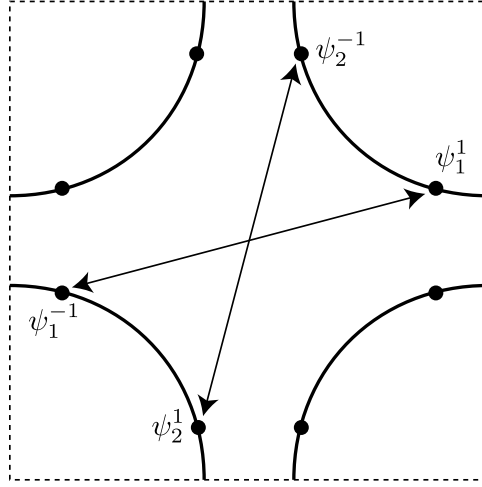


Figure 7.19: Pairing of the electrons at the $\ell = \pm 1$ hotspots of Fig. 7.1. Electrons at opposite ends of the arrows form spin-singlet pairs. The $\mu = +1$ ($\mu = -1$) pairing amplitude in Eq. (7.85) has the same (opposite) sign on the two arrows. Only the $\mu = -1$ spin singlet pairing is enhanced near the SDW critical point.

		μ	
		1	-1
ν	1	s	g
	-1	d_{xy}	$d_{x^2-y^2}$

Table 7.1: Symmetry properties of the pairing vertex.

The renormalization properties of the operator V can be determined from its insertion into the correlation function,

$$\epsilon_{\sigma\sigma'} \Gamma_{V\psi^\dagger\psi^\dagger}(k_1, k_{-1}) = \int d^D x_1 d^D x_{-1} \langle V(0) \psi_{1\sigma'}^{\dagger\ell=-1}(x_{-1}) \psi_{1\sigma}^{\dagger\ell=1}(x_1) \rangle_{1PI} e^{i(k_1 x_1 + k_{-1} x_{-1})} \quad (7.88)$$

At tree level, $\Gamma_{V\psi^\dagger\psi^\dagger} = 1$. Let us now consider the one-loop renormalization of V , shown in Fig. 7.20 a). This diagram is given by

$$\delta\Gamma_{V\psi^\dagger\psi^\dagger}(k_1, k_{-1}) = -3\mu \int \frac{d^3 l}{(2\pi)^3} D(l) G_2^1(k_1 - l) G_2^{-1}(k_{-1} + l). \quad (7.89)$$

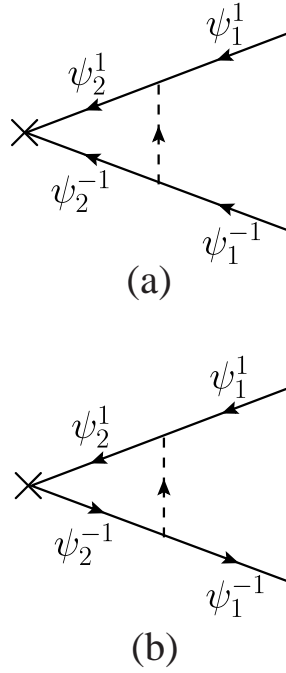


Figure 7.20: The leading corrections to (a) BCS pairing vertex, (b) density-wave vertex.

Details of the evaluation of (7.89) appear in Appendix F.2.3. Direct computation with bare fermion propagators gives rise to strong infra-red divergences, which are cured by using the one-loop dressed propagators. With this approach, we obtain to logarithmic accuracy

$$\delta\Gamma_{V\psi^\dagger\psi^\dagger} = -\frac{\mu\alpha}{\pi(\alpha^2 + 1)} \log^2\left(\frac{\Lambda^2}{\gamma\omega}\right) \quad (7.90)$$

Note that the one loop renormalization of the pairing vertex (7.90) is of order unity, and is not suppressed in $1/N$. Thus the naive counting in powers of $1/N$ is violated, as was already noted in Ref. [227]. Moreover, the one-loop contribution gives a suppression of the vertex for $\mu = 1$ (s and d_{xy} channels) and an enhancement for $\mu = -1$ ($d_{x^2-y^2}$, g channels) as expected. Finally, we find that the one-loop result

has a non-local \log^2 divergence. The origin of this non-local divergence is BCS pairing of the Fermi surface away from the hot spots. Indeed, as noted in Appendix F.2.3, the divergence comes from the regime where $\gamma|l_\tau| \ll l_\parallel^2$, with l_\parallel the component of \vec{l} along the Fermi surface of ψ_2 . This is precisely the regime in which one has good Landau-quasiparticles, suggesting that it may be possible to obtain Eq. (7.90) in a Fermi liquid computation.

We now show this is indeed the case, and obtain (7.90) in a physically transparent form. Let us approximate the propagators in Eq. (7.89) by the Fermi-liquid form Eq. (7.43),

$$\begin{aligned} \delta\Gamma_{V\psi^\dagger\psi^\dagger} &= \frac{3\mu}{N} \int \frac{dl_\parallel}{2\pi} \int_{\gamma|l_\tau| \lesssim l_\parallel^2} \frac{dl_\tau}{2\pi} \int \frac{dl_\perp}{2\pi} \frac{1}{\gamma|l_\tau| + l_\parallel^2} \frac{\mathcal{Z}(l_\parallel)}{i(l_\tau - \omega) - v_F(l_\parallel)l_\perp} \\ &\times \frac{\mathcal{Z}(l_\parallel)}{i(l_\tau + \omega) + v_F(l_\parallel)l_\perp} \end{aligned} \quad (7.91)$$

with the Fermi-liquid parameters given by Eq. (7.47). Note that due to the restriction $\gamma|l_\tau| \ll l_\parallel^2$ the bosonic propagator is static. Changing variables to $\epsilon = v_F(l_\parallel)l_\perp$,

$$\delta\Gamma_{V\psi^\dagger\psi^\dagger} = \frac{3\mu}{N} \int \frac{dl_\parallel}{2\pi} \frac{\mathcal{Z}^2(l_\parallel)}{v_F(l_\parallel)l_\parallel^2} \int_{\gamma|l_\tau| \lesssim l_\parallel^2} \frac{dl_\tau}{2\pi} \int \frac{d\epsilon}{2\pi} \frac{1}{i(l_\tau - \omega) - \epsilon} \frac{1}{i(l_\tau + \omega) + \epsilon} \quad (7.92)$$

The integral over l_τ, ϵ has the form familiar from Fermi-liquid theory and gives the usual BCS logarithm,

$$\int \frac{dl_\tau}{2\pi} \int \frac{d\epsilon}{2\pi} \frac{1}{i(l_\tau - \omega) - \epsilon} \frac{1}{i(l_\tau + \omega) + \epsilon} = -\frac{1}{2\pi} \log \frac{\Lambda_{FL}}{\omega} \quad (7.93)$$

where Λ_{FL} is the frequency/energy cut-off, which in the present case is $\Lambda_{FL} = l_\parallel^2/\gamma$.

Of course, for the above form to hold, we need $\omega \ll \Lambda_{FL}$. Thus,

$$\delta\Gamma_{V\psi^\dagger\psi^\dagger} = -\frac{3\mu}{2\pi^2 N} \int_{\sqrt{\gamma\omega}}^{\infty} dl_\parallel \frac{\mathcal{Z}^2(l_\parallel)}{v_F(l_\parallel)l_\parallel^2} \log \frac{l_\parallel^2}{\gamma\omega} = -\frac{\mu\alpha}{\pi(\alpha^2 + 1)} \log^2 \frac{\Lambda^2}{\gamma\omega} \quad (7.94)$$

which agrees with the result in Eq. (F.60) obtained from a more complete computation. Note that the prefactor of $1/N$ arising from the boson propagator has disappeared from the final result. A similar log-squared term has been noted for the pairing vertex in a theory of a Fermi surface coupled to a gauge field in three dimensions[232, 233] and in a theory of a Fermi surface interacting via a Chern-Simons gauge field and a $1/r$ potential in two dimensions.[206, 207]

The appearance of the log-squared term above indicates a breakdown of the present RG in analyzing the renormalization of the pairing vertex. It is clearly a consequence of two different physical effects. One is the familiar BCS logarithm of Fermi liquid theory, which appears here from the Fermi surface away from the hot spots. The second logarithm is a critical singularity associated with SDW fluctuations at the hot spot. Our RG approach, defined in terms of a cutoff Λ which measures distance from the hot spot, is unable to regulate the first logarithm: the Fermi surface is present at momenta all the way upto Λ .

An alternative RG is necessary to analyze the consequences of the log-squared term. One possible approach is that of Son [232], who worked with an RG defined in terms of momentum shells a fixed distance from the Fermi surface of fermions coupled to a gauge field. We leave such investigations for future work.

7.6 Density vertices

In this section we focus attention on one of the interesting consequences of the pseudospin symmetries of the critical theory of the SDW transition, specified by Eq. (7.6). Note that the pseudospin rotations can be performed independently on

different pairs of hotspots.

Under the operation in Eq. (7.6), the pairing operator (7.85) in the particle-particle channel becomes exactly degenerate with certain operators in the particle-hole channel which connect opposite patches of the Fermi surface. Indeed, consider spin-singlet operators that can be built out of fermions coming from hot spots ℓ and $-\ell$. Using the spinor representation (7.3), we may write these as,

$$V_{\alpha\beta}^{\ell} = M_{ij}\epsilon_{\sigma\sigma'}\Psi_{i\alpha}^{-\ell}\Psi_{j\beta}^{\ell} \quad (7.95)$$

The indices α, β of $V_{\alpha\beta}$ carry spin 1/2 under the independent $SU^{-\ell}(2)$ and $SU^{\ell}(2)$ particle-hole symmetries. Hence, we have a set of four degenerate operators. Choosing $\alpha = 1, \beta = 1$,

$$V_{11}^{\ell} = M_{ij}\epsilon_{\sigma\sigma'}\psi_{i\sigma}^{-\ell}\psi_{j\sigma'}^{\ell} \quad (7.96)$$

The mixing matrix M_{ij} is fixed by lattice symmetries to give operators,

$$V_{\mu}^{\ell, \vec{Q}=(0,0)} = \epsilon_{\sigma\sigma'} (\psi_{1\sigma}^{-\ell}\psi_{1\sigma'}^{\ell} + \mu\psi_{2\sigma}^{-\ell}\psi_{2\sigma'}^{\ell}) \quad (7.97)$$

$$V_{\mu}^{\ell, \vec{Q}=(\pi,\pi)} = \epsilon_{\sigma\sigma'} (\psi_{1\sigma}^{-\ell}\psi_{2\sigma'}^{\ell} + \mu\psi_{2\sigma}^{-\ell}\psi_{1\sigma'}^{\ell}) \quad (7.98)$$

which correspond to superconducting order parameters with momenta $(0, 0)$ and (π, π) respectively. The index $\mu = \pm 1$ determines the parity of the operator under a reflection about a lattice diagonal. The operator (7.97) was considered above. We will not discuss the other operator (7.98) below; due to kinematics, its renormalization at one-loop order contains neither the large- N enhancement, nor the unusual powers of logarithm squared.

Now, let us discuss the particle-hole partners of (7.97). Setting $\alpha = 2, \beta = 2$ in (7.95) simply gives rise to the Hermitian conjugate of (7.97). On the other hand

$\alpha = 2, \beta = 1$ gives the operators,

$$O_\mu^\ell = \psi_{1\sigma}^{-\ell\dagger} \psi_{1\sigma}^\ell + \mu \psi_{2\sigma}^{-\ell\dagger} \psi_{2\sigma}^\ell \quad (7.99)$$

The other choice $\alpha = 1, \beta = 2$ generates the Hermitian conjugates of (7.99). Following Fig. 7.19, the O_μ^ℓ operators are illustrated in Fig. 7.21. To determine the wavevectors

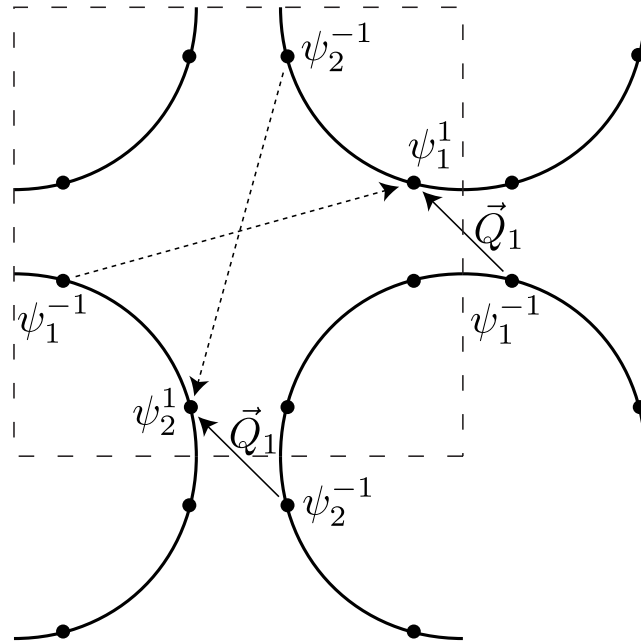


Figure 7.21: Spin singlet density operators ($\sim \psi^\dagger \psi$) of the electrons at the $\ell = \pm 1$ hotspots of Fig. 7.1 (see also Fig. 7.19), shown with an arrow pointing from the Brillouin zone location of ψ^\dagger to that of ψ . The dashed arrows are the density operators in the first Brillouin zone. The full arrows are in an extended zone scheme which shows that these operators have net momentum $\vec{Q}_1 = 2K_y(-1, 1)$, where (K_x, K_y) is the location of the $\ell = 1, i = 1$ hot spot. The density operator with opposite signs ($\mu = -1$) on the two arrows is enhanced near the SDW critical point. Similarly the $\ell = \pm 2$ hot spots contribute density operators at $\vec{Q}_2 = 2K_y(1, 1)$.

of these operators, let the $\ell = 1, i = 1$ hot spot be at $\vec{K}_1 = (K_x, K_y)$. (Note that here we are using the principal axes of the square lattice for the momentum co-ordinates, not the diagonal axes indicated in Fig. 7.1.) Then, from Fig. 7.1 we note that the

$\ell = 1, i = 2$ hot spot is at $(-K_y, -K_x)$, and so the value of the SDW wavevector $\vec{Q} = (\pi, \pi)$ implies that $K_x + K_y = \pi$. Also from Fig. 7.1, the $\ell = -1, i = 1$ hot spot is at $(-K_x, -K_y)$, and so we conclude that the ordering wavevector of the first term in O_μ^1 is $(2K_x, 2K_y)$. Similarly, the ordering wavevector of the second term in O_μ^1 is seen to be $(-2K_y, -2K_x)$. Using $K_x + K_y = \pi$, we observe that these two ordering wavevectors are actually equal, and take the common value $\vec{Q}_1 = 2K_y(-1, 1)$, which is therefore the momentum of the O_μ^1 order parameters, as shown in Fig. 7.19. Similarly, the momentum of the O_μ^2 order parameters is seen to be $\vec{Q}_2 = 2K_y(-1, -1)$. Thus the O_μ^ℓ represent density modulations along the diagonals of the square lattice.

For a clearer physical interpretation of the O_μ^ℓ orders, it is useful to express them in terms of the lattice fermions $c_{\vec{k}\sigma}$, where the momentum \vec{k} ranges over the full square lattice Brillouin zone. Then by looking at the transformations of Eq. (7.99) under all square lattice space group operations, and under time-reversal, we find that the O_+^ℓ are orders are characterized by

$$\left\langle c_{\vec{k}-\vec{Q}_\ell/2,\sigma}^\dagger c_{\vec{k}+\vec{Q}_\ell/2,\sigma} \right\rangle = O_+^\ell f_0(\vec{k}), \quad (7.100)$$

where $f_0(\vec{k})$ is any periodic function on the Brillouin zone that is invariant under the point group operations which leave the wavevector \vec{Q}_ℓ invariant *i.e.* under the little group of \vec{Q}_ℓ . Also time-reversal and inversion symmetries imply $f_0(\vec{k})$ is real and even. The little group consists only of reflections along the diagonals, and so a simple choice is $f_0(\vec{k}) = 1 + c_1 (\cos k_x + \cos k_y) + \dots$, where c_1 is a constant. By taking a Fourier transform of Eq. (7.100), it is clear that O_1^ℓ corresponds to an ordinary charge

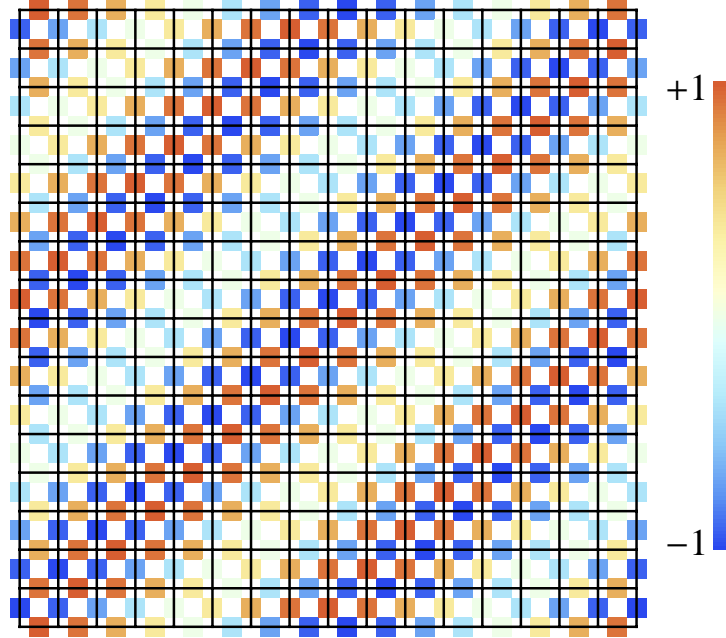


Figure 7.22: (Color online) Plot of the bond density modulations in Eq. (7.104). The lines are the links of the underlying square lattice. Each link contains a colored square representing the value of $\langle c_{\vec{r}\sigma}^\dagger c_{\vec{s}\sigma} \rangle$, where \vec{r} and \vec{s} are the sites at the ends of the link. We chose the ordering wavevector $\vec{Q}_1 = (2\pi/16)(1, -1)$. Notice the local Ising-nematic ordering, and the longer wavelength sinusoidal envelope along the diagonal.

density wave (CDW) on the sites of the square lattice:

$$\langle c_{\vec{r}\sigma}^\dagger c_{\vec{r}\sigma} \rangle = \sum_{\ell=1,2} \left(O_+^\ell e^{i\vec{Q}_\ell \cdot \vec{r}} + \text{c.c.} \right) \quad (7.101)$$

As we saw in Section 7.5, SDW fluctuations suppress pairing with $\mu = +1$, and so its particle-hole partner, the CDW order parameter O_+^ℓ will also be suppressed. We will therefore not consider it further.

By the same reasoning, the order parameter O_-^ℓ should be enhanced by the SDW fluctuations, and so it is of far greater interest. Following the steps leading

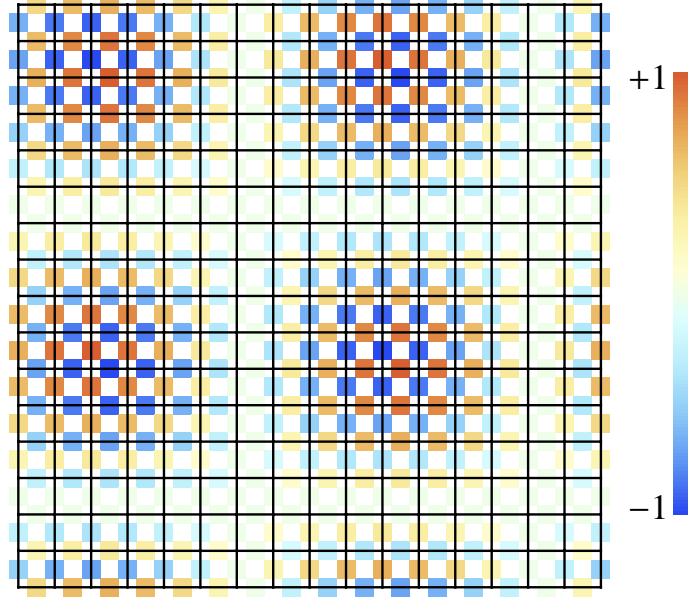


Figure 7.23: (Color online) As in Fig. 7.22, but for orderings along both $\vec{Q}_1 = (2\pi/16)(1, -1)$ and $\vec{Q}_2 = (2\pi/16)(1, 1)$.

to Eq. (7.100), we now find

$$\left\langle c_{\vec{k}-\vec{Q}_\ell/2,\sigma}^\dagger c_{\vec{k}+\vec{Q}_\ell/2,\sigma} \right\rangle = O_-^\ell \tilde{f}_0(\vec{k}) (\cos k_x - \cos k_y), \quad (7.102)$$

where $\tilde{f}_0(\vec{k})$ has the same structure as $f_0(\vec{k})$. Time-reversal symmetry played an important role in constraining the rhs: it is easily verified that Eq. (7.102) is invariant under time-reversal for general complex O_-^ℓ . The order in Eq. (7.102) is odd under reflections along the diagonals, and so it is a $p_{x\pm y}$ -density wave, in the nomenclature of Ref. [234]. Despite the d -wave-like factor on the rhs of Eq. (7.102), this order is not the popular d -density wave [235]; the latter is odd under time-reversal, and in the present notation takes the form

$$\left\langle c_{\vec{k}-\vec{Q}/2,\sigma}^\dagger c_{\vec{k}+\vec{Q}/2,\sigma} \right\rangle \sim i (\sin k_x - \sin k_y), \quad (7.103)$$

with $\vec{Q} = (\pi, \pi)$. The order in Eq. (7.103) is not enhanced near the SDW critical point, while that in Eq. (7.102) is. By taking the Fourier transform of Eq. (7.102), it is easy to see that O_-^ℓ does not lead to any modulations in the site charge density $\langle c_{\vec{r}\sigma}^\dagger c_{\vec{r}\sigma} \rangle$, and so it is not a CDW. The non-zero modulations occur in the off-site correlations $\langle c_{\vec{r}\sigma}^\dagger c_{\vec{s}\sigma} \rangle$ with $\vec{r} \neq \vec{s}$. For \vec{r} and \vec{s} nearest-neighbors, we have

$$\langle c_{\vec{r}\sigma}^\dagger c_{\vec{s}\sigma} \rangle = \sum_{\ell=1,2} \left(O_-^\ell e^{i\vec{Q}_\ell \cdot (\vec{r} + \vec{s})/2} + \text{c.c.} \right) [\delta_{\vec{r}-\vec{s}, \hat{x}} + \delta_{\vec{s}-\vec{r}, \hat{x}} - \delta_{\vec{r}-\vec{s}, \hat{y}} - \delta_{\vec{s}-\vec{r}, \hat{y}}], \quad (7.104)$$

where \hat{x} and \hat{y} are unit vectors corresponding to the sides of the square lattice unit cell. The modulations in the nearest neighbor bond variables $\langle c_{\vec{r}\sigma}^\dagger c_{\vec{r}+\hat{x}, \sigma} \rangle$ and $\langle c_{\vec{r}\sigma}^\dagger c_{\vec{r}+\hat{y}, \sigma} \rangle$ are plotted in Figs. 7.22 and 7.23. These observables measure spin-singlet correlations across a link: if there are 2 electrons on the 2 sites of a link, this observable takes different values depending upon whether the electrons are in a spin singlet or a spin triplet state. Thus O_-^ℓ has the character of a valence bond solid (VBS) order parameter. The first factor on the rhs of Eq. (7.104) shows that the VBS order has modulations at the wavevectors \vec{Q}_ℓ along the square lattice diagonals. However, from our discussion above, note that $|\vec{Q}_\ell| = 2\sqrt{2}K_y$, where the magnitude of K_y is quite small for the Fermi surface in Fig. 7.1: the $\ell = 1, i = 1$ hot spot is at (K_x, K_y) . Thus the first factor in Eq. (7.104) contributes a relatively long-wavelength modulation, as is evident from Figs. 7.22 and 7.23. This long-wavelength modulation serves as an envelope to the oscillations given by the second factor in Eq. (7.104). The latter indicates that the bond order has opposite signs on the x and y directed bonds: this short distance behavior corresponds locally to an *Ising-nematic* order, which is also evident in Figs. 7.22 and 7.23. The ordering in Eq. (7.104) becomes global Ising-nematic order in the limit $\vec{Q}_\ell \rightarrow 0$. Non-linear terms in the effective

action for the bond order will lock in commensurate values of \vec{Q}_ℓ , and so it is possible that strong-coupling effects will prefer $\vec{Q}_\ell = 0$.

As already remarked, the particle-hole symmetry of our theory guarantees a degeneracy between the d -wave superconducting vertex and the density-wave vertex. However, this degeneracy is lifted once effects which break the particle-hole symmetry are introduced. One such effect is the curvature of the Fermi surface at the hot spots. Nominally, the curvature is irrelevant under the scaling towards hot spots (7.16). However, we recall that the double-log structure in Eq. (7.90) originates from an interplay between scaling in a Fermi-liquid and quantum critical scaling. Moreover, we know that the scaling of the superconducting vertex and the density-wave vertex in a Fermi liquid are very different: at one loop the corrections to former are logarithmic, while corrections to latter are suppressed by $\omega^{1/2}$. Thus, one might expect that the Fermi surface curvature will play an important role in the renormalization of the density-wave vertex, reducing its enhancement compared to the BCS vertex and establishing superconductivity as the dominant instability of the SDW critical point. We check this by an explicit calculation below.

We introduce the Fermi-surface curvature into the theory via a perturbation,

$$L_c = \frac{1}{2m} \sum_{\ell,i} |(\nabla \cdot \hat{n}_{\parallel,i}^\ell) \psi_i^\ell|^2 \quad (7.105)$$

where $\hat{n}_{\parallel,i}^\ell = \hat{z} \times \hat{v}_i^\ell$ is the unit tangent to the Fermi surface of ψ_i^ℓ .

Let us define the insertion of the density-wave order parameter O_μ^ℓ into the fermion correlation function,

$$\Gamma_{O\psi\psi^\dagger}(k_1, k_{-1}) \delta_{\sigma\sigma'} = \int d^D x_1 d^D x_{-1} \langle O_\mu^\ell(0) \psi_{1\sigma}^{-\ell}(x_{-1}) \psi_{1\sigma'}^{\dagger\ell}(x_1) \rangle_{1PI} e^{i(k_1 x_1 - k_{-1} x_{-1})} \quad (7.106)$$

At tree level $\Gamma_{O\psi\psi^\dagger}(k_1, k_{-1}) = 1$. The one loop correction to the vertex is given by the diagram in Fig. 7.20b). We perform the calculations with propagators dressed by the one-loop fermion self-energy and by the curvature (7.105). Details are presented in Appendix F.2.4. To leading logarithmic accuracy we obtain,

$$\delta\Gamma_{O\psi\psi^\dagger} = -\frac{\mu\alpha}{3\pi(\alpha^2 + 1)} \log^2 \frac{\Lambda^2}{\gamma\omega} \quad (7.107)$$

which is a factor of 3 smaller than the corresponding expression for the superconducting vertex (7.90).

Finally, we note the resemblance between our results and those obtained by Halboth and Metzner,[179] and Honerkamp et. al,[236] using a functional renormalization group treatment of the Hubbard model. They find dominant instabilities to SDW order and d -wave pairing, along with a sub-dominant enhancement of Ising-nematic order. They assumed their Ising-nematic order was at $\vec{Q}_\ell = 0$, but their results could be limited by the finite resolution of Fermi surface points, and their specific Fermi surface configurations. It would be interesting if higher resolution studies of more generic Fermi surfaces lead to ordering compatible with Eq. (7.102).

7.7 Conclusion

Quantum phase transitions involving symmetry breaking in the presence of a Fermi surface can be associated with the appearance of a condensate of particle-hole pairs of the Fermi surface quasiparticles. Such transitions can be divided into two broad classes: those in which the particle-hole condensate carries net momentum $\vec{Q} \neq 0$, and those in which the particle-hole condensate is at $\vec{Q} = 0$. Both classes were considered

by Hertz in his 1976 paper [5], using a self-consistent RPA approach, formulated in terms of a RG analysis of an effective action for the condensate fluctuations. He argued that for both cases, and for all spatial dimensions $d \geq 2$, the condensate fluctuations were effectively Gaussian, and hence the leading critical behavior could be exactly calculated.

We have re-examined both classes of Fermi surface transitions in this and a previous chapter. While Hertz's conclusions are expected to be largely correct in $d = 3$, they break down [67] in both classes for the physically important case of $d = 2$. The previous chapter proposed and analyzed a critical theory in $d = 2$ for a paradigm of the $\vec{Q} = 0$ case: the onset of Ising-nematic order. This theory involved both the bosonic order parameter and the fermionic quasiparticles as fundamental degrees of freedom, which interact strongly at the quantum critical point. The present chapter has considered a typical case in $d = 2$ with $\vec{Q} \neq 0$, the onset of spin density wave (SDW) order, using a field theory for the bosonic order parameter and the fermions proposed by Abanov and Chubukov [226].

Our analysis for $\vec{Q} \neq 0$ begins by focusing on the vicinity of the “hot spots” on the Fermi surface shown in Fig. 7.1. Zooming in on a single pair of hot spots, and shifting one of the hot spots by a momentum \vec{Q} , we obtain the situation shown in Fig. 7.2, where we can approximate the two Fermi surfaces near the hot spots by two non-collinear straight lines. The two Fermi surfaces are coupled at the hot spot by the SDW order parameter ϕ , and the low energy physics is then described by the field theory in Eq. (7.1). In the phase with SDW order with $\langle \phi \rangle \neq 0$, the Fermi surfaces reconnect into the configuration shown in Fig. 7.3, leading to electron and

hole pockets appearing from the original large Fermi surface in Fig. 7.1.

Our RG analysis of Eq. (7.1) was performed using the $1/N$ expansion, where the fermions are endowed with an additional flavor index which runs over N values. Initially, it seems that the counting of powers of $1/N$ is simple: each boson propagator comes with a factor of $1/N$, and each fermion loop yields a factor N . Using this “naive” counting, all RG flow equations were computed to order $1/N$ in Section 7.3. We found a consistent renormalization of the couplings in the local field theory in Eq. (7.1); the damping parameter γ appearing in the boson propagator was tied to the local couplings via Eq. (7.9), and this relation was maintained under the RG. The flow of the spin-damping rate under RG implies that the dynamical critical exponent z renormalizes away from its RPA value $z = 2$. This is in stark contrast to Hertz theory[5] and previous studies of the present theory.[229] One of the main consequences of the RG flow in Section 7.3 was a logarithmic divergence in the ratio of Fermi velocity components with length scale: this implied that the Fermi surfaces at the quantum critical point took the shape in Fig 7.8. The effective dynamical nesting of the Fermi surfaces at low energies gives rise to a divergence of anomalous dimensions, which may lead to a first order phase transition.

Section 7.4 looked at higher loop effects which showed that the naive counting of powers of $1/N$ was not correct. The enhancements in powers of N arose from infrared singularities appearing when internal fermion lines were restricted to momenta on the Fermi surface, similar to the Fermi surface enhancements discovered by S.-S. Lee for the problem of a Fermi surface coupled to a U(1) gauge field. These enhancements distinguish the present problem from that considered in Refs. [195, 196]:

the Ising-nematic transition in a d -wave superconductor. Formally, the latter problem is described by a field theory similar to that of the present chapter: fermions with linear dispersion coupled via a Yukawa interaction to a scalar field ϕ . Also, in both problems we find a logarithmic divergence of velocity ratios in the infrared at order $1/N$ for the RG flows. However, for the d -wave superconductor, with Dirac fermions whose energy vanishes only at isolated “hot spots”, the $1/N$ expansion was found to be stable at higher loops. In contrast, for the present SDW problem, the fermion hot spots are connected to “cold” Fermi lines, and singularities associated with these lines lead to a breakdown in the naive $1/N$ counting. Because of this breakdown, the nature of the $N \rightarrow \infty$ limit of Eq. (7.1) remains unclear.

Next, we examined the instability of the SDW metal to the onset of superconductivity near the quantum critical point in Section 7.5. We found a strong tendency towards spin-singlet pairing, with pairing amplitude having opposite signs across a pair of hot spots. For the cuprate Fermi surface in Fig. 7.1 this includes $d_{x^2-y^2}$ pairing, while for the pnictide Fermi surfaces this includes s_{+-} pairing. This pairing instability was manifested in a log-squared divergence of the renormalization of the pairing vertex, arising from an interplay of the infrared singularities associated with the Fermi surfaces and the hot spot. This log-squared singularity cannot be resolved by the present RG approach, and other methods are needed to determine its consequences. An important problem for future research is to understand the feedback of the pairing fluctuations on the non-Fermi liquid singularities at the metallic hot spot. Clearly, superconductivity appears near the quantum critical point as $T \rightarrow 0$. The interesting question is the behavior above T_c , involving the interplay between the

metallic quantum criticality and the pairing fluctuations.

In our discussion of the critical theory for the SDW transition in Section 7.2, we noted that the field theory had emergent pseudospin $SU(2)$ symmetries (Eq. (7.6)) containing the particle-hole transformation; note that the pseudospin rotations can be carried out independently on different pairs of hot spots. Given the strong instability towards d -wave pairing near the SDW critical point described in Section 7.5, it is natural to examine the action of the $SU(2)$ pseudospin symmetries on the d -wave pairing order parameter. This was described in Section 7.6, where we found a similar log-squared enhancement of the susceptibility to a modulated valence bond solid (VBS) order parameter illustrated in Figs. 7.22 and 7.23. Notice that at short scales this ordering has an Ising-nematic character: this corresponds to the breaking of a 90 degree rotation symmetry of the square lattice by the values of the bond order parameter in Eq. (7.104). It would be interesting if future work supports a connection between the ordering instability of Section 7.6, and the bond and Ising-nematic ordering observed in experiments [10, 12, 166, 9, 11, 13]. While the present analysis has focused exclusively on the vicinity of the hot spots, it is quite possible that strong coupling physics away from the hot spot could lock in a preference for commensurate values, such as $\vec{Q}_\ell = 0$, in Eq. (7.104), leading to global Ising-nematic order. Also, it would be interesting to study the changes in the VBS ordering for the case of a SDW transition at an incommensurate ordering wavevector, like that found in the hole-doped cuprates.

Finally, we note an interesting possibility for future theoretical work. Given the breakdown of the $1/N$ expansion for the theory in Eq. (7.1) for the SDW critical point

in a two-dimensional metal, other systematic methods of analyzing this field theory are clearly needed. Following Ref. [206, 207], one possibility is to modify the $(\nabla\vec{\phi})^2$ term in Eq. (7.1) to $k^{1+x}\vec{\phi}^2$, where k is the momentum carried by ϕ . Then at the RPA level, we obtain a theory with $z = 1 + x$, and an expansion in small x appears possible.

Chapter 8

Entanglement entropy in the $O(N)$ model

It is generally believed that in spatial dimension $d > 1$ the leading contribution to the entanglement entropy $S = -\text{tr} \rho_A \log \rho_A$ scales as the area of the boundary of subsystem A . The coefficient of this “area law” is non-universal. However, in the neighbourhood of a quantum critical point S is believed to possess subleading universal corrections. In the present work, we study the entanglement entropy in the quantum $O(N)$ model in $1 < d < 3$. We use an expansion in $\epsilon = 3 - d$ to evaluate (i) the universal geometric correction to S for an infinite cylinder divided along a circular boundary; (ii) the universal correction to S due to a finite correlation length. Both corrections are different at the Wilson-Fisher and Gaussian fixed points, and the $\epsilon \rightarrow 0$ limit of the Wilson-Fisher fixed point is distinct from the Gaussian fixed point. In addition, we compute the correlation length correction to the Renyi entropy $S_n = \frac{1}{1-n} \log \text{tr} \rho_A^n$ in ϵ and large- N expansions. For $N \rightarrow \infty$, this correction generally scales as N^2 rather than the naively expected N . Moreover, the Renyi entropy has a phase transition as a function of n for d close to 3.

8.1 Introduction

One of the most fascinating and counterintuitive properties of a quantum system is the entanglement of its many-body wave-function. In recent years, there has been a lot of interest in using entanglement as a theoretical probe of ground state correlations.[237] It is hoped that this viewpoint will be particularly fruitful in studying quantum critical points, which realize some of the most non-classical, entangled states of matter.

A useful measure of entanglement is given by the entanglement entropy S , also known as von-Neumann entropy. To compute S , we divide the system into two parts, A and B , and determine the reduced density matrix $\rho_A = tr_B \rho$, where ρ is the full density matrix of the system. Then, the entanglement entropy,

$$S_A = -tr_A \rho_A \log \rho_A \quad (8.1)$$

If the system is in a pure state, then the entanglement entropy is “mutual”, i.e. $S_A = S_B$.

One may ask how does the entanglement entropy behave near a quantum critical point. This question has been addressed completely for one-dimensional critical points with dynamical critical exponent $z = 1$. Such critical points are described by $1 + 1$ dimensional conformal field theories (CFT’s). In these systems if A is chosen to be a segment of length l and B - its complement in the real line, the entanglement entropy is given by,[238, 6]

$$S = \frac{c}{3} \log l/a \quad (8.2)$$

where a is the short-distance cut-off and the constant c , known as the central charge,

is a fundamental property of the CFT. Moreover, if the system is perturbed away from the critical point, the entanglement entropy becomes,

$$S = \mathcal{A} \frac{c}{6} \log \xi/a \quad (8.3)$$

where ξ is the correlation length and \mathcal{A} is the number of boundary points of the region A . Here it is assumed that A and B are composed of intervals whose length is much larger than ξ .

The study of entanglement entropy at quantum critical points in dimension $d > 1$ has received much less attention. The leading contribution to S is believed to satisfy the “area law”, [239, 240]

$$S = C \frac{\mathcal{A}}{a^{d-1}} \quad (8.4)$$

where \mathcal{A} is the length/area of the boundary between the regions A and B . Physically, the area law implies that the entanglement in $d > 1$ is local to the boundary even at the critical point (for a recent review of the area law see Ref. [241]). The coefficient C entering the area law is sensitive to the short distance cut-off, and is, therefore, non-universal. So, in contrast to the one-dimensional case, the leading term (8.4) in the entanglement entropy in higher dimensions cannot be used to characterize various critical points.

Proceeding, more generally, beyond the leading area law term, at least for Lorentz-invariant theories that we study here it is expected that the entanglement entropy near a critical point has the scaling form, [242, 243, 244, 245, 246]

$$S = g_{d-1}[\mathcal{B}]a^{-(d-1)} + g_{d-2}[\mathcal{B}]a^{-(d-2)} + \dots + g_0[\mathcal{B}] \log(L/a) + S_0(L/\xi) \quad (8.5)$$

Here L is a characteristic finite size in the problem. The coefficients of the ultra-violet

divergent terms, $g_i[\mathcal{B}]$, are integrals of local geometric invariants over the boundary \mathcal{B} between regions A and B and scale as L^i under dilatations. In particular, the first coefficient $g_{d-1}[\mathcal{B}]$ is proportional to the area of the boundary \mathcal{A} . Clearly, the prefactors of extensive terms $g_i[\mathcal{B}]$ with $i \geq 1$ are non-universal, while the coefficient of the logarithmic term $g_0[\mathcal{B}]$ is universal. The finite piece S_0 is a function of the dimensionless ratio L/ξ and encodes geometric and correlation length corrections to the entanglement entropy. It is universal up to additive dilatation invariant geometric contributions from the boundary. If such contributions, $g_0[\mathcal{B}]$ in particular, vanish, S_0 becomes completely universal. There exists some evidence[247, 242, 243] that this, indeed, occurs when the boundary \mathcal{B} is closed and smooth and the spatial dimension $d = 2$. On the other hand, if the dimension $d = 3$ then $g_0[\mathcal{B}]$ is generally non-zero due to the extrinsic curvature of the boundary and S_0 contains additive non-universal contributions.[242, 243, 248] Likewise, $g_0[\mathcal{B}]$ is known to be non-zero even in $d = 2$ when the boundary contains corners/endpoints.[245, 246, 244]

We note that the above considerations have only been verified by explicit field theoretic calculations in free theories. These assertions were also confirmed in strongly coupled supersymmetric gauge theories using the AdS/CFT correspondence.[242, 243] Recently, universal corrections were found for a special class of quantum critical points in $d = 2$ which are described by dimensional reduction to a classical $d = 2$ field theory.[249, 250] However, such critical points are non-generic, and unstable [251, 252] in physical situations to quantum critical points described by interacting field theories in 3 space-time dimensions.

In the present work, we compute the geometric and correlation length corrections

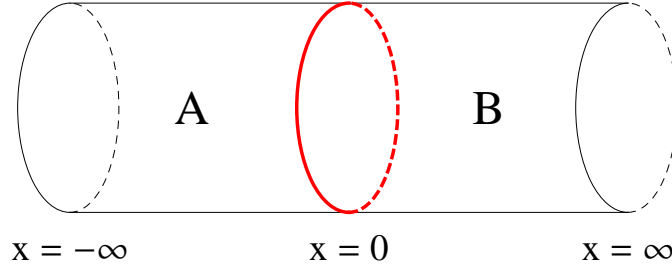


Figure 8.1: The cylindrical geometry considered in calculation of finite size correction to the entanglement entropy.

to the entanglement entropy in the simplest generic interacting CFT in $d = 2$ dimensions - the $O(N)$ model. We verify that these corrections are, indeed, universal. We perform our calculations using expansions in $\epsilon = 3 - d$ and $1/N$.

In the rest of this chapter we consider the following geometry. We take two semi-infinite regions A and B with a straight boundary at $x = 0$. The boundary extends along the remaining $d - 1$ spatial directions, each taken to have a length L . For technical reasons, we impose anti-periodic boundary conditions along each of these directions. We also consider more general boundary conditions with a twist by an arbitrary phase φ in a theory of $N/2$ complex scalar fields. So in the physical case $d = 2$, our space is an infinite cylinder divided into regions A and B along a circle of length L , see Fig. 8.1. For general d , the boundary \mathcal{B} between the regions A and B is a $d - 1$ dimensional torus. As \mathcal{B} is flat, the only geometric invariant on it is the area, $\mathcal{A} = L^{d-1}$. Hence, all the subleading coefficients $g_i[\mathcal{B}]$, $0 \leq i < d - 1$ in eq. (8.5) vanish and S_0 is universal in this geometry. In particular, at the critical point S_0 becomes a universal geometric constant γ and the entanglement entropy is given

by,

$$S = C \frac{L^{d-1}}{a^{d-1}} + \gamma \quad (8.6)$$

We explicitly compute the constant γ . To leading order in ϵ -expansion we obtain,

$$\gamma = -\frac{N\epsilon}{6(N+8)} \left(\log \left| \theta_1 \left(\frac{\varphi(1+i)}{2\pi}, i \right) \right| - \frac{\varphi^2}{4\pi} - \log \eta(i) \right),$$

$d = 3 - \epsilon$, Wilson-Fisher fixed point

(8.7)

Here θ_1 and η are Jacobi elliptic and Dedekind-eta functions and i is the square root of -1 . The sign of γ depends on the value of φ : it is negative for $\varphi = \pi$ (anti-periodic boundary conditions) and positive for $\varphi \rightarrow 0$. Note that eq. (8.7) is only valid for $\varphi \gg \epsilon^{1/2}$. For zero twist (periodic boundary conditions), we hypothesize that to leading order,

$$\gamma = -\frac{N\epsilon}{12(N+8)} \log \epsilon \quad (8.8)$$

The result (8.7) should be compared to the corresponding value at the Gaussian fixed point in $d = 3 - \epsilon$ dimensions,

$$\gamma = -\frac{N}{6} \left(\log \left| \theta_1 \left(\frac{\varphi(1+i)}{2\pi}, i \right) \right| - \frac{\varphi^2}{4\pi} - \log \eta(i) \right), \quad d = 3 - \epsilon, \text{ Gaussian fixed point}$$
(8.9)

We see that $|\gamma|$ is parametrically smaller at the Wilson-Fisher fixed point than at the Gaussian fixed point. Thus, entanglement entropy distinguishes these two fixed points already at leading order in ϵ -expansion.

If we perturb the system by tuning a relevant coupling t slightly away from the critical point $t = t_c$, the entanglement entropy obeys the scaling form,

$$S = C(t) \frac{L^{d-1}}{a^{d-1}} + S_0(L/\xi) \quad (8.10)$$

Here $C(t)$ is a non-universal, analytic function of t , while S_0 is a universal function of the dimensionless ratio L/ξ . In the limit $L/\xi \rightarrow 0$, the system is effectively critical and S_0 reduces to the geometric constant γ of eq. (8.6). In the opposite limit $L/\xi \rightarrow \infty$, the system obeys the area law, hence,

$$S = C(t) \frac{L^{d-1}}{a^{d-1}} + r \frac{L^{d-1}}{\xi^{d-1}} \quad (8.11)$$

where r is a universal coefficient that we compute. Note that both terms in eq. (8.11) contribute to the t dependence of the prefactor in the area law. The contribution of the first term is analytic and so to leading order scales as $t - t_c$. On the other hand, the contribution of the second term is non-analytic and scales as $(t - t_c)^{\nu(d-1)}$, where ν is the correlation length exponent. Since in the $O(N)$ model $\nu < 1$ for $d = 2$, the non-analytic contribution from the universal term dominates.

In general, the coefficient r is tied to the specific choice for the definition of the correlation length ξ . In the $O(N)$ model there is a very natural choice, $\xi = m^{-1}$, where m is the gap to the first excitation. Note that in the present work we only consider the phase of the $O(N)$ model with unbroken symmetry. The value of r to leading order in ϵ -expansion is found to be,

$$r = -\frac{N}{144\pi}, \quad d = 3 - \epsilon, \quad \text{Wilson-Fisher fixed point} \quad (8.12)$$

As with the finite size correction, $|r|$ is parametrically smaller at the Wilson-Fisher fixed point than at the Gaussian fixed point where,[6]

$$r = -\frac{N}{24\pi\epsilon}, \quad d = 3 - \epsilon, \quad \text{Gaussian fixed point} \quad (8.13)$$

We would like to note that the only corrections to the scaling forms in eqs. (8.6), (8.10) come from irrelevant operators and scale as L^{-p} , $p > 0$. Two operators compete

for the role of the leading correction to scaling. The first of these has the usual bulk correction-to-scaling exponent $p = \omega$. The second is an operator living on the boundary \mathcal{B} with $p = 2 - 1/\nu$. Numerically, $2 - 1/\nu < \omega$ for $d = 2$ and $N = 1, 2, 3$, so the corrections from the boundary operator dominate.[49]

In addition to the entanglement entropy, we study the Renyi entropy,

$$S_n = \frac{1}{1-n} \log \text{tr}_A \rho_A^n \quad (8.14)$$

The Renyi entropy always naturally appears in field-theoretic calculations as it is related to the partition function of the theory on an n -sheeted Riemann surface. One then obtains the entanglement entropy by taking the limit, $S = \lim_{n \rightarrow 1} S_n$. At least for n close to 1, the Renyi entropy is believed to possess the same universal properties as the entanglement entropy. In particular, the finite size and correlation length corrections are given by,

$$S_n = C_n \frac{L^{d-1}}{a^{d-1}} + \gamma_n \quad (8.15)$$

$$S_n = C_n(t) \frac{L^{d-1}}{a^{d-1}} + r_n \frac{L^{d-1}}{\xi^{d-1}} \quad (8.16)$$

where the non-universal coefficient C_n of the leading area law term, as well as the universal coefficients γ_n , r_n are now n dependent. We compute r_n in ϵ and large- N expansions. A careful renormalization group analysis demonstrates that r_n is parametrically enhanced in both of these limits. In particular, $r_n \sim O(\frac{1}{\epsilon})$ in the ϵ -expansion. However, the enhancement is most striking in the large- N expansion where we find $r_n \sim O(N^2)$. Such scaling is in contrast with the result $r_n \sim O(N)$ that one would obtain at each order in $1/N$ for fixed correlation length ξ , implying that the limits $\xi \rightarrow \infty$ and $N \rightarrow \infty$ do not commute. As far as we know, this is the

first violation of naive large- N counting in the $O(N)$ model. A common feature of the two expansions is that the leading term of r_n behaves as $r_n \sim n - 1$ for $n \rightarrow 1$ and does not contribute to the entanglement entropy S . Hence, $r \sim O(N)$ in the large N limit and $r \sim O(1)$ in the ϵ -expansion.

Another unusual phenomenon that we find in ϵ -expansion is non-analytic dependence of the coefficients γ_n, r_n on n . In fact, γ_n and r_n will have a discontinuity at $n = n^*$, where n^* is generally non-universal and lies in the range, $1 < n^* \leq 1 + \frac{3}{4} \frac{N+2}{N+8} \epsilon$. The n -dependence of γ_n and r_n for $n < n^*$ and $n > n^*$ is, however, universal. Thus, we have two universal branches for γ_n and r_n . We note that eqs. (8.15) and (8.16) are understood in the limit $L \rightarrow \infty, \xi \rightarrow \infty$. However, there appears a new divergent length-scale in the problem as $n \rightarrow n^*$, and the limits $n \rightarrow n^*$ and $L \rightarrow \infty, \xi \rightarrow \infty$ do not commute. In particular, if we fix the size of our regions L or the correlation length ξ , the n -dependence of the Renyi entropy S_n will be completely analytic. Moreover, due to the emergence of a new length-scale as $n \rightarrow n^*$, in the crossover region S_n is not entirely universal. We stress that any non-analyticity and non-universality only occurs away from the point $n = 1$. In particular, the entanglement entropy $S = \lim_{n \rightarrow 1} S_n$ is well defined and universal.

The non-analytic behaviour discussed above is also found to occur in the large- N expansion in dimensions $2.74 \lesssim d < 3$. The limited range of d suggests that this phenomenon might be absent in the $O(N)$ model in the physically relevant case $d = 2$. Nevertheless, we expect that such non-trivial n dependence will occur quite generically at other quantum critical points.

This chapter is organized as follows. In section 8.2, we remind the reader of the

replica trick, which relates the entanglement entropy to the partition function on an n -sheeted Riemann surface. In section 8.3, we show that the coefficient of the correlation length correction to the Renyi entropy r_n is parametrically enhanced in both expansions we consider. Sections 8.4 and 8.5 are respectively devoted to the evaluation of correlation length and finite size corrections in ϵ -expansion. In section 8.6 we compute the coefficient r_n in the large- N expansion. Some concluding remarks are given in section 8.7.

8.2 The replica trick

We consider the $O(N)$ model in $D = d + 1$ space-time dimensions. The action for the N -component real scalar field ϕ is given by ,

$$S = \int d^d x d\tau \left(\frac{1}{2} (\partial_\mu \phi)^2 + \frac{t}{2} \phi^2 + \frac{u}{4} \phi^4 \right) \quad (8.17)$$

We divide our space into two regions A and B with the boundary being a $d - 1$ dimensional plane at $x = 0$. We will denote the coordinates along the boundary directions by x_\perp . The Renyi entropy S_n may be calculated as,

$$S_n = \frac{1}{1-n} \log \frac{Z_n}{Z_1^n} \quad (8.18)$$

from which we obtain the entanglement entropy,

$$S = \lim_{n \rightarrow 1} S_n \quad (8.19)$$

Here Z_n is the partition function of the theory on an n -sheeted Riemann surface. This Riemann surface lies in the $x_\parallel = (\tau, x)$ plane and has a conical singularity at

$(\tau, \mathbf{x}) = (0, 0)$. The surface is invariant under translations along the x_\perp directions.

We may use the following metric for our space-time,

$$ds^2 = dr^2 + r^2 d\theta^2 + dx_\perp^2 \quad (8.20)$$

where r, θ are the polar coordinates in the (τ, \mathbf{x}) plane. Concentrating on this plane, we see that the metric is exactly the same as for the usual Euclidean plane; the only modification is that the angular variable θ has a period $\theta \sim \theta + 2\pi n$.

8.3 Parametric enhancement of correlation length correction

In this section, we show that the coefficient r_n of the correlation length correction to the Renyi entropy, eq. (8.16), is parametrically enhanced in both expansions that we consider. Moreover, we demonstrate that r_n can to leading order be extracted from the properties of the theory at the critical point.

We start with the $O(N)$ model perturbed away from the critical point $t = t_c$ by a finite $\tilde{t} = t - t_c > 0$ (we drop the tilde below). To compute r_n , we need to find the dependence of the partition function Z_n on the mass gap $m = \xi^{-1}$. Here we assume that the dimensions of the boundary $L \gg \xi$, so that we can take the limit $L \rightarrow \infty$. It is useful to differentiate,

$$\frac{d}{dt} \log \frac{Z_n}{Z_1^n} = -\frac{1}{2} \left(\int_{n\text{-sheets}} d^D x \langle \phi^2(x) \rangle_n - n \int_{1\text{-sheet}} d^D x \langle \phi^2(x) \rangle_1 \right) \quad (8.21)$$

$$= -\frac{1}{2} L^{d-1} \int_{n\text{-sheets}} d^2 x_\parallel (\langle \phi^2(x) \rangle_n - \langle \phi^2(x) \rangle_1) \quad (8.22)$$

where we have used the fact that the contribution to the integral from each of the sheets is the same (from here on, all integrals over d^2x_{\parallel} are understood to be over n -sheets). Now, recalling, $m \sim t^{\nu}$, we may convert the derivative with respect to t into a derivative with respect to m ,

$$m \frac{d}{dm} \log \frac{Z_n}{Z_1^n} = -\frac{1}{2\nu} L^{d-1} \int d^2x_{\parallel} t(\langle \phi^2(x) \rangle_n - \langle \phi^2(x) \rangle_1) \quad (8.23)$$

The expression $t(\langle \phi^2(x) \rangle_n - \langle \phi^2(x) \rangle_1)$ is renormalization group invariant.¹ Thus, we may write,

$$t(\langle \phi^2(x) \rangle_n - \langle \phi^2(x) \rangle_1) = m^D f_n(mr) \quad (8.24)$$

where f_n is a universal function. The function f_n is expected to decay exponentially for $mr \gg 1$, and the integral in (8.23) converges for $r \rightarrow \infty$. The short-distance asymptotic of f_n is controlled by the critical point. From the scaling dimension of the operator $\phi^2(x)$, $[\phi^2(x)] = D - \nu^{-1}$, we conclude,

$$f_n(u) \rightarrow \frac{d_n}{u^{D-1/\nu}}, \quad u \ll 1 \quad (8.25)$$

where d_n is a universal constant. So the integral in (8.23) converges for $r \rightarrow 0$, provided that $\nu^{-1} > D - 2$.² In the $O(N)$ model in both expansions we consider, $\nu^{-1} = D - 2 + \nu_1$, where the correction ν_1 is given to leading order by,

$$\nu_1 = \frac{6\epsilon}{N+8}, \quad D = 4 - \epsilon \quad (8.26)$$

$$\nu_1 = \frac{1}{N} \frac{8\Gamma(D)}{D\Gamma(2-D/2)\Gamma(D/2-1)^2\Gamma(D/2)}, \quad \nu_1(D=3) = \frac{32}{3\pi^2 N}, \quad N \rightarrow \infty \quad (8.27)$$

¹Two subtractions (constant and linear in t), in addition to the multiplicative renormalization, are needed to render the operator ϕ^2 finite. However, these subtractions cancel among the two expectation values in (8.23).

²Otherwise, a UV divergence appears which adds a piece analytic in t to the entanglement entropy, in addition to the singular contributions discussed below.

In particular, $\nu_1 > 0$ and ν^{-1} asymptotically approaches $D - 2$ from above in both limits. With these remarks in mind, we integrate eq. (8.23) with respect to m ,

$$\log \frac{Z_n}{Z_1^n}(t) - \log \frac{Z_n}{Z_1^n}(t=0) = -\frac{\pi n}{\nu(d-1)}(mL)^{d-1} \int_0^\infty du u f_n(u) \quad (8.28)$$

This is as far as we can proceed in general - to make further progress one needs the function $f_n(u)$. However, we have already noted that due to the fact, $\nu^{-1} \rightarrow D - 2$, the integral in (8.28) is very close to diverging in both expansions. Hence, to leading order in ϵ or $1/N$, this integral is saturated at short distances,

$$\int_0^\infty du u f_n(u) \rightarrow \frac{d_n}{\nu^{-1} - (D - 2)} = \frac{d_n}{\nu_1} \quad (8.29)$$

and

$$\log \frac{Z_n}{Z_1^n} \approx -\frac{\pi n}{\nu_1} d_n (mL)^{d-1} \quad (8.30)$$

where we've dropped the constant contribution at the critical point $t = 0$. So, the universal coefficient r_n of the correlation length correction, eq. (8.16), is given by,

$$r_n \approx -\frac{\pi n}{(1-n)\nu_1} d_n \quad (8.31)$$

Thus, to leading order the problem is reduced to evaluating the coefficient d_n in (8.25). Since this coefficient is a short distance property, we may work directly at the critical point. Note in particular that in the large N limit, $d_n \sim O(N)$, so our result for $\log \frac{Z_n}{Z_1^n}$ scales as N^2 . This is in contrast to the linear in N behaviour that one would obtain at any finite order in the $1/N$ expansion for a fixed correlation length ξ .

It turns out that the leading term (8.31) behaves as $r_n \sim (n - 1)$ for $n \rightarrow 1$ in both expansions and does not contribute to the entanglement entropy, eq. (8.19). Thus, the correlation length correction to the entanglement entropy has the expected

scaling $r \sim O(N)$. To proceed systematically beyond the leading order one needs to use renormalization group (RG) technology that will be developed explicitly in the context of ϵ -expansion in section 8.4.3.

8.4 ϵ - expansion: correlation length correction

In this section we compute the correlation length correction to the entanglement entropy in ϵ -expansion. Recall that for the interacting $O(N)$ model, $\nu_1 = \nu^{-1} - (D - 2) \sim O(\epsilon)$ in $D = 4 - \epsilon$ dimensions, hence the argument in section 8.3 can be applied. This is also true for the non-interacting (Gaussian) fixed point for $D = 4 - \epsilon$, where $\nu_1 = \epsilon$, allowing us to compare the predictions of our method to the exact calculations of Ref. [6]. We first consider the Gaussian fixed point and then proceed to the Wilson-Fisher fixed point.

8.4.1 Gaussian theory

Consider the Gaussian theory,

$$L = \frac{1}{2}(\partial_\mu \phi)^2 + \frac{t}{2}\phi^2 \quad (8.32)$$

where, $t = m^2$. We need to compute the expectation value,

$$\langle \phi^2(x) \rangle_n - \langle \phi^2(x) \rangle_1 \quad (8.33)$$

at the critical point, $t = 0$. To leading order we may work in $D = 4$. The massless propagator on an n -sheeted Riemann-surface in $D = 4$ is known to be,[152]

$$G_n(r, r', \theta, x_\perp) = \frac{\sinh(\eta/n)}{8\pi^2 n r r' \sinh \eta (\cosh(\eta/n) - \cos(\theta/n))} \quad (8.34)$$

where

$$\cosh \eta = \frac{r^2 + r'^2 + x_{\perp}^2}{2rr'} \quad (8.35)$$

Hence,

$$\langle \phi^2(x) \rangle_n - \langle \phi^2(x) \rangle_1 = \frac{N}{48\pi^2 r^2} \left(\frac{1}{n^2} - 1 \right) \quad (8.36)$$

So comparing to eqs. (8.24), (8.25), we obtain,

$$d_n = \frac{N}{48\pi^2} \left(\frac{1}{n^2} - 1 \right), \quad \text{Gaussian fixed point, } D = 4 - \epsilon \quad (8.37)$$

We can now use eq. (8.31) to compute the coefficient r_n of the correlation length correction. As noted above for the Gaussian theory, $\nu_1 = \epsilon$, so

$$r_n = -\frac{N}{48\pi\epsilon} \left(1 + \frac{1}{n} \right) \quad (8.38)$$

and for the entanglement entropy proper,

$$r = \lim_{n \rightarrow 1} r_n = -\frac{N}{24\pi\epsilon} \quad (8.39)$$

This can be compared to the exact result of Ref. [6],

$$r_n = N \frac{\Gamma(\frac{2-D}{2})}{24(4\pi)^{(D-2)/2}} \left(1 + \frac{1}{n} \right) \quad (8.40)$$

Eq. (8.40) is in agreement with our result (8.38) to leading order in ϵ , which is all that the discussion in section 8.3 guarantees.

8.4.2 Interacting theory

We now proceed to consider the interacting $O(N)$ model, eq. (8.17). We again need to compute the expectation value (8.33). Naively, one would expect that at leading order in ϵ , one can work with the mean-field approximation, $u = 0$, recovering

the result (8.37). Then, one would simply substitute (8.37) into eq. (8.31) and use the appropriate ν_1 , eq. (8.26), for the Wilson-Fisher fixed point. However, such reasoning turns out to be too simple minded, as it neglects “boundary perturbations.” Indeed, our conical singularity will generally induce local perturbations at $r = 0$. Of these, the term with the lowest engineering dimension is,

$$\delta S = \frac{c}{2} \int d^{D-2} x_{\perp} \phi^2(r = 0, x_{\perp}) \quad (8.41)$$

In the absence of the conical singularity this perturbation is known to be irrelevant in the $O(N)$ model as the scaling dimension $[c] = \nu^{-1} - 2 < 0$. [107] However, as we will now show, the presence of the conical singularity will modify the renormalization group flow of the coefficient c .

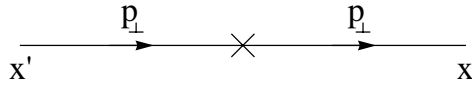


Figure 8.2: Leading correction to the propagator $\delta\mathcal{G}^{1,0}$ due to the boundary perturbation. Here and below, a cross denotes an interaction vertex of c .

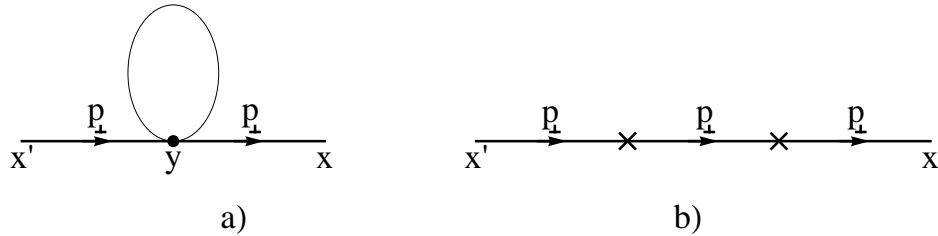
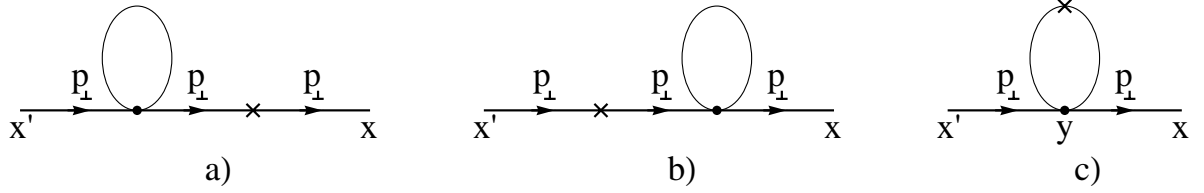


Figure 8.3: Corrections to the propagator, a) $\delta\mathcal{G}^{0,1}$ and b) $\delta\mathcal{G}^{2,0}$. Here and below, a dot denotes an interaction vertex of u .

The engineering dimension of the coupling constant c is zero in any space-time dimension D . We wish to compute the β -function, $\beta(c)$. Let us perform perturbation

Figure 8.4: Corrections to the propagator $\delta\mathcal{G}^{1,1}$.

theory in u and c for the two-point function $\langle\phi_\alpha(x)\phi_\beta(x')\rangle = \delta_{\alpha\beta}\mathcal{G}(x, x')$. It is sufficient to work in $D = 4$ dimensions to compute the leading terms in $\beta(c)$. We use a mixed momentum/position p_\perp, x_\parallel representation. To first order in c and zeroth order in u , we have the simple diagram in Fig. 8.2,

$$\delta^{1,0}\mathcal{G}(x_\parallel, x'_\parallel, p_\perp) = -c G_n(x_\parallel, 0, p_\perp) G_n(0, x'_\parallel, p_\perp) \quad (8.42)$$

where the superscripts on δ indicate the order in c and u . Notice that the bare propagator $G_n(x, x')$, eq. (8.34), remains finite as its arguments approach the conical singularity. In fact,

$$G_n(0, x) = \frac{1}{n} G_1(x) \quad (8.43)$$

Also, $G_n(x_\parallel, x'_\parallel, p_\perp)$ is just the two dimensional massive propagator $(-\nabla_2^2 + p_\perp^2)^{-1}$ on an n -sheeted Riemann surface. In particular, $G_n(x_\parallel, 0, p_\perp) = \frac{1}{n} K_0(p_\perp |x_\parallel|)$ (which implies that the relation (8.43) is actually correct in any dimension). Thus, the correction (8.42) is finite.

We next consider the Hartree-Fock (first order in u) correction to the propagator,

Fig. 8.3 a),

$$\delta^{0,1}\mathcal{G}(x_{\parallel}, x'_{\parallel}, p_{\perp}) = -(N+2)u \int d^2y_{\parallel} G_n(x_{\parallel}, y_{\parallel}, p_{\perp}) G_n(y_{\parallel}, x'_{\parallel}, p_{\perp}) (G_n(y, y) - G_1(y, y)) \quad (8.44)$$

We have already evaluated $G_n(y, y) - G_1(y, y) \sim \frac{1}{y_{\parallel}^2}$, eq. (8.36). Thus, the integral (8.44) has an ultraviolet divergence in the region $y_{\parallel} \rightarrow 0$,

$$\delta^{0,1}\mathcal{G}(x_{\parallel}, x'_{\parallel}, p_{\perp}) \stackrel{UV}{=} \frac{(N+2)u}{24\pi} \left(n - \frac{1}{n} \right) G_n(x_{\parallel}, 0, p_{\perp}) G_n(0, x'_{\parallel}, p_{\perp}) \log(\Lambda) \quad (8.45)$$

Notice that this divergence is local to the conical singularity and, as is evident from eq. (8.42), can be canceled by an additive renormalization of the coupling constant c . Hence, the perturbation (8.41) will be automatically induced by the presence of the conical singularity.

We also consider the second order contribution in c to the propagator, Fig. 8.3 b),

$$\delta^{2,0}\mathcal{G}(x_{\parallel}, x'_{\parallel}, p_{\perp}) = c^2 G_n(x_{\parallel}, 0, p_{\perp}) G_n(0, x'_{\parallel}, p_{\perp}) G_n(0, 0, p_{\perp}) \quad (8.46)$$

The quantity $G_n(0, 0, p_{\perp})$ is UV singular,

$$G_n(0, 0, p_{\perp}) = \int d^2y_{\perp} G_n(0, 0, y_{\perp}) e^{-ip_{\perp}y_{\perp}} = \frac{1}{4\pi^2 n} \int d^2y_{\perp} \frac{1}{y_{\perp}^2} e^{ip_{\perp}y_{\perp}} \stackrel{UV}{=} \frac{1}{2\pi n} \log(\Lambda/p_{\perp}) \quad (8.47)$$

so

$$\delta^{2,0}\mathcal{G}(x_{\parallel}, x'_{\parallel}, p_{\perp}) \stackrel{UV}{=} \frac{c^2}{2\pi n} G_n(x_{\parallel}, 0, p_{\perp}) G_n(0, x'_{\parallel}, p_{\perp}) \log(\Lambda) \quad (8.48)$$

The divergence of (8.48) is a manifestation of the well-known fact that the two-dimensional δ -function potential requires regularization. Again, from (8.42), we observe that the divergence can be eliminated by a renormalization of the coefficient c .

Finally, we consider corrections which are bilinear in c and u , Fig. 8.4. For c - small, these corrections are generally subleading compared to $\delta^{0,1}\mathcal{G}$, Fig. 8.3 a). However, for $n \rightarrow 1$, $\delta^{0,1}\mathcal{G}$ vanishes, and the diagram in Fig. 8.4 c) becomes important. On the other hand, the diagrams in Figs. 8.4 a,b) can be ignored to leading order for all n since they also vanish at $n = 1$.³ With this in mind, we only need to evaluate Fig. 8.4 c) at $n = 1$. We recognize, that this is just the diagram corresponding to the usual multiplicative renormalization of the ϕ^2 operator. Explicitly,

$$\begin{aligned} \delta^{1,1}\mathcal{G}(x_{\parallel}, x'_{\parallel}, p_{\perp}) &\stackrel{n=1}{=} (N+2)uc \int d^2y_{\parallel} G_1(x_{\parallel}, y_{\parallel}, p_{\perp}) G_1(y_{\parallel}, x'_{\parallel}, p_{\perp}) \int d^2z_{\perp} G_1(y_{\parallel}, z_{\perp})^2 \\ &= (N+2)uc \int d^2y_{\parallel} G_1(x_{\parallel}, y_{\parallel}, p_{\perp}) G_1(y_{\parallel}, x'_{\parallel}, p_{\perp}) \frac{1}{16\pi^3 y_{\parallel}^2} \\ &\stackrel{UV}{=} \frac{(N+2)uc}{8\pi^2} G_1(x_{\parallel}, 0, p_{\perp}) G_1(0, x'_{\parallel}, p_{\perp}) \log \Lambda \end{aligned} \quad (8.49)$$

We can now introduce counterterms to cancel the divergences considered above,

$$c = c_r + \left(\frac{(N+2)u_r}{24\pi} \left(n - \frac{1}{n} \right) + \frac{(N+2)u_r c_r}{8\pi^2} + \frac{c_r^2}{2\pi n} \right) \log(\Lambda/\mu) \quad (8.50)$$

where c_r and u_r are the renormalized coupling constants and μ is the renormalization scale. Note that the coefficient of the $u_r c_r$ term has been only computed at $n = 1$. So,

$$\beta(c_r) = \mu \frac{\partial}{\partial \mu} c_r \Big|_{c,u} = \frac{(N+2)u_r}{24\pi} \left(n - \frac{1}{n} \right) + \frac{(N+2)u_r c_r}{8\pi^2} + \frac{c_r^2}{2\pi n} \quad (8.51)$$

Note that the RG flow of u is not affected by the boundary perturbation or by the presence of the conical singularity,

$$\beta(u_r) = -\epsilon u_r + \frac{N+8}{8\pi^2} u_r^2 \quad (8.52)$$

and we have the usual Wilson-Fisher fixed point $u^* = \frac{8\pi^2\epsilon}{N+8}$.

³Technically, these diagrams contain $(\log \Lambda)^2$ divergences, and one needs to use a consistent regularization method to evaluate them.

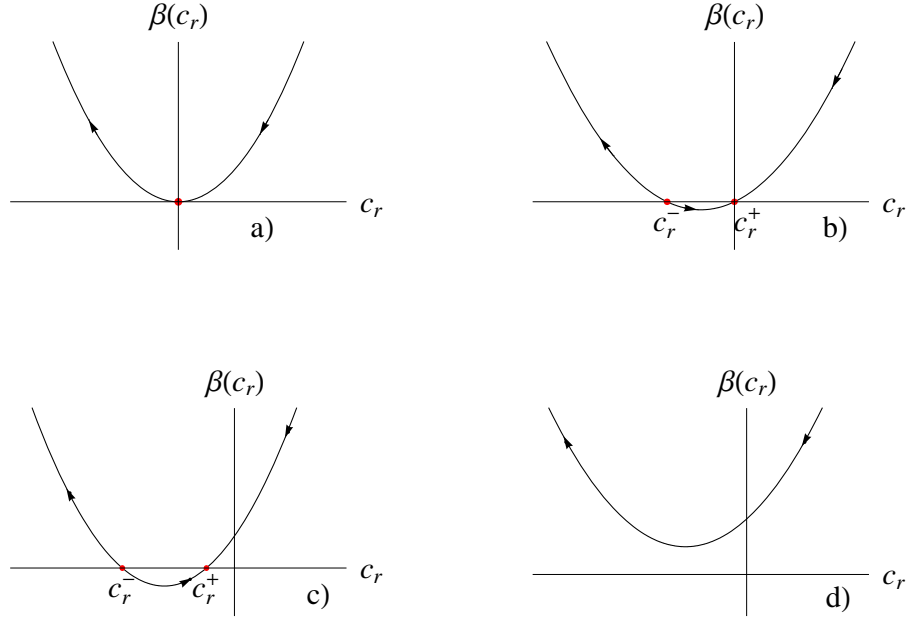


Figure 8.5: β -function of the boundary coupling c_r for a) Non-interacting theory ($u = 0$), b) Interacting theory, $n = 1$, c) Interacting theory, $n < n_c$, d) Interacting theory, $n > n_c$.

We now discuss the RG flow of c_r in detail. Let us start with the non-interacting theory, $u = 0$, which corresponds to the well-studied problem of a particle in a two-dimensional δ -function potential. Then, $\beta(c_r) = \frac{1}{2\pi n} c_r^2$. As demonstrated in Fig. 8.5 a), the coupling constant c_r flows logarithmically to zero for $c_r > 0$ and runs away to $-\infty$ for $c_r < 0$, signaling the formation of a bound state.

Next, consider turning on the interaction u , in the absence of conical singularity ($n = 1$). Then, $\beta(c_r) = -\eta_2(u_r)c_r + \frac{c_r^2}{2\pi}$, where η_2 is just the usual anomalous dimension of the ϕ^2 operator, ($[\phi^2] = D - 2 - \eta_2$),

$$\eta_2(u_r) = -\frac{(N+2)u_r}{8\pi^2} \quad (8.53)$$

The RG flow of c is sketched in Fig. 8.5 b). We find two fixed-points: $c_r^+ = 0$

and $c_r^- = -\frac{N+2}{N+8}(2\pi\epsilon)$. The first fixed point $c_r^+ = 0$ is stable, due to $\beta'(c_r = 0) = -\eta_2(u^*) > 0$, which implies that for c -small, the perturbation (8.41) is irrelevant.[107] This conclusion can be immediately reached by consideration of scaling dimensions at the interacting fixed point, since $[c] = D - 2 - [\phi^2] = \eta_2 < 0$.

The second fixed point c_r^- is unstable, and for $c_r < c_r^-$ the RG flow runs away to $c_r = -\infty$. Naively, such a flow may be interpreted as a tendency of ϕ to condense in the vicinity of $r = 0$. However, this would result in a condensate that is effectively $D - 2 < 2$ dimensional, which, at least for $N \geq 2$ and $t > 0$, is prohibited by the Mermin-Wagner theorem. Exactly at the critical point, long-range forces could, in principle, stabilize the condensate. However, as we will discuss in section 8.6, large- N expansion suggests that no such condensation occurs even at $t = 0$, and the flow actually terminates at a scale invariant fixed-point, which is inaccessible in our perturbative expansion. However, this fixed point can likely be interpreted in terms of a fluctuating “boundary” order parameter.

Finally, we proceed to the interacting case in the presence of a conical singularity. For $n < n_c \approx 1 + \frac{3}{4}\frac{N+2}{N+8}\epsilon$ we again obtain two fixed points, Fig. 8.5 c),

$$c_r^\pm = \pi \left(-\frac{N+2}{N+8}n\epsilon \pm \sqrt{\left(\frac{N+2}{N+8}\right)^2 n^2 \epsilon^2 - \frac{2}{3}\frac{N+2}{N+8}(n^2-1)\epsilon} \right) \quad (8.54)$$

The fixed point c_r^+ is stable, while c_r^- is unstable. In the limit $n \rightarrow 1$, which is relevant for the computation of entanglement entropy, c_r^+ smoothly evolves to the $c_r^+ = 0$ stable fixed point, which we obtained in the absence of the conical singularity. Moreover, for $n \rightarrow 1$, we expect the starting point of the RG flow $c_r \rightarrow 0$. Hence, for n close to 1 the RG flow will terminate at the fixed point c_r^+ . The stability exponent of this fixed point $\beta'(c_r^+) \rightarrow [\phi^2] - (D - 2) = 2 - 1/\nu$ as $n \rightarrow 1$. This boundary

exponent, as well as the usual bulk exponent, $\omega = \beta'(u_r^*)$, will control corrections to scaling for the entanglement entropy S .

Thus, the main effect of the conical singularity is to shift c_r^+ away from 0. The parametric magnitude of this shift depends on whether $1 - n \gg \epsilon$ or $|1 - n| \ll \epsilon$:

$$c_r^+ \approx \pi \sqrt{\frac{2N+2}{3N+8}} (1-n^2)\epsilon, \quad 1-n \gg \epsilon \quad (8.55)$$

$$c_r^+ \approx -\frac{2\pi}{3}(n-1) - \frac{2\pi N+8}{9} \frac{(n-1)^2}{N+2} \frac{1}{\epsilon}, \quad |1-n| \ll \epsilon \quad (8.56)$$

Thus, for $1 - n \gg \epsilon$, $c_r^+ \sim O(\sqrt{\epsilon})$: this is the regime in which the $u_r c_r$ term in the β -function (8.51) can be ignored. On the other hand, for $|n - 1| \ll \epsilon$, $c_r^+ \sim (n - 1) \ll \epsilon$ and the $u_r c_r$ term in $\beta(c_r)$ becomes important. Note that in both regimes, c_r^+ is parametrically small and the perturbative expansion in c_r is justified.

For $n > n_c$, both fixed points disappear and the RG flow runs away to $c_r = -\infty$, Fig. 8.5 d). As discussed above for the case $n = 1$, large N analysis suggest that the flow is towards another fixed point (which itself evolves as a function of n). Now there are two possibilities. If as n increases from 1 to n_c , the initial value of c_r , determined by the microscopic details of the theory, satisfies $c_r(n) > c_r^-(n)$ then the run-off to the $c_r = -\infty$ fixed point will occur precisely at $n = n^* = n_c$. On the other hand, if the initial value of the coupling $c_r(n) < c_r^-(n)$ for $n > n^*$ where $1 < n^* < n_c$, the runaway to $c_r = -\infty$ will occur before n reaches n_c . Note that the value of n^* is generally non-universal. In either case, the long-distance physics is controlled by the c_r^+ fixed point for $n < n^*$ and the $c_r = -\infty$ fixed point for $n > n^*$. Thus, the constants γ_n, r_n , eqs. (8.15), (8.16) will always have a discontinuity at some $n = n^*$, $1 < n^* \leq n_c$. Note that eqs. (8.15), (8.16) are understood in the limit when the size of the regions whose entanglement entropy we are computing and the correlation length ξ tend to infinity.

However, as $n \rightarrow n^*$ a new divergent length scale emerges in the problem. In fact, we can think of the point $n = n^*$, $t = 0$ as a multicritical point. Thus, the limits L , $\xi \rightarrow \infty$ and $n \rightarrow n^*$ do not commute. In particular, if we fix L or ξ , the dependence of the Renyi entropy on n will be completely analytic. Moreover, the emergence of a new length-scale as $n \rightarrow n^*$ implies that the Renyi entropy in the cross-over region is not entirely universal.

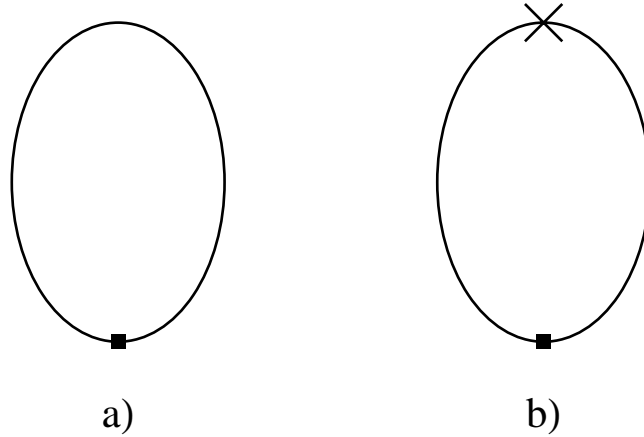


Figure 8.6: Leading contributions to $\langle \phi^2(x) \rangle_n$ (denoted by a black square here and below): a) Mean-field result, b) Correction due to the boundary perturbation.

Having discussed the non-trivial n -dependence of the Renyi entropy that occurs for n away from 1, we come back to the range $n < n_c$ and concentrate on the c_r^+ fixed point. We will from here on denote c_r^+ as c_r^* . Let us now compute the value of $\langle \phi^2(x) \rangle$ at this fixed point. The leading correction to the mean-field result, Fig. 8.6 a), eq. (8.36), is given by the diagram in Fig. 8.6 b),

$$\delta^{1,0} \langle \phi^2(x) \rangle = -Nc_r \int d^{D-2}y_{\perp} G_n^2(x, y) = -\frac{Nc_r}{16\pi^3 n^2} \frac{1}{r^2} \quad (8.57)$$

Since to leading order we still have $t = m^2$, from eqs. (8.24) and (8.25),

$$d_n \approx N \left[\frac{1}{48\pi^2} \left(\frac{1}{n^2} - 1 \right) - \frac{c_r^+}{16\pi^3 n^2} \right] \quad (8.58)$$

and from eqs. (8.26), (8.31), the coefficient of the correlation length correction to the Renyi entropy is,

$$r_n \approx -\frac{\pi n(N+8)}{6\epsilon(1-n)} d_n \quad (8.59)$$

As we see, in the regime $1-n \gg \epsilon$, taking the boundary perturbation into account only weakly modifies the mean-field result for d_n , eq. (8.37), by a term of order $\sqrt{\epsilon}$. Note that r_n is still strongly modified due to a different value of ν_1 .

However, in the regime $|1-n| \ll \epsilon$,

$$d_n \approx \frac{N(N+8)}{(N+2)} \frac{(n-1)^2}{72\pi^2\epsilon}, \quad |1-n| \ll \epsilon \quad (8.60)$$

$$r_n \approx \frac{N(N+8)^2}{N+2} \frac{n-1}{432\pi\epsilon^2}, \quad |1-n| \ll \epsilon \quad (8.61)$$

Thus, for $n \rightarrow 1$, the behavior of d_n at the Wilson-Fisher is drastically different from the mean-field result, eq. (8.37). In particular, notice that to the present order in ϵ , the correction due to the boundary perturbation precisely cancels the term linear in $n-1$ coming from eq. (8.36). The technical reason for this remarkable cancellation is as follows. For $n \rightarrow 1$, we expect $c_r \sim O(n-1)$, and we can work just to first order in c . Then, in considering the corrections to the propagator, we can drop the diagram in Fig. 8.3 b), keeping only Figs. 8.3 a) and 8.4 c). These diagrams are, essentially, Hartree-Fock corrections to the propagator, and the ‘‘Hartree-Fock potential’’ at y is just $\langle \phi^2(y) \rangle_n - \langle \phi^2(y) \rangle_1 \sim 1/y_{\parallel}^2$. As a result, the diagrams diverge for $y_{\parallel} \rightarrow 0$. The β -function for the coupling constant c_r vanishes precisely when this divergence is absent, i.e. $\langle \phi^2(y) \rangle_n - \langle \phi^2(y) \rangle_1 = 0$.

The crucial consequence of eq. (8.60) is that to this order the correction to entanglement entropy proper, $r = \lim_{n \rightarrow 1} r_n = 0$. Thus,

$$r \sim O(1), \quad D = 4 - \epsilon \quad (8.62)$$

We conclude that the correlation length dependent contribution to the entanglement entropy at the Wilson-Fisher fixed point is parametrically smaller than at the Gaussian fixed point in $D = 4 - \epsilon$, eq. (8.39). As a result, we have to proceed to higher order in ϵ to evaluate it. This will be done in the next section.

Before we perform the higher order computation, let us ask how do the correlation functions of the field $\phi(x)$ behave as x approaches the conical singularity. This question is connected to the effective boundary conditions on the field ϕ that are generated at the singularity. In accordance with the general theory of boundary critical phenomena,[138] we expect the field ϕ to satisfy the operator product expansion (OPE),

$$\phi(x_{\parallel}, x_{\perp}) \sim r^{\alpha} \phi(0, x_{\perp}), \quad r \rightarrow 0 \quad (8.63)$$

where $\phi(0, x_{\perp})$ is an operator living on the conical singularity. The exponent α can be extracted from the two-point function $\mathcal{G}(x, x')$. Combining the free propagator with the boundary correction, eq. (8.42),

$$\mathcal{G}(x_{\parallel}, x'_{\parallel}, p_{\perp}) \stackrel{x_{\parallel} \rightarrow 0}{=} \left(1 + \frac{c_r}{2\pi n} \log(p_{\perp} r)\right) G_n(0, x'_{\parallel}, p_{\perp}) \quad (8.64)$$

from which we conclude,

$$\alpha = \frac{c_r^*}{2\pi n} \quad (8.65)$$

Note that from eq. (8.54) the exponent α is positive for $n < 1$, implying effective Dirichlet boundary conditions on $\phi(x)$ at the conical singularity. On the other hand,

α is negative for $1 < n < n_c$ and correlation functions of $\phi(x)$ exhibit a power-law divergence as x_{\parallel} approaches the origin.

8.4.3 Beyond the leading order in ϵ

The inhomogeneous renormalization group equation

At leading order in ϵ , our calculation has relied on the integral in eq. (8.28) being saturated at short distances, $u = mr \rightarrow 0$, allowing us to work directly at the critical point. However, we saw that the coefficient d_n of the short-distance asymptotic of f_n , eq. (8.25), behaved as $d_n \sim (n-1)^2/\epsilon$ for $n \rightarrow 1$, giving no contribution to the entanglement entropy. We expect that to next order in ϵ , d_n will acquire a term linear in $n-1$, $d_n \sim \epsilon(n-1)$, which by eq. (8.30) will give a contribution of $O(1)$ to S . Notice that this is of the same order as the contribution of the long distance, $u \rightarrow \infty$, part of the integral (8.28), which now has to be taken into account. Thus, we need to compute the long distance part of f_n to leading order in ϵ and the short distance part to subleading order. Although the separation between short and long distance contributions is unambiguous to present order, it is convenient to introduce a formalism that allows one to consistently treat the problem order by order in ϵ .⁴

Let us define,

$$\Phi(p) = n \int_{1\text{-sheet}} d^2x_{\parallel} \left(\langle [\phi^2(x)]_r \rangle_n - \langle [\phi^2(x)]_r \rangle_1 \right) e^{-i\vec{p}\vec{x}} \quad (8.66)$$

⁴We note that the discussion below closely parallels the renormalization group technology used to calculate the specific heat in the classical $O(N)$ model.

Here, we have introduced the usual renormalization of the ϕ^2 operator,

$$[\phi^2(x)]_r = \frac{Z_2}{Z} \phi^2(x), \quad t_r = \left(\frac{Z_2}{Z} \right)^{-1} t \quad (8.67)$$

We are considering Φ at a finite momentum p in order to make Φ well-defined even at the critical point, $t = 0$. We are actually interested in computing Φ at $p = 0$ in the gapped phase, $t \neq 0$, as from eq. (8.22),

$$t_r \frac{\partial}{\partial t_r} \log \frac{Z_n}{Z^n} = -\frac{1}{2} t_r \Phi(p=0) L^{D-2} \quad (8.68)$$

As already observed in section 8.3, although the integrand in (8.66) is finite, the integral diverges logarithmically for $|x| \rightarrow 0$ at each order in u . Thus, $\Phi(p)$ requires an additive renormalization,

$$\Phi(p) = \Phi_r(p) + C(u_r, c_r, \mu/\Lambda) \mu^{-\epsilon} \quad (8.69)$$

where C is a renormalization constant. We will use dimensional regularization below, so that C is, in fact, just a function of u_r and c_r . Then Φ_r satisfies the inhomogeneous renormalization group equation,

$$\left(\mu \frac{\partial}{\partial \mu} + \beta(u_r) \frac{\partial}{\partial u_r} + \beta(c_r) \frac{\partial}{\partial c_r} - \eta_2(u_r) \left(1 + t_r \frac{\partial}{\partial t_r} \right) \right) \Phi_r = B(u_r, c_r) \mu^{-\epsilon} \quad (8.70)$$

with

$$B(u_r, c_r) = - \left(\beta(u_r) \frac{\partial}{\partial u_r} + \beta(c_r) \frac{\partial}{\partial c_r} - (\eta_2(u_r) + \epsilon) \right) C(u_r, c_r) \quad (8.71)$$

where as usual,

$$\eta_2(u_r) = \mu \frac{\partial}{\partial \mu} \bigg|_u \log \frac{Z_2}{Z} \quad (8.72)$$

Note that B must be finite, as the left hand side of eq. (8.70) is finite. The solution to (8.70) can be represented as a sum of the solution to the homogeneous RG equation and a particular solution. In the scaling limit, $t_r \rightarrow 0$,

$$\Phi_r(p=0) = A_s \mu^{-\epsilon} \left(\frac{t_r}{\mu^2} \right)^{-(\epsilon+\eta_2)/(2+\eta_2)} + A_{ns}(u_r, c_r) \mu^{-\epsilon} \quad (8.73)$$

where the coefficient of the particular solution A_{ns} satisfies,

$$\left(\beta(u_r) \frac{\partial}{\partial u_r} + \beta(c_r) \frac{\partial}{\partial c_r} - (\eta_2(u_r) + \epsilon) \right) A_{ns}(u_r, c_r) = B(u_r, c_r) \quad (8.74)$$

Hence, at the critical point,

$$A_{ns}(u_r^*, c_r^*) = -\frac{1}{\eta_2 + \epsilon} B_* = -\frac{1}{\nu_1} B_* \quad (8.75)$$

where we recall our definition in section 8.3, $\nu_1 = \nu^{-1} - (D-2)$ and $\nu^{-1} = 2 + \eta_2$.

Thus, from eq. (8.68),

$$\log \frac{Z_n}{Z^n} = -\frac{A_s}{2\nu(D-2)} \left(\mu \left(\frac{t_r}{\mu^2} \right)^\nu \right)^{D-2} L^{D-2} \quad (8.76)$$

where we've dropped terms analytic in t_r . Note that the mass gap m is related to $\mu \left(\frac{t_r}{\mu^2} \right)^\nu$ via a finite proportionality constant, which at leading order in ϵ is just 1. So to leading order,

$$r_n \approx -\frac{A_s}{2(1-n)} \quad (8.77)$$

Hence, we must compute A_s . To do so, we perturbatively calculate $\Phi_r(p=0)$ and $B(u_r, c_r)$. A_s can then be determined by matching the perturbative expansion with the solution to the RG equation (8.73) at the critical point, where the corrections to scaling vanish. Notice that we always need to compute B to one higher order in ϵ than $\Phi_r(p=0)$ due to the factor ν_1 in the denominator of eq. (8.75). Moreover,

since Φ_r is finite for $\epsilon \rightarrow 0$, while $A_{ns} = -B_*/\nu_1$ behaves as $1/\epsilon$, to leading order $A_s = -A_{ns} = B_*/\nu_1$. Precisely this fact was utilized in section 8.3, and we identify to leading order $B_* = 2\pi n d_n$.

Regularization

For the purpose of computing the entanglement entropy S we can work to linear order in $n - 1$. Since the fixed point value $c_* \sim O(n - 1)$, we also work to linear order in c . Therefore, all diagrams that include an insertion of c can be evaluated at $n = 1$. In addition, power counting indicates that if we work to linear order in c , all diagrams will be finite for $D < 4$ (by contrast, higher order diagrams in c , such as Fig. 8.3 b) diverge even for $D < 4$). Thus, we use dimensional regularization and minimal subtraction below. We remind the reader that in dimensional regularization the bare coupling constant $u = \mu^\epsilon u_r Z_u / Z^2$. We list below the renormalization constants in the MS scheme to the order that they will be needed in our calculation.

$$\frac{Z_u}{Z^2} = 1 + \frac{(N+8)}{\epsilon} \frac{u_r}{8\pi^2} \quad (8.78)$$

$$\frac{Z_2}{Z} = 1 + \frac{(N+2)}{\epsilon} \frac{u_r}{8\pi^2} + \frac{(N+2)(N+5)}{\epsilon^2} \left(\frac{u_r}{8\pi^2}\right)^2 - \frac{5(N+2)}{4\epsilon} \left(\frac{u_r}{8\pi^2}\right)^2 \quad (8.79)$$

Correspondingly,

$$\beta(u_r) = -\epsilon u_r + \frac{(N+8)u_r^2}{8\pi^2} \quad (8.80)$$

$$\eta_2(u_r) = -(N+2) \frac{u_r}{8\pi^2} \left(1 - \frac{5}{2} \frac{u_r}{8\pi^2}\right) \quad (8.81)$$

As we saw, the boundary coupling constant c will also require renormalization.

To linear order in c ,

$$c = D(u_r) + \frac{Z_2}{Z} c_r \quad (8.82)$$

where we observe that the multiplicative renormalization of c to zeroth order in $(n-1)$ is just Z_2/Z . On the other hand, the additive renormalization, which behaves as $D(u_r) \sim (n-1)$ for $n \rightarrow 1$, needs to be computed explicitly. So the β -function,

$$\beta(c_r) = - \left(\frac{Z_2}{Z} \right)^{-1} \beta(u_r) \frac{\partial D}{\partial u_r} - \eta_2(u_r) c_r \quad (8.83)$$

Entanglement entropy to $O(1)$

To calculate the entanglement entropy to $O(1)$ in ϵ , we need to find the finite part of $\Phi(p=0)$, eq. (8.66), at $t \neq 0$ to $O(1)$ in u and the divergent part of $\Phi(p)$, which determines B , eq. (8.71), to $O(u)$.

$\Phi(p)$ to $O(1)$ in u is given by the two diagrams in Fig. 8.6. The diagram Fig. 8.6 a) is just the mean field contribution computed in Ref. [6],

$$\begin{aligned} \Phi(p=0)_{MF} &= N \int d^2 x_{\parallel} (G_n(x, x) - G_1(x, x)) \\ &= N \int \frac{d^{D-2} k_{\perp}}{(2\pi)^{D-2}} \int d^2 x_{\parallel} (G_n^{D=2}(x, x; k_{\perp}^2 + m^2) - n \rightarrow 1) \\ &= -\frac{N}{12} \left(n - \frac{1}{n} \right) \int \frac{d^{D-2} k_{\perp}}{(2\pi)^{D-2}} \frac{1}{k_{\perp}^2 + m^2} \\ &= -\frac{N}{12} \left(n - \frac{1}{n} \right) \frac{\Gamma(2 - D/2)}{(4\pi)^{D/2-1}} m^{D-4} \end{aligned} \quad (8.84)$$

where $G_n^{D=2}(x, x'; M^2)$ is the two dimensional massive propagator on the n -sheeted Riemann surface, and we have used the result proved in Ref. [6],

$$\int d^2 x_{\parallel} (G_n^{D=2}(x, x; M^2) - G_1^{D=2}(x, x; M^2)) = -\frac{1}{12} \left(n - \frac{1}{n} \right) \frac{1}{M^2} \quad (8.85)$$

The diagram in Fig. 8.6 b) is the boundary correction,

$$\delta^{1,0} \Phi(p=0) = -N c_r \int d^2 x_{\parallel} \int d^{D-2} y_{\perp} G_1^2(x_{\parallel}, y_{\perp}) = -N c_r \frac{\Gamma(2 - D/2)}{(4\pi)^{D/2}} m^{D-4} \quad (8.86)$$

Combining eqs. (8.84), (8.86),

$$\Phi(p=0) \stackrel{O(1)}{=} -N \left(\frac{n-1}{12\pi} + \frac{c_r}{8\pi^2} \right) \left(\frac{1}{\epsilon} + \frac{1}{2} \log 4\pi - \frac{\gamma}{2} - \log(m/\mu) \right) \mu^{-\epsilon} \quad (8.87)$$

where we keep only terms linear in $n-1$.

Subtracting the pole, we obtain for the additive renormalization constant C , eq. (8.69),

$$C \stackrel{O(1)}{=} -N \left(\frac{n-1}{12\pi} + \frac{c_r}{8\pi^2} \right) \frac{1}{\epsilon} \quad (8.88)$$

and consequently from eq. (8.71),

$$B \stackrel{O(1)}{=} \epsilon C = -N \left(\frac{n-1}{12\pi} + \frac{c_r}{8\pi^2} \right) \quad (8.89)$$

and

$$\Phi_r(p=0) \stackrel{O(1)}{=} -N \left(\frac{n-1}{12\pi} + \frac{c_r}{8\pi^2} \right) \left(\frac{1}{2} \log 4\pi - \frac{\gamma}{2} - \log(m/\mu) \right) \mu^{-\epsilon} \quad (8.90)$$

In particular, at the critical point, by eq. (8.56),

$$c_r^* \stackrel{O(1)}{=} -\frac{2\pi}{3}(n-1) \quad (8.91)$$

and

$$\Phi_r^*(p=0) = O(\epsilon), \quad B_* = O(\epsilon) \quad (8.92)$$

Thus, in the minimal subtraction scheme $\Phi_r^*(p=0)$ vanishes at the critical point to $O(1)$ in ϵ . The fact that $B_* = 2\pi n d_n$ vanishes to $O(1)$ in ϵ has already been observed in section 8.4.2. Thus, from eqs. (8.73), (8.75),

$$A_s \stackrel{O(1)}{=} \frac{B_*}{\nu_1} \quad (8.93)$$

We now proceed to evaluate B to $O(\epsilon)$. To do this, we compute $\Phi(p)$ at the critical point. We first evaluate $\langle [\phi^2]_r \rangle_n - \langle [\phi^2]_r \rangle_1$ and use it to determine the renormalization

of the coupling c in dimensional regularization. We then perform the Fourier transform, eq. (8.66), to find the subtraction constant C and hence B . To leading order, we have the two familiar diagrams in Fig. 8.6,

$$\langle \phi^2(x) \rangle_n - \langle \phi^2(x) \rangle_1 \stackrel{O(1)}{=} N \left[J(D) - c_r \frac{\Gamma(D/2 - 1)^3}{16\pi^{D/2+1}\Gamma(D-2)} \right] \frac{1}{r^{D-2}} \quad (8.94)$$

where we've defined,

$$G_n(x, x) - G_1(x, x) = \frac{J(D)}{r^{D-2}} \quad (8.95)$$

Note that in dimensional regularization $\langle \phi^2 \rangle_1 = NG_1(x, x) = 0$ at the critical point.

We will show in section 8.4.3 that to linear order in $n - 1$,

$$J(D) = (n - 1) \frac{\Gamma(D/2)^3}{4\pi^{D/2}(1 - D/2)\Gamma(D)} \quad (8.96)$$

In particular, $J(D = 4) = -\frac{n-1}{24\pi^2}$ in agreement with eq. (8.36). We note that the diagrams that contain the tadpole (8.95) can effectively be evaluated with $n = 1$.

The computation is simplest in position space, where one uses,

$$G_1(x, x') = \frac{\Gamma(D/2 - 1)}{4\pi^{D/2}|x - x'|^{D-2}} \quad (8.97)$$

At order u , $\langle [\phi^2] \rangle_n - \langle [\phi^2] \rangle_1$ receives contributions from the diagrams in Fig. 8.7.

Note that the diagram c) is the renormalization of the coupling constant $c_0 = c_r + \delta^1 c + \dots$. Taking the multiplicative renormalization of the operator ϕ^2 into account, we obtain,

$$\begin{aligned} \langle [\phi^2]_r \rangle_n - \langle [\phi^2]_r \rangle_1 &\stackrel{O(u)}{=} N \left(\frac{Z_2}{Z} \frac{1}{r^{D-2}} - \frac{\Gamma(D/2 - 1)\Gamma(2 - D/2)^2 (N + 2)u_r \mu^\epsilon}{16\pi^{D/2}(D - 3)\Gamma(4 - D)} \frac{1}{r^{2(D-3)}} \right) \\ &\times \left(J - \frac{\Gamma(D/2 - 1)^3}{16\pi^{D/2+1}\Gamma(D-2)} c_r \right) - N \frac{\Gamma(D/2 - 1)^3}{16\pi^{D/2+1}\Gamma(D-2)} \frac{\delta^1 c}{r^{D-2}} \end{aligned} \quad (8.98)$$

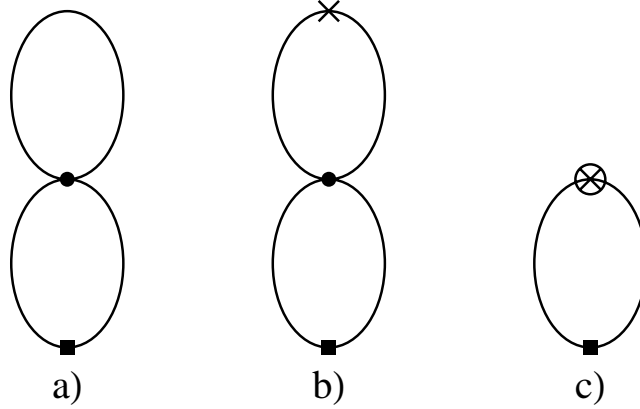


Figure 8.7: Contributions to $\langle \phi^2(x) \rangle_n - \langle \phi^2(x) \rangle_1$ at order u . The counterterm $\delta^1 c$ is denoted by a circled cross here and below.

Performing minimal subtraction,

$$\delta^1 c = \frac{(N+2)u_r}{\epsilon} \left(\frac{n-1}{12\pi} + \frac{c_r}{8\pi^2} \right) \quad (8.99)$$

Notice that the coefficient of the multiplicative renormalization is precisely Z_2/Z as expected. We also obtain the additive renormalization constant, eq. (8.82),

$$D(u_r) = \frac{(N+2)u_r}{\epsilon} \frac{n-1}{12\pi} \quad (8.100)$$

Hence, from eq. (8.83), to first order in u ,

$$\beta(c_r) \stackrel{O(u)}{=} (N+2)u_r \left(\frac{n-1}{12\pi} + \frac{c_r}{8\pi^2} \right) \quad (8.101)$$

in agreement with the expression (8.51) obtained earlier using cut-off regularization.

By Fourier transforming eq. (8.98), we can compute $\Phi(p)$ at the critical point to order u . From the divergent part, we obtain the additive renormalization constant C (8.69),

$$C(u_r, c_r) = -N \left(\frac{1}{\epsilon} + \frac{N+2}{\epsilon^2} \frac{u_r}{8\pi^2} \right) \left(\frac{n-1}{12\pi} + \frac{c_r}{8\pi^2} \right) \quad (8.102)$$

which gives the $O(u)$ correction to our previous result (8.88). Substituting into eq. (8.71), we obtain

$$B \stackrel{O(u)}{=} -N \left(\frac{n-1}{12\pi} + \frac{c_r}{8\pi^2} \right) \quad (8.103)$$

Comparing the above result to eq. (8.89), we observe that B receives no additional contributions at $O(u)$. Thus, from eq. (8.93),

$$A_s \stackrel{O(1)}{=} -\frac{N(N+8)}{6\epsilon} \left(\frac{n-1}{12\pi} + \frac{c_r^*}{8\pi^2} \right) \quad (8.104)$$

which, upon determination of c_r^* to order ϵ would yield the entanglement entropy, eq. (8.77).

$\beta(c_r)$ to order u^2

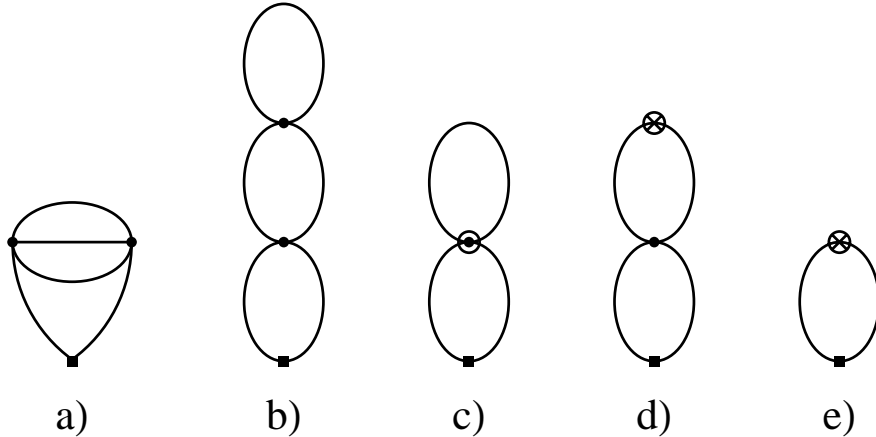


Figure 8.8: Contributions to $\langle \phi^2(x) \rangle_n - \langle \phi^2(x) \rangle_1$ at order u^2 (diagrams involving insertions of c_r are not shown). The counterterm for the coupling u is shown as a circled dot.

To complete our calculation, we need the value of the fixed point coupling c_r^* to order ϵ . This requires the knowledge of $\beta(c_r)$ to order u^2 . As before, we will determine

the renormalization of c by computing the expectation value $\langle[\phi^2]_r\rangle_n - \langle[\phi^2]_r\rangle_1$. As explained in section 8.4.3, we need to find only the additive renormalization of c . Hence, we ignore all diagrams with vertices proportional to c_r . At order u^2 , we obtain the graphs shown in Fig. 8.8.

Now we are faced with a new technical difficulty. Up to this point, to linear order in $n - 1$, the conical singularity entered our calculations through the tadpole term $G_n(x, x) - G_1(x, x)$, whose form was fixed by dimensional analysis, eq. (8.95), up to an overall constant $J(D)$. Moreover, the renormalization constants only depended on $J(D = 4)$, which could be extracted from the explicit form of the propagator, eq. (8.34). However, at the present order, we are faced with the diagram in Fig. 8.8 a), which requires the full position dependence of the propagator $G_n(x, x')$. Yet, as far as we know, there is no simple expression for $G_n(x, x')$ in arbitrary dimension, and even in $D = 4$ eq. (8.34) is rather awkward to work with.

To address this problem, we expand the propagator $G_n(x, x')$ to linear order in $n - 1$ in terms of the usual propagators $G_1(x, x')$, eq. (8.97). The simplest way to do this is to consider the $O(N)$ model in the presence of an arbitrary metric $g_{\mu\nu}$,

$$S = \int d^D x \sqrt{\det g} \left(g^{\mu\nu} \partial_\mu \phi \partial_\nu \phi + \frac{t}{2} \phi^2 + \frac{u}{4} \phi^4 \right) \quad (8.105)$$

It is convenient to parameterize the n -sheeted Riemann surface using rescaled variables,

$$\tilde{r} = \sqrt{nr}, \quad \varphi = \theta/n \quad (8.106)$$

Then, the angular variable $\varphi \sim \varphi + 2\pi$. We may also define,

$$\tilde{\tau} = \tilde{r} \cos \varphi, \quad \tilde{x} = \tilde{r} \sin \varphi \quad (8.107)$$

The coordinates $(\tilde{\tau}, \tilde{x})$ form the usual two dimensional Euclidean plane and uniquely specify each point on the Riemann surface. With this choice of variables, the metric (8.20) in the x_{\parallel} plane becomes,

$$g_{\alpha\beta} = n\delta_{\alpha\beta} + \left(\frac{1}{n} - n\right) \frac{\tilde{x}_{\alpha}\tilde{x}_{\beta}}{\tilde{x}^2} \quad (8.108)$$

where α, β run over $\tilde{\tau}, \tilde{x}$. Note that we have chosen to rescale r in such a way that,

$$\det g = 1 \quad (8.109)$$

Moreover, expanding g in powers of $n - 1$, $g_{\alpha\beta} = \delta_{\alpha\beta} + \delta g_{\alpha\beta}$,

$$\delta g_{\alpha\beta} \approx (n - 1) \left(\delta_{\alpha\beta} - \frac{2\tilde{x}_{\alpha}\tilde{x}_{\beta}}{\tilde{x}^2} \right) \quad (8.110)$$

We drop the tildes on variables τ, x in what follows. We can now obtain the usual Feynman graph expansion for the theory (8.105), treating $\delta g_{\alpha\beta}$ as a perturbation. Note that all the integrals in the resulting expansion are over the usual D -dimensional Euclidean space. In particular, note that the bare propagator becomes,

$$G_n(x, x') \approx G_1(x, x') + \delta G_n(x, x') \quad (8.111)$$

$$\delta G_n(x, x') = (n - 1) \int d^D y \left(\delta_{\alpha\beta} - \frac{2y_{\alpha}y_{\beta}}{y_{\parallel}^2} \right) \partial_{\alpha} G_1(x - y) \partial_{\beta} G_1(x' - y) \quad (8.112)$$

By performing the integral, we immediately obtain eq. (8.96) for $G_n(x, x) - G_1(x, x)$.

Using the expansion (8.112) we compute the divergent part of the diagrams in Fig. 8.8 to linear order in $n - 1$. After accounting for the multiplicative renormalization of the ϕ^2 operator, eq. (8.79), we extract the additive renormalization of the coupling constant c , eq. (8.82) to $O(u^2)$,

$$D(u_r) = \frac{n - 1}{12\pi} \left(\frac{(N + 2)u_r}{\epsilon} + \frac{(N + 2)(N + 5)}{\epsilon^2} \frac{u_r^2}{8\pi^2} - \frac{7(N + 2)}{4\epsilon} \frac{u_r^2}{8\pi^2} \right) \quad (8.113)$$

and from eq. (8.83),

$$\beta(c_r) = (N+2)u_r \left(1 - \frac{7}{2} \frac{u_r}{8\pi^2}\right) \frac{n-1}{12\pi} + (N+2) \frac{u_r}{8\pi^2} \left(1 - \frac{5}{2} \frac{u_r}{8\pi^2}\right) c_r \quad (8.114)$$

Hence,

$$c_r^* = -\frac{2\pi}{3} \left(1 - \frac{u_r^*}{8\pi^2}\right) (n-1) = -\frac{2\pi}{3} \left(1 - \frac{\epsilon}{N+8}\right) (n-1) \quad (8.115)$$

and from eq. (8.104),

$$A_s = -\frac{N}{72\pi} (n-1) \quad (8.116)$$

which by eq. (8.77) finally yields the coefficient of the correlation length correction to the entanglement entropy,

$$r = -\frac{N}{144\pi} \quad (8.117)$$

8.5 ϵ - expansion: finite size correction

In this section we compute the geometric corrections γ , γ_n to the entanglement entropy and the Renyi entropy, eqs. (8.6), (8.15), at the critical point.

As before, we consider two semi-infinite regions A and B with a boundary at $x = 0$. However, we now take the remaining $D - 2$ spatial directions to have a finite length L . In order to avoid dealing with the zero mode, we use twisted boundary conditions along these directions.

$$\phi(x + L\hat{n}_i) = e^{i\varphi_i} \phi(x) \quad (8.118)$$

where \hat{n}_i are unit vectors along the boundary. If the fields ϕ are real, then $\varphi_i = 0$ or π . On the other hand, in an $O(N)$ model with N even, we can group our fields

into $N/2$ complex pairs - then, an arbitrary twist is allowed (however, this breaks the $O(N)$ symmetry down to $U(1) \times SU(N/2)$). We note that when accessing $D = 3$ via ϵ -expansion, we will choose all φ_i 's to be equal.

Thus, the boundary between regions A and B is a $D - 2$ dimensional torus. Since this manifold is smooth we expect the constants γ, γ_n to be universal. Moreover, we don't have to take into account divergences which appear as $D \rightarrow 4$ when the boundary has a finite curvature,[243] since this manifold is flat.

8.5.1 Gaussian theory

Let us begin with the free theory. We wish to compute,

$$\log \frac{Z_n}{Z^n} = -\frac{N}{2} (Tr \log(-\partial^2)_n - n Tr \log(-\partial^2)_1) \quad (8.119)$$

$$= -\frac{N}{2} \sum_{\vec{k}_\perp} \left[Tr_{\parallel} \log(-\partial_{\parallel}^2 + \vec{k}_\perp^2)_n - n Tr_{\parallel} \log(-\partial_{\parallel}^2 + \vec{k}_\perp^2)_1 \right] \quad (8.120)$$

where $k_\perp^i = \frac{2\pi n_i + \varphi_i}{L}$ and n_i are integers. We leave the regularization of eq. (8.120) implicit for now (we will later use dimensional regularization). Eq. (8.120) involves the partition function of the two-dimensional massive gaussian theory evaluated in Ref. [6],

$$\log \frac{Z_n}{Z^n} \Big|_{D=2} = -\frac{1}{2} (Tr_{\parallel} \log(-\partial_{\parallel}^2 + m^2) - n Tr_{\parallel} \log(-\partial_{\parallel}^2 + m^2)_1) = \frac{1}{24} \left(n - \frac{1}{n} \right) \log(m^2) \quad (8.121)$$

Thus,

$$\log \frac{Z_n}{Z^n} = \frac{N}{24} \left(n - \frac{1}{n} \right) \sum_{\vec{k}_\perp} \log(\vec{k}_\perp^2) = -N \frac{\pi}{6} \left(n - \frac{1}{n} \right) L^{D-2} G_1^L(x, x) \quad (8.122)$$

Here, $G_n^L(x, x')$ is the free propagator on an n -sheeted Riemann surface, which incorporates the finite size effects in the transverse direction. Explicitly,

$$G_n^L(x, x') = \frac{1}{L^{D-2}} \sum_{\vec{k}_\perp} G_n^{D=2}(x_\parallel, x'_\parallel; k_\perp^2) e^{i\vec{k}_\perp(\vec{x}_\perp - \vec{x}'_\perp)} \quad (8.123)$$

In particular, for $n = 1$,

$$G_1^L(x, x') = \frac{1}{L^{D-2}} \sum_{\vec{k}_\perp} \int \frac{d^2 k_\parallel}{(2\pi)^2} \frac{1}{k_\parallel^2 + k_\perp^2} e^{ik(x-x')} \quad (8.124)$$

justifying the last step in eq. (8.122).

An alternative representation for the propagator (8.123) on the torus can be obtained by Poisson resumming \vec{k}_\perp , which is equivalent to “periodizing” the infinite volume propagator,

$$G_n^L(x, x') = \sum_{\vec{l}} e^{i\vec{l}\vec{\varphi}} G_n(x + \vec{l}L, x') \quad (8.125)$$

where \vec{l} is a vector of $D - 2$ integers in the plane parallel to the boundary. Note that when $x = x'$, only the $l = 0$ term in eq. (8.125) is ultra-violet divergent and $G_n^L(x, x) - G_n(x, x)$ is finite. Moreover, since the $l = 0$ term, $G_1(x, x) \sim \Lambda^{D-2}$, is L independent, it gives a non-universal contribution to $\log(Z_n/Z^n)$, eq. (8.122), proportional to the area of the boundary. Concentrating on the universal constant term,

$$\log \frac{Z_n}{Z^n} = -N \frac{\pi}{6} \left(n - \frac{1}{n} \right) L^{D-2} (G_1^L(x, x) - G_1(x, x)) \quad (8.126)$$

where from eqs. (8.97), (8.125),

$$L^{D-2} (G_1^L(0) - G_1(0)) = \frac{\Gamma(D/2 - 1)}{4\pi^{D/2}} \sum_{\vec{l} \neq 0} \frac{e^{i\vec{l}\vec{\varphi}}}{|\vec{l}|^{D-2}} \quad (8.127)$$

Here and below we abbreviate $G_1^L(x, x)$ by $G_1^L(0)$.

We can now explicitly evaluate the universal constant contribution γ_n to the entanglement entropy for $D = 3$ and $D = 4$.

$$\gamma_n = -\frac{N}{12} \left(1 + \frac{1}{n}\right) \log(2|\sin \varphi/2|), \quad D = 3 \quad (8.128)$$

$$\gamma = -\frac{N}{6} \log(2|\sin \varphi/2|), \quad D = 3 \quad (8.129)$$

For $D = 4$, we note that the sum

$$\sum_{\vec{l} \neq 0} \frac{e^{i\vec{l}\vec{\varphi}}}{\vec{l}^2} = (2\pi)^2 G^{D=2}(\vec{\varphi}) \quad (8.130)$$

where $G^{D=2}(\vec{\varphi})$ is the massless two-dimensional propagator (with the zero-mode removed) on a torus with side-length 2π . This propagator can be expressed in terms of the Jacobi-theta function θ_1 ,

$$G^{D=2}(\vec{\varphi}) = -\frac{1}{2\pi} \left(\log \left| \theta_1 \left(\frac{\varphi_1 + i\varphi_2}{2\pi}, i \right) \right| - \frac{\varphi_2^2}{4\pi} - \log \eta(i) \right) \quad (8.131)$$

where η is the Dedekind-eta function.

Thus,

$$\gamma_n = \frac{\pi N}{6} \left(1 + \frac{1}{n}\right) G^{D=2}(\vec{\varphi}), \quad D = 4 \quad (8.132)$$

$$\gamma = \frac{\pi N}{3} G^{D=2}(\vec{\varphi}), \quad D = 4 \quad (8.133)$$

8.5.2 ϵ - expansion

We now compute the universal finite size correction to leading order in ϵ -expansion. The leading correction to the free theory behaviour comes from the boundary perturbation (8.41), as at the fixed point $c_r^* \sim \sqrt{\epsilon}$ for $1 - n \gg \epsilon$ and $c_r^* \sim (n - 1)$ for

$|1 - n| \ll \epsilon$. Thus,

$$\begin{aligned} \delta^{1,0} \log \frac{Z_n}{Z^n} &= -\frac{c_r}{2} \int d^{D-2} x_\perp \langle \phi^2(r=0) \rangle_n = -\frac{N c_r}{2} L^{D-2} G_n^L(r=r'=0) \\ &= -\frac{N c_r}{2n} L^{D-2} G_1^L(x, x) \end{aligned} \quad (8.134)$$

where in the last step we've used eqs. (8.43), (8.125). Again, subtracting the non-universal area law piece $\sim L^{D-2} G_1(0)$, and combining eq. (8.134) with the free theory result (8.126),

$$\log \frac{Z_n}{Z^n} = -N \left(\frac{\pi}{6} \left(n - \frac{1}{n} \right) + \frac{c_r}{2n} \right) L^{D-2} (G_1^L(0) - G_1(0)) \quad (8.135)$$

Now replacing c_r by its fixed point value and taking $D \rightarrow 4$,

$$\gamma_n = N \left(\frac{\pi}{6} \left(1 + \frac{1}{n} \right) + \frac{c_r^*}{2n(n-1)} \right) G^{D=2}(\varphi, \varphi) \quad (8.136)$$

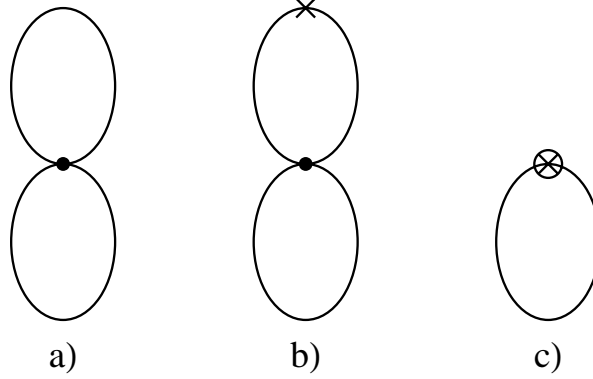
Here we've set all the twists φ_i equal. For $1 - n \gg \epsilon$, eq. (8.55), the c^* term gives a correction of order $\sqrt{\epsilon}$ to the free theory result. However, in the limit $|1 - n| \ll \epsilon$, eq. (8.56), the correction due to the boundary perturbation cancels with the free theory result to leading order in $n - 1$, leaving,

$$\gamma_n \stackrel{n \rightarrow 1}{\approx} -\frac{\pi N(N+8)}{9(N+2)} \frac{n-1}{\epsilon} G^{D=2}(\varphi, \varphi) \quad (8.137)$$

This implies that at the Wilson-Fisher fixed point the universal finite size correction to the entanglement entropy,

$$\gamma \sim O(\epsilon) \quad (8.138)$$

parametrically smaller than at the Gaussian fixed point in $D = 4 - \epsilon$.

Figure 8.9: Contributions to the partition function at order u .

8.5.3 Beyond the leading order in ϵ

We now evaluate the universal finite size correction to the entanglement entropy γ to order ϵ . As before, we only work to leading order in $n - 1$. To order u the partition function receives contributions from the diagrams in Fig. 8.9. The diagram in Fig. 8.9 a) is given by,

$$\begin{aligned}
 \delta^{0,1} \log \frac{Z_n}{Z^n} &= -\frac{N(N+2)u_r\mu^\epsilon}{4} \int d^D x (G_n^L(x, x) - G_1^L(x, x)) \times \\
 &\quad [(G_n^L(x, x) - G_1(x, x)) + (G_1^L(x, x) - G_1(x, x))] \\
 &\stackrel{n \rightarrow 1}{\approx} -\frac{N(N+2)u_r\mu^\epsilon}{2} (G_1^L(0) - G_1(0)) \times \\
 &\quad \sum_{\vec{k}_\perp} \int d^2 x (G_n^{D=2}(x, x; k_\perp^2) - G_1^{D=2}(x, x; k_\perp^2)) \\
 &= \frac{N(N+2)(n-1)u_r\mu^\epsilon}{12} (G_1^L(0) - G_1(0)) \sum_{\vec{k}_\perp} \frac{1}{\vec{k}_\perp^2} \quad (8.139)
 \end{aligned}$$

where in the last step we've used eq. (8.85).

The diagram in Fig. 8.9 b) can be evaluated with $n = 1$ propagators,

$$\begin{aligned} \delta^{1,1} \log \frac{Z_n}{Z^n} &= \frac{N(N+2)u_r c_r \mu^\epsilon}{2} (G_1^L(0) - G_1(0)) \int d^{D-2}x_\perp \int d^D x' G_1^L(x_\perp, x')^2 \\ &= \frac{N(N+2)u_r c_r \mu^\epsilon}{8\pi} (G_1^L(0) - G_1(0)) \sum_{\vec{k}_\perp} \frac{1}{k_\perp^2} \end{aligned} \quad (8.140)$$

Finally, the diagram in Fig. 8.9 c) can be obtained from eq. (8.134) by substituting the counterterm for c , eq. (8.99). Combining all the diagrams in Fig. 8.9 with the $O(1)$ result, eq. (8.135),

$$\begin{aligned} \log \frac{Z_n}{Z^n} &= -\frac{N}{2} \left(\frac{2\pi}{3}(n-1) + c_r \right) L^{D-2} (G_1^L(0) - G_1(0)) \\ &\quad \times \left[1 - \frac{(N+2)u_r}{4\pi} \left((\mu L)^\epsilon \sum_{\vec{k}_\perp} \frac{1}{(Lk_\perp)^2} - \frac{1}{2\pi\epsilon} \right) \right] \end{aligned} \quad (8.141)$$

Applying the usual technique for analytically continuing sums over D -dimensional vectors,

$$\sum_{\vec{k}_\perp} \frac{1}{(Lk_\perp)^2} = \int_0^\infty ds T(s)^{D-2} \quad (8.142)$$

where

$$T(s) = \sum_n e^{-s(2\pi n + \varphi)^2} \quad (8.143)$$

The function $T(s)$ has the following asymptotics,

$$T(s) \rightarrow \frac{1}{\sqrt{4\pi s}}, \quad s \rightarrow 0 \quad (8.144)$$

$$T(s) \rightarrow e^{-s\varphi^2}, \quad s \rightarrow \infty \quad (8.145)$$

Hence, for finite φ the integral in eq. (8.142) converges in the $s \rightarrow \infty$ region. Moreover, the $s \rightarrow 0$ region contributes a pole for $D \rightarrow 4$,

$$\sum_{\vec{k}_\perp} \frac{1}{(Lk_\perp)^2} \rightarrow \frac{1}{2\pi\epsilon} + \text{finite terms} \quad (8.146)$$

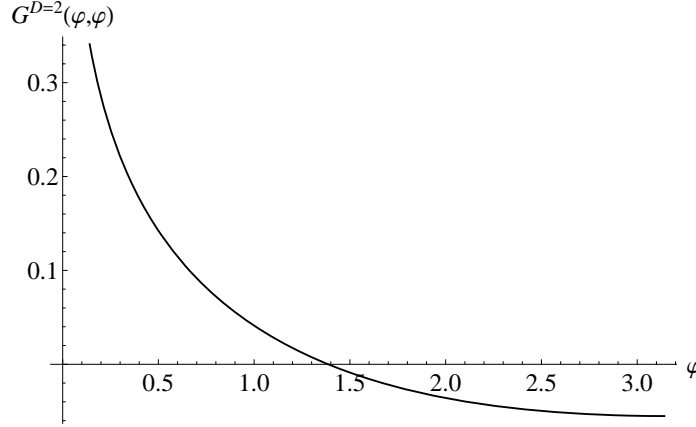


Figure 8.10: The function $G^{D=2}(\varphi, \varphi)$ determining the dependence of γ on the twist φ , eq. (8.148).

As expected, this pole precisely cancels with the c counterterms, so that the expression (8.141) is finite. Moreover, setting c_r to its fixed point value, eq. (8.115), the prefactor in eq. (8.141) is already $O(\epsilon)$, so that we can neglect the $O(u)$ terms in the square brackets. Thus,

$$\log \frac{Z_n}{Z^n} = -\frac{N\pi\epsilon(n-1)}{3(N+8)} L^{D-2} (G_1^L(0) - G_1(0)) \quad (8.147)$$

and

$$\gamma = \frac{N\pi\epsilon}{3(N+8)} G^{D=2}(\varphi, \varphi) \quad (8.148)$$

Note that the result (8.148) is of $O(1)$ in N for $N \rightarrow \infty$, instead of the naively expected $O(N)$. It is not clear if this is an artifact of working to leading order in ϵ .

The function $G^{D=2}(\varphi, \varphi)$ which determines the φ dependence of γ is shown in Fig. 8.10. We observe that γ is a monotonically decreasing function of φ for $0 < \varphi < \pi$.

In particular, for $\varphi = \pi$,

$$\gamma = -\frac{N\epsilon}{12(N+8)} \log 2 \quad (8.149)$$

Thus, γ is negative for anti-periodic boundary conditions. On the other hand, for $\varphi \rightarrow 0$,

$$\gamma \approx -\frac{N\epsilon}{6(N+8)} \log \varphi, \quad \varphi \rightarrow 0 \quad (8.150)$$

suggesting that γ is positive for periodic boundary conditions. Note that our expression for γ becomes invalid for φ sufficiently small. The value of φ where the breakdown of direct perturbative expansion occurs can be estimated as follows. Let us separate out the quasi-zero mode ϕ_0 of the field ϕ ,

$$\phi(x) = \frac{1}{L^{(D-2)/2}} \phi_0(x_{\parallel}) e^{i\vec{\varphi} \cdot \vec{x}_{\perp}/L} + \tilde{\phi}(x) \quad (8.151)$$

where $\tilde{\phi}(x)$ has the $\vec{k}_{\perp} = \frac{\vec{\varphi}}{L}$ mode omitted. At the mean-field level, the effective action for ϕ_0 is a two dimensional ϕ^4 field theory, with an effective mass $m_{2D}^2 \sim \frac{\varphi^2}{L^2}$ and quartic coupling $u_{2D} \sim \frac{u}{L^{D-2}}$. We know that perturbative expansion in a $2D$ theory is valid for $u_{2D}/m_{2D}^2 \ll 1$. Thus, setting $D = 4$ and $u = u^*$, we obtain,

$$\varphi^2 \gg \epsilon \quad (8.152)$$

as the domain of validity of perturbation theory. For smaller values of φ , the zero mode must be treated separately and non-perturbatively. This result can be checked in the $1/N$ expansion where one obtains a slightly stronger condition $\varphi^2 \gg \epsilon \log \varphi$. Cutting off the logarithmic divergence of (8.150) at the value of φ where perturbation theory breaks down, we obtain,

$$\gamma \approx -\frac{N\epsilon}{12(N+8)} \log \epsilon \quad (8.153)$$

We conjecture that eq. (8.153) is the leading order result for the case of zero twist (periodic boundary conditions).

8.6 Large N limit

In this section we compute the correlation length correction to the Renyi entropy S_n , eq. (8.16), in the large N limit. Although we are mainly interested in the physical case $D = 3$, we will keep the dimension of space-time arbitrary in our discussion in order to compare the results of the large- N and ϵ -expansions.

When working in the large- N limit, it is more convenient to use the non-linear σ -model version of the $O(N)$ model (8.17), where the quartic interaction is replaced by a local constraint $\phi^2(x) = \frac{1}{g}$. Enforcing this constraint with the help of the Lagrange multiplier $\lambda(x)$, the action takes the form,

$$S = \int d^D x \left(\frac{1}{2} (\partial_\mu \phi)^2 + \frac{1}{2} i\lambda (\phi^2 - \frac{1}{g}) \right) \quad (8.154)$$

Our discussion in section 8.3 is then directly transcribed into the present case with the replacement, $t \rightarrow -(\frac{1}{g} - \frac{1}{g_c})$, $\phi^2 \rightarrow i\lambda$. In particular, to determine the coefficient r_n of the correlation length correction to leading order in $1/N$, we need to find the behaviour of $\langle i\lambda(x) \rangle$ at the critical point.

We tune the $O(N)$ model to criticality $g = g_c$. At $N = \infty$, the problem is reduced to finding the saddle-point value of the Lagrange multiplier $\langle i\lambda(x) \rangle_n$ such that the gap equation,

$$G_n(x, x) = \frac{1}{N} \langle \phi^2(x) \rangle_n = \frac{1}{Ng_c} \quad (8.155)$$

is satisfied. Here $G_n(x, x')$ is the Green's function of the operator $-\partial^2 + \langle i\lambda(x) \rangle_n$

on the n -sheeted Riemann surface. The quantity $G_n(x, x)$ requires regularization; we will implicitly use point splitting regularization. It is convenient to rewrite the gap equation as,

$$G_n(x, x) - G_1(x, x) = 0 \quad (8.156)$$

We note that at $N = \infty$ the scaling dimension of $\lambda(x)$ is 2, so,

$$\langle i\lambda(x) \rangle_n = \frac{a_n}{r^2} \quad (8.157)$$

From (8.24), with the appropriate replacement $\phi^2 \rightarrow i\lambda$, $t \rightarrow g_c^{-1} - g^{-1}$, the constant a_n is related to the constant d_n (8.25) as

$$d_n = \frac{1}{m^{D-2}} \left(\frac{1}{g_c} - \frac{1}{g} \right) a_n \quad (8.158)$$

Now from the gap equation at finite m ,

$$\frac{1}{Ng} - \frac{1}{Ng_c} = \int \frac{d^D p}{(2\pi)^D} \left(\frac{1}{p^2 + m^2} - \frac{1}{p^2} \right) = \frac{1}{(4\pi)^{D/2}} \Gamma(1 - D/2) m^{D-2} \quad (8.159)$$

and

$$d_n = -\frac{N}{(4\pi)^{D/2}} \Gamma(1 - D/2) a_n \quad (8.160)$$

In particular in $D = 3$, $d_n = \frac{N}{4\pi} a_n$. Thus, the problem of computing the entanglement entropy at $N = \infty$ reduces to finding the constants a_n .

We now need to find the Green's function G_n . The main observation is that the angular harmonics on an n -sheeted Riemann surface are $\frac{1}{\sqrt{2\pi n}} e^{il\theta/n}$, where l is an integer. Hence,

$$G_n(x, x') = \int \frac{d^{D-2} k_\perp}{(2\pi)^{D-2}} e^{ik_\perp(x_\perp - x'_\perp)} G_n^{D=2}(r, r', \theta; k_\perp^2) \quad (8.161)$$

where the two-dimensional massive propagator on an n -sheeted Riemann surface is given by,

$$G_n^{D=2}(r, r', \theta; m^2) = \sum_l \frac{e^{il(\theta-\theta')/n}}{2\pi n} g_l(r, r'; m^2) \quad (8.162)$$

Here,

$$\left(-\frac{1}{r} \frac{\partial}{\partial r} \left(r \frac{\partial}{\partial r} \right) + \frac{(l/n)^2 + a_n}{r^2} + m^2 \right) g_l(r, r'; m^2) = \frac{1}{r} \delta(r - r') \quad (8.163)$$

We use spectral decomposition for g_l ,

$$g_l(r, r'; m^2) = \int dE \frac{1}{E + m^2} \phi_{l,E}(r) \phi_{l,E}^*(r') \quad (8.164)$$

where

$$\left(-\frac{1}{r} \frac{\partial}{\partial r} \left(r \frac{\partial}{\partial r} \right) + \frac{(l/n)^2 + a_n}{r^2} \right) \phi_{l,E} = E \phi_{l,E} \quad (8.165)$$

and $\phi_{l,E}$ are normalized to

$$\int dr r \phi_{l,E}^*(r) \phi_{l,E'}(r) = \delta(E - E') \quad (8.166)$$

The constant a_n must be positive in order to avoid the presence of negative energy states, which would render our saddle point unstable. Let us call the quantity $l^2/n^2 + a_n = \nu^2$. Eq. (8.165) admits two linearly independent solutions,

$$\phi(r) = \frac{1}{\sqrt{2}} J_{|\nu|}(\sqrt{E}r) \quad (8.167)$$

$$\phi(r) = \frac{1}{\sqrt{2}} J_{-|\nu|}(\sqrt{E}r) \quad (8.168)$$

We recall that

$$J_\nu(x) \sim |x|^\nu, \quad x \rightarrow 0 \quad (8.169)$$

When working in free space (in the absence of conical singularity and potential (8.157)) one chooses only the solutions with a positive index $|\nu| = |l|$, so that $\phi_E(r)$

is finite and differentiable at $r = 0$. However, in the present problem there is no *a priori* physical reason why the solutions (and hence the propagator) have to remain finite as $r \rightarrow 0$.

In fact, a particle in a $1/r^2$ potential is a famous problem known as conformal quantum mechanics. Note that the potential (8.157) is highly singular and requires regularization at short distances. Such regularization will automatically appear in the linear $O(N)$ model, which can be obtained from (8.154) by adding a term $\lambda^2/4u$ to the Lagrangian. In that case, eq. (8.157) only holds for $ur^{4-D} \gg 1$ and the saddle point value $\langle i\lambda \rangle$ is modified at short distances. We note that even after this regularization, the $l \neq 0$ states still experience an l^2/r^2 centrifugal barrier and we must choose positive index solutions (8.167) for them. We now concentrate on the $l = 0$ sector. For simplicity, imagine cutting the $1/r^2$ divergence off at some radius $r = r_0$ and replacing it by a finite potential. Generally, the resulting scattering states will approach the positive index solutions (8.167) for $\sqrt{E}r_0 \rightarrow 0$. However, non-trivial behaviour can occur if the potential is close to developing a bound state. In that case, for $|\nu| < 1$, one “dynamically” generates a length-scale ξ and the scattering solutions become linear combinations of (8.167) and (8.168) with coefficients (and, thus, the phase-shifts) depending on $\sqrt{E}\xi$. Since we are looking for a scale invariant solution to the gap equation, we need $\xi \rightarrow \infty$, i.e. the system is exactly at the threshold of bound state formation. At this threshold, for $\sqrt{E}r_0 \rightarrow 0$ one obtains negative index solutions (8.168). Note, that this behaviour is special to the range $|\nu| < 1$ and does not occur for $|\nu| > 1$. This fact could be anticipated as the negative index solutions are square integrable at short distances for $|\nu| < 1$ but not for $|\nu| > 1$.

Thus, applying RG terminology to the simple quantum mechanics problem (8.165), we conclude that there are two fixed points - one stable (8.167) and one unstable (8.168). However, we are allowed to choose the unstable fixed point solutions as we are fine tuning both the long and short distance parts of $\langle i\lambda \rangle$ to solve the gap equation.

With these remarks in mind,

$$g_l(r, r'; m^2) = \int_0^\infty k dk \frac{1}{k^2 + m^2} J_{\nu_l}(kr) J_{\nu_l}(kr') \quad (8.170)$$

where $\nu_l = \alpha$ for $l = 0$ and $\nu_l = \sqrt{l^2/n^2 + \alpha^2}$ for $|l| > 0$, with $a_n = \alpha^2$. The constant α can be either positive or negative. We note that as discussed in Ref [165], α enters the operator product expansion of the field $\phi(x)$ as x approaches the conical singularity,

$$\phi(x_{\parallel}, x_{\perp}) \sim r^\alpha \phi(0, x_{\perp}), \quad r \rightarrow 0 \quad (8.171)$$

Combining eqs. (8.161),(8.162) and (8.170), and performing the integrals over k_{\perp} , k we obtain

$$G_n(r = r', \theta, x_{\perp} = x'_{\perp}) = \frac{\Gamma((3-D)/2)}{2\pi n(4\pi)^{(D-1)/2} r^{D-2}} \sum_l \frac{\Gamma(D/2 - 1 + \nu_l)}{\Gamma(2 - D/2 + \nu_l)} e^{il\theta/n} \quad (8.172)$$

Since we are mostly interested in $G_n(x = x')$, we have set $r = r'$, $x_{\perp} = x'_{\perp}$ in (8.172); we have left $\theta \neq 0$ as a regulator.

As an aside that will be of some interest later, we note that (8.172) is meaningful only for $\alpha > -(D/2 - 1)$. For $\alpha \leq -(D/2 - 1)$ one obtains an infrared divergence in the $k_{\perp}, k \rightarrow 0$ region of integrals (8.161),(8.170). We note that at $\alpha = -(D/2 - 1)$, eq. (8.165) has a zero energy solution,

$$\phi(r) = \frac{1}{r^{D/2-1}} \quad (8.173)$$

The solution (8.173) could, in principle, correspond to a saddle point with a non-zero expectation value $\langle \phi(x) \rangle$. Note that the r dependence of (8.173) is consistent with the scaling dimension $[\phi(x)] = D/2 - 1$ in the $N \rightarrow \infty$ limit. Alternatively, observe that the scaling dimension of the “boundary” operator, $[\phi(0, x_\perp)] = D/2 - 1 + \alpha \rightarrow 0$ as $\alpha \rightarrow -(D/2 - 1)$, indicating a tendency to condense. However, the infrared divergence of the propagator (8.172) indicates that condensation of $\phi(x)$ at the conical singularity is unstable to fluctuations. This is not unexpected, as the condensate would be $D - 2 < 2$ dimensional. Such a condensate certainly cannot exist for any $g > g_c$, as it would violate the Mermin-Wagner theorem. Long range interactions could potentially stabilize the condensate exactly at the critical point, however, the above discussion shows that this does not occur (at least in the large- N limit).

We use contour integration to write (8.172) in a somewhat more convenient form,

$$\begin{aligned}
 G_n(r = r', \theta, x_\perp = x'_\perp) &= \frac{1}{4\pi^{D/2}\Gamma(2 - D/2)r^{D-2}} \left(\int_0^\infty d\nu \frac{\nu}{\sqrt{\nu^2 + \alpha^2}} U_{\sqrt{\nu^2 + \alpha^2}}(\theta) R(\nu) + \theta(-\alpha) \frac{iR(i\alpha)}{n} \right) \\
 & \tag{8.174}
 \end{aligned}$$

with

$$U_\nu(\theta) = \frac{\cosh(\nu(\pi n - |\theta|))}{\sinh(\pi n \nu)} \tag{8.175}$$

$$R(\nu) = -i\Gamma(3 - D) \left[\frac{\Gamma(-i\nu + D/2 - 1)}{\Gamma(-i\nu + 2 - D/2)} - \frac{\Gamma(i\nu + D/2 - 1)}{\Gamma(i\nu + 2 - D/2)} \right] \tag{8.176}$$

$$= \frac{2\pi\Gamma(3 - D) \sin(\pi(3 - D)/2) \sinh(\pi\nu)}{\cosh^2 \pi\nu - \sin^2(\pi(3 - D)/2)} \frac{1}{|\Gamma(i\nu + 2 - D/2)|^2} \tag{8.177}$$

In particular, for $D = 3$, $R(\nu) = \pi \tanh(\pi\nu)$. We note that despite the presence of the $\theta(-\alpha)$ term in eq. (8.174), $G_n(r = r', \theta, x_\perp = x'_\perp)$ is analytic at $\alpha = 0$ as is evident

from eq. (8.172). Thus, the gap equation (8.156) takes the form,

$$\begin{aligned} & (G_n - G_1)|_{x=x'} \\ &= \frac{1}{4\pi^{D/2}\Gamma(2 - D/2)r^{D-2}} \left[\int_0^\infty d\nu \left(\frac{\nu}{\sqrt{\nu^2 + \alpha^2}} \coth(\pi n \sqrt{\nu^2 + \alpha^2}) - \coth(\pi \nu) \right) R(\nu) \right. \\ & \quad \left. + \theta(-\alpha) \frac{i}{n} R(i\alpha) \right] = 0 \end{aligned} \quad (8.178)$$

The function $R(\nu)$ is positive for real values of ν . So the left-handside of the gap equation goes to $-\infty$ as $\alpha \rightarrow \infty$ and to ∞ as $\alpha \rightarrow -(D/2 - 1)^+$. Hence, the gap equation always has at least one solution, and more generally, an odd number of solutions. Numerically, we find that the gap equation has a unique solution for all n for $D < D_c$, $D_c \approx 3.74$. For $D > D_c$, there are one or three solutions depending on the value of n , as we will discuss below.

As we are mainly interested in the entanglement entropy, let us consider the limit $n \rightarrow 1$. Then we expect $\alpha \rightarrow 0$. The integral in (8.178) is non-analytic at $\alpha = 0$, due to singular behaviour in the $\nu \rightarrow 0$ region. Noting that $R(\nu) \approx R'(0)\nu$, as $\nu \rightarrow 0$, we obtain to leading order in α ,

$$\begin{aligned} & (G_n - G_1)|_{x=x'} - (G_n - G_1)|_{x=x', \alpha=0} \\ & \approx \frac{R'(0)}{4n\pi^{D/2}\Gamma(2 - D/2)r^{D-2}} \left(\frac{1}{\pi} \int_0^\infty d\nu \left(\frac{\nu^2}{\nu^2 + \alpha^2} - 1 \right) - \theta(-\alpha)\alpha \right) \\ & = \frac{R'(0)}{4n\pi^{D/2}\Gamma(2 - D/2)r^{D-2}} \left(-\frac{1}{2}|\alpha| - \theta(-\alpha)\alpha \right) = -\frac{\Gamma(D/2 - 1)^2\Gamma(D/2)}{4\pi^{D/2}\Gamma(D - 1)r^{D-2}} \frac{\alpha}{n} \end{aligned} \quad (8.179)$$

where the contributions from the integral and the θ function have combined to produce a result analytic in α . Now using eqs. (8.95), (8.96) for $(G_n - G_1)|_{x=x', \alpha=0}$,

$$\alpha \approx -\frac{D-2}{2(D-1)}(n-1), \quad n \rightarrow 1 \quad (8.180)$$

Note that the exponent α controlling the OPE (8.171) of the field $\phi(x)$ at the conical singularity is positive for $n < 1$ and negative for $n > 1$. Now, from (8.180),

$$a_n = \frac{(D-2)^2}{4(D-1)^2} (n-1)^2, \quad n \rightarrow 1 \quad (8.181)$$

Therefore, combining eqs. (8.31) and (8.158), we find that

$$r_n \propto \frac{a_n}{1-n} \propto n-1, \quad n \rightarrow 1 \quad (8.182)$$

and the correlation length correction to the entanglement entropy proper vanishes at leading order in N ,

$$r = \lim_{n \rightarrow 1} r_n = 0 \quad (8.183)$$

Thus, for all dimensions $2 < D < 4$

$$r \sim O(N) \quad (8.184)$$

even though $r_n \sim O(N^2)$ for all $n \neq 1$.

So far we have concentrated on the solution to the gap equation in the $n \rightarrow 1$ limit for arbitrary dimension. However, we can also obtain an analytic solution for arbitrary n in the limit $D = 4 - \epsilon$. Such a solution is useful for comparison to the results of the ϵ -expansion presented in section 8.4.

When $D = 4 - \epsilon$, the function $R(\nu) = -2\nu^{1-\epsilon}\Gamma(-1 + \epsilon)$. The divergence of the Γ function is not important here as it is just an overall factor in the gap equation (which anyway cancels with $\Gamma(2 - D/2)$ in (8.174)). However, the integral (8.178) now diverges for $\nu \rightarrow \infty$ if $\epsilon = 0$. Hence, for generic n and $D = 4 - \epsilon$ the leading α -dependent contribution to the gap equation comes from the region $\nu \gg 1$ and is of order, $\frac{1}{\epsilon}\alpha^2$. This suggests that α will be at most of order $\epsilon^{1/2}$. However, for α very

small (i.e. $n \rightarrow 1$), we already know from the previous discussion that the leading contribution to the integral scales as $|\alpha|$ and comes from the $\nu \rightarrow 0$ region. Keeping these two contributions (one non-analytic in α and the other analytic, but with a diverging coefficient) and setting $\alpha = 0$ in the rest of the integral, we reduce the gap equation to

$$\begin{aligned} \frac{1}{\pi n} \int_0^\infty d\nu \left(\frac{\nu^2}{\nu^2 + \alpha^2} - 1 \right) + \int_0^\infty d\nu \nu \left(\frac{\cosh(\pi n \nu)}{\sinh(\pi n \nu)} - \frac{\cosh(\pi \nu)}{\sinh(\pi \nu)} \right) \\ - \frac{1}{2} \alpha^2 \int_{\nu \gg 1}^\infty d\nu \nu^{-\epsilon-1} - \theta(-\alpha) \frac{\alpha}{n} = 0 \end{aligned} \quad (8.185)$$

$$\frac{\alpha}{n} + \frac{\alpha^2}{\epsilon} - \frac{1}{6} \left(\frac{1}{n^2} - 1 \right) = 0 \quad (8.186)$$

The quadratic has two solutions,

$$\alpha_\pm = -\frac{\epsilon}{2n} \pm \frac{1}{2n} \sqrt{\epsilon^2 + \frac{2\epsilon}{3}(1-n^2)} \quad (8.187)$$

and the corresponding values of d_n , eq. (8.160), are,

$$d_n^\pm = \frac{N}{8\pi^2} \left[\frac{1}{6} \left(\frac{1}{n^2} - 1 \right) + \frac{\epsilon \mp \sqrt{\epsilon^2 + \frac{2\epsilon}{3}(1-n^2)}}{2n^2} \right] \quad (8.188)$$

Eq. (8.188) is in agreement with the result of the ϵ -expansion, eq. (8.58), and we can identify the α_\pm saddle points with the c_τ^\pm fixed points. Moreover, we see that the predictions of the large- N (8.187) and ϵ -expansion (8.65) for the OPE exponent α also agree. Note that both saddle points (8.187) disappear for $n > n_c \approx 1 + 3\epsilon/4$. This coincides with the value of n at which runaway of RG flow is observed in the ϵ -expansion. However, as we noted earlier, the gap equation always has an odd number of solutions. Thus, we have missed a solution in our discussion above. This solution has $\alpha \approx -(D/2 - 1) \rightarrow -1$, i.e. α is not small. Its existence is possible due to a

cancellation of $1/\epsilon$ divergences between the large ν part of the integral and the $\theta(-\alpha)$ term in (8.178). Keeping these two contributions to the gap equation, we obtain in the $\alpha \rightarrow -(D/2 - 1)$ limit,

$$\frac{\alpha^2}{\epsilon} - \frac{\epsilon}{n} \frac{1}{\alpha + D/2 - 1} = 0 \quad (8.189)$$

So,

$$\alpha = -1 + \frac{1}{2}\epsilon + \frac{1}{n}\epsilon^2 \quad (8.190)$$

Eqs. (8.187), (8.190) comprise the three solutions to the gap equation for $1 < n < n_c$, and eq. (8.190) is the only solution for $n > n_c$. We speculate that the runaway of the RG flow observed in ϵ -expansion for $n > n_c$ is towards the fixed point (8.190). As we noted above, the value $\alpha = -(D/2 - 1)$ corresponds to the would be condensation of the ϕ field at the conical singularity. Thus, for $\epsilon \rightarrow 0$, the saddle-point (8.190) is proximate to such condensation. This is consistent with our interpretation of the RG flow $c \rightarrow -\infty$ as the tendency to formation of $\langle \phi(x) \rangle \neq 0$. However, the large- N analysis demonstrates that no true spontaneous symmetry breaking at the conical singularity occurs for $D < 4$.

To our knowledge no such non-trivial n -dependence has been previously observed in any theories. Still, in the large- N expansion such behaviour is only present for $D > D_c \approx 3.74$ and its relevance to the physical case $D = 3$ is doubtful. Moreover, the non-analyticity occurs away from $n = 1$ and, thus, is unimportant for computing the entanglement entropy proper. Indeed, the behaviour of the theory for $n \rightarrow 1$ (8.180) is found to evolve smoothly as the dimension D increases from 2 to 4.

We now come back to the physical case $D = 3$, where the solution to the gap equation is unique. The numerical solution for the first few integers n is listed in

n	α_n
2	-0.16515
3	-0.26594
4	-0.32905
5	-0.36743

Table 8.1: Solution to the gap equation in the large- N limit for $D = 3$.

Table 8.1. Then, from (8.30) and (8.158),

$$r_n = \frac{3\pi^2 N^2}{128} \frac{n\alpha_n^2}{n-1}, \quad D = 3 \quad (8.191)$$

The coefficient (8.191) can be, in principle, obtained numerically by performing classical Monte-Carlo simulations of the $O(N)$ model in the spirit of Refs. [253, 254].

So far our large- N computation has been confined to the correlation length correction to the Renyi entropy. At leading order the calculation was technically fairly simple, as utilizing the discussion in section 8.3, we could work at the critical point. In particular, the form of the Lagrange multiplier $\langle i\lambda(r) \rangle$ was fixed by scale invariance up to an overall constant. To proceed beyond the leading order, as is required for the calculation of the correlation length correction to the entanglement entropy proper, we would have to work in the gapped phase. The Lagrange multiplier $\langle i\lambda(r) \rangle$ would now be a non-trivial function of r with a length scale determined by the correlation length $\xi = m^{-1}$. Similarly, if we wish to compute the finite size correction γ to the entanglement entropy, $\langle i\lambda(r) \rangle$ will again vary non-trivially with a length scale determined by the size L of the compact direction. In both cases, we have to solve the gap equation for a whole function $\langle i\lambda(r) \rangle$ rather than a single number a_n . In principle, this problem can be addressed numerically. It would be particularly interesting to

check whether $\gamma \sim O(1)$ for $N \rightarrow \infty$ as suggested by the ϵ -expansion, eq. (8.148).

8.7 Conclusion.

In the present work we have computed the universal finite size and correlation length corrections to the entanglement entropy and the Renyi entropy for the $O(N)$ model. The evaluation of this entropy required a study of the $O(N)$ field theory on a n -sheeted Riemann surface for general n , and an understanding of the nature of the $n \rightarrow 1$ limit. For $n \neq 1$, there is a conical singularity at the origin of the Riemann surface and we have presented a detailed analysis of the structure of the “boundary” excitations of the $O(N)$ CFT at this singularity. (A closely related CFT with vortex boundary conditions was studied in Ref. [165] with a very different physical motivation.) In particular, we showed that in the context of $\epsilon = 3 - d$ expansion, the RG flow of the boundary coupling c in Eq. (8.41) was the key to a determination of the entanglement entropy. The RG flow of c had two possible structures shown in Figs. 8.5 c) and d). For n greater than a critical n_c , we had flow in the infrared to $c = -\infty$ as in Fig. 8.5 d). In contrast for $n < n_c$, we had three possible fixed points, and the $n \rightarrow 1$ limit was controlled by the non-zero fixed point $c = c_r^+$, at which all strong hyperscaling assumptions were obeyed. All our computations in the ϵ and $1/N$ expansions were consistent with this RG flow and fixed-point structure. One crucial consequence of the boundary perturbation and the subtle limit $n \rightarrow 1$ is that the finite size and correlation length corrections to the entanglement entropy are different at the Wilson-Fisher and Gaussian fixed points already at leading order in ϵ -expansion.

Here we have considered a geometry with a smooth, straight boundary between regions A and B . Therefore, we can make no strong claims regarding possible presence of non-universal terms in the entanglement entropy associated with the curvature of the boundary. Nevertheless, we generally expect such terms to be absent in spatial dimension $d = 2$. Indeed, as we discussed in the introduction, any non-universal contributions of the entanglement entropy must involve integrals of local geometric quantities over the length of the boundary. The simplest geometric object for a one dimensional boundary is the curvature vector $\vec{\kappa}$. Assuming that the integrand is analytic in $\vec{\kappa}$, the leading correction due to the boundary curvature that we can construct is,

$$\Delta S \sim \int_B ds \vec{\kappa}^2 \quad (8.192)$$

which scales as $1/L$ under dilatations. Such a behaviour is subleading not only to the universal terms in the entanglement entropy, but also to corrections to scaling coming from irrelevant operators.

One possible extension of our work is to consider boundaries with sharp corners. In such geometries, it is expected that the entanglement entropy will contain a universal logarithmically divergent term.[245, 246, 244, 249, 250] Moreover, we have only studied the correlation length correction to the entanglement entropy in the symmetry unbroken region $t > 0$. It would be interesting to extend our treatment to the symmetry broken phase $t < 0$.

As this work was being completed, we learned of the numerical study of entanglement entropy in the $d = 2$ quantum Ising model in Ref. [255]. At the quantum critical point the authors of Ref. [255] find evidence for a finite size correction γ as

in Eq. (8.6) in the case when the boundary between regions A and B is smooth. We note that the geometry studied in Ref. [255] is an $L \times L$ torus divided into two equal cylinders rather than the infinite cylinder cut in half that we have considered here. Thus, the two results cannot be compared directly. Nevertheless, the value of γ in Ref. [255] is found to be positive, as in our conjecture in Eq. (8.8) for the case of periodic boundary conditions along the cylinder.

Appendix A

Appendix to Chapter 2

A.1 Functions $G_q(b^2)$ and $F_q(b^2)$

The purpose of this appendix is to compute the behaviour of functions $G_q(b^2)$ [Eq. (2.30)], and $F_q(b^2)$ [Eq. (2.41)], in the limit $b \rightarrow \infty$.

We begin with G_q . First, we consider the case q -even. Then,

$$G_q(b^2) = \sum_{l=0}^{\infty} \left(\frac{l+1/2}{((l+1/2)^2 + b^2)^{\frac{1}{2}}} - 1 \right) - \sum_{l=0}^{q/2-1} \left(\frac{l+1/2}{((l+1/2)^2 + b^2)^{\frac{1}{2}}} - 1 \right). \quad (\text{A.1})$$

In what follows, we will drop all the corrections to $G_q(b^2)$ that vanish as b^{-1} or faster.

Thus, simplifying the second term above,

$$G_q(b^2) = \sum_{l=0}^{\infty} \left(\frac{l+1/2}{((l+1/2)^2 + b^2)^{\frac{1}{2}}} - 1 \right) + q/2. \quad (\text{A.2})$$

Now we utilize the symmetry of the summand under $l \rightarrow -l-1$, obtaining

$$G_q(b^2) = \frac{1}{2} \sum_{l=-\infty}^{\infty} \left(\frac{|l+1/2|}{((l+1/2)^2 + b^2)^{\frac{1}{2}}} - 1 \right) + q/2. \quad (\text{A.3})$$

Upon Poisson-resumming the l 's, we have

$$\begin{aligned}
 G_q(b^2) &= \frac{1}{2} \sum_{n=-\infty}^{\infty} (-1)^n \int_{-\infty}^{\infty} dl \left(\frac{|l|}{(l^2 + b^2)^{\frac{1}{2}}} - 1 \right) e^{2\pi i n l} + q/2 \\
 &= \int_0^{\infty} dl \left(\frac{l}{(l^2 + b^2)^{\frac{1}{2}}} - 1 \right) + \\
 &\quad + 2 \sum_{n=1}^{\infty} (-1)^n \int_0^{\infty} dl \left(\frac{l}{(l^2 + b^2)^{\frac{1}{2}}} - 1 \right) \cos(2\pi n l) + q/2. \quad (\text{A.4})
 \end{aligned}$$

As usual, the leading (divergent) contribution in the $b \rightarrow \infty$ limit comes from the $n = 0$ term in Eq (A.4), which is

$$\int_0^{\infty} dl \left(\frac{l}{(l^2 + b^2)^{\frac{1}{2}}} - 1 \right) = -b. \quad (\text{A.5})$$

As for the $n \geq 1$ terms, we rotate the contour of integration as follows:

$$\begin{aligned}
 &\int_0^{\infty} dl \left(\frac{l}{(l^2 + b^2)^{\frac{1}{2}}} - 1 \right) \cos(2\pi n l) = b \operatorname{Re} \int_0^{\infty} dl \left(\frac{l}{(l^2 + 1)^{\frac{1}{2}}} - 1 \right) e^{2\pi i n b l} \\
 &= b \operatorname{Re} \int_0^{\infty} i dy \left(i y (\theta(1-y)(1-y^2)^{-\frac{1}{2}} + \theta(y-1)(y^2-1)^{-\frac{1}{2}} e^{-i\pi/2}) - 1 \right) e^{-2\pi n b y} \\
 &= -b \int_0^1 dy \frac{y}{(1-y^2)^{\frac{1}{2}}} e^{-2\pi n b y} = -b \left(\frac{1}{(2\pi n b)^2} + O\left(\frac{1}{(n b)^4}\right) \right). \quad (\text{A.6})
 \end{aligned}$$

Hence,

$$2 \sum_{n=1}^{\infty} (-1)^n \int_0^{\infty} dl \left(\frac{l}{(l^2 + b^2)^{\frac{1}{2}}} - 1 \right) \cos(2\pi n l) \sim \frac{2}{(2\pi)^2 b} \sum_{n=1}^{\infty} (-1)^{n+1} \frac{1}{n^2} \sim O(b^{-1}), \quad (\text{A.7})$$

and this can be dropped in the limit $b \rightarrow \infty$. Therefore,

$$G_q(b^2) \sim -b + q/2 \quad (\text{A.8})$$

Repeating this analysis for q -odd and $b \rightarrow \infty$,

$$\begin{aligned}
 G_q(b^2) &= \sum_{l=\frac{q+1}{2}}^{\infty} \left(\frac{l}{(l^2 + b^2)^{\frac{1}{2}}} - 1 \right) = \sum_{l=0}^{\infty} \left(\frac{l}{(l^2 + b^2)^{\frac{1}{2}}} - 1 \right) - \sum_{l=0}^{\frac{q-1}{2}} \left(\frac{l}{(l^2 + b^2)^{\frac{1}{2}}} - 1 \right) \\
 &= \frac{1}{2} \sum_{l=-\infty}^{\infty} \left(\frac{|l|}{(l^2 + b^2)^{\frac{1}{2}}} - 1 \right) - 1/2 + \frac{q+1}{2} = \frac{1}{2} \sum_{l=-\infty}^{\infty} \left(\frac{|l|}{(l^2 + b^2)^{\frac{1}{2}}} - 1 \right) + q/2 \\
 &= \frac{1}{2} \sum_{n=-\infty}^{\infty} \int dl \left(\frac{|l|}{(l^2 + b^2)^{\frac{1}{2}}} - 1 \right) e^{2\pi i n l} + q/2. \tag{A.9}
 \end{aligned}$$

Comparing Eq. (A.9) to its q -even counterpart Eq. (A.4), we see that the only difference is the absence of the factor $(-1)^n$ in the sum. Recalling that in the $b \rightarrow \infty$ limit the only finite contribution came from the $n = 0$ term in the sum, we obtain the same result as in the q -even case [Eq. (A.8)].

Now, we proceed to the function F_q . We again begin with the case of q even:

$$F_q(b^2) = \sum_{l=0}^{\infty} \left((l+1/2)((l+1/2)^2 + b^2)^{\frac{1}{2}} - (l+1/2)^2 - \frac{1}{2}b^2 \right) \tag{A.10}$$

$$- \sum_{l=0}^{q/2-1} \left((l+1/2)((l+1/2)^2 + b^2)^{\frac{1}{2}} - (l+1/2)^2 - \frac{1}{2}b^2 \right). \tag{A.11}$$

As before, we drop all the terms decaying as b^{-1} or faster. Thus,

$$F_q(b^2) \sim \frac{1}{2} \sum_{l=-\infty}^{\infty} \left(|l+1/2|((l+1/2)^2 + b^2)^{\frac{1}{2}} - (l+1/2)^2 - \frac{1}{2}b^2 \right) \tag{A.12}$$

$$+ \frac{1}{2}b^2 \sum_{l=0}^{q/2-1} 1 - b \sum_{l=0}^{q/2-1} (l+1/2) + \sum_{l=0}^{q/2-1} (l+1/2)^2. \tag{A.13}$$

Poisson-resumming the first sum, we have

$$\begin{aligned}
F_q(b^2) &\sim \frac{1}{2} \sum_{n=-\infty}^{\infty} (-1)^n \int_{-\infty}^{\infty} dl \left(|l|(l^2 + b^2)^{\frac{1}{2}} - l^2 - \frac{1}{2}b^2 \right) e^{2\pi i n l} \\
&+ \frac{q}{4}b^2 - \frac{q^2}{8}b + \frac{1}{24}q(q^2 - 1) \\
&= \int_0^{\infty} dl \left(l(l^2 + b^2)^{\frac{1}{2}} - l^2 - \frac{1}{2}b^2 \right) \\
&+ 2 \sum_{n=1}^{\infty} (-1)^n \int_0^{\infty} dl \left(l(l^2 + b^2)^{\frac{1}{2}} - l^2 - \frac{1}{2}b^2 \right) \cos(2\pi n l) \\
&+ \frac{q}{4}b^2 - \frac{q^2}{8}b + \frac{1}{24}q(q^2 - 1). \tag{A.14}
\end{aligned}$$

As before, the most divergent piece in the $b \rightarrow \infty$ limit comes from the $n = 0$ term in the Poisson-resummed series, which is

$$\int_0^{\infty} dl \left(l(l^2 + b^2)^{\frac{1}{2}} - l^2 - \frac{1}{2}b^2 \right) = -\frac{1}{3}b^3. \tag{A.15}$$

The integral for the $n \neq 0$ terms can again be analyzed by rotating the integration contour:

$$\begin{aligned}
&\int_0^{\infty} dl \left(l(l^2 + b^2)^{\frac{1}{2}} - l^2 - \frac{1}{2}b^2 \right) \cos(2\pi n l) \\
&= b^3 \operatorname{Re} \int_0^{\infty} dl \left(l(l^2 + 1)^{\frac{1}{2}} - l^2 - \frac{1}{2} \right) e^{2\pi i n b l} \\
&= b^3 \operatorname{Re} \int_0^{\infty} i dy \left(i y(\theta(1-y)(1-y^2)^{\frac{1}{2}} + \theta(y-1)(y^2-1)^{\frac{1}{2}} e^{i\pi/2}) + y^2 - \frac{1}{2} \right) e^{-2\pi n b y} \\
&= -b^3 \int_0^1 dy y(1-y^2)^{\frac{1}{2}} e^{-2\pi n b y} \rightarrow -b^3 \left(\frac{1}{(2\pi n b)^2} + O\left(\frac{1}{(n b)^4}\right) \right). \tag{A.16}
\end{aligned}$$

Here, unlike for the gap equation, we cannot limit ourselves to just the $n = 0$ term in the $b \rightarrow \infty$ limit, and

$$F_q(b^2) \sim -\frac{1}{3}b^3 + \frac{2}{(2\pi)^2}b \sum_{n=1}^{\infty} \frac{(-1)^{n+1}}{n^2} + \frac{q}{4}b^2 - \frac{q^2}{8}b + \frac{1}{24}q(q^2 - 1) \tag{A.17}$$

$$= -\frac{1}{3}b^3 + \frac{q}{4}b^2 + \left(\frac{1}{24} - \frac{q^2}{8}\right)b + \frac{1}{24}q(q^2 - 1). \tag{A.18}$$

Performing a similar analysis for q -odd, we find

$$\begin{aligned}
F_q(b^2) &= \sum_{l=0}^{\infty} \left(l(l^2 + b^2)^{\frac{1}{2}} - l^2 - \frac{1}{2}b^2 \right) - \sum_{l=0}^{(q-1)/2} \left(l(l^2 + b^2)^{\frac{1}{2}} - l^2 - \frac{1}{2}b^2 \right) \\
&\sim \frac{1}{2} \sum_{l=-\infty}^{\infty} \left(l(l^2 + b^2)^{\frac{1}{2}} - l^2 - \frac{1}{2}b^2 \right) \\
&\quad - \frac{1}{4}b^2 + \frac{1}{2}b^2 \sum_{l=0}^{(q-1)/2} 1 - b \sum_{l=0}^{(q-1)/2} l + \sum_{l=0}^{(q-1)/2} l^2 \\
&= \frac{1}{2} \sum_{n=-\infty}^{\infty} \int dl \left(l(l^2 + b^2)^{\frac{1}{2}} - l^2 - \frac{1}{2}b^2 \right) e^{2\pi i n l} \\
&\quad + \frac{q}{4}b^2 - \frac{1}{8}(q^2 - 1)b + \frac{1}{24}q(q^2 - 1) \\
&\sim -\frac{1}{3}b^3 - \frac{2}{(2\pi)^2}b \sum_{n=1}^{\infty} \frac{1}{n^2} + \frac{q}{4}b^2 - \frac{1}{8}(q^2 - 1)b + \frac{1}{24}q(q^2 - 1) \\
&= -\frac{1}{3}b^3 + \frac{q}{4}b^2 + \left(\frac{1}{24} - \frac{q^2}{8} \right)b + \frac{1}{24}q(q^2 - 1). \tag{A.19}
\end{aligned}$$

which is equal to the result [Eq. (A.18)] we obtained for q -even.

A.2 Comparison to Murthy-Sachdev expression

Murthy and Sachdev[3] have expressed their result for the scaling dimension of the monopole operator as

$$\frac{\Delta_q}{N} = -\Omega_q + \Xi_q + \frac{q^3}{24} + \frac{q}{12}, \tag{A.20}$$

where

$$\Omega_q = \frac{q^4}{4} \sum_{l=q/2}^{\infty} \left(\frac{1}{(\sqrt{(2l+1)^2 - q^2} + 2l + 1)^2} \right), \tag{A.21}$$

and

$$\begin{aligned} \Xi_q = & - \sum_{l=q/2}^{\infty} (2l+1) \left(((l+1/2)^2 - q^2/4)^{\frac{1}{2}} \right. \\ & \left. - ((l+1/2)^2 - q^2/4 - \alpha_q)^{\frac{1}{2}} - \frac{\alpha_q}{2((l+1/2)^2 - q^2/4 - \alpha_q)^{\frac{1}{2}}} \right). \end{aligned} \quad (\text{A.22})$$

Using the identification $\alpha_q = -q^2/4 - a_q^2$ to convert this to the notation used in our analysis, and summing the last term in Eq. (A.22) using the gap equation Eq. (2.34), we have

$$\Xi_q = 2 \sum_{l=q/2}^{\infty} \left((l+1/2) \left((l+1/2)^2 + a_q^2 \right)^{\frac{1}{2}} - (l+1/2)^2 - \frac{q}{2} \right) + \frac{q}{2} \alpha_q. \quad (\text{A.23})$$

For Ω_q , we can eliminate the irrationality in the denominator to obtain

$$\Omega_q = -2 \sum_{l=q/2}^{\infty} \left((l+1/2) \left((l+1/2)^2 - q^2/4 \right)^{\frac{1}{2}} - (l+1/2)^2 + \frac{1}{8} q^2 \right). \quad (\text{A.24})$$

Thus, adding Eq. (A.23) and Eq. (A.24),

$$\frac{\Delta_q}{N} = 2 \sum_{l=q/2}^{\infty} \left((l+1/2) \left((l+1/2)^2 + a_q^2 \right)^{\frac{1}{2}} - (l+1/2)^2 - \frac{1}{2} a_q^2 \right) - \frac{q}{2} a_q^2 - \frac{1}{12} q (q^2 - 1) \quad (\text{A.25})$$

which is identical to our result [Eq. (2.46)].

Appendix B

Appendix to Chapter 3

B.1 $U(1)$ charge density

Throughout Chapter 2 we have concentrated on computing matrix elements of uniform and staggered magnetization $Q^a(x)$, $n^a(x)$. However, for the deconfined critical point, it is also interesting to compute the charge density associated with the $U(1)$ local symmetry of the \mathbb{CP}^{N-1} model. This charge density is the zeroth component of the current,

$$j_\mu(x) = z^\dagger D_\mu z - (D_\mu z)^\dagger z \quad (\text{B.1})$$

As we shall see this computation serves as an additional test of our procedure for projecting onto the single spinon state.

Consider the \mathbb{CP}^{N-1} model coupled to an external current,

$$\mathcal{S} = \mathcal{S}_b^z + i \int d^3x A_\mu J_\mu^{\text{ext}} \quad (\text{B.2})$$

As in the rest of the chapter, we set $e^2 = \infty$, so that the gauge field has no bare

kinetic term. Then, by equations of motion,

$$0 = \frac{\delta \mathcal{S}}{\delta A_\mu} = i(j^\mu + J_\mu) \tag{B.3}$$

$$j_\mu = -J_\mu^{\text{ext}} \tag{B.4}$$

Thus, the dynamical current completely screens (locally!) the external current. Eq. (B.4) is an operator identity, and should, in particular, hold in the ground state of the system with a single impurity. Let's check this statement in the $1/N$ expansion.

We start from Eq. (3.9), with $O(x) = j_0(x)$. We write,

$$\langle \alpha | j_0(\vec{x}) | \beta \rangle = \rho(\vec{x}) \delta_{\alpha\beta} \tag{B.5}$$

with $\rho(\vec{x}) = \frac{1}{L^2} \sum_{\vec{q}} \rho(\vec{q}) e^{i\vec{q}\vec{x}}$. The Wilson line term in Eq. (3.9) can be incorporated into the action as coupling to an external current, $J_\mu^{\text{ext}}(\vec{x}, \tau) = \delta_{\mu 0} \delta^3(\vec{x}) \theta(\mathcal{T}/2 - \tau) \theta(\tau + \mathcal{T}/2)$. At leading order in $1/N$ the numerator of Eq. (3.9) is given by diagrams shown in Fig. B.1, while the denominator is given by the bare propagator $D(\vec{x} = 0, \mathcal{T})$.

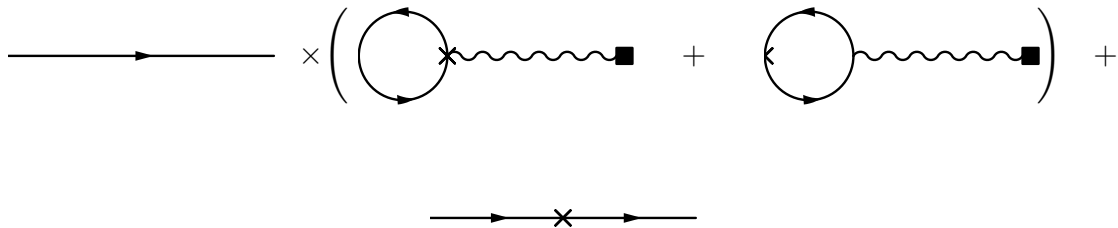


Figure B.1: Diagrams contributing to $U(1)$ charge induced

Thus, we can distinguish two contributions: the disconnected one, $\rho^1(\vec{q})$, coming from the first line in Fig. B.1, and the connected one, $\rho^2(\vec{q})$, coming from the second

line. We note that the scalar loops contributing to $\rho^1(\vec{q})$ are precisely the same as those contributing to the self-energy of A_μ field, thus,

$$\rho^1(\vec{q}) = - \int \frac{dq_\tau}{2\pi} K_{0\nu}(\vec{q}, q_\tau) \mathcal{D}_{\nu\lambda}(\vec{q}, q_\tau) J_\lambda^{\text{ext}}(\vec{q}, q_\tau) \quad (\text{B.6})$$

Now,

$$K_{\mu\nu}(q) \mathcal{D}_{\nu\lambda}(q) = \delta_{\mu\lambda} - \frac{q_\mu q_\lambda}{q^2} \quad (\text{B.7})$$

Thus,

$$\rho^1(\vec{q}) = - \int \frac{dq_\tau}{2\pi} \frac{\vec{q}^2}{q_\tau^2 + \vec{q}^2} J^{\text{ext}}(\vec{q}, q_\tau) \quad (\text{B.8})$$

Noting, $J^{\text{ext}}(\vec{q}, q_\tau) \xrightarrow{T \rightarrow \infty} 2\pi\delta(q_\tau)$,

$$\rho^1(\vec{q}) = -(1 - \delta_{\vec{q},0}) \quad (\text{B.9})$$

For the $\vec{q} = 0$ part, the order of the limits $\vec{q} \rightarrow 0$, $q_\tau \rightarrow 0$ is very important. In our finite system the $\vec{q} = 0$ mode is isolated, and, moreover, in our present treatment the Wilson line is of finite length, so we must take the $\vec{q} = 0$ limit first and then $q_\tau \rightarrow 0$. Hence, $\rho^1(\vec{q} = 0) = 0$. This is not surprising. In perturbation theory, we start with the vacuum which has charge 0. Unless we manually project the system into a finite charge subspace (as we do in our treatment by acting on the vacuum with z , z^\dagger operators), we will never be able to see global screening of charge. Since the diagrams contributing to $\rho^1(\vec{q})$ are disconnected from the external z line, $\rho^1(\vec{q} = 0) = 0$.

Now, the connected contribution, simply gives the charge density of one spinon in the $\vec{k} = 0$ state,

$$\rho^2(\vec{q}) = -\delta_{\vec{q},0} \quad (\text{B.10})$$

Putting the two contributions together,

$$\rho(\vec{q}) = 1 \quad (\text{B.11})$$

$$\rho(\vec{x}) = \delta^2(\vec{x}) \tag{B.12}$$

as expected by equations of motion (B.4).

Thus, we have been able to check exact screening of external charge, which follows from equation of motion (B.4), to leading order in $1/N$. We see that local and global parts of the screening charge come from very different Feynman diagrams.

Appendix C

Appendix to Chapter 4

C.1 Electric field in the free theory

We wish to use eq. (4.78) to compute the electric field in the free theory. We start from the equation for the propagator (4.61) and promote the ω integral to run over $D - 2$ dimensions, as discussed in section 4.3.3, obtaining

$$D(r, \theta) = \frac{\Gamma(2 - D/2)}{(4\pi)^{(D-2)/2}} \sum_l \frac{e^{il\theta}}{2\pi} \int du u^{D-3} J_{|l|}(ur)^2 \quad (\text{C.1})$$

$$= \frac{\Gamma((3 - D)/2)}{(4\pi)^{(D-1)/2}} \frac{1}{r^{D-2}} \sum_l \frac{e^{il\theta}}{2\pi} \frac{\Gamma(|l| + D/2 - 1)}{\Gamma(|l| - D/2 + 2)} \quad (\text{C.2})$$

We see that the prefactor diverges for $D = 3$. However, at $D = 3$ the sum over angular momenta becomes $\sum_l \frac{e^{il\theta}}{2\pi} = \delta(\theta)$. So, we have to first perform the sum over angular momenta and then take the limit $D \rightarrow 3$. The sum over angular momenta

can be performed in terms of hypergeometric functions, giving for $0 < Q < 1$,

$$\begin{aligned}
D(r, \theta) &= \frac{\Gamma((3-D)/2) e^{-iQ\theta}}{2^D \pi^{(D+1)/2} r^{D-2}} \left(e^{i\theta} \frac{\Gamma(D/2 - Q)}{\Gamma(3 - D/2 - Q)} \right. \\
&\times F(\{1, D/2 - Q\}, \{3 - D/2 - Q\}, e^{i\theta}) \\
&+ \left. \frac{\Gamma(D/2 - 1 + Q)}{\Gamma(2 - D/2 + Q)} F(\{1, -1 + D/2 + Q\}, \{2 - D/2 + Q\}, e^{-i\theta}) \right)
\end{aligned} \tag{C.3}$$

where F denotes the Barnes extended hypergeometric function. One can check that for $D = 3$ the expression in brackets in (C.3) vanishes, cancelling the pole in the prefactor. Now, differentiating with respect to θ ,

$$\begin{aligned}
-i\partial_\theta D(r, \theta) &= \frac{\Gamma((3-D)/2) e^{-iQ\theta}}{2^D \pi^{(D+1)/2} r^{D-2}} \left(\frac{(1-Q)\Gamma(D/2 - Q)}{\Gamma(3 - D/2 - Q)} e^{i\theta} \right. \\
&\times F(\{1, D/2 - Q\}, \{3 - D/2 - Q\}, e^{i\theta}) \\
&+ \frac{\Gamma(D/2 + 1 - Q)}{\Gamma(4 - D/2 - Q)} e^{2i\theta} F(\{2, D/2 - Q + 1\}, \{4 - D/2 - Q\}, e^{i\theta}) \\
&- \frac{Q\Gamma(D/2 - 1 + Q)}{\Gamma(2 - D/2 + Q)} F(\{1, D/2 - 1 + Q\}, \{2 - D/2 + Q\}, e^{-i\theta}) \\
&\left. - \frac{\Gamma(D/2 + Q)}{\Gamma(3 - D/2 + Q)} e^{-i\theta} F(\{2, D/2 + Q\}, \{3 - D/2 + Q\}, e^{-i\theta}) \right)
\end{aligned} \tag{C.4}$$

According to (4.78), to compute the electric field we need to take the limit as $\theta \rightarrow 0$ of (C.4). Strictly speaking this limit does not exist as the hypergeometric functions blow up as $\theta \rightarrow 0$ (that is when the last argument goes to 1). However, we note that only the imaginary part of (C.4) becomes infinite as $\theta \rightarrow 0$, while the real part has a well-defined limit. The expectation value of electric field $\langle -iE_r \rangle = -\langle -iF_\theta \rangle$ should be real. Thus, we can drop the infinite imaginary part. Moreover, the imaginary part is antisymmetric under $\theta \rightarrow -\theta$, so the ‘‘symmetrized’’ limit of (C.4) exists. It turns

out that this symmetrized limit can be obtained by the formal summation formulas,

$$F(\{1, a\}, \{b\}, 1) = \frac{1 - b}{a - b + 1} \quad (\text{C.5})$$

$$F(\{2, a\}, \{b\}, 1) = \frac{(b - 1)(b - 2)}{(a - b + 1)(a - b + 2)} \quad (\text{C.6})$$

So, taking $\theta \rightarrow 0$, plugging (C.5) into (C.4) and performing a few manipulations,

$$\begin{aligned} -i\partial_\theta D(\theta = 0, r) &= \frac{(2Q - 1)\Gamma((1 - D)/2)\Gamma(D/2 + Q - 1)}{2^{D+2}\pi^{(D+1)/2}\Gamma(1 - D/2 + Q)} \\ &\times \left(\frac{\sin(\pi(D/2 + Q))}{\sin(\pi(D/2 - Q))} - 1 \right) \frac{1}{r^{D-2}} \end{aligned} \quad (\text{C.7})$$

Taking the limit $D \rightarrow 3$,

$$-i\partial_\theta D(\theta = 0, r) = -\frac{1}{32\pi r}(2Q - 1)^2 \tan(\pi Q) \quad (\text{C.8})$$

Finally, plugging into (4.78) we recover (4.43) with

$$C(Q) = \frac{1}{8}(1 - 2Q)^2 \tan(\pi Q), \quad 0 < Q < 1 \quad (\text{C.9})$$

We remind the reader that all the manipulations above have been performed for $0 < Q < 1$. The function $C(Q)$ can then be extended to other values of Q by periodicity. In particular, extending to the range $|Q| < 1$,

$$C(Q) = \frac{1}{8}(1 - 2|Q|)^2 \tan(\pi Q), \quad |Q| < 1 \quad (\text{C.10})$$

C.2 Integral form of the twisted propagator

In this section we review the derivation of the integral form of the twisted propagator (4.81) given in Ref. [152]. We use this integral form to compute the electric field (4.78) and show that it is in agreement with the result obtained using spectral

representation of the propagator (see Appendix C.1). We also indicate how the free twisted propagator should be modified in the strongly interacting $M = \infty$ theory.

Recall the free massive propagator in $2D$ (without any twisted b.c.) obeys,

$$(-\partial^2 + m^2)D(\vec{x}, \vec{x}') = \delta(\vec{x} - \vec{x}') \quad (\text{C.11})$$

and is given by,

$$D_2(\vec{x}, \vec{x}') = \frac{1}{2\pi} K_0(m|\vec{x} - \vec{x}'|) = \frac{1}{2\pi^2} \int_{-\infty}^{\infty} d\nu K_{i\nu}(mr) K_{i\nu}(mr') e^{\pi\nu} e^{-\nu|\theta - \theta'|} \quad (\text{C.12})$$

where the integral representation is valid for $|\theta - \theta'| < 2\pi$. The BesselK functions of imaginary argument satisfy the equation,

$$\left(-\frac{1}{r} \frac{d}{dr} \left(r \frac{d}{dr} \right) - \frac{\nu^2}{r^2} + m^2 \right) K_{i\nu}(mr) = 0 \quad (\text{C.13})$$

Hence the functions $K_{i\nu}(mr)e^{\pm\nu\theta}$ are in the kernel of the operator $-\partial_2^2 + m^2 = -\frac{1}{r} \frac{\partial}{\partial r} \left(r \frac{\partial}{\partial r} \right) - \frac{1}{r^2} \frac{\partial^2}{\partial \theta^2} + m^2$. Applying this operator to $D_2(\vec{x}, \vec{x}')$ we learn,

$$\frac{1}{\pi^2 r^2} \int_{-\infty}^{\infty} d\nu \nu K_{i\nu}(mr) K_{i\nu}(mr') e^{\pi\nu} = \frac{1}{r} \delta(r - r') \quad (\text{C.14})$$

This identity will be useful to us later.

Now, we want to modify the propagator (C.12) in such a way that it satisfies the twisted boundary conditions (4.42). Let's first symmetrize equation (C.12) with respect to ν by noting $K_{i\nu} = K_{-i\nu}$. Then,

$$D_2(r, r', \theta - \theta') = \frac{1}{2\pi^2} \int_{-\infty}^{\infty} d\nu K_{i\nu}(mr) K_{i\nu}(mr') \cosh(\nu(\pi - |\theta - \theta'|)) \quad (\text{C.15})$$

Now, we can generalize,

$$D_2(r, r', \theta, Q) = \frac{1}{2\pi^2} \int_{-\infty}^{\infty} d\nu K_{i\nu}(mr) K_{i\nu}(mr') \sinh(\pi\nu) U_\nu(\theta) \quad (\text{C.16})$$

where

$$U_\nu(\theta) = \frac{\cosh(\nu(\pi - |\theta|))}{\sinh(\pi\nu)} + c(\nu)e^{\nu\theta} - c(-\nu)e^{-\nu\theta} \quad (\text{C.17})$$

$D_2(r, r', \theta, Q)$ still satisfies eq. (C.11) since, as noted above, the functions $K_{i\nu}(mr)e^{\pm\nu\theta}$ are in the kernel of $-\partial_2^2 + m^2$. It remains to find $c(\nu)$ such that the propagator (C.16) obeys boundary conditions (4.42). After a few manipulations one arrives at,

$$U_\nu(\theta) = \frac{e^{-2\pi i Q \text{sgn}(\theta)} \sinh(\nu|\theta|) + \sinh(\nu(2\pi - |\theta|))}{\cosh(2\pi\nu) - \cos(2\pi Q)} \quad (\text{C.18})$$

Next, one uses the identity,

$$\sinh(\pi\nu)K_{i\nu}(mr)K_{i\nu}(mr') = \frac{\pi}{2} \int_{\xi_2}^{\infty} du J_0(m(2rr')^{\frac{1}{2}}(\cosh(u) - \cosh \xi_2)^{\frac{1}{2}}) \sin(\nu u) \quad (\text{C.19})$$

where $\xi_2 > 0$ is defined by,

$$\cosh \xi_2 = \frac{r^2 + r'^2}{2rr'} \quad (\text{C.20})$$

Substituting this into (C.16),

$$D_2(r, r', \theta, Q) = \frac{1}{2\pi} \int_{\xi_2}^{\infty} du J_0(m(2rr')^{\frac{1}{2}}(\cosh(u) - \cosh \xi_2)^{\frac{1}{2}}) \int_0^{\infty} d\nu U_\nu(\theta) \sin(\nu u) \quad (\text{C.21})$$

We are mostly interested in the propagator with $r = r'$,

$$D_2(r = r', \theta, Q) = \frac{1}{2\pi} \int_0^{\infty} du J_0(mr\sqrt{2}(\cosh u - 1)^{\frac{1}{2}}) \int_0^{\infty} d\nu U_\nu(\theta) \sin(\nu u) \quad (\text{C.22})$$

In principle, it is possible to perform the integral over ν analytically in (C.21) (see Ref. [152]). This, however, will not be very beneficial for our purposes. Instead, let's proceed directly to the three-dimensional massless propagator, obtained by integrating over the mass parameter of the two dimensional propagator (4.61),

$$D(r, \theta) = \frac{1}{2\pi^2 r \sqrt{2}} \int_0^{\infty} du \frac{1}{(\cosh u - 1)^{\frac{1}{2}}} \int_0^{\infty} d\nu U_\nu(\theta) \sin(\nu u) \quad (\text{C.23})$$

where we have computed only the 3 dimensional propagator with $r = r'$, $\tau = \tau'$.

Now, performing the integral over u ,

$$D(r, \theta) = \frac{1}{4\pi r} \int_0^\infty d\nu \tanh(\pi\nu) U_\nu(\theta) \quad (\text{C.24})$$

To find the electric field we again use eq. (4.78),

$$\begin{aligned} -i\partial_\theta D(r, \theta) &= -\frac{1}{4\pi r} \int_0^\infty d\nu \nu \tanh(\pi\nu) \left(\frac{\sin(2\pi Q) \cosh(\nu\theta)}{\cosh(2\pi\nu) - \cos(2\pi Q)} \right. \\ &\quad \left. + i\text{sgn}(\theta) \frac{(\cos(2\pi Q) \cosh(\nu\theta) - \cosh(\nu(2\pi - |\theta|)))}{\cosh(2\pi\nu) - \cos(2\pi Q)} \right) \end{aligned} \quad (\text{C.25})$$

Again, the real part of $-i\partial_\theta D(r, \theta)$ has a well-defined limit as $\theta \rightarrow 0$, while the imaginary part is antisymmetric under $\theta \rightarrow -\theta$ and diverges as $\theta \rightarrow 0$. So the “symmetrized” limit is given by,

$$-i\partial_\theta D(r, \theta = 0) = -\frac{1}{4\pi r} \int_0^\infty d\nu \nu \frac{\sin(2\pi Q) \tanh(\pi\nu)}{\cosh(2\pi\nu) - \cos(2\pi Q)} = -\frac{1}{32\pi r} (2|Q| - 1)^2 \tan(\pi Q) \quad (\text{C.26})$$

in agreement with an earlier computation (C.8) based on spectral decomposition.

Thus, $C(Q)$ is again given by expression (4.79).

Now we generalize the above derivation of the twisted propagator to the strongly interacting $M = \infty$ theory. The strongly interacting theory differs from the free theory by the additional space-varying potential $\langle i\lambda(\vec{x}, \tau) \rangle$, so that the propagator satisfies,

$$\left(-\partial^2 + \frac{a(Q)}{|\vec{x}|^2} \right) D(x, x', Q) = \delta(x - x') \quad (\text{C.27})$$

We again rewrite $D(x, x', Q)$ in terms of the two dimensional massive propagator $D_2(\vec{x}, \vec{x}', m^2, Q)$ as in eq. (4.61). The two dimensional propagator satisfies,

$$\left(-\frac{1}{r} \frac{\partial}{\partial r} \left(r \frac{\partial}{\partial r} \right) - \frac{1}{r^2} \frac{\partial^2}{\partial \theta^2} + \frac{a}{r^2} + m^2 \right) D_2(r, r', \theta, \theta') = \delta(\vec{x} - \vec{x}') \quad (\text{C.28})$$

We need to generalize the two-dimensional, massive, twisted, free propagator (C.16) so that it obeys the above equation. We observe that the function $U_\nu(\theta)$ (C.17), (C.18) satisfies,

$$\frac{\partial^2 U_\nu}{\partial \theta^2} = \nu^2 U_\nu(\theta) - 2\nu \delta(\theta) \quad (\text{C.29})$$

Now combining eqs. (C.13), (C.14) and (C.29), we find that,

$$D_2(r, r', \theta, Q) = \frac{1}{\pi^2} \int_0^\infty d\nu K_{i\nu}(mr) K_{i\nu}(mr') \sinh(\pi\nu) \frac{\nu}{\sqrt{\nu^2 + a}} U_{\sqrt{\nu^2 + a}}(\theta) \quad (\text{C.30})$$

satisfies (C.28) as needed. Proceeding as above from two to three dimensional propagator, and setting $r = r'$, $\tau = \tau'$

$$D(r, \theta) = \frac{1}{4\pi r} \int_0^\infty d\nu \tanh(\pi\nu) \frac{\nu}{\sqrt{\nu^2 + a}} U_{\sqrt{\nu^2 + a}}(\theta) \quad (\text{C.31})$$

Appendix D

Appendix to Chapter 5

D.1 Eigenfunctions of Bogoliubov quasiparticles

First, we define for fixed energy λ ,

$$\begin{pmatrix} u \\ v \end{pmatrix} = \frac{1}{\sqrt{2\lambda}} \begin{pmatrix} -\sqrt{1+\lambda} \\ \sqrt{1-\lambda} \end{pmatrix} \quad (\text{D.1})$$

Now, the eigenstates can be expressed as,

Normalizable solution:

$$\begin{aligned} \lambda &= \frac{1}{\sqrt{2}} |\sin k_y|, \quad -\pi/2 < k_y < \pi/2 \\ \phi(j_x) &= c_1 \begin{pmatrix} u \\ v \end{pmatrix} e^{-s_1 j_x} + c_2 \begin{pmatrix} -u \\ v \end{pmatrix} (-1)^{j_x} e^{-s_2 j_x} \\ e^{s_1} &= (\sqrt{2} + 1)(\sqrt{1 + \cos^2 k_y} - \cos k_y) \\ e^{s_2} &= (\sqrt{2} + 1)(\sqrt{1 + \cos^2 k_y} + \cos k_y) \end{aligned}$$

$$\begin{pmatrix} c_1 \\ c_2 \end{pmatrix} = \frac{2^{-\frac{3}{4}}(\sqrt{2}-1)|\sin k_y|}{\sqrt{1-|\sin k_y|}\sqrt{1+\cos^2 k_y}} \begin{pmatrix} e^{s_2}\sqrt{1-\lambda}-\sqrt{1+\lambda} \\ e^{s_1}\sqrt{1-\lambda}-\sqrt{1+\lambda} \end{pmatrix} \quad (\text{D.2})$$

Continuum solutions:

$$\gamma = \frac{1}{2}(\cos(k_x) + \cos(k_y)), \quad \lambda = \sqrt{1-\gamma^2}, \quad 0 < k_x < \pi - |k_y|, \quad -\pi/2 < k_y < \pi/2 \quad (\text{D.3})$$

Branch 1: $0 < k_x < \cos^{-1}(1 - 2 \cos k_y)$

$$\begin{aligned} \phi(j_x) &= \frac{1}{|\alpha|} \begin{pmatrix} (\alpha e^{ik_x j_x} + \alpha^* e^{-ik_x j_x} - (-1)^{j_x} e^{-s j_x}) u \\ (\alpha e^{ik_x j_x} + \alpha^* e^{-ik_x j_x} + (-1)^{j_x} e^{-s j_x}) v \end{pmatrix} \\ s &= \cosh^{-1}(\cos k_x + 2 \cos k_y) \\ \alpha &= -\frac{1}{2\lambda} \left(\gamma e^s - 1 - \frac{i}{\sin k_x} ((\gamma \cos k_x - 1)e^s + \gamma - \cos k_x) \right) \end{aligned} \quad (\text{D.4})$$

Branch 2: $\cos^{-1}(1 - 2 \cos k_y) < k_x < \pi - |k_y|$

$$\begin{aligned} \tilde{k}_x &= \pi - \cos^{-1}(\cos(k_x) + 2 \cos(k_y)), \quad \pi - |k_y| < \tilde{k}_x < \pi \\ \phi_1(j_x) &= A \left(c_{11} \cos(k_x(j_x + 1/2)) \begin{pmatrix} u \\ v \end{pmatrix} + c_{12} \cos(\tilde{k}_x(j_x + 1/2)) \begin{pmatrix} -u \\ v \end{pmatrix} \right) \\ \phi_2(j_x) &= A \left(c_{21} \sin(k_x(j_x + 1/2)) \begin{pmatrix} u \\ v \end{pmatrix} + c_{22} \sin(\tilde{k}_x(j_x + 1/2)) \begin{pmatrix} -u \\ v \end{pmatrix} \right) \\ A &= (\sin k_x)^{\frac{1}{2}} (\sin((k_x + \tilde{k}_x)/2) + \gamma \sin((k_x - \tilde{k}_x)/2))^{-\frac{1}{2}} \\ c_{11} &= (1 + \gamma)^{\frac{1}{2}} \left(\frac{2 \cos \tilde{k}_x/2}{\cos k_x/2} \right)^{\frac{1}{2}}, \quad c_{12} = (1 - \gamma)^{\frac{1}{2}} \left(\frac{2 \cos k_x/2}{\cos \tilde{k}_x/2} \right)^{\frac{1}{2}} \\ c_{21} &= (1 - \gamma)^{\frac{1}{2}} \left(\frac{2 \sin \tilde{k}_x/2}{\sin k_x/2} \right)^{\frac{1}{2}}, \quad c_{22} = (1 + \gamma)^{\frac{1}{2}} \left(\frac{2 \sin k_x/2}{\sin \tilde{k}_x/2} \right)^{\frac{1}{2}} \end{aligned} \quad (\text{D.5})$$

The division of the continuum spectrum into two branches is clear when we look at a plot of $\lambda(k_x)$ (D.3) for k_y fixed. For $\sqrt{1 - \cos^4(k_y/2)} < \lambda < \sqrt{1 - \sin^4(k_y/2)}$ there is only one corresponding value of k_x in the range $0 < k_x < \pi$ (there is always a solution with opposite k_x , as well). This is our branch 1. On the other hand, for $\sqrt{1 - \sin^4(k_y/2)} < \lambda < 1$ there are two solutions with $0 < k_x < \pi$, which we label by k_x and \tilde{k}_x . These two solutions are mixed by the edge and form the two linearly independent eigenstates ϕ_1, ϕ_2 in branch 2.

Appendix E

Appendix to Chapter 6

E.1 Decoupling of non-collinear momenta

In this section we will argue that the fluctuations of the order parameter at non-collinear momenta effectively decouple. We focus for simplicity on the case of an Ising-nematic transition. We follow the standard Hertz approach, integrating out the fermions to obtain an effective action for ϕ ,

$$S[\phi] = \sum_{n=2}^{\infty} \frac{1}{n!} \int d^D x_1 \dots d^D x_n \Gamma^n(x_1, x_2, \dots, x_n) \phi(x_1) \phi(x_2) \dots \phi(x_n) \quad (\text{E.1})$$

The n -point effective vertex Γ^n is given by,

$$\Gamma^n(q_1, q_2, \dots, q_n) = \frac{N}{n} f^n(q_1, q_2, \dots, q_n) + \text{permutations of } q_1, q_2, \dots, q_n \quad (\text{E.2})$$

with

$$f^n(q_1, q_2, \dots, q_n) = \int \frac{dk_\tau d^2 k}{(2\pi)^3} \prod_{i=0}^{n-1} \left[G(k + l_i) d_{\vec{k} + \frac{\vec{l}_i + \vec{l}_{i+1}}{2}} \right] \quad (\text{E.3})$$

where $l_i = \sum_{j=1}^i q_j$. For now we work with “undressed” propagators,

$$G(\omega, \vec{k}) = \frac{1}{-i\omega + v_F(\theta)k} \quad (\text{E.4})$$

with k - the distance to the Fermi surface and $v_F(\theta)$ - the local Fermi velocity. As is well-known, for $\omega \ll v_F|\vec{q}|$ and $|\vec{q}| \ll k_F$ the two-point vertex has a Landau-damped form,

$$\Gamma^2(\omega, \vec{q}) = N \left[\gamma(\hat{q}) \frac{|\omega|}{|\vec{q}|} + \frac{\vec{q}^2}{e^2} + r \right] \quad (\text{E.5})$$

where the coefficient of the non-analytic term $\gamma(\hat{q}) = Kd^2/(2\pi v_F^2)$ with the Fermi-surface curvature radius K , Fermi-velocity v_F and form-factor d evaluated at the point on the Fermi surface to which \vec{q} is tangent. On the other hand, the coefficients of the analytic terms r and $1/e^2$ come from the entire Fermi-surface.

If we truncate the series (E.1) at the quadratic order,

$$S_2 = \frac{N}{2} \int \frac{d\omega d^2\vec{q}}{(2\pi)^3} \left[\gamma(\hat{q}) \frac{|\omega|}{|\vec{q}|} + \frac{\vec{q}^2}{e^2} + r \right] |\phi(\vec{q}, \omega)|^2 \quad (\text{E.6})$$

then at the critical point $r = 0$ the action (E.6) is invariant under the scale transformation,

$$\phi(\vec{x}, \tau) \rightarrow s^{3/2} \phi(s\vec{x}, s^3\tau) \quad (\text{E.7})$$

Note that here, in contrast to Eq. (6.14), all components of \vec{q} are scaled in the same way as we are not studying the effects of fluctuations with collinear wave-vectors. We can regard the terms in Eq. (E.1) with $n > 2$ as perturbations to the Hertz action (E.6). Hertz noted that if the effective vertices Γ^n possess a regular expansion in frequencies and momenta, such that the corresponding operators can be represented as polynomials in the order parameter ϕ and its derivatives, then the perturbations with $n > 2$ are irrelevant due to the large effective dimensionality, $D_{eff} = d + z = 5$, with $d = 2$ - spatial dimension and $z = 3$ - the dynamical critical exponent. Indeed, the perturbation $\int d^2\vec{x} d\tau \phi^n(x)$ scales as $s^{3n/2-5}$ under (E.7) (in the special case $n = 3$,

the operator ϕ^3 is actually prohibited by the 90° lattice rotation symmetry. The lowest dimension local operators with three powers of ϕ that are allowed by symmetry are $\phi((\partial_x\phi)^2 - (\partial_y\phi)^2)$ in the $d_{x^2-y^2}$ case and $\phi\partial_x\phi\partial_y\phi$ in the d_{xy} case, which scale as $s^{3/2}$).

However, due to the presence of low-energy excitations on the Fermi-surface there is no reason to expect that the effective vertices Γ^n would possess a regular expansion in momenta. Indeed, we have already seen that the two-point vertex has the non-analytic Landau-damped form (E.5). As we now show, similar non-analyticities occur in the higher order vertices.

Let us estimate the vertices (E.2) when the external frequencies and momenta obey the Hertz scaling (E.7), $\omega \sim |\vec{q}|^3$, $\vec{q} \rightarrow 0$. In this regime,

$$f^n(q_1, q_2, \dots, q_n) = \int \frac{dk_\tau dk d\theta}{(2\pi)^3} \left| \frac{d\vec{k}_F}{d\theta} \right| d(\theta)^n \prod_{i=0}^{n-1} \frac{1}{-i(k_\tau + l_{i\tau}) + v_F(\theta)(k + \hat{v}_F(\theta) \cdot \vec{l}_i)} \quad (\text{E.8})$$

Let us perform the integral over k . Observe that if $|k_\tau| > \Omega$, with $\Omega = \max_i |l_{i\tau}|$ then the integral vanishes as all the poles of the integrand are in the same half-plane. Thus, the range of the internal frequency is limited by the external ones. With this in mind,

$$f^n(q_1, q_2, \dots, q_n) = i \int_{|k_\tau| < \Omega} \frac{dk_\tau}{2\pi} \int \frac{d\theta}{2\pi} \left| \frac{d\vec{k}_F}{d\theta} \right| \frac{d(\theta)^n}{v_F(\theta)} \times \sum_{j=0}^{n-1} \vartheta(k_\tau + l_{j\tau}) \prod_{i=0, i \neq j}^{n-1} \frac{1}{-i(l_{i\tau} - l_{j\tau}) + \hat{v}_F(\theta) \cdot (\vec{l}_i - \vec{l}_j)}, \quad (\text{E.9})$$

where we have used the symbol ϑ for the step function, to avoid confusion with the angular variable θ . Now, since $q_\tau \sim |\vec{q}|^3/(\gamma e^2) \ll v_F|\vec{q}|$, for general θ we can ignore the

frequency dependence in the denominator of Eq. (E.9). Then the angular integration yields a factor of $\mathcal{O}(1)$ and the integral over k_τ yields a factor of external frequency, so that

$$\Gamma^n(q_1, q_2, \dots, q_n) \sim \frac{q_\tau}{|\vec{q}|^{n-1}} \quad (\text{E.10})$$

Note that the momentum dependence in Eq. (E.10) is far from analytic. Also, note that for $n = 2$ the result is consistent with the standard Landau damping.

The only possible caveat to the estimate (E.10) is associated with regions of angular integration where $\hat{v}_F(\theta) \cdot (\vec{l}_i - \vec{l}_j) \rightarrow 0$, i.e some combination of external momenta becomes tangent to the Fermi surface. Then the angular integration acquires poles just off the real axis, with the imaginary parts of the poles provided by the frequency dependence in the denominator of Eq. (E.9). As long as the real parts of the poles do not coalesce, i.e no two momenta $\vec{l}_i - \vec{l}_j$ and $\vec{l}_{i'} - \vec{l}_j$ are collinear, the angular integration still yields a factor of $\mathcal{O}(1)$ and the estimate (E.10) remains correct. This is the regime that we are considering in the present appendix. The rest of the paper is devoted to the opposite limit, where all the external momenta are nearly collinear and the angular integral in Eq. (E.9) is dominated by the vicinity of two antipodal points on the Fermi surface to which the external momenta are tangent. This observation motivates the introduction of the two patch theory in Section 6.2 and all the subsequent development of the present work.

Returning to the non-collinear regime, upon combining Eq. (E.10) with the Hertz scaling (E.7), we conclude that the n -th term in the series (E.1) scales as $s^{n/2-1}$. Therefore, all terms with $n > 2$ represent non-local *irrelevant* perturbations, which confirms that the fluctuations with non-collinear momenta decouple.

We would like to point out that the argument above still holds if one dresses the fermion propagator by the one-loop self-energy, $\Sigma(\omega, k) \sim -i \text{sgn} \omega |\omega|^{2/3}$. This modifies the frequency dependence in the denominator of Eq. (E.9) via, $-i(l_{i\tau} - l_{j\tau}) \rightarrow \Sigma(k_\tau + l_{i\tau}) - \Sigma(k_\tau + l_{j\tau})$. However, since $\Sigma(\omega) \ll v_F |\vec{q}|$ for typical $\omega \sim |\vec{q}|^3$, the estimate (E.10) is still correct.

E.2 Computations of Feynman diagrams

Here we provide some details of the computations of the diagrams in Section 6.5.

E.2.1 Boson self-energy

We begin by evaluating the two-loop polarization correction in Fig. 6.4,

$$\delta^2 \Pi(q) = N \sum_s \int \frac{dp_\tau d^2 p}{(2\pi)^3} \frac{dl_\tau d^2 l}{(2\pi)^3} D(l) G_s(p) G_s(p+q) G_s(p-l) G_s(p+q-l) \quad (\text{E.11})$$

The contributions to the integral from the two patches are equal. Thus, integrating over p_x, l_x we obtain,

$$\begin{aligned} \delta^2 \Pi(q) &= 2N \int \frac{dp_\tau dp_y}{(2\pi)^2} \frac{dl_\tau dl_y}{(2\pi)^2} D(l) \frac{\theta(p_\tau) - \theta(p_\tau + q_\tau)}{\frac{ic_f}{N}(\{p\} - \{p+q\}) + 2q_y p_y + q_x + q_y^2} \\ &\times \frac{\theta(l_\tau - p_\tau) - \theta(l_\tau - p_\tau - q_\tau)}{\frac{ic_f}{N}(\{l-p-q\} - \{l-p\}) + 2q_y(p_y - l_y) + q_x + q_y^2} \end{aligned} \quad (\text{E.12})$$

where here and below we use the notation $\{p\} = \text{sgn}(p_\tau) |p_\tau|^{2/3}$. We observe that the poles of the p_y integral are always in the same half-plane. Thus, $\delta^2 \Pi(q) = 0$. This is consistent with Ref. [205], which found that the two loop corrections to Eq. 6.10 are suppressed by factors of $|\omega|^{2/3}$ or $|\omega|/|q_y| \sim |\omega|^{2/3}$.

Now, let us proceed to compute the Aslamazov-Larkin diagrams, Fig. 6.6. We begin by evaluating the three point-function $f_s(q, l, -(l+q))$ in Eq. (6.81). Note that $f_-(q, l, -(l+q)) = f_+(P_x q, P_x l, -P_x(l+q))$ where $P_x(k_0, k_x, k_y) = (k_0, -k_x, k_y)$. The calculation of f is simplified when $q_\tau = 0$. Then, performing the integral over p_x and, subsequently, p_y , in Eq. (6.81),

$$\begin{aligned}
f_+(q, l, -(l+q)) &\stackrel{q_\tau=0}{=} \int \frac{dp_\tau dp_y}{(2\pi)^2} \frac{i(\theta(p_\tau + l_\tau) - \theta(p_\tau))}{\frac{ic_f}{N}(\{p+l\} - \{p\}) - l_x - 2l_y p_y - l_y^2} \\
&\times \frac{1}{\frac{ic_f}{N}(\{p+l\} - \{p\}) - q_x - l_x - 2(q_y + l_y)p_y + q_y^2 - l_y^2} \\
&= \frac{1}{2q_y} \int \frac{dp_\tau}{2\pi} \frac{|\theta(p_\tau + l_\tau) - \theta(p_\tau)|(\theta(l_y) - \theta(q_y + l_y))}{\frac{-ic_f}{N}(\{p+l\} - \{p\}) + l_x - \frac{q_x}{q_y}l_y + l_y(q_y + l_y)}
\end{aligned} \tag{E.13}$$

Thus,

$$\begin{aligned}
\delta^3 \Pi(q_\tau = 0, \vec{q}) &= \frac{\lambda_+ \lambda_- N^2}{4q_y^2} \int \frac{dl_\tau d^2 \vec{l}}{(2\pi)^3} \frac{dp_\tau}{2\pi} \frac{dp'_\tau}{2\pi} D(l) D(l+q) \\
&\times \frac{|\theta(p_\tau + l_\tau) - \theta(p_\tau)| |\theta(p'_\tau + l_\tau) - \theta(p'_\tau)| |\theta(l_y) - \theta(l_y + q_y)|}{\frac{-ic_f}{N}(\{p+l\} - \{p\}) + l_x - \frac{q_x}{q_y}l_y + l_y(q_y + l_y)} \\
&\times \left(\frac{1}{\frac{-ic_f}{N}(\{p'+l\} - \{p'\}) - l_x + \frac{q_x}{q_y}l_y - l_y(q_y + l_y)} \right. \\
&\left. - \frac{1}{\frac{-ic_f}{N}(\{p'+l\} - \{p'\}) - l_x + \frac{q_x}{q_y}l_y + l_y(q_y + l_y)} \right) + (q \rightarrow -q)
\end{aligned} \tag{E.14}$$

Finally, integrating over l_x ,

$$\begin{aligned}
\delta^3\Pi(q_\tau = 0, \vec{q}) &= \frac{\lambda_+\lambda_-N^2}{4q_y^2} \int \frac{dl_\tau dl_y}{(2\pi)^2} \frac{dp_\tau}{2\pi} \frac{dp'_\tau}{2\pi} D(l)D(l+q) \\
&\times i\text{sgn}(l_\tau)|\theta(p_\tau+l_\tau)-\theta(p_\tau)||\theta(p'_\tau+l_\tau)-\theta(p'_\tau)||\theta(l_y)-\theta(l_y+q_y)| \\
&\times \left(\frac{1}{\frac{-ic_f}{N}(\{p+l\}-\{p\}+\{p'+l\}-\{p'\})} \right. \\
&\left. - \frac{1}{\frac{-ic_f}{N}(\{p+l\}-\{p\}+\{p'+l\}-\{p'\})+2l_y(q_y+l_y)} \right) + (q \rightarrow -q)
\end{aligned} \tag{E.15}$$

The integral is invariant under $q \rightarrow -q$. Moreover, the integrals in the regions $l_0 > 0$ and $l_0 < 0$ are related by complex conjugation. Thus,

$$\begin{aligned}
\delta^3\Pi(q_\tau = 0, \vec{q}) &= -\frac{\lambda_+\lambda_-N}{q_y^2} \int_0^\infty \frac{dl_\tau}{2\pi} \int_0^{l_\tau} \frac{dp_\tau}{2\pi} \int_0^{l_\tau} \frac{dp'_\tau}{2\pi} \int_0^{|q_y|} \frac{dl_y}{2\pi} \\
&\frac{1}{c_b \frac{l_\tau}{l_y} + \frac{l_y^2}{e^2}} \frac{1}{c_b \frac{l_\tau}{|q_y|-l_y} + \frac{(|q_y|-l_y)^2}{e^2}} \\
&\times \left(\frac{1}{c_f((l-p)_\tau^{2/3} + p_\tau^{2/3} + (l-p')_\tau^{2/3} + p_\tau'^{2/3})} \right. \\
&\left. - \frac{c_f((l-p)_\tau^{2/3} + p_\tau^{2/3} + (l-p')_\tau^{2/3} + p_\tau'^{2/3})}{c_f^2((l-p)_\tau^{2/3} + p_\tau^{2/3} + (l-p')_\tau^{2/3} + p_\tau'^{2/3})^2 + 4N^2l_y^2(|q_y|-l_y)^2} \right)
\end{aligned}$$

Notice that the integral over l_y is bounded by the external momentum q_y . This leads to a violation of the naive power counting, which would predict that each diagram in Fig. 6.6 has a superficial degree of divergence $\Lambda_y^2 \sim \Lambda_\tau^{2/3}$. Instead, we find that for $l_\tau \rightarrow \infty$, the two diagrams behave as,

$$\delta^{3a}\Pi(0, \vec{q}) = -\delta^{3b}\Pi(0, \vec{q}) \sim -\lambda_+\lambda_-N|q_y| \left(\frac{\Lambda_\tau}{e^4} \right)^{1/3} \tag{E.16}$$

(In reality, the divergence is cut once we exit the two patch regime where the momentum $l_x \ll l_y$. This occurs when $l_x \sim l_\tau^{2/3}$ becomes of order l_y . However, for

the Aslamazov-Larkin diagrams the internal momentum l_y is controlled by external momentum q_y . Hence, $\Lambda_\tau \sim q_y^{3/2}$ and $\delta^{3a}\Pi = -\delta^{3b}\Pi \sim q_y^{3/2}$, as found in Ref. [186]).

However, as expected for problems involving a boson field coupled to the charge sector of the Fermi-surface, the divergence cancels when we add the two diagrams. In fact, for $N \gg 1$, the divergence is cut-off at $\frac{c_f}{N}l_\tau^{2/3} \sim q_y^2$, *i.e.*

$$l_\tau \sim N^{3/2}q_y^3/e^2 \quad (\text{E.17})$$

so that

$$\delta^3\Pi(0, \vec{q}) \sim -\lambda_+\lambda_-N^{3/2}\frac{q_y^2}{e^2} \quad (\text{E.18})$$

Note that the result is parameterically larger in the large- N limit than the bare boson polarization, Eq. (6.7) (although it has the same scaling as the bare term). Also observe that the sign of the contribution (E.18) is positive for the spin-liquid and negative for the Ising-nematic transition.

One may ask whether the enhancement in (E.18) is an artifact of taking $q_\tau = 0$. However, since the integral in Eq. (E.18) is saturated in the region (E.17), we expect the result (E.18) to be valid for, $q_\tau \ll N^{3/2}q_y^3/e^2$, which is certainly satisfied by the typical bosonic momenta $q_\tau \sim q_y^3/e^2$.

We can compute the proportionality factor in Eq. (E.18) in the large- N limit. Changing variables to $l_\tau = \left(\frac{N}{c_f}\right)^{3/2} |q_y|^3 \bar{l}_\tau$, $p_\tau = l_\tau x$, $p'_\tau = l_\tau x'$, $l_y = |q_y|y$,

$$\delta^3\Pi(0, \vec{q}) = C\lambda_+\lambda_-\frac{q_y^2}{e^2} \quad (\text{E.19})$$

$$C = \frac{2^{5/2}3^{3/4}N^{3/2}}{\pi} \frac{\int_0^\infty d\bar{l}_\tau \int_0^1 dx \int_0^1 dx' \int_0^1 dy}{\bar{l}_\tau^{4/3} y^3 (1-y)^3} \frac{1}{(\bar{l}_\tau + \left(\frac{2}{N\sqrt{3}}\right)^{3/2} y^3)(\bar{l}_\tau + \left(\frac{2}{N\sqrt{3}}\right)^{3/2} (1-y)^3) A(A^2\bar{l}_\tau^{4/3} + 4y^2(1-y)^2)}$$

with,

$$A = x^{2/3} + (1-x)^{2/3} + x'^{2/3} + (1-x')^{2/3} \quad (\text{E.20})$$

For $N \gg 1$, the integral over \bar{l}_τ is saturated in the region $\bar{l}_\tau \sim 1$, so,

$$C \approx -\frac{2^{5/2}3^{3/4}N^{3/2}}{\pi} \int_0^\infty \frac{d\bar{l}_\tau}{\bar{l}_\tau^{2/3}} \int_0^1 dx \int_0^1 dx' \int_0^1 dy \frac{y^3(1-y)^3}{A(A^2\bar{l}_\tau^{4/3} + 4y^2(1-y)^2)} \quad (\text{E.21})$$

After a change of variables, $z = A\bar{l}_\tau^{2/3}/(2y(1-y))$,

$$\begin{aligned} C &\approx -\frac{3^{7/4}N^{3/2}}{\pi} \int_0^\infty \frac{dz}{z^{1/2}(z^2+1)} \int_0^1 dy y^{3/2}(1-y)^{3/2} \int_0^1 dx \int_0^1 dx' \frac{1}{A^{3/2}} \\ &= \frac{3^{11/4}\pi N^{3/2}}{2^{15/2}} \int_0^1 dx \int_0^1 dx' \frac{1}{A^{3/2}} \end{aligned} \quad (\text{E.22})$$

The integral over x, x' can be evaluated numerically,

$$\int_0^1 dx \int_0^1 dx' \frac{1}{A^{3/2}} = 0.269653 \quad (\text{E.23})$$

so that

$$C \approx -0.09601N^{3/2}, \quad N \rightarrow \infty \quad (\text{E.24})$$

We may also compute the constant C in Eq. (E.19) for the physical value $N = 2$,

$$C \approx -0.04455 \quad (\text{E.25})$$

E.2.2 Fermion self-energy

We next compute the three loop corrections to the fermion self-energy in diagrams Fig. 6.10 b), c):

$$\begin{aligned} \delta^{3b}\Sigma(p_\tau = 0, \vec{p}) &= N\lambda_+^3\lambda_-^3 \int \frac{dk_\tau d^2k}{(2\pi)^3} \frac{dl_{1\tau} d^2l_1}{(2\pi)^3} \frac{dl_{2\tau} d^2l_2}{(2\pi)^3} G_+(p-l_1)G_+(p-l_2)G_-(k) \\ &\times G_-(k+l_1)G_-(k+l_2)D(l_1)D(l_2)D(l_1-l_2) \end{aligned} \quad (\text{E.26})$$

$$\begin{aligned}
\delta^{3c}\Sigma(p_\tau = 0, \vec{p}) &= N\lambda_+^3\lambda_-^3 \int \frac{dk_\tau d^2k}{(2\pi)^3} \frac{dl_{1\tau} d^2l_1}{(2\pi)^3} \frac{dl_{2\tau} d^2l_2}{(2\pi)^3} G_+(p+l_1)G_+(p+l_2)G_-(k) \\
&\times G_-(k+l_1)G_-(k+l_2)D(l_1)D(l_2)D(l_1-l_2) \quad (\text{E.27})
\end{aligned}$$

Integrating over l_{1x} and l_{2x} we obtain,

$$\begin{aligned}
\delta^{3b}\Sigma(p_\tau = 0, \vec{p}) &= -N\lambda_+\lambda_- \int \frac{dk_\tau d^2k}{(2\pi)^3} \frac{dl_{1\tau} dl_{1y}}{(2\pi)^2} \frac{dl_{2\tau} dl_{2y}}{(2\pi)^2} D(l_1)D(l_2)D(l_1-l_2) \\
&\times \frac{1}{-\frac{ic_f}{N}k_\tau^{2/3} + \delta_k^-} \frac{\theta(l_{1\tau} + k_\tau) - \theta(-l_{1\tau})}{-\frac{ic_f}{N}((l_1+k)_\tau^{2/3} + l_{1\tau}^{2/3}) + \delta_k^- + 2(k+p)_y l_{1y} - \delta_p^+} \\
&\times \frac{\theta(l_{2\tau} + k_\tau) - \theta(-l_{2\tau})}{-\frac{ic_f}{N}((l_2+k)_\tau^{2/3} + l_{2\tau}^{2/3}) + \delta_k^- + 2(k+p)_y l_{2y} - \delta_p^+} \quad (\text{E.28})
\end{aligned}$$

$$\begin{aligned}
\delta^{3e}\Sigma(p_\tau = 0, \vec{p}) &= -N\lambda_+\lambda_- \int \frac{dk_\tau d^2k}{(2\pi)^3} \frac{dl_{1\tau} dl_{1y}}{(2\pi)^2} \frac{dl_{2\tau} dl_{2y}}{(2\pi)^2} \\
&D(l_1)D(l_2)D(l_1-l_2) \frac{1}{-\frac{ic_f}{N}k_\tau^{2/3} + \delta_k^-} \\
&\times \frac{\theta(l_{1\tau} + k_\tau) - \theta(-l_{1\tau})}{-\frac{ic_f}{N}((l_1+k)_\tau^{2/3} + l_{1\tau}^{2/3}) + \delta_k^- + 2(k+p)_y l_{1y} + 2l_{1y}^2 + \delta_p^+} \\
&\times \frac{\theta(l_{2\tau} + k_\tau) - \theta(-l_{2\tau})}{-\frac{ic_f}{N}((l_2+k)_\tau^{2/3} + l_{2\tau}^{2/3}) + \delta_k^- + 2(k+p)_y l_{2y} + 2l_{2y}^2 + \delta_p^+} \quad (\text{E.29})
\end{aligned}$$

where $\delta_p^\pm = \pm p_x + p_y^2$. Note the cancellation of the fermi-surface curvature terms $l_{1y,2y}^2$ in the ‘‘planar graph’’ $\delta^{3b}\Sigma$.

We can reduce the integration range to $k_\tau > 0$, as the region $k_\tau < 0$ is related by complex conjugation. There are then four different kinematic regimes: i) $l_{1\tau} > 0, l_{2\tau} > 0$, ii) $l_{1\tau} < -k_\tau, l_{2\tau} > 0$, iii) $l_{1\tau} > 0, l_{2\tau} < -k_\tau$, iv) $l_{1\tau} < -k_\tau, l_{2\tau} < -k_\tau$. The integral over k_x in the regime i) vanishes as all the poles are in the same half-

plane. The regimes ii) and iii) are related by $l_1 \leftrightarrow l_2$. Thus,

$$\begin{aligned}
\delta^{3b}\Sigma(p_\tau = 0, \vec{p}) &= -N\lambda_+\lambda_- \left[-2 \int_0^\infty \frac{dk_\tau}{2\pi} \int \frac{d^2k}{(2\pi)^2} \int_{k_\tau}^\infty \frac{dl_{1\tau}}{2\pi} \int_0^\infty \frac{dl_{2\tau}}{2\pi} \int \frac{dl_{1y}dl_{2y}}{(2\pi)^2} \right. \\
&\quad D(l_1)D(l_2)D(l_{1\tau} + l_{2\tau}, l_{1y} - l_{2y}) \frac{1}{-\frac{ic_f}{N}k_\tau^{2/3} + \delta_k^-} \\
&\quad \times \frac{1}{\frac{ic_f}{N}((l_1 - k)_\tau^{2/3} + l_{1\tau}^{2/3}) + \delta_k^- + 2(k+p)_yl_{1y} - \delta_p^+} \\
&\quad \times \frac{1}{-\frac{ic_f}{N}((l_2 + k)_\tau^{2/3} + l_{2\tau}^{2/3}) + \delta_k^- + 2(k+p)_yl_{2y} - \delta_p^+} \\
&\quad + \int_0^\infty \frac{dk_\tau}{2\pi} \int \frac{d^2k}{(2\pi)^2} \int_{k_\tau}^\infty \frac{dl_{1\tau}}{2\pi} \int_{k_\tau}^\infty \frac{dl_{2\tau}}{2\pi} \int \frac{dl_{1y}dl_{2y}}{(2\pi)^2} \\
&\quad D(l_1)D(l_2)D(l_1 - l_2) \frac{1}{-\frac{ic_f}{N}k_\tau^{2/3} + \delta_k^-} \\
&\quad \times \frac{1}{\frac{ic_f}{N}((l_1 - k)_\tau^{2/3} + l_{1\tau}^{2/3}) + \delta_k^- + 2(k+p)_yl_{1y} - \delta_p^+} \\
&\quad \times \left. \frac{1}{\frac{ic_f}{N}((l_2 - k)_\tau^{2/3} + l_{2\tau}^{2/3}) + \delta_k^- + 2(k+p)_yl_{2y} - \delta_p^+} \right] + h.c. \quad (E.30)
\end{aligned}$$

$$\begin{aligned}
\delta^{3c}\Sigma(p_\tau = 0, \vec{p}) &= -N\lambda_+\lambda_- \left[-2 \int_0^\infty \frac{dk_\tau}{2\pi} \int \frac{d^2k}{(2\pi)^2} \int_{k_\tau}^\infty \frac{dl_{1\tau}}{2\pi} \int_0^\infty \frac{dl_{2\tau}}{2\pi} \int \frac{dl_{1y}dl_{2y}}{(2\pi)^2} \right. \\
&\quad D(l_1)D(l_2)D(l_{1\tau} + l_{2\tau}, l_{1y} - l_{2y}) \frac{1}{-\frac{ic_f}{N}k_\tau^{2/3} + \delta_k^-} \\
&\quad \times \frac{1}{\frac{ic_f}{N}((l_1 - k)_\tau^{2/3} + l_{1\tau}^{2/3}) + \delta_k^- + 2(k+p)_yl_{1y} + 2l_{1y}^2 + \delta_p^+} \\
&\quad \times \frac{1}{-\frac{ic_f}{N}((l_2 + k)_\tau^{2/3} + l_{2\tau}^{2/3}) + \delta_k^- + 2(k+p)_yl_{2y} + 2l_{2y}^2 + \delta_p^+} \\
&\quad + \int_0^\infty \frac{dk_\tau}{2\pi} \int \frac{d^2k}{(2\pi)^2} \int_{k_\tau}^\infty \frac{dl_{1\tau}}{2\pi} \int_{k_\tau}^\infty \frac{dl_{2\tau}}{2\pi} \int \frac{dl_{1y}dl_{2y}}{(2\pi)^2} \\
&\quad D(l_1)D(l_2)D(l_1 - l_2) \frac{1}{-\frac{ic_f}{N}k_\tau^{2/3} + \delta_k^-} \\
&\quad \times \frac{1}{\frac{ic_f}{N}((l_1 - k)_\tau^{2/3} + l_{1\tau}^{2/3}) + \delta_k^- + 2(k+p)_yl_{1y} + 2l_{1y}^2 + \delta_p^+} \\
&\quad \times \left. \frac{1}{\frac{ic_f}{N}((l_2 - k)_\tau^{2/3} + l_{2\tau}^{2/3}) + \delta_k^- + 2(k+p)_yl_{2y} + 2l_{2y}^2 + \delta_p^+} \right] + h.c. \quad (E.31)
\end{aligned}$$

Integrating over k_x and shifting $k_y \rightarrow k_y - p$,

$$\begin{aligned}
\delta^{3b}\Sigma(p_\tau = 0, \vec{p}) &= -N\lambda_+\lambda_- \left[2i \int_0^\infty \frac{dk_\tau}{2\pi} \int \frac{dk_y}{2\pi} \int_{k_\tau}^\infty \frac{dl_{1\tau}}{2\pi} \int_0^\infty \frac{dl_{2\tau}}{2\pi} \int \frac{dl_{1y}dl_{2y}}{(2\pi)^2} \right. \\
& D(l_1)D(l_2)D(l_{1\tau} + l_{2\tau}, l_{1y} - l_{2y}) \frac{1}{-\frac{ic_f}{N}(k_\tau^{2/3} + (l_1 - k)_\tau^{2/3} + l_{1\tau}^{2/3}) - 2k_y l_{1y} + \delta_p^+} \\
& \times \frac{1}{-\frac{ic_f}{N}((l_1 - k)_\tau^{2/3} + l_{1\tau}^{2/3} + (l_2 + k)_\tau^{2/3} + l_{2\tau}^{2/3}) + 2k_y(l_2 - l_1)_y} \\
& + i \int_0^\infty \frac{dk_\tau}{2\pi} \int \frac{dk_y}{2\pi} \int_{k_\tau}^\infty \frac{dl_{1\tau}}{2\pi} \int_{k_\tau}^\infty \frac{dl_{2\tau}}{2\pi} \int \frac{dl_{1y}dl_{2y}}{(2\pi)^2} D(l_1)D(l_2)D(l_1 - l_2) \\
& \times \frac{1}{\frac{ic_f}{N}(k_\tau^{2/3} + (l_1 - k)_\tau^{2/3} + l_{1\tau}^{2/3}) + 2k_y l_{1y} - \delta_p^+} \\
& \left. \times \frac{1}{\frac{ic_f}{N}(k_\tau^{2/3} + (l_2 - k)_\tau^{2/3} + l_{2\tau}^{2/3}) + 2k_y l_{2y} - \delta_p^+} \right] + h.c. \tag{E.32}
\end{aligned}$$

$$\begin{aligned}
\delta^{3c}\Sigma(p_\tau = 0, \vec{p}) &= -N\lambda_+\lambda_- \left[2i \int_0^\infty \frac{dk_\tau}{2\pi} \int \frac{dk_y}{2\pi} \int_{k_\tau}^\infty \frac{dl_{1\tau}}{2\pi} \int_0^\infty \frac{dl_{2\tau}}{2\pi} \int \frac{dl_{1y}dl_{2y}}{(2\pi)^2} \right. \\
& D(l_1)D(l_2)D(l_{1\tau} + l_{2\tau}, l_{1y} - l_{2y}) \\
& \times \frac{1}{-\frac{ic_f}{N}(k_\tau^{2/3} + (l_1 - k)_\tau^{2/3} + l_{1\tau}^{2/3}) - 2k_y l_{1y} - 2l_{1y}^2 - \delta_p^+} \\
& \times \frac{1}{-\frac{ic_f}{N}((l_1 - k)_\tau^{2/3} + l_{1\tau}^{2/3} + (l_2 + k)_\tau^{2/3} + l_{2\tau}^{2/3}) + 2k_y(l_2 - l_1)_y + 2(l_{2y}^2 - l_{1y}^2)} \\
& + i \int_0^\infty \frac{dk_\tau}{2\pi} \int \frac{dk_y}{2\pi} \int_{k_\tau}^\infty \frac{dl_{1\tau}}{2\pi} \int_{k_\tau}^\infty \frac{dl_{2\tau}}{2\pi} \int \frac{dl_{1y}dl_{2y}}{(2\pi)^2} D(l_1)D(l_2)D(l_1 - l_2) \\
& \times \frac{1}{\frac{ic_f}{N}(k_\tau^{2/3} + (l_1 - k)_\tau^{2/3} + l_{1\tau}^{2/3}) + 2k_y l_{1y} + 2l_{1y}^2 + \delta_p^+} \\
& \left. \times \frac{1}{\frac{ic_f}{N}(k_\tau^{2/3} + (l_2 - k)_\tau^{2/3} + l_{2\tau}^{2/3}) + 2k_y l_{2y} + 2l_{2y}^2 + \delta_p^+} \right] + h.c. \tag{E.33}
\end{aligned}$$

The integration regions $l_{1y} > 0$ and $l_{1y} < 0$ give the same contribution. So, integrating

over k_y ,

$$\begin{aligned}
\delta^{3b}\Sigma(p_\tau = 0, \vec{p}) &= N\lambda_+\lambda_- \left[2 \int_0^\infty \frac{dk_\tau}{2\pi} \int_{k_\tau}^\infty \frac{dl_{1\tau}}{2\pi} \int_0^\infty \frac{dl_{2\tau}}{2\pi} \int_0^\infty \frac{dl_{1y}}{2\pi} \int_{l_{1y}}^\infty \frac{dl_{2y}}{2\pi} \right. \\
&D(l_1)D(l_2)D(l_{1\tau} + l_{2\tau}, l_{1y} - l_{2y}) \\
&\times \frac{1}{-\frac{ic_f}{N}(l_{2y}((l_1 - k)_\tau^{2/3} + l_{1\tau}^{2/3} + k_\tau^{2/3}) + l_{1y}((l_2 + k)_\tau^{2/3} + l_{2\tau}^{2/3} - k_\tau^{2/3})) + (l_2 - l_1)_y\delta_p^+} \\
&+ \int_0^\infty \frac{dk_\tau}{2\pi} \int_{k_\tau}^\infty \frac{dl_{1\tau}}{2\pi} \int_{k_\tau}^\infty \frac{dl_{2\tau}}{2\pi} \int_0^\infty \frac{dl_{1y}}{2\pi} \int_0^\infty \frac{dl_{2y}}{2\pi} D(l_1)D(l_2)D(l_{1\tau} - l_{2\tau}, l_{1y} + l_{2y}) \\
&\times \left. \frac{1}{-\frac{ic_f}{N}(l_{2y}((l_1 - k)_\tau^{2/3} + l_{1\tau}^{2/3} + k_\tau^{2/3}) + l_{1y}((l_2 - k)_\tau^{2/3} + l_{2\tau}^{2/3} + k_\tau^{2/3})) + (l_1 + l_2)_y\delta_p^+} \right] \\
&+ h.c. \tag{E.34}
\end{aligned}$$

$$\begin{aligned}
\delta^{3c}\Sigma(p_\tau = 0, \vec{p}) &= N\lambda_+\lambda_- \left[2 \int_0^\infty \frac{dk_\tau}{2\pi} \int_{k_\tau}^\infty \frac{dl_{1\tau}}{2\pi} \int_0^\infty \frac{dl_{2\tau}}{2\pi} \int_0^\infty \frac{dl_{1y}}{2\pi} \int_{l_{1y}}^\infty \frac{dl_{2y}}{2\pi} \right. \\
&\left(-\frac{ic_f}{N}(l_{2y}((l_1 - k)_\tau^{2/3} + l_{1\tau}^{2/3} + k_\tau^{2/3}) + l_{1y}((l_2 + k)_\tau^{2/3} + l_{2\tau}^{2/3} - k_\tau^{2/3})) \right. \\
&+ \left. \left. 2l_{1y}l_{2y}(l_2 - l_1)_y - (l_2 - l_1)_y\delta_p^+ \right)^{-1} D(l_1)D(l_2)D(l_{1\tau} + l_{2\tau}, l_{1y} - l_{2y}) \right. \\
&+ \int_0^\infty \frac{dk_\tau}{2\pi} \int_{k_\tau}^\infty \frac{dl_{1\tau}}{2\pi} \int_{k_\tau}^\infty \frac{dl_{2\tau}}{2\pi} \int_0^\infty \frac{dl_{1y}}{2\pi} \int_0^\infty \frac{dl_{2y}}{2\pi} \\
&\left(-\frac{ic_f}{N}(l_{2y}((l_1 - k)_\tau^{2/3} + l_{1\tau}^{2/3} + k_\tau^{2/3}) + l_{1y}((l_2 - k)_\tau^{2/3} + l_{2\tau}^{2/3} + k_\tau^{2/3})) \right. \\
&\left. \left. - 2l_{1y}l_{2y}(l_1 + l_2)_y - (l_1 + l_2)_y\delta_p^+ \right)^{-1} D(l_1)D(l_2)D(l_{1\tau} - l_{2\tau}, l_{1y} + l_{2y}) \right] + h.c. \\
&\tag{E.35}
\end{aligned}$$

Expanding the self-energy in δ_p^+ and performing a change of variables $l_{1\tau} = k_\tau x_1$,

$$l_{2\tau} = k_\tau x_2, l_{1y} = (c_b e^2 k_\tau)^{1/3} y_1, l_{2y} = (c_b e^2 k_\tau)^{1/3} y_2,$$

$$\delta^{3b}\Sigma_+(p_\tau = 0, \vec{p}) = \lambda_+\lambda_-(J_1 + J_2)\delta_p^+ \int_0^\infty \frac{dk_\tau}{k_\tau} \tag{E.36}$$

$$\delta^{3c}\Sigma_+(p_\tau = 0, \vec{p}) = \delta^{3c}\Sigma_+(p_\tau = 0, \vec{p} = 0) + \lambda_+\lambda_-(J_3 + J_4)\delta_p^+ \int_0^\infty \frac{dk_\tau}{k_\tau} \tag{E.37}$$

where

$$J_1 = \frac{6}{\pi^2} \int_1^\infty dx_1 \int_0^\infty dx_2 \int_0^\infty dy_1 \int_{y_1}^\infty dy_2 \frac{y_1 y_2 (y_2 - y_1)^2}{(x_1 + y_1^3)(x_2 + y_2^3)(x_1 + x_2 + (y_2 - y_1)^3)} \times \frac{1}{(y_2((x_1 - 1)^{2/3} + x_1^{2/3} + 1) + y_1((x_2 + 1)^{2/3} + x_2^{2/3} - 1))^2} \quad (\text{E.38})$$

$$J_2 = \frac{3}{\pi^2} \int_1^\infty dx_1 \int_1^\infty dx_2 \int_0^\infty dy_1 \int_0^\infty dy_2 \frac{y_1 y_2 (y_1 + y_2)^2}{(x_1 + y_1^3)(x_2 + y_2^3)(|x_1 - x_2| + (y_1 + y_2)^3)} \times \frac{1}{(y_2((x_1 - 1)^{2/3} + x_1^{2/3} + 1) + y_1((x_2 - 1)^{2/3} + x_2^{2/3} + 1))^2} \quad (\text{E.39})$$

$$J_3 = \frac{6}{\pi^2 N^2} \int_1^\infty dx_1 \int_0^\infty dx_2 \int_0^\infty dy_1 \int_{y_1}^\infty dy_2 \frac{y_1 y_2 (y_2 - y_1)^2}{(x_1 + y_1^3)(x_2 + y_2^3)(x_1 + x_2 + (y_2 - y_1)^3)} \times \frac{3y_1^2 y_2^2 (y_2 - y_1)^2 - \frac{1}{N^2} (y_2((x_1 - 1)^{2/3} + x_1^{2/3} + 1) + y_1((x_2 + 1)^{2/3} + x_2^{2/3} - 1))^2}{(3y_1^2 y_2^2 (y_2 - y_1)^2 + \frac{1}{N^2} (y_2((x_1 - 1)^{2/3} + x_1^{2/3} + 1) + y_1((x_2 + 1)^{2/3} + x_2^{2/3} - 1))^2} \quad (\text{E.40})$$

$$J_4 = \frac{3}{\pi^2 N^2} \int_1^\infty dx_1 \int_1^\infty dx_2 \int_0^\infty dy_1 \int_0^\infty dy_2 \frac{y_1 y_2 (y_1 + y_2)^2}{(x_1 + y_1^3)(x_2 + y_2^3)(|x_1 - x_2| + (y_1 + y_2)^3)} \times \frac{3y_1^2 y_2^2 (y_1 + y_2)^2 - \frac{1}{N^2} (y_2((x_1 - 1)^{2/3} + x_1^{2/3} + 1) + y_1((x_2 - 1)^{2/3} + x_2^{2/3} + 1))^2}{(3y_1^2 y_2^2 (y_1 + y_2)^2 + \frac{1}{N^2} (y_2((x_1 - 1)^{2/3} + x_1^{2/3} + 1) + y_1((x_2 - 1)^{2/3} + x_2^{2/3} + 1))^2} \quad (\text{E.41})$$

Cutting off the UV divergence in (E.36), (E.37) at $k_\tau = \Lambda_\tau \sim \Lambda_y^3/e^2$, we obtain to logarithmic accuracy,

$$\delta^{3b}\Sigma_+(p_\tau = 0, \vec{p}) = \lambda_+ \lambda_- (J_1 + J_2) \delta_p^+ \log \frac{\Lambda_y^3}{|\delta_p^+|^{3/2}} \quad (\text{E.42})$$

$$\delta^{3c}\Sigma_+(p_\tau = 0, \vec{p}) = \delta^{3c}\Sigma_+(p_\tau = 0, \vec{p} = 0) + \lambda_+ \lambda_- (J_3 + J_4) \delta_p^+ \log \frac{\Lambda_y^3}{|\delta_p^+|^{3/2}} \quad (\text{E.43})$$

which is equivalent to Eqs. (6.86), (6.87) with $J_b = 3(J_1 + J_2)$, $J_c = 3(J_3 + J_4)$. Note

that J_1 and J_2 are constants independent of N ,

$$J_1 \approx 0.01276 \quad (\text{E.44})$$

$$J_2 \approx 0.02264 \quad (\text{E.45})$$

On the other hand, the constants J_3 and J_4 are N dependent. In the large- N limit we can evaluate these constants analytically to leading logarithmic accuracy by setting $N = \infty$ in the integrand.

$$J_3 \approx \frac{2}{\pi^2 N^2} \int_1^\infty dx_1 \int_0^\infty dx_2 \int_0^\infty dy_1 \int_{y_1}^\infty dy_2 \frac{1}{y_1 y_2 (x_1 + y_1^3)(x_2 + y_2^3)(x_1 + x_2 + (y_2 - y_1)^3)} \quad (\text{E.46})$$

The above integral diverges logarithmically when $y_1, y_2, x_2 \rightarrow 0$. Hence,

$$\begin{aligned} J_3 &\approx \frac{2}{\pi^2 N^2} \int_1^\infty \frac{dx_1}{x_1^2} \int_0^1 dx_2 \int_0^1 dy_1 \int_{y_1}^1 dy_2 \frac{1}{y_1 y_2 (x_2 + y_2^3)} \\ &\approx \frac{2}{\pi^2 N^2} \int_0^1 \frac{dy_2}{y_2} \log(y_2^{-3}) \int_0^{y_2} \frac{dy_1}{y_1} \end{aligned} \quad (\text{E.47})$$

Inspecting the original integral (E.40), we observe that the logarithmic divergence in (E.47) is cut-off when $y_1(y_2 - y_1) \sim \frac{1}{N}$. Hence,

$$J_3 \approx \frac{2}{\pi^2 N^2} \int_{N^{-\frac{1}{2}}}^1 \frac{dy_2}{y_2} \log(y_2^{-3}) \int_{(Ny_2)^{-1}}^{y_2} \frac{dy_1}{y_1} \approx \frac{1}{4\pi^2 N^2} \log^3 N \quad (\text{E.48})$$

Similarly,

$$\begin{aligned} J_4 &\approx \frac{1}{\pi^2 N^2} \int_1^\infty dx_1 \int_1^\infty dx_2 \int_0^\infty dy_1 \int_0^\infty dy_2 \frac{1}{y_1 y_2 (x_1 + y_1^3)(x_2 + y_2^3)(|x_1 - x_2| + (y_1 + y_2)^3)} \\ &\approx \frac{4}{\pi^2 N^2} \int_1^\infty \frac{dx_1}{x_1^2} \int_0^1 \frac{dy_2}{y_2} \int_0^{y_2} \frac{dy_1}{y_1} \log((y_1 + y_2)^{-3}) \end{aligned} \quad (\text{E.49})$$

Inspecting Eq. (E.41), we see that the logarithmic divergence in (E.49) is cut-off when $y_1 y_2 \sim \frac{1}{N}$. Writing, $y_1 = y_2 z$,

$$J_4 \approx -\frac{12}{\pi^2 N^2} \int_{N^{-\frac{1}{2}}}^1 \frac{dy_2}{y_2} \int_{(Ny_2^2)^{-1}}^1 \frac{dz}{z} (\log y_2 + \log(1+z)) \approx \frac{1}{2\pi^2 N^2} \log^3 N \quad (\text{E.50})$$

We note that expressions (E.48), (E.50) do not include subleading polynomial corrections in $\log N$. We can also calculate the constants J_3, J_4 numerically for $N = 2$,

$$J_3 \approx -0.004491 \quad (\text{E.51})$$

$$J_4 \approx -0.008158 \quad (\text{E.52})$$

Finally, we compute the insertion of the ϕ^2 operator into the fermion two-point function, which determines the renormalization of the chemical potential δ away from criticality. The UV contribution at three loop order comes from the diagrams in Figs. 6.10 b) c) and can be obtained by expanding the bosonic propagators in Eqs. (E.34), (E.35) to linear order in r . This yields,

$$\begin{aligned} \delta^{3b} \frac{\partial \Sigma}{\partial r} \stackrel{UV}{=} & -N \left[2 \int_0^\infty \frac{dk_\tau}{2\pi} \int_{k_\tau}^\infty \frac{dl_{1\tau}}{2\pi} \int_0^\infty \frac{dl_{2\tau}}{2\pi} \int_0^\infty \frac{dl_{1y}}{2\pi} \int_{l_{1y}}^\infty \frac{dl_{2y}}{2\pi} \right. \\ & (D(l_1) + D(l_2) + D(l_{1\tau} + l_{2\tau}, l_{1y} - l_{2y})) D(l_1) D(l_2) D(l_{1\tau} + l_{2\tau}, l_{1y} - l_{2y}) \\ & \times \left(-\frac{ic_f}{N} (l_{2y} ((l_1 - k)_\tau^{2/3} + l_{1\tau}^{2/3} + k_\tau^{2/3}) + l_{1y} ((l_2 + k)_\tau^{2/3} + l_{2\tau}^{2/3} - k_\tau^{2/3})) \right)^{-1} \\ & + \int_0^\infty \frac{dk_\tau}{2\pi} \int_{k_\tau}^\infty \frac{dl_{1\tau}}{2\pi} \int_{k_\tau}^\infty \frac{dl_{2\tau}}{2\pi} \int_0^\infty \frac{dl_{1y}}{2\pi} \int_0^\infty \frac{dl_{2y}}{2\pi} \\ & (D(l_1) + D(l_2) + D(l_{1\tau} - l_{2\tau}, l_{1y} + l_{2y})) D(l_1) D(l_2) D(l_{1\tau} - l_{2\tau}, l_{1y} + l_{2y}) \\ & \times \left(-\frac{ic_f}{N} (l_{2y} ((l_1 - k)_\tau^{2/3} + l_{1\tau}^{2/3} + k_\tau^{2/3}) + l_{1y} ((l_2 - k)_\tau^{2/3} + l_{2\tau}^{2/3} + k_\tau^{2/3})) \right)^{-1} \left. \right] \\ & + h.c. \quad (\text{E.53}) \end{aligned}$$

$$\begin{aligned}
\delta^{3c} \frac{\partial \Sigma}{\partial r} \stackrel{UV}{=} & -N \left[2 \int_0^\infty \frac{dk_\tau}{2\pi} \int_{k_\tau}^\infty \frac{dl_{1\tau}}{2\pi} \int_0^\infty \frac{dl_{2\tau}}{2\pi} \int_0^\infty \frac{dl_{1y}}{2\pi} \int_{l_{1y}}^\infty \frac{dl_{2y}}{2\pi} \right. \\
& (D(l_1) + D(l_2) + D(l_{1\tau} + l_{2\tau}, l_{1y} - l_{2y})) D(l_1) D(l_2) D(l_{1\tau} + l_{2\tau}, l_{1y} - l_{2y}) \\
& \times \left(-\frac{ic_f}{N} (l_{2y}((l_1 - k)_\tau^{2/3} + l_{1\tau}^{2/3} + k_\tau^{2/3}) + l_{1y}((l_2 + k)_\tau^{2/3} + l_{2\tau}^{2/3} - k_\tau^{2/3})) \right. \\
& + \left. 2l_{1y}l_{2y}(l_2 - l_{1y})_y \right)^{-1} + \int_0^\infty \frac{dk_\tau}{2\pi} \int_{k_\tau}^\infty \frac{dl_{1\tau}}{2\pi} \int_{k_\tau}^\infty \frac{dl_{2\tau}}{2\pi} \int_0^\infty \frac{dl_{1y}}{2\pi} \int_0^\infty \frac{dl_{2y}}{2\pi} \\
& (D(l_1) + D(l_2) + D(l_{1\tau} - l_{2\tau}, l_{1y} + l_{2y})) D(l_1) D(l_2) D(l_{1\tau} - l_{2\tau}, l_{1y} + l_{2y}) \\
& \times \left(-\frac{ic_f}{N} (l_{2y}((l_1 - k)_\tau^{2/3} + l_{1\tau}^{2/3} + k_\tau^{2/3}) + l_{1y}((l_2 - k)_\tau^{2/3} + l_{2\tau}^{2/3} + k_\tau^{2/3})) \right. \\
& \left. \left. - 2l_{1y}l_{2y}(l_1 + l_{2y})_y \right)^{-1} \right] + h.c. \tag{E.54}
\end{aligned}$$

We observe that the contribution from the diagram in Fig. 6.10 b) vanishes, while the diagram in Fig. 6.10 c) gives upon switching to dimensionless variables,

$$\delta^3 \frac{\partial \Sigma}{\partial r} \stackrel{UV}{=} J_r e^2 \log \Lambda_y \tag{E.55}$$

with

$$\begin{aligned}
J_r = & -\frac{36}{\pi^2 N^2} \int_1^\infty dx_1 \int_0^\infty dx_2 \int_0^\infty dy_1 \int_{y_1}^\infty dy_2 \frac{y_1^2 y_2^2 (y_2 - y_1)^2}{(x_1 + y_1^3)(x_2 + y_2^3)(x_1 + x_2 + (y_2 - y_1)^3)} \\
& \left(\frac{y_1}{x_1 + y_1^3} + \frac{y_2}{x_2 + y_2^3} + \frac{y_2 - y_1}{x_1 + x_2 + (y_2 - y_1)^3} \right) \\
& \frac{1}{3y_1^2 y_2^2 (y_2 - y_1)^2 + \frac{1}{N^2} (y_2((x_1 - 1)^{2/3} + x_1^{2/3} + 1) + y_1((x_2 + 1)^{2/3} + x_2^{2/3} - 1))^2} \\
+ & \frac{18}{\pi^2 N^2} \int_1^\infty dx_1 \int_1^\infty dx_2 \int_0^\infty dy_1 \int_0^\infty dy_2 \frac{y_1^2 y_2^2 (y_1 + y_2)^2}{(x_1 + y_1^3)(x_2 + y_2^3)(|x_1 - x_2| + (y_1 + y_2)^3)} \\
& \left(\frac{y_1}{x_1 + y_1^3} + \frac{y_2}{x_2 + y_2^3} + \frac{y_1 + y_2}{|x_1 - x_2| + (y_1 + y_2)^3} \right) \\
& \frac{1}{3y_1^2 y_2^2 (y_1 + y_2)^2 + \frac{1}{N^2} (y_2((x_1 - 1)^{2/3} + x_1^{2/3} + 1) + y_1((x_2 - 1)^{2/3} + x_2^{2/3} + 1))^2} \tag{E.56}
\end{aligned}$$

Evaluating the above integral, we obtain Eq. (6.95).

Appendix F

Appendix to Chapter 7

F.1 RG computations

In this appendix we give the details of our calculations in Sections 7.2 and 7.3.

F.1.1 RPA polarization

We begin with the RPA polarization bubble,

$$\Pi^{ab}(q) = 2N\delta^{ab} \sum_{\ell} \int \frac{dl_{\tau} d^2\vec{l}}{(2\pi)^3} (G_1^{\ell}(l+q)G_2^{\ell}(l) + G_2^{\ell}(l+q)G_1^{\ell}(l)) \quad (\text{F.1})$$

The two terms in brackets come from the two graphs in Fig. 7.4 with different directions of the particle flow. As discussed in Section 7.2 such graphs are equal by the emergent particle-hole symmetry. Thus, focusing on the contribution from $\ell = 1$,

$$\Pi^{\ell=1}(q) = 2N \int \frac{dl_{\tau} d^2\vec{l}}{(2\pi)^3} \frac{1}{(i\eta(l_{\tau} + q_{\tau}) - \vec{v}_1 \cdot (\vec{l} + \vec{q})) (i\eta l_{\tau} - \vec{v}_2 \cdot \vec{l})} + (q \rightarrow -q) \quad (\text{F.2})$$

We change variables to $l_1 = \hat{v}_1 \cdot (\vec{l} + \vec{q})$, $l_2 = \hat{v}_2 \cdot \vec{l}$, and take the limit $\eta \rightarrow 0$ using the relation,

$$\frac{1}{x + i\eta} = \frac{P}{x} - \pi i \text{sgn}(\eta) \delta(x) \quad (\text{F.3})$$

which yields,

$$\Pi^{\ell=1}(q) = \frac{N}{v_x v_y} \int \frac{dl_\tau d^2 \vec{l}}{(2\pi)^3} \left(\frac{P}{l_1} + \pi i \text{sgn}(l_\tau + q_\tau) \delta(l_1) \right) \left(\frac{P}{l_2} + \pi i \text{sgn}(l_\tau) \delta(l_2) \right) + (q \rightarrow -q) \quad (\text{F.4})$$

Evaluating the integrals over l_1 , l_2 ,

$$\Pi^{\ell=1}(q) = -\frac{N}{8\pi v_x v_y} \int dl_\tau \text{sgn}(l_\tau + q_\tau) \text{sgn}(l_\tau) + (q \rightarrow -q) \quad (\text{F.5})$$

Here, we've taken the principal value integral to be zero, as it would be if we used a particle-hole symmetric regularization. Otherwise, one can check that any terms generated by the pv integral are of the form iq_τ and are cancelled by the $(q \rightarrow -q)$ term of Eq. F.5. Now, subtracting the value of the polarization bubble at $q = 0$, we obtain,

$$\begin{aligned} \Pi^{\ell=1}(q) - \Pi^{\ell=1}(q=0) &= -\frac{N}{8\pi v_x v_y} \int dl_\tau (\text{sgn}(l_\tau + q_\tau) \text{sgn}(l_\tau) - 1) + (q \rightarrow -q) \\ &= \frac{N}{2\pi v_x v_y} |q_\tau| \end{aligned} \quad (\text{F.6})$$

which, taking into account contributions from the other hot spots, gives,

$$\Pi(q) = \Pi(q=0) + \frac{Nn}{2\pi v_x v_y} |q_\tau| \quad (\text{F.7})$$

F.1.2 Fermion self energy

We next proceed to the self-energy of fermion $\psi_1^{\ell=1}$, Fig. 7.5,

$$\begin{aligned}\Sigma_{1,\sigma\sigma'}(p) &= \tau_{\sigma\rho}^a \tau_{\rho\sigma'}^a \int \frac{dl_\tau d^2\vec{l}}{(2\pi)^3} G_2(p-l) D(l) \\ &= \frac{3}{N} \delta_{\sigma\sigma'} \int \frac{dl_\tau d^2\vec{l}}{(2\pi)^3} \frac{1}{i\eta(p_\tau - l_\tau) - \vec{v}_2 \cdot (\vec{p} - \vec{l})} \frac{1}{\gamma|l_\tau| + \vec{l}^2}\end{aligned}\quad (\text{F.8})$$

We take the limit $\eta \rightarrow 0$ and use Eq. (F.3). Moreover, we change variables, so that $l_\perp = \hat{v}_2 \cdot \vec{l}$ and l_\parallel is the momentum component along the Fermi surface of ψ_2 (i.e. perpendicular to \hat{v}_2). Then,

$$\Sigma_1(p) = \frac{3}{N|\vec{v}|} \int \frac{dl_\tau dl_\perp dl_\parallel}{(2\pi)^3} \left(\frac{P}{l_\perp - \hat{v}_2 \cdot \vec{p}} + \pi i \text{sgn}(l_\tau - p_\tau) \delta(l_\perp - \hat{v}_2 \cdot \vec{p}) \right) \frac{1}{\gamma|l_\tau| + l_\perp^2 + l_\parallel^2}\quad (\text{F.9})$$

Thus, the imaginary part of Σ is given by,

$$\text{Im}\Sigma_1(p) = \frac{3}{N|\vec{v}|} \int \frac{dl_\tau}{8\pi} \text{sgn}(l_\tau - p_\tau) \frac{1}{\sqrt{\gamma|l_\tau| + |\hat{v}_2 \cdot \vec{p}|^2}}\quad (\text{F.10})$$

where we have performed the integral over l_\perp, l_\parallel . Since, $\text{Im}\Sigma(p_\tau = 0) = 0$,

$$\begin{aligned}\text{Im}\Sigma_1(p) &= \frac{3}{N|\vec{v}|} \int \frac{dl_\tau}{8\pi} (\text{sgn}(l_\tau - p_\tau) - \text{sgn}(l_\tau)) \frac{1}{\sqrt{\gamma|l_\tau| + |\hat{v}_2 \cdot \vec{p}|^2}} \\ &= -\frac{3}{2\pi N|\vec{v}|\gamma} \text{sgn}(p_\tau) \left(\sqrt{\gamma|p_\tau| + (\hat{v}_2 \cdot \vec{p})^2} - |\hat{v}_2 \cdot \vec{p}| \right)\end{aligned}\quad (\text{F.11})$$

On the other hand, the real part of Σ is given by,

$$\text{Re}\Sigma_1(p) = -\frac{3\hat{v}_2 \cdot \vec{p}}{2N|\vec{v}|} \int \frac{dl_\tau dl_\parallel}{(2\pi)^2} \frac{1}{\sqrt{\gamma|l_\tau| + l_\parallel^2}} \frac{1}{\gamma|l_\tau| + l_\parallel^2 + (\hat{v}_2 \cdot \vec{p})^2}\quad (\text{F.12})$$

Changing variables to $u = \sqrt{\gamma|l_\tau| + l_\parallel^2}$,

$$\begin{aligned}\text{Re}\Sigma_1(p) &= -\frac{3(\hat{v}_2 \cdot \vec{p})}{2\pi^2 N \gamma |\vec{v}|} \int dl_\parallel \int_{|l_\parallel|}^{\infty} du \frac{1}{u^2 + (\hat{v}_2 \cdot \vec{p})^2} \\ &= -\frac{3(\hat{v}_2 \cdot \vec{p})}{2\pi^2 N \gamma |\vec{v}|} \int \frac{dl_\parallel}{|\hat{v}_2 \cdot \vec{p}|} \tan^{-1} \left(\frac{|\hat{v}_2 \cdot \vec{p}|}{|l_\parallel|} \right)\end{aligned}\quad (\text{F.13})$$

The integral over l_{\parallel} is ultra-violet divergent. Cutting off the integral at $|l_{\parallel}| = \Lambda$, we obtain to logarithmic accuracy,

$$\text{Re}\Sigma_1(p) = -\frac{3\hat{v}_2 \cdot \vec{p}}{\pi^2 N |\vec{v}| \gamma} \log \frac{\Lambda}{|\hat{v}_2 \cdot \vec{p}|} \quad (\text{F.14})$$

Combining eqs. (F.11), (F.14) we obtain the self-energy (7.45).

F.1.3 Boson-fermion vertex

Proceeding to the first correction in $1/N$ to the boson-fermion vertex, Fig. 7.6,

$$\delta\Gamma_{\sigma\sigma'}^a(p, q) = (\tau^b \tau^a \tau^b)_{\sigma\sigma'} \int \frac{dl_{\tau} d^2\vec{l}}{(2\pi)^3} G_2(l+p) G_1(l+p+q) D(l) \quad (\text{F.15})$$

Evaluating the matrix product,

$$\begin{aligned} \delta\Gamma(p, q) = & -\frac{1}{N} \int \frac{dl_{\tau} d^2\vec{l}}{(2\pi)^3} \frac{1}{\vec{v}_2 \cdot (\vec{l} + \vec{p}) - i\eta(l_{\tau} + p_{\tau})} \frac{1}{\vec{v}_1 \cdot (\vec{l} + \vec{p} + \vec{q}) - i\eta(l_{\tau} + p_{\tau} + q_{\tau})} \\ & \times \frac{1}{\gamma|l_{\tau}| + \vec{l}^2} \end{aligned} \quad (\text{F.16})$$

The integral (F.16) is logarithmically divergent in the UV. To extract this divergence, we may set all external momenta to zero:

$$\delta\Gamma(p, q) \stackrel{UV}{=} -\frac{1}{N} \int \frac{dl_{\tau} d^2\vec{l}}{(2\pi)^3} \frac{1}{(-v_x l_x + v_y l_y - i\eta l_{\tau})(v_x l_x + v_y l_y - i\eta l_{\tau})} \frac{1}{\gamma|l_{\tau}| + l_x^2 + l_y^2} \quad (\text{F.17})$$

The poles in l_y coming from the two fermion propagators in Eq. (F.17) are in the same half-plane; we may choose to close the l_y integration contour in the opposite half-plane, picking up the pole from the bosonic propagator:

$$\begin{aligned} \delta\Gamma(p, q) \stackrel{UV}{=} & -\frac{1}{N} \int \frac{dl_{\tau} dl_x}{(2\pi)^2} \frac{1}{-v_x l_x - i v_y \text{sgn}(l_{\tau}) \sqrt{\gamma|l_{\tau}| + l_x^2}} \\ & \times \frac{1}{v_x l_x - i v_y \text{sgn}(l_{\tau}) \sqrt{\gamma|l_{\tau}| + l_x^2}} \frac{1}{2\sqrt{\gamma|l_{\tau}| + l_x^2}} \end{aligned} \quad (\text{F.18})$$

Changing variables to $u = \sqrt{\gamma|l_\tau| + l_x^2}$,

$$\delta\Gamma(p, q) \stackrel{UV}{=} \frac{2}{N\gamma} \int_{-\infty}^{\infty} \frac{dl_x}{2\pi} \int_{|l_x|}^{\infty} \frac{du}{2\pi} \frac{1}{v_x^2 l_x^2 + v_y^2 u^2} \quad (\text{F.19})$$

We now go to polar coordinates, $v_x l_x + i v_y u = |\vec{v}| \rho e^{i\theta}$,

$$\delta\Gamma(p, q) \stackrel{UV}{=} \frac{1}{N\pi(2\pi v_x v_y \gamma)} \int_0^{\infty} \frac{d\rho}{\rho} \int_{\tan^{-1} \alpha}^{\pi - \tan^{-1} \alpha} d\theta \quad (\text{F.20})$$

The integral over ρ is logarithmically divergent in the UV ; cutting off the integral at $\rho \sim \Lambda$,

$$\delta\Gamma(p, q) \stackrel{UV}{=} \frac{2}{\pi n N} \tan^{-1} \frac{1}{\alpha} \log \Lambda \quad (\text{F.21})$$

F.1.4 Boson self energy

We now proceed to the $1/N$ corrections to the boson self-energy, Fig. 7.7. We first analyze the contribution of diagrams a), b) and c), which we label $\delta\Pi_I$. Utilizing the expression (7.15) for the fermion induced quartic coupling, we obtain,

$$\begin{aligned} \delta\Pi_I^{ab}(q) &= \frac{1}{2} \int \frac{dl_\tau d^2 \vec{l}}{(2\pi)^3} \Gamma^{abcc}(q, -q, l, -l) D(l) \\ &= \int \frac{dl_\tau d^2 \vec{l}}{(2\pi)^3} (f^{abcc}(q, -q, l, -l) + f^{accb}(q, l, -l, -q) + f^{acbc}(q, l, -q, -l)) D(l) \end{aligned} \quad (\text{F.22})$$

The first two terms in Eq. (F.22) vanish (these terms correspond to the diagrams in Fig. 7.7 a), b)). Thus, only the diagram in Fig. 7.7 c) contributes,

$$\delta\Pi_I(q_\tau, \vec{q}) = |q_\tau| A(q_\tau, \vec{q}) + B(q_\tau, \vec{q}) \quad (\text{F.23})$$

with

$$A(q_\tau, \vec{q}) = -\frac{N}{\pi v_x v_y} \sum_\ell \int \frac{dl_\tau d^2 \vec{l}}{(2\pi)^3} G_1^\ell(l-q) G_2^\ell(l+q) D(l) \quad (\text{F.24})$$

$$B(q_\tau, \vec{q}) = \frac{N}{\pi v_x v_y} \sum_\ell \int \frac{dl_\tau d^2 \vec{l}}{(2\pi)^3} |l_\tau| G_1^\ell(l-q) G_2^\ell(l+q) D(l) \quad (\text{F.25})$$

The quantity $A(q_\tau, \vec{q})$ is logarithmically divergent in the UV . The coefficient of the divergence may be extracted by setting the external momenta and r to zero. Then, from Eq. (F.16), we recognize,

$$A(q_\tau, \vec{q}) \stackrel{UV}{=} \frac{N}{\pi v_x v_y} \sum_\ell \delta\Gamma(p, q) = \frac{4\gamma}{n\pi} \tan^{-1} \frac{1}{\alpha} \log \Lambda \quad (\text{F.26})$$

Now, let us evaluate B . We temporarily keep only the contribution from the hot spot pair $\ell = 1$.

$$\begin{aligned} B^{\ell=1}(q_\tau, \vec{q}) &= \frac{1}{\pi v_x v_y} \int \frac{dl_\tau d^2 \vec{l}}{(2\pi)^3} \frac{1}{(v_x l_x + v_y l_y - \vec{v}_1 \cdot \vec{q} - i\eta(l_\tau - q_\tau))} \\ &\quad \times \frac{1}{(-v_x l_x + v_y l_y + \vec{v}_2 \cdot \vec{q} - i\eta(l_\tau + q_\tau))} \frac{|l_\tau|}{(\gamma |l_\tau| + l_x^2 + l_y^2 + r)}. \end{aligned} \quad (\text{F.27})$$

Note that the region $|l_\tau| < |q_\tau|$ does not contain any UV divergences. Thus, to compute the UV divergent part, we can confine our attention to the region $|l_\tau| > |q_\tau|$. In this case, the two poles in l_y coming from the fermion propagators in Eq. (F.27) lie in the same half-plane; we may choose to close the l_y integration contour in the opposite half-plane, picking up the pole from the bosonic propagator:

$$\begin{aligned} B^{\ell=1}(q_\tau, \vec{q}) &\stackrel{UV}{=} \frac{1}{\pi v_x v_y} \int_{|l_\tau| > |q_\tau|} \frac{dl_\tau dl_x}{(2\pi)^2} \frac{1}{v_x l_x - i v_y \text{sgn}(l_\tau) \sqrt{\gamma |l_\tau| + l_x^2 + r} - \vec{v}_1 \cdot \vec{q}} \\ &\quad \times \frac{1}{-v_x l_x - i v_y \text{sgn}(l_\tau) \sqrt{\gamma |l_\tau| + l_x^2 + r} + \vec{v}_2 \cdot \vec{q}} \frac{|l_\tau|}{2\sqrt{\gamma |l_\tau| + l_x^2 + r}} \end{aligned} \quad (\text{F.28})$$

Note that we may extend the integration over l_τ in Eq. (F.28) back to the whole real line without influencing the UV part of the result. Thus,

$$B^{\ell=1}(q_\tau, \vec{q}) \stackrel{UV}{=} -\frac{1}{\pi v_x v_y} \int_0^\infty \frac{dl_\tau}{2\pi} \int_{-\infty}^\infty \frac{dl_x}{2\pi} \frac{1}{(v_x l_x - i v_y \sqrt{\gamma l_\tau + l_x^2 + r} - \vec{v}_1 \cdot \vec{q})} \\ \times \frac{1}{(v_x l_x + i v_y \sqrt{\gamma l_\tau + l_x^2 + r} - \vec{v}_2 \cdot \vec{q})} \frac{l_\tau}{2\sqrt{\gamma l_\tau + l_x^2 + r}} + c.c. \quad (\text{F.29})$$

It is convenient to change variables to $u = \sqrt{\gamma |l_\tau| + l_x^2 + r}$,

$$B^{\ell=1}(q_\tau, \vec{q}) \stackrel{UV}{=} -\frac{1}{\pi v_x v_y \gamma^2} \int_{-\infty}^\infty \frac{dl_x}{2\pi} \int_{\sqrt{l_x^2 + r}}^\infty \frac{du}{2\pi} \\ \frac{u^2 - l_x^2 - r}{(v_x l_x - i v_y u - \vec{v}_1 \cdot \vec{q})(v_x l_x + i v_y u - \vec{v}_2 \cdot \vec{q})} + c.c. \quad (\text{F.30})$$

The r in the lower limit of the integral over u may be dropped without influencing the UV behaviour. We now go to polar coordinates, $v_x l_x + i v_y u = |\vec{v}| \rho e^{i\theta}$,

$$B^{\ell=1}(q_\tau, \vec{q}) \stackrel{UV}{=} -\frac{1}{\pi (2\pi v_x v_y \gamma)^2} \frac{|\vec{v}|^2}{v_x v_y} \int \rho d\rho \int_{\tan^{-1} \alpha}^{\pi - \tan^{-1} \alpha} d\theta \frac{\rho^2 (\frac{1}{\alpha} \sin^2 \theta - \alpha \cos^2 \theta) - \frac{v_x v_y}{|\vec{v}|^2} r}{(\rho e^{i\theta} - \hat{v}_2 \cdot \vec{q})(\rho e^{-i\theta} - \hat{v}_1 \cdot \vec{q})} \\ + c.c. \quad (\text{F.31})$$

The integral over ρ is quadratically divergent. Expanding the divergent part in \vec{q} and r ,

$$B^{\ell=1}(q_\tau, \vec{q}) \stackrel{UV}{=} -\frac{2}{\pi n^2} \frac{|\vec{v}|^2}{v_x v_y} \int \rho d\rho \int_{\tan^{-1} \alpha}^{\pi - \tan^{-1} \alpha} d\theta \left[\left(\frac{1}{\alpha} \sin^2 \theta - \alpha \cos^2 \theta \right) \right. \\ \times \left(1 + \frac{1}{\rho} (\hat{v}_1 + \hat{v}_2) \cdot \vec{q} \cos \theta \right. \\ \left. \left. + \frac{1}{\rho^2} ((\hat{v}_1 \cdot \vec{q})(\hat{v}_2 \cdot \vec{q}) + ((\hat{v}_1 \cdot \vec{q})^2 + (\hat{v}_2 \cdot \vec{q})^2) \cos 2\theta) \right) - \frac{v_x v_y}{|\vec{v}|^2} \frac{r}{\rho^2} \right] \quad (\text{F.32})$$

As usual, the term constant in \vec{q} corresponds to a shift in the position of the critical point and will be dropped below. The term linear in \vec{q} vanishes under $\theta \rightarrow \pi - \theta$, *i.e.*

$l_x \rightarrow -l_x$ (more rigorously, this term must vanish by symmetry, once the contributions from all 4 pairs of hot spots are summed). Finally, the term quadratic in \vec{q} and the term linear in r give logarithmic divergences. Cutting off the integral over ρ at $\rho \sim \Lambda$,

$$B^{\ell=1}(q_\tau, \vec{q}) \stackrel{UV}{=} \frac{4}{\pi n^2} \log \Lambda \left[\frac{q_x^2}{\alpha^2} \left(\tan^{-1} \frac{1}{\alpha} + \frac{\alpha}{1 + \alpha^2} \right) + \alpha^2 q_y^2 \left(\tan^{-1} \frac{1}{\alpha} - \frac{\alpha}{1 + \alpha^2} \right) + r \tan^{-1} \frac{1}{\alpha} \right] \quad (\text{F.33})$$

Now, summing over the four pairs of hot spots, we restore rotational invariance,

$$B(q_\tau, \vec{q}) = \frac{2}{\pi n} \left[\frac{1}{\alpha} - \alpha + \left(\frac{1}{\alpha^2} + \alpha^2 \right) \tan^{-1} \frac{1}{\alpha} \right] \vec{q}^2 \log \Lambda + \frac{4}{\pi n} \tan^{-1} \frac{1}{\alpha} r \log \Lambda \quad (\text{F.34})$$

We now compute the diagram in Fig. 7.7 d), which we label $\delta\Pi_{II}$. This diagram is present already in the Hertz-Millis theory and, being momentum independent, leads only to a renormalization of r ,

$$\begin{aligned} \delta\Pi_{II}(q) &= 5u \int \frac{dl_\tau d^2\vec{l}}{(2\pi)^3} D(l) \stackrel{UV}{=} -\frac{5}{N} ur \int \frac{dl_\tau d^2\vec{l}}{(2\pi)^3} \frac{1}{(\gamma|l_\tau| + \vec{l}^2)^2} = -\frac{5ur}{\pi N \gamma} \int \frac{d^2\vec{l}}{(2\pi)^2} \frac{1}{\vec{l}^2} \\ &= -\frac{5}{2\pi^2 N} \tilde{u} r \log \Lambda \end{aligned} \quad (\text{F.35})$$

Now combining Eqs. (F.23), (F.26), (F.34), (F.35) we obtain the UV part of the correction to the boson propagator, Eq. (7.53).

F.2 Violations of large- N counting

F.2.1 Boson-fermion vertex correction at three loops

In this section we compute the vertex correction in Fig. 7.9. As shown in section 7.4, an attempt to evaluate this graph directly with bare fermion propagators results

in infra-red divergences. To cure this problem, we dress the fermion propagators by the one-loop self-energy (7.45). For simplicity, we include only the imaginary part of the self-energy responsible for the dynamics. The frequency independent real part responsible for the logarithmic running of the velocity v will be ignored here. Thus, we use,

$$G_i^\ell(\omega, \vec{k}) = \frac{1}{-i\frac{c_f}{N}g(\omega, \hat{v}_i^\ell \cdot \vec{k}) + \vec{v}_i^\ell \cdot \vec{k}} \quad (\text{F.36})$$

where $\bar{1} = 2$, $\bar{2} = 1$ and

$$g(\omega, k) = \text{sgn}(\omega)(\sqrt{\gamma|\omega| + k^2} - |k|), \quad c_f = \frac{3}{2\pi|\vec{v}|\gamma} \quad (\text{F.37})$$

Then, the diagram in Fig. 7.9 is given by,

$$\begin{aligned} \delta\Gamma_{\phi\psi_2\psi_1^\dagger} &= -28N \int \frac{d^3k}{(2\pi)^3} \frac{d^3l_1}{(2\pi)^3} \frac{d^3l_2}{(2\pi)^3} G_1^{-1}(k)G_2^{-1}(k-l_1)G_1^{-1}(k-l_2)G_2^{-1}(k) \\ &\quad \times G_2^1(l_1)G_1^1(l_2)D(l_1)D(l_2)D(l_2-l_1) \end{aligned} \quad (\text{F.38})$$

The external fermions are taken to have hot spot index $\ell = 1$, while the fermions in the loop are taken to have $\ell' = -1$. As discussed in section 7.4, the contributions from $\ell' = 2$ and $\ell' = 4$ are not enhanced in N , while $\ell' = 1$ contributes a UV finite term of $O(1)$ when the external fermion momenta are chosen to lie on the Fermi surface. As we are mainly interested in corrections to mean-field scaling, we only retain UV divergent contributions below. Hence, all the external momenta of the diagram have

been set to 0. Substituting the one-loop corrected propagators (F.36), we obtain,

$$\begin{aligned}
\delta\Gamma_{\phi\psi_2\psi_1^\dagger} &= -28N \int \frac{d^3k}{(2\pi)^3} \frac{d^3l_1}{(2\pi)^3} \frac{d^3l_2}{(2\pi)^3} \frac{1}{-i\frac{c_f}{N}g(k_\tau, \hat{v}_1 \cdot \vec{k}) - \vec{v}_2 \cdot \vec{k}} \\
&\times \frac{1}{-i\frac{c_f}{N}g(k_\tau, \hat{v}_2 \cdot \vec{k}) - \vec{v}_1 \cdot \vec{k}} \frac{1}{-i\frac{c_f}{N}g(k_\tau - l_{1\tau}, \hat{v}_1 \cdot (\vec{k} - \vec{l}_1)) - \vec{v}_2 \cdot (\vec{k} - \vec{l}_1)} \\
&\times \frac{1}{-i\frac{c_f}{N}g(k_\tau - l_{2\tau}, \hat{v}_2 \cdot (\vec{k} - \vec{l}_2)) - \vec{v}_1 \cdot (\vec{k} - \vec{l}_2)} \frac{1}{-i\frac{c_f}{N}g(l_{1\tau}, \hat{v}_1 \cdot \vec{l}_1) + \vec{v}_2 \cdot \vec{l}_1} \\
&\times \frac{1}{-i\frac{c_f}{N}g(l_{2\tau}, \hat{v}_2 \cdot \vec{l}_2) + \vec{v}_1 \cdot \vec{l}_2} D(l_1)D(l_2)D(l_1 - l_2)
\end{aligned} \tag{F.39}$$

We may divide the spatial momenta into two groups: $\hat{v}_1 \cdot \vec{k}$, $\hat{v}_2 \cdot \vec{k}$, $\hat{v}_2 \cdot \vec{l}_1$, $\hat{v}_1 \cdot \vec{l}_2$ and $\hat{v}_1 \cdot \vec{l}_1$, $\hat{v}_2 \cdot \vec{l}_2$. The singular manifold of the diagram is given by setting the momenta in the first group to zero and can be parameterized by the two variables in the second group. We begin by integrating over the first set of variables, picking up the contribution from the poles of the fermion propagators. As this integration is saturated at momenta of $\mathcal{O}(1/N)$, we can neglect the dependence of the boson propagators and fermion self-energies on these momenta. We then obtain the result in terms of an integral over the singular manifold.

Due to the symmetry, $G(l) = -G(-l)$, the contributions to the integral from $k_\tau > 0$ and $k_\tau < 0$ are equal. Now, changing momentum variables to $\hat{v}_1 \cdot \vec{p}$, $\hat{v}_2 \cdot \vec{p}$, and

integrating over $\hat{v}_2 \cdot \vec{l}_1, \hat{v}_1 \cdot \vec{l}_2$,

$$\begin{aligned}
\delta\Gamma_{\phi\psi_2\psi_1^\dagger} &= -7N \frac{|\vec{v}|^4}{(v_x v_y)^3} \int_0^\infty \frac{dk_\tau}{2\pi} \int \frac{d(\hat{v}_1 \cdot \vec{k})d(\hat{v}_2 \cdot \vec{k})d(\hat{v}_1 \cdot \vec{l}_1)d(\hat{v}_2 \cdot \vec{l}_2)}{(2\pi)^4} \\
&\quad \left[\int_{k_\tau}^\infty - \int_{-\infty}^0 \right] \frac{dl_{1\tau}}{2\pi} \left[\int_{k_\tau}^\infty - \int_{-\infty}^0 \right] \frac{dl_{2\tau}}{2\pi} D(l_1)D(l_2)D(l_1 - l_2) \Big|_{\hat{v}_1 \cdot \vec{l}_2 = \hat{v}_2 \cdot \vec{l}_1 = 0} \\
&\quad \times \frac{1}{-i \frac{c_f}{N} (g(l_{1\tau}, \hat{v}_1 \cdot \vec{l}_1) - g(k_\tau - l_{1\tau}, \hat{v}_1 \cdot (\vec{k} - \vec{l}_1))) + \vec{v}_2 \cdot \vec{k}} \\
&\quad \times \frac{1}{-i \frac{c_f}{N} (g(l_{2\tau}, \hat{v}_2 \cdot \vec{l}_2) - g(k_\tau - l_{2\tau}, \hat{v}_2 \cdot (\vec{k} - \vec{l}_2))) + \vec{v}_1 \cdot \vec{k}} \\
&\quad \times \frac{1}{i \frac{c_f}{N} g(k_\tau, \hat{v}_1 \cdot \vec{k}) + \vec{v}_2 \cdot \vec{k}} \frac{1}{i \frac{c_f}{N} g(k_\tau, \hat{v}_2 \cdot \vec{k}) + \vec{v}_1 \cdot \vec{k}} \tag{F.40}
\end{aligned}$$

Now, performing the integral over $\hat{v}_1 \cdot \vec{k}, \hat{v}_2 \cdot \vec{k}$,

$$\begin{aligned}
\delta\Gamma_{\phi\psi_2\psi_1^\dagger} &= -7N^3 \frac{|\vec{v}|^2}{(v_x v_y)^3 c_f^2} \int_0^\infty \frac{dk_\tau}{2\pi} \int_{k_\tau}^\infty \frac{dl_{1\tau}}{2\pi} \int_{k_\tau}^\infty \frac{dl_{2\tau}}{2\pi} \int \frac{d(\hat{v}_1 \cdot \vec{l}_1)d(\hat{v}_2 \cdot \vec{l}_2)}{(2\pi)^2} \\
&\quad \frac{1}{g(k_\tau, 0) + g(l_{1\tau}) + g(l_{1\tau} - k_\tau, \hat{v}_1 \cdot \vec{l}_1)} \\
&\quad \times \frac{1}{g(k_\tau, 0) + g(l_{2\tau}) + g(l_{2\tau} - k_\tau, \hat{v}_2 \cdot \vec{l}_2)} D(l_1)D(l_2)D(l_1 - l_2) \Big|_{\hat{v}_1 \cdot \vec{l}_2 = \hat{v}_2 \cdot \vec{l}_1 = 0}
\end{aligned}$$

Changing variables to $l_{1,2\tau} = k_\tau x_{1,2}$, $l_{1,2y} = \sqrt{\gamma k_\tau} y_{1,2}$,

$$\delta\Gamma_{\phi\psi_2\psi_1^\dagger} = \frac{1}{2} X(\alpha) \int_0^\infty \frac{dk_\tau}{k_\tau} = X(\alpha) \log \Lambda_y \tag{F.41}$$

with

$$\begin{aligned}
X(\alpha) &= -\frac{7}{18\pi^2 n} \left(\frac{1}{\alpha} + \alpha \right)^2 \int_1^\infty dx_1 \int_1^\infty dx_2 \int_{-\infty}^\infty dy_1 \int_{-\infty}^\infty dy_2 \\
&\quad \frac{1}{\sqrt{x_1 + y_1^2} + \sqrt{x_1 - 1 + y_1^2} - 2|y_1| + 1} \frac{1}{x_1 + \frac{1}{4}(\frac{1}{\alpha} + \alpha)^2 y_1^2} \\
&\quad \times \frac{1}{\sqrt{x_2 + y_2^2} + \sqrt{x_2 - 1 + y_2^2} - 2|y_2| + 1} \frac{1}{x_2 + \frac{1}{4}(\frac{1}{\alpha} + \alpha)^2 y_2^2} \\
&\quad \times \frac{1}{|x_1 - x_2| + \frac{1}{4}(\frac{1}{\alpha} + \alpha)^2 (y_1^2 + y_2^2) - \frac{1}{2}(\frac{1}{\alpha^2} - \alpha^2) y_1 y_2} \tag{F.42}
\end{aligned}$$

F.2.2 Quartic vertex

In this section we evaluate the five loop correction to the boson four-point function shown in Fig. 7.18. We recall that by the particle-hole symmetry of our theory, diagrams with a reversed direction of the two fermion loops have the same value. We focus only on the diagrams where the fermions in the two loops come from opposite hot spots as these give a result, which is of $\mathcal{O}(N^3)$ and logarithmically divergent. To identify the coefficient of the logarithmic divergence we may set all the external momenta to zero. Then by rotational invariance each hot spot pair gives the same contribution. Moreover, we can also consider the diagram as in Fig. 7.18 but with fermions 1 and 2 interchanged. By reflection symmetry, this has the same UV divergence. Finally, we should be able to absorb the UV divergence into the coefficient of the quartic vertex $\vec{\phi}^2$, which specifies the spin structure,

$$\delta\Gamma_4^{a_1 a_2 a_3 a_4} \stackrel{UV}{=} \frac{1}{3} (\delta^{a_1 a_2} \delta^{a_3 a_4} + \delta^{a_1 a_3} \delta^{a_2 a_4} + \delta^{a_1 a_4} \delta^{a_2 a_3}) \delta\Gamma_4^{3333} \quad (\text{F.43})$$

and

$$\begin{aligned} \delta\Gamma_4^{3333} &= -4 \cdot 6 \cdot 2 \cdot n \cdot S \cdot N^2 \int \frac{d^3 p_1 d^3 p_2 d^3 l_1 d^3 l_2 d^3 l_3}{(2\pi)^{15}} D(l_1) D(l_3) D(l_1 - l_2) D(l_2 - l_3) \\ &\times G_1^1(p_1) G_2^1(p_1)^2 G_1^1(p_1 - l_1) G_2^1(p_1 - l_2) G_1^1(p_1 - l_3) \\ &\times G_1^{-1}(p_2) G_2^{-1}(p_2)^2 G_1^{-1}(p_2 - l_1) G_2^{-1}(p_2 - l_2) G_1^{-1}(p_2 - l_3) \end{aligned} \quad (\text{F.44})$$

with

$$S = \text{tr}(\tau^3 \tau^3 \tau^a \tau^b \tau^c \tau^d) \text{tr}(\tau^3 \tau^3 \tau^a \tau^b \tau^c \tau^d) = 84 \quad (\text{F.45})$$

We will use the same strategy for evaluating the integral (F.44) as for computing the vertex correction in section F.2.1. The singular manifold in the present case is

specified by vanishing $\vec{p}_1, \vec{p}_2, \hat{v}_1 \cdot \vec{l}_1, \hat{v}_2 \cdot \vec{l}_2, \hat{v}_1 \cdot \vec{l}_3$ and can be parameterized by the three momenta $\hat{v}_2 \cdot \vec{l}_1, \hat{v}_1 \cdot \vec{l}_2, \hat{v}_2 \cdot \vec{l}_3$. We will integrate explicitly over the first set of momenta and leave the result as an integral over the later three momenta.

Let us call $I(p_{1\tau}, p_{2\tau})$ the result of integrating over all momenta and frequencies in Eq. (F.44), except $p_{1\tau}$ and $p_{2\tau}$. Then, using the particle-hole symmetry, $G(p) = -G(-p)$, and the inversion symmetry, $G^{-1}(p_\tau, \vec{p}) = G^1(p_\tau, -\vec{p})$, we obtain $I(p_{1\tau}, p_{2\tau}) = I(-p_{1\tau}, -p_{2\tau})$ and $I(p_{1\tau}, p_{2\tau}) = I(p_{2\tau}, p_{1\tau})$. Thus,

$$\begin{aligned} \delta\Gamma_4^{3333} &= -2^{10} \cdot 3^2 \cdot 7 \cdot N^2 \left(\frac{|\vec{v}|^2}{2v_x v_y} \right)^5 \int_0^\infty \frac{dp_{1\tau}}{2\pi} \int_{-p_{1\tau}}^{p_{1\tau}} \frac{dp_{2\tau}}{2\pi} \int \frac{dl_{1\tau} dl_{2\tau} dl_{3\tau}}{(2\pi)^3} \\ &\int \frac{d(\hat{v}_1 \cdot \vec{l}_1) d(\hat{v}_2 \cdot \vec{l}_1) d(\hat{v}_1 \cdot \vec{l}_2) d(\hat{v}_2 \cdot \vec{l}_2) d(\hat{v}_1 \cdot \vec{l}_3) d(\hat{v}_2 \cdot \vec{l}_3)}{(2\pi)^6} \\ &\int \frac{d(\hat{v}_1 \cdot \vec{p}_1) d(\hat{v}_2 \cdot \vec{p}_1) d(\hat{v}_1 \cdot \vec{p}_2) d(\hat{v}_2 \cdot \vec{p}_2)}{(2\pi)^4} \frac{1}{-i\frac{c_f}{N}g(p_{1\tau}, 0) + \vec{v}_1 \cdot \vec{p}_1} \\ &\times \frac{1}{(-i\frac{c_f}{N}g(p_{1\tau}, 0) + \vec{v}_2 \cdot \vec{p}_1)^2} \frac{1}{-i\frac{c_f}{N}g(p_{1\tau} - l_{1\tau}, \hat{v}_2 \cdot \vec{l}_1) + \vec{v}_1 \cdot (\vec{p}_1 - \vec{l}_1)} \\ &\times \frac{1}{-i\frac{c_f}{N}g(p_{1\tau} - l_{2\tau}, \hat{v}_1 \cdot \vec{l}_2) + \vec{v}_2 \cdot (\vec{p}_1 - \vec{l}_2)} \frac{1}{-i\frac{c_f}{N}g(p_{1\tau} - l_{3\tau}, \hat{v}_2 \cdot \vec{l}_3) + \vec{v}_1 \cdot (\vec{p}_1 - \vec{l}_3)} \\ &\times \frac{1}{-i\frac{c_f}{N}g(p_{2\tau}, 0) - \vec{v}_1 \cdot \vec{p}_2} \frac{1}{(-i\frac{c_f}{N}g(p_{2\tau}, 0) - \vec{v}_2 \cdot \vec{p}_2)^2} \\ &\times \frac{1}{-i\frac{c_f}{N}g(p_{2\tau} - l_{1\tau}, \hat{v}_2 \cdot \vec{l}_1) - \vec{v}_1 \cdot (\vec{p}_2 - \vec{l}_1)} \frac{1}{-i\frac{c_f}{N}g(p_{2\tau} - l_{2\tau}, \hat{v}_1 \cdot \vec{l}_2) - \vec{v}_2 \cdot (\vec{p}_2 - \vec{l}_2)} \\ &\times \frac{1}{-i\frac{c_f}{N}g(p_{2\tau} - l_{3\tau}, \hat{v}_2 \cdot \vec{l}_3) - \vec{v}_1 \cdot (\vec{p}_2 - \vec{l}_3)} D(l_1)D(l_3)D(l_1 - l_2)D(l_2 - l_3) \end{aligned}$$

Integrating over $\hat{v}_1 \cdot \vec{l}_1, \hat{v}_2 \cdot \vec{l}_2, \hat{v}_1 \cdot \vec{l}_3$,

$$\begin{aligned} \delta\Gamma_4^{3333} &= -i2^{10} \cdot 3^2 \cdot 7 \cdot N^2 \frac{|\vec{v}|^7}{(2v_x v_y)^5} \int_0^\infty \frac{dp_{1\tau}}{2\pi} \int_{-p_{1\tau}}^{p_{1\tau}} \frac{dp_{2\tau}}{2\pi} \\ &\left[\int_{p_{1\tau}}^\infty - \int_{-\infty}^{p_{2\tau}} \right] \frac{dl_{1\tau}}{2\pi} \left[\int_{p_{1\tau}}^\infty - \int_{-\infty}^{p_{2\tau}} \right] \frac{dl_{2\tau}}{2\pi} \left[\int_{p_{1\tau}}^\infty - \int_{-\infty}^{p_{2\tau}} \right] \frac{dl_{3\tau}}{2\pi} \\ &\int \frac{d(\hat{v}_1 \cdot \vec{p}_1) d(\hat{v}_2 \cdot \vec{p}_1) d(\hat{v}_1 \cdot \vec{p}_2) d(\hat{v}_2 \cdot \vec{p}_2) d(\hat{v}_2 \cdot \vec{l}_1) d(\hat{v}_1 \cdot \vec{l}_2) d(\hat{v}_2 \cdot \vec{l}_3)}{(2\pi)^7} \end{aligned}$$

$$\begin{aligned}
& \frac{1}{-i\frac{c_f}{N}g(p_{1\tau}, 0) + \vec{v}_1 \cdot \vec{p}_1} \frac{1}{(-i\frac{c_f}{N}g(p_{1\tau}, 0) + \vec{v}_2 \cdot \vec{p}_1)^2} \\
& \times \frac{1}{-i\frac{c_f}{N}g(p_{2\tau}, 0) - \vec{v}_1 \cdot \vec{p}_2} \frac{1}{(-i\frac{c_f}{N}g(p_{2\tau}, 0) - \vec{v}_2 \cdot \vec{p}_2)^2} \\
& \times \frac{1}{-i\frac{c_f}{N}(g(p_{1\tau} - l_{1\tau}, \hat{v}_2 \cdot \vec{l}_1) + g(p_{2\tau} - l_{1\tau}, \hat{v}_2 \cdot \vec{l}_1)) + \vec{v}_1 \cdot (\vec{p}_1 - \vec{p}_2)} \\
& \times \frac{1}{-i\frac{c_f}{N}(g(p_{1\tau} - l_{2\tau}, \hat{v}_1 \cdot \vec{l}_2) + g(p_{2\tau} - l_{2\tau}, \hat{v}_1 \cdot \vec{l}_2)) + \vec{v}_2 \cdot (\vec{p}_1 - \vec{p}_2)} \\
& \times \frac{1}{-i\frac{c_f}{N}(g(p_{1\tau} - l_{3\tau}, \hat{v}_2 \cdot \vec{l}_3) + g(p_{2\tau} - l_{3\tau}, \hat{v}_2 \cdot \vec{l}_3)) + \vec{v}_1 \cdot (\vec{p}_1 - \vec{p}_2)} \\
& \times D(l_1)D(l_3)D(l_1 - l_2)D(l_2 - l_3)|_{\hat{v}_1 \cdot \vec{l}_1 = \hat{v}_2 \cdot \vec{l}_2 = \hat{v}_1 \cdot \vec{l}_3 = 0} \tag{F.46}
\end{aligned}$$

Now, integrating over $\hat{v}_1 \cdot \vec{p}_1, \hat{v}_2 \cdot \vec{p}_1,$

$$\begin{aligned}
\delta\Gamma_4^{3333} &= -i2^{10} \cdot 3^2 \cdot 7 \cdot N^2 \frac{|\vec{v}|^5}{(2v_x v_y)^5} \int_0^\infty \frac{dp_{1\tau}}{2\pi} \int_{-p_{1\tau}}^{p_{1\tau}} \frac{dp_{2\tau}}{2\pi} \int_{p_{1\tau}}^\infty \frac{dl_{2\tau}}{2\pi} \\
& \int \frac{d(\hat{v}_1 \cdot \vec{p}_2)d(\hat{v}_2 \cdot \vec{p}_2)d(\hat{v}_2 \cdot \vec{l}_1)d(\hat{v}_1 \cdot \vec{l}_2)d(\hat{v}_2 \cdot \vec{l}_3)}{(2\pi)^5} \\
& \left(-i\frac{c_f}{N}g(p_{2\tau}, 0) - \vec{v}_1 \cdot \vec{p}_2\right)^{-1} \left(-i\frac{c_f}{N}g(p_{2\tau}, 0) - \vec{v}_2 \cdot \vec{p}_2\right)^{-2} \\
& \times \left(-i\frac{c_f}{N}(g(p_{1\tau}, 0) + g(l_{2\tau} - p_{1\tau}, \hat{v}_1 \cdot \vec{l}_2) + g(l_{2\tau} - p_{2\tau}, \hat{v}_1 \cdot \vec{l}_2)) + \vec{v}_2 \cdot \vec{p}_2\right)^{-2} \\
& \times \left[\int_{p_{1\tau}}^\infty \frac{dl_{1\tau}}{2\pi} \int_{p_{1\tau}}^\infty \frac{dl_{3\tau}}{2\pi} \left(i\frac{c_f}{N}(g(p_{1\tau}, 0) + g(l_{1\tau} - p_{1\tau}, \hat{v}_2 \cdot \vec{l}_1) + g(l_{1\tau} - p_{2\tau}, \hat{v}_2 \cdot \vec{l}_1)) \right. \right. \\
& \left. \left. - \vec{v}_1 \cdot \vec{p}_2 \right)^{-1} \left(i\frac{c_f}{N}(g(p_{1\tau}, 0) + g(l_{3\tau} - p_{1\tau}, \hat{v}_2 \cdot \vec{l}_3) + g(l_{3\tau} - p_{2\tau}, \hat{v}_2 \cdot \vec{l}_3)) - \vec{v}_1 \cdot \vec{p}_2 \right)^{-1} \right. \\
& \left. + \int_{p_{1\tau}}^\infty \frac{dl_{1\tau}}{2\pi} \int_{-\infty}^{p_{2\tau}} \frac{dl_{3\tau}}{2\pi} \left(-i\frac{c_f}{N}(g(p_{1\tau}, 0) + g(l_{1\tau} - p_{1\tau}, \hat{v}_2 \cdot \vec{l}_1) + g(l_{1\tau} - p_{2\tau}, \hat{v}_2 \cdot \vec{l}_1)) \right. \right. \\
& \left. \left. + \vec{v}_1 \cdot \vec{p}_2 \right)^{-1} \left(-i\frac{c_f}{N}(g(l_{1\tau} - p_{1\tau}, \hat{v}_2 \cdot \vec{l}_1) + g(l_{1\tau} - p_{2\tau}, \hat{v}_2 \cdot \vec{l}_1) \right. \right. \\
& \left. \left. + g(p_{1\tau} - l_{3\tau}, \hat{v}_2 \cdot \vec{l}_3) + g(p_{2\tau} - l_{3\tau}, \hat{v}_2 \cdot \vec{l}_3)) \right)^{-1} \right)
\end{aligned}$$

$$\begin{aligned}
 & + \int_{-\infty}^{p_{2\tau}} \frac{dl_{1\tau}}{2\pi} \int_{p_{1\tau}}^{\infty} \frac{dl_{3\tau}}{2\pi} \left(-i \frac{c_f}{N} (g(p_{1\tau}, 0) + g(l_{3\tau} - p_{1\tau}, \hat{v}_2 \cdot \vec{l}_3) + g(l_{3\tau} - p_{2\tau}, \hat{v}_2 \cdot \vec{l}_3)) \right. \\
 & \left. + \vec{v}_1 \cdot \vec{p}_2 \right)^{-1} \left(-i \frac{c_f}{N} (g(p_{1\tau} - l_{1\tau}, \hat{v}_2 \cdot \vec{l}_1) + g(p_{2\tau} - l_{1\tau}, \hat{v}_2 \cdot \vec{l}_1) \right. \\
 & \left. + g(l_{3\tau} - p_{1\tau}, \hat{v}_2 \cdot \vec{l}_3) + g(l_{3\tau} - p_{2\tau}, \hat{v}_2 \cdot \vec{l}_3)) \right)^{-1} \Big] \\
 & \times D(l_1)D(l_3)D(l_1 - l_2)D(l_2 - l_3)|_{\hat{v}_1 \cdot \vec{l}_1 = \hat{v}_2 \cdot \vec{l}_2 = \hat{v}_1 \cdot \vec{l}_3 = 0}
 \end{aligned} \tag{F.47}$$

Observe that under $l_1 \leftrightarrow l_3$ the first term in the square brackets is invariant, while the second and third terms map into each other. Utilizing this fact and integrating over $\hat{v}_1 \cdot \vec{p}_2$, $\hat{v}_2 \cdot \vec{p}_2$,

$$\begin{aligned}
 \delta\Gamma_4^{3333} &= -2^{12} \cdot 3^2 \cdot 7 \cdot N^7 \frac{|\vec{v}|^3}{(2v_x v_y c_f)^5} \int_0^{\infty} \frac{dp_{1\tau}}{2\pi} \int_0^{p_{1\tau}} \frac{dp_{2\tau}}{2\pi} \int_{p_{1\tau}}^{\infty} \frac{dl_{1\tau}}{2\pi} \int_{p_{1\tau}}^{\infty} \frac{dl_{2\tau}}{2\pi} \\
 & \int \frac{d(\hat{v}_2 \cdot \vec{l}_1) d(\hat{v}_1 \cdot \vec{l}_2) d(\hat{v}_2 \cdot \vec{l}_3)}{(2\pi)^3} \left(g(p_{1\tau}, 0) + g(p_{2\tau}, 0) + g(l_{1\tau} - p_{1\tau}, \hat{v}_2 \cdot \vec{l}_1) \right. \\
 & \left. + g(l_{1\tau} - p_{2\tau}, \hat{v}_2 \cdot \vec{l}_1) \right)^{-1} \left(g(p_{1\tau}, 0) + g(p_{2\tau}, 0) + g(l_{2\tau} - p_{1\tau}, \hat{v}_1 \cdot \vec{l}_2) \right. \\
 & \left. + g(l_{2\tau} - p_{2\tau}, \hat{v}_1 \cdot \vec{l}_2) \right)^{-3} \left[\int_{p_{1\tau}}^{l_{1\tau}} \frac{dl_{3\tau}}{2\pi} \left(g(p_{1\tau}, 0) + g(p_{2\tau}, 0) \right. \right. \\
 & \left. \left. + g(l_{3\tau} - p_{1\tau}, \hat{v}_2 \cdot \vec{l}_3) + g(l_{3\tau} - p_{2\tau}, \hat{v}_2 \cdot \vec{l}_3) \right)^{-1} + \int_{-\infty}^{p_{2\tau}} \frac{dl_{3\tau}}{2\pi} \left(g(l_{1\tau} - p_{1\tau}, \hat{v}_2 \cdot \vec{l}_1) \right. \right. \\
 & \left. \left. + g(l_{1\tau} - p_{2\tau}, \hat{v}_2 \cdot \vec{l}_1) + g(p_{1\tau} - l_{3\tau}, \hat{v}_2 \cdot \vec{l}_3) + g(p_{2\tau} - l_{3\tau}, \hat{v}_2 \cdot \vec{l}_3) \right)^{-1} \right] \\
 & \times D(l_1)D(l_3)D(l_1 - l_2)D(l_2 - l_3)|_{\hat{v}_1 \cdot \vec{l}_1 = \hat{v}_2 \cdot \vec{l}_2 = \hat{v}_1 \cdot \vec{l}_3 = 0}
 \end{aligned} \tag{F.48}$$

We now introduce dimensionless variables, $p_{2\tau} = xp_{1\tau}$, $l_{i\tau} = y_i p_{1\tau}$, $\hat{v}_2 \cdot \vec{l}_1 = \sqrt{\gamma p_{1\tau}} z_1$, $\hat{v}_1 \cdot \vec{l}_2 = \sqrt{\gamma p_{1\tau}} z_2$, $\hat{v}_2 \cdot \vec{l}_3 = \sqrt{\gamma p_{1\tau}} z_3$. Then,

$$\delta\Gamma_4^{3333} = \frac{1}{2} N^3 Y(\alpha) \gamma \int_0^{\infty} \frac{dp_{1\tau}}{p_{1\tau}} = N^3 Y(\alpha) \gamma \log \Lambda \tag{F.49}$$

with

$$\begin{aligned}
Y(\alpha) = & -\frac{56}{27\pi^2} \left(\frac{1}{\alpha} + \alpha\right)^4 \int_0^1 dx \int_1^\infty dy_1 \int_1^\infty dy_2 \int_{-\infty}^\infty dz_1 \int_{-\infty}^\infty dz_2 \int_{-\infty}^\infty dz_3 \\
& \left(1 + \sqrt{x} + \sqrt{y_1 - 1 + z_1^2} + \sqrt{y_1 - x + z_1^2} - 2|z_1|\right)^{-1} \\
& \times \left(1 + \sqrt{x} + \sqrt{y_2 - 1 + z_2^2} + \sqrt{y_2 - x + z_2^2} - 2|z_2|\right)^{-3} \\
& \left[\int_1^{y_1} dy_3 \left(1 + \sqrt{x} + \sqrt{y_3 - 1 + z_3^2} + \sqrt{y_3 - x + z_3^2} - 2|z_3|\right)^{-1} \right. \\
& + \int_{-\infty}^x dy_3 \left(\sqrt{y_1 - 1 + z_1^2} + \sqrt{y_1 - x + z_1^2} + \sqrt{1 - y_3 + z_3^2} \right. \\
& \left. \left. + \sqrt{x - y_3 + z_3^2} - 2|z_1| - 2|z_3|\right)^{-1} \right] \left(y_1 + \frac{1}{4}\left(\frac{1}{\alpha} + \alpha\right)^2 z_1^2\right)^{-1} \\
& \times \left(|y_3| + \frac{1}{4}\left(\frac{1}{\alpha} + \alpha\right)^2 z_3^2\right)^{-1} \left(|y_1 - y_2| + \frac{1}{4}\left(\frac{1}{\alpha} + \alpha\right)^2 (z_1^2 + z_2^2) + \frac{1}{2}\left(\alpha^2 - \frac{1}{\alpha^2}\right) z_1 z_2\right)^{-1} \\
& \times \left(|y_2 - y_3| + \frac{1}{4}\left(\frac{1}{\alpha} + \alpha\right)^2 (z_2^2 + z_3^2) + \frac{1}{2}\left(\alpha^2 - \frac{1}{\alpha^2}\right) z_2 z_3\right)^{-1} \tag{F.50}
\end{aligned}$$

F.2.3 Pairing vertex

This appendix will describe the direct evaluation of the pairing vertex correction in Eq. (7.89). We first attempt to perform the calculation using bare fermion propagators,

$$\begin{aligned}
\delta\Gamma_{V\psi^\dagger\psi^\dagger} = & \frac{-3\mu}{N|\vec{v}|^2} \int \frac{dl_\tau dl_\perp dl_\parallel}{(2\pi)^3} \frac{1}{\gamma|l_\tau| + l_\perp^2 + l_\parallel^2} \frac{1}{l_\perp - \hat{v}_2 \cdot \vec{k}_1 - i\frac{\eta}{|\vec{v}|}(l_\tau - k_{1\tau})} \\
& \times \frac{1}{l_\perp + \hat{v}_2 \cdot \vec{k}_{-1} + i\frac{\eta}{|\vec{v}|}(l_\tau + k_{-1\tau})}
\end{aligned}$$

where we've introduced variables $l_\perp = \hat{v}_2 \cdot \vec{l}$, $l_\parallel = \epsilon_{ij}(\hat{v}_2)_i l_j$. For simplicity, let us choose $k_{1\tau} = k_{-1\tau} = \omega > 0$. We now perform the integral over l_\perp . For $|l_\tau| < \omega$ both poles in the fermion propagators are in the same half-plane and we can pick up

just the pole from the bosonic propagator. In the opposite regime, $|l_\tau| > \omega$, we get contributions from both the bosonic and fermionic poles. Thus,

$$\delta\Gamma_{V\psi^\dagger\psi^\dagger} = -\frac{3\mu}{N|\vec{v}|^2} \left[-\int_0^\infty \frac{dl_\tau}{2\pi} \int \frac{dl_\parallel}{2\pi} \frac{1}{\sqrt{\gamma l_\tau + l_\parallel^2}} \frac{1}{\sqrt{\gamma l_\tau + l_\parallel^2 + i\hat{v}_2 \cdot \vec{k}_1}} \right. \\ \left. \times \frac{1}{\sqrt{\gamma l_\tau + l_\parallel^2 - i\hat{v}_2 \cdot \vec{k}_{-1}}} \right] \quad (\text{F.51})$$

$$+ \frac{|\vec{v}|}{2\eta} \int_\omega^\infty \frac{dl_\tau}{2\pi} \int \frac{dl_\parallel}{2\pi} \left(\frac{1}{l_\tau - i\frac{\hat{v}_2}{\eta} \cdot (\vec{k}_1 + \vec{k}_{-1})} \frac{1}{\gamma l_\tau + l_\parallel^2 + (\hat{v}_2 \cdot \vec{k}_1)^2} \right. \\ \left. + \frac{1}{l_\tau + i\frac{\hat{v}_2}{\eta} \cdot (\vec{k}_1 + \vec{k}_{-1})} \frac{1}{\gamma l_\tau + l_\parallel^2 + (\hat{v}_2 \cdot \vec{k}_{-1})^2} \right) \quad (\text{F.52})$$

$$\left. \right] \quad (\text{F.53})$$

The contribution from the bosonic pole in Eq. (F.51) gives an expected logarithmic divergence,

$$\delta^{bos}\Gamma_{V\psi^\dagger\psi^\dagger} \sim \frac{3\mu}{N\pi^2\gamma|\vec{v}|^2} \log \frac{\Lambda}{|\hat{v}_2 \cdot \vec{k}|} \quad (\text{F.54})$$

On the other hand, the contribution from the fermionic poles in Eqs. (F.52),(F.53) gives a much stronger infra-red singularity. If we set the total momentum of the fermion pair $\vec{k}_1 + \vec{k}_{-1}$ to zero, then

$$\delta^{fer}\Gamma_{V\psi^\dagger\psi^\dagger} \sim -\frac{3\mu}{4\pi N\eta|\vec{v}_2 \cdot \vec{k}_1|} f\left(\frac{\gamma|\omega|}{|\hat{v}_2 \cdot \vec{k}_1|^2}\right) \quad (\text{F.55})$$

with

$$f(a) = \int_a^\infty dx \frac{1}{x\sqrt{x+1}} \quad (\text{F.56})$$

If the total pair momentum is non-vanishing, in particular, if $\frac{\gamma}{\eta}|\vec{v}_2 \cdot (\vec{k}_1 + \vec{k}_{-1})| \gg (\hat{v}_2 \cdot \vec{k}_1)^2, \gamma\omega$, then,

$$\delta^{fer}\Gamma_{V\psi^\dagger\psi^\dagger} = -\frac{3\mu}{4N|\vec{v}|\sqrt{2\gamma\eta}} \frac{1}{\sqrt{|\vec{v}_2 \cdot (\vec{k}_1 + \vec{k}_{-1})|}} \quad (\text{F.57})$$

As usual, we cure the strong infra-red divergences by using a one-loop dressed fermion propagator (F.36). Then,

$$\begin{aligned} \delta\Gamma_{V\psi^\dagger\psi^\dagger}(k_1, k_{-1}) &= -\frac{3\mu}{N|\vec{v}|^2} \int \frac{d^3l}{(2\pi)^3} \frac{1}{\hat{v}_2 \cdot (\vec{l} - \vec{k}_1) - i\frac{c_f}{N|\vec{v}|} g(l_\tau - k_{1\tau}, \hat{v}_1 \cdot (\vec{l} - \vec{k}_1))} \\ &\times \frac{1}{\hat{v}_2 \cdot (\vec{l} + \vec{k}_{-1}) + i\frac{c_f}{N|\vec{v}|} g(l_\tau + k_{-1\tau}, \hat{v}_1 \cdot (\vec{l} + \vec{k}_{-1}))} \frac{1}{\gamma|l_\tau| + \vec{l}^2} \end{aligned}$$

For simplicity, we take the external fermion momenta to lie at the hot spots, $\vec{k}_1 = \vec{k}_{-1} = 0$. Moreover, as before, we choose the external frequencies, $k_{1\tau} = k_{-1\tau} = \omega > 0$. Switching to variables, l_\perp, l_\parallel , we perform the integral over l_\perp . As we saw above, the contribution from the pole in the bosonic propagator could be calculated without dressing the fermion Green's function and was of $\mathcal{O}(1/N)$ - we drop this piece below. On the other hand, as we will see the contribution from the poles in fermionic propagators is of $\mathcal{O}(1)$ in N . Moreover, since $l_\perp \sim \mathcal{O}(1/N)$ at these poles, we may ignore the dependence of the fermion self-energy on l_\perp , which gives, $\hat{v}_1 \cdot \vec{l} = \frac{2\alpha}{\alpha^2+1} l_\parallel$. In this manner, we obtain,

$$\begin{aligned} \delta\Gamma_{V\psi^\dagger\psi^\dagger} &= -\frac{6\mu}{c_f|\vec{v}|} \int_\omega^\infty \frac{dl_\tau}{2\pi} \int \frac{dl_\parallel}{2\pi} \frac{1}{\gamma l_\tau + l_\parallel^2} \\ &\times \frac{1}{g(l_\tau - \omega, \frac{2\alpha}{\alpha^2+1} l_\parallel) + g(l_\tau + \omega, \frac{2\alpha}{\alpha^2+1} l_\parallel)} \end{aligned} \quad (\text{F.58})$$

We now perform the integral over l_τ . This integral is convergent in the ultra-violet. However, when $\omega \rightarrow 0$, it is logarithmically divergent in the infra-red. This infra-red divergence comes from the region $\gamma l_\tau \ll l_\parallel^2$. Changing variables to $\gamma l_\tau = x l_\parallel^2$, we

obtain,

$$\delta\Gamma_{V\psi^\dagger\psi^\dagger} = -\frac{3\mu}{\pi^2\gamma|\vec{v}|c_f} \int_0^\infty \frac{dl_\parallel}{l_\parallel} \int_{\frac{\gamma\omega}{l_\parallel^2}} \frac{dx}{x+1} \frac{1}{\sqrt{x + \left(\frac{2\alpha}{\alpha^2+1}\right)^2 - \frac{\gamma\omega}{l_\parallel^2}} + \sqrt{x + \left(\frac{2\alpha}{\alpha^2+1}\right)^2 + \frac{\gamma\omega}{l_\parallel^2} - \frac{4\alpha}{\alpha^2+1}}} \quad (\text{F.59})$$

For $l_\parallel^2 \gg \gamma\omega$, performing the integral over x to logarithmic accuracy,

$$\delta\Gamma_{V\psi^\dagger\psi^\dagger} \approx -\frac{6\mu\alpha}{\pi^2\gamma|\vec{v}|c_f(\alpha^2+1)} \int_{\sqrt{\gamma\omega}}^\infty \frac{dl_\parallel}{l_\parallel} \log\left(\frac{l_\parallel^2}{\gamma\omega}\right) = -\frac{\mu\alpha}{\pi(\alpha^2+1)} \log^2\left(\frac{\Lambda^2}{\gamma\omega}\right) \quad (\text{F.60})$$

F.2.4 Density vertex

In this appendix, we compute the one-loop renormalization of the density-wave vertex, shown in Fig. 7.20b),

$$\delta\Gamma_{O\psi\psi^\dagger}(k_1, k_{-1}) = 3\mu \int \frac{d^3l}{(2\pi)^3} D(l) G_2^1(k_1 - l) G_2^{-1}(k_{-1} - l). \quad (\text{F.61})$$

If we ignore the effects of Fermi-surface curvature, $G(l) = -G(-l)$, and Eq. (F.61) reduces to its counterpart in the superconducting channel with $k_{-1} \rightarrow -k_{-1}$. In the present calculation, we will keep the effects of the Fermi-surface curvature using a propagator,

$$G_i^\ell(l) = \frac{1}{-\frac{ic_f}{N}g(l_\tau, \hat{v}_i^\ell \cdot \vec{l}) + \vec{v}_i^\ell \cdot \vec{l} + (\hat{n}_{\parallel,i}^\ell \cdot \vec{l})^2} \quad (\text{F.62})$$

Here, we ignore any dressing of the curvature by the interactions.

For simplicity, we set external momenta to zero and choose $k_{1\tau} = -k_{-1\tau} = \omega > 0$. As in Appendix F.2.3, we introduce variables $l_\perp = \hat{v}_2 \cdot \vec{l}$, $l_\parallel = \epsilon_{ij}(\hat{v}_2)_i l_j$. Proceeding as in Section 7.5, we keep only the contribution to the integral (F.61) from the Fermi

liquid regime, $\gamma l_\tau \ll l_\parallel^2$. Then,

$$\delta\Gamma_{O\psi\psi^\dagger} = \frac{3\mu}{N} \int \frac{dl_\parallel}{2\pi} \int_{\gamma|l_\tau| \lesssim l_\parallel^2} \frac{dl_\tau}{2\pi} \int \frac{dl_\perp}{2\pi} \frac{1}{l_\parallel^2} \frac{1}{i\mathcal{Z}^{-1}(l_\parallel)(l_\tau - \omega) - |\vec{v}|l_\perp - \frac{1}{2m}l_\parallel^2} \frac{1}{i\mathcal{Z}^{-1}(l_\parallel)(l_\tau + \omega) + |\vec{v}|l_\perp - \frac{1}{2m}l_\parallel^2} \quad (\text{F.63})$$

Performing the integral over l_\perp ,

$$\delta\Gamma_{O\psi\psi^\dagger} = -\frac{3\mu}{N|\vec{v}|} \int \frac{dl_\parallel}{2\pi} \int_\omega^{l_\parallel^2/\gamma} \frac{dl_\tau}{2\pi} \frac{\mathcal{Z}(l_\parallel)}{l_\parallel^2} \frac{l_\tau}{l_\tau^2 + \left(\frac{\mathcal{Z}(l_\parallel)l_\parallel^2}{2m}\right)^2} \quad (\text{F.64})$$

Notice that the Fermi-surface curvature is present in the denominator of Eq. (F.64).

This is in contrast to the corresponding calculation in the superconducting channel,

where the Fermi-surface curvature drops out. Performing the integral over l_τ ,

$$\delta\Gamma_{O\psi\psi^\dagger} = -\frac{3\mu}{2\pi N|\vec{v}|} \int_{\sqrt{\gamma\omega}}^\infty \frac{dl_\parallel}{2\pi} \frac{\mathcal{Z}(l_\parallel)}{l_\parallel^2} \log \frac{l_\parallel^4}{(\gamma\omega)^2 + \left(\frac{\gamma\mathcal{Z}(l_\parallel)l_\parallel^2}{2m}\right)^2} \quad (\text{F.65})$$

where we have ignored terms subleading in l_\parallel in the numerator of the logarithm.

Recall, $\mathcal{Z}(l_\parallel) \sim N|\vec{v}|l_\parallel$. Hence, for $l_\parallel \ll (m\omega/N|\vec{v}|)^{1/3}$ the l_τ integral is cut-off

in the infrared by the external frequency and the Fermi surface curvature may be

neglected. On the other hand, for $l_\parallel \gg (m\omega/N|\vec{v}|)^{1/3}$ the integral is cut-off by the

curvature. By comparison, in the superconducting channel the integral is cut-off by

the external frequency in both regimes resulting in a stronger enhancement. Notice

that the cross-over scale $(m\omega/N|\vec{v}|)^{1/3}$ is much larger than the infra-red cut-off of the

l_\parallel integral $\sqrt{\gamma\omega}$. Evaluating the integral over l_\parallel to leading logarithmic accuracy,

$$\delta\Gamma_{O\psi\psi^\dagger} = -\frac{\mu\alpha}{3\pi(\alpha^2 + 1)} \log^2 \left(\frac{\Lambda^2}{\gamma\omega} \right) \quad (\text{F.66})$$

Bibliography

- [1] T. Senthil, A. Vishwanath, L. Balents, S. Sachdev, and M. Fisher, *Science* **303**, 1490 (2004)
- [2] T. Senthil, L. Balents, S. Sachdev, A. Vishwanath, and M. P. A. Fisher, *Phys. Rev. B* **70**, 144407 (2004)
- [3] G. Murthy and S. Sachdev, *Nuclear Physics B* **344**, 557 (1990)
- [4] K. H. Höglund and A. W. Sandvik, *Phys. Rev. B* **79**, 020405 (2009)
- [5] J. A. Hertz, *Phys. Rev. B* **14**, 1165 (1976)
- [6] P. Calabrese and J. L. Cardy, *J.Stat.Mech.* **0406**, P06002 (2004)
- [7] S. Chakravarty, B. I. Halperin, and D. R. Nelson, *Phys. Rev. Lett.* **60**, 1057 (1988)
- [8] D. Haug, V. Hinkov, Y. Sidis, P. Bourges, N. B. Christensen, A. Ivanov, T. C. Keller, T. Lin, and B. Keimer, *New. J. Phys.* **12**, 105006 (2010)
- [9] V. Hinkov, D. Haug, B. Fauqu, P. Bourges, Y. Sidis, A. Ivanov, C. Bernhard, C. T. Lin, and B. Keimer, *Science* **319**, 597 (2008)
- [10] Y. Ando, K. Segawa, S. Komiya, and A. N. Lavrov, *Phys. Rev. Lett.* **88**, 137005 (2002)
- [11] R. Daou, J. Chang, D. LeBoeuf, O. Cyr-Choinire, F. Lalibert, N. Doiron-Leyraud, B. J. Ramshaw, R. Liang, D. A. Bonn, W. N. Hardy, and L. Taillefer, *Nature* **463**, 519 (2010)
- [12] Y. Kohsaka, C. Taylor, K. Fujita, A. Schmidt, C. Lupien, T. Hanaguri, M. Azuma, M. Takano, H. Eisaki, H. Takagi, S. Uchida, and J. C. Davis, *Science* **315**, 1380 (2007)
- [13] M. J. Lawler, K. Fujita, J. Lee, A. Schmidt, Y. Kohsaka, C. K. Kim, H. Eisaki, S. Uchida, J. Davis, J. Sethna, and E.-A. Kim, *Nature* **466**, 347 (2010)

-
- [14] M. Fujita, H. Goka, K. Yamada, J. M. Tranquada, and L. P. Regnault, *Phys. Rev. B* **70**, 104517 (2004)
- [15] J. M. Tranquada, G. D. Gu, M. Hücker, Q. Jie, H.-J. Kang, R. Klingeler, Q. Li, N. Tristan, J. S. Wen, G. Y. Xu, Z. J. Xu, J. Zhou, and M. v. Zimmermann, *Phys. Rev. B* **78**, 174529 (2008)
- [16] N. Ichikawa, S. Uchida, J. M. Tranquada, T. Niemöller, P. M. Gehring, S.-H. Lee, and J. R. Schneider, *Phys. Rev. Lett.* **85**, 1738 (2000)
- [17] W. D. Wise, M. C. Boyer, K. Chatterjee, T. Kondo, T. Takeuchi, H. Ikuta, Y. Wang, and E. W. Hudson, *Nature Physics* **4**, 696 (2008)
- [18] B. Fauqué, Y. Sidis, V. Hinkov, S. Pailhès, C. T. Lin, X. Chaud, and P. Bourges, *Phys. Rev. Lett.* **96**, 197001 (2006)
- [19] Y. Li, V. Baldent, N. Bariii, Y. Cho, B. Fauqu, Y. Sidis, G. Yu, X. Zhao, P. Bourges, and M. Greven, *Nature* **455**, 372 (2008)
- [20] J. Xia, E. Schemm, G. Deutscher, S. A. Kivelson, D. A. Bonn, W. N. Hardy, R. Liang, W. Siemons, G. Koster, M. M. Fejer, and A. Kapitulnik, *Phys. Rev. Lett.* **100**, 127002 (2008)
- [21] N. Read and S. Sachdev, *Phys. Rev. Lett.* **62**, 1694 (1989)
- [22] N. Read and S. Sachdev, *Phys. Rev. B* **42**, 4568 (1990)
- [23] R. K. Kaul, A. Kolezhuk, M. Levin, S. Sachdev, and T. Senthil, *Phys. Rev. B* **75**, 235122 (2007)
- [24] R. K. Kaul, Y. B. Kim, S. Sachdev, and T. Senthil, *Nature Physics* **4**, 28 (2008)
- [25] R. K. Kaul, M. A. Metlitski, S. Sachdev, and C. Xu, *Phys. Rev. B* **78**, 045110 (2008)
- [26] V. Galitski and S. Sachdev, *Phys. Rev. B* **79**, 134512 (2009)
- [27] E. G. Moon and S. Sachdev, *Phys. Rev. B* **80**, 035117 (2009)
- [28] S. Sachdev, M. A. Metlitski, Y. Qi, and C. Xu, *Phys. Rev. B* **80**, 155129 (2009)
- [29] Y. Qi and S. Sachdev, *Phys. Rev. B* **81**, 115129 (2010)
- [30] S. Sachdev, *Quantum Phase Transitions* (Cambridge University Press, NY, 1999)

- [31] D. van der Marel, H. J. A. Molegraaf, J. Zaanen, Z. Nussinov, F. Carbone, A. Damascelli, H. Eisaki, M. Greven, P. H. Kes, and M. Li, *Nature* **425**, 271 (2003)
- [32] A. Kaminski, S. Rosenkranz, H. M. Fretwell, Z. Z. Li, H. Raffy, M. Randeria, M. R. Norman, and J. C. Campuzano, *Phys. Rev. Lett.* **90**, 207003 (2003)
- [33] N. Doiron-Leyraud, P. Auban-Senzier, S. René de Cotret, C. Bourbonnais, D. Jérôme, K. Bechgaard, and L. Taillefer, *Phys. Rev. B* **80**, 214531 (2009)
- [34] L. Fang, H. Luo, P. Cheng, Z. Wang, Y. Jia, G. Mu, B. Shen, I. I. Mazin, L. Shan, C. Ren, and H.-H. Wen, *Phys. Rev. B* **80**, 140508 (2009)
- [35] L. Taillefer, *Annual Review of Condensed Matter Physics* **1**, 51 (2010)
- [36] R. Daou, N. Doiron-Leyraud, D. LeBoeuf, S. Y. Li, F. Lalibert, O. Cyr-Choinire, Y. J. Jo, L. Balicas, J.-Q. Yan, J.-S. Zhou, J. B. Goodenough, and L. Taillefer, *Nature Physics* **5**, 31 (2009)
- [37] S. Nakamae, K. Behnia, N. Mangkorntong, M. Nohara, H. Takagi, S. J. C. Yates, and N. E. Hussey, *Phys. Rev. B* **68**, 100502 (2003)
- [38] R. A. Cooper, Y. Wang, B. Vignolle, O. J. Lipscombe, S. M. Hayden, Y. Tanabe, T. Adachi, Y. Koike, M. Nohara, H. Takagi, C. Proust, and N. E. Hussey, *Science* **323**, 603 (2009)
- [39] S. A. Kivelson, E. Fradkin, and V. J. Emery, *Nature* **393**, 550 (1998)
- [40] M. E. Simon and C. Varma, *Phys. Rev. Lett.* **89**, 247003 (2002)
- [41] S. Sachdev, *Physica Status Solidi b* **247**, 537 (2010)
- [42] E. Demler, S. Sachdev, and Y. Zhang, *Phys. Rev. Lett.* **87**, 067202 (2001)
- [43] J. Chang, C. Niedermayer, R. Gilardi, N. B. Christensen, H. M. Rønnow, D. F. McMorrow, M. Ay, J. Stahn, O. Sobolev, A. Hiess, S. Pailhes, C. Baines, N. Momono, M. Oda, M. Ido, and J. Mesot, *Phys. Rev. B* **78**, 104525 (2008)
- [44] N. Doiron-Leyraud, C. Proust, D. LeBoeuf, J. Levallois, J.-B. Bonnemaïson, R. Liang, D. A. Bonn, W. N. Hardy, and L. Taillefer, *Nature* **447**, 565 (2007)
- [45] D. J. Scalapino, E. Loh, and J. E. Hirsch, *Phys. Rev. B* **34**, 8190 (1986)
- [46] D. J. Scalapino, *Physics Reports* **250**, 329 (1995)
- [47] A. W. Sandvik and H. G. Evertz, *Phys. Rev. B* **82**, 024407 (2010)

- [48] L. Wang, K. S. D. Beach, and A. W. Sandvik, Phys. Rev. B **73**, 014431 (2006)
- [49] A. Pelissetto and E. Vicari, Phys.Rept. **368**, 549 (2002)
- [50] F. D. M. Haldane, Phys. Rev. Lett. **61**, 1029 (1988)
- [51] O. I. Motrunich and A. Vishwanath, Phys. Rev. B **70**, 075104 (2004)
- [52] M. Peskin, Annals Phys. **113**, 122 (1978)
- [53] C. Dasgupta and B. I. Halperin, Phys. Rev. Lett. **47**, 1556 (1981)
- [54] O. I. Motrunich and A. Vishwanath, Phys. Rev. Lett. **101**, 050405 (2008)
- [55] A. B. Kuklov, M. Matsumoto, N. V. Prokof'ev, B. V. Svistunov, and M. Troyer, Phys. Rev. Lett. **101**, 050405 (2008)
- [56] A. M. Polyakov, Phys.Lett. **B59**, 82 (1975)
- [57] A. W. Sandvik, Phys. Rev. Lett. **98**, 227202 (2007)
- [58] R. G. Melko and R. K. Kaul, Phys. Rev. Lett. **100**, 017203 (2008)
- [59] A. W. Sandvik, Phys. Rev. Lett. **104**, 177201 (2010)
- [60] J. Polchinski(1992), hep-th/9210046
- [61] R. Shankar, Physica A: Statistical Mechanics and its Applications **177**, 530 (1991)
- [62] R. Shankar, Rev. Mod. Phys. **66**, 129 (1994)
- [63] C. J. Halboth and W. Metzner, Phys. Rev. B **57**, 8873 (1998)
- [64] A. V. Chubukov, D. L. Maslov, S. Gangadharaiah, and L. I. Glazman, Phys. Rev. B **71**, 205112 (2005)
- [65] A. V. Chubukov, C. Pépin, and J. Rech, Phys. Rev. Lett. **92**, 147003 (2004)
- [66] A. J. Millis, Phys. Rev. B **45**, 13047 (1992)
- [67] A. Abanov and A. Chubukov, Phys. Rev. Lett. **93**, 255702 (2004)
- [68] M. A. Metlitski and S. Sachdev, Phys. Rev. B **82**, 075127 (2010)
- [69] T. Grover and T. Senthil, Phys. Rev. Lett. **100**, 156804 (2008)
- [70] Y. Ran, A. Vishwanath, and D. H. Lee, arXiv:0806.2321 [cond-mat.str-el] (2008)

- [71] I. Affleck and J. B. Marston, Phys. Rev. B **37**, 3774(R) (1988)
- [72] J. B. Marston and I. Affleck, Phys. Rev. B **39**, 11538 (1989)
- [73] P. A. Lee and N. Nagaosa, Phys. Rev. B **46**, 5621 (1992)
- [74] B. I. Halperin, P. A. Lee, and N. Read, Phys. Rev. B **47**, 7312 (1993)
- [75] J. Polchinski, Nucl. Phys. B **422**, 617 (1994)
- [76] W. Rantner and X.-G. Wen, Phys. Rev. Lett. **86**, 3871 (2001)
- [77] W. Rantner and X.-G. Wen, Phys. Rev. B **66**, 144501 (2002)
- [78] M. Hermele, T. Senthil, M. P. A. Fisher, P. A. Lee, N. Nagaosa, and X.-G. Wen, Phys. Rev. B **70**, 214437 (2004)
- [79] S.-S. Lee, Phys. Rev. B **78**, 085129 (2008)
- [80] Y. Shimizu, K. Miyagawa, K. Kanoda, M. Maesato, and G. Saito, Phys. Rev. Lett. **91**, 107001 (2003)
- [81] O. I. Motrunich, Phys. Rev. B **72**, 045105 (2005)
- [82] S. S. Lee and P. A. Lee, Phys. Rev. Lett. **95**, 036403 (2005)
- [83] J. S. Helton, K. Matan, M. P. Shores, E. A. Nytko, B. M. Bartlett, Y. Yoshida, Y. Takano, A. Suslov, Y. Qiu, J.-H. Chung, D. G. Nocera, and Y. S. Lee, Phys. Rev. Lett. **98**, 107204 (2007)
- [84] O. Ofer, A. Keren, E. A. Nytko, M. P. Shores, B. M. Bartlett, D. G. Nocera, C. Baines, and A. Amato, “Ground state and excitation properties of the quantum kagome system $\text{ZnCu}_3(\text{OH})_6\text{Cl}_2$ investigated by local probes,” arXiv:cond-mat/0610540 (2006)
- [85] P. Mendels, F. Bert, M. de Vries, A. Olariu, A. Harrison, F. Duc, J. Trombe, J. Lord, A. Amato, and C. Baines, Phys. Rev. Lett. **98**, 077204 (2007)
- [86] Y. Ran, M. Hermele, P. A. Lee, and X.-G. Wen, Phys. Rev. Lett. **98**, 117205 (2007)
- [87] Y. Okamoto, M. Nohara, H. Aruga-Katori, and H. Takagi, Phys. Rev. Lett. **99**, 137207 (2007)
- [88] Y. Zhou, P. A. Lee, T.-K. Ng, and F.-C. Zhang, Phys. Rev. Lett. **101**, 197201 (2008)

-
- [89] M. Lawler, A. Paramakanti, Y. B. Kim, and L. Balents, “Gapless spin liquids on the three dimensional hyper-kagome lattice of $\text{Na}_4\text{Ir}_3\text{O}_8$,” arXiv:0806.4395 [cond-mat.str-el] (2008)
- [90] A. M. Polyakov, Nucl. Phys. **B120**, 429 (1977)
- [91] V. Borokhov, A. Kapustin, and X. Wu, J. High Energy Phys. **2002**, 049 (2002)
- [92] P. Di Francesco, P. Mathieu, and D. Senechal, *Conformal Field Theory* (Springer, 1999)
- [93] J. Polchinski, *String Theory, Vol. 1: An Introduction to the Bosonic String* (Cambridge University Press, 1998)
- [94] T. T. Wu and C. N. Yang, Nucl. Phys. B **107**, 365 (1976)
- [95] A. DAdda, P. Di Vecchia, and M. Lüscher, Nucl. Phys. B **146**, 63 (1978)
- [96] K. H. Höglund, A. W. Sandvik, and S. Sachdev, Phys. Rev. Lett. **98**, 087203 (2007)
- [97] K. Manabe, H. Ishimoto, N. Koide, Y. Sasago, and K. Uchinokura, Phys. Rev. B **58**, R575 (1998)
- [98] J. Bobroff, H. Alloul, W. A. MacFarlane, P. Mendels, N. Blanchard, G. Collin, and J.-F. Marucco, Phys. Rev. Lett. **86**, 4116 (2001)
- [99] S. Ouazi, J. Bobroff, H. Alloul, M. Le Tacon, N. Blanchard, G. Collin, M. H. Julien, M. Horvatić, and C. Berthier, Phys. Rev. Lett. **96**, 127005 (2006)
- [100] A. Yazdani, B. A. Jones, C. P. Lutz, M. F. Crommie, and D. M. Eigler, Science **275**, 1767 (1997)
- [101] S. H. Pan, E. W. Hudson, K. M. Lang, H. Eisaki, S. Uchida, and J. C. Davis, Nature (London) **403**, 746 (2000)
- [102] E. W. Hudson, K. M. Lang, V. Madhavan, S. H. Pan, H. Eisaki, S. Uchida, and J. C. Davis, Nature (London) **411**, 920 (2001)
- [103] O. P. Vajk, P. K. Mang, M. Greven, P. M. Gehring, and J. W. Lynn, Science **295**, 1691 (2002)
- [104] N. Nagaosa, Y. Hatsugai, and M. Imada, J. Phys. Soc. Jpn **58**, 978 (1989)
- [105] A. W. Sandvik, E. Dagotto, and D. J. Scalapino, Phys. Rev. B **56**, 11701 (1997)
- [106] S. Sachdev, C. Buragohain, and M. Vojta, Science **286**, 2479 (1999)

-
- [107] M. Vojta, C. Buragohain, and S. Sachdev, Phys. Rev. B **61**, 15152 (2000)
- [108] O. P. Sushkov, Phys. Rev. B **62**, 12135 (2000)
- [109] A. L. Chernyshev, Y. C. Chen, and A. H. Castro Neto, Phys. Rev. B **65**, 104407 (2002)
- [110] M. Troyer, Prog. Theor. Phys. Supplement **145**, 326 (2002)
- [111] K. H. Höglund and A. W. Sandvik, Phys. Rev. Lett. **91**, 077204 (2003)
- [112] S. Sachdev and M. Vojta, Phys. Rev. B **68**, 064419 (2003)
- [113] A. Lüscher and O. P. Sushkov, Phys. Rev. B **71**, 064414 (2005)
- [114] A. V. Syromyatnikov and S. V. Maleyev, Phys. Rev. B **74**, 184433 (2006)
- [115] F. Anfuso and S. Eggert, Phys. Rev. Lett. **96**, 017204 (2006)
- [116] S. Eggert and F. Anfuso, Physica B **384**, 192 (2006)
- [117] K. H. Höglund and A. W. Sandvik, Phys. Rev. Lett. **99**, 027205 (2007)
- [118] V. N. Kotov, O. Sushkov, Z. Weihong, and J. Oitmaa, Phys. Rev. Lett. **80**, 5790 (1998)
- [119] M. Matsumoto, C. Yasuda, S. Todo, and H. Takayama, Phys. Rev. B **65**, 014407 (2001)
- [120] E. Witten, Nucl. Phys. B **149**, 285 (1979)
- [121] A. Kolezhuk, S. Sachdev, R. R. Biswas, and P. Chen, Phys. Rev. B **74**, 165114 (2006)
- [122] S. Sachdev, Phys. Rev. B **55**, 142 (1997)
- [123] V. Y. Irkhin, A. A. Katanin, and M. I. Katsnelson, Phys. Rev. B **54**, 11953 (1996)
- [124] A. Banerjee, K. Damle, and F. Alet, Phys. Rev. B **82**, 155139 (2010)
- [125] A. Banerjee, K. Damle, and F. Alet(2010), [arXiv:1012.3691](https://arxiv.org/abs/1012.3691)
- [126] M. Vershinin, S. Misra, S. Ono, Y. Abe, Y. Ando, and A. Yazdani, Science **303**, 1995 (2004)
- [127] J. E. Hoffman, E. W. Hudson, K. M. Lang, V. Madhavan, S. H. Pan, H. Eisaki, S. Uchida, and J. C. Davis, Science **295**, 466 (2002)

-
- [128] B. W. Hoogenboom, K. Kadowaki, B. Revaz, M. Li, C. Renner, and O. Fischer, Phys. Rev. Lett. **87**, 267001 (2001)
- [129] G. Levy, M. Kugler, A. A. Manuel, O. Fischer, and M. Li, Phys. Rev. Lett. **95**, 257005 (2005)
- [130] A. Del Maestro, B. Rosenow, and S. Sachdev, Phys. Rev. B **74**, 024520 (2006)
- [131] J. A. Robertson, S. A. Kivelson, E. Fradkin, A. C. Fang, and A. Kapitulnik, Phys. Rev. B **74**, 134507 (2006)
- [132] M. Raczkowski, M. Capello, D. Poilblanc, R. Frésard, and A. M. Oleś, Phys. Rev. B **76**, 140505 (2007)
- [133] M. Vojta and O. Rösch, Phys. Rev. B **77**, 094504 (2008)
- [134] L. Balents, L. Bartosch, A. Burkov, S. Sachdev, and K. Sengupta, Phys. Rev. B **71**, 144508 (2005)
- [135] L. Bartosch, L. Balents, and S. Sachdev, Annals of Physics **321**, 1528 (2006)
- [136] L. Balents and S. Sachdev, Annals of Physics **322**, 2635 (2007)
- [137] M. Levin and T. Senthil, Phys. Rev. B **70**, 220403 (2004)
- [138] H. W. Diehl, Int. J. Mod. Phys. B **11**, 3503 (1997)
- [139] A. Bray and M. Moore, J. Phys. A **10**, 1927 (1977)
- [140] H. W. Diehl and M. Smock, Phys. Rev. B **47**, 5841 (1993)
- [141] T. W. Burkhardt and H. W. Diehl, Phys. Rev. B **50**, 3894 (1994)
- [142] S. Florens, L. Fritz, and M. Vojta, Phys. Rev. Lett. **96**, 036601 (2006)
- [143] M. A. Metlitski and S. Sachdev, Phys. Rev. B **76**, 064423 (2007)
- [144] K. H. Höglund and A. W. Sandvik, Phys. Rev. B **70**, 024406 (2004)
- [145] S. Sachdev and R. Jalabert, Mod. Phys. Lett. B **4**, 1043 (1990)
- [146] K. Kajantie, M. Laine, T. Neuhaus, A. Rajantie, and K. Rummukainen, Nucl. Phys. B **699**, 632 (2004)
- [147] D. Son, JHEP **0202**, 023 (2002)
- [148] M. A. Metlitski, Phys. Rev. D **77**, 085011 (2008)
- [149] S. Samuel, Nucl. Phys. B **154**, 62 (1979)

- [150] R. Fazio and D. Zappalà, *Phys. Rev. B* **53**, R8883 (1996)
- [151] M.-C. Cha, M. P. A. Fisher, S. M. Girvin, M. Wallin, and A. P. Young, *Phys. Rev. B* **44**, 6883 (1991)
- [152] M. E. X. Guimaraes and B. Linet, *Commun. Math. Phys.* **165**, 297 (1994)
- [153] S. Sachdev, in *Lecture Notes in Physics*, edited by D. J. J. F. U. Schollwock, J. Richter and R. A. Bishop (Springer, Berlin, 2004)
- [154] J. Smiseth, E. Smørgrav, and A. Sudbø, *Phys. Rev. Lett.* **93**, 077002 (2004)
- [155] J. Smiseth, E. Smørgrav, E. Babaev, and A. Sudbø, *Phys. Rev. B* **71**, 214509 (2005)
- [156] E. Babaev, *Phys. Rev. Lett.* **89**, 067001 (2002)
- [157] E. Babaev, *Nucl. Phys. B* **686**, 397 (2004)
- [158] J. Zaanen and O. Gunnarsson, *Phys. Rev. B* **40**, 7391 (1989)
- [159] K. Machida, *Physica C* **158**, 192 (1989)
- [160] M. Kato, K. Machida, H. Nakanishi, and M. Fujita, *J. Phys. Soc. Japan* **59**, 1047 (1990)
- [161] M. Inui and P. B. Littlewood, *Phys. Rev. B* **44**, 4415 (1991)
- [162] S. A. Kivelson, I. P. Bindloss, E. Fradkin, V. Oganesyan, J. M. Tranquada, A. Kapitulnik, and C. Howald, *Rev. Mod. Phys.* **75**, 1201 (2003)
- [163] A. V. Chubukov and S. Sachdev, *Phys. Rev. Lett.* **71**, 169 (1993)
- [164] R. K. Kaul, R. G. Melko, M. A. Metlitski, and S. Sachdev, *Phys. Rev. Lett.* **101**, 187206 (2008)
- [165] M. A. Metlitski and S. Sachdev, *Phys. Rev. B* **77**, 054411 (2008)
- [166] R. A. Borzi, S. A. Grigera, J. Ferrell, R. S. Perry, S. J. S. Lister, S. L. Lee, D. A. Tenant, Y. Maeno, and A. P. Mackenzie, *Science* **315**, 214 (2007)
- [167] C. Fang, H. Yao, W.-F. Tsai, J. Hu, and S. A. Kivelson, *Phys. Rev. B* **77**, 224509 (2008)
- [168] C. Xu, M. Müller, and S. Sachdev, *Phys. Rev. B* **78**, 020501 (2008)
- [169] T.-M. Chuang, M. P. Allan, J. Lee, Y. Xie, N. Ni, S. L. Bud'ko, G. S. Boebinger, P. C. Canfield, and J. C. Davis, *Science* **327**, 181 (2010)

-
- [170] J.-H. Chu, J. G. Analytis, K. De Greve, P. L. McMahon, Z. Islam, Y. Yamamoto, and I. R. Fisher, *Science* **329**, 824 (2010)
- [171] J. Zaanen, *J. Phys. Chem. Solids* **59**, 1769 (1998)
- [172] S. Sachdev, *Rev. Mod. Phys.* **75**, 913 (2003)
- [173] M. Vojta, *Adv. Phys.* **58**, 699 (2009)
- [174] P. Chandra, P. Coleman, and A. I. Larkin, *Phys. Rev. Lett.* **64**, 88 (1990)
- [175] L. Capriotti and S. Sachdev, *Phys. Rev. Lett.* **93**, 257206 (2004)
- [176] N. Read and S. Sachdev, *Phys. Rev. Lett.* **66**, 1773 (1991)
- [177] S. Sachdev and N. Read, *J. Mod. Phys. B* **5**, 219 (1991)
- [178] H. Yamase and H. Kohno, *J. Phys. Soc. Jpn.* **69**, 2151 (2000)
- [179] C. J. Halboth and W. Metzner, *Phys. Rev. Lett.* **85**, 5162 (2000)
- [180] V. Oganesyan, S. A. Kivelson, and E. Fradkin, *Phys. Rev. B* **64**, 195109 (2001)
- [181] W. Metzner, D. Rohe, and S. Andergassen, *Phys. Rev. Lett.* **91**, 066402 (2003)
- [182] H.-Y. Kee, E. H. Kim, and C.-H. Chung, *Phys. Rev. B* **68**, 245109 (2003)
- [183] H. Yamase, V. Oganesyan, and W. Metzner, *Phys. Rev. B* **72**, 035114 (2005)
- [184] L. Dell'Anna and W. Metzner, *Phys. Rev. B* **73**, 045127 (2006)
- [185] L. Dell'Anna and W. Metzner, *Phys. Rev. Lett.* **98**, 136402 (2007)
- [186] J. Rech, C. Pépin, and A. V. Chubukov, *Phys. Rev. B* **74**, 195126 (2006)
- [187] M. J. Lawler, D. G. Barci, V. Fernández, E. Fradkin, and L. Oxman, *Phys. Rev. B* **73**, 085101 (2006)
- [188] M. J. Lawler and E. Fradkin, *Phys. Rev. B* **75**, 033304 (2007)
- [189] P. Jakubczyk, P. Strack, A. A. Katanin, and W. Metzner, *Phys. Rev. B* **77**, 195120 (2008)
- [190] M. Zacharias, P. Wölfle, and M. Garst, *Phys. Rev. B* **80**, 165116 (2009)
- [191] D. L. Maslov and A. V. Chubukov, *Phys. Rev. B* **81**, 045110 (2010)
- [192] H. v. Löhneysen, A. Rosch, M. Vojta, and P. Wölfle, *Rev. Mod. Phys.* **79**, 1015 (2007)

-
- [193] M. Vojta, Y. Zhang, and S. Sachdev, Phys. Rev. Lett. **85**, 4940 (2000)
- [194] M. Vojta, Y. Zhang, and S. Sachdev, Int. J. Mod. Phys. B **14**, 3719 (2000)
- [195] E.-A. Kim, M. J. Lawler, P. Oreto, S. Sachdev, E. Fradkin, and S. A. Kivelson, Phys. Rev. B **77**, 184514 (2008)
- [196] Y. Huh and S. Sachdev, Phys. Rev. B **78**, 064512 (2008)
- [197] B. L. Altshuler, L. B. Ioffe, and A. J. Millis, Phys. Rev. B **50**, 14048 (1994)
- [198] S.-S. Lee, Phys. Rev. B **80**, 165102 (2009)
- [199] A. Luther, Phys. Rev. B **19**, 320 (1979)
- [200] A. Houghton and J. B. Marston, Phys. Rev. B **48**, 7790 (1993)
- [201] H.-J. Kwon, A. Houghton, and J. B. Marston, Phys. Rev. Lett. **73**, 284 (1994)
- [202] H. F. D. M., in *International School of Physics "Enrico Fermi", Course CXXI "Perspectives in Many-Particle Physics"*, edited by R. A. Broglia and J. R. Schrieffer (North-Holland, Amsterdam, 1994) cond-mat/0505529
- [203] A. H. Castro Neto and E. H. Fradkin, Phys. Rev. B **51**, 4084 (1995)
- [204] E. Berg, C.-C. Chen, and S. A. Kivelson, Phys. Rev. Lett. **100**, 027003 (2008)
- [205] Y. B. Kim, A. Furusaki, X.-G. Wen, and P. A. Lee, Phys. Rev. B **50**, 17917 (1994)
- [206] C. Nayak and F. Wilczek, Nucl. Phys. B **417**, 359 (1994)
- [207] C. Nayak and F. Wilczek, Nucl. Phys. B **430**, 534 (1994)
- [208] Y. B. Kim, P. A. Lee, and X.-G. Wen, Phys. Rev. B **52**, 17275 (1995)
- [209] A. Stern and B. I. Halperin, Phys. Rev. B **52**, 5890 (1995)
- [210] A. Stern, B. I. Halperin, F. von Oppen, and S. H. Simon, Phys. Rev. B **59**, 12547 (1999)
- [211] N. Read, Phys. Rev. B **58**, 16262 (1998)
- [212] R. Shankar and G. Murthy, Phys. Rev. Lett. **79**, 4437 (1997)
- [213] T. Senthil, Phys. Rev. B **78**, 035103 (2008)
- [214] T. Senthil, Phys. Rev. B **78**, 045109 (2008)

- [215] S.-S. Lee, Phys. Rev. D **79**, 086006 (2009)
- [216] M. Cubrovic, J. Zaanen, and K. Schalm, Science **325**, 439 (2009)
- [217] H. Liu, J. McGreevy, and D. Vegh, Phys. Rev. D **83**, 065029 (2011)
- [218] F. Denef, S. A. Hartnoll, and S. Sachdev, Phys. Rev. D **80**, 126016 (2009)
- [219] S. A. Hartnoll and D. M. Hofman, Phys. Rev. B **81**, 155125 (2010)
- [220] N. Ni, M. E. Tillman, J.-Q. Yan, A. Kracher, S. T. Hannahs, S. L. Bud'ko, and P. C. Canfield, Phys. Rev. B **78**, 214515 (2008)
- [221] S. Nandi, M. G. Kim, A. Kreyssig, R. M. Fernandes, D. K. Pratt, A. Thaler, N. Ni, S. L. Bud'ko, P. C. Canfield, J. Schmalian, R. J. McQueeney, and A. I. Goldman, Phys. Rev. Lett. **104**, 057006 (2010)
- [222] R. M. Fernandes, D. K. Pratt, W. Tian, J. Zarestky, A. Kreyssig, S. Nandi, M. G. Kim, A. Thaler, N. Ni, P. C. Canfield, R. J. McQueeney, J. Schmalian, and A. I. Goldman, Phys. Rev. B **81**, 140501 (2010)
- [223] G. Knebel, D. Aoki, and J. Flouquet(2009), [arXiv:0911.5223](https://arxiv.org/abs/0911.5223)
- [224] M. T. Béal-Monod and K. Maki, Phys. Rev. Lett. **34**, 1461 (1975)
- [225] S. Pankov, S. Florens, A. Georges, G. Kotliar, and S. Sachdev, Phys. Rev. B **69**, 054426 (2004)
- [226] A. Abanov and A. V. Chubukov, Phys. Rev. Lett. **84**, 5608 (2000)
- [227] A. Abanov, A. V. Chubukov, and A. M. Finkel'stein, Europhys. Lett. **54**, 488 (2001)
- [228] A. Abanov, A. V. Chubukov, and J. Schmalian, Europhys. Lett. **55**, 369 (2001)
- [229] A. Abanov, A. V. Chubukov, and J. Schmalian, Advances in Physics **52**, 119 (2003)
- [230] A. J. Millis, Phys. Rev. B **48**, 7183 (1993)
- [231] S.-W. Tsai, A. H. Castro Neto, R. Shankar, and D. K. Campbell, Phys. Rev. B **72**, 054531 (2005)
- [232] D. T. Son, Phys. Rev. D **59**, 094019 (1999)
- [233] T. Schäfer and K. Schwenzler, Phys. Rev. Lett. **97**, 092301 (2006)
- [234] C. Nayak, Phys. Rev. B **62**, 4880 (2000)

-
- [235] S. Chakravarty, R. B. Laughlin, D. K. Morr, and C. Nayak, *Phys. Rev. B* **63**, 094503 (2001)
- [236] C. Honerkamp, M. Salmhofer, and T. M. Rice, *Eur. Phys. J. B* **27**, 127 (2002)
- [237] L. Amico, R. Fazio, A. Osterloh, and V. Vedral, *Rev. Mod. Phys.* **80**, 5176 (2008)
- [238] L. Amico, R. Fazio, A. Osterloh, and V. Vedral, *Nucl. Phys. B* **424**, 443 (1994)
- [239] L. Bombelli, R. K. Koul, J. Lee, and R. D. Sorkin, *Phys. Rev. D* **34**, 373 (1986)
- [240] M. Srednicki, *Phys. Rev. Lett.* **71**, 666 (1993)
- [241] J. Eisert, M. Cramer, and M. B. Plenio, *Rev. Mod. Phys.* **82**, 277 (2010)
- [242] S. Ryu and T. Takayanagi, *Phys. Rev. Lett.* **96**, 181602 (2006)
- [243] S. Ryu and T. Takayanagi, *JHEP* **0608**, 045 (2006)
- [244] D. V. Fursaev, *Phys. Rev. D* **73**, 124025 (2006)
- [245] H. Casini and M. Huerta, *Nucl. Phys. B* **764**, 183 (2007)
- [246] H. Casini, M. Huerta, and L. Leitaó, *Nucl. Phys. B* **814**, 594 (2009)
- [247] H. Casini and M. Huerta, *J. Stat. Mech.* **0512**, P012 (2005)
- [248] S. N. Solodukhin, *Phys. Lett. B* **665**, 305 (2008)
- [249] E. Fradkin and J. E. Moore, *Phys. Rev. Lett.* **97**, 050404 (2006)
- [250] B. Hsu, M. Mulligan, E. Fradkin, and E.-A. Kim, *Phys. Rev. B* **79**, 115421 (2009)
- [251] A. Vishwanath, L. Balents, and T. Senthil, *Phys. Rev. B* **69**, 224416 (2004)
- [252] E. Fradkin, D. A. Huse, R. Moessner, V. Oganesyan, and S. L. Sondhi, *Phys. Rev. B* **69**, 224415 (2004)
- [253] P. V. Buividovich and M. I. Polikarpov, *Phys. Rev. B* **69**, 224415 (2004)
- [254] M. Caraglio and F. Gliozzi, *JHEP* 0811 **0811**, 076 (2008)
- [255] L. Tagliacozzo, G. Evenbly, and G. Vidal, *Phys. Rev. B* **80**, 235127 (2009)